Acta Geodaetica, Geophysica et Montanistica Hungarica

VOLUME 24, NUMBERS 1–2, 1989

Akadémiai Kiadó, Budapest
AGGM 24 (1–2) 1–212 (1989) HU ISSN 0236-5758

ACTA GEODAETICA, GEOPHYSICA et MONTANISTICA HUNGARICA
A Quarterly Journal of the Hungarian Academy of Sciences

Acta Geodaetica, Geophysica et Montanistica (AGGM) publishes original reports on geodesy, geophysics and minings in English.

AGGM is published in yearly volumes of four numbers by

AKADÉMIAI KIADÓ
Publishing House of the Hungarian Academy of Sciences
H–1054 Budapest, Alkotmány u. 21.

Manuscripts and editorial correspondence should be addressed to

AGGM Editorial Office
H–9401 Sopron P.O. Box 5

Subscription information

Orders should be addressed to KULTURA Foreign Trading Company
H–1389 Budapest P.O. Box 149

Acta Geodaetica, Geophysica et Montanistica Hungarica is abstracted/indexed in Geographical Abstracts, GeoRef Information System, Science Abstracts

INSTRUCTIONS TO AUTHORS

Manuscripts should be sent to the editors (MTA Geodéziai és Geofizikai Kutató Intézete, AGGM Editorial Office. H–9401 Sopron, P.O. Box 5. HUNGARY) Only articles not submitted for publication elsewhere are accepted.

Manuscripts should be typewritten in duplicate, double-spaced, 25 lines with 50 letters each. The papers generally include the following components, which should be presented in the order listed.

1. Title, name of author(s), affiliation, dateline, abstract, keywords
2. Text, acknowledgements
3. References
4. Footnotes
5. Legends
6. Tables and illustrations

1. The *affiliation* should be as concise as possible and should include the complete mailing address of the authors. The *date of receipt* of the manuscript will be supplied by the editors. The abstract should not exceed 250 words and should clearly and simply summarize the most important methods and results. 5–10 significant expressions describing the content are used as *keywords*. Authors may recommend these keywords.

2. The *text* should be generally in English and as short and clear as possible. From Hungarian authors papers are also accepted in Hungarian.

The section heading should *not* be underlined or in capitals.

Please note that underlining denotes special types:

– single underlining: italics
– double underlining: bold-face roman

ACTA GEODAETICA, GEOPHYSICA et MONTANISTICA HUNGARICA

A Quarterly Journal of the Hungarian Academy of Sciences

VOLUME 24

Akadémiai Kiadó, Budapest

1989

KEYWORD INDEX

CONTENTS

AUTHOR INDEX

CONTENTS

Borsodi Nyomda
PRINTED IN HUNGARY
Grafityp Gm

Acta Geod. Geoph. Mont. Hung., Vol. 24 (1-2), pp. 3-55 (1989)

ENERGY BALANCE OF UNDERGROUND GAS STORAGE

Gy Zoltán†

Mining Chemical Research Laboratory of the Hungarian Academy of Sciences,
H-3515 Miskolc, Egyetemváros, POB 2, Hungary

[Manuscript received September 12, 1984]

Mass and state of a porous reservoir determine the energy content of the system. However, according to the principles of thermodynamics the absolute value of the energy content of a system cannot be calculated and changes of the mass and state of a system can only characterize the direction and rate of the change of energy content. The paper analyzes the energy of the reservoir and the energy stored as functions of the state of reservoir. The specific energy of the saturation is determined as a function of volume. Apparent energy optimum of underground gas storage is dealt with. It is proved that the specific energy of storage is independent of the structure of the reservoir. Finally, the order and proportions of the components of the full energy content in fluid-bearing reservoirs is determined.

Keywords: capillary pressure; compressibility; fluid-bearing porous reservoir; formation pressure; formation water; energy of storage; "high-energy" pore space; interfacial properties; porosity; saturation; specific energy of storage

SYMBOLS

A	surface area, interfacial area
A_c	capillary cross-section
A_{sg}	solid-gas interfacial area
d	capillary diameter
F	force
F_c	capillary resistance
g	acceleration due to gravity
h	height
i	number of observation (subscript)
J	$J(S_g) = p_g/Z$
K	$K(S_g) = (p_g/Z)S_g$
n	mole number
p	pressure
p_g	gas pressure = $p_w + P_c$
p_w	water pressure, constant (= 2, 4, 6, 8, 10 MPa)
P_c	capillary pressure = $P_c(S_g) = P_c'(S_g)$
r	capillary radius
R	gas constant

S	saturation
S_g	gas saturation
S_w	water saturation
S_{wres}	residual water saturation
S_{gI}	gas saturation at the point of inflexion of function $P_c(S_g)$
T	temperature
T_{norm}	normal temperature
V	volume
V_k	volume, non-variable
V_v	volume, variable
V_g	gas volume
V_w	water volume
V_{gk}	gas volume, constant, in laboratory (= 14700 cm^3)
V_{gv}	gas volume, variable
V_{mol}	mole volume
V_p	pore volume
V_{pk}	pore volume, in laboratory (= 147.7475 cm^3)
V_{gkt}	gas volume, non-variable, in reservoir
V_{pkt}	pore volume, in reservoir
W	energy (work)
W_{stg}	energy of storage
W_{std}	energy stored
Z	$Z(S_g) = Z\,[p_g;T;\varepsilon]$ compressibility
ε	factor relating to composition of natural gas
ϱ	density
σ	interfacial tension
Θ	contact angle
β	elastic compressibility of water

Energy resources near agglomerations of civilization have mostly been exhausted, the distance between energy-consuming areas and newly developed energy resources (e.g. oil and gas fields in Siberia and Alaska) is rapidly increasing. Therefore transport of oil, gas and coal is becoming a more difficult technical and economic task and, in many cases, requires the utmost skill of scientists and engineers.

Interests of consumers and producers are common as to meet energy demands under acceptable conditions, i.e. reasonable prices and sufficient profits. Losses that do not cost money on either side are neglected. It is not difficult to estimate the financial consequences of this kind of indifference which is by no means deliberate and, seemingly, one does not pay for it. All these losses will, undoubtedly, be measured in the near future and attention will be paid to all kinds of energy changes and losses since mankind will depend on a positive energy balance for its existence.

As one of the most advanced measures of energy management

in the last decades, the underground gas storage was introduced to eliminate the gap between the characteristics of gas production and the requirements of the consumers. A buffer system was needed between producers and consumers to maintain production at its optimum while meeting excessively varying needs of consumers. This seems to sufficiently underline the necessity of establishing storage systems. Underground gas storage solves the technical side of the problem, and, in addition, provides especially advantageous features concerning economics due to its large storage capacity: specific operating costs are much lower than those of conventional surface storage. Though the operation of these storage systems has to face all the problems reservoir engineering is encountered in controlling changes of state in the reservoir, advanced techniques and methods used in oil and gas production can provide attractive solutions for these difficult technical-economic tasks.

1. ENERGY OF THE RESERVOIR AND ENERGY STORED AS FUNCTIONS OF THE STATE OF RESERVOIR

Although underground gas storage seems a purely technical activity at first sight, if all things are considered it is an economic undertaking: energy is stored at an "energy price". It might appear slightly unusual to consider the costs of a process in terms of energy used to carry out the very process, but in this special case it seems to be the most suitable way of treatment.

A previous equation (Zoltán 1986 b, Eq. 7) describes changes in the state of energy related to place and task, the change being a consequence of an interference with the mass of the system. Let us now rewrite this equation to express the change of energy in terms of the geometrical volumes in which the change has taken place. It holds for all states of the system that

$$V_g = V_{pk}\, S_g$$

hence

$$dV_g = V_{pk}\, dS_g$$

Using these expressions, Eq. (7) in Zoltán (1986b) can be rewritten as

$$V_{pk}\int_{S_{go}}^{S_g} p_w dS_g + V_{pk}\int_{S_{go}}^{S_g} P_c dS_g + V_{gk}\int_{p_{go}}^{p_g} dp_g + V_{pk}\int_{p_{go}}^{p_g} S_g dp_g = \tag{1}$$

$$= V_{gk}\int_{Z_o}^{Z} J\, dZ + V_{pk}\int_{Z_o}^{Z} K\, dZ + V_{gk}\int_{J_o}^{J} Z\, dJ + V_{pk}\int_{K_o}^{p_{go}} Z\, dK\ .$$

Equation (7) in Zoltán (1986b) and Eq. (1) here express the change of energy content equivalent to the change of mass and state of the experimental system. To achieve the highest accuracy, the results obtained from the laboratory experiments have been expressed in CGS-units, but in order to make them more accessible for engineers they have been converted into SI--units too. Instead of displaying numerical values, more plausible diagrams are used to show the changes of energy content in volumes V_{gk} and V_{pk} due to changes of state as a function of the state of saturation in the system. Formation pressure in the reservoir is represented by water pressures 2, 4, 6, 8 and 10 MPa. The curves give the change of energy content per unit volume (1 m^3) of V_{gkt} and V_{pkt}

$$W_I = C_I\, V_{gk}\int_{J_o}^{J} Z\, dJ \tag{2}$$

and

$$\Delta W_{II} = C_{II}\, V_{pk}\int_{K_o}^{K} Z\, dK \tag{3}$$

with the aforementioned formation pressures as parameters. C_I and C_{II} are coefficients used to convert energy values of the

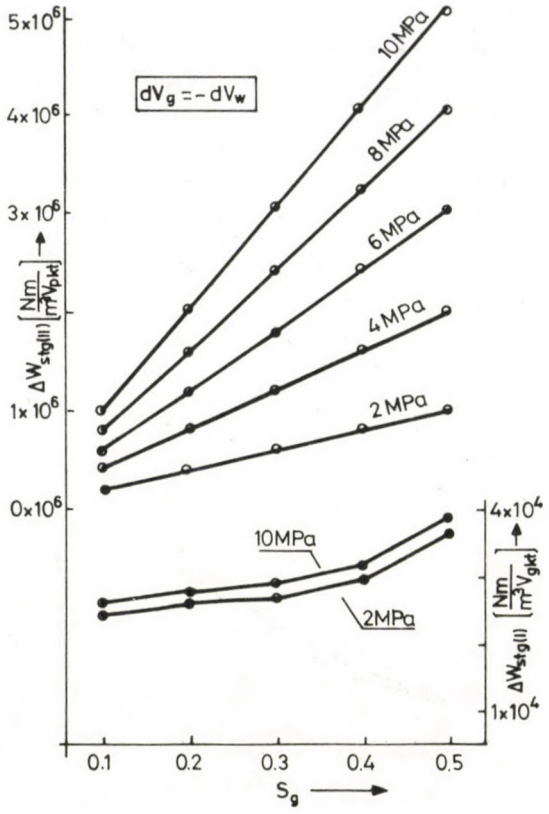

Fig. 1. Energy of storage as a function of reservoir state in terms of units of pore volumes V_{pkt} and V_{gkt} at $dV_g = -dV_w$

total constant gas volume V_{gk} and the likewise constant pore volume V_{pk} expressed in terms of CGS-units into SI-units for unit volume (1 m^3) of the reservoir. Figures 1 to 4 express the same in terms of numerical values given earlier in Eq. (23) by Zoltán (1986b) using theoretical considerations. As noted,

$$dW_I(S_{gi}) < dW_{II}(S_{gi})$$

holds for the changes of energy content in unit volume of the reservoir if $i > 1$, and the equivalent state is $0 < S_g < 1-S_{wres}$. If the change of energy content in unit volumes of V_{gk} and V_{pk} takes place within this saturation interval according to Eq. (25)

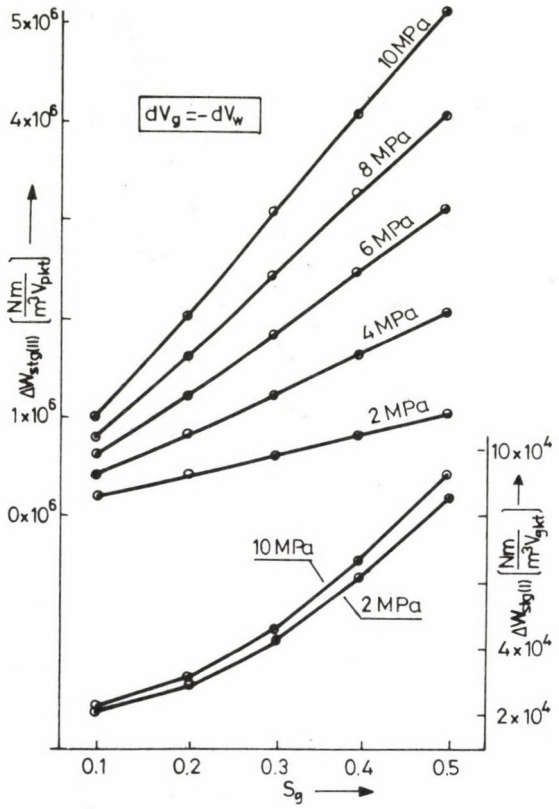

Fig. 2. Energy of storage as a function of reservoir state in terms of units of volumes V_{pkt} and V_{gkt} of a "high energy pore space" at $dV_g = -dV_w$

(Zoltán 1986b) then the sum of these elemental energy components must coincide with those in Figs 1 to 4.

In addition to the energy requirement of changes of state in volumes V_{gkt} and V_{pkt} it is of interest to know the amount of energy stored in these volumes. The "price" of storage of this energy is the energy requirement of the change of state. The amount of energy stored is illustrated in Figs 5 to 8 which indicate how the stored energy depends on the state of the system and the parameters of state.

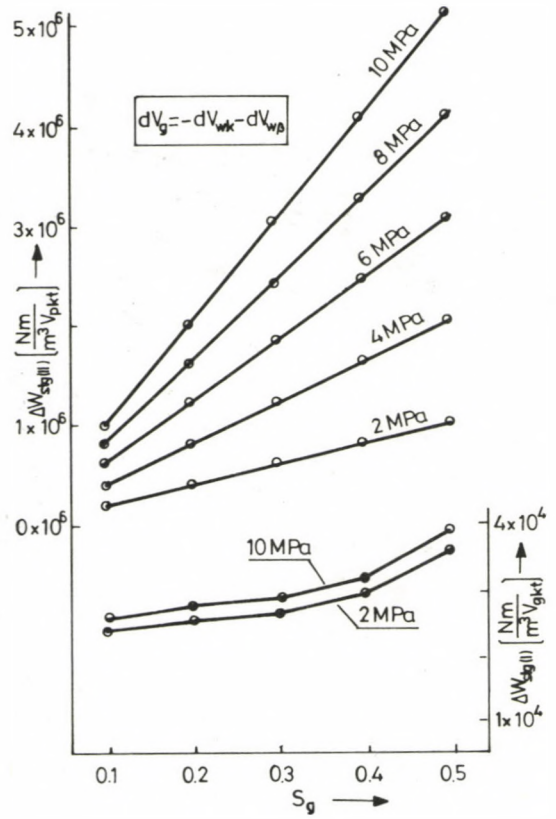

Fig. 3. The same as Fig. 1 at $dV_g = -dV_{wk}-dV_{w\beta}$

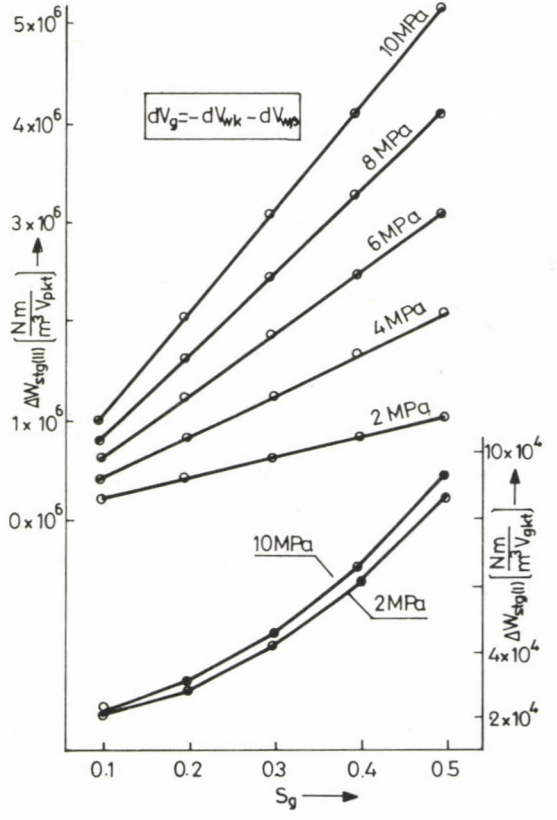

Fig. 4. The same as Fig. 2 at $dV_g = -dV_{wk}-dV_{w\beta}$

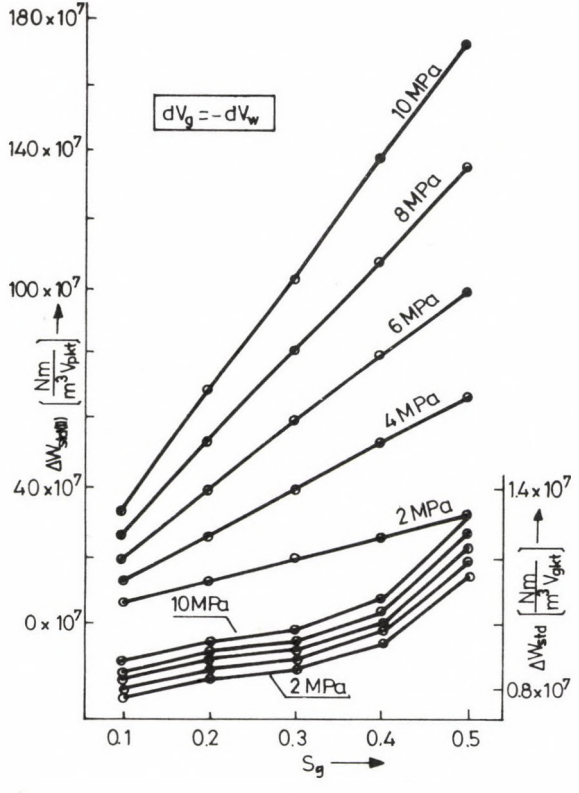

Fig. 5. The same as Fig. 1

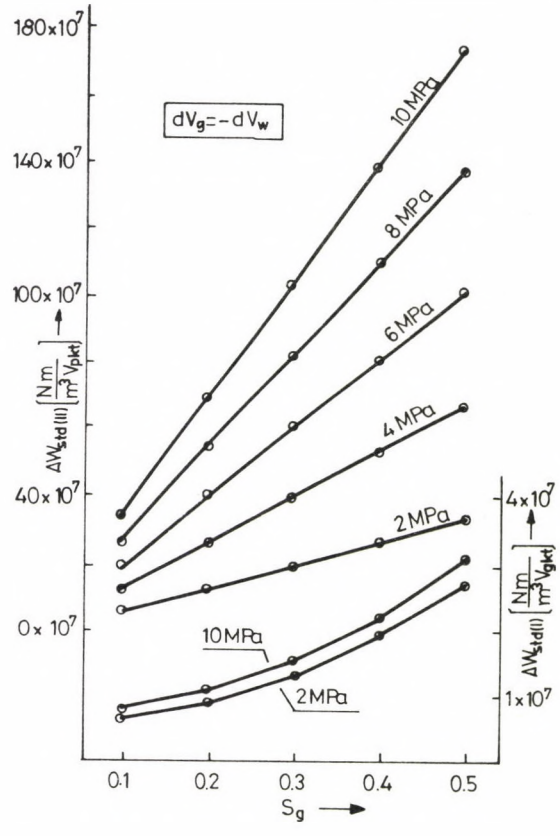

Fig. 6. The same as Fig. 2

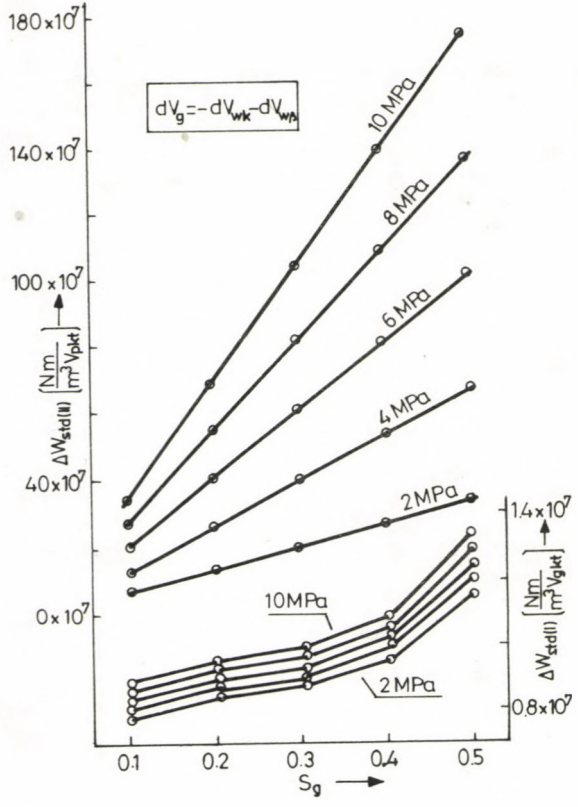

Fig. 7. The same as Fig. 3

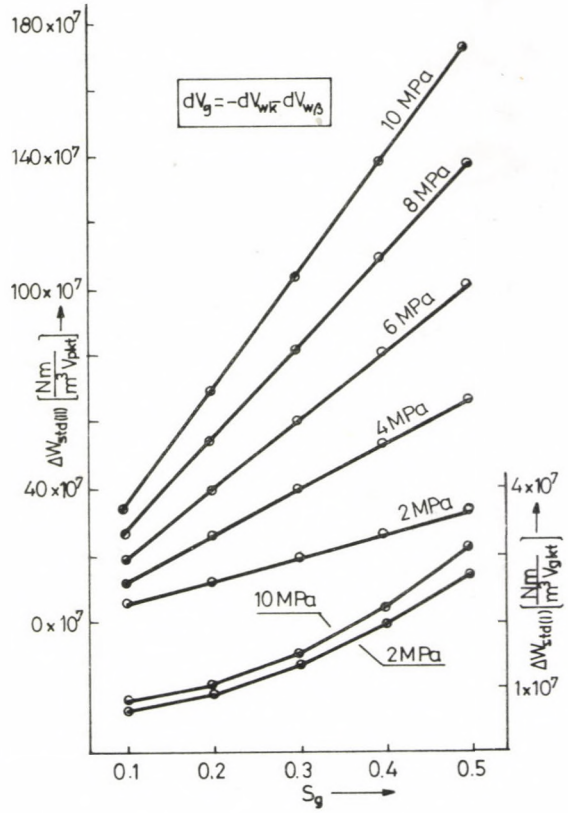

Fig. 8. The same as Fig. 4

2. SPECIFIC ENERGY OF THE SATURATION AS A FUNCTION OF VOLUME. APPARENT ENERGY OPTIMUM OF UNDERGROUND GAS STORAGE

Equations (8), (10) and (11) (Zoltán 1986b) describe the state of energy of the fluid-bearing reservoir i.e. the energy of storage needed to certain change of state. Using these equations one gets:

$$dW(S_g) = dW_I(S_g) + dW_{II}(S_g) = V_{gk} \; Z \; dJ + V_{pk} \; Z \; dK \; . \qquad (4)$$

Equation (4) indicates that $dW(S_g)$ has a minimum, which is illustrated in Fig. 2 (Zoltán 1986b) referring to a laboratory system. Only $dW_I(S_g)$ of the two terms of $dW(S_g)$ possesses a minimum while $dW_{II}(S_g)$ increases strictly monoton as a function of saturation. In Eq. (4) of $dW(S_g)$ describing the laboratory system, geometrical volumes V_{gk} and V_{pk} where elemental changes dW take place, are involved. Therefore these volumes influence the shape of $dW(S_g)$. Calculating components dW_I and dW_{II} in terms of unit volumes of V_{gk} and V_{pk}, they maintain their character since they only have to be divided by a constant. Figures 9 to 14 show energy changes dW_I, dW_{II} and $dW_I + dW_{II} = dW$ as functions of saturation.

Since laboratory pore volumes V_{gk} and V_{pk} never happen to coincide with the volumes V_{gkt} and V_{pkt} of the natural reservoir, it seems to be suitable to analyse the effect of the laboratory volumes V_{gk} and V_{pk} on energy components dW_I and dW_{II}. One of the most interesting questions in this analysis is to find the specific energy requirement of saturation changes as a function of the ratio of V_{gkt} to V_{pkt} as these volumes change between their maxima and minima. With

$$V_{gkt} + V_{pkt} = V_{gt} \qquad (5)$$

the ratio

$$V_{gkt}/V_{pkt} \qquad (6)$$

changes between 99/1 and 1/99.

The results provide tools to operate the underground gas

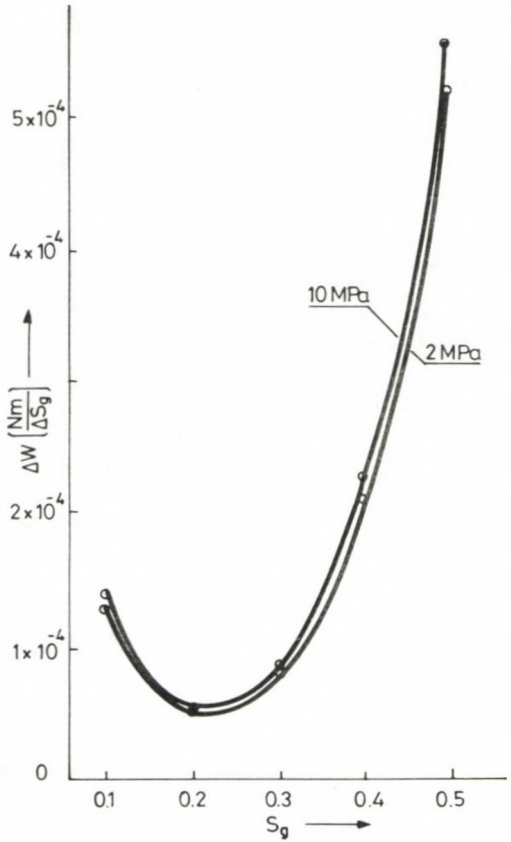

Fig. 9. Energy elements dW_I in terms of unit volumes (= 1 cm^3) of the experimental system in laboratory as a function of reservoir state at $dV_g = -dV_w$

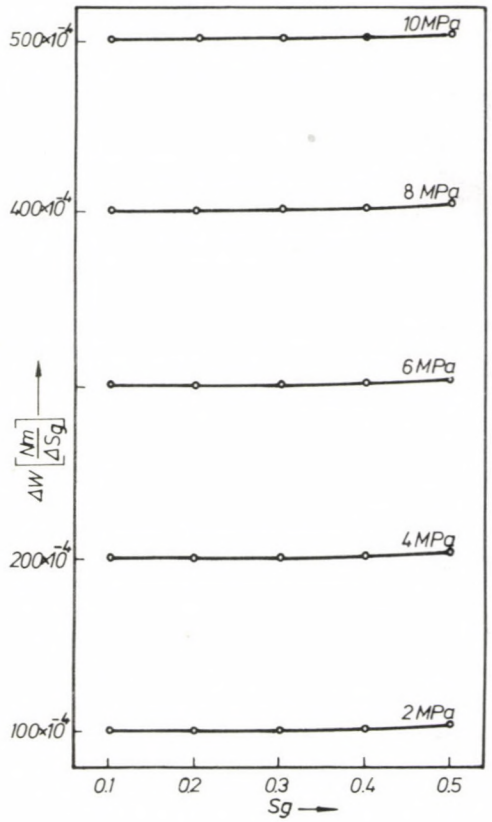

Fig. 10. Energy elements dW_{II} in the same terms as in Fig. 9

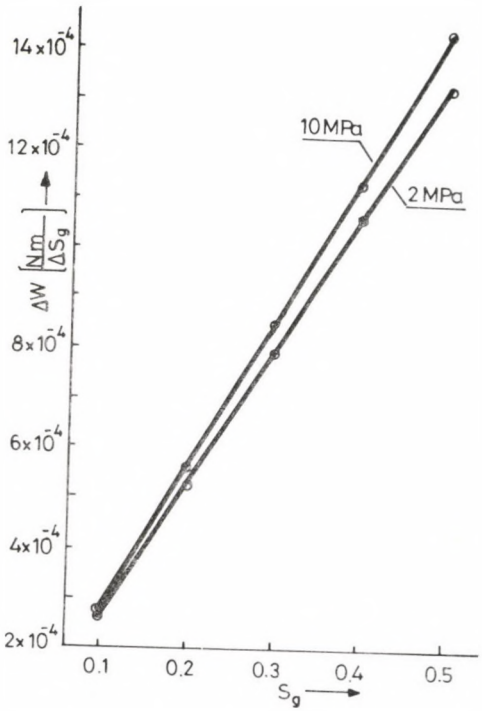

Fig. 11. Energy elements dW_I in terms of unit volumes (= 1 cm^3) of the experimental system in laboratory as a function of the state of the "high energy pore space" at $dV_g = -dV_w$

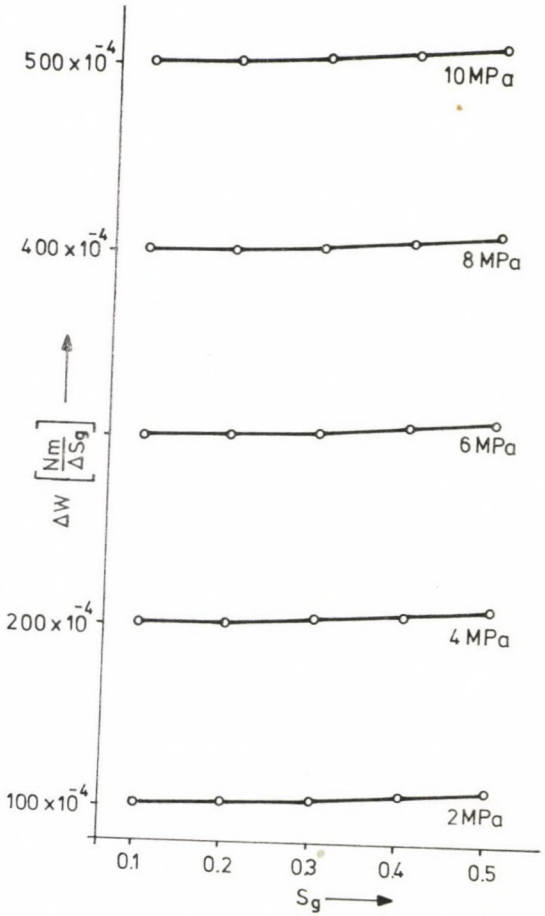

Fig. 12. Energy elements dW_{II} in the same terms as in Fig. 11

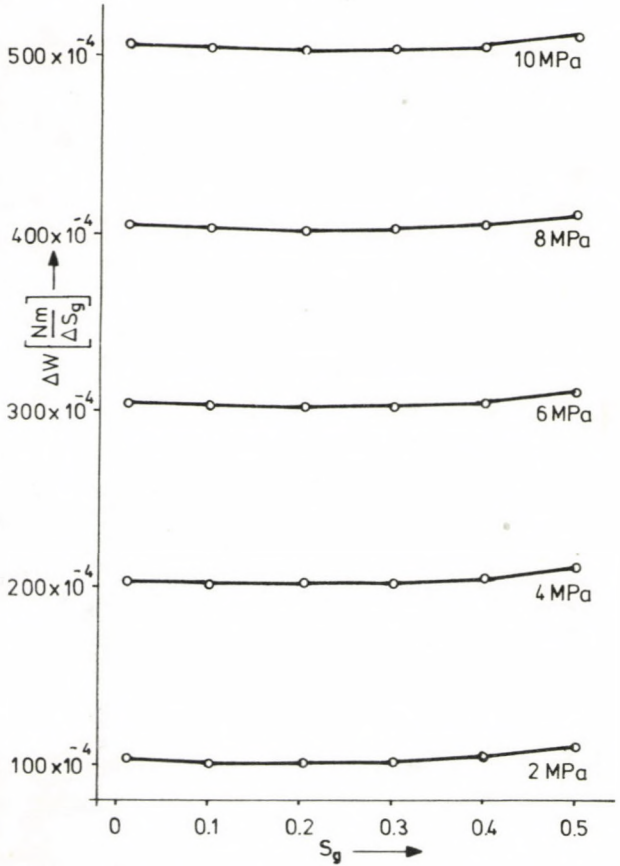

Fig. 13. Elementary energy components $dW = dW_I + dW_{II}$ as functions of the parameters of state in Figs 9 and 10

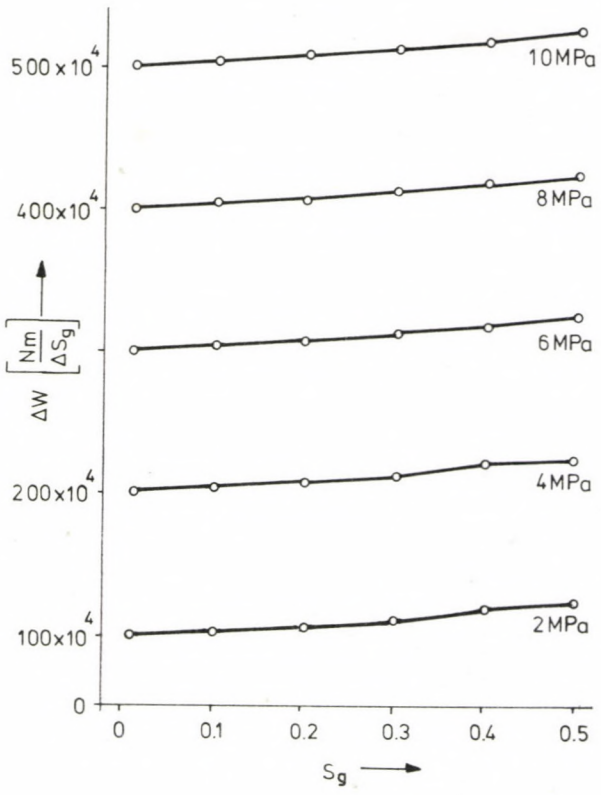

Fig. 14. The same as Fig. 13 for the parameters of state in Figs 11 and 12

reservoir around its energy optimum. Numerical values of dW vs. S_g are illustrated in Figs 15 to 16. Formation pressure has been chosen in 2 and 10 MPa. The curve with the highest ratio of V_{gkt}/V_{pkt} exhibits most clearly the minimum in the specific energy of the change of saturation. With increasing V_{pkt}, i.e. with decreasing ratio V_{gkt}/V_{pkt}, however, the minimum becomes hardly noticeable. And, finally, numerical values of the curve with ratio V_{gkt}/V_{pkt} = 1/99 fail to show the signs of the minimum. This phenomenon observed at both formation pressures 2 and 10 MPa indicates that the initial saturation may influence the energy requirement of gas injection.

Figures 17 and 18 show a totally different picture from those of Figs 15 and 16. Although the principles are similar, Figs 17 and 18 refer to "high-energy" reservoirs. As Zoltán (1986b) has shown in Fig. 3 the specific energy of the "high--energy" capillary system in the experimental reservoir shows a strictly monoton tendency with increasing gas saturation. Here no trace of a minimum can be found and the "energy price" of unit change of saturation is plotted in Fig. 17 for 2 MPa formation pressure and in Fig. 18 for 10 MPa.

The minimum of function $dW(S_g)$ is determined by the point of inflexion of function $P_c(S_g)$. Function $P_c(S_g)$ is the measurable resultant of interfacial and structural properties of the pores. Here the function value changes as a function of the arbitrarily selected independent variable, i.e. the state of saturation under the effect of natural factors. The natural factors may be such that the inflexion of function $P_c(S_g)$ lies at a small gas saturation or near S_w = 1.

Energetical considerations suggest that the most advantageous state of saturation of the reservoir is the value corresponding to the point of inflexion of function $P_c(S_g)$, because energy requirement of change of saturation is minimum in this range, i.e. this value of saturation can be maintained at minimum work. Consequently, if consumer demands and natural properties of the underground gas reservoir, viz. absolute value of consumption and its distribution in time as well as reservoir capacity enable us to maintain the state of the reservoir at

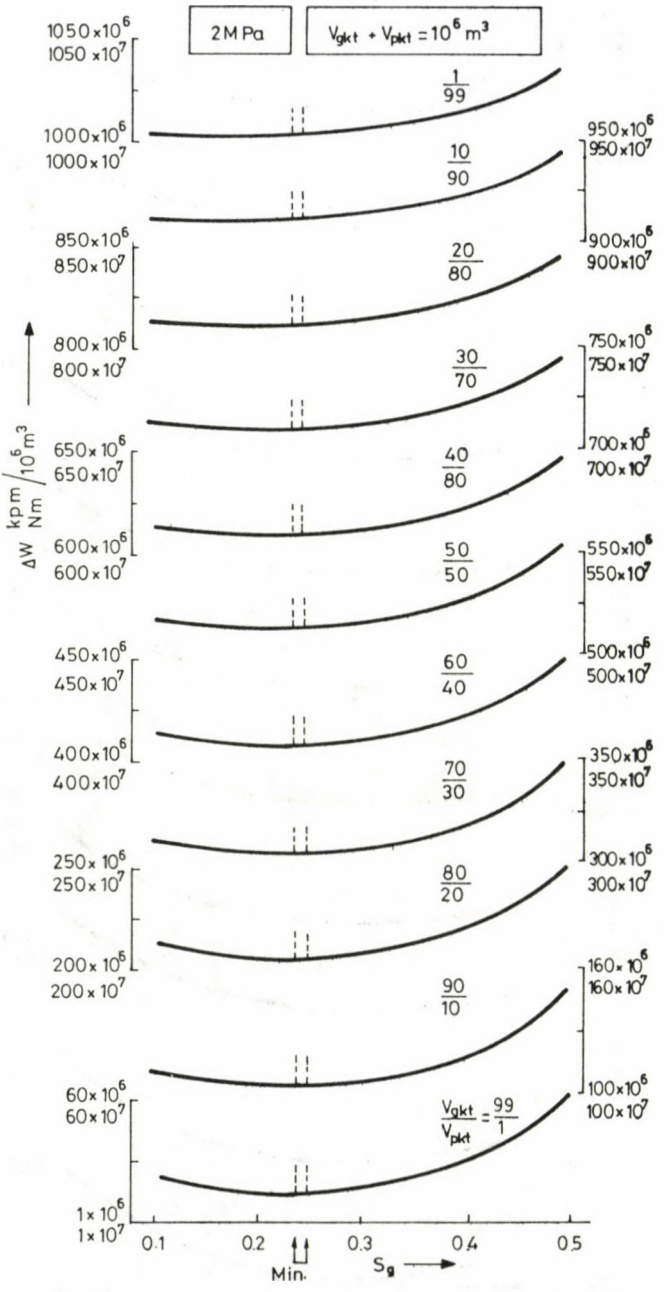

Fig. 15. $dW(S_g)$ as a function of V_{gkt}/V_{pkt} in a reservoir of 10^6 m^3 volume at 2 MPa formation pressure

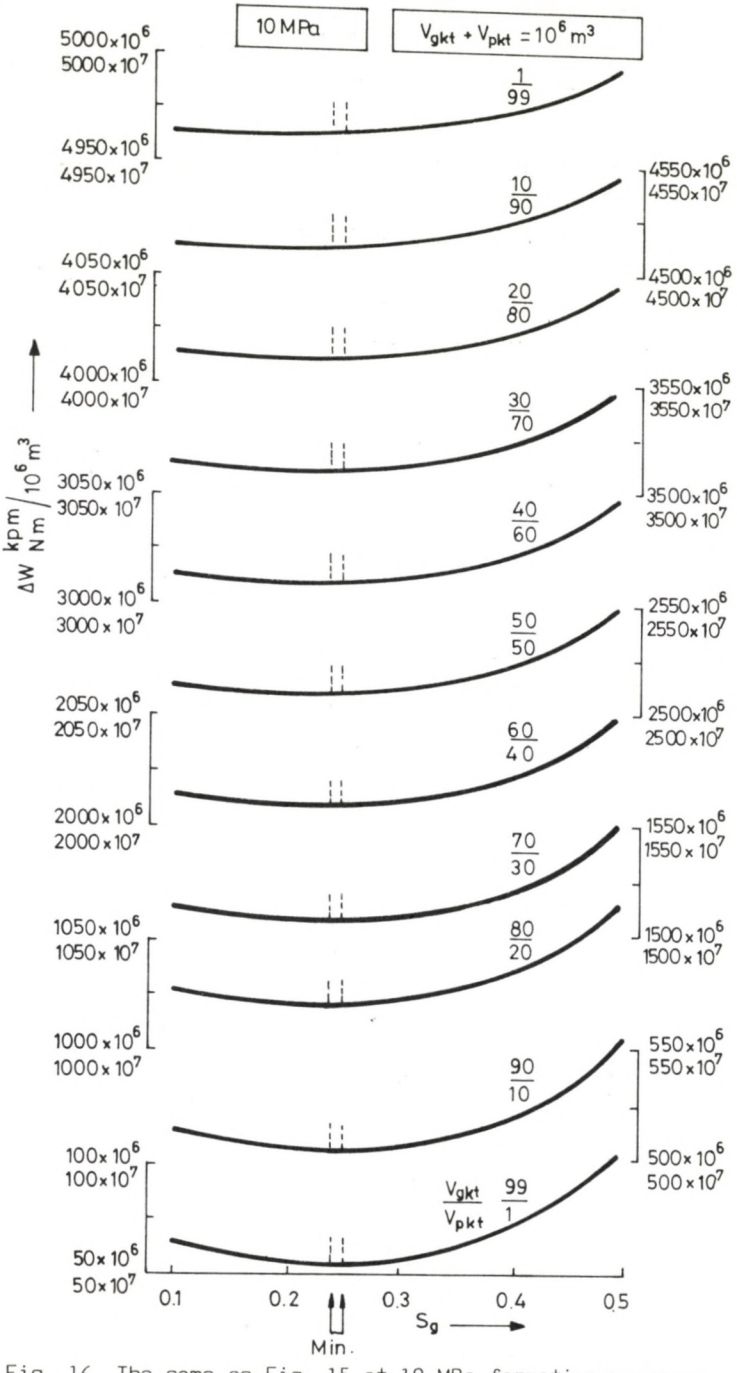

Fig. 16. The same as Fig. 15 at 10 MPa formation pressure

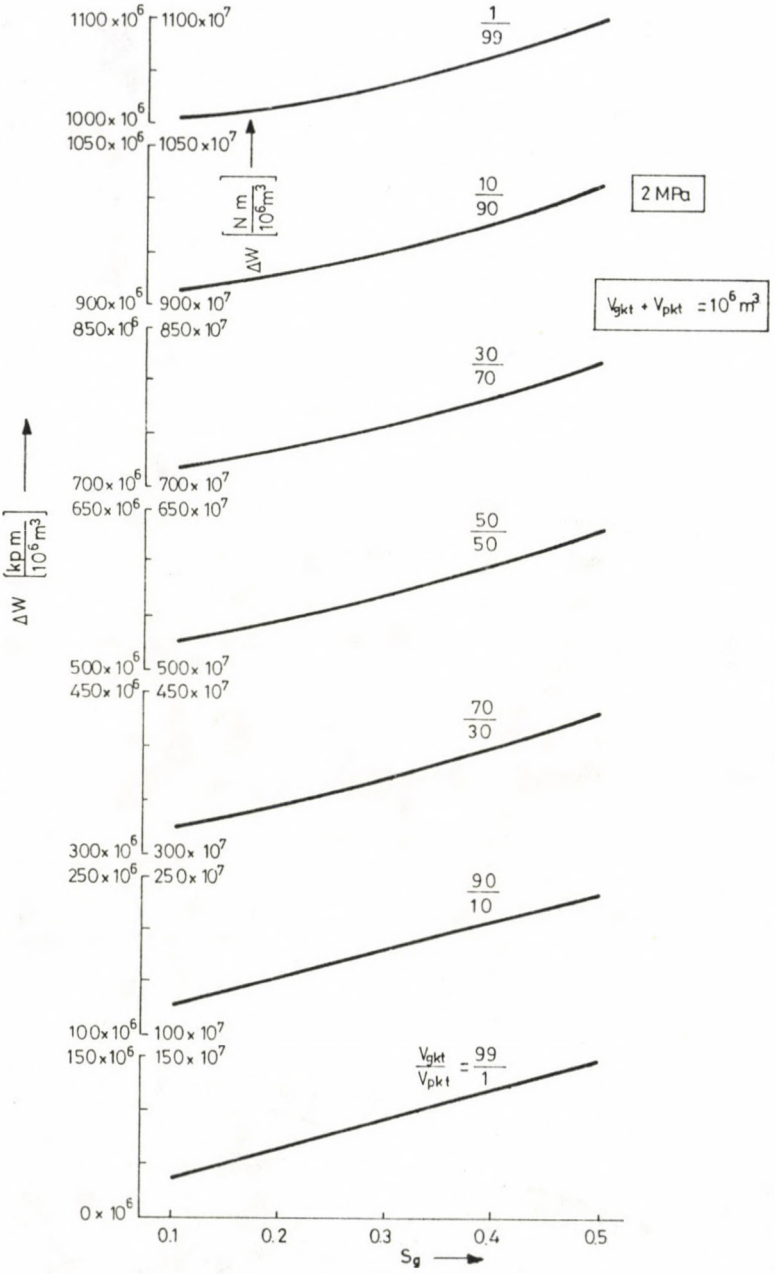

Fig. 17. $dW(S_g)$ as a function of V_{gkt}/V_{pkt} in a reservoir of 10^6 m^3 volume with "high energy" pore space at 2 MPa formation pressure

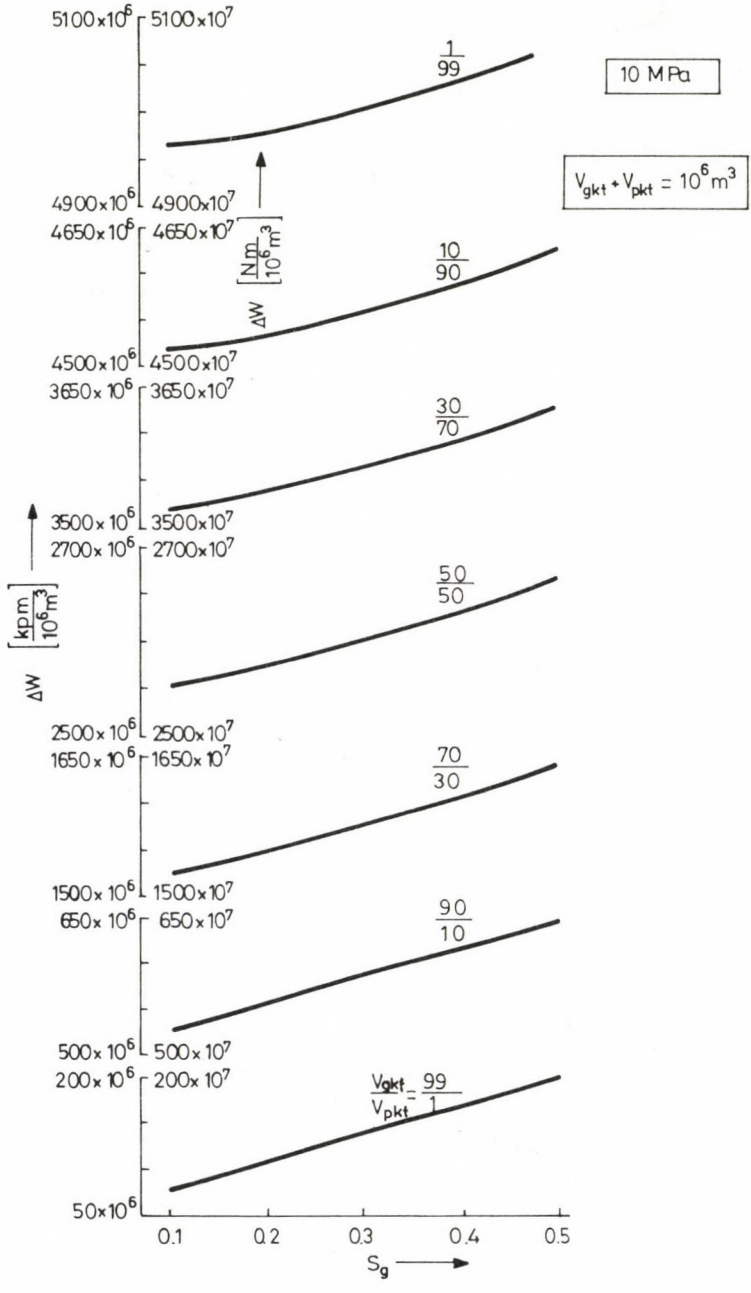

Fig. 18. The same as Fig. 17 at 10 MPa formation pressure

minimum dW, then the system is ideal from the energetical point of view, i.e. the cost of energy is minimum. But if the reservoir has the characteristics mentioned in the previous paragraph, i.e. the point of inflexion of the function $P_c(S_g)$ is disadvantageous, the reservoir has to be operated under uneconomical conditions. In this case a state of saturation can only meet the size and distribution of consumption that can be maintained in energetically unfavourable conditions.

This contradiction, however, is apparent only, as the "energy price" of changes in the state of saturation is only one of the important parameters. If not only the work needed for the change of state is taken into account but the energy costs are regarded as the "sine qua non" condition of storage, a fully new view will emerge. Our following discussion is meant to prove this statement. The optimum state of energy characterized by the saturation value of the point of inflexion of the function $P_c(S_g)$ is an apparent optimum only if the energy of storage is regarded as the specific energy of storage and not as the energy requirement. The energy optimum bears only exceptionally importance, e.g. in the case of limited technical possibilities.

3. INDEPENDENCE OF SPECIFIC ENERGY OF STORAGE ON THE STRUCTURE OF THE RESERVOIR

An evaluation of computer data of laboratory experiments has suggested that the ratio of the energy stored (the energy represented by the variable gas mass stored in the reservoir) to the energy of storage (energy needed to change the mass of gas) is independent of the structure of the reservoir:

$$\frac{\Delta W_{\text{stored(I)}}}{\Delta W_{\text{storage(I)}}} \simeq \frac{\Delta W_{\text{stored(II)}}}{\Delta W_{\text{storage(II)}}} , \qquad (7)$$

where indices I and II refer to reservoirs of basically different structure. The ratio of energy stored to that of storage is illustrated in Figs 19 to 22 at various formation pressures. To achieve the highest possible accuracy, different diagrams refer

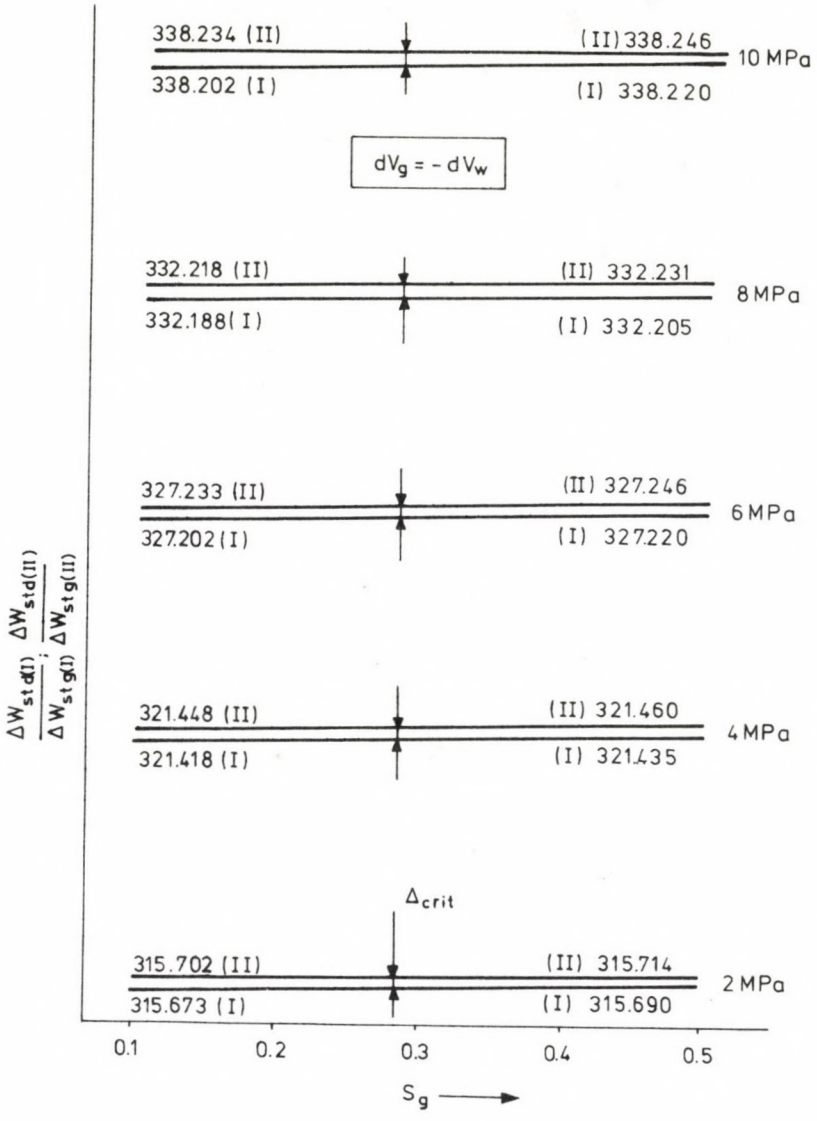

Fig. 19. Ratio of energy stored to that of storage as a function of reservoir state at $dV_g = -dV_w$

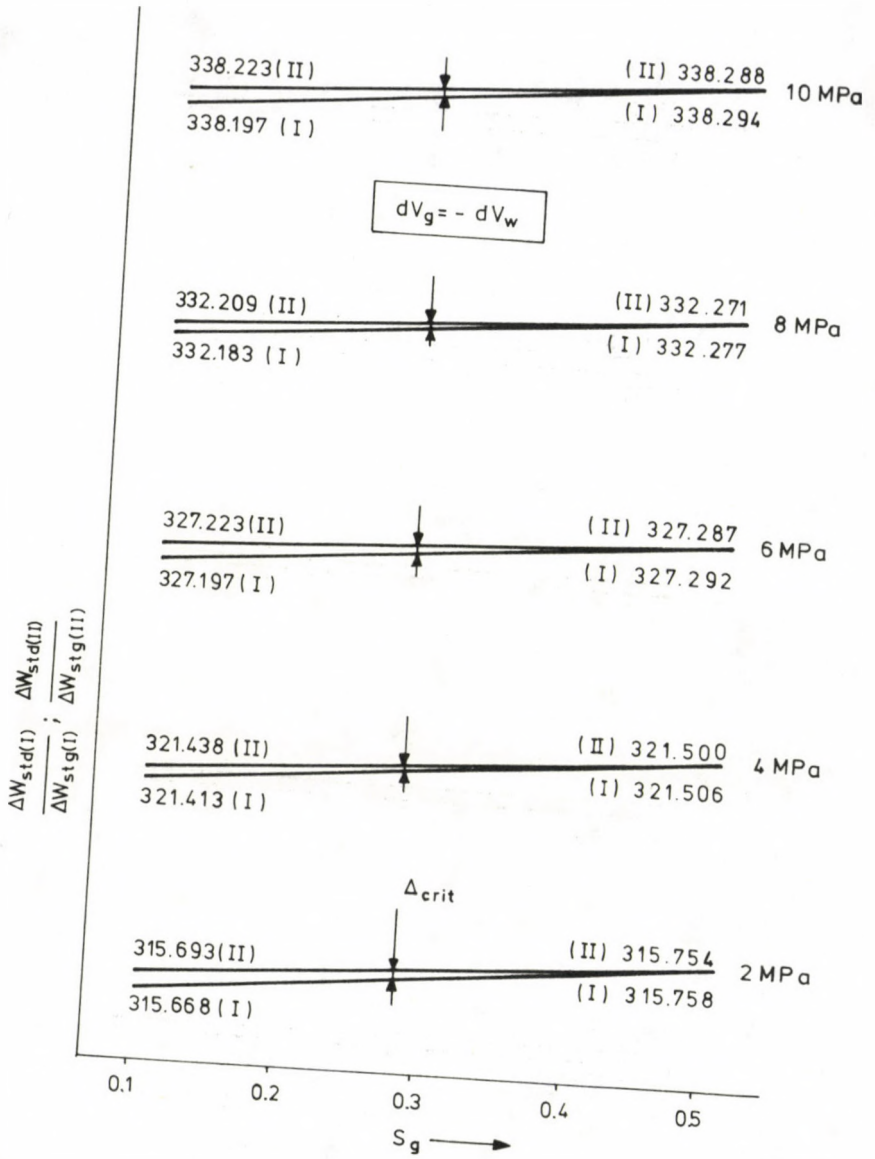

Fig. 20. Ratio of energy stored to that of storage as a function of reservoir state in a "high energy" pore space at $dV_g = -dV_w$

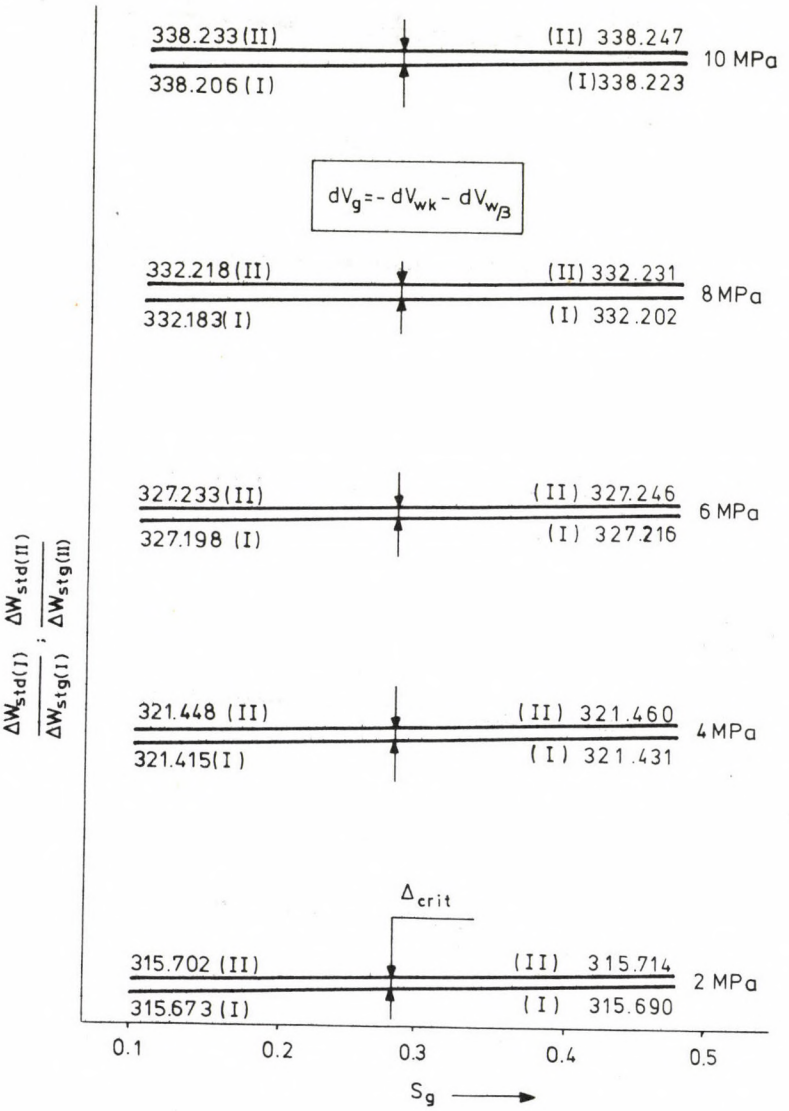

Fig. 21. The same as Fig. 19 at $dV_g = -dV_{wk} - dV_w$

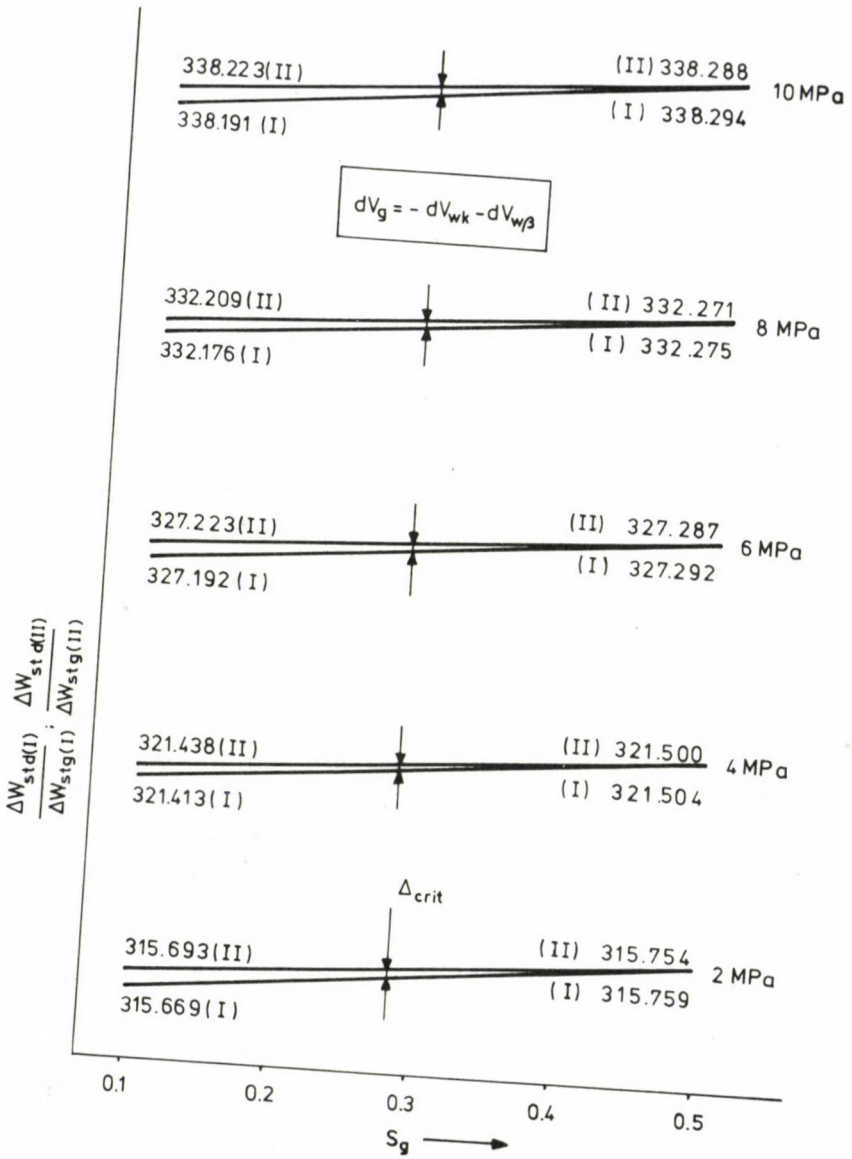

Fig. 22. The same as Fig. 20 at $dV_g = -dV_{wk} - dV_w$

to the cases

$$dV_g = -dV_w$$

and

$$dV_g = -dV_{wk} - dV_{w\beta} ,$$

while "common" and "high-energy" pore spaces are also distinguished.

The difference between L.H.S. and R.H.S. of Eq. (7) is so small that it cannot be illustrated in Figs 19 to 22. A comparison of numerical values of ΔW_{std} (stored) and ΔW_{stg} (storage) for reservoirs of different structures has shown that they are fully different. The ratios $\Delta W_{std}/\Delta W_{stg}$, however, were the same for different reservoirs and they hardly showed any change with changing saturation. To indicate small differences, the numerical values corresponding to saturation values $S_g = 0.1$ and $S_g = 0.5$ are placed near the curves, e.g. in Fig. 19 for reservoir II: 315.702 and 315.714 at 2 MPa formation pressure. Since Figs 1 to 8 illustrating the curves of energy stored and that of storage did not make it possible to decide whether the regularity in Eq. (7) has a random character or represents some law, an attempt has been made to prove or disprove them. This question is important since the reciprocal of the expression in Eq. (7) gives the specific energy of storage, i.e. the work needed to store unit energy, and it is of basic theoretical and practical importance whether the specific energy of storage is the same or different in different kinds of reservoirs.

Figure 23 illustrates the reservoir used to carry out our mental experiment. Gas-water interface prior to observation is denoted by $\frac{g}{w}$. Above this interface in the gas a space volume V_{gkt}, below the interface a pore volume V_{pkt} are considered. It holds for these volumes: $V_{gkt} = V_{pkt}$, and, water saturation of this pore volume above the gas-water interface equals residual water saturation S_{wr}. This yields $V_{gkt} = V'_{pkt}(1-S_{wr})$ while the volume V_{pkt} is perfectly saturated with water. The volume V_{gkt} can also be thought of as a cave-like structure instead of the pore space of a porous rock but it still equals the pore volume

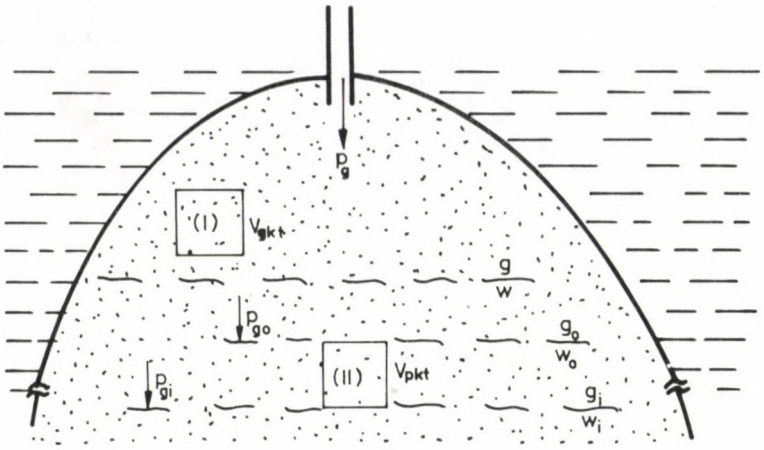

Fig. 23. Theoretical experimental reservoir with the parameters of state

V_{pkt} saturated with water. Gas injection takes continuously place and for the beginning of observation we choose the instant when the gas-water interface reaches pore space V_{pkt}, i.e. when the state of saturation in this space starts changing. The observed value at this instant is p_{go}. At the last instant of an arbitrary time interval, in the i-th state of the reservoir we finish our observation: the pressure of the reservoir now equals p_{gi}. Using elementary laws of physics, mass changes of the observed volumes enable us to determine the changes of normal volumes of the gas masses from state i=0 to state i being the end of observation. Substituting pressure, compressibility and saturation values into Eq. (7), we obtain

$$\frac{\frac{p_{gi}}{Z_i} - \frac{p_{go}}{Z_o}}{\int_{J_o}^{J_i} Z\, dJ} \gtreqless \frac{\frac{p_{gi}}{Z_i} S_{gi} - \frac{p_{go}}{Z_o} S_{go}}{\int_{K_o}^{K_i} Z\, dK} \tag{8}$$

L.H.S. of Eq. (8) refers to volume V_{gkt} while R.H.S. to V_{pkt}. Zoltán (1986a, b) has shown that functions characterizing

the gas mass in the reservoir are available in form of distinct measurement points only. Therefore, numerical methods have to be applied to calculate the integrals in the denominators of Eq. (8) in order to express the change of energy content of the gas-bearing reservoir comprising reservoir space, formation fluids and state of reservoir. The integrals can be written:

$$\int_{J_o}^{J_i} Z\, dJ \cong \bar{Z}_i(j_i J_{i-1}) + \bar{Z}_{i-1}(J_{i-1}-J_{i-2}) + \ldots$$

$$\ldots + \bar{Z}_2(J_2-J_1) + \bar{Z}_1(J_1-J_o) \quad ,$$

where

$$\bar{Z}_i = \frac{Z_i + Z_{i-1}}{2} \quad .$$

Similarly,

$$\int_{K_o}^{K_i} Z\, dK \cong Z_i(K_i-K_{i-1}) + \bar{Z}_{i-1}(K_{i-1}-K_{i-2}) + \ldots$$

$$\ldots + \bar{Z}_2(K_2-K_1) + \bar{Z}_1(K_1-K_o) \quad .$$

As earlier mentioned (Zoltán 1986a, b)

$$\frac{p_{gi}}{Z_i} = J_i \quad ,$$

$$\frac{p_{go}}{Z_o} = J_o \quad ,$$

and

$$\frac{p_{gi}}{Z_i} S_{gi} = K_i \quad ,$$

$$\frac{p_{go}}{Z_o} S_{go} = K_o \quad .$$

Substituting the approximate values for the integrals of Eq. (8), one gets

$$J_i - J_o$$

and

$$K_i - K_o$$

in the numerators. Without changing the values of the numerators, we can add and subtract the same quantities J_{i-1}, J_{i-2}, ..., J_2, J_1 yielding

$$J_i - J_{i-1} + J_{i-1} - J_{i-2} + J_{i-2} - J_{i-3} + J_{i-3} - \ldots$$
$$\ldots - J_3 + J_3 - J_2 + J_2 - J_1 + J_1 - J_o \,, \tag{9}$$

and similarly:

$$K_i - K_{i-1} + K_{i-1} - K_{i-2} + K_{i-2} - K_{i-3} + K_{i-3} - \ldots$$
$$\ldots - K_3 + K_3 - K_2 + K_2 - K_1 + K_1 - K_o \,. \tag{10}$$

Plotting functions

$$J = J(S_g) \qquad \text{and} \qquad K = K(S_g)$$

in a co-ordinate system $J\text{-}S_g$ and $K\text{-}S_g$ in Fig. 24 on the abscissa S_g one can find intervals

$$\Delta S_{gi} = S_{gi} - S_{gi-1}$$

for which

$$J_i - J_{i-1} = J_{i-1} - J_{i-2} = J_1 - J_o$$

and

$$K_i - K_{i-1} = K_{i-1} - K_{i-2} = K_1 - K_o$$

hold.

Thus Eq. (8) can be written as

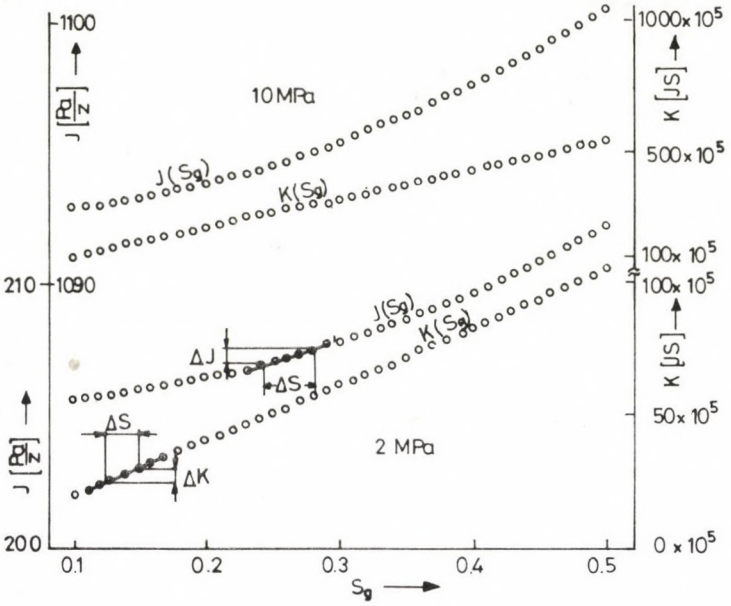

Fig. 24. Functions $J(S_g)$ and $K(S_g)$ in the experimental reservoir in laboratory

$$\frac{n(J_i-J_{i-1})}{(J_i-J_{i-1})\sum_{i=0}^{n}\bar{Z}_i} \lessgtr \frac{n(K_i-K_{i-1})}{(K_i-K_{i-1})\sum_{i=0}^{n}\bar{Z}_i} . \qquad (11)$$

This expression does not exclude the possibility that the two sides are equal but does not prove it either. Obviously, for functions $j(S_g)$ and $K(S_g)$ one can always find differences ΔJ_i and ΔK_i which are strictly equal. But since $J(S_g)$ and $K(S_g)$ are not parallel, or differential quotients of functions $J(S_g)$ and $K(S_g)$ are equal for a single value of S_g only and nowhere else, we may choose ΔJ_i and ΔK_i anywhere, the corresponding ΔS_{gi}-s are not equal thus end points S_{gi} and S_{gi-1} are not the same for them either. Therefore, terms $\bar{Z}_i$ given by function

$$Z = Z\left[p_g(S_g);\ T;\varepsilon\right]$$

in the sum of Eq. (11) are not the same, thus the correct form of Eq. (11) has to be written as

$$\frac{n}{\sum_{i=0}^{n} \bar{Z}_i} = \frac{n}{\sum_{i=0}^{n} \bar{Z}'_i} \quad . \tag{12}$$

If n is sufficiently large, i.e. a great number of differences ΔJ and ΔK are involved in the calculation, the sums of different compressibility factors $\bar{Z}_i$ and $\bar{Z}'_i$ may happen to be equal or nearly equal. This was the case with our observation in connection with Eq. (7).

However, considering equation

$$\frac{\int_{J_o}^{J_i} dJ}{\int_{J_o}^{J_i} Z\, dJ} = \frac{\int_{K_o}^{K_i} dK}{\int_{J_o}^{K_i} Z\, dK} \tag{13}$$

with the same physical content as that of Eq. (8) but expressed in a more exact form, the inequality will be replaced by an equality since the more the number n of equal differences $J_i - J_{i-1}$ and $K_i - K_{i-1}$ increases, the more holds that $\Delta J \to dJ$ and $\Delta K \to dK$. Differentials dJ and dK require differential changes dS, therefore elements Z_i and $\bar{Z}'_i$ to be summarized in Eq. (12) differ by differential amounts only, thus Eqs (7) and (8) can be written as a strict equality

$$\frac{\Delta W_{std(I)}}{\Delta W_{stg(I)}} = \frac{\Delta W_{std(II)}}{\Delta W_{stg(II)}} \quad . \tag{14}$$

The fact that Eq. (7) has shown a near-equality, can be explained by the great number of points of observation in the saturation interval S_g=0 to S_g=0.5 with differences ΔS_g=0.005. This resulted in a high accuracy of the results - at the expense of a labourous evaluation. The difference between the two

sides of Eq. (7) giving the total change of energy content was less than 5-10 ergs while the total change of energy content mounted to several thousand million ergs.

Similarly to Eq. (14) a new result can be obtained by restricting the analysis to the saturation interval $S_g=0$ to $S_g=1-S_{wr}$. Let us consider saturation difference

$$\Delta S_{gi} = S_{gi} - S_{gi-1}$$

and write Eq. (8) using this difference:

$$\frac{\frac{p_{gi}}{Z_i} - \frac{p_{gi-1}}{Z_{i-1}}}{\int_{J_{i-1}}^{J_i} Z\, dJ} \lessgtr \frac{\frac{p_{gi}}{Z_i} S_{gi} - \frac{p_{gi-1}}{Z_{i-1}} S_{gi-1}}{\int_{K_{i-1}}^{K_i} Z\, dK} .$$

Hence

$$\frac{2\,(J_i-J_{i-1})}{(Z_i+Z_{i-1})\,(J_i-J_{i-1})} \lessgtr \frac{2\,(K_i-K_{i-1})}{(Z_i+Z_{i-1})\,(K_i-K_{i-1})} .$$

It can now be written in form of an equality

$$\frac{2}{Z_i+Z_{i-1}} = \frac{2}{Z_i+Z_{i-1}} . \qquad (15)$$

Since Eq. (15) has been obtained from Eq. (7) the physical meaning of Eq. (15) is obvious. The same refers to the reciprocal of Eq. (15), i.e.

$$\frac{Z_i+Z_{i-1}}{2} = \frac{Z_i+Z_{i-1}}{2} . \qquad (16)$$

From the results of our analyses of gas storage the final conclusion can be drawn that the ratio of the energy stored to that of storage does not depend on the structure of the reservoir or container. Or, vice versa: the specific energy of

storage, i.e. the work needed to store unit energy is independent of the fact whether the gas is stored in a steel container, underground excavation or porous reservoir where the injected gas has to first displace formation water primarily saturating pore space.

Since function $p_g(S_g)$ strictly monoton increases as a function of the independent variable S_g, and $Z(S_g)$ is a strictly monoton decreasing function of gas saturation, it follows that the specific energy of gas storage is the smaller, the greater the energy requirement of gas storage is. This statement is valid for the interval $S_g < S_g \mid Z_{min}$.

In proving the independence of the specific energy of storage the limiting condition $V_{gkt} = V_{pkt}$ has been applied where V_{gkt} denotes the part of the reservoir pore space that is filled with gas at the instant of observation. This volume will be regarded as a constant geometric volume. During gas injection only the mass of gas changes in this space and the mass change is necessarily accompanied with a change of gas pressure. On the other hand, V_{pkt} is the part of the pore space whose water saturation continuously reduces in this process and the primary saturating phase, i.e. formation water is displaced by gas. Therefore the amount of gas steadily increases in this space from the beginning to the end of the observation of the change of state of saturation. At any time of the process and for the whole pore space of the reservoir it holds that

$$V_{gt} = V_{gkt} + V_{gvt} \tag{17}$$

i.e. the whole pore space filled with gas is considered as to be made up by the initial volume V_{gkt} which is constant and by the increasing or decreasing volume V_{gvt} which keeps changing during the observation.

The aforementioned strict limitation, i.e. the geometrical equality of volumes V_{gkt} and V_{pkt} is never met in nature and cannot be produced under real operating conditions. Therefore the theorem of the independence of the specific energy of storage has to be generalized for natural conditions when it is not

limited by given volumetric ratios and the law is valid for the whole reservoir irrespective of time and geometric boundaries.

Let the whole volume of the geological structure suitable for gas storage be V and its porosity Φ , thus the effective pore space is $V\Phi$. Let us consider reservoir parameters of the (i-1)th and i-th observations:

(i-1):

S_g :		$S_{g(i-1)} = s_{gk}$ (= initial)
p_g :	$p_g = p_g(S_g)$	$p_{g(i-1)} = p_{gk}$
Z :	$Z = Z\,[p_g(S_g)]$	$Z_{(i-1)} = Z_k$
V_g :	$V_g = V\Phi\, S_g$	$V_{g(i-1)} = V\Phi\, S_{g(i-1)} = V\Phi\, S_{gk}$
n :		$n_{(i-1)} = n_k$
T :	T = constant	T

Taking account of the parameters of state in the (i-1)th stage

$$p_{g(i-1)}\, V_{g(i-1)} = n_{(i-1)}\, Z_{(i-1)}\, RT\ .$$

The state of the gas will be changed while its mass remains constant, and the new state is regarded as the normal state:

$$p'_{g\ norm}\, V_{g\ norm} = n_{(i-1)}\, Z'_{norm}\, RT_{norm}.$$

$V_{g\ norm}$ and T_{norm} refer to the physical normal state while $p'_{g\ norm}$ is calculated from these two values because the gas cannot be considered ideal. From the last two equations, if

$$V_{g(i-1)} = V\Phi\, S_{g(i-1)} = V\Phi\, S_{gk} = V_{gk}$$

and $V_{g\ norm} = n_{(i-1)}\, V_{mol}$ are taken into account, the normal volume of the gas mass in the geometrical volume V_{gkt} is obtained:

$$n_k\, V_{mol} = \frac{Z'_{norm}\, T_{norm}}{p'_{g\ norm}\, T}\, V\Phi\, S_{gk}\, \frac{p_{gk}}{Z_k}\ . \qquad (18)$$

Let us now take the next set of parameters of state and write the equation of the i-th state:

$$p_{g(k1)} V_{gk} = n_{(k1)} Z_{(k1)} RT ,$$

where index k1 refers to the first set of data after beginning the observation. Correspondingly,

$$n_{k1} V_{mol} = \frac{Z'_{norm} T_{norm}}{p'_{g\ norm} T} v\Phi S_{gk} \frac{p_{gk1}}{Z_{k1}} . \qquad (19)$$

From Eqs (18) and (19)

$$n_{k1} V_{mol} = \frac{Z'_{norm} T_{norm}}{p'_{g\ norm} T} V\Phi S_{gk} \left\{ J_{k1} - J_k \right\} . \qquad (20)$$

Equation (20) gives the change of gas mass in volume V_{gkt} for the interval between observations (i-1) and i in terms of normal volume. Taking into account the calorific value and heat-work equivalence, the change of energy content $\Delta W_{std(V_{gk})}$ due to change of the gas mass can be written:

$$\Delta W_{std(V_{gk})} =$$

$$= 10^{-6} \cdot c \cdot 426.9 \cdot 9.80665 \frac{Z'_{norm} T_{norm}}{p'_{g\ norm} T} V\Phi S_{gk} \left\{ J_{k1} - J_k \right\} \quad [N\ m] \quad (21)$$

where C denotes calorific value. The work of storage needed for this change is

$$\Delta W_{stg(V_{gk})} =$$

$$= V_{gk} \int_{J_k}^{J_{k1}} Z\, dJ \simeq V\Phi S_{gk} \frac{Z_k + Z_{k1}}{2} \left\{ J_{k1} - J_k \right\} 10^{-7} \quad [N\ m] . \qquad (22)$$

Dividing Eq. (21) by Eq. (22) and denoting all constans by

N, we get for the ratio of the energy stored to that of storage in volume V_{gkt}:

$$\frac{\Delta W_{std}}{\Delta W_{stg}} (V_{gk}) = \frac{N}{Z_k + Z_{k1}} . \qquad (23)$$

The reciprocal of the expression in Eq. (23) gives the specific energy of storage, i.e. the work needed to store unit energy:

$$\frac{W_{stg}}{W_{std}} (V_{gk}) = \frac{Z_k + Z_{k1}}{N} . \qquad (24)$$

Similar considerations lead to the energy equation of the changes in volume V_{gvt} (s. Eq. (17)). Our basic equations of the k-th and k_1-th observations furnish the change of gas mass in volume V_{gvt} from which the change of energy content can be calculated in volume V_{gvt}:

$$\Delta W_{std(V_{gv})} =$$

$$= 10^{-6} \cdot C \cdot 426.9 \cdot 9.80665 \frac{Z'_{norm} T_{norm}}{p'_{g\ norm} T} V \Phi \left\{K_{k1} - K_1\right\} \quad [N\ m] . \qquad (25)$$

"Energy price" of this change becomes

$$W_{stg(V_{gv})} =$$

$$= V_{pk} \int_{K_k}^{K_{k1}} Z\, dK \simeq V \Phi \frac{Z_k + Z_{k1}}{2} (K_{k1} - K_k) 10^{-7} \quad [N\ m] . \qquad (26)$$

From Eqs (25) and (26)

$$\frac{\Delta W_{std}}{\Delta W_{stg}} (V_{gv}) = \frac{N}{Z_k + Z_{k1}} . \qquad (27)$$

Equations (21) to (27) express energy changes accompanying

changes in the saturation interval

$$S_{gi} - S_{gi-1} = \Delta S_{gi} ,$$

i.e. the ratio of the energy stored to that of storage and, in form of its reciprocal, the specific energy of storage. Using the same mathematical and physical principles, a numerical analysis proved that the theorem holds for the possible widest saturation interval from $S_g = 0$ to $S_g = S_{gn}$. The conclusions of the analyses can be summed up as

$$\left\{ \frac{\Delta W_{std}}{\Delta W_{stg}} (V_{gk}) \right\}_i = \frac{N}{Z_i + Z_{i-1}} = \left\{ \frac{\Delta W_{std}}{\Delta W_{stg}} (V_{gv}) \right\}_i ,$$

and

$$\left\{ \frac{\Delta W_{std}}{\Delta W_{stg}} (V_{gk}) \right\}_i = \left\{ \frac{N (J_i - J_k)}{\sum_{i=k}^{n} (Z_i + Z_{i-1}) (J_i - J_{i-1})} \right\}_i =$$

$$= \left\{ \frac{N (K_i - K_k)}{\sum_{i=k}^{n} (Z_i + Z_{i-1}) (K_i - K_{i-1})} \right\}_i = \left\{ \frac{\Delta W_{std}}{\Delta W_{stg}} (V_{gv}) \right\}_i .$$

4. PROPORTIONS OF COMPONENTS OF THE FULL ENERGY CONTENT IN FLUID-BEARING POROUS RESERVOIRS

Any change of the gas mass in an underground reservoir changes the energy content which is reflected by the state of the system. Instantaneous values of the parameters of state characterize the actual state of energy, through their changes the changes of state of energy can be followed: energy needed to increase the mass of gas, or, conversely, energy needed to produce a new state of the reservoir if the gas mass decreases.

As earlier mentioned, components of the change of energy can separately be analysed ensuring an assessment of underground

gas storage. Comparing various components of energy, disadvantageous parts can be spotted and more suitable operating conditions can be provided. Components of energy are used to decide about the necessity of changes in the operation of the reservoir and to assess the effectivity of measures taken.

The components of energy are as follows (see details in Table I):

a) Energy needed to produce changes of state, i.e. to inject gas into the reservoir, is equal to the work done against the formation pressure.
b) The second-largest component is the energy requirement of interfacial changes, i.e. work to be done against capillary resistance.
c) Compression work of the gas mass injected into the reservoir.
d) Energy requirement of increasing the internal energy of the gas mass is the last component of energy.
e) Energy needed to produce elastic change of volume of the formation water if water compressibility is also taken into account.

The figures of Table II are characteristic of changes of energy content in terms of $V_{pkt} = 1\ m^3$ of the varying gas space, i.e. they give the limits of changes of energy content corresponding to the saturation interval between $S_g = 0.1$ and $S_g = 0.5$. Changes of state are independent of external actions within the volume V_{gv} only, because there dominate natural conditions of change. Volume V_{gv} can be chosen under a certain influence of our will, thus energy values within this space change according to our influence, therefore they have not been determined in terms of V_{gkt}. Figures 25 to 32 show the percentages of the energy components as functions of the saturation of the reservoir for maximum and minimum formation pressures. Values for pressures other than 2 and 10 MPa have been omitted in the figures. The difference between the illustrated two curves is so small that further details would not have given additional information.

Figures 33 to 40 illustrating the changes of state in the experimental system, provide a summary of underground gas storage. The show formation pressure, capillary pressure,

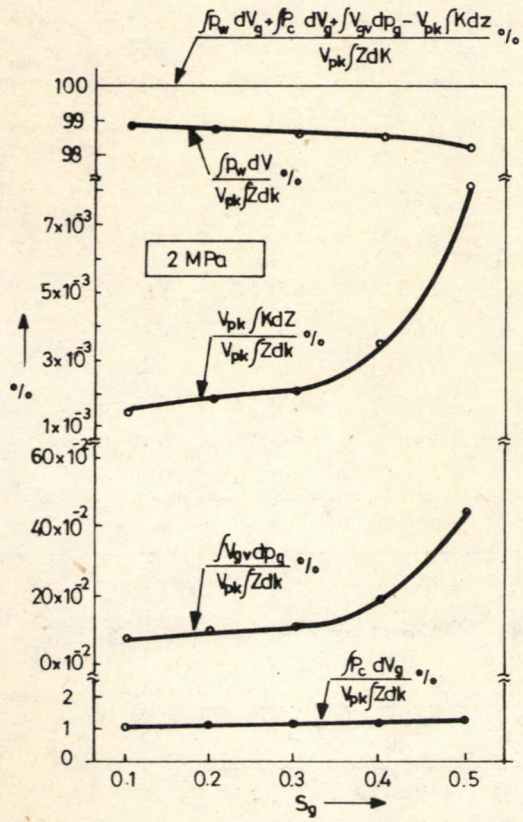

Fig. 25. Components of total energy requirement in gas volume V_{gv} at 2 MPa formation pressure

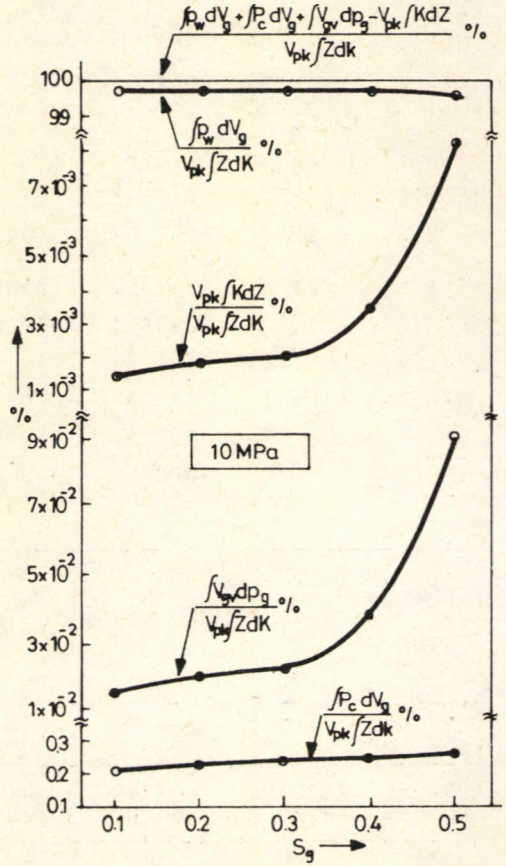

Fig. 26. The same as Fig. 25 at 10 MPa formation pressure

Table I. Energy of storage (= state of energy) in the porous fluid reservoir in terms of units of pore volumes V_{gkt} and V_{pkt} as a function of reservoir state

		Puszta-földvár	High energy	Puszta-földvár	High energy	Puszta-földvár	High energy	Puszta-földvár	High energy
		$dV_g = -dV_w$		$dV_g = -dV'_{wk} - dV_{w\beta}$		$dV_g = -dV_w$		$dV_g = -dV'_{wk} - dV_{w\beta}$	
i	S_{gi}	$W_{stg(I)} = V_{gkt} \int_{J_o}^{J} Z\, dJ \left[\frac{Nm}{n^3}\right]$				$W_{stg(II)} = V_{pkt} \int_{K_o}^{K} Z\, dK \left[\frac{Nm}{m^3}\right]$			
2 MPa									
0	0.000	0.000	0.000	0.000	0.000	0.000	0.000	0.000	0.000
1	0.000	1.854	1.854	1.854	1.854	0.000	0.000	2	2
2	0.005	2.100	1.855	2.100	1.855	1.030	1.029	1.031	1.030
6	025	2.221	1.871	2.221	1.871	5.153	5.145	5.155	5.146
11	050	2.302	1.922	2.302	1.922	10.310	10.292	10.312	10.293
16	0.075	2.380	2.007	2.380	2.007	15.471	15.444	15.473	15.445
21	0.100	2.450	2.126	2.450	2.126	20.635	20.604	20.637	20.605
26	125	2.508	2.280	2.508	2.280	25.801	25.773	25.803	25.775
31	150	2.558	2.467	2.558	2.467	30.969	30.956	30.971	30.958
36	175	2.598	2.688	2.598	2.688	36.137	36.154	36.139	36.156
41	0.200	2.629	2.944	2.629	2.944	41.306	41.370	41.308	41.372
46	225	2.657	3.233	2.657	3.233	46.475	46.605	46.477	46.608
51	250	2.682	3.557		3.557	51.646	51.864		51.867

56	275	2.709	3.914	2.709	3.914	56.817	57.148	56.819	57.151
61	0.300	2.740	4.306	2.741	4.306	61.992	62.461	61.994	62.463
66	0.325	2.778	4.731	2.778	4.731	67.170	67.803	67.172	67.806
71	350	2.834	5.191	2.834	5.191	72.356	73.179	72.358	73.182
76	375		5.685	2.905	5.685		78.590	77.553	78.593
81	0.400	2.998	6.213	2.998	6.213	82.758	84.039	82.760	84.042
86	425	3.114	6.775	3.114	6.775	87.980	89.529	87.981	89.532
91	450	3.263	7.371	3.263	7.371	93.222	95.062	93.223	95.066
96	475	3.441	8.001	3.441	8.001	98.485	100.641	98.487	100.644
101	0.500	3.673	8.666	3.673	8.666	103.784	106.268	103.786	106.272
106	0.525	4.007	9.364	4.007	9.364	109.148	111.946	109.150	111.950
111	550	7.237	10.096	7.237	10.097	116.121	117.677	116.124	117.681
112	0.553	10.384	10.384	10.384	10.384	118.495	118.477	118.499	118.482
10 MPa									
0	0.000	0.000	0.000	0.000	0.000	0.000	0.000	0.000	0.000
1	0.000	1.986	1.986	1.986	1.986	0.000	0.000	8	8
2	0.005	2.250	1.987	2.250	1.987	5.109	5.108	5.118	5.116
6	025	2.380	2.005	2.380	2.005	25.548	25.539	25.557	25.547
11	050	2.467	2.059	2.467	2.059	51.099	51.080	51.109	51.088
16	0.075	2.550	2.150	2.550	2.151	76.655	76.627	76.665	76.635
21	0.100	2.625	2.278	2.625	2.278	102.214	102.182	102.223	102.190
26	125	2.687	2.442	2.687	2.442	127.775	127.748	127.784	127.756
31	150	2.740	2.643	2.740	2.643	153.337	153.326	153.346	153.336
36	175	2.784	2.880	2.784	2.880	178.900	178.921	178.910	178.931

Table I (contd.)

		Puszta-földvár	High energy	Puszta-földvár	High energy	Puszta-földvár	High energy	Puszta-földvár	High energy
		$dV_g = -dV_w$		$dV_g = -dV'_{wk} - dV_{w\beta}$		$dV_g = -dV_w$		$dV_g = -dV'_{wk} - dV_{w\beta}$	
i	S_{gi}	$W_{stg(I)} = V_{gkt} \int_{J_o}^{J} Z\, dJ \left[\frac{Nm}{n^3}\right]$				$W_{stg(II)} = V_{pkt} \int_{K_o}^{K} Z\, dK \left[\frac{Nm}{m^3}\right]$			
41	0.200	2.817	3.154	2.817	3.154	204.464	204.535	204.473	204.545
46	225	2.847	3.464	2.847	3.464	230.028	230.169	230.037	230.180
51	250	2.874	3.810	3.874	3.810	255.593	255.828	255.601	255.839
56	275	2.903	4.193	2.903	4.193	281.159	281.513	281.168	281.525
61	0.300	2.936	4.613	2.936	4.613	306.729	307.227	306.737	307.240
66	325	2.976	5.069	2.976	5.069	332.302	332.974	332.310	332.988
71	350	3.036	5.562	3.036	5.562	357.884	358.755	357.892	358.769
76	375	3.112	6.091	3.112	6.091	383.475	384.573	383.483	384.588
81	0.400	3.212	6.656	3.212	6.656	409.079	410.431	409.087	410.447
86	0.425	3.336	7.258	3.337	7.259	434.698	436.332	434.706	436.349
91	450	3.496	7.897	3.496	7.897	460.339	462.278	460.347	462.295
96	475	3.687	8.572	3.687	8.572	486.003	488.272	486.011	488.290
101	0.500	3.935	9.284	3.935	9.284	511.704	514.316	511.712	514.335
106	0.525	4.293	10.032	4.293	10.032	537.475	540.414	537.483	540.433
111	550	7.753	10.817	7.753	10.817	564.968	566.568	564.982	566.587
112	0.553	11.125	11.125	11.125	11.125	569.912	569.827	569.933	569.847

Table II. Percentages of components of energy change in porous fluid reservoirs at formation pressures 10 and 2 MPa and at saturation values S_g=0.1 and S_g=0.5 in the volume V_{pkt}

	Formation pressure	$dV_g = -dV_w$ characterizing the change of state of the systems			
		Pusztaföldvár		High energy	
	MPa	S_g = 0.1	0.5	0.1	0.5
Energy requirement of the resistance	10	99.763 1	99.639 3	99.794 0	99.133 2
of the formation pressure p_w	2	98.832 4	98.253 8	98.984 6	95.957 3
Energy requirement of changes in	10	0.219 9	0.262 1	0.187 0	0.393 8
the interfacial surfaces P_c	2	1.089 2	1.292 2	0.927 3	1.906 1
Energy requirement of gas	10	0.015 6	0.090 4	0.017 4	0.433 5
compression dp	2	0.077 0	0.445 9	0.086 5	2.098 0
Change of the internal energy	10	0.001 4	0.008 2	0.001 6	0.039 5
of the gas mass dZ	2	0.001 4	0.008 1	0.001 6	0.038 6
Energy requirement of the elastic change of volume of the wetting	-	-	-	-	-
phase $w\beta$	-	-	-	-	-
		100.000 0	100.000 0	100.000 0	100.000 0
		100.000 0	100.000 0	100.000 0	100.000 0

Table II (contd.)

	Formation pressure	$dV_g = -dV_{wk} - dV_w$ characterizing the change of state of the systems			
		Pusztaföldvár		High energy	
	MPa	S_g = 0.1	0.5	0.1	0.5
Energy requirement of the resistance of the formation pressure p_w	10	99.752 8	99.636 6	99.785 1	99.127 8
	2	98.822 0	98.251 1	98.976 0	95.952 1
Energy requirement of changes in the interfacial surface P_c	10	0.219 9	0.262 1	0.187 0	0.393 8
	2	1.089 3	1.292 2	0.927 4	1.906 0
Energy requirement of gas compression dp	10	0.015 6	0.090 4	0.017 4	0.433 5
	2	0.077 0	0.445 9	0.086 4	2.098 1
Change of the internal energy of the gas mass dZ	10	0.001 4	0.008 2	0.001 6	0.039 5
	2	0.001 5	0.008 1	0.001 5	0.038 6
Energy requirement of the elastic change of volume of the wetting phase w/β	10	0.010 3	0.002 7	0.008 9	0.005 4
	2	0.010 2	0.002 7	0.008 7	0.005 3
		100.000 0	100.000 0	100.000 0	100.000 0
		100.000 0	100.000 0	100.000 0	100.000 0

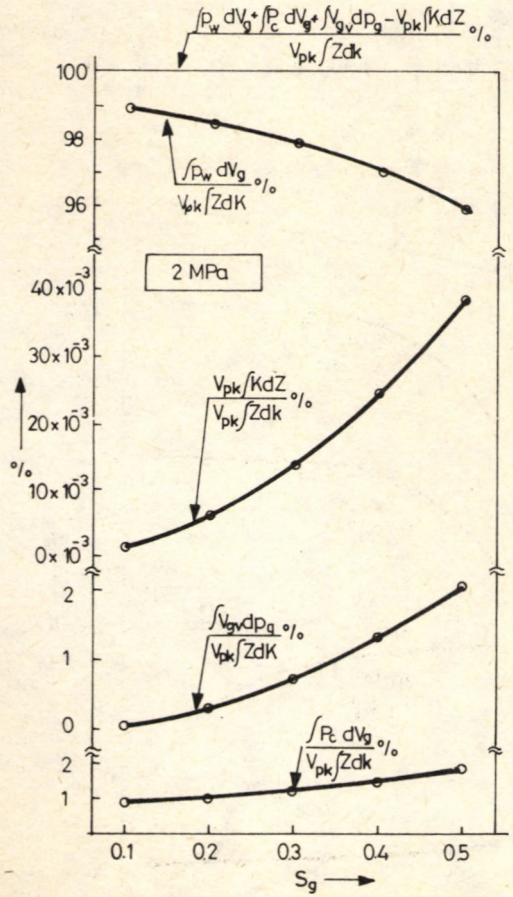

Fig. 27. Components of total energy resuirement in gas volume V_{gv} of "high energy" pore space at 2 MPa formation pressure

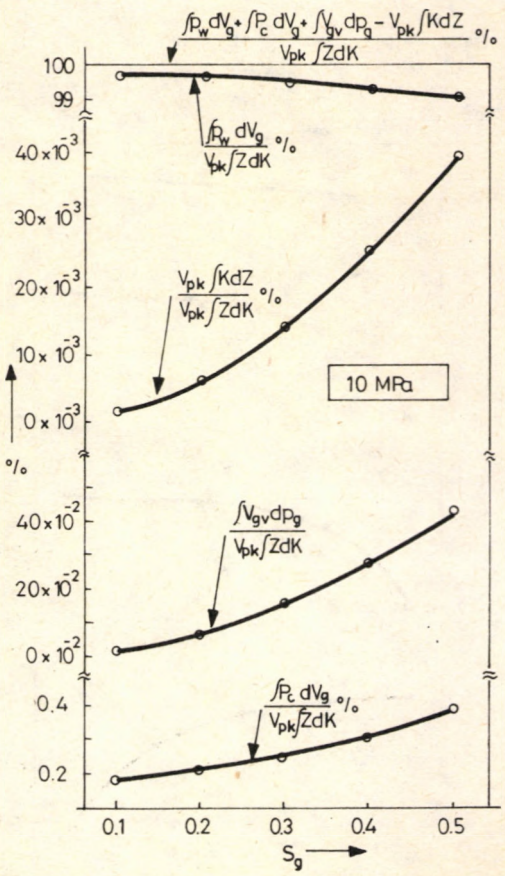

Fig. 28. The same as Fig. 27 at 10 MPa formation pressure

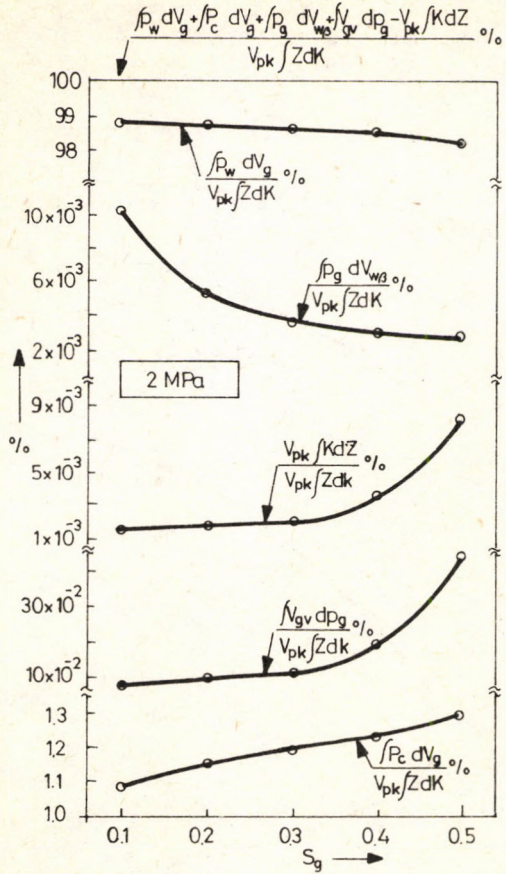

Fig. 29. Components of total energy requirement in gas volume V_{gv} at 2 MPa formation pressure taking account of elastic compressibility of formation water

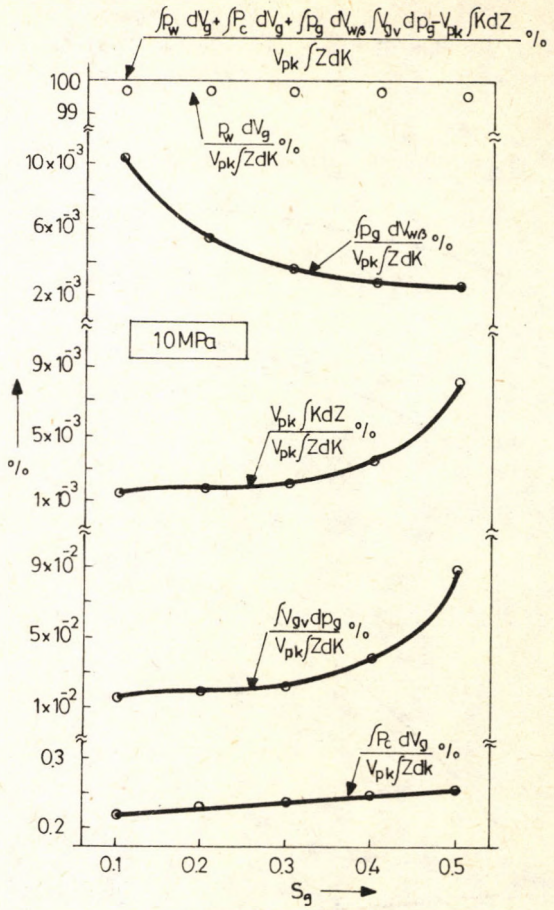

Fig. 30. The same as Fig. 29 at 10 MPa formation pressure

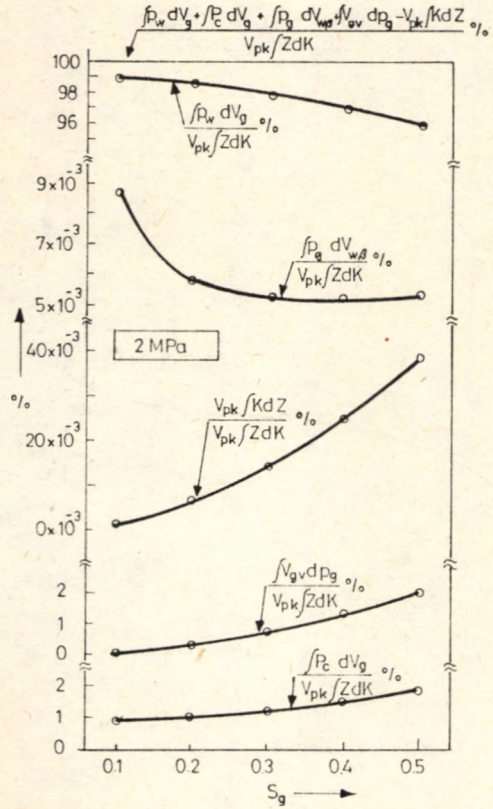

Fig. 31. Components of total energy requirement in gas volume V_{gv} at 2 MPa formation pressure in a "high energy" pore space taking account of elastic compressibility of formation water

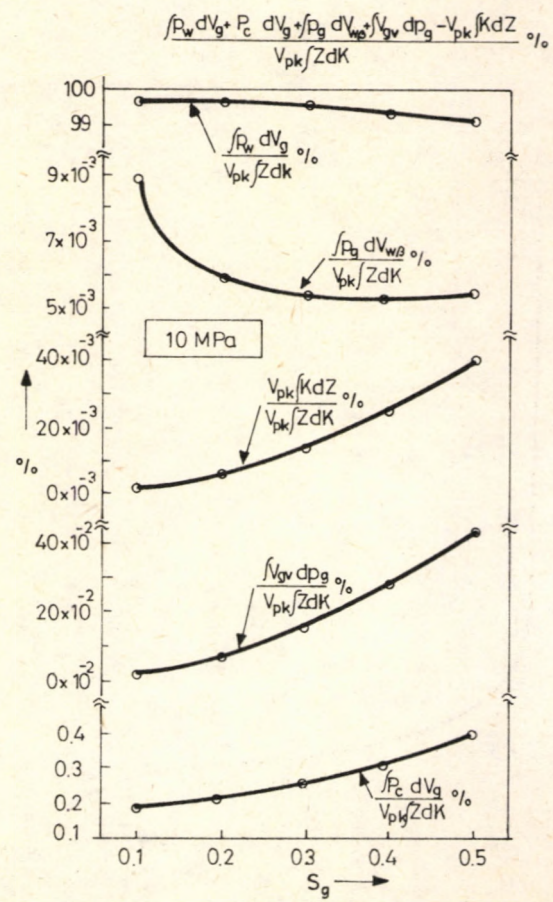

Fig. 32. The same as Fig. 31 at 10 MPa formation pressure

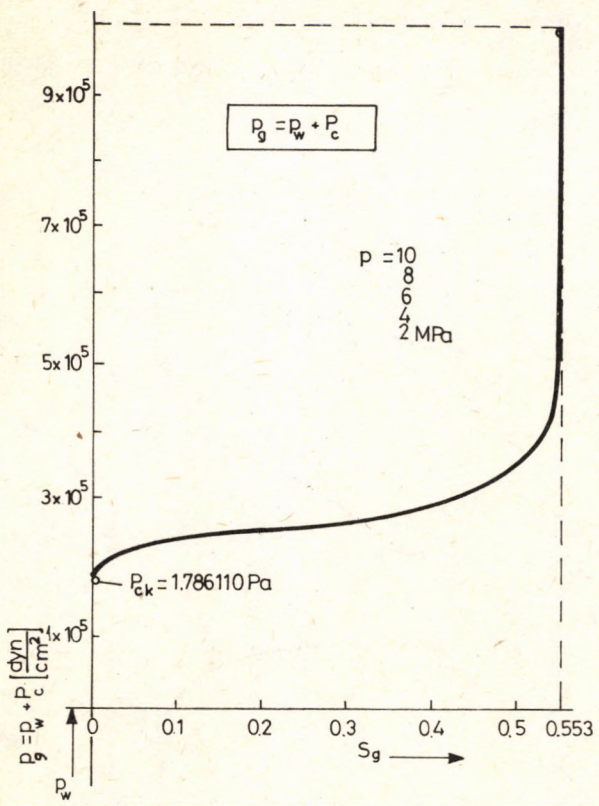

Fig. 33. Functions $P_C = P_C(S_g)$ and $p_g = p_g(S_g)$ in the Pusztaföldvár system

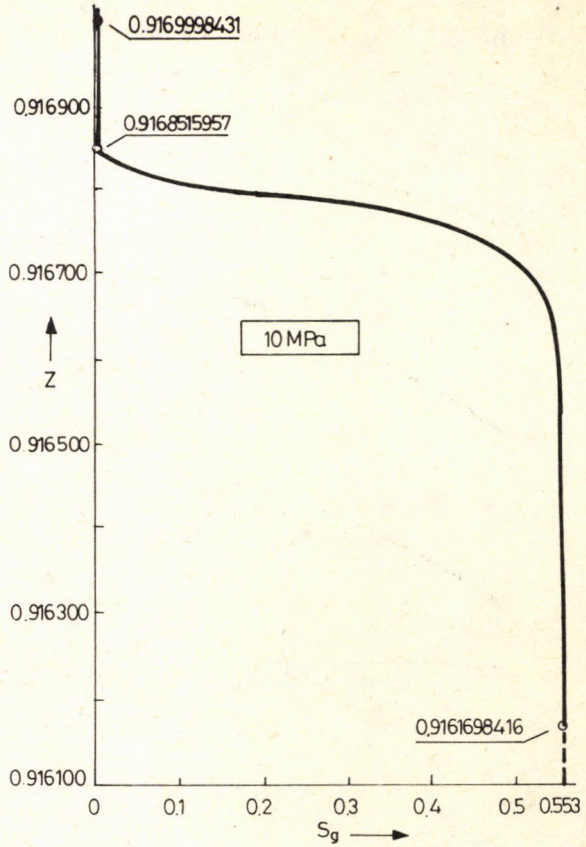

Fig. 34. Function $Z = Z(S_g)$ in the Pusztaföldvár system

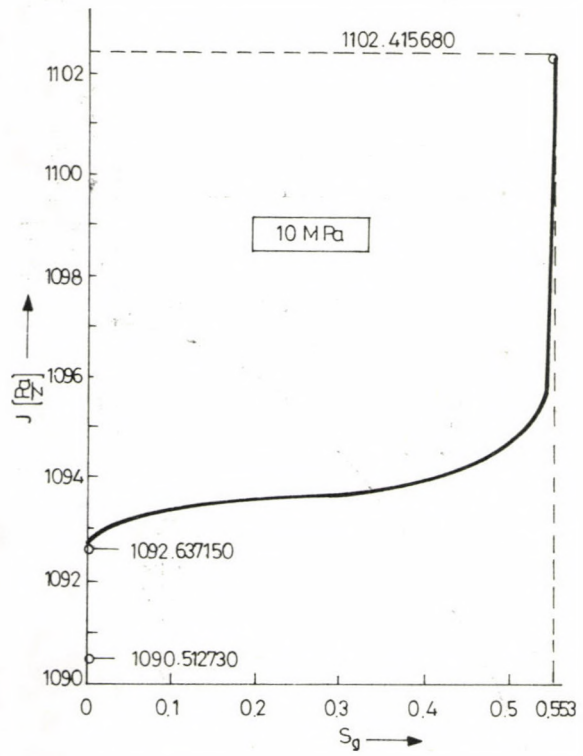

Fig. 35. Function $J = J(S_g)$ in the Pusztaföldvár system

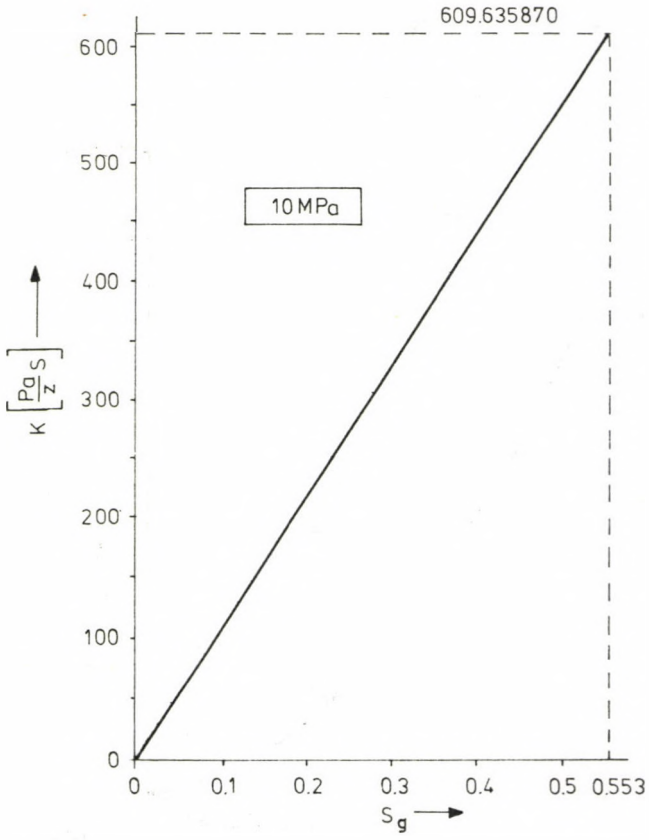

Fig. 36. Function $K = K(S_g)$ in the Pusztaföldvár system

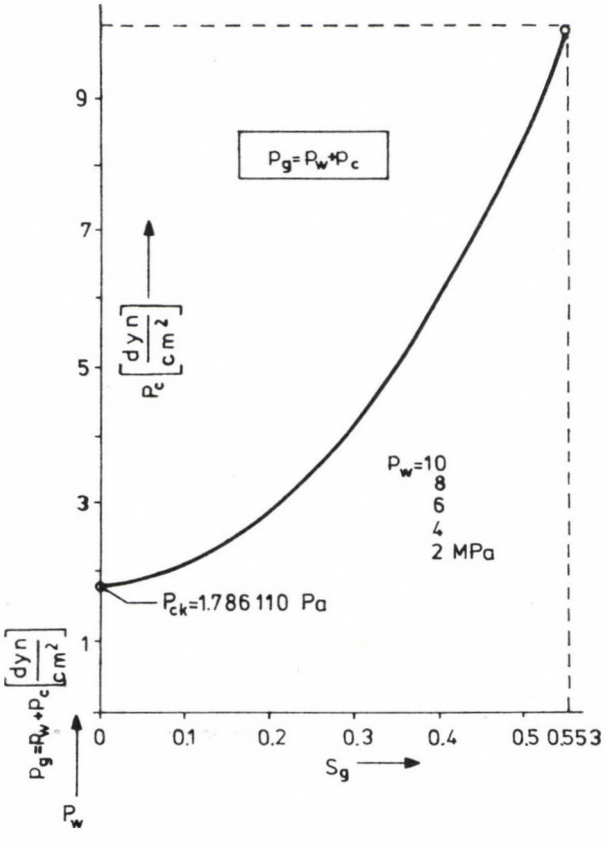

Fig. 37. Functions $P_c = P_c(S_g)$ and $p_g = p_g(S_g)$ in the "high energy" system

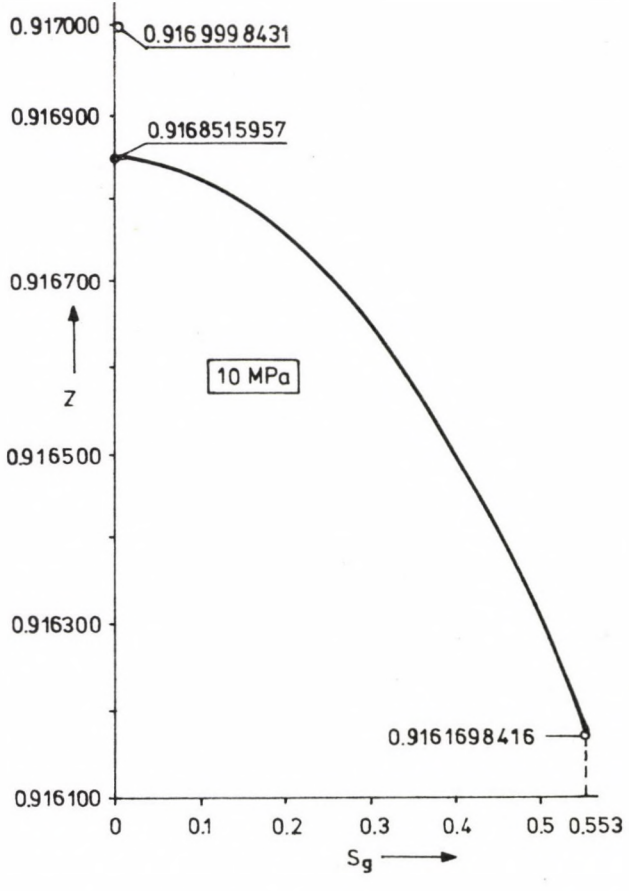

Fig. 38. Function $Z = Z(S_g)$ in the "high energy" system

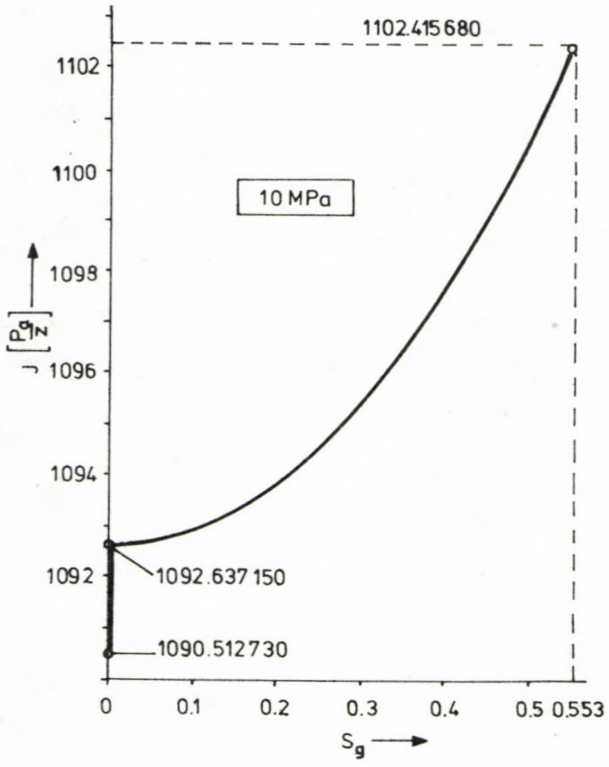

Fig. 39. Function $J = J(S_g)$ in the "high energy" system

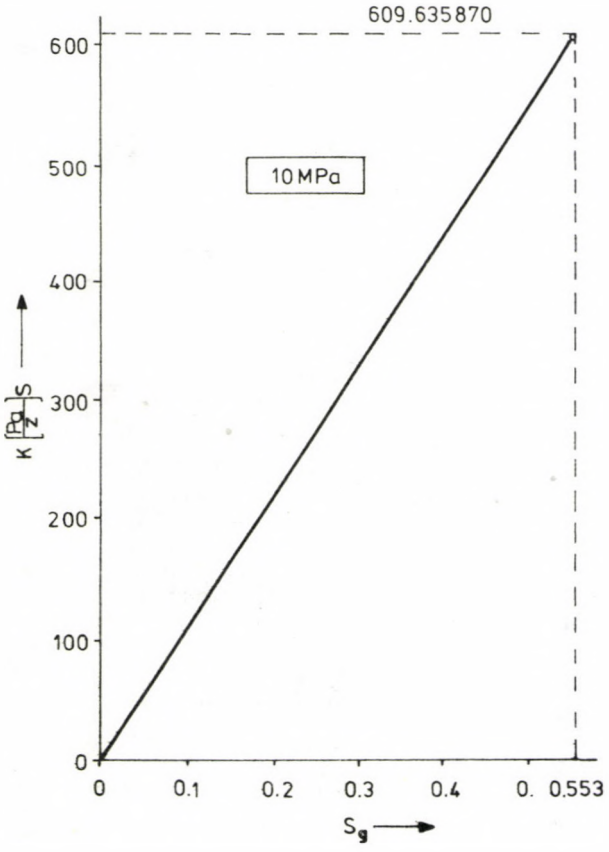

Fig. 40. Function $K = K(S_g)$ in the "high energy" system

gas pressure and further quantities defined earlier as functions of gas saturation. Figure 41 gives a layout of the high--pressure, high-temperature experimental apparatus used in laboratory.

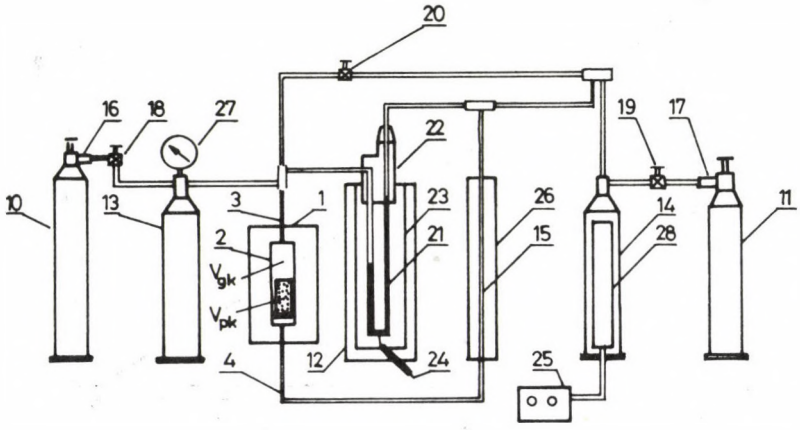

Fig. 41

SUMMARY

The most general independent variable of the system is the mass of the system. The geometrical volume of a geological structure suitable for fluid storage where changes caused by external effects take place, is regarded as a system.

Energy components making up the change of energy content which is equivalent to the change of state due to changes of a fluid-bearing reservoir, are of strictly local and functional character.

If the volumetric elements of the system and the direction and measure of the intended changes are known, the amount of energy needed for the change can be predicted, either work is done on the system or it arrives at a further state through spontaneous changes of state.

If would be difficult to handle the change of state of the

system as a function of the mass of the system. Therefore the state of saturation is regarded as independent variable instead of the mass of the system.

The specific energy of the change of the state of saturation, i.e. work needed to produce unit change of saturation has a minimum. This minimum is determined by the point of inflexion of the function $P_c(S)$ depending on the interfacial properties and the state of the pores of the system.

The total volume of the reservoir consists of a constant volume V_k and a varying volume V_v. The elementary energy components of volume V_k change through a minimum while those of volume V_v show a strictly monoton increase. For the total system $V_k + V_v = V$ the total elementary change

$$dW(S) = dW_I(S) + dW_{II}(S)$$

has a minimum.

The reservoir engineer has to know the minimum of function dW(S) if he intends to carry out changes in the state of the reservoir that require work to be done on the system.

The apparent energy optimum of the change of state of the system is determined by the minimum of function dW(S). The work needed to change the saturation and the mass of the system is minimum around this saturation and this state can be maintained at the expense of minimum work. The energy optimum is apparent because it means an optimum only if the value of the change of saturation is compared to the energy requirement of this change. In another aspect it is no optimum.

For practical purposes it is of great importance to note that within saturation limits interesting for engineering, the same change of state in unit volume (1 cm^3) of V_v requires less energy than in unit volume of V_k: thus rationality and necessity of energy management may become controversial.

In order to compromise natural conditions and technical aims, operational parameters have to be chosen with regard to the character of the reservoir. The investigations carried out have shown that function $P_c(S)$ determined by interfacial

properties and the pore structure play a characteristic role in forming the energy pattern of the system.

In capillary systems with functions $P_c(S)$ lacking the point of inflexion, energy varies strictly monoton. Thus the elementary components of energy fail to show any minimum, and there is no apparent energy optimum either. The elementary energy components show a monoton increasing or decreasing tendency depending on the direction of the change of gas mass.

These capillary systems arbitrarily called "high-energy" systems are rather rare in nature. Strictly speaking there is no function $P_c(S)$ which perfectly lacks the point of inflexion, because that would mean that the curve of the function would touch the abscissa axis at $S_w = 1$. Since natural fluid-bearing reservoirs have the tendency to retard the wetting fluid phase, i.e. they prohibit a zero threshold pressure, a capillary pressure-saturation function with a tangential character is not possible.

The ratio of the energy stored to that of storage does not depend on the structure of the reservoir. Therefore the specific energy of storage, i.e. the work needed to store unit energy is independent of the fact whether a steel container, an underground excavation or a porous rock is used to store the gas from which latter the gas first has to displace the formation water primarily saturating it.

The specific energy of storage, apart from being independent of the structure of the reservoir, does not depend on the ratio of the volume V_k to V_v either. Thus for any ratio of these volumes the specific energy of storage $\Delta W_{stg}/\Delta W_{std}$ is independent of the ratio of the geometrical dimensions of the above mentioned parts of the reservoir. This theorem solves the contradiction between technical and energetic aspects created by the physical state of "energy optimum", i.e. between rationality and necessity of operation due to the existence of the minimum of $dW(S_g)$.

The higher the energy requirement of storage, the smaller the specific energy.

It follows from this statement that the energy accumulated

by the storage of gas increases more rapidly, than the energy requirement of the technical operation.

The order of the components of the change of energy content accompanying changes of mass and state in the porous fluid-bearing system can be given as follows:

1. Energy of formation pressure.
2. Energy of interfacial properties.
3. Energy connected to the state of the wetting phases which also includes energy needed to change interactions among the smallest parts of matter, i.e. molecules.

Numerical values of energy components for various natural capillary systems may differ from those given in this paper, but their order remains the same.

REFERENCES

Zoltán Gy 1986a: Acta Geod. Geoph. Mont. Hung., 21, 297-314.
Zoltán Gy 1986b: Acta Geod. Geoph. Mont. Hung., 21, 315-343.

Acta Geod. Geoph. Mont. Hung., Vol. 24 (1-2), pp. 57-77 (1989)

EFFECT OF LONGWALL DIMENSIONS ON MINE FIRE HAZARD

F Kovács

Technical University for Heavy Industry, H-3515 Miskolc, Egyetemváros, Hungary

[Manuscript received April 3, 1985]

Frequency of endogenous mine fires is analysed as a function of working dimensions in longwalls of the Mecsek Coal Mines in Southern Hungary.

With increasing face length of the workings the average rate of advance decreases and the expected frequency of fires increases.

An increase of panel dimensions along the strike and of the life of face substantially increase the frequency of fires. Mine fire hazard increases with the life of face more rapidly in advancing workings than in retreating operations. The reason for this is in all probability the different ventilation pattern due to the direction of advance.

With increasing extracted seam thickness and thickness of caved top coal the rate of advance decreases, coal loss increases and the frequency of fires becomes greater.

A forecast method has been established to estimate frequency of mine fires on the basis of connection between working dimensions, rate of advance and coal loss. The expected measure of mine fire hazard is given as a function of face length and extracted seam thickness.

Frequency number estimated on the basis of natural and technical parameters can be used to decide about the method of fire protection and the increase of protection intensity.

Keywords: advancing working; coal loss; endogenous heatings; extracted seam thickness; face length; frequency number; life of face; mine fire hazard; panel dimensions; rate of advance; retreating working; thickness of caved top coal

SYMBOLS

D_v estimated error of the rate of advance
H length of face
K life of face
M extracted seam thickness
M_o open (supported) height of workings
M' thickness of caved top coal
p frequency number
r correlation factor
v rate of advance
V working loss
X = 2.4-v mpd

$Y = V$ percent
$Z = f(X,Y)$ regression function
$x = \frac{2.4 - v}{1.15}$
$y = \frac{V}{10.4}$
$z = f(x,y)$ regression function

SUBSCRIPTS

crit critical
max maximum

Endogenous mine fires require three conditions to be met (Lindenau 1977, Veselovsky 1975): sufficient amount of oxidable material with suitable grain size characteristic which is usually coal in the mining industry; sufficient amount of available oxygen in the various phases of oxidation; the heat produced by oxidation should gradually increase the temperature of the oxidable material and its surroundings. Latter condition is met if the air flowing through the gob does not exert an intensive cooling effect.

Analysing the frequency of fires it has been found that coal loss in the gob, rate of advance of the face, ventilation parameters and direction of advance play a major role in producing fires. An investigation of statistical data has also shown that the frequency of fires in longwalls is directly influenced by the dimensions of workings. The indirect effect of the parameters of workings is felt through parameters having a direct effect on fire hazard, viz. loss, rate of advance and ventilation pattern (Dept. Mining Engng. Techn. Univ. Heavy Ind. 1984, 1985).

Length of face H, life of face K and extracted seam thickness M have been regarded as the three principal dimensions of longwalls in the analysis. The data used in the investigation were taken from the Mecsek coal basin in Southern Hungary, and according to the local geological conditions, length of face coincides with the dipping dimension of the panels and life of face equals the striking dimension. Extracted seam thickness equals the open (supported) height M_o of workings in thin layers and in slicing of thick layers and it is equal to $M = M_o + M'$

in top coal cavings where M' denotes the thickness of the caved top coal. The volume H× K× M gives the output of the working--taking account of working loss and coal density.

Theoretical considerations suggest that the average rate of advance depends on the length of face of the workings, the life of face has primarily an effect on the parameters of ventilation and the extracted seam thickness influences working losses and the rate of advance, especially in top coal caving due to problems in caving control. However, it has to be taken into account that the effect of each parameter on the fire hazard cannot be separately registered. Geological properties of the deposits (mechanical characteristics of the layers and adjacent rocks) determine the parameters of roadway maintenance, caving etc. to a large extent.

The effect of the parameters of workings on the frequency of mine fires has been analysed using the data of longwalls of the Mecsek Coal Mines worked between 1979 and 1983. The data of 208 workings have been analysed altogether. There were operating 74 workings in Pécsbánya, 12 in Vasas Mine, 50 in Kossuth Mine and 72 in Zobák Mine in the time interval investigated. Thin layers were mined by 98 workings, slicing in thick layers was used in 59 workings and 51 workings applied top coal caving. 29 percent of the total were advancing, 63 percent retreating and 16 workings were partly advancing partly retreating. Data of the workings were provided by the Mecsek Coal Mines (Dept. of Mining Engng. Tech. Univ. of Heavy Ind. 1985).

The measure of fire hazard is characterized by the frequency of endogenous heatings and fires. Frequency parameter p is obtained by dividing the number of fires by the number of workings.

The frequency of fires has been first investigated as a function of the length of face. In addition to the analysis of the frequency of fires the rate of advance has also been looked into. Similar tendencies have been found from the data of Pécsbánya, Kossuth and Zobák Mines. The frequency of fires rises with increasing length of face while the average rate of advance decreases. Figure 1 shows diagrams based on data of Zobák Mine,

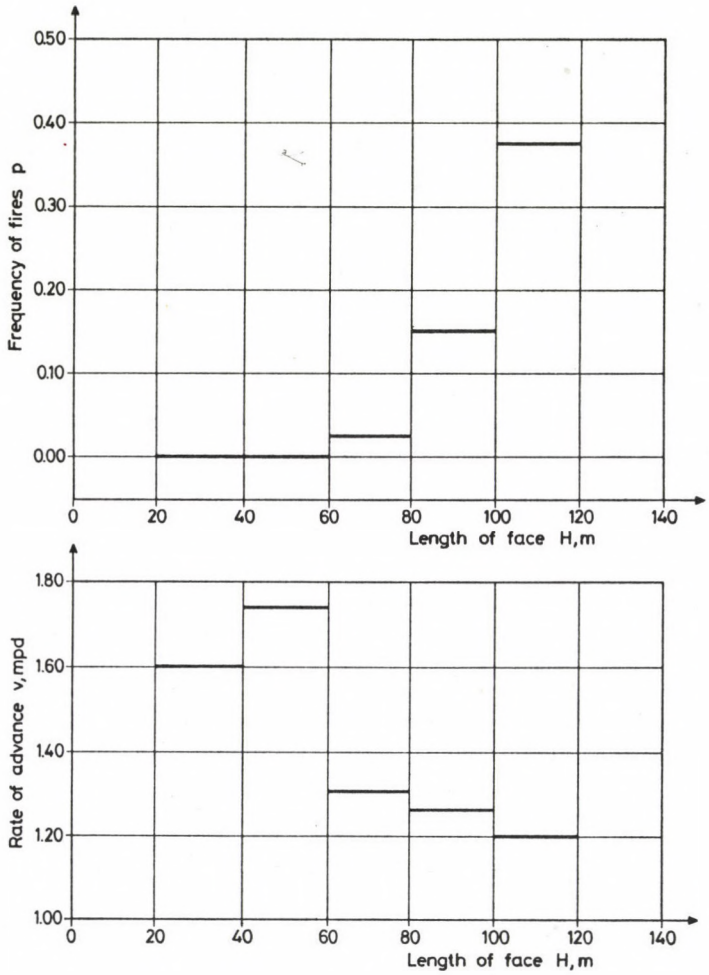

Fig. 1. Frequency of fires and rate of advance as functions of the length of face in Zobák Mine

while Fig. 2 illustrates those of all four mines. Increasing the pitch to 40 m the bar charts become more regular. Using this unit in Fig. 3, data of the four mines indicate a continuous linear change for the frequency of fires as a function of the length of face. While the expected frequency is p = 0.10 for an 80-m length of face indicating fires to be expected in every tenth working, the frequency mounts to p = 0.20 to 0.22 in

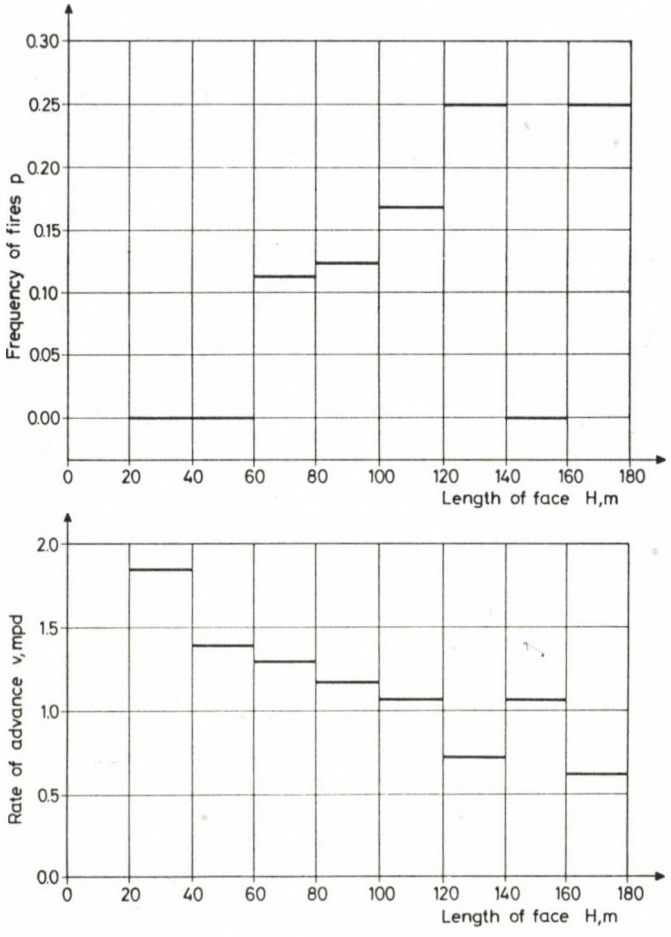

Fig. 2. Frequency of fires and rate of advance as functions of the length of face (Pécsbánya, Vasas, Kossuth and Zobák Mines)

workings with 160 m long faces forecasting fires or heatings in every fifth working.

The effect of the face length on the increase of fire hazard is obviously the consequence of the fact that with increasing length of face the rate of advance decreases and the coal left behind in the gob is exposed to the effect of oxidation. A longer face has, of course, other effects as well, e.g. greater air loss due to greater depression.

From the data used in the lower diagram of Fig. 3 the

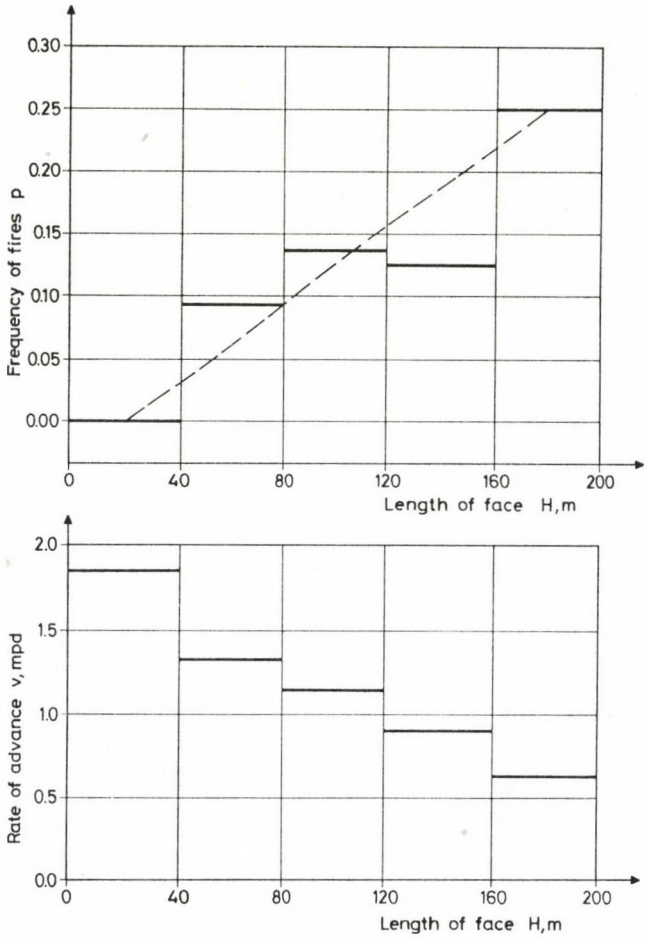

Fig. 3. Frequency of fires and rate of advance as functions of the length of face (Pécsbánya, Vasas, Kossuth and Zobák Mines)

equation of the regression correlation can be determined between the rate of advance v and the length of face H:

$$v = 1.86 - 0.00712\ H \qquad r = 91\ \% \qquad D_v = 15\ \% \ .$$

Rate of advance considerably decreases with the increase of the length of face. For an 80-m long face a rate of advance v = 1.2 to 1.4 mpd can be expected while for 160 m only 0.6 to 0.8 mpd.

Analysing the effect of the life of face, frequency values for the individual mines have been first determined. The tendencies obtained were the same for Pécsbánya, Kossuth and Zobák Mines. Figure 4 illustrates the data of Pécsbánya, while Fig. 5 shows those of Zobák mine. The bar chart of Fig. 4 indicates a steeper increase. Figure 6 displays frequency values as a function of the life of face based on the data of all mines. Definite increasing tendency has been observed in all cases.

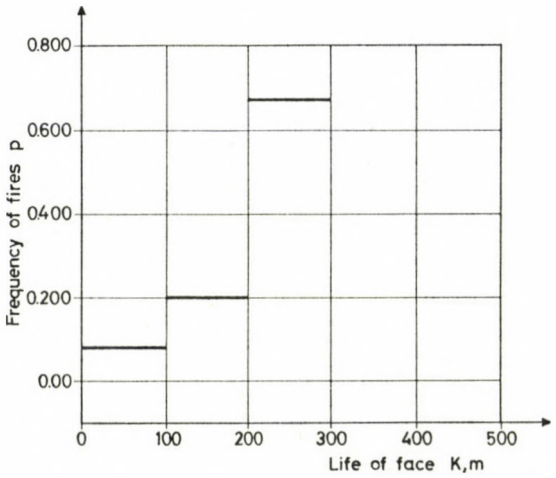

Fig. 4. Frequency of fires as a function of the life of face in Pécsbánya Mine

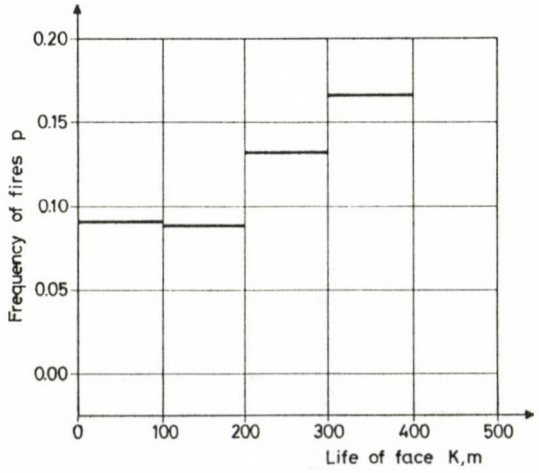

Fig. 5. Frequency of fires as a function of the life of face in Zobák Mine

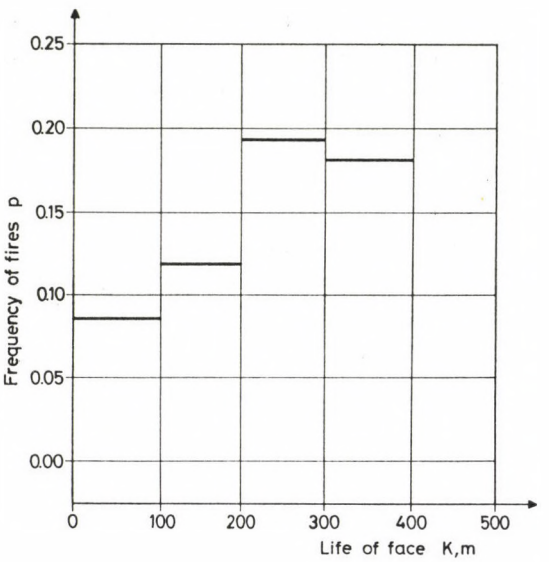

Fig. 6. Frequency of fires as a function of the life of face (Pécsbánya, Vasas, Kossuth and Zobák Mines)

A comparison of Figs 4 and 5 suggests that the diagram based on the Pécsbánya data is steeper, i.e. higher frequencies occur at smaller values of life of face. Therefore, to perform a more differentiated analysis of the effect of the life of face, the frequency of fires has been investigated according to the direction of advance. For advancing workings the data of Pécsbánya Mine, for retreating direction those of Pécsbánya, Kossuth and Zobák Mines have been used in the statistical analysis. Figure 7 illustrates frequencies for various directions of advance in the different mines as functions of the life of face. The figure indicates that the frequency of fires increases more steeply in advancing workings. Practically the same is illustrated by Fig. 8 using the data of all mines. For advancing workings the rate of increase of the frequency of fires (the slope of the regression line) is about twice that for retreating workings.

The disadvantageous tendency of fire hazard as a function of the life of face can also be experienced in the practice of advancing workings. Among 61 advancing workings the life of face

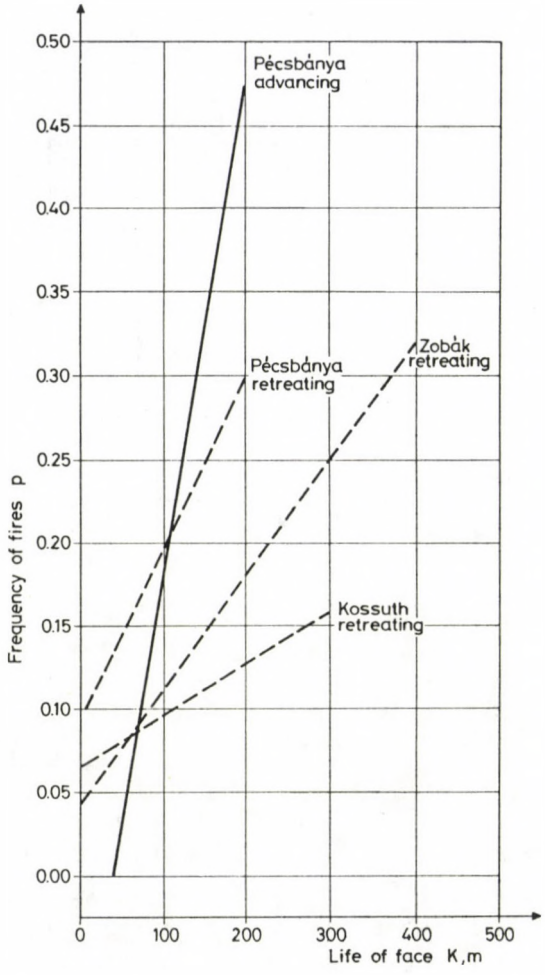

Fig. 7. Frequency of fires as a function of the life of face in various mines

exceeded 200 m in 8 cases only, there was no working with a life of face of 300 m. Among retreating workings there were some with 500 to 700 m life of face, although the frequency of fires was here rather high: p = 0.50. The average life of face of the advancing workings was 99 m while that of retreating ones 139 m. These data prove that advancing direction is generally regarded safe at shorter life of face only. A more detailed analysis has also shown that the frequency of fire in retreating workings

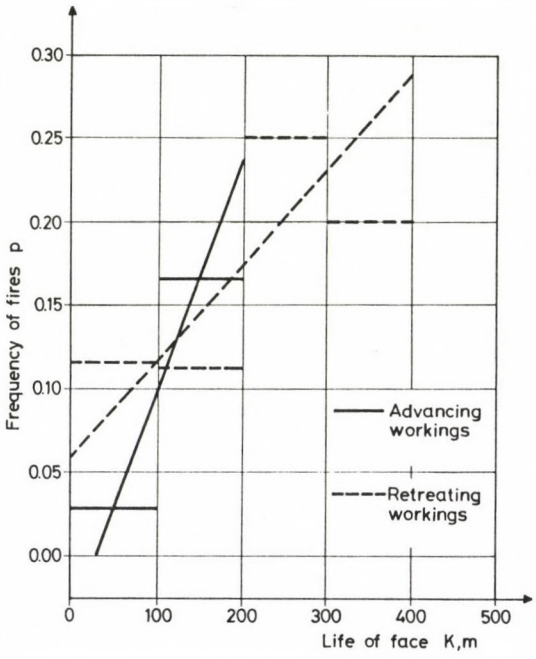

Fig. 8. Frequency of fires as a function of the life of face (Pécsbánya, Vasas, Kossuth and Zobák Mines)

was 3 to 4 times that of advancing workings.

It has also been analysed through which parameters the life of face influenced fire hazard. The statistical analysis has shown that the rate of advance and air velocity at the face is not in connection with the life of face.

Based on observations about the origin of endogenous mine fires it can be assumed that the life of face exerts its effect on the fire hazard partly through the coal in the gob which experiences the effect of oxygen at longer life of face for a long time especially if the rate of advance is low. Another factor increasing fire danger is the high depression between the intake and return sides which, especially in advancing workings, increases air losses through the gob.

Our results suggest that retreating direction is more suitable to choose - especially for longer life of face. However, short life of face is not advantageous from economic

aspects (longwall installation, beginning of working), therefore other means have to be selected to reduce fire hazard. Fire hazard can be reduced by increasing the rate of advance, moderating coal losses and optimizing ventilation parameters (minimum air velocity and depression allowed from the point of view of firedamp hazard). In addition, perfect caving on the intake side and the sealing of the gob in retreating workings, and a perfect sealing around the drifts near the workings considerably reduce potential hazard.

The third principal dimension of the working panel is the extracted seam thickness. In thin layers this parameter is fixed, while in slicing of thick layers the support limits M_o to 3 to 3.5m according to the technology applied. The thickness can be varied within wider limits in top coal caving methods. Top coal caving, however, has several disadvantages concerning fire hazard: dilution increases, coal losses are high due to problems in roof coal control the rate of advance is low because of the complicated technology, time needed to provoke roof coal and other problems. All these disadvantages contribute to increasing potential fire hazard.

Using data of the Mecsek coal basin, coal loss and rate of advance have been analysed as functions of the seam thickness. The statistical analysis has shown each for Vasas, Kossuth and Zobák mines that with increasing caved top coal thickness M' and extracted seam thickness M the working loss V shows a definite increasing tendency while the rate of advance v decreases. Figure 9 shows the working loss in Vasas Mine, Fig. 10 illustrates the rate of advance in Zobák Mine as functions of the thickness of the caved top coal. Since higher losses and lower rates of advance increase fire hazard, increasing extracted seam thickness increases the frequency of endogenous mine fires.

Relationship between working loss, rate of advance, length of face and extracted seam thickness, as well as frequency of mine fires enable us to develop a forecast method to predict the expected measure of fire hazard.

As a first step frequencies of fires and heatings have

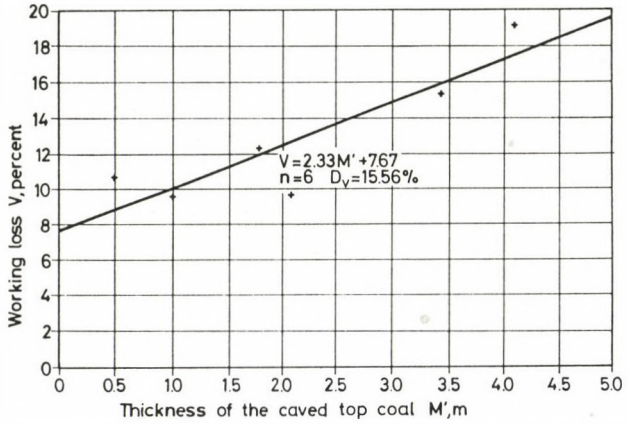

Fig. 9. Working loss as a function of the thickness of the caved top coal (Vasas Mine)

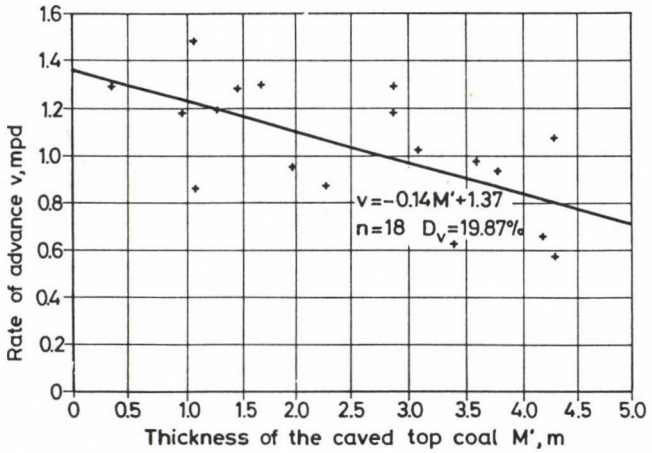

Fig. 10. Rate of advance vs the thickness of the caved top coal (Zobák Mine)

been determined for various ranges of loss and rate. From the frequency values the equation of the function of frequency p has been calculated using the regression method. Instead of variable v, since with its increase p decreases, independent variable X = 2.4 - v has been introduced while the other independent variable was Y = V (in percentage).

The two-variable regression function with general exponents has the form:

$$Z = 0.00002\ X^{3.95}\ Y^{2.87}, \qquad I = 71 \text{ percent}$$

or

$$p = 0.0002\ (2.4-v)^{3.95}\ V^{2.87}, \qquad I = 71 \text{ percent.}$$

From the set of points the equation of the regression plane has been calculated:

$$Z = 0.1865\ X + 0.0204\ Y - 0.2271, \qquad I = 72 \text{ percent}$$

or

$$p = 0.1865\ (2.4-v) + 0.0204\ Y - 0.2271, \qquad I = 72 \text{ percent.}$$

To ensure a more reliable assessment of the effects of the independent variables, the function has been transformed into a dimensionless form by dividing the variables by the co-ordinates of the centre of gravity, which are

$$\bar{v} = 1.15 \text{ mpd} \qquad \text{and} \qquad \bar{V} = 10.4 \text{ percent.}$$

The new dimensionless variables become

$$x = \frac{2.4 - v}{1.15} \qquad \text{and} \qquad y = \frac{V}{10.4}\ .$$

The equation of the regression function can be written as

$$z = 0.0203\ x^{4.53}\ y^{2.81}, \qquad I = 73 \text{ percent}$$

or

$$p = 0.0203\ \left(\frac{2.4-v}{1.15}\right)^{4.53}\ \left(\frac{V}{10.4}\right)^{2.81} \qquad I = 73 \text{ percent}\ .$$

The sketch of the regression function is illustrated in Fig. 11.

Using the equations of the regression plane and the general surface, the frequency of fires can be illustrated in a v-V co-ordinate system. The line of intersection of the regression plane with plane p=0 gives the line of frequency p=0. In

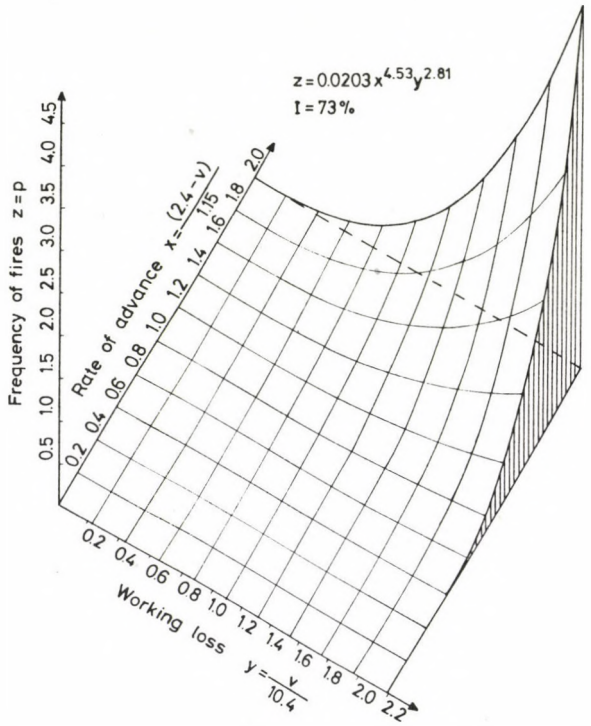

Fig. 11. Frequency of fires as a function of the working loss V and the rate of advance v

the field to the left from this line the probability is zero indicating that no heating or fire can be expected. The lines and areas of various frequencies are determined by the projections of the lines of intersection of the regression plane with the planes p=0.1; 0.2; ...; 0.9; 1.0 on the v-V plane (Fig. 12). From the figure it can be seen that for v=1.5 mpd rate of advance and 27.5 percent loss the frequency of heatings and fires is p=0.5 i.e. its probability 50 percent. Data of the investigated fires v,V have been plotted on the diagram. Reality of the diagram is proved by the fact that heating or fire can be observed in the field of probability higher than p=0.05 only and that no working took place in the field of probability higher than 50 percent. The equation of the regression plane can be used for forecast purposes in those fields of the v-V

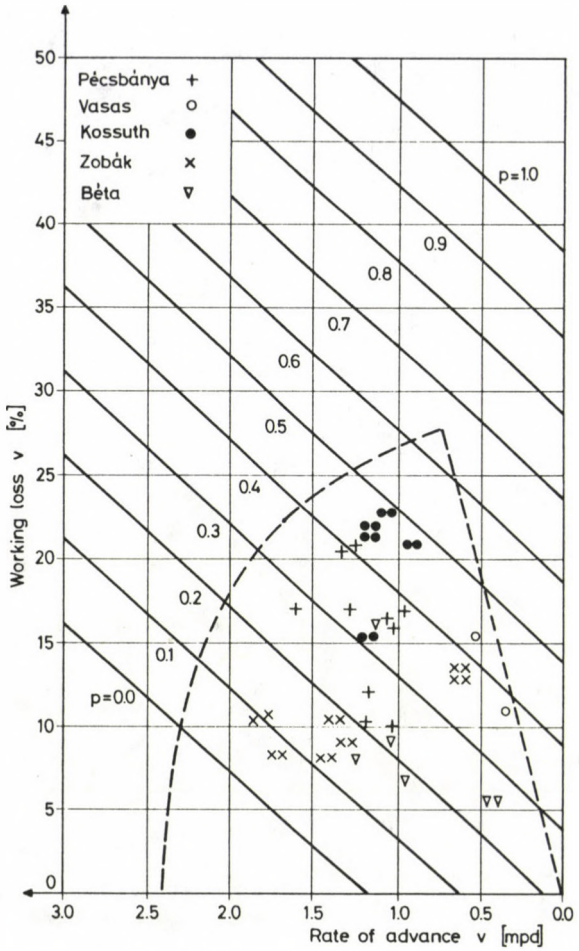

Fig. 12. Frequency (probability p) of endogenous heatings and fires as functions of the rate of advance and working loss

plane where the data of the investigated workings can be found. This field is indicated by dotted lines in Fig. 12.

The lines and fields of frequency parameters determined from the regression surface with general exponents are indicated in Fig. 13. The field of zero frequency is bounded by the lines V=0 and v=2.4. The shape of the frequency parameter lines reflects the high exponents 4.53 and 2.81 of both variables v and V. At certain parameter values - below v=1.6 to 1.5 mpd

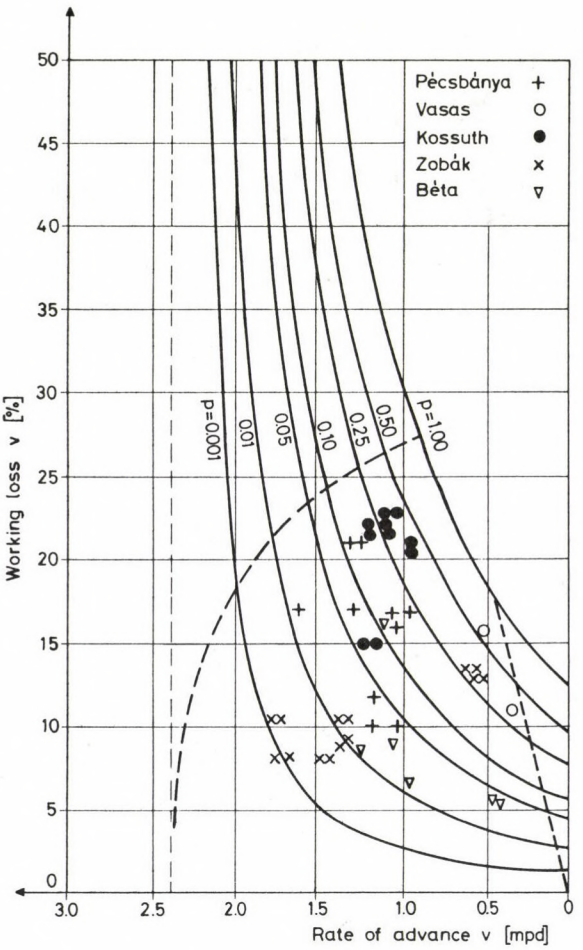

Fig. 13. Frequency (probability p) of endogenous heatings and fires as functions of the rate of advance and working loss

and above V=9 to 10 percent - the parameter of hazard shows an abrupt increase. Points corresponding to actual fires have also been plotted in the diagram. Majority of the fires lie in the field between the probability limits 1 to 50 percent. In the field below zero probability neither heating nor fire took place which proves the feasibility of a forecast method based on the function determined. There was one working with heating in Vasas Mine only that fell into the field above 50 percent

(v=0.51 mpd and V= 15.2 percent). Apart from that, the data of three workings fell beyond the line p=0.5.

The function with general exponents illustrated in Fig. 13 can better reflect the effects of the parameters and their differences owing to the values of the exponents than the unit exponents of the regression plane. Parameter lines obtained from the power function show that the hazard abruptly increases below a certain rate of advance when the coal in the goaf has contact with oxygen for a time longer than the incubation time. Figure 13 also proves that below a coal loss of 3 to 5 percent fire hazard is minimum and that fires have not to be expected above the rate of advance 1.7 to 2.0 mpd because the coal in the goaf is sealed off the oxygen within a short time.

Using the functions and diagrams, the expected frequency can be calculated for a prescribed or selected (designed) pair of parameters according to regression function

$$p = 0.0203 \left(\frac{2.4-v}{1.15}\right)^{4.53} \left(\frac{V}{10.4}\right)^{2.81}$$

as

p=0.00015= 0.015 %	for	v=2 mpd	and	V=10 %,
p=0.3108 =31.08 %	for	v=1.0 mpd	and	V=20 %,
p=0.9713 =97.13 %	for	v=1.0 mpd	and	V=30 %.

Naturally, the coefficient and the exponents of the regression functions may be different under different natural conditions. Also, if the number of data available increases or basically new technologies are applied, they have to be determined anew.

The second step of the forecast method may be the estimation of the frequency as a function of the length of face H and the extracted seam thickness using the functions rate of advance vs. length of face, working loss vs. extracted seam thickness and rate of advance vs. extracted seam thickness. From the data displayed in Figs 1 to 3 and 9 to 10 regression functions

$$v = f(m, H) \quad \text{and} \quad V = f(M)$$

can be determined. On substitution in function p=f(v,V) the

expected frequency can be expressed as a function of H and M.

Functions v=f(M,H) and V=f(M) can be determined for certain areas using characteristic averages of data. However, if sufficient data are available, the functions can be calculated for each mine or each mining method.

For all workings using either slicing or top coal caving method and the data of four mines (Pécsbánya, Vasas, Kossuth and Zobák), the functions can be written:

$$v = -0.0567\ M - 0.0045\ H + 1.84 \quad \text{mpd}$$
$$V = 2.0873\ M + 3.60 \quad \text{percent}$$

where M and H have been substituted in metre.

For the slicing workings of Zobák Mine hold

$$v = -0.2174\ M - 0.0030\ H + 2.14\ ,$$
$$V = 1.3640\ M + 5.34.$$

For the workings of Zobák Mine using top coal caving method we have

$$v = 0.0552\ M - 0.0066\ H + 1.90\ ,$$
$$V = 1.8191\ M + 4.04.$$

For all workings of Zobák Mine with any of the aforementioned two technologies hold

$$v = -0.1022\ M - 0.0044\ H + 1.97$$
$$V = 1.3331\ M + 5.93.$$

The value of M can vary within 1.5 to 3.5 m for workings with slicing and within 2.5 to 10.0 m for top coal caving. The length of face H of the workings is between 20 and 200 m.

Function constants calculated can only be used for forecast purposes under given technical and natural conditions, but first of all under those where the data used for calculating regression constants come from. Thus conditions of using the functions are: identical or similar

- natural circumstances (seam and adjacent strata properties),
- technological properties (support, cutting, ventilation etc.),
- protection method (chemicals, sandfill etc.).

The theoretical background of the forecast method is the fact that working loss and rate of advance together are capable of suitably characterizing the measure of fire hazard, and, at the same time, rate of advance is a function of the length of face and the extracted seam thickness while working loss depends on the caved thickness - given the same technology and support.

Let us now have a few examples of application for Zobák Mine.

For slicing let be $M \cong 2.5$ m and H = 70 m. Then v=1.39 mpd and V=8.75 percent. From the equation of the regression plane we have for the expected frequency p=0.14=14 percent. At the same thickness but with double length of face, i.e. H = 140 m the rate of advance becomes v=1.18 mpd and the loss V=8.75 percent. The expected frequency will be p=0.18=18 percent. Doubling the length of face increases the expected frequency from p=0.14 to p=0.18 i.e. by 4 percent.

For top coal caving let us first have M = 5 m and H = 75 m. We now find v=1.13 mpd and V=13.5 percent. The expected frequency is p=0.29=29 percent. The loss V=13.5 percent for the extracted seam thickness of 5 m ($M' \cong 2.5$ m) forecast a high frequency for even medium length of face: heating or fire can be expected in every third working. If the length of face doubles (at identical seam dip the height of level becomes twice as much i.e. H = 150 m), the rate of advance decreases to v= =0.63 mpd while the expected frequency of fires increases to $p \cong 0.38 = 38$ percent.

Having the same pitch of level, i.e. a length of face H = 150 m and a seam of M = 10 m thickness ($M' \approx 7.5$ m) is worked with top coal caving then the loss becomes V = 23 percent and the expected frequency of fires p=0.57=57 percent which indicates that the frequency for the case of M = 5 m and H = 75 has doubled. Thus, in every second working a heating - which is difficult to localise in top coal caving - or a fire can be

expected.

For the parameters M = 10 m and H = 150 m the function with general exponents illustrated in Fig. 13 forecasts a frequency p > 1.0 which indicates that applying chemicals only, heating or fire cannot be prevented at v=0.63 mpd and V=23 percent.

Further research can provide an economic assessment technique which could be used in selecting the suitable method of reducing fire hazard or increasing production safety.

The first possibility to be mentioned is to carry out top coal caving of the 10 m thick seam in two parts, 5 m thick each. This method reduces the frequency of fires from 57 percent to 38 percent. Another possibility is to reduce the pitch of level to its half (by applying auxiliary levels or sublevels), i.e. to work the seam with a length of face of H = 75 m and at M = 10 m. The expected frequency is p=0.4789=0.48=48 percent in this case, thus this measure reduces fire frequency by 9 percent only. The third possibility is to apply slicing with 150 m long faces, i.e. to work the same seam in four slices 2.5 m thick each. The rate of advance now is v=1.15 mpd, working loss V=8.75 percent and the expected frequency p=18 percent. This method may reduce fire hazard to one third, i.e. from 57 percent to 18 percent which ensures a reasonable situation.

A change in technology keeping M and H unchanged but increasing the rate of advance and reducing working losses, may decrease fire hazard. The measure of fire hazard can also be reduced by considerably intensifying protection techniques (sandfill, optimum ventilation, perfect sealing of air). Changes in technology or basically new protection methods are accompanied with new regression constants and forecast parameters.

An economic assessment can decide whether the hazard characterised by given frequency parameter can be tolerated for the technology and equipment applied, or more intensive and reliable fire protection has to be introduced in order to reduce hazard. Based on economic considerations a critical or

limiting frequency p_{crit} or p_{max} can be determined taking into account the value of equipment, the output of the working, costs and safety aspects of closing and re-opening the working etc. If a hazard higher than that is forecast then by changing the parameters of working or intensifying protection, the expected measure of hazard can be lowered below the permitted level.

In choosing between slicing or top coal caving methods, one of the aspects can be the expected measure of fire hazard (which is usually higher for top coal caving due to lower rates of advance and higher losses). The other aspect in taking the choice is to consider the economic advantages of the top coal caving method (output, productivity, drivage requirement, specific costs).

REFERENCES

Department of Mining Engineering, Technical University for Heavy Industry 1984: Critical analysis of top coal caving methods and firedampproof blasts in the Mecsek Coal Mines. Proposals to increase safety (in Hungarian). Research Report for the Ministry of Industry, Miskolc

Department of Mining Engineering, Technical University for Heavy Industry 1985: Connection of mine fire hazard with natural and technical parameters using longwall data in the Mecsek Coal Mines (in Hungarian). Research Report for the Mecsek Coal Mines, Miskolc

Lindenau N I 1977: Origin, prevention and extinguishment of endogenous mine fires (in Russian). Publisher "Nedra", Moscow

Veselovsky V S 1975: Forecast and prevention of endogenous fires (in Russian). Publisher "Nauka", Moscow

Acta Geod. Geoph. Mont. Hung., Vol. 24 (1-2), pp. 79-86 (1989)

ON THE CONNECTION BETWEEN QUALITY PARAMETERS DETERMINING THE CALORIFIC VALUE OF COAL

I Osváth[1] and Sz Pethő[2]

[1]Coal Mining Union, Tatabánya

[2]Technical University for Heavy Industry, H-3515 Miskolc, Egyetemváros, Hungary

[Manuscript received May 17, 1985]

Energy content of coal expressed in terms of calorific value is a linear function of the calorific value of the combustible pure coal without ash and moisture, as well as ash content, heat of burning, moisture content and heat of evaporation. All these parameters, including heat of burning, which is different for various coal types, can be determined from the results of analyses carried out by the mining companies, if the mathematical methods of the study are applied. Analysing Hungarian coal types, the authors have found that not only their ash and moisture contents but the calorific value of the pure coal without ash and moisture, as well as the heat of burning of ash producing minerals are different (Pethő et al. 1972). The authors intend to take account of the results of the paper in their suggestions for a new coal price system.

Keywords: ash content; ash producing minerals; calorific value; combustible pure coal; heat of burning; heat of evaporation; moisture content

Symbols:
- a ash content
- A constant, explained by Eq. (7)
- b heat of burning
- B constant, explained by Eq. (6)
- C calorific value of coal
- C_o calorific value of coal without ash and moisture content
- D coefficient of moisture content, see Eq. (11)
- g mass ratio of ash producing minerals to ash
- m moisture content

1. CALCULATION OF QUALITY PARAMETERS DETERMINING CALORIFIC VALUE

To calculate calorific value of coal with ash content a and moisture content m, most handbooks suggest the following equation:

$$C = \frac{100 - (a + m)}{100} C_o - 24.62\ m. \qquad (1)$$

In Eq. (1) C_o denotes the calorific value of coal without ash and moisture content. 2,462 kJ/kg is the heat of evaporation of the water and 24.62 is its one hundredth part since m and a are expressed in terms of mass percentage.

Equation (1) fails, however, to take account of the heat requirement of burning minerals and rocks contained by the coal into ash. Therefore, instead of Eq. (1), the following equation is suggested to reflect natural circumstances (Tarján 1974):

$$C = \frac{100 - m - ga}{100} C_o - 24.62\ m - gab. \qquad (2)$$

In Eq. (2) g denotes the ratio of the mass of the ash producing minerals in the coal to that of ash, $g \gtrless 1$; b stands for the specific heat requirement of burning these minerals into ash. In our next discussions b will be called heat of burning with a dimension of kJ/0.01 kg.

Since the mineral content and g are rather difficult to determine, assumption g = 1 will be used in Eq. (2):

$$C = \frac{100 - m - a}{100} C_o - 24.62\ m - ab. \qquad (3)$$

In Eq. (3) all variables, among them ash content are linear functions of the calorific value, therefore

$$C = B - Aa \qquad (4)$$

holds (Pethő 1981). B and A are constants characteristic of the coal types.

Rearranging Eq. (3) according to Eq. (4) gives

$$C = \left(1 - \frac{m}{100}\right) C_o - 24.62\ m - \left(\frac{C_o}{100} + b\right) a. \qquad (5)$$

A comparison of Eqs (4) and (5) enables us to express constants B and A as

$$B = \left(1 - \frac{m}{100}\right) C_o - 24.62\ m, \qquad (6)$$

$$A = \frac{C_o}{100} + b\ . \qquad (7)$$

Constant B as expressed by (6) gives the calorific value of the coal without ash, and A in Eq. (7) stands for the change of calorific value due to a one-percent change of ash content at constant moisture content.

Both constants are linear functions of C_o. In addition, constant B is linearly proportional to the moisture content and the heat of evaporation of the water. Apart from C_o, constant A also depends on b. For endogeneous minerals b is positive, while for endotherm ones it is negative. For example, limestone is an endogeneous mineral, pyrite is endotherm.

Table I contains the numerical values of constants B and A for various types of coal. The constants have been calculated for Hungarian Liassic, Eocene, Cretaceous and Miocene coals, as well as for lignites at average moisture contents. Average moisture contents are, in the above sequence, 8; 16; 22; 26 and 46 percent. As Eq. (5) indicates, calorific value of coal is a linear function of the ash content at constant moisture content.

Table I. Function constants of various coal types at average moisture contents

Parameters	Coal types				
	Liassic	Eocene	Cretaceous	Miocene	Lignite
Average moisture content m, %	8	16	22	26	46
Function constants					
B, kJ/kg	31,663	24,244	23,672	19,386	12,325
A, kJ/0.01 kg	381	335	430	282	260
Correlation coefficient r	0.999	0.991	0.993	0.996	0.996

B and A are the parameters of the straight lines. The last row of Table I displays the correlation coefficients indicating the closeness of this linear connection between the calorific value and ash content. The value of the correlation coefficient exceeds 0.99 for all types of coal which indicates a functional connection. - Linear connection between calorific value and ash content is regarded as a functional one both in Hungarian and foreign technical literature without exception.

Since constants in Eqs (6) and (7) can analytically be determined and the average moisture contents of the various coal basins are known, C_o and b can be determined from the two equations:

$$C_o = \frac{B + 24.62\ m}{1 + \frac{m}{100}} \tag{8}$$

and

$$b = A - \frac{C_o}{100} \ . \tag{9}$$

Equation (5) can also be rearranged as follows:

$$C = C_o - \left(\frac{C_o}{100} + b \right) a - \left(\frac{C_o}{100} + 24.62 \right) m \ . \tag{10}$$

In Eq. (10) a and m are variables, their coefficients being constant for each type of coal. The coefficient of moisture content, i.e.

$$D = \frac{C_o}{100} + 24.62 \tag{11}$$

gives the change of calorific value due to a one-percent change of moisture content at constant ash content. Taking account of Eqs (7) and (11), Eq. (10) can be simplified as

$$C = C_o - Aa - Dm \ . \tag{12}$$

It can be seen that the calorific value is a linear

function of ash and moisture contents. The coefficients in Eq. (12), which are constant for the same type of coal, give the change of calorific value due to one-percent changes in the ash and moisture contents.

2. ANALYSIS OF QUALITY PARAMETERS DETERMINING CALORIFIC VALUE OF HUNGARIAN COAL TYPES

Table II displays for the various coal types the numerical values of C_o calculated by Eq. (8) and b according to Eq. (9), as well as b/24.62 i.e. the ratio of the heat of burning to the heat of evaporation and, finally, constants A and B, their differences and their ratios.

Table II. Parameters determining the calorific value of Hungarian coals

Parameters	Coal types				
	Liassic	Eocene	Cretaceous	Miocene	Lignite
C_o, kJ/kg	34,630	29,331	31,043	27,062	24,921
b, kJ/0.01 kg	35	42	120	11	11
b/24.62	1.4	1.7	4.9	0.45	0.45
A, kJ/0.01 kg	381	335	430	282	260
D, kJ/0.01 kg	371	318	335	295	274
A-D	10	17	95	-13	-14
A/D	1.027	1.053	1.284	0.956	0.949

Using above equations and the numerical values of parameters in both tables, one can determine energy content and components of various coal types and the effect of changes of quality parameters viz. ash and moisture contents on the change of energy content in general form, and, numerically, for Hungarian coal types.

Energy content expressed in terms of calorific value C is a linear function of the calorific value of the combustible pure coal without ash and moisture C_o, ash content a and heat of burning b, as well as moisture content m and heat of evaporation 24.62 kJ/0.01 kg. If the ash content changes, energy content of coal varies as a function of calorific value C_o and heat of burning b - both being different for various coal types. If moisture content changes, energy content changes as a function of different C_o and constant heat of evaporation of the water.

Table II indicates that calorific value of pure combustible coal is maximum for Liassic coals among Hungarian coal types; the further order is Cretaceous, Eocene, Miocene and lignite. C_o of Liassic and Cretaceous coals exceeds 30,000 kJ/kg, the difference between C_o of Liassic coals and that of lignites (34,630-24,921 = 9,709) is almost as high as 10,000 kJ/kg. - Heat of burning b is positive for all Hungarian coal types, thus ash producing minerals and rocks are endotherm. There are, however, very great differences between the heat of burning of ash producing minerals and rocks of various types of coal. Heat of burning is the greatest for Cretaceous coal types with 120 kJ/kg: this value is 4.9-fold of the heat of evaporation. For Eocene coals, heat of burning is 1.7 times the heat of evaporation, while that of Liassic coal types is 1.4-fold of the heat of evaporation. Miocene coals and lignites have, however, a heat of burning less than the heat of evaporation: it is for both types only 0.45 times the heat of evaporation.

Since heat absorption caused by one mass percent of ash content is directly proportional to C_o and b, constant A with 430 kJ/0.01 kg is maximum for Cretaceous coals. For Liassic coals this constant is by 50 kJ/0.01 kg less while for Eocene and Miocene ones by 100 and 150 kJ/0.01 kg. Lignites have the smallest constant A: 260 kJ/0.01 kg. - Heat absorption caused by one mass percent of moisture content is proportional to C_o which is different for various types of coal, and to the constant heat of evaporation; therefore the order of constans D coincides with that of the values of C_o. This constant is

maximum for Liassic coals with 371 kJ/0.01 kg and minimum for lignites with 274 kJ/0.01 kg, the difference being almost 100 kJ/0.01 kg. - The data of Table II indicate that for Cretaceous, Eocene and Liassic coals constant A of ash content is greater while for Miocene coals and lignites coefficient D of moisture content exceeds the other one. From our findings the conclusion can be drawn that for Cretaceous, Eocene and Liassic coals the reduction of ash content, while for Miocene coals and lignites the reduction of moisture content is more efficient in increasing energy content - assuming a separation without heat loss. Difference and ratio of the two constants are especially great for Cretaceous coals: 95 kJ/0.01 kg and 1.284. Therefore, reduction of ash content of Cretaceous coals can be expected to produce a more significant increase of energy content, if compared with other Hungarian coal types.

3. FURTHER ASPECTS OF ANALYSIS

The results achieved so far show that the Hungarian coal types differ not only in their ash and moisture contents but also in the calorific value of pure combustible coal and the heat of burning of the ash producing minerals. Numerical values published by the paper are averages of coal types selected by the authors. Quality parameters of single mines or layers may strongly differ from these averages.

To most effectively utilize coal types in Hungary, it seems necessary to investigate the rate of increase of calorific value to be achieved by reducing moisture and ash contents. The results obtained so far enable us to determine the rate of increase of the calorific value due to the reduction of moisture content. To be able to calculate the increase of calorific value due to the reduction of ash content, one has to determine the coefficient g for each type of coal, rock and mineral. To carry out this determination, well organized laboratory analysis is required.

REFERENCES

Pethő Sz 1981: Comminution and classification I. Tankönyvkiadó, Budapest (in Hungarian)

Pethő Sz, Nagy Z, Schultz Gy, Tompos E 1972: Laboratory analyses in mineral dressing. Tankönyvkiadó, Budapest (in Hungarian)

Tarján G 1974: Mineral dressing I. Tankönyvkiadó, Budapest (in Hungarian)

Acta Geod. Geoph. Mont. Hung., Vol. 24 (1-2), pp. 87-98 (1989)

NUMERICAL EXAMINATION OF LAWS OF MOTION OF A BODY MOVING VERTICALLY IN A STATIONARY MEDIUM

Sz Pethő[1], Z Szarka[2], M Ács[3]

[1]Technical University for Heavy Industry, Mineral Dressing Department, H-3515 Miskolc, Hungary

[2]Technical University for Heavy Industry, Mathematical Institute, H-3515 Miskolc, Hungary

[3]Technical University for Heavy Industry, Faculty of Mechanical Engineering, H-3515 Miskolc, Hungary

[Manuscript received March 13, 1986]

Considering the grain motions occurring during the processes of mineral dressing, only those of downwards direction have been studied so far. A common feature of the examinations performed so far is that the phoronomic functions describing the laws of motion are determined by analytical methods, they are of a closed form but are only valid on the concerning range of the Reynolds number.

If a grain is thrown up with a fairly high velocity, its motion is first turbulent, then laminar finally sometimes turbulent again. Thus the Reynolds number decreases from a very high value (e.g. from 200000) to almost zero then it starts to rise again. If the values of the resistance of the medium are given on this whole range, the solution of the differential equation describing the motion is valid along the full range of velocity. However, this solution can only be found with numeric methods.

By means of a programme for a Commodore-64 computer, the differential equation of the velocity can be solved with several numerical methods and the acceleration and the path of the grain are also obtained.

Keywords: grain motion vertically upwards; mineral dressing; resistance of the medium; Reynolds number

1. DIFFERENTIAL EQUATION OF VERTICAL MOVEMENT

The movement of a body of m mass thrown off vertically with an initial velocity v_0 in a medium at rest can be described with the differential equation (Finkey 1924)

$$m \frac{dv}{dt} = mg_0 + F \qquad (1)$$

v is the velocity of the body, t time, g_0 acceleration of the body in the medium and F the force resulting from the

resistance of medium.

If the density of the body (grain) is γ, and the density of the medium ϱ,

$$g_o = g \frac{\gamma - \varrho}{\gamma} , \tag{2}$$

where g is the gravitational acceleration. Acceleration g_o has been proposed by Pethő and Szarka (1985) to be called Finkey's number. mg_o is the weight force in the medium.

If the moving grain is spherical and its diameter is d, the force F resulting from the resistance of medium acting against the movement is:

$$F = -c \frac{d^2 \pi \varrho}{4} \frac{v^2}{2} \operatorname{sgn} v . \tag{3}$$

Here c is the factor of resistance of the medium (Pethő and Szarka 1985). The downwards direction of the force of gravity, is selected to be positive (Finkey 1924, Tarján 1954, Fejes and Tarján 1973).

As the force resulting from the resistance of the medium is described by the sign function vertical movements of both directions can be discussed. The density of grain can be higher or lower than the density of the medium but it can also be equal to it.

The resistance factor of the medium of convex bodies bordered by smooth, arched surfaces is only a function of Reynolds number:

$$c = c\,(Re) , \tag{4}$$

and Re, Reynolds number is

$$Re = \frac{\varrho d}{\eta} |v| , \tag{5}$$

where η is the dynamic viscosity of the medium.

The solution of differential equation (1) fulfilling the initial condition of $v(0) = v_o$ provides the velocity of the grain thrown away vertically with starting velocity v_o in the

function of time. According to the above selection, the velocity of a grain going vertically upwards is negative, that of a grain going downwards is positive. The first derivative of the velocity function gives the acceleration, its first integral provides the path of the grain, also in function of time.

So far an analytical solution of differential equation (1) was looked for with classical methods. Due to the nature of the empirical function $c = c(Re)$, however, the possibility of finding an analytical solution is excluded which can characterize the motion with both high and low velocities. Therefore it has been a practice so far that function $c = c(Re)$ has been approximated in some parts of its range by a function of relatively easy handling which has allowed the analytical solution of differential equation (1). For certain theoretical studies this method is used at present as well. The following three approximations are generally used:

In Stokes' laminar range of flow

$$c = \frac{24}{Re} , \qquad 0 < Re \leq 1 , \tag{6}$$

in the transitional section examined by Allen

$$c = \frac{10}{\sqrt{Re}} , \qquad 30 \leq Re \leq 300 , \tag{7}$$

while in Newton's turbulent flow range:

$$c = 0.43 , \qquad 600 \leq Re \leq 200000 . \tag{8}$$

By using these approximations, the force resulting from the resistance of medium is

$$F = -\beta |v|^{\alpha} \operatorname{sgn} v , \tag{9}$$

where the value of α according to the different ranges of flow are, successively 1, 1.5, 2, while the values of β are:

$$3\pi\eta d; \qquad 1.25\pi(\eta\varrho)^{1/2} d^{3/2}; \qquad 0.5375\pi\varrho d^2 .$$

On the basis fo Eq. (5), a range of velocity corresponds to each flow range which depends on the density and viscosity of the medium as well as on the grain size. Thus, the range of velocity corresponding to range $0 < Re \leqq 1$ can be e.g. very large if the diameter of the grain is very small. So it may happen that the flow, even in case of a relatively high velocity, remains still laminar or with a very low velocity it may become turbulent.

By using approximations of Eqs (6), (7) and (8), the solution of differential equation (1) is well applicable in the proper ranges of velocity. However, during its motion, a grain can pass all three ranges, therefore different solutions are necessary to describe its motion according to the different ranges of velocity. It would be necessary to connect these solutions at the boundary of the ranges with a smooth transition in order that the motion be characterized acceptably. This is not possible, because with approximations (6), (7) and (8), even the ranges themselves do not join each other. But even if these ranges are extended to meet each other, a smooth connection is not possible.

In addition to these approximations, a very large number of empirical functions is known from the technical literature and the ranges of the Reynolds number which they approximate (Tarján 1954, Fejes and Tarján 1973, Schubert 1975) are wider than the previous ones. But not even with these can a smooth transition be ensured on the boundary of the ranges.

So it is hopeless to approach $c = c(Re)$ by a function in such a way that it should approximate in the range $0 < Re \leqq \leqq 200000$ occurring in the practice of mineral dressing and at the same time, it should allow an analytical solution of the differential equation.

2. NUMERICAL DETERMINATION OF THE ACCELERATION, VELOCITY AND PATH

Now a numerical solution of differential equation (1) seems to be obvious. When using these methods, function $c = c(Re)$ can

be of any shape only the actual value of c should be computable or it should be provided in a tabular form.

There are several methods for the computerized numerical solution of differential equations. Typical of those to be applied here is that starting from value v_o given at time $t = 0$, the value of the velocity is calculated at Δt ($\Delta t > 0$); when this is known, advancing further with a step Δt at time $2\,\Delta t$ then at $3\,\Delta t$, etc. Let v_1, v_2, v_3, ... indicate the velocity values obtained in this way.

The numerical solution of differential equation (1) was carried out by three simple methods which, however, meet the demands of practice: by the Euler, second-order Runge-Kutta and P1-C1 predictor-corrector methods (Ralston 1969). For the computer-type solution to be described here, any of these can be used and thus the results can be compared too.

Simultaneously with the point-by-point calculation of velocity, the acceleration

$$a = \frac{dv}{dt} = g_o + \frac{1}{m} F \tag{10}$$

to be obtained from Eq. (1) has also been calculated at the previous times $K\Delta t$ ($k = 0; 1; 2; 3; \ldots$).

The path of the grain has been calculated by using the integral

$$s = s(t) \int_o^t v(T)\, dT \tag{11}$$

with the approximation

$$s_{k+1} = s\left((k+1)\,\Delta t\right) = s\,(k\,\Delta t) + \frac{1}{2}\,(v_{k+1} + v_k) \tag{12}$$

as $s(0) = 0$.

For the solution the function $c = c(Re)$ or its acceptable approximation should be given. From the large number of relations in the literature, the approximate function

$$c = \frac{24}{Re} + \frac{4.565}{3\sqrt{Re}} - \frac{0.491}{\sqrt{Re}} (1 - \text{th } 0.00025\ Re) + \\ + 0.42\text{th } 0.00025\ Re + 0.02\text{th } 0.00001\ Re \qquad (13)$$

has been selected which, in accordance with experience shows a good approximation in the range

$$0 < Re = 200000$$

(Idelchik 1975) as verified with test calculations. It is as suitable for computers as any formally simpler function.

The process of the solution is as follows:

1. For the initial value v_0 the value of Re is calculated by means of Eq. (5).
2. From Re, on the basis of Eq. (13), the value of c is calculated.
3. From c and $v = v_0$, the force F resulting from the resistance of the medium is calculated with Eq. (3).
4. By means of Eq. (10), acceleration a_0 is calculated.
5. By using differential equation (1), the value of v_1 is calculated.
6. With Eq. (12), the path s_1 is calculated.

After that, the previous six-step cycle is repeated so that v_1 is used for the calculation instead of v_0. Thus the values of a_1, v_2 and s_2 are obtained. The calculation is repeated with v_2. After the k^{th} repetition, values a_k, v_{k+1} and s_{k+1} will be obtained.

So this method of solution calculates, at time intervals Δt, the Reynolds number belonging to the relevant velocity, i.e. it eliminates the inflexibility of the analytic methods that the solutions cannot be smoothly connected at the boundary of the ranges. The numerical solution obtained in this way can be used on the whole range of velocity as the calculation of all the values of velocity is performed with the corresponding Reynolds number.

3. THE COMPUTER PROGRAM

The calculations have been performed by means of a programme written for a Commodore-64 type computer (Ács 1985).

The programme is constructed so that for the approximation of function $c = c(Re)$, any of the functions of Eqs (6), (7), (8) or (13) can be applied. All the alternatives of the calculation are performed so it is possible to compare the results.

The computer displays the velocity, the acceleration and the path vs. time on the screen, plots these diagrams with dotted line on paper, writes the function values on paper or on the screen in a tabular form. It stores the results which can be displayed, plotted and written again.

The input data are as follows:

- density (ϱ) and dynamical viscosity (η) of the medium;
- diameter (d) and density (γ) of the grain;
- initial velocity (v_0);
- length and number of the step intervals (max. 320).

Within reasonable limits, the data should be given in SI dimensions. For instance, the density of the medium must not be negative and higher than 10000 kg/m^3, similarly, the density of grain must not be negative and exceed 20000 kg/m^3, etc.

The time required for a problem is 2-5 minutes. During this time, the computer calculates in 80-100 points the velocity, acceleration and path and displays the diagrammes of these on screen. In few additional minutes, it writes the results on paper tabularly and plots the diagrammes.

In case of 320 points, the plotted diagrammes appear practically as a continuous line. Even before the solution of differential equation (1), approximations Eqs (6), (7) and (8) enable the determination of the final falling velocity v_m. That is, in fact, necessary while searching for an analytical solution since after the proper modification of the differential equation, one of its parameters is just v_m. Approximation (13) or the tabular presentation of function $c = c(Re)$ would not allow this. But for the numerical solution, this is not required. In spite of that, the falling final velocity can be determined

since, during the progress of calculation, the velocity becomes constant in a short time. This constant velocity is the final falling velocity which gets soon visible on the screen. It is practicable to choose the step interval Δt and the number of the step intervals n so that the velocity be practically constant even before the nth step. After that, it is not worth continuing the calculation. If the number of steps was not selected well, it is to be changed immediately after the interpretation on screen of the acceleration and velocity and the programme be run again.

The programme is highly flexible in the sense that data can be changed by pushing a button and thus the different alternatives can be run within minutes and the results can be compared immediately. Besides, that part of the programme that solves the differential equation can be replaced by a sub-program of higher accuracy.

Interpretation of the results is facilitated by clear arrangement, the proper readability of the written characters, insertion of explanatory or supplementary words (texts) and, last but not least, the pleasant, restful colour composition of the VDU screen.

4. A NUMERICAL EXAMPLE

For a demonstration a numerical example is given hereby. A grain of a diameter of $d = 0.05$ m and a density of $\gamma = 7500$ kg/m^3 is thrown up with a velocity of $v_0 = -2$ m/s. Density of the medium is $\varrho = 1000$ kg/m^3, viscosity is $\eta = 0.001$ kg/ms. Values of the velocity, acceleration and path have been calculated in 85 points in steps of $\Delta t = 0.012$ s.

Table I includes results where factor c of resistance of the medium has been regarded for by relation (13). The 1st column of the table indicates the serial number of the points, columns 2, 3 and 4 contain the values of path, velocity and acceleration. The calculation has been made with the P1-C1 method.

The results of Table II have also been calculated with the

Table I. Values of the path velocity and acceleration if c is from Eq. (13)

No.	s [m]	v [m/s]	a [m/s^2]
1	0.000000	-2.000000	12.022000
2	-0.023152	-1.858616	11.541920
3	-0.044639	-1.722684	11.113522
4	-0.064525	-1.591615	10.731249
⋮			
17	-0.195600	-0.144488	8.519644
18	-0.196721	-0.042350	8.503404
19	-0.196617	0.059666	8.499240
20	-0.195289	0.161540	8.479735
⋮			
35	-0.036206	1.542464	6.408308
36	-0.017242	1.618102	6.197937
37	0.002613	1.691200	5.985062
38	0.023331	1.761735	5.770737
⋮			
54	0.447596	2.560070	2.734516
55	0.478508	2.592015	2.589682
⋮			
82	1.404410	3.014106	0.507344
83	1.440615	3.020007	0.476013
84	1.476888	3.025542	0.446563
85	1.513226	3.030735	0.418888

P1-C1 method assuming that c = 0.43 that is, by Newton's law of resistance of the medium.

Results contained in Table III are also the values of path, velocity and acceleration valid if c = 0.43 but they have been calculated by phoronomical functions (Pethő and Szarka 1985) resulting from the analytical solution of differential equation (1).

Table II. Values of the path velocity and acceleration if c = 0.43

No.	s [m]	v [m/s]	a [m/s^2]
1	0.000000	-2.000000	11.942000
2	-0.023157	-1.859494	11.475638
3	-0.044660	-1.724287	11.058921
4	-0.064568	-1.593813	10.686607
⋮			
17	-0.196224	-0.148627	8.520997
18	-0.197395	-0.046478	8.503858
19	-0.197340	0.055541	8.499347
20	-0.196063	0.157421	8.480688
⋮			
35	-0.037491	1.542360	6.456167
36	-0.018525	1.618591	6.248940
37	0.001341	1.692319	6.039009
38	0.022076	1.763517	5.827406
⋮			
54	0.447882	2.574650	2.801214
55	0.478974	2.607389	2.655311
⋮			
82	1.412594	3.044109	0.532722
83	1.449161	3.050307	0.500237
84	1.485799	3.056127	0.469675
85	1.522506	3.061591	0.440929

So the results of Tables II and III can be compared. They are in a surprisingly good accordance. In Table III the values have been calculated in 100 points instead of 85. Thus a comparison is available for the degree of approximation of the theoretical $v_m = 3.1443$ m/s falling final velocity and for the degree of approximation possible by increasing the number

Table III. Values of the path, velocity and acceleration calculated by means of phoronomic functions if c = 0.43

No.	s [m]	v [m/s]	a [m/s^2]
1	0.000000	-2.000000	11.942000
2	-0.023152	-1.859546	11.475803
3	-0.044650	-1.724382	11.059206
4	-0.064556	-1.593947	10.686975
⋮			
17	-0.196230	-0.149030	8.521101
18	-0.197406	-0.046898	8.503892
19	-0.197356	0.055135	8.504614
20	-0.196083	0.157023	8.480796
⋮			
35	-0.037535	1.542203	6.456585
36	-0.018568	1.618442	6.249356
37	0.001298	1.692176	6.039424
38	0.022034	1.763381	5.827819
⋮			
54	0.447854	2.574536	2.801717
55	0.478947	2.607275	2.655819
⋮			
82	1.412561	3.044039	0.533091
83	1.449127	3.050239	0.500595
84	1.485765	3.056061	0.470023
85	1.522471	3.061527	0.441265
⋮			
99	2.041536	3.110615	0.180703
100	2.078876	3.112715	0.169462

of points.

It is worth mentioning that the results of Tables I and II

show a fairly good accordance, too.

REFERENCES

Ács M 1985: Numerical analysis of laws of motion taking place in mineral dressing equipments with Commodore-64 type computer. Paper made by scientific group of undergraduates. Technical University for Heavy Industry, Mineral Dressing Department, Miskolc

Fejes G, Tarján G 1973: Machines and operations in the chemical industry. Takönyvkiadó, Budapest

Finkey J 1924: Die wissenschaftlichen Grundlagen der nassen Erzaufbereitung. Verlag von Julius Springer, Berlin

Idelʹtchik I E 1975: Po gidravlitcheskim soprotivleniam. Mashinostroenie, Moscow

Pethő Sz 1982: Bányászati és Kohászati Lapok, Bányászat, 115, 472-473.

Pethő Sz, Szarka Z 1985: Építőanyag, 37, 376-384.

Ralston A 1969: Introduction into the numerical analysis. Műszaki Könyvkiadó, Budapest

Schubert H 1975: Aufbereitung fester mineralischer Rohstoffe. VEB Deutscher Verlag für Grundstoff-Industrie, Leipzig

Tarján G 1954: Mineral dressing. Tankönyvkiadó, Budapest

Acta Geod. Geoph. Mont. Hung., Vol. 24 (1-2), pp. 99-114 (1989)

ESTIMATE OF GAS RESERVE WITH THE MONTE-CARLO METHOD

R Drágossy[1], M Kristóf[2], B Mating[1], J Tóth[3], T Miklós[2]

[1]Department of Petroleum Recovery, Technical University for Heavy Industry, H-3515 Miskolc, Egyetemváros, Hungary

[2]Petroleum and Natural Gas Production Company Nagyalföld, H-5001 Szolnok, POB 86, Hungary

[3]Mining Chemical Research Laboratory of the Hungarian Academy of Sciences, H-3515 Miskolc, Egyetemváros, POB 2, Hungary

[Manuscript received April 11, 1988]

In the estimation of hydrocarbon reserves, the degree of uncertainty is the function of the quantity and accuracy of the data available. Utilizing an actual Hungarian example and applying the probability curve of the reserve determined by the Monte-Carlo method, the authors analyse the effect of the parameters serving as bases of reserve determination to define the efficiency of the reserve estimates.

Keywords: gas reserve estimation; geological reserve field; Monte-Carlo method; Sarkadkeresztur hydrocarbon

SYMBOLS

G	Geological gas reserve
G_p	Reserve recovered up to pressure P
B_g	Seam volumetric factor of the gas
B_{gi}	The initial gas seam volumetric factor
B_w	The seam volumetric factor of the water
W_e	Degree of water intrusion
W_p	The amount of water produced with the gas up to pressure P
z	The deviation factor of the gas
z_i	The initial deviation factor of the gas
T	Temperature
T_n	Temperature of the normal condition (15.6°)
p_i	The initial formation pressure of the seam studied
P_n	Normal pressure (1.013 bar)
AME	material balance equation

INTRODUCTION

The national economic demand on the rational exploitation of hydrocarbons (petroleum and natural gas) in order to bring the seams into production as soon as possible, has made it

unavoidable to connect the exploration and exploitation phases. One of the features is that the different reserve calculation methods should be applied in an early state of the development in order to ensure that the working project should be better founded. In the experience gained during the recent years considerable differences can be observed between the data of the different volumetric statistical (output decrease) and material balance estimates.

The above mentioned differences make the comparative examination of the reserve calculation parameters and methods necessary, with special regard to the fractured, double porosity metamorphic reservoirs. The well known reserve calculation methods are methodically simple. The difference in views, the effect of the "personal ego" which affect the calculation or reserves are natural and necessary as the results of calculations are expected to be provided by the reservoir engineer when hardly more than the data of some wells are available. Considering that the observations of a reservoir engineer obtained from the first wells of a newly discovered hydrocarbon field should be interpreted after extrapolation for the whole reservoir, it is clear that the volume of the "dreamt" reserve can only be categorized into the following groups: "certain", "probable" and "possible". With regard to a particular seam, the quantity of the reserves considered as "certain", "probable" and "possible" naturally cannot be unequivocally formulated the following considerations may be, however, of help in the categorization:

a) Only observations and measurements connected to the test wells are taken as a basis of the evaluation of the probable and possible reserves.
b) The parameters are taken into account with their average and reliability depending on the distance from the borehole and method of determination (laboratory-geophysics).

Individual reserve calculation data contain a large number of subjective value judgement. These deviations from the reality are ancient problems of natural science. The question was asked a long time ago: "how is it possible to equalize the unavoidable

errors of measurements, observations so that the most probable values be obtained?" A possible answer to the question is given by the method of the mathematical statistics. It should only be mentioned in brief that the basic idea comes from Jacob Bernouilli-, Pascal applied it in practice in case of games. Its further development is found in Gauss's mathematical studies, his best known formulations are the "Gaussian curve" and the "normal curve of error frequency". The above methods which describe the future behaviour of a given system can be applied when the system does not allow an accurate observation of the measurable changes. It is also the above mentioned difficulties which occur during the estimation of hydrocarbon reserves. In the present study, the determination of the most probable value of the hydrocarbon reserve of the Sarkadkeresztur field is described with a method which takes into consideration the probable value of the different parameters and the mistakes possible in the reserve estimation resulting from the error made.

The exploration of the hydrocarbon field discovered in the region of Sarkadkeresztur started in 1976. The reconnaissance survey report made on the basis of the results of exploration determined a C_2 category cap- and dissolved gas reserve of 10.2 billion m^3. The field is located at the Roumanian-Hungarian boundary striking in East-West direction, it is 11 km long, 2 km wide. The etage height of the seam is 360 m. Its regional location and geological section and profile are shown in Figs 1 and 2.

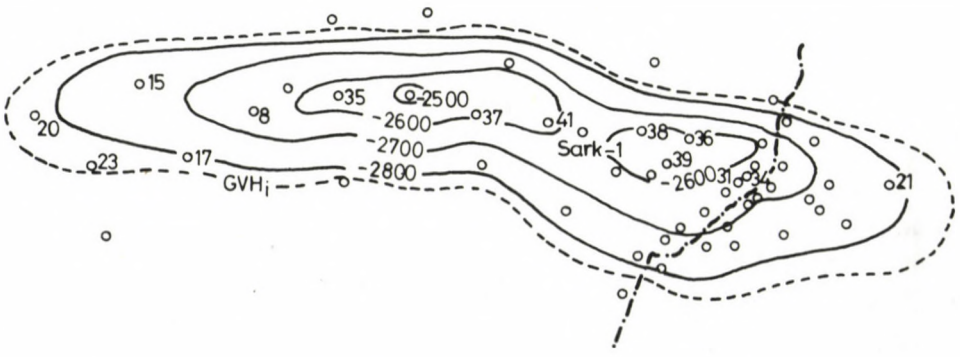

Fig. 1. Structural map on top of the Sarkadkeresztur seam

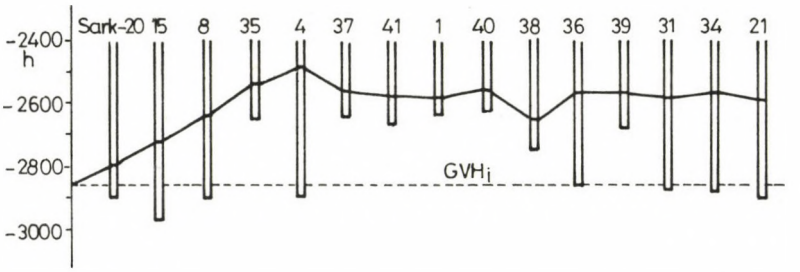

Fig. 2. Sarkadkeresztur - Outlined geological profile

1. DETERMINATION OF THE GEOLOGICAL RESERVE

There are three periods of estimate during the lifetime of a hydrocarbon field. Figure 3 shows the reserve determination methods applicable in the lifetime of an assumed field and the tendency of their probable errors during the life of the field. In the first stage of development, geological-geophysical profiles and sections, countour maps and data obtained from core analysis are available for the volumetric estimate. In the subsequent period of estimate a continuously increasing number of production parameters is available which allow a more and more accurate reserve determination as the numbers of the data increase. In the final state of the life of the field, for the determination of the industrial reserve, statistical processing of the production data can be of decisive importance.

Irrespective of the method of reserve determination, it is evident that each of the basic data has errors to some degree. The effect of uncertainty of the basic parameter on the reserve determination can be expressed with a so-called "reserve probability curve" (Mayer-Gürr 1976) (Fig. 4).

The probability curve can be determined with the Monte-Carlo method.

2. APPLICATION OF THE MONTE-CARLO METHOD

The reliability of the individual data utilized for the

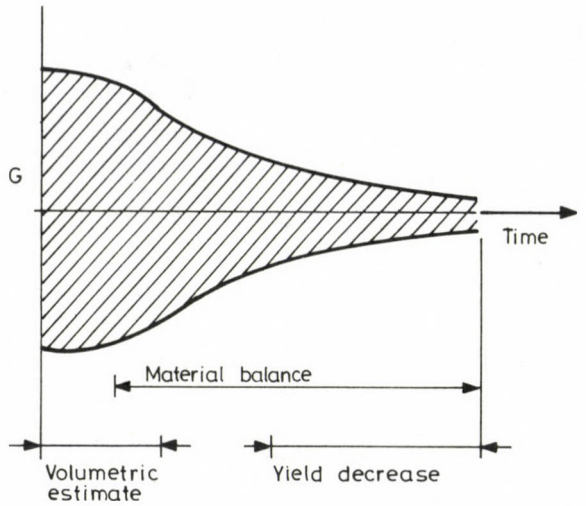

Fig. 3.

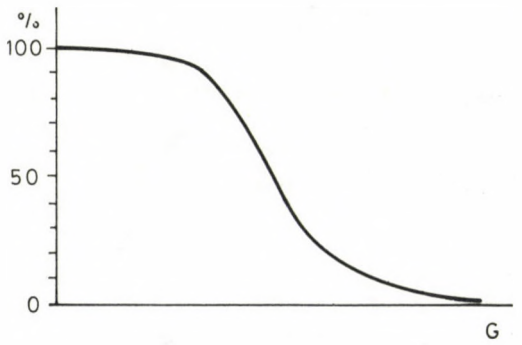

Fig. 4.

determination of hydrocarbon reserves can only be expressed with its distribution around an expected value. The more uncertain a basic data is, the "smoother" is the distribution curve which characterizes it. The distribution of the different data (porosity, average pressure,seam-volumetric factor), their most probable minimum and maximum values can be estimated by the reservoir engineering practice or, in certain cases, in possession of the required number of data they can be determined.

The joint study of all the parameters which affect the reserve can be performed by the Monte-Carlo method. The basis of the method is to simulate by means of a computer the error made in the determination of the parameters and the "erroneous" data are used for the reserve determination. If the method is repeated several times a great number of the values concerning the reserve will be obtained; their distribution depends on the type of the distribution of the basic parameters as well as on the relations applied.

Walstrom and Mueller (1967) recommend the application of the uniform - and triangular - distribution in order to solve the reservoir-engineering problems with the Monte-Carlo method if the nature of the actual distribution is unknown. For the generation of the random numbers of uniform distribution computers have built-in function and generate R_i random number in the range between 0 - 1.

By denoting the value range of any of the parameters with X_{min}, X_{max}, the expected value with X_{aver}, the triangular distribution for the given value range can be obtained from the uniform distribution between 0-1 with the following functions:

$$X_i = (2R_i-1)\,(X_{aver}-X_{min}) + X_{aver}, \qquad \text{if } R_i > 0.5$$

and (1)

$$X_i = (1 - 2(1-R_i))\,(X_{max}-X_{aver}) + X_{aver}, \quad \text{if } R_i < 0.5 \ .$$

The reserve probability curve can be obtained by arranging according to their magnitude the reserve-values obtained and by their subsequent illustration. The smoother the curve obtained is, the more uncertain is the value of the reserve, in a theoretical limit case - in case of a certain reserve - the probability curve would be a vertical straight line. In case of a symmetrical distribution, the estimated value of the geological reserve of the field can be read off directly with the 50 % probability, in case of an asymmetrical distribution the estimated value should be determined as an integrated average. The integrated average can be approximated with a sufficient accuracy as the arithmetical average of the values belonging to

the 10, 30, 50, 70 and 90 percent probabilities, that is

$$G_{estimated} = \frac{G_{10} + G_{30} + G_{50} + G_{70} + G_{90}}{5} \qquad (2)$$

3. BASIC DATA

The range of the basic data available for the reserve estimate is continuously expanded during exploration and development. After the delimitating boreholes have been drilled, the geological-geophysical data as well as the observation concerning the possible gas-water boundary allows the determination of the rock volume containing the geological reserve. Since the position of the overburden is known with a sufficient reliability, the accuracy of the rock volume is in case of seams with water phase the function of the accuracy of the gas-water boundary.

In case of the field Sarkadkeresztur, the initial gas-water boundary was found in 2846 m, the rock volume belonging to it is 2.077×10^6 m^3. An error of ± 2 m in the gas-water boundary position results in a rock volume error of ± 1.3 percent on the basis of the rock volume-depth curve of the field.

The determination of porosity is made on the basis of laboratory and geophysical data. Before September 1979 laboratory tests were performed on 35 core samples, the values measured ranged from 0.78 to 8.3 percent with an arithmetical mean of 1.9 percent.

On the basis of the interpretation of well-logging results, the weighted average value of the porosity is 5.11 percent.

The value of water saturation ranges on the basis of laboratory measurements from 22.9 to 93.4 percent, on the average 68.2 percent - while the weighted average on the basis of the well-logging measurements is 50 percent.

The determination of the initial formation pressure was performed on the basis of the measurements by NKFV (Petroleum and Natural Gas Production Company Nagyalföld) and by OGIL (Research Laboratory for Oil and Gas Industry). The lowest value measured was 305.8 bar, the largest one 324.0 bar. The

measured values taken into consideration for the determination of the average pressure range from 321.0 to 324.2 bar (the average value was 322.2 bar at 2846 m).

Due to the great etage height, the value of the formation temperature varies, the average value is 152°C.

37 well-flow composition data as well as the production data allowed the determination of the initial composition and the moisture content. The processing showed that the composition resulting from the formation measurement and the moisture content differ from the data determined on the basis of production accepted value of the average composition results from exploitation data.

With regard to the different basic data of formation pressure, formation temperature and composition, the initial seam volume factor B_{gi} ranges between 0.004666 m^3/m^3 and 0.004718 m^3/m^3 what means an error of $\pm$0.5 % percent being negligible.

During production from the field the following values are available in addition to the data utilized for the initial reserve estimate: monthly produced gas quantity, formation pressure measured annually, data of water saturation measured periodically.

4. CHANGE OF THE PROBABILITY CURVE ON THE BASIS OF VOLUMETRIC RESERVE ESTIMATE

For the volumetric reserve estimate of the Sarkadkeresztur field, the following data have been applied:

rock volume: $2.077 \cdot 10^6$ m^3 $\pm$1.3 percent

porosity: laboratory: 0.78 percent - 1.9 percent - 8.31 percent

geophysics: 0.78 percent - 5.11 percent - 8.31 percent

water saturation: laboratory: 22.9 percent - 68.2 percent - - 93.4 percent

geophysics: 22.9 percent - 50 percent - - 93.4 percent

initial seam-volumetric factor: 0.004666 m^3/m^3 - - 0.004718 m^3/m^3.

The limiting values of the porosity and water saturation measured in laboratory were taken into account together with extreme values of the geophysical data. An error of uniform distribution has been attributed to the initial seam-volumetric factor, while the error of other parameters was supposed to be of triangular distribution. The reserve probability curve has been determined on the basis of 2500-2500 calculations each using on the one hand the geophysical, on the other hand the laboratory data applying in both cases the same error to the rock-volumetric and the seam-volumetric factors. The reserve probability curve thus obtained is shown in Fig. 5.

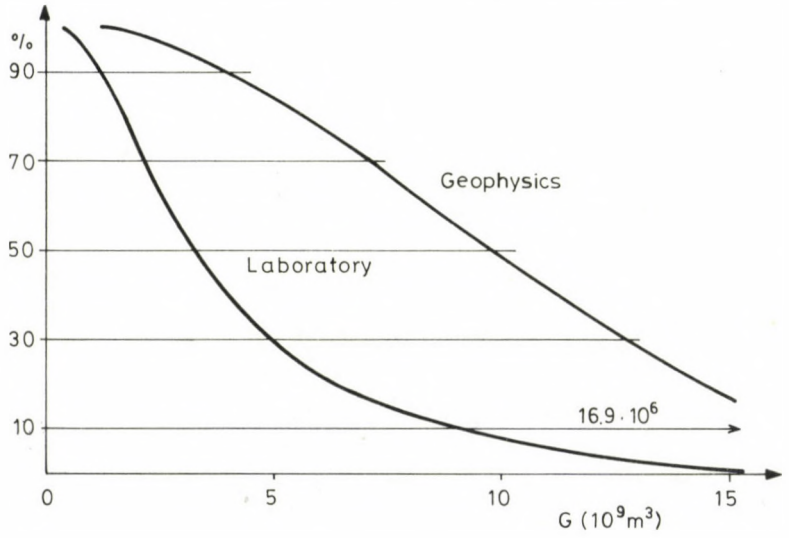

Fig. 5.

There is a considerable difference between the falling edges of the two curves if laboratory or geophysical data are applied.

The estimated value of the geological reserve on the basis of the curve from the laboratory data is

4.2×10^9 m^3, while

the same value determined on the basis of geophysical data is

$$10.2 \times 10^9 \ m^3.$$

Thus both curves show a very great reserve uncertainty.

Considering that the bearing rock is weathered and the fracture porosity cannot be determined with laboratory measurements, it is assumed that laboratory basic data result in the underestimation of the actual geological reserve but even this fact cannot justify such a great difference between the laboratory and the geophysical results. The result obtained fits into the hypothesis about the uncertainty of the initial estimate as in Fig. 3.

5. DETERMINATION OF THE GEOLOGICAL RESERVE WITH THE MATERIAL-BALANCE METHOD

The finite form of the material-balance equation referring to the gas field, disregarding the compressibility of the adherent water and the pore-space, can be written in the following, simple form:

$$G_p \cdot B_g + W_p \cdot B_w = G(B_g - B_{gi}) + W_e \cdot B_w \cdot \qquad (3)$$

Substituting the relation for the seam volume factor:

$$B_g = a \frac{z \cdot T}{p}$$

(where $a = \frac{p_n}{T_n}$)

and using the approximation $B_w = 1$, Eq. (3) gets the following form:

$$\frac{p}{z} = \frac{p_i}{z_i} \left(1 - \frac{G_p}{G} + \frac{W_e - W_p}{G \cdot a \cdot T} \cdot \frac{p}{z} \right). \qquad (4)$$

Assuming a closed reservoir the equation in the coordinate system $p/z = f(G_p)$ yields a straight-line the intersection point of which with the horizontal axis provides the initial reserve value.

If the reservoir is not closed, i.e. if there is a water inflow, the geological gas reserve is certainly smaller than the value obtained with the assumption of a closed reservoir.

The Havlena-Odeh form of the material-balance equation serves for a simultaneous determination of the geological reserve and the degree of water inflow, which rearranging Eq. (3) and by the assumption $B_w = 1$ with the properly selected water-body parameters gets the form:

$$\frac{G_p \cdot B_g + W_p}{B_g - B_{gi}} = G + \frac{W_e}{B_g - B_{gi}} \qquad (5)$$

i.e. a straight line.

For the evaluation of the position of mining of the Sarkadkeresztur field performed at the Department of Petroleum Recovery in 1985, Eq. (5) has been applied after rearranging:

$$\frac{G_p \cdot B_g}{B_g - B_{gi}} = G + \frac{W_e - W_p}{B_g - B_{gi}} \qquad (6)$$

which form hints at the following function relation:

$$\frac{G_p \cdot B_g}{B_g - B_{gi}} = f(G_p) \; . \qquad (7)$$

As the second term on the right side of Eq. (6) before starting production equals zero, since then no water could flow into the seam ($W_e = 0$), and water cannot be produced either ($W_p = 0$) therefore if the relation written on the left side of Eq. (7) is extrapolated backwards up to $G_p = 0$, the value of G is obtained as the limit value of Eq. (6).

In the forthcoming, we review the geological reserve values determined for the Sarkadkeresztur field in chronological order, in the function of the time since the development and in that of the produced gas output (Figs 6, 7).

The initial optimistic estimate resulted in a considerable error in the determination of the values of the reserve which

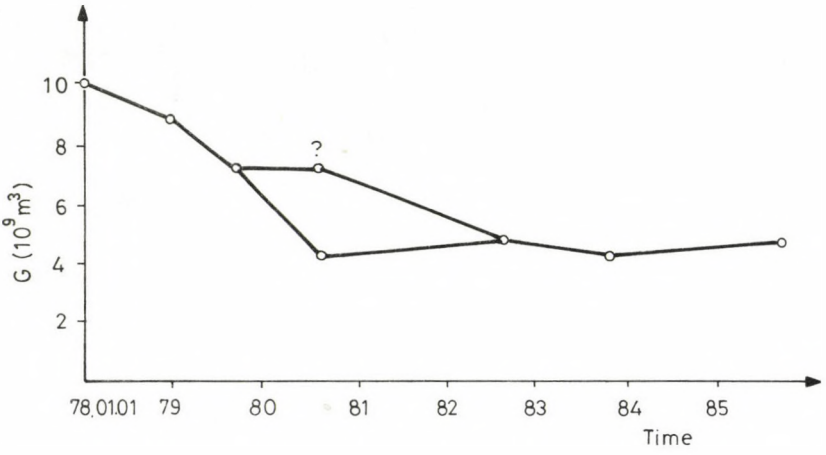

Fig. 6.

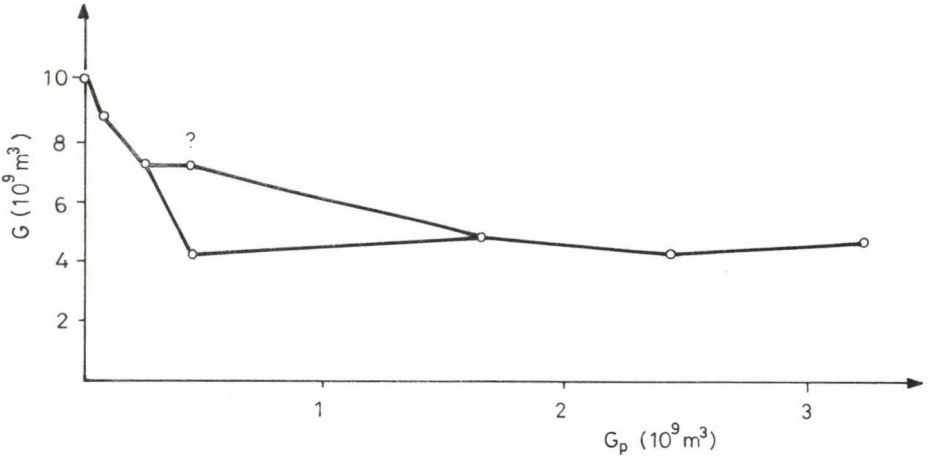

Fig. 7.

is probable on the basis of the present knowledge. Here we refer back to the curves shown in Fig. 5 which have been drawn on the basis of the data known in 1977. On the basis of Figs 6-7, according to the present knowledge, a gas reserve of 4.3-4.9 billion m^3 is possible which compared with the 1977 data proves the assumption that laboratory data resulted in the

underestimation, geophysical data in the overestimation of the actual reserve. Considering the measurements performed on not more than 35 core samples, it is possibly a coincidence, nevertheless it is a fact that the reserve determined by using the laboratory data has much less error than that determined with the geophysical data.

Regarding the methods of material balance reserve determination, it is possible to use the Monte-Carlo simulation within a realistic computer time period for the determination of the geological reserve with the assumption of a closed seam.

As it is obvious on the basis of the production well observation data, this assumption is not true, however, the error in reserve determination can be examined in the function of the errors of formation pressure, produced quantities and the information available.

Omitting from Eq. (4) the W_e term representing water inflow one has:

$$\frac{p}{z} = \frac{p_i}{z_i} \left[1 - \frac{1}{G} \cdot \left(G_p + \frac{W_p}{B_g}\right)\right] .$$

The above form of the equation has been used to study the effect of the error made in the reserve estimate. Using the same 2500 calculations applied for the volumetric estimate, the following alternatives have been examined:

a) The error of the average pressure obtained from the formation pressure measurements is ± 2 bar, the measuring accuracy of the volumes recovered: ± 2 percent.
b) Error of the average pressure is ± 1 bar, the measuring accuracy of the amounts recovered: ± 1 percent.

In both cases we examined the effect of the increasing number of data on the shape of the reserve probability curve, i.e. we determined the curve by using the data of the initial formation pressure and the pressure data of the year

1979, together with the relevant production data,
1979-80, " " "
1979-82, " " "
1979-84, " " "

Table I

Time (year)	Gas output (10^9 m^3)	Calculated reserve (10^9 m^3)	Method of determination
1977	0	10.2 (KV)	volumetric
December 1978	0.073	8.98 (KV)	volumetric
September 1979	0.255	7-7.5 (NKFV)	Material balance We = 0 felt
August 1980	0.468	Reserve modification not justified (SZKFI)	Material balance We 0
		4.3 (NME)	Material balance We 0
September 1982	1.63	4.9 (SZKFI)	Material balance We 0
November 1983	2.43	4.3 (NKFV)	Material balance We
October 1985	3.256	4.9 (NME)	Limit value of AME

KV - Petroleum Company
NKFV - Petroleum and Natural Gas Production Company Nagyalföld
SZKFI - Research and Development Institute for Hydrocarbons
NME - Technical University for Heavy Industry

The results obtained are presented in Figs 8-9.

The initial erroneous but necessary assumption that the seam is closed affected the absolute value of the results but it is suitable for the determination of the tendencies. With the advancement of time and production the uncertainty of the determination radically decreases, at the same time it changes in proportion with the uncertainty of the quantities measured. In Figs 8-9 from the probability curves made by using the 1979 data, the reserve maximum estimated according to Eq. (2) is 5.7 billion m^3 - and since the fact of the water inflow is known, i.e. the actual reserve can only be smaller than that - even from these data it could have been suggested that the reserve estimates at that time were overoptimistic. The shift of the curve referring to later times towards greater reserve is

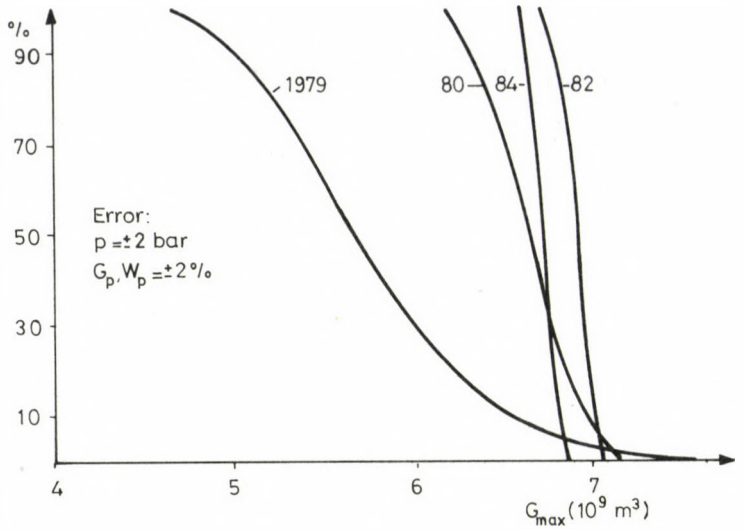

Fig. 8.

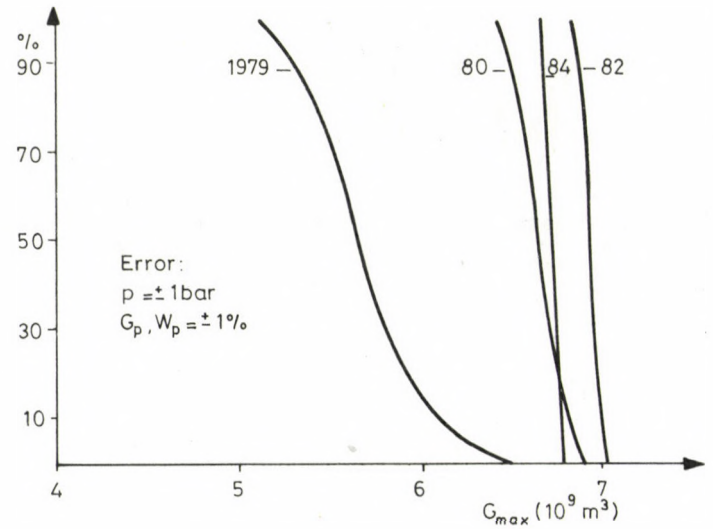

Fig. 9.

due to the increased quantity of the water inflow.

6. SUMMARY

The practice of the estimation of hydrocarbon reserves has proved several times the uncertainty of the initial estimate of the reserve discovered. In the present study we have tried to answer the question to what degree this uncertainty is necessary and unavoidable and whether it can be reduced. By using the Monte-Carlo method for the first time in the domestic practice, we illustrated with the example of the Sarkadkeresztur natural gas field that even in case of careful and precise engineer's work, the uncertainty of the initial estimates is unavoidable, at the same time we proved that by using the probability curve, the degree of uncertainty can be estimated and by using carefully the data available, it can even be reduced.

REFERENCES

Analysis of the test production of Sarkadkeresztur field. NKFV Report, 1979

Estimation of the initial geological reserve and further production possibilities of the Sarkad seam of Sarkadkeresztur field on the basis of the history of production. NKFV Report, 1983

Mayer-Gürr A 1976: Petroleum Engineering. Ferdinand Enke Publishers, Stuttgart

Study of the present operation conditions of the Sarkadkeresztur gas field, a more accurate forecast of production. NME Report, 1985

Walstrom and Mueller: JPT, 1967, 1595.

Acta Geod. Geoph. Mont. Hung., Vol. 24 (1-2), pp. 115-138 (1989)

PROBLEMS IN FORECASTING OF MINE DANGERS AND THEIR SOLUTION IN PREDICTION OF METHANE EMISSION

L Szirtes

Information and Computing Services Company for the Mining Industry (BISZT), Tatabánya, Hungary

[Manuscript received August 27, 1986]

Forecasting of dangers has been a substantial problem of mining for centuries. Automatic forecasting using measurement data associated with mine dangers is a new possibility enabled by the widespread use of computers. This paper provides a perspective of forecasting through examples of methane emission estimation. After a short introduction defining the basic notions of danger, forecasting, and computer their relation is examined. The use of differential equations for methane emission analysis is briefly reviewed and a proposition is outlined for a new formulation of the production scheduling problem for gassy coal mines. This formulation has been used in the generation of long-term emission forecasts, and it reflects interactions with other mine dangers (e.g. gas outbursts or endogenous fires) through extra constraints or sequencing in model formulation and solution on computers. The methane forecasting is suggested to be performed through cooperation of separately developed models. Separation is possible because of large differences in emission dynamics, due to different mining processes which accompany the emission of methane. The structure of a mine field is used in long-term, the failure of rocks and production dynamics in medium-term, and the coal clearance and ventilation parameters in short-term forecasting. Data generation problems and comparison of forecasted variables with actual data through examples are discussed.

Keywords: coal mines; danger; endogenous fires; forecasting; gas outburst; methane emission

1. DANGERS, FORECASTS AND COMPUTERS

Danger is defined as a subspace of state-variables in the state-space of mine workings. The subspace is constructed by rules on the state variables. Most common rules are defined by intervals on the variables. Forecasting is used in this paper in such cases, when most of the variables are measured automatically and for state estimation a mathematical model has been developed. Forecasting by computers means that estimation of

future states can be done automatically and within a short time period. Computers for forecasting mining processes have to be equipped with appropriate forecasting software.

A more sophisticated method for analysis of mine dangers can be performed using notions of safety and reliability analysis. Although these disciplines use a lot of ideas in their analysis safety, security and availability are the most basic ones and they have to be described in more detail. Their definitions according to the "European Purdue Workshop" TC "Safety and Security" (Frey 1979):

Safety: avoidance of or protection against, danger to life and limb, the environment and property arising from failures.

Security: protection against all classes of threat, whether accidental or deliberate to an installation or to the plant which it controls.

Reliability: the ability of an item to perform a required function under stated conditions for a stated period of time.

By using these definitions we can state that our goal in mine management is to assure reliable mining operations protecting against mine dangers by maintaining security measures (Szirtes 1986a). Besides some hardwared schemes cost effective security can be assured by computer-aided forecasting of mine dangers using both mine survey and measurement data and forecasting software.

The most important factors in forecasting model selection include the following:

- The time horizon for decision making: immediate-, short-, medium- and long-term.
- The pattern of data: seasonal, horizontal, trend (non-stationary), cyclical, or random.
- The type of model desired: time series or causal.
- The value of the forecast, and thus the amount of time and money that can be spent in obtaining it.
- The accuracy that is required and justified.
- The complexity that can be tolerated.
- The availability of historical data.

The central theme of quantitative techniques of forecasting is that the future can be predicted by discovering the

patterns in the past. Such patterns are generally assumed to take one of two forms: first, is a pattern that is determined solely as a function of time. Such a pattern can be identified directly from historical data for the variable to be forecast and related variables. Time series forecasting techniques assume that the pattern is of such a nature. The alternative pattern that is often assumed to exist consists of a relationship between two or more variables. Multiple regression assume this type of pattern.

For purposes of forecasting, the underlying pattern is assumed to be constant over at least two subsequent sets of time periods, the first being the period in which data are collected and analyzed to identify the pattern and the second being that time in the future when the identified pattern will be used as the basis for forecasting. Even following the basic guidelines of modelling described in textbooks on forecasting model development is not an easy and straightforward task in most cases. After formulating the initial model improvements are usually required by iterations in model building and making the necessary corrections on the models.

Using computers for forecasting some help in form of computer programs is required and assured on most machines. Besides programs of data input and output (including graphics), data series manipulation, and some matrix operations the basic procedures required - and generally available - on modern computers for time-series analysis are:

- Elementary operations in time or frequency domain. Addition, subtraction, scaling, multiplication, normalization, etc., of series.
- Correlation, cross-correlation, convolution of time series.
- Filtering and windowing in time or frequency domain.
- Statistics of time series, probability curves, maxima and minima distributions.
- Least-square estimation, ARIMA models, hypothesis tests.

In the development of casual models software packages for multiple linear regression, stepwise linear regression or ordinary least square estimation are generally provided.

Forecasting of mine dangers can be performed on computers in general use in coal mines. First experiments for short-term forecasting were realized on computers in mine-dispatching systems. State of the art mini and micro computers in computer networks can be used for assisting practically every aspects of forecasting. Personal computers in local-area networks can be used effectively even on mine level.

2. THE USE OF DIFFERENTIAL EQUATIONS FOR FORECASTING OF MINE DANGERS

Transport equations of physics describing material and energy transport in mining systems have been solved for the most widely used mining technologies. Special importance was devoted for the description of rock-gas and rock-fluid interaction. Although solution of these equations is possible even on contemporary mini-cimputers acquisition of equation parameters is complicated in most cases.

The flow equations used for simulation of methane emission are second order non-linear partial differential equations which are solved by computer based numerical analysis. The required input to the computer program includes parameters to define the model size, the initial and boundary conditions, including the pressure distribution, properties of the coal seams and strata, including directional permeabilities, and the properties of the flowing gas. These programs usually terminate when the flow equations have been solved or when the required number of iterations have been made. The output gives the predicted gas pressure distribution, the methane flow rates on a time basis (e.g. m^3/d), etc. (Manula et al. 1984). Figure 1 describes the most widely used solutions of partial differential equations of methane deliberation. Solution of these equations is usually possible only on off-line computers (computers which are not connected directly to mine dispatching systems) that is they can not be used for automatic forecasting of mine dangers.

I. Mining technology

1. No adjacent seam
   a) longwall, thin seam
   b) longwall, thick seam (more slides)
   c) room and pillar
   d) drivage in thin seam
   e) drivage in thick seam
2. Methane is released from adjacent seams and strata

II. Type of non-linearity

1. Anisotropy in direction of advance only
2. Anisotropy in both directions of advance and along the face

III. Dynamics of gas emission

1. Advance rate (longwall standing, constant rate of advance, variable rate of advance)
2. Methane emission during coal clearance considered
3. Dynamics due to rock-failure considered

Fig. 1. Main engineering parameters of methane emission models using solutions of partial differential equations

3. PROPOSED SYSTEM OF METHANE EMISSION FORECASTING

Both production control and mine safety need efficient and reliable methane emission forecasts in longwall faces of gassy coal mines. Prediction of methane emission is generally performed on three time scales (Szirtes 1986b), reflecting three aspects of production and adjacent seam and rock strata interaction (Fig. 2):

- Long-term forecasting is based on general description of zones of gas emission. All gassy coal seams and strata lying within the effected zone are considered, and typical forecasts are made for a year ahead. Predictions are made for a whole mine field. Used mainly for mine planning and only static relations are formulated.
- Medium-term forecasting produces estimates of gas emission on a monthly or weekly basis. Forecasting models on both time-scales reflect the influence of production rate on gas emission, but only in weekly estimation is the production variation between working days considered. Medium-term forecasts are used for ventilation and production control.

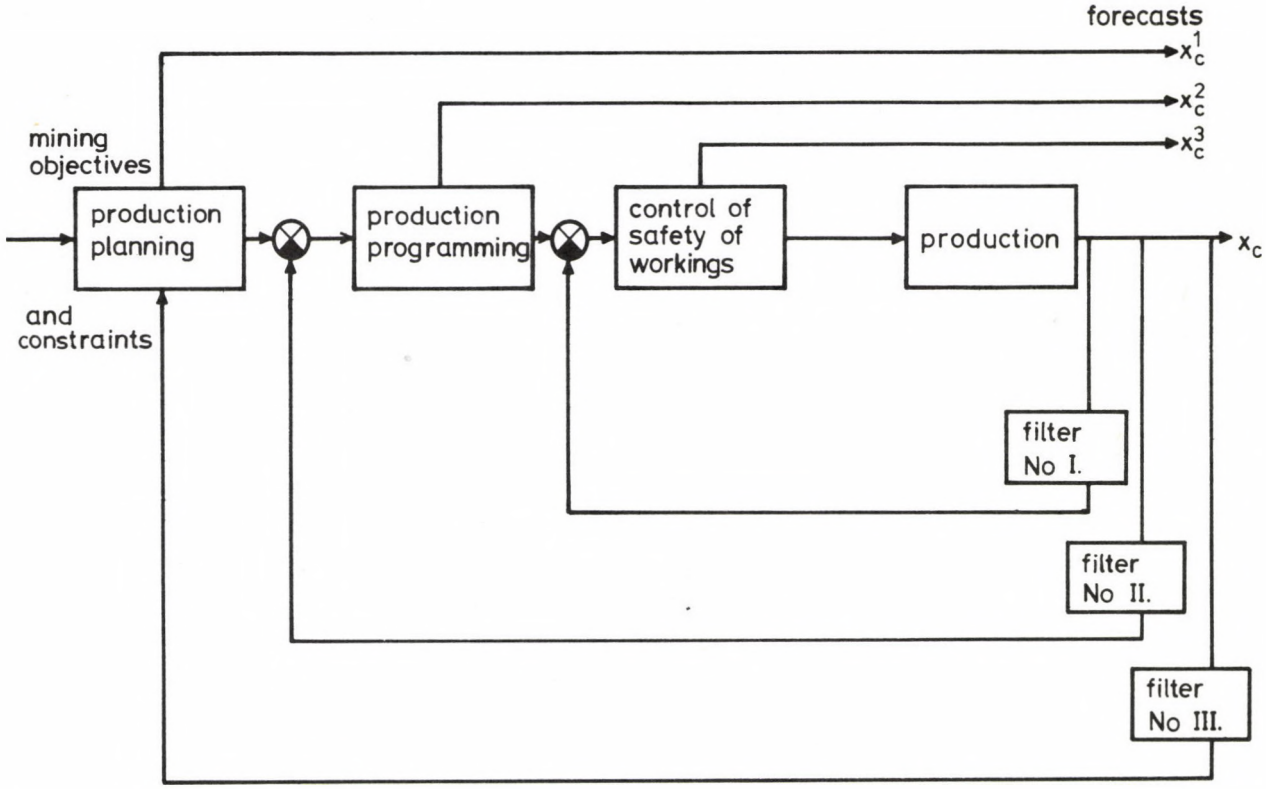

Fig. 2. Proposed structure of forecasting model interaction

- Short-term forecasting is based on real-time measurement of methane concentration and of some ventilation parameters. Forecasts are made for some minutes/hours. Direct use in safety and production control.

Both forecasting model structure needed and forecasting error produced are influenced by geologic structure, dimensions, mining methods used in a given coal mine. In Fig. 2 Xc stands for the state-variable vector of a mine working and its environment. Filtered values of Xc are used for model identification and model update. Three filters are used for the three time-scales. Estimates of future values of methane emission are generated by the models on the three time-scales. Figure 2 illustrates our opinion that the three models has to be connected in order to get better forecasts of the state-variables (Szirtes 1981).

Methane forecasting models used on the three time-scales have different dynamic properties. Response characteristics to production 'steps' of the three models are illustrated in Fig. 3. Long-term forecasting models make static forecasts of emission; they can be used for determination of the best long-term mean methane emission. Medium-term forecasting models reflect 'dynamic' behavior of methane emission. Short-term models have a very clear stochastic behavior which has to be filtered for efficient control of safety of equipments and miners. The structure of methane emission forecasting system proposed can be used for forecasting other mine dangers as well. This structure can be used for all dangers, where the interaction of two or more mining (geotechnical, ventilation, etc.) processes with different dynamic properties take place.

4. CHARACTERISTICS OF LONG-TERM METHANE EMISSION MODELS

General characteristics

Prediction of methane emission for longwall mining is performed for almost every gassy coal mine. The methods used for prediction differ from country to country which reflect differences among coal basins. Some basic parameters are used in

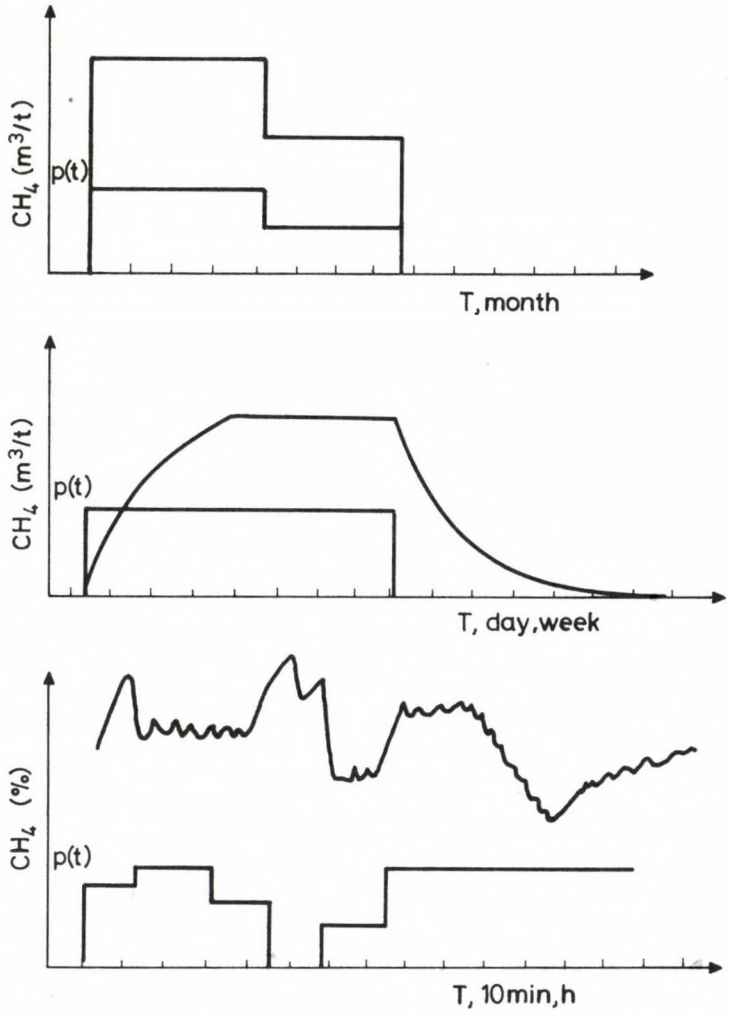

Fig. 3. Response characteristics of methane forecasting models

almost every method (Curl 1978, UN Economic and Social Council, ECU, Coal Committee 1982):

1. the stratigraphy above and below the worked seam,
2. the desorbable gas content (m^3/t) of the worked coal seam and, if possible, of adjacent seams and strata,
3. the zone of gas emission in both the roof and floor strata,

4. the degree of gas emission from adjacent seams and strata.

A detailed knowledge of the position and thickness of the strata surrounding the worked coal seam is essential for all the prediction methods. The extent of the stratigraphic column to be considered depends on the height and depth of the zone of gas emission. This zone is the three dimensional area surrounding the workings from which gas is released as a result of mining and flows into the mine workings or the methane drainage system. Not all the gas in the emission zone is necessarily released. The degree of gas emission is the percentage of the gas contained within the strata at a specific level which flows into the workings.

The proposed model

In the model developed in Hungary for long-term forecasting of methane emission a special function describing the zone of gas emission and the assumed variation of the degree of gas emission within the zone was used. These functions are different for various coal basins. Because each discrete seam or bed of strata is considered separately in the model relatively large data matrices are used in the calculations (Szirtes 1982).

The distance of the seam or bed of strata from the worked seam is applied to a relationship between the degree of gas emission and the distance from the worked seam. This relationship is defined graphically in the model. The degree of gas emission is given for every 10 m in roof and floor direction and a linear interpolation is used for distances between points on the graph. No direct use of the so called relative thickness is employed in the model. Gas emission from coal during clearance from the working district is not considered in the model because its dynamics is described by short-term forecasting. The long-term emission forecasting model can be used for production scheduling as well. Main activities of production scheduling are illustrated in Fig. 4. Long-term forecasting data are used in a system of unequalities describing mine safety regulations. Optimal production plans are formulated using linear programming (Szirtes 1984).

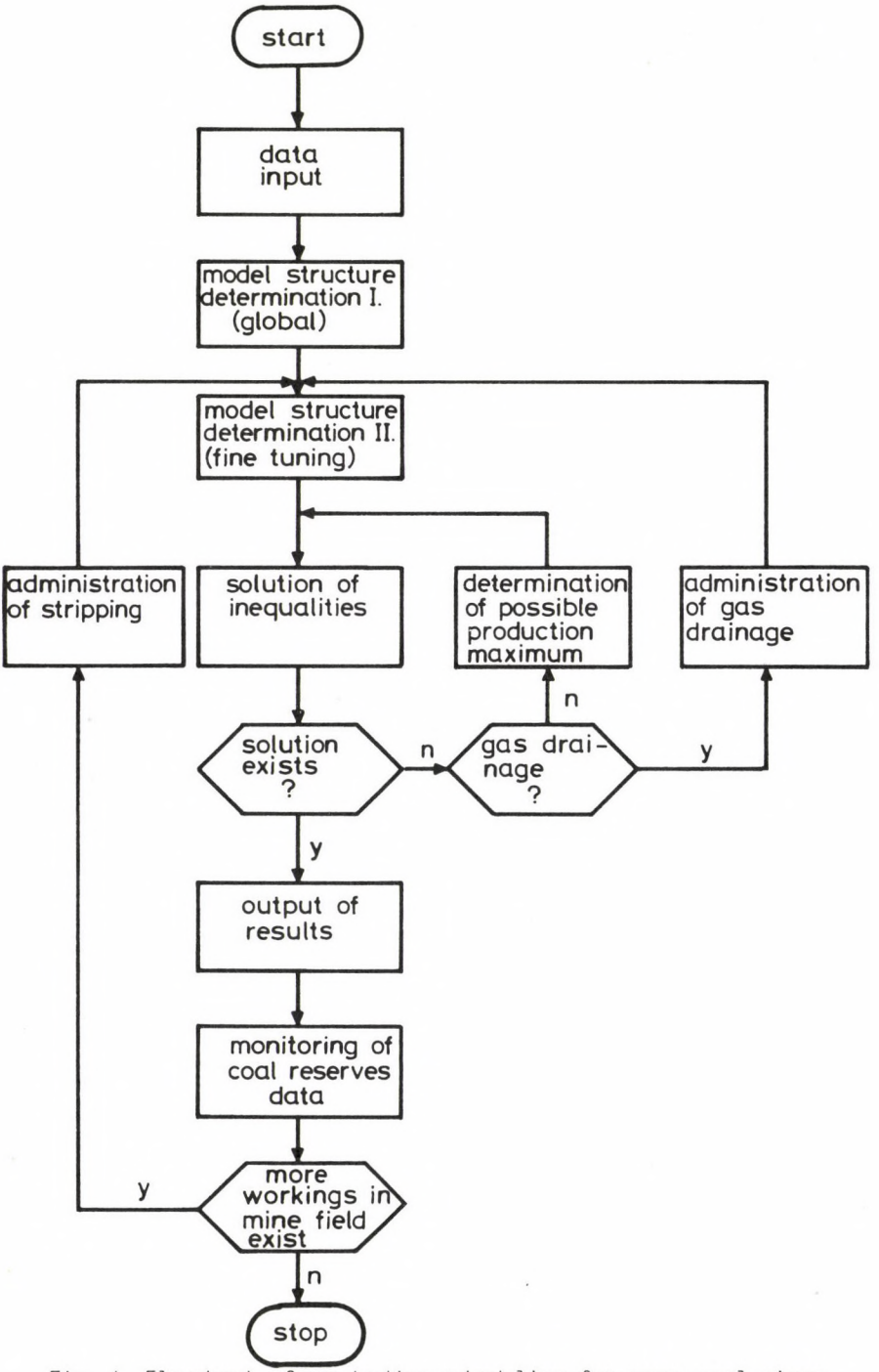

Fig. 4. Flowchart of production scheduling for gassy coal mines

In linear programming we maximize

$$z = f(x_1,\ldots,x_n) = \sum_{j=1}^{n} c_j x_j \qquad (1)$$

subject to the constraints

$$g_i\ (x_1,\ldots,x_n) = \sum_{j=1}^{n} a_{ij} x_j \leqq b_i \quad \text{for} \quad i = 1,\ldots,m \qquad (2)$$

and also subject to the nonnegative restrictions

$$x_j \geqslant 0, \quad \text{for} \quad j=1,\ldots,n. \qquad (3)$$

This problem has n unknowns and m constraints. Consequently, the linear programming problem can be characterized by the following essential parts: Optimize (maximize or minimize) a linear objective function, often called criterion function, subject to

a) a set of linear constraints which may be expressed as equalities or inequalities ($\leqslant$ or $\geqslant$),
b) a set of nonnegative restrictions for the unknowns of the problem.

In the long term emission forecasting and production scheduling problem a linear programming model with $3 \cdot n+m+1$ constraints was used according to the 5 constraint types (production goal for a mine field, production maxima and minima for all faces, maximal CH_4 concentrations in the return air of the faces, maximal CH_4 concentration allowed in return air for a group of faces (n is the number of faces, m is the number of groups of faces)).

The effect of gas drainage can be analysed in an interactive man-computer dialogue. Simulation of long-term methane emission and its comparison with actual production data is possible for model evaluation. Simulation is performed within time-intervals where main characteristics of mine workings are considered to be constant. Distinct changes in parameters of the workings can be considered only on boundaries of the mine elements. Changes in parameters can be performed either interactively or automatically using stored parameter-lists. Several

mine dangers can be considered in one production scheduling model (eg. for gas emission and fires), and mining sequences accomplishing relieving seam mining can be realised. Stochastic behavior of methane emission is considered through the use of the so called irregularity coefficients.

Short description of the Mecsek coal basin

Parametrization and verification of forecasting properties of the proposed model was performed using data from the Mecsek coal basin located in South-Hungary. Main characteristics of this basin are the following (Banhegyi and Rado 1984): In the basin black coal is produced. The coal bearing strata are 300 to 500 m thick and are of Liassic age. The underlying rock is made up of Triassic limestone and Rhaetian sandstone, the seams being overlain with shales, sandstone and limestone. Some 170 coal seams are thicker than 0.2 m, although only 10-15 seams are mineable. The thickness of the economically mineable seams is 1.5-12 m and the dirt bands between the seams contain shale and sandstone. There are considerable geologic disturbances. The many faults, disturbing the seam continuity, and foldings result in a wide range of dips, which vary from 10 to 70 degrees (characteristic value is between 40-45 degrees). Six mines are operated in the basin with 500 to 2500 t daily productions. Total annual production of the six mines is $3 \cdot 10^6$ t. The methane entering the roadways from the coal being mined and the adjacent strata averages 20-30 m^3/t of coal, whereas 40-100 m^3/t may be released in individual faces. Gas outbursts are common in the mines.

Output of the long-term methane emission forecasting program

Output of a computer program generating long-term methane emission forecasts can be seen on Fig. 5. Emission is forecasted for V-th level, 1-st mine field East of István shaft of Mecsek Coal Mines. The output on Fig. 5 was used for simulation of a given production sequence and for model verification. The computer program can be run on PDP-11 mini-computers widely used in Hungarian coal mines.

Report N^{O} 3

Results of long term forecasting

Seam	Production (T/D)	Methane conc. (%)	Air volume (m^3/min)
25	108	115	600
Seam N^{O} Ø	Slide N^{O} Ø	Concluded	
Methane emission		$248.7 \cdot 10^3$ m^3	
Coal production		$2.7 \cdot 10^3$ t	
Elapsed time		64 (25) day	
Specific gas emission		92.1 m^3/t	
Total methane emission and production:		$438 \cdot 10^3$ m^3	$4.75 \cdot 10^3$ t

Fig. 5. Computer output of long-term forecasting model

5. CHARACTERISTICS OF MEDIUM-TERM METHANE EMISSION

While fairly good estimates can be produced for long-term planning, the nature of rock failure, and so the dynamics of gas emission can not be estimated by these methods. A combined method is suggested for monthly forecasting, where the gas dynamics in outlet air concentration is modelled, measuring production rate at the face. Steps of this combined method:

1. Using information on geology (stratigraphy), geometry, and mining technology assumptions are derived on forecasting model structure.
2. Model parameters are estimated using statistically controlled measurement data. E.g. monthly average methane concentration and average production rate data as time series can be used for ordinary least-square estimation of model parameters.
3. Steps 1 and 2 are repeated until minimal degree model is attained at acceptable error limits.

Searching for the most appropriate model structure representing medium-term methane emission characteristics a special class of stochastic models, the transfer function model has special importance. We suppose that pairs of observations (X_t, Y_t) are available at equispaced intervals of time of an input X and

an output Y from some dynamic system (Box and Jenkins 1970). We can refer to the steady state level of the output obtained when the input is held at some fixed value. By this we mean the value $Y_\infty(X)$ at which the discrete output from a stable system eventually comes to equilibrium when the input is held at the fixed level X. Very often, over the range of interest, the relationship between $Y_\infty(X)$ and X will be approximately linear. Hence, if we use Y and X to denote deviations from convenient origins, we can write the steady state relationship as

$$Y = gX \tag{4}$$

where g is called the steady state gain, and it is understood that Y is a function of X.

Now, suppose the level of the input is being varied and that X_t and Y_t represent deviations at time t from equilibrium. Then it frequently happens that, to an adequate approximation, the inertia of the system can be represented by a linear filter of the form

$$\begin{aligned} Y_t &= v_o X_t + v_1 X_{t-1} + v_2 X_{t-2} + \ldots \\ &= (v_o + v_1 B + v_2 B^2 + \ldots) X_t \\ &= v(B) X_t \end{aligned} \tag{5}$$

in which the output deviation at some time t is represented as a linear aggregate of input deviations at times t,t-1,.... The operator v(B) is called the transfer function of the filter.

Parameters of the filter can be determined by calculating regression parameters of X on Y. The regression parameters used for medium-term methane emission forecasting were computed by ordinary least squares algorithm of the time-series analysis computer program package RATS.

Results of choosing the appropriate model are given for five medium-term methane forecasting models (Fig. 6). The figure depicts cumulative absolute forecasting errors for five linear regression models of the type-prod 0 2; -prod 0 2 prod 2 0 2; -prod 0 2 -ltef 0 2; -prod 0 3; -prod 0 4. The 1-st,

4-th and 5-th regression models are of autoregresive nature.

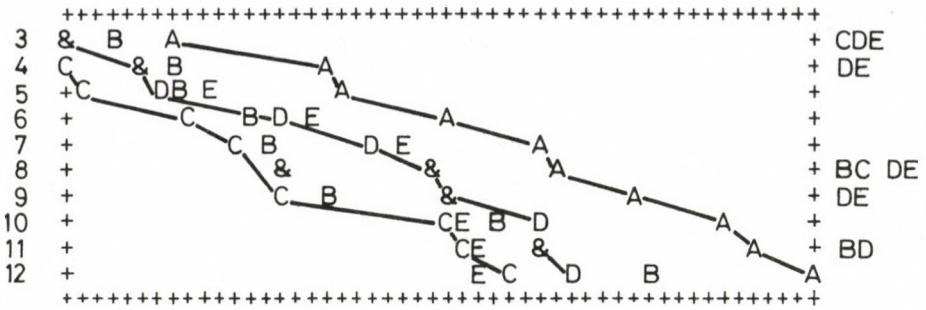

Fig. 6. Summary of cumulated absolute forecasting error for medium-term methane emission forecasting models

Model structure is described using the notation of time--series analysis. Prod stands for production, prod 2 for squared production, ltef for long-term emission forecasts. The fourth model (marked with D on Fig. 6) was chosen for medium-term forecasting because its relatively small error and low order. Letter E in the 12-th month represents cumulative absolute forecasting error of 2.5 E5 m^3 methane for the longwall face at István shaft mentioned in Chapter 4. In medium-term forecasting deseasonalisation (removing daily and weekly cycles) is often used in the model-building process.

6. PROBLEMS OF DATA ACQUISITION IN MODEL-BUILDING

With so many classes of model available one must search for general principles that help to choose the most cost-effective approach. It is generally accepted that, no "best" approach exists. Consequently, questions of data quality and availability, model complexity, and the possible effect of selecting the wrong model have to be used to limit the search to plausible alternatives. If a forecasting model is unduly sensitive to the data on which it is based, it must be used circumspectly, since

the magnitude and consistency of data errors remains unknown. Although most data includes sampling errors data revisions within the modelling process can correct them. Data quality is such a basic problem in modelling technical systems that researchers pay great attention to data problems and have developed names and categories for the most frequently occurring ones (Intriligator 1972): Among the more important problems are that there is simply not enough data (the degrees of freedom problem); that the data tend to be bunched together (the multicollinearity problem); that because changes occur slowly over time, the data from time periods close together tend to be similar (the serial correlation problem); that there may be a discontinuous change in the real world so that the data refer to different populations (the structural change problem); and that there are many inaccuracies and biases in measuring variables (the errors of measurement problem).

For forecasting of mine dangers and first of all methane emission the degrees of freedom, the structural change and the errors of measurement problems are of great importance.

Engineers determine the validity of their models by the use of statistical tests of model generated data against real-world data and by the informal comparison of model results with their mental models of "reasonable" values for their variables.

Data delivery for the long-term and medium-term forecasting model building process can be very time consuming because data collection can be performed using data bases of various mine departments and services. Production and mine geometry data come from mine-surveying, geologic data from the geology, ventilation and gas drainage data from the ventilation service. For the long-term methane forecasting program called SIMUL 28 kind of data is needed. 12 of them describe geometrical and physical, 9 technological, 6 ventilation parameters. For a larger model describing 30 coal-seams and layers some 5000 input data has to be delivered for complicated technology. These data are partly redundant. Many data used in daily work of various mine services can not be directly read into forecasting

models. Long-term forecasting models use data which are supposed to be characteristic for a given region in the mine. The definition of these regions can be performed using similar principles mentioned in Section 2 for parametrization of differential equations. For mathematically correct estimation of system parameters for various regions geostatistics can be applied. The use of geostatistical procedures for input parameter estimation is usually hindered by the lack of sufficient amount of data. For input data generation of long-term emission forecasting models the microcomputer software package "Mining Geometry" developed in Hungary was used in examples of this paper (Szirtes 1985). This package performed determination of equivalent seam-thickness e.g. thickness of a seam modelled by a paralellepipedon with equal volume as the original seam mined.

Attention has to be devoted to preliminary data analysis by short-term forecasting as well. Missing data in time-series have to be substituted. Data substitution can be performed with repetition of the last measured data, with the mean of the time-series for a given time period, or statistical continuation is also possible. Corrected time-series have to be filtered in most cases. Results of raw methane measurement data, its corrected and filtered values using a 10 element moving-average filter with equal weights can be seen on Fig. 7. Statistical parameters of raw-data may be very different from the corrected or corrected and filtered series. Standard deviation of raw data of Fig. 7 is more than 10 times larger then for the corrected data.

7. SCHORT-TERM FORECASTING

Short-term forecasting is used first of all for prediction of safety level violations. Linear forecasts (extrapolations) of methane emission data can be used for this purpose. The main problem with extrapolations is that they depend very heavily on the beginning and length of the interval from which the extrapolation was determined. Ordinary least square estimates of time-series can be used for determination of the time interval

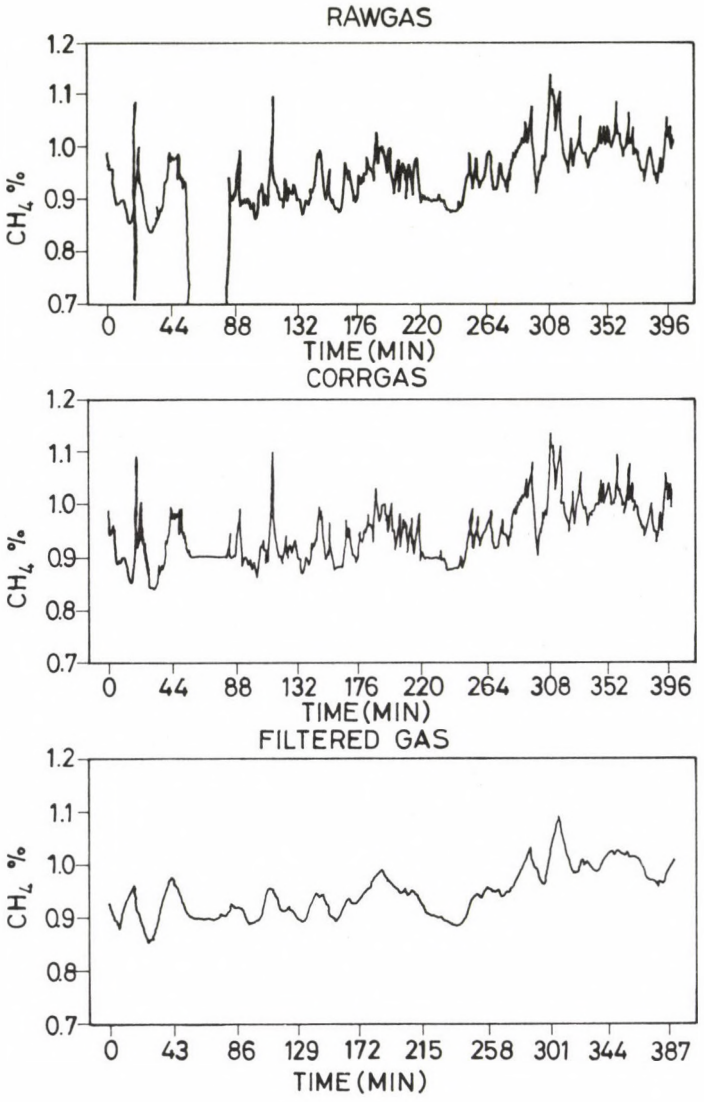

Fig. 7. Raw, corrected and filtered methane time-series for short-term forecasts

through which violation of safety boundaries is probable. The dependence of extrapolations on the beginning and length of forecasting intervals is illustrated on Fig. 8.

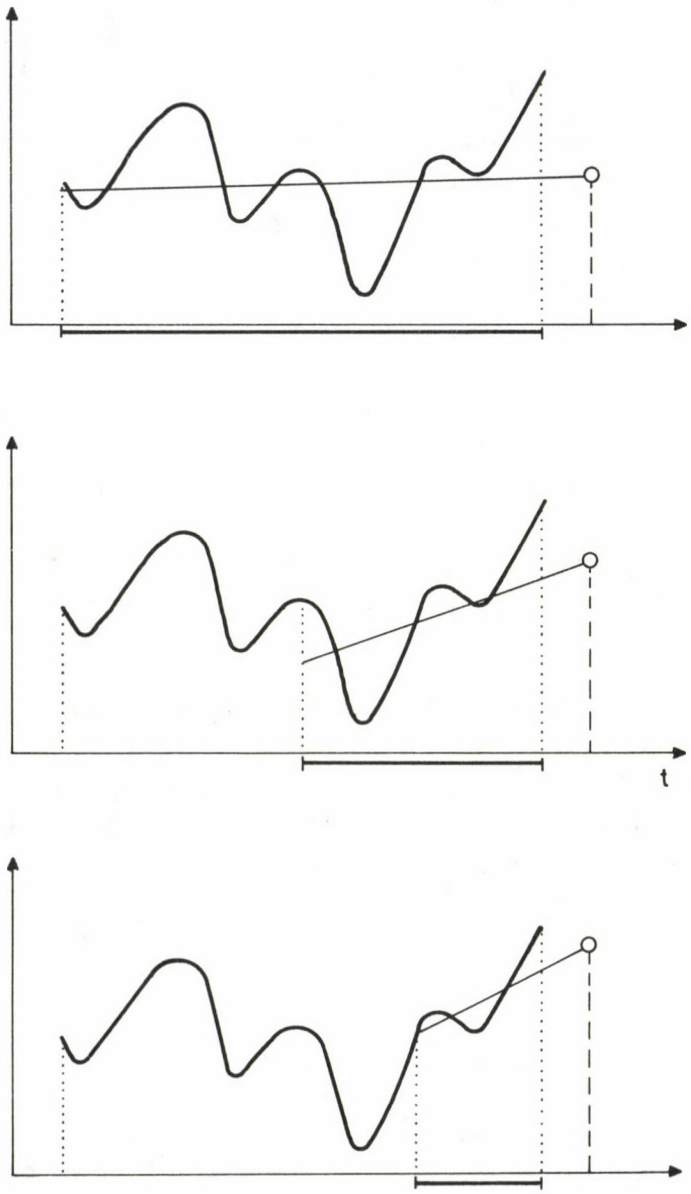

Fig. 8. Dependence of extrapolations on beginning and length of forecasting interval

In practical mining situations nonlinear extrapolations

may outperform linear ones for several reasons. E.g. convex nature of time series used for extrapolations in the vicinity of safety bounds may hinder many false alarms. With automatic detection and correction of special mining events (e.g. roof falls) in methane concentration time series the quality of short-term forecasts can be raised considerably.

8. COMPARISON OF METHANE EMISSION FORECASTS

On Fig. 9 results of various forecasting models are presented for methane emission in István shaft. Corrected methane emission data were used because of gas-drainage from the neighbourhood of the modelled longwall face. The difference between long-term and medium-term forecasts can be explained by the static nature of long-term forecasts and the relative short time-span of comparison. The absence of forecasts for the first three month is explained by the autoregressive nature of the forecasting model (Fig. 10).

9. SUMMARY OF MATHEMATICAL METHODS OF FORECASTING

The range of existing forecasting methodologies can be described by considering their classification. One of the simplest classification is summarized in Table I (Makridakis and Wheelwright 1979).

This framework employs two dimensions for describing forecasting situations - the type of pattern experienced and the type of information available. The upper left-hand quadrant of the table represent situations for which time series methods are appropriate - where quantitative historical data are available and where it is anticipated that the historical pattern will continue into the future. The lower left-hand quadrant represents situations for which explanatory or causal approaches - based on quantitative historical data - are appropriate, where the pattern depends on external factors as well as historical data on the item being forecast. The methodologies in both upper and lower left-hand quadrants assume a continuation

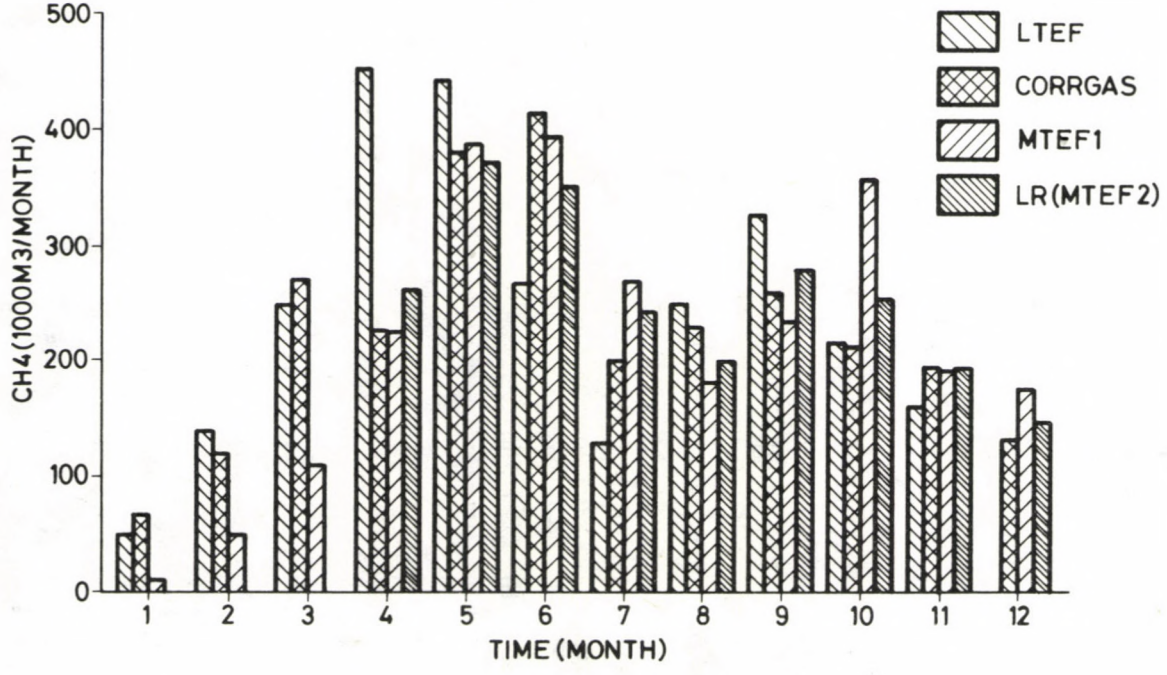

Fig. 9. Comparison of methane emission forecasts for long and medium-term models

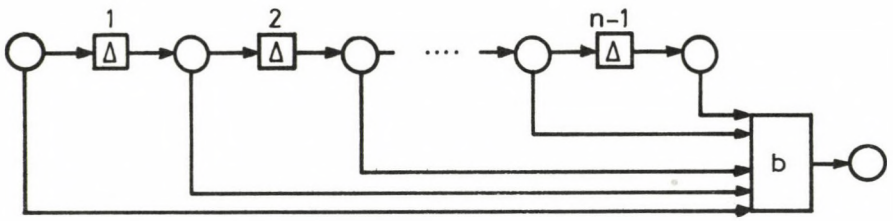

Fig. 10. Schematics of medium-term (autoregressive) forecasting model

into the future of a historical pattern, although the number of variables used in identifying and predicting that pattern is different for the two quadrants.

The upper right-hand quadrant of Table I presents those methods commonly referred to as exploratory, the lower right-hand quadrant shows those normative methodologies which, while based on qualitative or subjective data, consider the impact of factors chosen by management on the future outcome of specific event.

In forecasting of mining dangers the methods underlined in Table I are of most interest and were used throughout examples of this paper.

10. FORECASTING OF METHANE EMISSION IS A REALITY

Comparison of forecasts with actual emission data for István shaft prove the reality of methane emission for production control and mine design. No mathematical or computing problem hinders widespread use of these methods in coal mines. Because of mine safety regulations very many data are stored temporarily in coal mines but few of them are used for engineering analysis of mine state. Modeling of methane emission requires a very sound data-acquisition and analysis but good forecasts can sink mining costs and enhance the safety of mining operations effectively. Through further experiments in automatic analysis of time series of measured data automatic detection of safety

degradation can be reached for some mining processes.

Table I. Classification of forecasting techniques

Type of pattern	Type of information available	
	Quantitative	Qualitative or technological
History repeats itself	Time series methods Exponential smoothing Decomposition/census II Filters Autoregressive/moving average Leading indicators Various forms of trend extrapolations	Exploratory method Anticipatory surveys Catastrophe theory Delphi Historical analogies Life-cycle analysis Morphological research Jury of executive opinion Sales force composite
External factors determine events	Explanatory methods Regression Econometric models Multivariate ARMA Input/output	Normative methods Cross-impact matrices Relevance trees Delphi System dynamics Market research

REFERENCES

Banhegyi M, Rado A 1984: In: Proc. of the 3-rd Int. Mine Ventilation Congress, Harrogate, p. 183-186.

Box G E P, Jenkins G M 1970: Time series analysis forecasting and control Holden-Day, San Francisco

Curl S J 1978: Methane prediction in coal mines. IEA Coal Research, London, Report No ICTIS/TR04

Frey H H 1979: In: Proceedings of the IFA Workshop, Stuttgart, 3-10.

Intriligator M D 1972: Econometrics and economic forecasting. In: Economics of engineering and social systems (Ed. English J M), New-York, Interscience

Makridakis S, Wheelwright S C 1979: In: TIMS Studies in the Management Sciences. North-Holland, No 12, 1-15.

Manula C B et al. 1984: A master environmental control and mine system simulator for underground coal mining. Volume II. Methane Generator. The Pennsylvania State University. University Park, Pennsylvania, Bureau of Mines Open File Report 84(6)-76.

Methods of eliminating firedamp and the utilization of firedamp from mines as a source of energy. 1982, UN Economic and Social Council, ECU, Coal Committee, Geneva, Report No Coal/GE.1/R.44

Szirtes L 1981: In: Publications of the Hungarian Central Institute for the Development of Mining (KBFI), No. 24, 170-182.

Szirtes L 1982: Systems analysis and design for enhancement of mine safety through examples from control of methane emission. KBFI, Budapest

Szirtes L 1984: BKL, Bányászat, 117, No 1, 27-37.

Szirtes L (ed.) 1985: Computer programs for the analysis of mining geometry. BISZT, Tatabánya

Szirtes L 1986a: FTPRPI, Novosibirsk, No 2, 116-121.

Szirtes L 1986b: Forecasting of methane emission dynamics with combined method. Paper submitted for ICAMC 86, Dubrovnik, Yugoslavia

Acta Geod. Geoph. Mont. Hung., Vol. 24 (1-2), pp. 139-153 (1989)

DETERMINATION OF WATER SATURATION IN ROCKS WITH DIELECTRIC METHODS

K Bauer and Z Mosonyi

Research Laboratory for Mining Chemistry of the Hungarian Academy of Sciences, H-3515 Miskolc, University Campus, POB 2, Hungary

[Manuscript received November 17, 1986]

In course of modelling at the pressure and temperature of the reservoir the water saturation can be determined in the simplest way and with the lowest costs by means of the dielectric methods. For this purpose, however, a certain amount of consistent information would be needed about the area. In this paper the results of studies are discussed which were carried out in natural and artificial rocks with condensers having both insulated and uninsulated armatures. These studies had the aim to overcome the lack of information mentioned.

On the basis of the results authors conclude that an unambiguous and well defined functional connection exists between water saturation and permittivity in the frequency range where the frequency dependence of the rock saturated totally or partially with water can already be neglected. This frequency range changes in function of the characteristics of the porous system as well as of the salt content of the model water.

For the prediction of the functional connection $\Sigma(S_w)$ Odelevsky's statistical method has been applied.

Keywords: dielectric method; frequency dependence of dielectricity; permettivity; water saturation

SYMBOLS

C	capacity (F)
G	conductivity (s)
S	fluid saturation
f	frequency (s^{-1})
ε'	relative dielectric constant
ε''	relative dielectric loss
ω	angular velocity (s^{-1})

INDICES

- 10 value measured at 10 KHz
- x value measured at the frequency concerned
- w water
- x in test conducted with insulated armature, the value measured at the concerning frequency

Acta Geod. Geoph. Mont. Hung. 24, 1989
Akadémiai Kiadó, Budapest

INTRODUCTION

Model tests conducted in laboratories form integral part of both the new methods of crude oil recovery and of those which are more efficient than the traditional ones. In addition to the linear models, areal and volumetric models are also applied as their system of conditions can be better adjusted to the real conditions. In all cases, it is also necessary to be aware of the intra-model fluid-saturation distributions and their change in time since the fluid saturation conditions developed on completion of the secondary recovery are preconditions of the tertiary intervention.

For the determination of fluid saturation in a rock model, a relatively wide range of measuring methods are currently available (Uhlman 1972). The majority of these require high expenditure and special safety measures, however, they are only suitable for measuring average saturation of samples of small size (Hornyos 1973) under nearly atmospheric pressure and temperature conditions. So the result does not justify the high expenditure.

With regard to the above methods, for the conditions approximating the reservoir dielectric methods would be relatively less cost-intensive, which belong to the non-tracing, direct measuring methods and have been used for a fairly long time to the fast control and measurement of the moisture content of liquids and solids in several fields of technology (Berliner 1960, Kritchevskovo 1980, Stuchly and Stuchly 1983). They also have traditions in reservoir-mechanical tests (Dunlap et al. 1949, Simandoux 1963, Csernyák 1964). However, their wider application has been and is aggravated by the fact that in many cases the information are contradictional and inefficient.

Therefore, keeping in mind the task of "in situ" measurement of water saturation values in the rock model as well, tests have been conducted on natural and artificial rocks to gain information on their permittivity and frequency-dependence as well as, knowing their permittivity, on the degree to which their water saturation can be forecast.

INSTRUMENTS AND MATERIALS USED FOR THE TESTS

For the tests, 4775A type, Hewlett-Packard LCR meter has been applied. With the LCR meter, the capacity and conductivity of the condensers outlined in Fig. 1 were simultaneously measured in the frequency band of 10 KHz < f < 10 MHz.

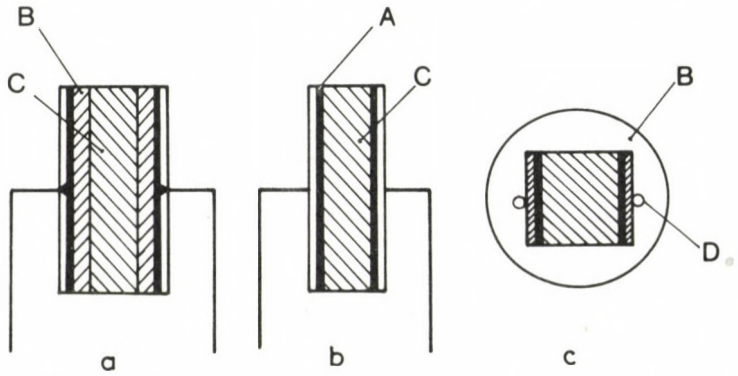

Fig. 1. Structural build of the measuring condensers used for the tests, with insulated (a) and uninsulated electrode connections (b,c). A - plastic covered with copper foil, B - epoxy resin, C - rock, D - stainless steel pipe

The dielectric medium of the above condensers have been formed from the following natural and artificial rocks. Armatures of the condensers against the rock have been either insulated or uninsulated fixed to the rock samples so that they could not be moved.

The natural rock used in the test: sandstone from water-containing zone of a hydrocarbon seam (Transdanubia, Kiscsehi). The permeability ranged from 10^{-3} μm^2 and 1 μm^2, its porosity from 0.06 to 0.25.

Regarding the artificial rocks, for that of synthetic resinous bond, Tipox resin has been applied to cement the grains of the washed sand from Miskolc. The specific resin consumption calculated for the non-consolidated sand volume has had a ratio of 0.05-0.16. Their porosity ranged from 0.2 to 0.36, permeability from 0.01 μm^2 to 10 μm^2.

The frame grains of artificial rock of silicate binding consisted of washed sand from Fehérvárcsurgó. For binding of

the sand grains, the mix of glass grits of grain sizes below 45 μm and calcium fluoride has been applied. The weight of the calcium fluoride has been 0.005-0.02 times lower than that of the powdered glass while the proportion of the latter has accounted for 0.03 to 0.14 of the powder bed. After the sintering of the sand mixed with binder, the rock material had a porosity of 0.35-0.46 and a permeability of 0.1 μm^2-30μm^2. For water saturation of the rocks, distilled water has been applied. In some cases, rocks saturated with ethyl alcohol and/or acetone have also been tested.

RESULTS AND THEIR INTERPRETATION

For tests with uninsulated electrodes, to characterize the general frequency-dependence of the results, C_x/C_{10} and G_{10}/G_x dimensionless parameters have been applied. Considering these parameter ratios, capacities are typical of the dielectric constants, conductivities of the specific conductivities of the proper frequency. The results concerning the dry and water-saturated condition of the rock - for natural rocks - can be seen in Figs 2 and 5, those concerning the silicate bonded type artificial rocks in Figs 3 and 6 as well as those of the resin bond type artificial rocks in Figs 4 and 7.

The trend to be observed within the individual types of rocks in the frequency-dependence of the reduced parameters characterized by the maximum and minimum values indicated on the curves of the above figures, can also be observed between the different types of rocks.

The latter similarity is reflected in the frequency curves of the complex permettivity of the rocks studied, too, as can be seen from the change in their real and imaginary components as well, on the basis of Figs 8 and 9. The only difference observed is between the values of these parameters. For instance, regarding the dielectric permeabilities shown in Fig. 8, on frequencies below 10 KHz, that of the artificial-resin bonded rock is minimum compared to the natural sandstone. This in itself, however, can still be of a considerable value having

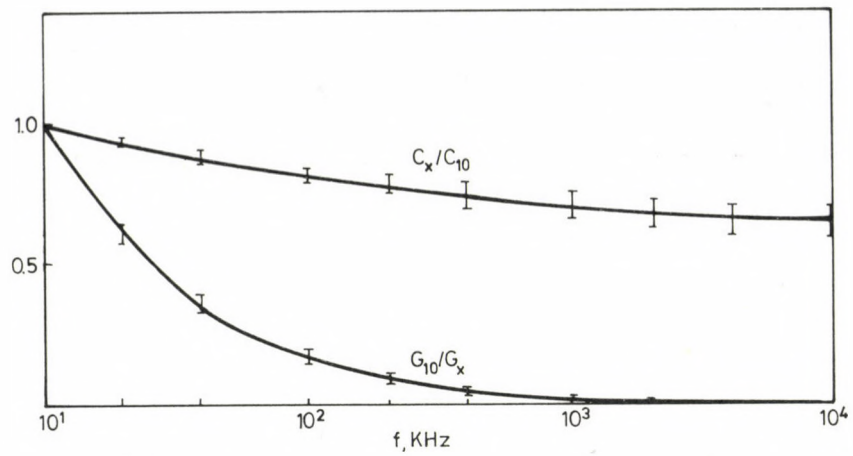

Fig. 2. In dry condition of natural sandstones, change of the reduced capacity and conductivity in the function of frequency

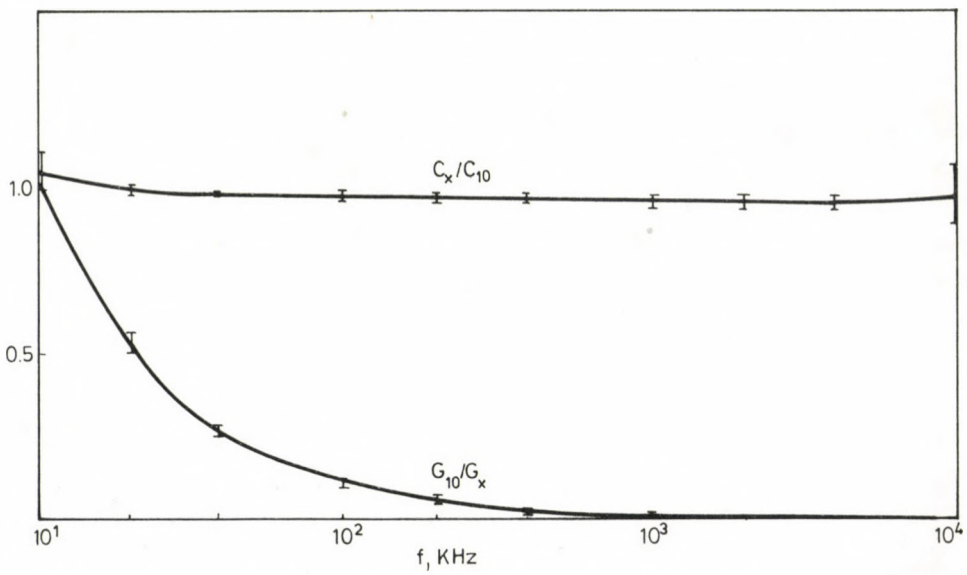

Fig. 3. With the silicate-bond type artifical rocks in dry condition, the change of the reduced capacity and conductivity in the function of frequency

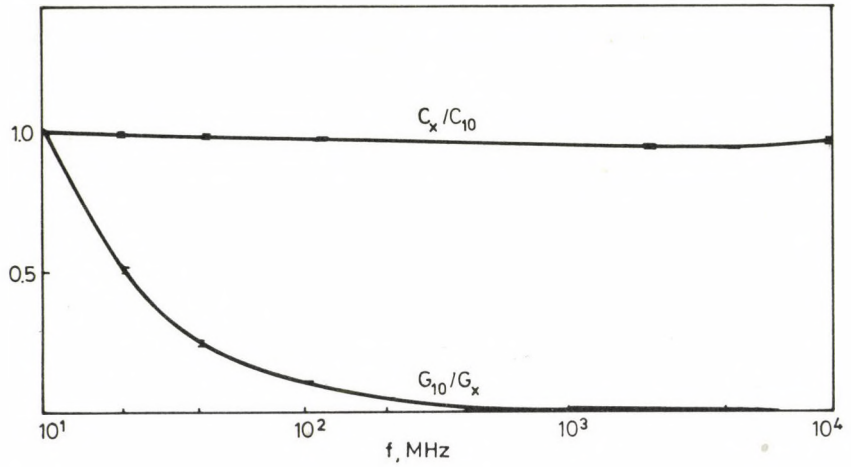

Fig. 4. In the dry condition of synthetic resin bonded artificial rocks, change of reduced capacity and conductivity according to the frequency

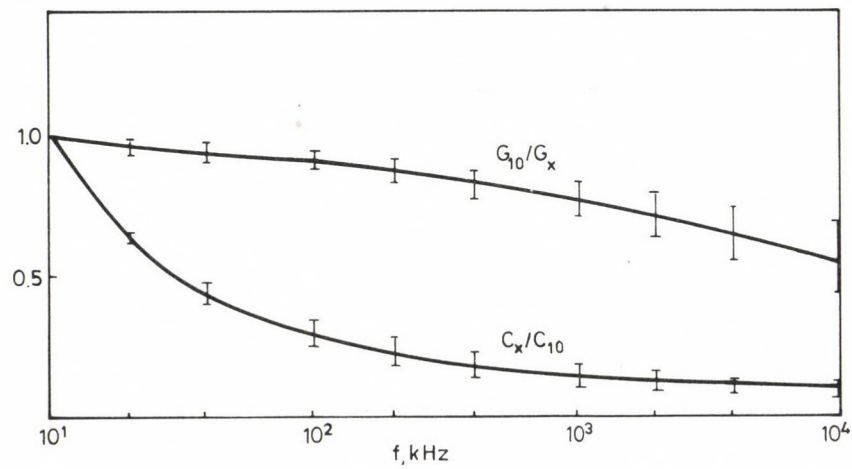

Fig. 5. In water-saturated condition of natural sandstones, change of the reduced capacity and conductivity according to the frequency

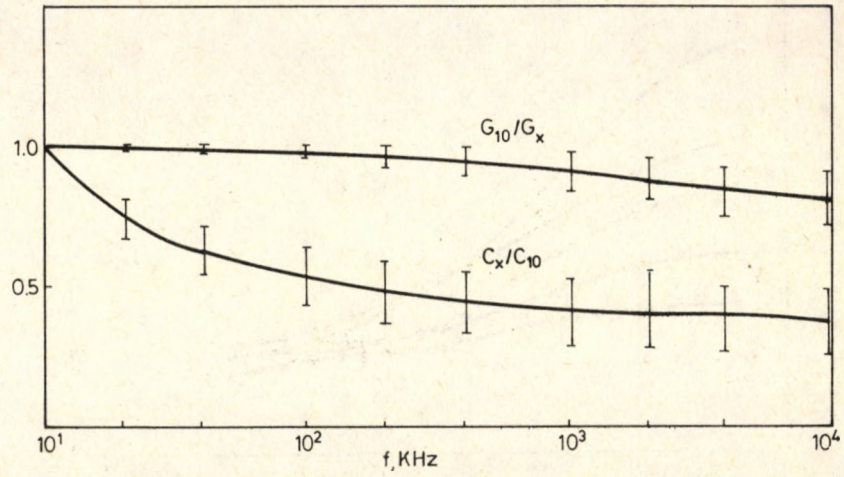

Fig. 6. With the silicate-bonded artificial rocks in water-saturated condition, change of the reduced capacity and conductivity in the function of frequency

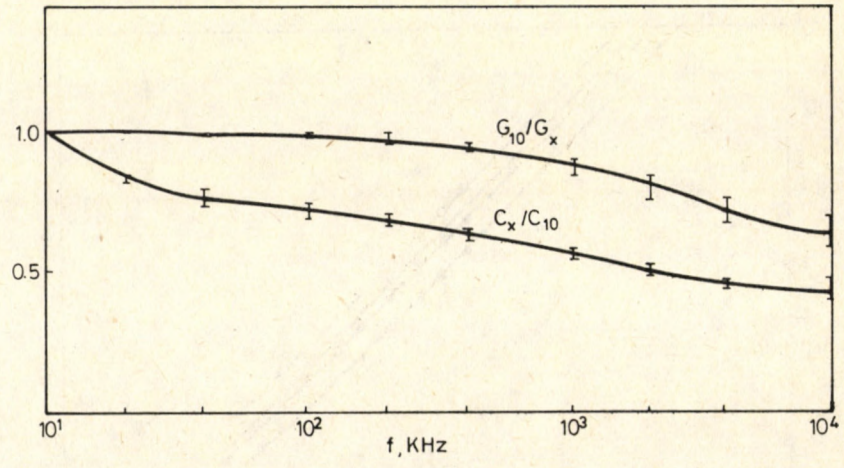

Fig. 7. With the synthetic resin bonded artificial rocks in water-saturated condition, change of the reduced capacity and conductivity according to the frequency

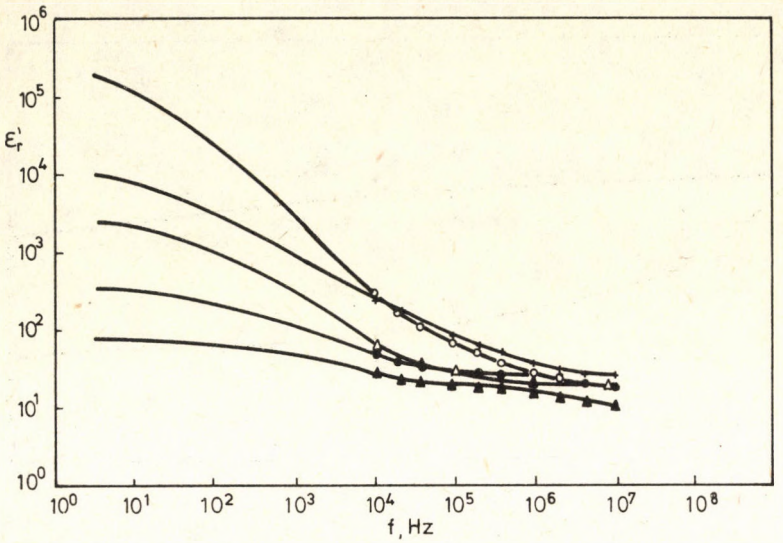

Fig. 8. Change of the dielectric permeability of natural and artificial rocks in the function of frequency. o - natural sandstone (Kiscsehi), + - low-porosity artificial rock (of silicate binding), Δ , ● - high-porosity artificial rock (of silicate binding), ▲ - artificial rock of synthetic resin binding

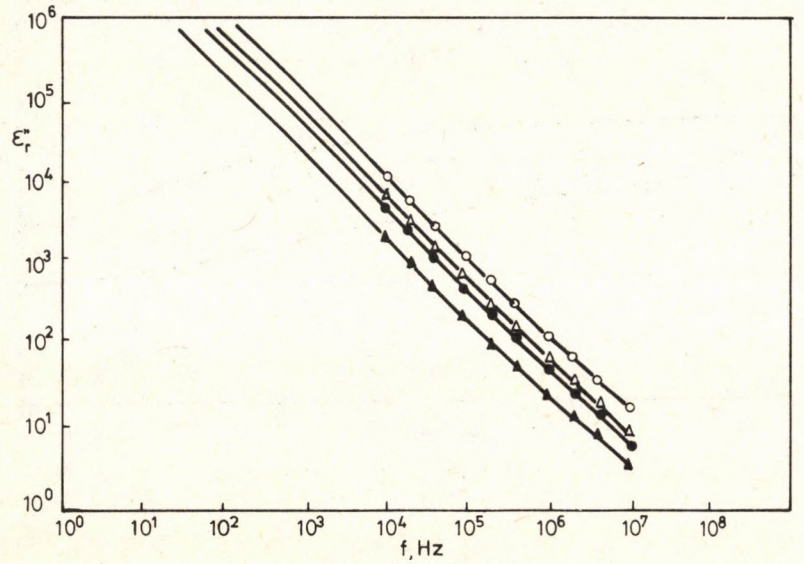

Fig. 9. For the rocks shown in Fig. 8, change of the dielectric loss in the function of frequency

regard for the fact that it is considerably higher than that of the water which is one of its components ($\varepsilon_{resin} = 3$; $\varepsilon_{quartz\text{-}sand} = 3$; $\varepsilon_{water} = 80$).

In the uninsulated armature type tests of water saturated rocks, micro-heterogeneity and anisotropy can also account for the very high dielectric permeabilities observable at the lower frequencies. An example of this can be seen in Fig. 10, making use of the results by Sen (1980). The permettivity change in case of a narrow frequency band is primarily expected for rocks of granular structure similar to those in Fig. 11. The considerable shift to the right in the direction of the high frequencies of the transitional zone is in connection with the highly increased conductivity resulting from the electrolite content of pore-filling water.

In our own tests, this transitional zone, as shown in Fig. 8, has been highly displaced to the left, into the direction of the KHz frequency values. The displacement to this direction of the transitional zones is assumed to have resulted from the low conductivity of the distilled water applied for the

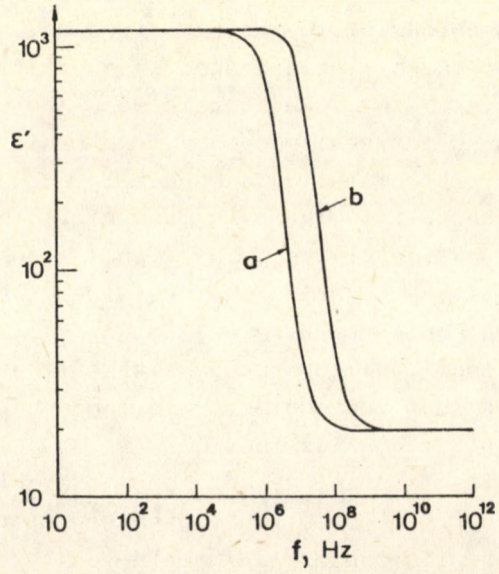

Fig. 10. Change of the dielectric permeability of water-saturated sandstone with grain-size similar to that schematically shown in Fig. 11 in the function of the frequency of the electric field perpendicular to the stratification Sen (1980). a - = 1 mho/m; b - = 10 mho/m

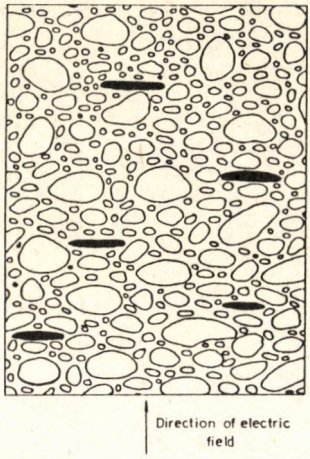

Fig. 11. Schematic drawing of rock containing laminarly flat, disc-form grains too, where the dielectric constant can be of particarly high value as well if the electric field is perpendicular to the stratification Sen (1980)

saturation of the rocks. What could only account for the increase of the water conductivity here have been the ions of the hydrating clay minerals, to a small degree, in case of the natural rocks and the ions of the metal oxides soluble in pore-water in case of the silicate bonded type artificial rocks. The differences resulting from this between the conductivities of rocks, taking some given frequency as a basis, can also be reflected in the dielectric losses shown in Fig. 9. Consequently, the differences within the rock conductivities have also determined the location of the transitional zones compared to one another. The transitional zone much wider than that in Fig. 10, covering frequencies of even 0.1 KHz $< f <$ 100 KHz can also result from the fact that the rock grains here are only of slightly oriented location and also the laminarly flat grains to be seen in Fig. 11 are lacking.

In the non-insulated electrode type tests of the rock containing ionic fluid, the previously observed extreme permittivity changes can be limited if the metal electrodes of the condenser are connected to the rock by the insertion of a loss-free dielectric medium (insulator).

This, however, can result in the frequency dependence

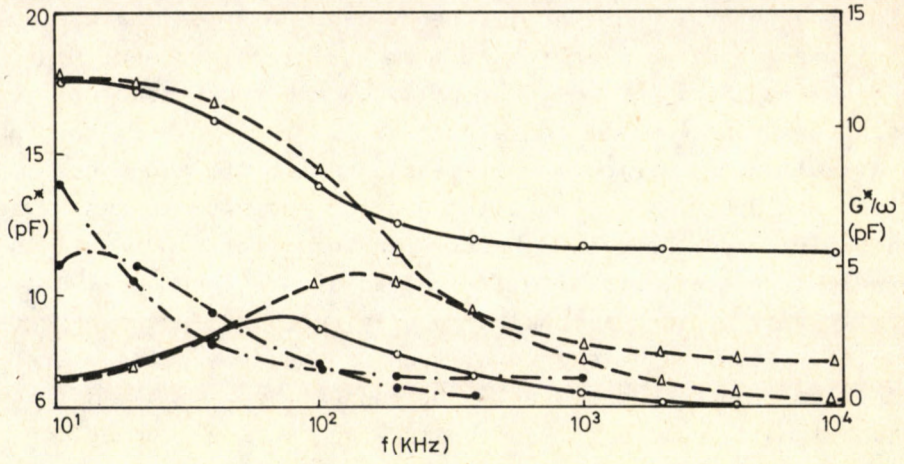

Fig. 12. When a measuring condenser with insulated armament is applied, change of parameters C^* and G^*/ω proportional to the dielectric properties in the function of frequency for synthetic resin bonded artificial rocks saturated with water (o), acetone (•) and/or ethyl alcohol (Δ)

shown in Fig. 12 in case of the component of the complex permittivity and of the values proportional to them, also, it means a considerably lower apparent dielectric constant than the original in the sound frequency range.

Such a frequency dependence having been measured, e.g., for the conditions of synthetic resin bond type sand saturated with water, ethyl alcohol and/or acetone results from the polarization on the contact surface of loss-involving and loss-free materials differing in their dielectric permeabilities and as such, it can also be interpreted as one of the cases of Maxwell's surface effects. This phenomenon has already been studied by Simandoux (1973), in connection with the determination of the radio-frequency type capacitive water saturation. He has pointed out that in the tests using insulated electrodes, the dielectric loss in connection with the rock conductivity

distorts the values measured, similarly to the case when a separating condenser is inserted into the measuring circle, as it is proved by the tests conducted by Csernyák (1964), too.

In a general case the frequency-dependence of the dielectric parameters can also result from the micro and semi-micro (intra-stratification) heterogeneity of the rock structure and also from point mode of the electrode. In these cases, the ion polarizations occurring in the micro, semi-micro and macroscopic regions of the separating surfaces between the water as ionic fluid and the solid phase as an insulator can result in Maxwell-Wagner effects of different origins, consequently, the permittivity of such a complex material with different heterogeneities can also have several such frequency spectra where its volume can be considerably changed (Alvarez 1973). With regard to all these points, for studying the real connection between the water saturation and the dielectric constant, only the results of the measurements performed with uninsulated measuring condensers have been applied. As can be seen in Figs 5-9, the frequency dependence of the capacity and the dielectric constant has been negligible above 1 MHz. Thus, on the basis of the tests conducted at 10 MHz, relation S_w (ε') can change according to Fig. 13 for the different rock types. For the numerical forecast of relation S_w (ε'), Odelevsky's (1951) statistical model with several components have been applied. The only modification we have performed in the latter is that we have assumed the particles of the three-component system to be of non-spherical form. Therefore, during matching to the measuring points, the average depolarization factor has ranged from 0.1 to 0.2. Although the frequency dependence of the values measured is not considerably any more, the relation between water saturation and the dielectric constant is not linear for rocks of medium porosity, it can only be made linear if the rock porosity is very low - $\phi < 0.1$ - or very high: $\phi > 0.5$, as well as if the dielectric constant of the solid components is high, $\varepsilon_s > 15$. The latter results unequivocally follow from the generalizations to be made with the mathematical model adapted to the measuring results.

What we could also observe during the tests is that in the

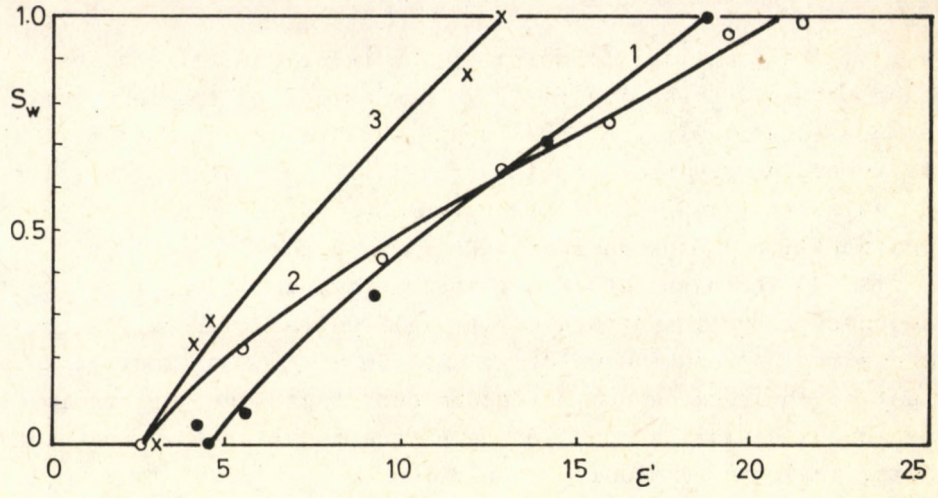

Fig. 13. Curves showing the relation between the water saturation and the dielectric permeability at 10 MHz frequency on the basis of tests conducted with uninsulated electrode type measuring condenser. 1. Natural sandstone (Kiscsehi), 2. Silicate bond type artificial rock, 3. Synthetic resin bonded artificial rock

fields of the dielectric constants which highly depend on frequencies, it is difficult to forecast water saturation on the basis of the dielectric parameter measured, for lack of a clear relation between the water saturation and the apparent dielectric constant. On the basis of the measurements performed at 10 MHz, however, a well reproducable relation could be outlined for all three types of rocks. Naturally, in case of these rocks as well, if the water has a considerable electrolite content, the frequency of the measurements should be increased. Generally this is possible up to abt. 500 MHz as above this, the effect of the orientation polarization of the water molecule is beginning to be felt. This frequency is at the same time, the upper frequency limit of the applicability of conduction type

dielectric measuring methods.

CONCLUSIONS

1. The numerical forecast of the relations between the water saturation and the dielectric constant of the rock will be more accurate if, in addition to being aware of the permittivity of the dry rock and the rock fully saturated with water, the anisotropy typical of the porous system is also taken into consideration in the Odelevsky-Csernyák model.

2. On the basis of merely speculative considerations, that frequency range in which a clear, well-definable relation can be assumed between the water saturation and the dielectric constant of the rock cannot be determined, therefore, concerning the porous systems of the would-be rock model of the laboratory tests, preliminary studies should be made in order to identify the frequency range suitable for the forecast of the water saturation, that frequency range in which the frequency-dependence of the dielectric permeability of the rock fully or partially saturated with water is negligible. This frequency range can vary according to the properties of the porous system and the salt content of the model water too.

REFERENCES

Alvarez R 1973: Geophysics, 38, 920-940.

Berliner M A 1960: Elektricheskie metodi i pribori dlya izmereniya i regulirovaniya vlazhnosti. Gosenergoizdat, Moscow

Csernyak G J 1964: Dielektricheskie metodi issledovaniya vlazhnikh gruntov. Nedra, Moscow

Dunlap H I, Bilhartz H L, Schuler E, Bailey C R 1949: Trans, AIME, 210, 259.

Hornyos I, Őri V, Lendvai J 1973: OGIL Műsz. Tud. Közlöny, 10, 69.

Krichevskiy E S 1980: Teoriya i praktika eksperessnogo kontrolya vlazhnosti tvordih i zhidkikh materialov. 7-18, 47-66.

Odelevskiy V I 1951: Zhurnal Tekhnicheskoy Fiziki, 21, 667-677.

Sen P N 1980: AIME, SPE 9379.

Simandoux P 1963: Revue de l'Inst. Fran. de Petr., 193-215.
Stuchly M A, Stuchly S S 1983: IEE Proceedings, 130, 467-497.
Uhlmann N 1972: Kőolaj és Földgáz, 309-313.

Acta Geod. Geoph. Mont. Hung., Vol. 24 (1-2), pp. 155-174 (1989)

EFFECT OF CHANGE IN MOISTURE CONTENT ON QUANTITY AND QUALITY PARAMETERS OF COALS

Sz Pethő

Mineral Dressing Department of the Technical University for Heavy Industry, H-3515 Miskolc, Egyetemváros, Hungary

[Manuscript received June 17, 1986, revised: June 15, 1987]

The study contains the functions describing the change of ash- and ballast contents vs. moisture content of coals as well as the changes of mass recovery, calorific value, total energy and specific ballast and a discussion of them. By means of the relations and parameters deduced, the domestic types of coals are analyzed in details.

The relations deduced in this paper and the rules determined by them are valid if, during the change in moisture content, the extract content of coal does not undergo any physical or chemical change and if the mass of the dry coal material remains the same. This also means that the other product of dewatering will be pure water.

The study has been made with the support of the National Scientific Research Foundation of the Hungarian Academy of Sciences.

Keywords: ash content; ballast; calorific value of coals; combustible content; moisture content

1. INTRODUCTION

Table I shows the commercial ash- and moisture contents A_r and W_r of Hungarian coals of easy distinction both geologically and according to the quality parameter values as well as the ballast contents $b_r = A_r + W_r$ and combustible contents $e_r = 100 - b_r$ which can be directly calculated from them. Liassic, Eocene, Cretaceous and Miocene coals as well as lignites have been distinguished. The data of the table are from Osváth and Pethő (1985) where the dependence of the calorific value on the ash- and moisture contents is given with a linear function-like relation of two variables.

Values a, w and Q_o contained in the other parts of Table I are also taken from the same paper. a means the change in calorific value resulting from a 1 % change of ash content and w

Table I. Some quality parameters of the different types of coals in Hungary

Type of coal	A_r	W_r	$b_r=A_r+W_r$	$e_r=100-b_r$	a	w	Q_o	Q_r	k	$A_{rf}=10^4\frac{A_r}{Q_r}$	$b_{rf}=10^4\frac{A_r+W_r}{Q_r}$
Liassic	42	8	50	50	381	371	34630	15660	34.70	26.82	31.93
Eocene	27	16	43	57	335	318	29331	15198	41.69	17.77	28.29
Cretaceous	23	22	45	55	430	335	31043	13783	119.57	16.69	32.65
Miocene	26	26	52	48	282	295	27062	12060	11.38	21.56	43.12
Lignite	22	46	68	32	260	274	24921	6597	10.79	33.35	103.08

means that resulting from a 1 % change of moisture content. Q_o is the heating value of the ash-free and moisture-free coal, i.e. of the combustible part.

Q_r is a function of two variables referring to the commercial heating value

$$Q_r = Q_o - aA_r - wW_r \quad . \tag{1}$$

Multipliers a and w can also be provided with a physical interpretation:

$$a = \left(\frac{Q_o}{100} + k \right) g \qquad \text{and} \quad w = \frac{Q_o}{100} + 24.62 \quad , \tag{2}$$

where k means the combustion heat, i.e. the heat required to burn the waste minerals and rocks contained in the coal into ash; 24.62 is the evaporation heat. The dimension of both the combustion and the evaporation heats is kJ/0.01 kg. Equation (2) also includes the mineral raw material factor g which is the quotient of the mass of minerals and rocks in the coal and that of the ash resulting from the burning.

The sign of combustion heat k is positive if the waste consists of minerals and rocks of endothermal properties. Limestone is a mineral of endothermal property. When waste of exothermal properties is burned, k has a negative sign in Eq. (2). Pyrite is a mineral of exothermal property.

It is worth determining the values of constants Q_o, a and w in Eq. (1) by means of mathematical statistic methods for each coal seam and mine basin. Then, by determining Q_r and A_r, the calorific value Q_r can be calculated and compared with the measuring result.

The last two columns of the table show the specific ash- and specific ballast values. Both are given in g/1000 kJ. The specific ash A_{rf} is the ash - g - per 1000 kJ while specific ballast b_{rf} is the joint mass in g of ash and water per 1000 kJ.

The relations and rules determined in the study are valid for the mechanical dewatering process. It means that during dewatering, there is no physical and chemical change in the coal. It is also assumed that the water removed does not contain

solid material.

2. CHANGE OF ASH- AND BALLAST CONTENTS OF COALS AND OF MASS EXTRACTION IN FUNCTION OF MOISTURE CONTENT

In the function of moisture content W, the change of ash content A can be calculated with the following relation if the test values W_r and A_r mentioned are known

$$A = \frac{100-W}{100-W_r} A_r = \frac{100\ A_r}{100-W_r} - \frac{A_r}{100-W_r} W = A_d - \frac{A_d}{100} W \ . \qquad (3)$$

According to the transposed equation, the change of ash content in function of moisture content W can be expressed with a straight line of negative inclination the ordinate intercept of which is dry ash-content A_d and the dimension of the direction factor is one hundredth of this dry ash content.

Ballast content b_r is the sum of the ash-content and moisture content: $b_r = A_r + W_r$. The change of this in the function of the moisture content:

$$b = \frac{100-W}{100-W_r} A_r + W = \frac{100\ A_r}{100-W_r} + \frac{100 - (A_r+W_r)}{100-W_r} W = A_d + \frac{e_d}{100} W \ . \qquad (4)$$

So the change of b ballast content vs. moisture content can be given with a straight line of positive inclination the intercept y of which is also the dry ash content and the value of the direction factor is one hundredth of the combustible content e_d referred to the dry coal material.

As a result of the change in moisture content, the mass also changes. Mass recovery m_h vs. moisture content is as follows:

$$m_h = \frac{100 - W_r}{100 - W} \ . \qquad (5)$$

According to the equation, the change of mass extraction is described by an equilateral hyperbola. With a moisture content of W = 0, $m_{hd} = (100 - W_r)/100$ where m_{hd} is mass recovery of

the extract content. It follows from a comparison of Eqs (3) and (5) that the relation between the ash content and the mass recovery is:

$$m_h A = A_r \qquad (6)$$

i.e. the product of the mass recovery resulting from the varying moisture content and the ash content equals to the test ash content to be cosidered as constant.

3. CHANGE OF THE CALORIFIC VALUE IN THE FUNCTION OF MOISTURE CONTENT

In addition to the test values, the heating value Q_r of the coals has been given with Eq. (1), the values of a and w included in it with Eq. (2). With a view to determine the calorific value vs. moisture content, the values of the latter factors are needed.

If the moisture content of the coal changes from W_r to W and, together with this, the ash content changes from A_r to A, heating value Q valid for the latter case can be calculated by substituting Eq. (3) into Eq. (1):

$$Q = Q_o - \frac{100\ a\ A_r}{100 - W_r} - \left(w - \frac{a\ A_r}{100 - W_r} \right) W = Q_o - a\ A_d - w'\ W\ . \qquad (7)$$

According to this equation the calorific value vs. moisture content changes according to a straight line of negative direction factor the ordinate intercept of which is the first two terms of Eq. (7), calorific value Q_d of the moisture-free coal. This calorific value, considering the value of a according to Eq. (2) is as follows:

$$Q_d = Q_o - \frac{100\ a\ A_r}{100 - W_r} = Q_o \frac{100 - (g\ A_r + W_r)}{100 - W_r} - \frac{100\ g\ A_r}{100 - W_r} k\ . \qquad (8)$$

In Eq. (7), multiplier w' of the moisture content W means the change in calorific value resulting from a 1 % change of moisture content. This w' multiplier, by the substitution of a and w, is

$$w' = w - \frac{a\,A_r}{100-W_r} = \frac{Q_o}{100} \cdot \frac{100 - (g\,A_r + W_r)}{100 - W_r} - \frac{g\,A_r}{100-W_r}\,k + 24.62\ . \qquad (9)$$

In the previous two equations the multiplier of Q_o and $Q_o/100$ is equally the waste and moisture-free coal content referred to the extract content and this is denoted by e_{gd}. In the same equations the multiplier of k is the waste content of the dry coal material: gA_d. With regard to these quality parameters substituting Eqs (8) and (9) into Eq. (7) in function of the moisture content, the calorific value can be described as follows

$$Q = \frac{e_{gd}}{100}\,Q_o - g\,A_d\,k - \left(\frac{e_{gd}}{100}\,\frac{Q_o}{100} - \frac{g\,A_d}{100}\,k + 24.62\right)W = Q_d - \frac{Q_d}{100} + 24.62\ \ W\ . \qquad (10)$$

The change of Q calorific value vs. moisture content W according to Eq. (1) can be described with a straight line of negative direction factor the intercept y of which is heating value Q_d of the moisture-free (W = 0) coal material, the value of the direction factor is the sum of the hundredth part of this heating value and the evaporation heat. The moisture free coal material consists of two parts: e_{gd} combustible material and $g\,A_d$ waste content. The sum of these is 100 %. The thermal energy $e_{gd}\,Q_o/100$ represented by the combustible material is reduced by $g\,A_d k$, that is, the thermal energy necessary to burn the ash-forming waste minerals if it is an endothermic burning process.

4. CHANGE OF TOTAL ENERGY IN THE FUNCTION OF MOISTURE CONTENT

Equations (7) and (10) express the thermal energy of the material of unit mass. However, when the moisture content changes, the mass also changes and thus the absolute value of the thermal energy available is equal to the product of the mass extraction and the calorific value. Total energy ΣQ of the coal of 1 kg mass and W_r moisture content can be written by using Eqs (5), (7) and (10) if its moisture content changes to W and therefore its mass also changes:

$$\Sigma Q = m_h\, Q = \frac{100-W_r}{100-W}\left[Q_o - \frac{100\ a\ A_r}{100-W_r} - \left(w - \frac{a\ A_r}{100-W_r}\right) W\right] = \tag{11}$$

$$= \frac{100-W_r}{100-W}\left[Q_d - \left(\frac{Q_d}{100} + 24.62\right) W\right].$$

Thus the change of total thermal energy vs. moisture content is expressed by a general hyperbola. Besides, its volume is also affected by moisture W_r and calorific values Q_d in a way to be determined by means of Eq. (11). In case of a moisture content of zero, the value of the energy is

$$\Sigma Q_d = \frac{100-W_r}{100}\, Q_d = m_{hd}\, Q_d\ , \tag{12}$$

that is, the product of the mass recovery and calorific value of the extract content.

By means of Eq. (10) and with regard to Q = 0, in case of a moisture content of

$$W_o = \frac{Q_d}{\frac{Q_d}{100} + 24.62} \tag{13}$$

the calorific value is zero.

The specific value of the total energy change which results from a 1 % change of the moisture content is:

$$\Sigma Q' = \frac{d\,\Sigma Q}{dW} = -\frac{2462\ (100-W_r)}{(100-W)^2}\ . \tag{14}$$

ΣQ has a negative sign. So the shape of function (11) expressing the total energy change between moisture contents 0 and W_o, is convex from above, so with a decreasing moisture content, the specific energy change gets smaller and smaller. $\Sigma Q'$ is independent of the calorific value.

The energy change is the greatest in case of a moisture content W according to Eq. (13)

$$\Sigma Q' = -\left(\frac{Q_d}{100} + 24.62\right)^2 \frac{100-W_r}{2462}\ . \tag{15}$$

With a test moisture content $W = W_r$, the value of the specific change is

$$\Sigma Q' = \frac{2462}{100-W_r} . \qquad (16)$$

According to this equation, at the beginning of the dewatering process, the higher the moisture content of the run-of-mine coal is, the higher is the value of the specific change. The degree of change is always higher than the evaporation heat if $W_r > 0$.

$$\Sigma Q' = - \frac{2462}{10^4} (100-W_r) . \qquad (17)$$

On the other hand, according to this latter function, in case of a zero moisture content the change decreases linearly with W_r. In case of moisture contents of zero or low values, the specific value of the total energy change is at the same time lower than the evaporation heat if $W_r > 0$. Because of all these facts, it is practicable to determine a moisture content W_p where the concerning specific energy change is exactly the same as the evaporation heat. Substituting $\Sigma Q' = 24.62$ into Eq. (14)

$$24.62 = - \frac{2462\ (100-W_r)}{(100-W_p)^2} . \qquad (18)$$

In this equation W_p is the moisture content where thus the specific energy change equals to the evaporation heat

$$W_p = 100 - 10\sqrt{100-W_r} . \qquad (19)$$

As this latter function shows, $W_r = 0$ and in case of its 100 % value $W_p = W_r$; with $0 < W_r < 100$ %, $W_p < W_r$.

The most important rules of energy change can be summarized according to the above. With the decrease of moisture content, the total thermal energy increases so that the value of its specific change continuously decreases. Although the absolute value of the energy is in a linear connection with the

calorific value Q and Q_d of the coal, the degree of change is independent of the heating value, it is only in connection with the initial and the momentary moisture contents.

In case of a well definable moisture content, the value of the specific change equals to the evaporation heat. In case of a lower moisture content, the energy change is less than the evaporation heat.

5. CONNECTION BETWEEN THE SPECIFIC BALLAST AND THE MOISTURE CONTENT

In the Hungarian practice, the utility value of coals is expressed with the specific ash value. Specific ash, as mentioned, means the ash mass in g per 1000 kJ. The wholesale price of thermal coals, in a way regulated by law, is specified in function of the specific ash value.

In the forthcoming, the relation between the specific ballast and the moisture content will be discussed. Specific ballast b_{rf} can be described as follows

$$b_{rf} = 10^4 \frac{A_r + z W_r}{Q_o - a A_r - w W_r} . \qquad (20)$$

The test moisture content W_r in the numerator appears in a product with z, $0 = z \leq 1$. If $z \leq 0$, the specific ash value is considered. If z = 1, the actual specific ballast can be determined, that is, the joint mass in g of the ash and water per 1000 kJ, b_{rf} as Eq. (20) shows is called modified specific ballast (Osváth and Pethő 1985). The denominator of the relation concerned is the calorific value Q_r according to Eq. (1).

If the moisture content of the coal changes, i.e., it has a moisture content W, its ash content is of the value according to Eq. (3), its calorific value is that according to Eqs (7) and (10). With regard to these facts,the dependence of the modified specific ballast of on the moisture content is expressed with the following equation:

$$b_f = 10^4 \frac{\frac{100\,A_r}{100-W_r} + \left(z - \frac{A_r}{100-W_r}\right)W}{Q_o - \frac{100\,a\,A_r}{100-W_r} - \left(w - \frac{a\,A_r}{100-W_r}\right)W} = 10^4 \frac{A_d + Z\,W}{Q_d - \left(\frac{Q_d}{100} + 24.62\right)W}, \quad (21)$$

thus the modified specific ballast changes vs. moisture content according to a general hyperbola. In Eq. (21) $Z = z - A^r/(100-W_r)$. The value of the function, with a moisture content of $W = 0$, is given by the quotient of the dry ash content and the heating value referring to the extract content, thus $b_{fd} = 10^4\,A_d/Q_d$. With the moisture content given by Eq. (3) belonging to $Q = 0$, the modified specific ballast approaches infinity.

Direction factor b_f, of Eq. (21) provides the specific change of the specific ballast depending on the moisture content

$$b'_f = 10^4 \frac{Z\,Q_d + \left(\frac{Q_d}{100} + 24.62\right)A_d}{\left[Q_d - \left(\frac{Q_d}{100} + 24.62\right)W\right]^2} \quad . \quad (22)$$

With the moisture contents possible in practice ($0 \leqq W \leqq W_o$) the direction factor is a positive value which is also inversely proportional to the square of the calorific value depending on the moisture content.

If the moisture content is $W = 0$, the directional tangent is

$$b'_f = 10^4 \frac{Z\,Q_d + \left(\frac{Q_d}{100} + 24.62\right)A_d}{Q_d^2} \quad . \quad (23)$$

With moisture W_o the value of b_f approaches infinity where the directional tangent is $b'_f = \infty$ by substituting the moisture content according to Eq. (13) into Eq. (22). The shape of function b_f in the moisture range of $0 \leqq W \leqq W_o$ is from above concave.

6. DETAILED STUDY OF HUNGARIAN TYPES OF COAL

In this section Hungarian coal types characterized with

data of Table I will be considered in more details.

Table II. Values of the parameters in connection with the change in moisture content

Type of coal	A_d	$e_d=\frac{e_r}{100-W_r}100$	m_{hd}	a A_d	$Q_d=Q_o-aA_d$	$w'\frac{Q_d}{100}$ + 24.62
Liassic	45.65	54.35	0.92	17393	17237	197.0
Eocene	32.14	67.86	0.84	10767	18564	210.3
Cretaceous	29.49	70.51	0.78	12681	18362	208.2
Miocene	35.14	64.86	0.74	9909	17153	196.1
Lignite	40.74	59.26	0.54	10592	14329	167.9

Table II contains the parameters connected to the change of ash- and ballast contents as well as of the calorific value, such as A_d ash contents referred to the extract content, e_d combustible contents and m_{hd} mass extraction, besides, the products ($a \cdot A_d$), Q_d calorific value of the dry coal material and finally directional tangents $w' = Q_d/100 + 24.62$. The sum of values A_d and e_d is 100 %. The Cretaceous coals of Ajka have the highest dry combustible contents, because of the high ash content, e_d value of the Liassic coals is the lowest. Apart from the latter, the dry combustible content of the other coals of Hungary ranges from 60 to 70 %. Due to the high moisture content, m_{hd} mass recovery of lignites is the lowest. The heat extraction of the waste in the coals is indicated by values a A_d referred to the dry ash content. Due to the high ash content, this is far the highest for the Liassic coals which, because of the great a parameter, are followed by the Cretaceous coals. Although the moisture- and ash-free coal material of the same coals has the highest Q_o calorific value, due to the great heat extraction of the waste rocks, it is still the Eocene coals which have the highest Q_d heating value (18564 kJ/kg). The others in succession are: Cretaceous, Liassic, Miocene coals and lignites. The order of succession of the change of w' calorific value belonging to 1 % change in the moisture content

as proved is the same as that of Q_d calorific values. The values of w' in case of the Hungarian coals range from 210 to 196 kJ/0.01 kg, this value for lignites is 168 kJ/0.01 kg.

The e_{gd} and g A_d values in Eq. (10) (the sum of these is also 100 %) have not been determined because of the uncertainty of the factors g (Takács 1985).

In Fig. 1 the straight lines referring to the change of the ash- and ballast contents in the function of the moisture content of lignites and a hyperbola showing the change in the mass recovery can be seen. Intercept y of both straights is 40.74 %, the dry ash content of lignites. With any value of moisture content content to be 100 %, the combustible content can be determined by supplementing the ballast. Mass recovery m_{hd} of the extract content is 0.54.

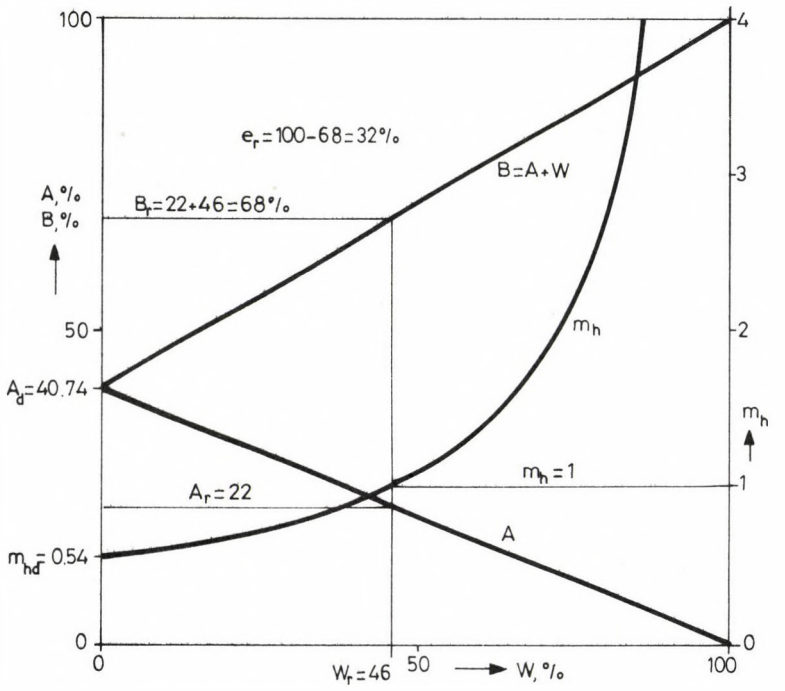

Fig. 1. Ash- and ballast contents as well as the mass recovery for lignites vs. moisture content

Figures 2 and 3 show the straight lines referring to the

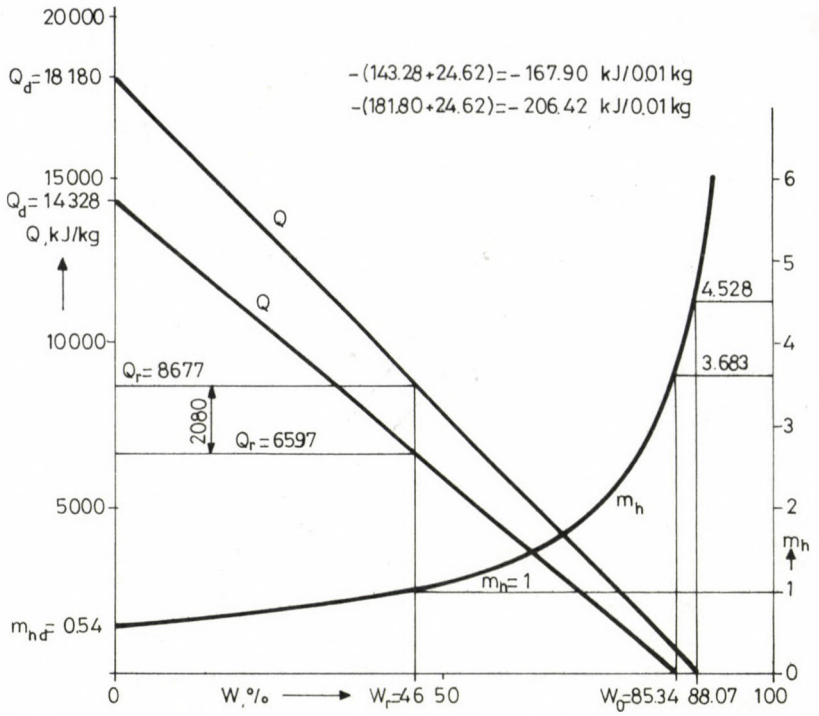

Fig. 2. Calorific value and mass recovery of lignites of different ash contents vs. moisture content

change in calorific value. Both figures show two straight lines. In Fig. 2, one of them has been plotted with the original selling properties of the lignite: W_r = 46 %, A_r = 22 % and Q_r = = 6597 kJ/kg. The so-called test values of the other straight line are: W_r = 46 %, A_r = 14 % and Q_r = 8677 kJ/kg, that is the raw material is of an 8 % lower ash content and of a 2080 kJ/kg higher calorific value. Figure 3 shows the change of calorific value resulting from the change in moisture content of Cretaceous coals. One straight line has also been drawn with the marketing data included in Table I: W_r = 22 %, A_r = 23 % and

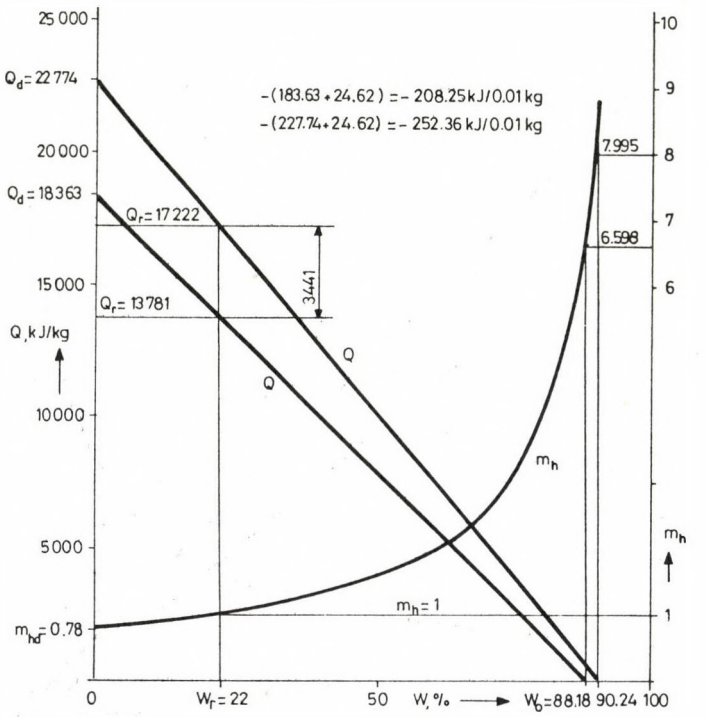

Fig. 3. Heating value and mass recovery of Cretaceous coals with different ash contents vs. moisture content

Q_r = 13781 kJ/kg. In the same figure the second straight line has also been plotted with the assumption of a raw material of an 8 % lower ash content. Thus the testing calorific value Q_r belonging to moisture W_r = 22 % and ash content A_r = 15 % is 17222 kJ/kg, by 3441 kJ/kg higher than the previous value. As it can be pointed out by means of relation (10) as well, with the preliminary reduction of the ash content, drying is more effective: the directional tangent showing the moisture content change of the higher quality raw materials is larger. If the burning heat k is great, such as, e.g. for the Hungarian Cretaceous coals shown in Fig. 3, by separating the waste content in advance, the moisture content can be reduced more effectively. Both figures indicate the change in mass recoveries as well and

the numerical values of mass recoveries where the calorific value is zero.

Table III shows all the parameters in connection with the energy change for the types of coals considered so far. These are energies ($m_{hd} \cdot Q_d$) belonging to the zero moisture content, moisture contents W_o belonging to zero heating value, the dimension of the same and, in case of the test moisture values, that of the directional tangent and finally those moisture contents W_p where the absolute value of the energy change is exactly the same as the evaporation heat. - According to the Table, if the moisture content is zero, the Liassic coals have the greatest thermal energy ($m_{hd} \cdot Q_d$ = 15859 kJ). The Eocene and Cretaceous coals have hardly lower energies than that and lignites have the lowest thermal energy (7737 kJ). Since lignites have the highest W_r test moisture content, it is this type of coal which has the highest initial energy change - that according to Eq. (16) - on the other hand, with a moisture content of zero, in case of the same coal the specific change calculable with Eq. (17) is the least.

Table III. Values of parameters in connection with the energy change

Type of coal	$m_{hd} Q_d$	W_o	$-\frac{2462}{10^4}(100-W_r)$	$-\left(\frac{Q_d}{100}+24.62\right)^2 \frac{100-W_r}{2462}$	$-\frac{2462}{100-W_r}$	W_p
Liassic	15859	87.50	-22.65	-1450	-26.76	4.08
Eocene	15594	88.27	-20.68	-1508	-29.31	8.35
Cretaceous	14322	88.19	-19.20	-1374	-31.56	11.68
Miocene	12692	87.47	-18.22	-1156	-33.27	13.98
Lignite	7737	85.34	-13.29	- 618	-45.59	26.52

Figure 4 shows all the energy changes for the types of coals also considered in Figs 2 and 3 in function of the moisture content. The functions 1 and 2 relate to the two lignites while curves 3 and 4 refer to Cretaceous coals. The types of coal of the same moisture content but of different ash contents maintain the differences in the calorific values during the

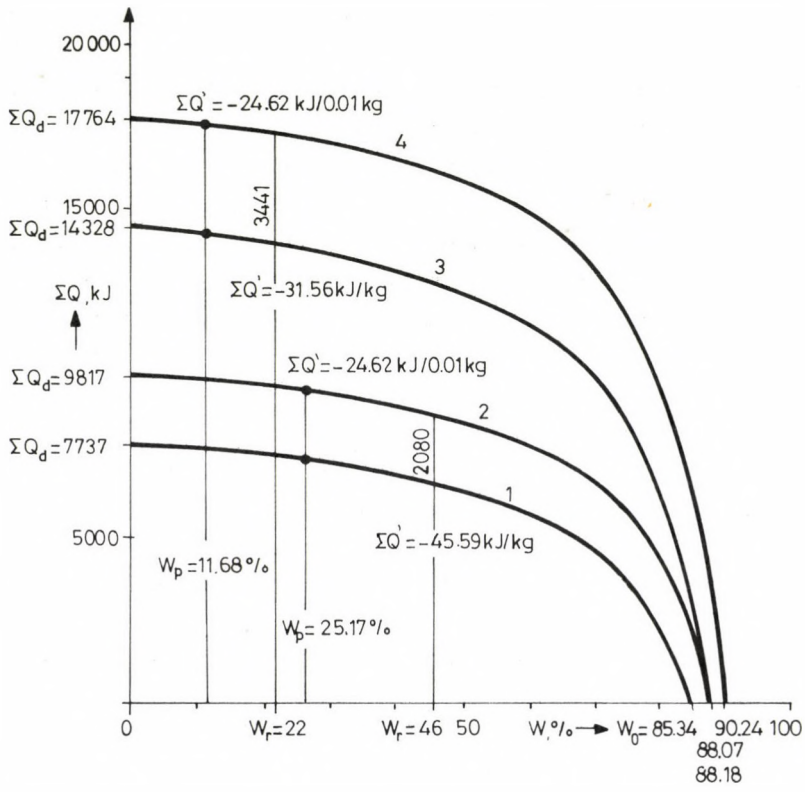

Fig. 4. Total thermal energy of lignites and Cretaceous coals vs. moisture content

change of moisture content. For instance, the difference of the calorific values of Cretaceous coals with 15 and 23 % ash contents and of 22 % moisture content is 3441 kJ/kg. If the moisture content is higher or lower than this, the thermal energy difference remains the same.

In case of lignites, the thermal energy increase is relatively large due to the high moisture content, during the dewatering processes. This particularly holds true for peats. If the high moisture content is connected to high calorific value of the pure coal material, with the decrease of the moisture content, while the calorific value rises, the total thermal energy increase is also considerable.

Figure 5 shows for lignites of 22 and 14 % ash contents,

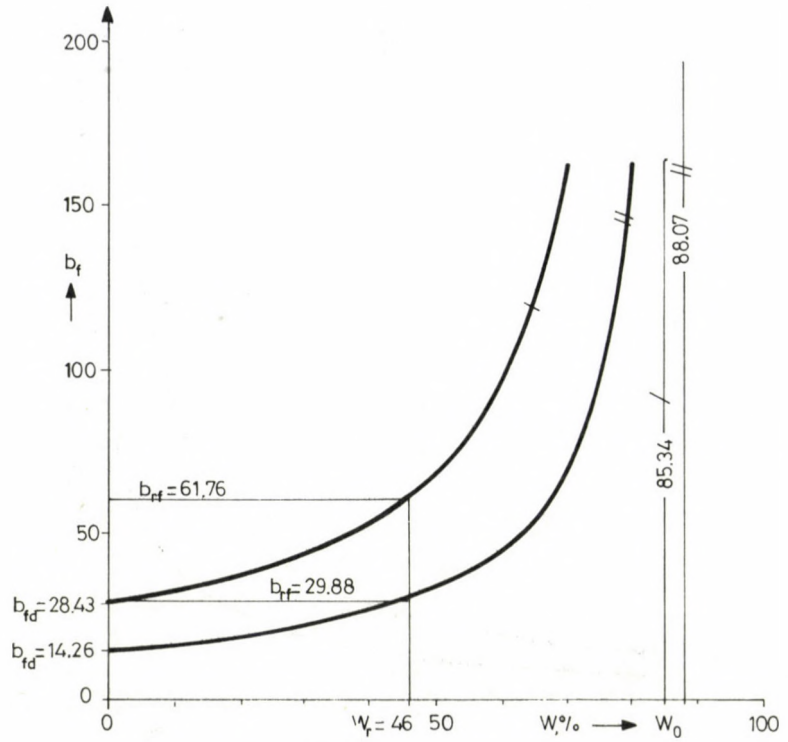

Fig. 5. Modified specific ballast vs. moisture content for lignites of different ash contents

Fig. 6. for Cretaceous coals of 23 and 15 % ash contents, the change of b_f modified specific ballast vs. moisture content. For plotting the curves, Z to be found in Eq. (21) has been chosen to be zero, therefore in the same relation, z the multiplier of the moisture content

$$z = \frac{A_r}{100-W_r} = \frac{A_d}{100} \tag{24}$$

is one hundredth of the dry ash content. The curves in Figs 5 and 6 correspond to function

$$b = 10^4 \frac{A_d}{Q_d - \left(\frac{Q_d}{100} + 24.62\right) W} \tag{25}$$

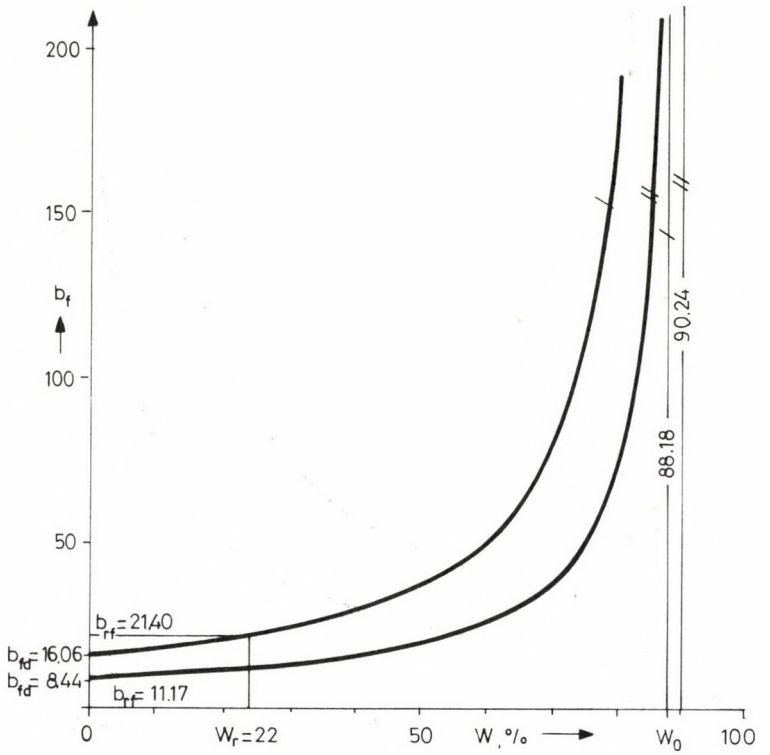

Fig. 6. Modified specific ballast vs. moisture content in case of Cretaceous coals of different ash contents

which means they are equilateral hyperbolas vs. moisture content. The curves and the numerical values also show the effect of ash content on the modified specific ballast as Eq. (25). E.g., if W_r = 46 %, the modified specific ballast of the lignites with two different ash contents will be 61.76 and 29.88 respectively; the same values in dry condition are 28.43 and 14.26.

7. SUMMARY OF THE BASIC RELATIONS AND RULES IN CONNECTION WITH THE CHANGE OF MOISTURE CONTENT OF COALS

In function of the moisture content, the ash content of coals changes according to a straight line of negative

inclination while the ballast content, that is the sum of the ash- and moisture contents changes according to a straight line of positive inclination. The ordinate intercept of both straight lines is the ash content of the dry coal material. The directional factor of the straight line relating to the ash content is a hundredth of the previous dry ash content, that of the straight line describing the change in ballast content is one hundredth of the combustible content of the dry coal material. - The mass recovery changes vs. moisture content according to an equilateral hyperbola.

In connection with the change of calorific value and the total thermal energy, regularities have been determined as follows:

The change in calorific value vs. moisture content is described by a straight line of negative inclination, the ordinate intercept of which is the calorific value of the moisture-free coal while the inclination is the sum of one hundredth of this calorific value and the evaporation heat (24.62 kJ/0.01 kg).

The product of the mass recovery and the calorific value that is the total thermal energy changes vs. moisture content according to a general hyperbola so that with a decreasing moisture content the degree of energy increase is gradually less. Its value depends on the moisture content obtained during the dewatering process, the initial moisture content of the raw material as well as on the calorific value of the dry coal material. On the other hand, the specific value of the total energy change is independent of the heating value of the dry coal material, it is only the function of the obtained and the initial moisture contents. The higher the value of the initial moisture content of the coal is, the higher is the value of specific energy increase at the beginning of the dewatering process. However, this specific change gradually decreases as the moisture content decreases; at a given moisture content it is equal to the evaporation heat, near a moisture content of zero, it is generally much lower than the evaporation heat. With a moisture content of zero, the specific value of energy increase linearly decreases vs. initial moisture content.

On the basis of the above, quality improvement by reducing the moisture content (dewatering, drying in heat, dehydration) are only effective if, in addition to the high water content, the combustible content referred to the dry coal material is also high and this dry coal material has at the same time a high calorific value. If the coal has high waste content or the burning heat k of the waste is high, with the preliminary removal of the waste, the efficiency of dewatering improves.

The relations deduced in this paper and the rules determined by means of them refer to a mechanical water removal. As shown by general practice, the quality parameters of coals after dehydration are better, when drying in heat they are behind the results achieved with mechanical dewatering.

REFERENCES

Bőhm J, Csőke B, Schultz Gy, Tompos E 1984: Mineral dressing measurements and laboratory practices. Manuscript. Educational Publishers, Budapest

Káplár Zs 1968: Journals of Mining and Metallurgy, Mining, 101, 182-189.

Osváth I, Pethő Sz 1985: Journals of Mining and Metallurgy, 9, 584-586.

Takács P 1985: Referee's comment. Manuscript

Acta Geod. Geoph. Mont. Hung., Vol. 24 (1-2), pp. 175-184 (1989)

ANALYSIS OF RHEOLOGICAL FEATURES FOR THE REGULATION OF HYDRAULIC CHARACTERISTICS OF NON-NEWTONIAN OILS

T Sh Salavatov[1], G M Panahov[2], T Bódi[3]

[1]Petroleum Engineering Department, "Azizbekov" Azerbaidjan Institute of Petroleum and Chemistry, Baku, Scientific Probationer of Petroleum Engineering Department, Technical University for Heavy Industry, H-3515 Miskolc, Egyetemváros, Hungary

[2]Petroleum Engineering Department, "Azizbekov" Azerbaidjan Institute of Petroleum and Chemistry, Baku, USSR

[3]Petroleum Engineering Department, Technical University for Heavy Industry, H-3515 Miskolc, Egyetemváros, Hungary

[Manuscript received June 23, 1987]

The present paper gives experimental data on the effect of different patterns of pressure application on the rheological properties of non--Newtonian crude oils.

The evaluation of the changes in rheological behaviour was based on measurements carried out with rotational viscometers.

Keywords: barotreatment; changes; depressurizing; non-Newtonian crude oils; rheological properties; pressurizing

1. INTRODUCTION

One way of increasing the technological efficiency of oil production and transport processes of non-Newtonian oils is the regulation of rheological properties. An improvement in rheological properties can be reached by using methods as thermal treatment, barotreatment, preheating, pumping over in hot conditions and others (Mirzadjanzade 1976, 1977, Mirzadjanzade et al. 1973, 1984, 1985, Szilas 1985, 1986, Mamedzade and Makhmud--Il-Batanauni 1982).

Previously proved facts on changes of rheological properties and their regulation forms by pressure treatment necessitate to study peculiarities of barotreatment in case of both pressure increase and decrease (Mirzadjanzade et al. 1985).

They are firstly connected with the appearance of different conditions such as stopping or pipeline diameter changes,

through which a certain pressure drop in the system takes place; on the other side with situations when the well is starting slowly, i.e. gradual depressurizing in the flow line.

2. EXPERIMENTAL RESULTS

An experimental installation was set up consisting of a high pressure bomb (pVT) - 2, a liquid container - 1, a hand pump - 3, pressure gages - 4, needle valves - 5, a thermostat - - 6, a glycol container - 7, and a vacuum pump - 8 (Fig. 1).

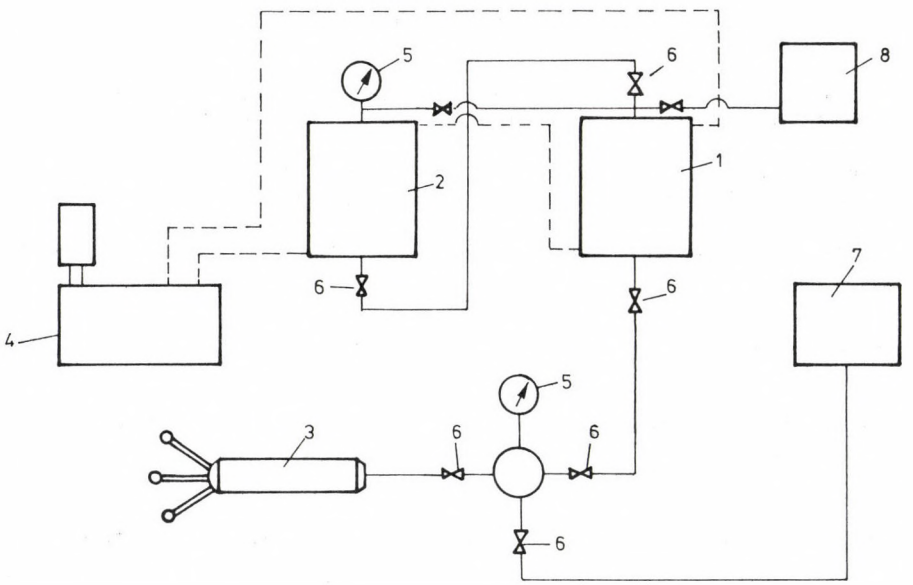

Fig. 1. Schematic experimental setup

Oils from Mishovdag and Kyursangya Oil Fields (Oil Department of Azerbaidjan-USSR, Shirvanneft), with remarkable high contents of bitumen (correspondingly up to 16.3 % and 7.56 %), and asphaltenes (up to 4.56 % and 3.91 %) and parafines (up to 3.98 % and 3.54 %), were used in the experiments.

With the aim of eliminating the influence of gas and air

on the barotreatment process, the oils were carefully vacuumed in the bomb pVT-2 for over 2 hours.

This process was followed by thermostation of the whole system at t = 295 K.

The pressure in the system was created by nearly momentanous feeding under the working liquid piston with the help of a hydraulic pump.

The pressure was recorded in the system by a high accuracy gage with an upper limit 10 MPa and a scale point $3.33 \cdot 10^{-2}$ MPa.

Having reached the pressure of 10 MPa in pVT-2 its lower bomb valve was closed and gage-5 showed some pressure-fall P = P(t) within 660 sec. Without waiting for the pressure to stabilize, the system was pressurized up to 10 MPa for the second time. Again a pressure fall was recorded but it was less than previously. This cycle was repeated several times.

After a certain cycle (in our case after the 8th), no further pressure fall was recorded. The oil was then considered to be barotreated.

In Fig. 2 the results of pressure treatment are given for the barotreatment of the oil from the Mishovdag layer.

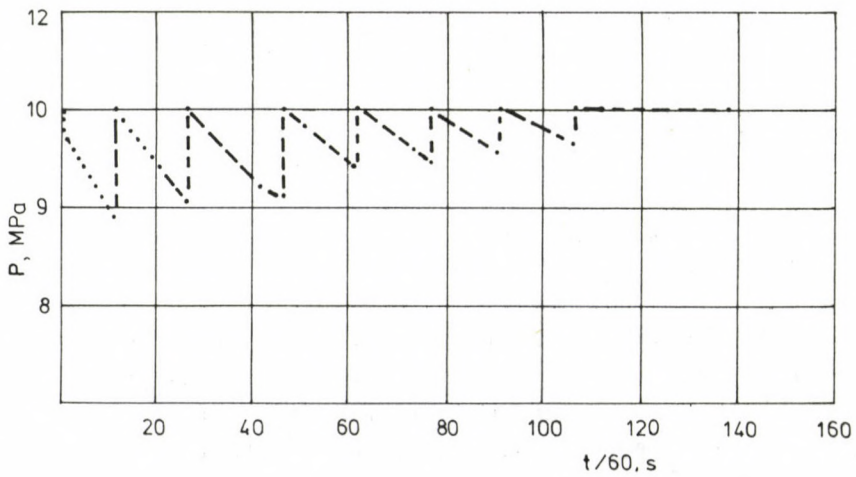

Fig. 2. Pressure changes after consecutive pressurizing of oil from the Mishovdag field

The oil sample was then barotreated by decreasing the pressure in pVT-2. In this case the experimental condition (i.e. oil thermostating and vacuuming) were the same as previously.

The pressure in the bomb pVT-2 was in this case the same as in the first cycle of the previous experiment, then the system was depressurized to a certain point within a few seconds, at last valve-6 was closed.

Gage-5 recorded an increase in the pressure for several minutes. Later on the system was again depressurized to a certain point and the pressure changes were again recorded.

This was continued in several cycles until achieving a minimum pressure value (Fig. 3).

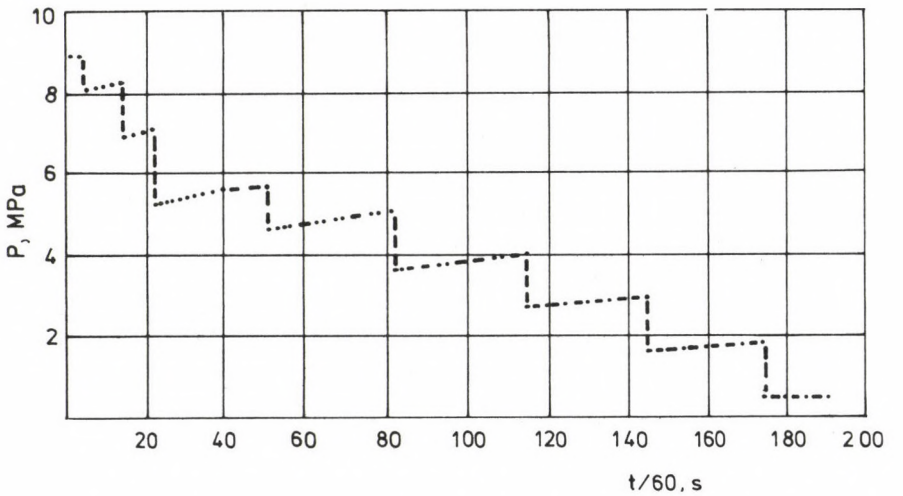

Fig. 3. Pressure changes after consecutive depressurizing of oil from the Mishovdag field

Several series of experiments were carried out on the rheological properties of non-Newtonian oils. Figures 4 and 5 give results obtained with the rotation viscosimeter Rheotest-2. A depressurizing of the system improved rheological characteristics (curve 3) to a greater extent then pressurizing (curve 2).

The changes of viscoelastic properties of the system were estimated by Cross' method (1968). The effective viscosity is

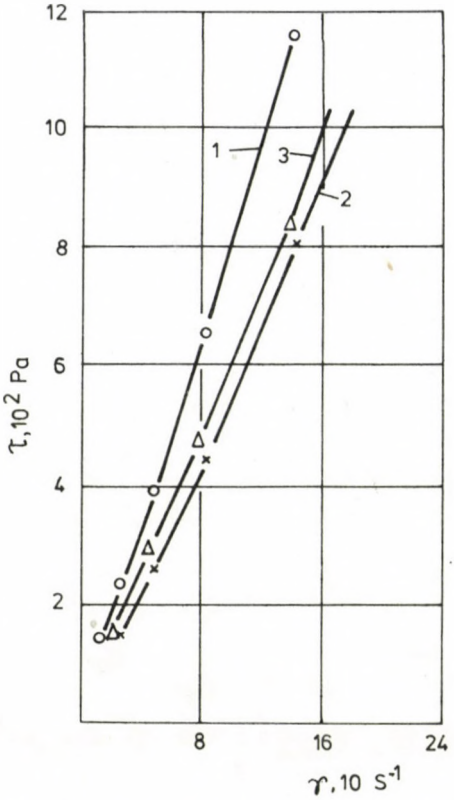

Fig. 4. Function $\tau = \tau(\dot{\gamma})$ for Mishovdag Oil

obtained by $\eta_{ef} = \tau_{12}/\dot{\gamma}$ vs. shear rate $\dot{\gamma}$ in the form

$$\eta_t = \eta_{ef}\left(1 + \frac{\tau_{12}^2}{4\,G^2}\right)^{1/2}$$

where G is the modulus of liquid elasticity. In an other form:

$$\frac{1}{\eta_{ef}^2} = \frac{1}{\eta_t^2} + \frac{\tau_{12}^2}{4\,G^2\,\eta_t^2}\,.$$

The formula shows that the results of rheological studies in coordinates $1/\eta_{ef}^2 - \tau_{12}^2$ correspond to straight lines, from

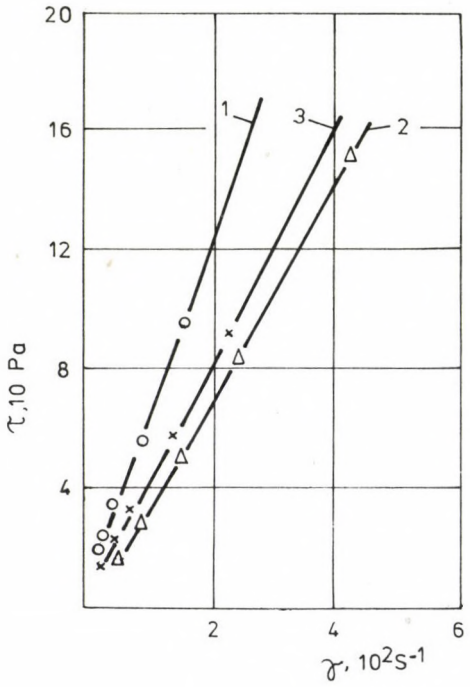

Fig. 5. Function $\tau = \tau(\dot{\gamma})$ for Kyursangya Oil

which the viscosity factor η_t and the elasticity modulus G can be found. The parameter continuity is in agreement with the linear viscoelastic liquid model. The results are given in Figs 6 and 7. The system revealed after barotreatment by pressurizing mainly Newtonian properties (curve 2, Figs 6 and 7), while after barotreatment by depressurizing, properties were better and only the nonlinear viscoelasticity was kept (curve 3, Figs 6 and 7). In the same way relaxation periods of these oils before and after barotreatment were estimated.

The relaxation period (Θ) was determined by Mukuk's (1980) method. The results are given in Table I. They show that the system can be barotreated by pressurizing or depressurizing. Here a question arises: does barotreatment take place by itself or only while operating the oil pump? This question can be answered by comparing the rates of pressure changes in the

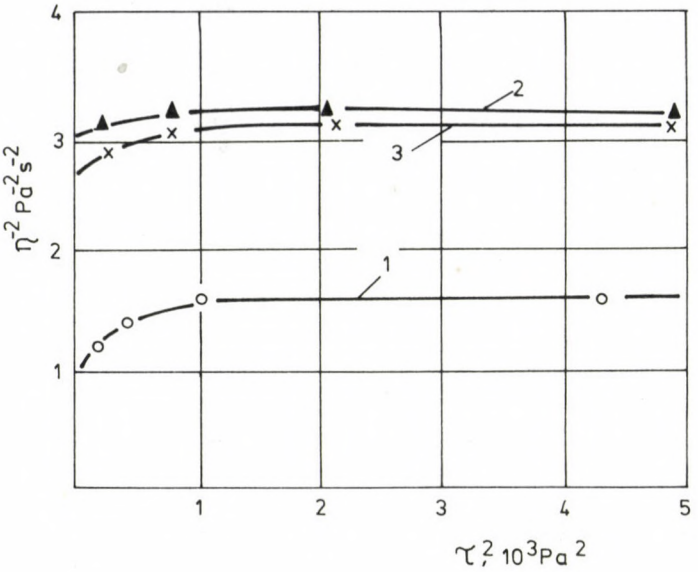

Fig. 6. Results obtained by Cross' method in the viscosimeter for the Mishovdag oilfield. 1 - before barotreatment, 2 - after pressurizing, 3 - after depressurizing

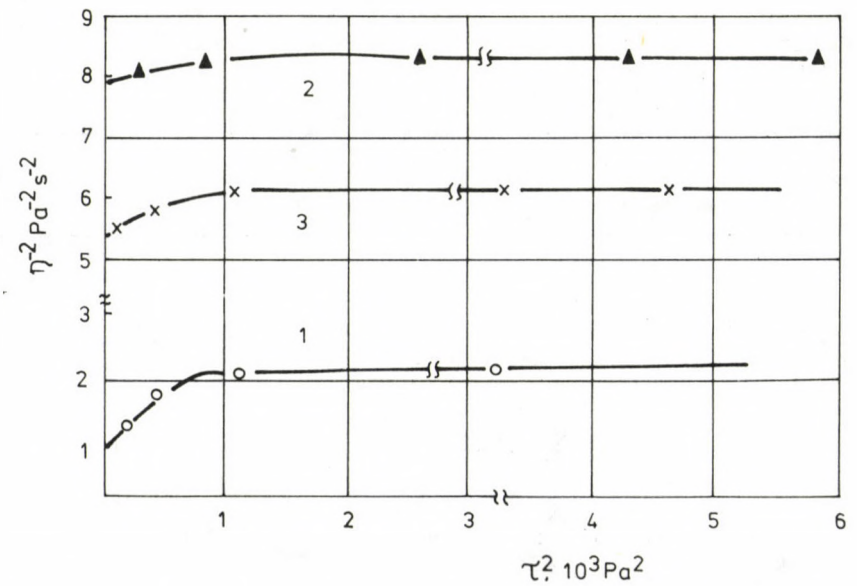

Fig. 7. Results obtained by Cross' method in the viscosimeter for the Kyursangya oilfield. 1 - before barotreatment, 2 - after pressurizing, 3 - after depressurizing

Table I

Crude types	Before treatment			After barotreatment by pressurizing			After barotreatment by depressurizing		
	η_t Pa s	G Pa	Θ 10^{-2}s	η_t Pa s	G Pa	Θ 10^{-2}s	η_t Pa s	G Pa	Θ 10^{-2}s
Kyursangya Oil Field	0.817	37.5	2.2	0.356	98.8	0.4	0.423	59.2	0.8
Mishovdag Oil Field	0.913	30.0	3.0	0.577	76.0	0.8	0.603	54.7	1.1

experimental pressure bomb and in actual transportation.

Table II contains data measured in an operating pipeline.

Table II

Length of the pipeline 10^3 m	Diameter of the pipeline m	Flow rate m^3/s	Flow velocity m/s	Oil density kg/m^3	Reynolds number	λ	p MPa
222	1.020	0.452	0.553	830	3902	0.04	1.106

The time of pressure changes in the pressure bomb and in the pipeline were calculated by the equation:

$$\frac{dp}{dt} = \frac{\partial p}{\partial x} v + \frac{\partial p}{\partial t} .$$

The results for the oil pipeline are:

$$\frac{dp}{dt} = \frac{1.106}{2.22 \cdot 10^5} \cdot 0.553 = 0.276 \cdot 10^{-5} \text{ MPa/s}$$

for the pressure bomb in case of pressurizing:

$$\frac{dp}{dt} = \frac{4.7}{140 \cdot 60} = 0.560 \cdot 10^{-3} \text{ MPa/s}$$

and for the pressure bomb in case of depressurizing:

$$\frac{dp}{dt} = \frac{2.0}{200 \cdot 60} = 0.170 \cdot 10^{-3} \text{ MPa/s} .$$

Thus the pressure in the pressure bomb and in the pipeline differ by two or more orders of magnitude.

Results for an oil from Sávoly (Hungary) are given in Fig. 8. In this case measurements were carried out with a rotational viscometer "HAAKE RV-11".

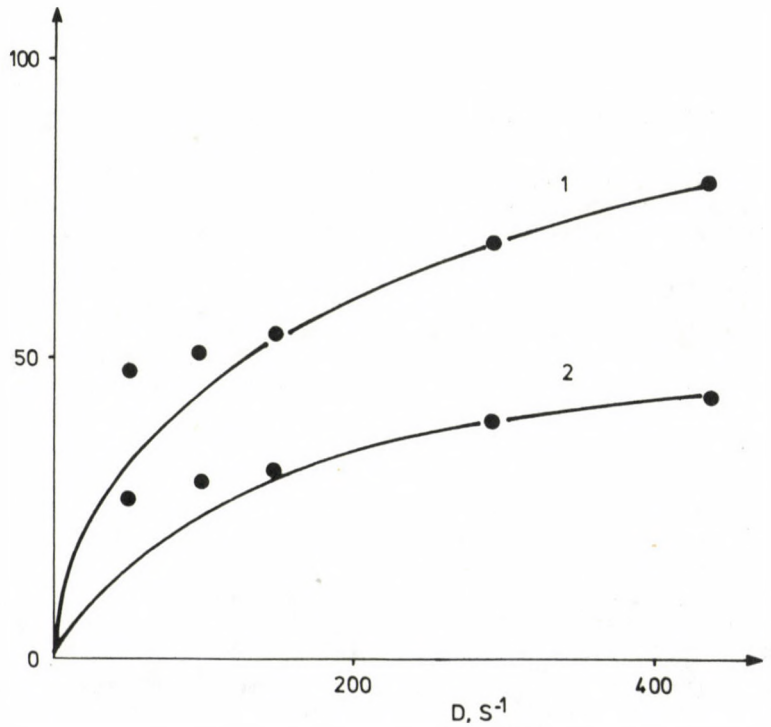

Fig. 8. Function $\tau = \tau(D)$ for Sávoly Oil. 1 - before barotreatment, 2 - after barotreatment

3. CONCLUSIONS

The present results suggest to use an oil transport technology which assures the required barotreatment of the transported crude, as it will increase the effectivity of pipeline transport operations.

The evaluation of the phenomena described in this article needs further investigations. First of all the role of the paraffins seems to be important. The research is continued and the results will later be published.

ACKNOWLEDGEMENT

The task was put and carried out under the guidance of Professor A Kh Mirzadjanzade.

REFERENCES

Cross M 1968: Journal of Colloid and Interface Science, 27, 84-90.

Mamedzade R Bu, Makhmud-Il-Batanauni 1982: In: Gasohydrodynamic foundation analysis of oil and gas field exploitation. Ed.: Azerbaidjan Institute of Oil and Chemistry, Baku, 16-18.

Mirzadjanzade A Kh 1976: Studies of kinetic effects in viscoelastic systems. Neft i gas (Oil and Gas)

Mirzadjanzade A Kh 1977: Changes of rheological characteristics of non-Newton systems within pressure treatment. Rheology (polymers and oil) Institute of Thermal Physics, Novosibirsk

Mirzadjanzade A Kh, Kovalev A G, Zaitsev J V 1973: Exploitation Peculiarities of abnormal Oils (in Russian). M. Nedra

Mirzadjanzade A Kh, Galyamov A K, Maron V I, Yufin V A 1984: Hydrodynamics of pipeline oil transport and oil products (in Russian). M. Nedra

Mirzadjanzade A Kh, Maksudov F K, Nigmatulin R I, Salavatov T Sh 1985: Theory and practice of application of unequal systems in oil production. Baku, "Elm"

Mukuk K V 1980: Elements of relaxing anomalous systems. Hydraulics. Tashkent, edit. "Fan" Uz.SSR

Szilas A P 1985: Production and transport of oil and gas (Part A). Akadémiai Kiadó, Budapest

Szilas A P 1986: Production and transport of oil and gas (Part B). Akadémiai Kiadó, Budapest

Acta Geod. Geoph. Mont. Hung., Vol. 24 (1-2), pp. 185-194 (1989)

REDOX POTENTIAL MEASUREMENTS AS A METHOD FOR THE INVESTIGATION OF THE STATE OF CARBONIZATION

J Milley-Tóth[1] and M Hetényi[2]

[1]Research Laboratory for Mining Chemistry of the Hungarian Academy of Sciences, H-3515 Miskolc, Egyetemváros, Hungary

[2]Department of Mineralogy, Geochemistry and Petrology of József Attila Scientific University, H-6701 Szeged, POB 651, Hungary

[Manuscript received October 15, 1987]

The theoretical bases and the practical method of the redox potential measurements had been summarized by J Milley (1985) including the general fields of the applicability.

In this work special attention was paid to the investigation of the degree of carbonization. For this reason the most characteristic values of the redox potential curves were compared with the results of Rock-Eval measurements, and coal petrological data (huminite or vitrinite reflection) - these values are generally accepted for the determination of the state of carbonization - to give evidence for the applicability of this method for coal-geochemical investigations.

Keywords: carbonization; coal petrology; huminite; redox potential; vitrinite

SYMBOLS

A	integral value of the redox potential curves, h·mV
E	redox potential, mV
t_i	time of the inflection point in the redox potential curves, min
T_{max}	temperature of maximum of hydrocarbon generation during pyrolysis in Rock-Eval measurements, ^oC
A^a	ash content, w %
W^a	humidity content, w %
C^a	organic carbon content, w %
H^a	hydrogen content, w %
ϱ	specific gravity, g/cm^3
$\bar{R}_m$ %	mean huminite or vitrinite reflection
t	time, min or h

Recently a lot of efforts have been made to replace the very tedious and often time consuming analyses of coals (C, H, S, O analysis, determination of volatiles, ash and humidity content, measurement of the reflections of the coal minerals, etc.) by modern methods for classifying, qualifying, ranking of

coals, and determination of their degree of carbonization. These methods, however, usually require expensive instrumentation (Rock-Eval apparatus) and sometimes serious preparative work (Verheyen et al. 1984).

Measurements of the redox potential to determine rock characteristic in sediment petrology were firstly applied by Krumbein and Garrels (1948). Somewhat later a Russian school was established for this method, especially Pustovalov and Sokolova (1957). The general of these measurements is Nernst's law. For the measurements Pt or Au were used as measuring electrodes, and calomel as a reference one. They were put into the wetted rock powders, and the change of the redox potential was measured vs. time, until equilibrium was reached.

Bod and Bárdossy (1959) introduced in Hungary a new method using an aqueous solution of a strong oxidizing agent, and from the change of the redox potential of the solution in time, a general idea about the oxidizing process could be obtained.

This method was applied for coals by Kossuth (1982). The redox potential measurements were developed and the measuring technique was improved and refined in our laboratory (Milley 1985), so that it became applicable for the general qualification of coals being in different chemical, physical state. The accuracy and reproducibility have been increased so that chemically and/or physically treated coal samples can be distinguished even if they originated from the same source and had the same maturity.

EXPERIMENTAL

For redox potential measurements an aqueous solution of $K_2Cr_2O_7/H_2SO_4$ was used as oxidizing agent, and they were carried out with on OP-208/1 Precision Digital pH Meter (Radelkis). The data were printed by a data logger. Saturated calomel and PT electrodes were used as reference and measuring ones, respectively. The measurements were made in a thermostated, closed vessel which had two tube connections for the electrodes and one to introduce the sample. For thorough mixing of the solvent-

-coal suspension during the measurement a magnetic stirrer was used.

Before the measurements the coal samples were ground and sieved. Because the redox potential curves are different for different particle sizes, the same fraction of particle sizes was used during one run of measurements.

A Girde Type Rock-Eval apparatus was applied for the pyrolysis of the coals. The samples were put into the boat without any preparation, except sieving, particle size $< 63\ \mu m$. The measurements were performed under the same conditions described by Verheyen et al. (1984). The only difference was that the CO_2 trap was closed at 390 ^{o}C.

The C and H analyses needed to the Rock-Eval investigations were made on a Hewlett-Packard C, H, N analyser Type 185 B.

The coal petrological investigations were carried out on polished microsection with coal material ground to 1 mm particle size using a Reichert Zetopan Type Microphotometric Microscope magnified 400-600 times.

All chemicals used were of analytical grade.

RESULTS AND DISCUSSION

The most characteristic numerical values of the redox potential curves are: 1. the time (in minutes) at which the inflection point is reached; 2. the integral value of the curves.

As the first step the results for four coals of different carbonization states are given in Figs 1-3 and in Tables I-II, comparing the most characteristic values of the redox potential curves with the results of Rock-Eval pyrolysis (T_{max}). Figure 1 shows that with increasing degree of carbonization the inflection points of the redox potential curves are shifted to longer times. In Fig. 2 the relationship between the time of inflection and T_{max} is shown, while in Fig. 3 the relationship between the integral values of curves and T_{max} from the Rock-Eval measurements is indicated.

The numerical data to Figs 2-3 are summarized in Table I.

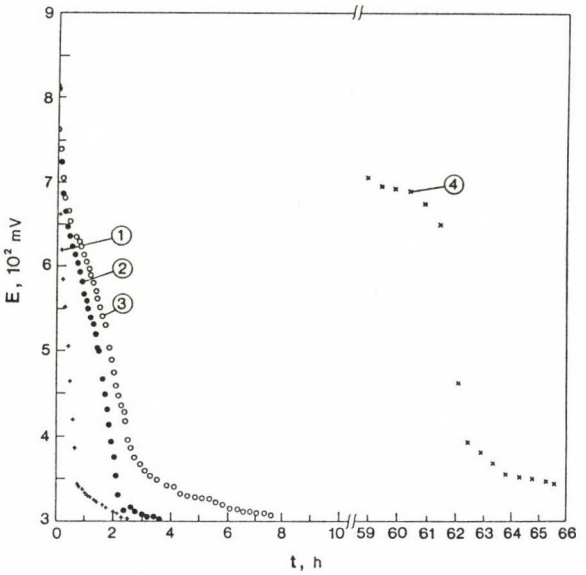

Fig. 1. Redox potential curves of coals of different geological age. Curve 1: lignite from Gyöngyösvisonta, Pliocene; Curve 2: brown coal from Lyuko, Miocene; Curve 3: brown coal from Tatabánya, Eocene; Curve 4: black coal from Pécs, Jurassic. The curves were measured on particle size below 71 μm

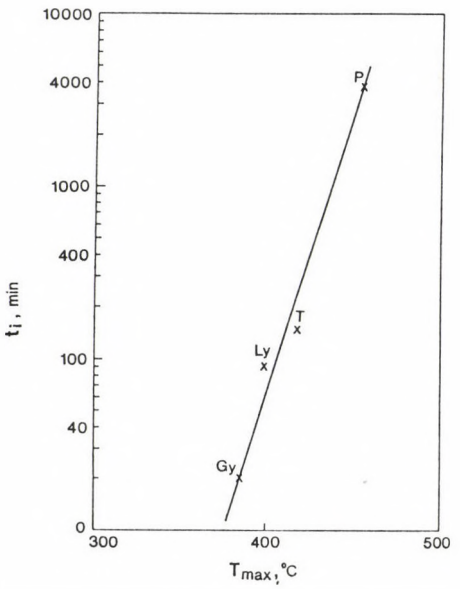

Fig. 2. Relationship between t_i and T_{max}

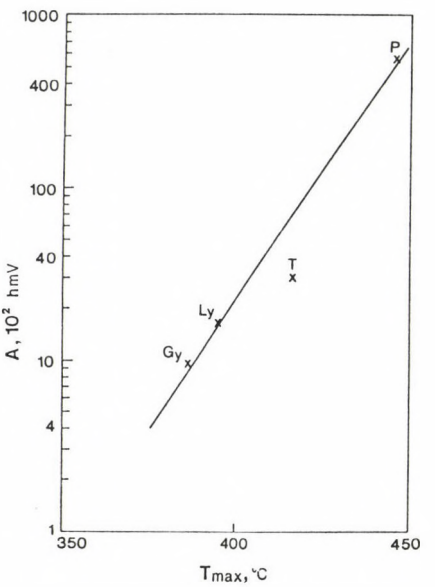

Fig. 3. Relationship between A and T_{max}

Table I. Characteristic values of the redox potential curves and the values of the Rock-Eval measurements for the samples of Fig. 1

Age of samples	A, h·mV	t, min	T_{max}, ^{o}C
1. Pliocene	960	20	385
2. Miocene	1617	90	395
3. Eocene	2987	150	417
4. Jurassic	54100	3700	446

Table II. Analytical values for the samples, used in Fig. 1

Age of samples	A^a, %	W^a, %	C^a, %	H^a, %	ϱ, g/cm^3
1. Pliocene	17.3	11.0	50.4	4.7	1.5467
2. Miocene	9.2	8.0	58.2	4.5	1.5216
3. Eocene	20.1	11.5	49.6	3.7	1.5093
4. Jurassic	21.4	1.5	60.9	3.7	1.5057

Table II contains some analytical data of coals regarding to Fig. 1.

From Figs 1-3 and from Table I a definite relationship between the values of the redox potential curves and the data of Rock-Eval pyrolysis (T_{max}) can be seen, but the data in Table II do not give a basis for a well defined relationship with the redox potential curves.

From these facts it can be seen that the main character of the coals affecting the place (in time) of the redox potential curves is the state of carbonization.

This run of measurements was made with a particle size < 63 µm. In another investigation the results of coal petrological measurements were compared with the character of the redox potential curves. A short description of the coal petrological characteristic:

1. Lignite from Gyöngyösvisonta: bituminous wood, earthy, soft coal of Pliocene age, with fractions of detrital texture. Medium quantity of wooden telite is present in the form of mediotelite. The degree of carbonization is low. The huminite reflection was measured on humotelite and humocollinite $\bar{R}_m$ = 0.27 %.

2. Coal from Borsod district of Miocene age: lustreless, hard brown coal with bituminous wood (xilitol) mixtures. The degree of carbonization is moderate. It contains a high portion of geotelite and mediotelite, rubbed detrite. The huminite reflection: $\bar{R}_m$ = 0.35 %.

3. Coal from Nógrád district: lustrous brown coal of Miocene age. Contains dunn bass and quartz and carbominerite. The main coal minerals: telogelite, gelite and detrite. The vitrinite reflection: $\bar{R}_m$ = 0.45 %.

4. Coal from Dorog district: lustrous brown coal of Eocene age. Contains mainly detrite and gelite with some percents of clarite. The vitrinite reflection: $\bar{R}_m$ = 0.46 %.

5. Coal from Mecsek district: black (bituminous) coal, nephelite type of Jurassic age. Constitutes mainly vitrinite, but some carbominerite and clay are present, too as well as half-coke and coke. The vitrinite reflection: $\bar{R}_m$ = 1.46 %.

The huminite and vitrinite reflection values were choosen for comparison with the characteristic values of the redox potential curves. The results are summarized in Figs 4-6 and Tables III-IV.

Figure 7 shows the reproducibility of the redox potential measurements, where two redox potential curves of the same coal sample are given.

SUMMARY

Rock-Eval pyrolysis and petrological investigations (reflection of mineral constituents) are most usually applied in organic geochemistry to determine the degree of carbonization of coals.

On the basis of the good correlations shown in Figures and

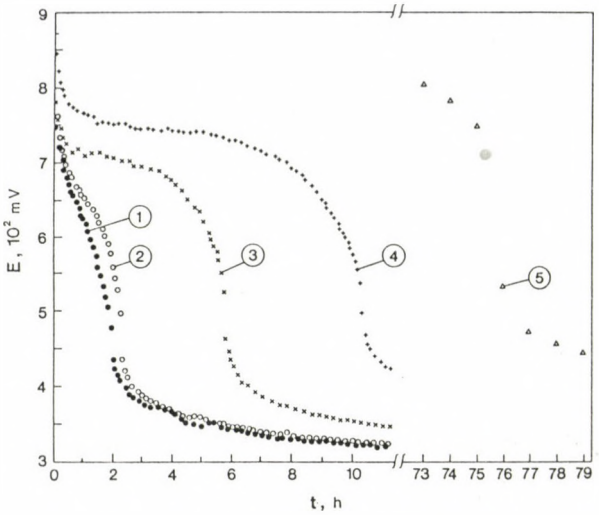

Fig. 4. Redox potential curves of coals from different ages and sources. Curve 1: lignite from Gyöngyösvisonta, Pliocene; Curve 2: brown coal from Borsod district, Miocene; Curve 3: brown coal from Nógrád district, Miocene; Curve 4: brown coal from Dorog district, Eocene; Curve 5: black coal from Mecsek district, Jurassic. The curves were made on particle size below 200 μm

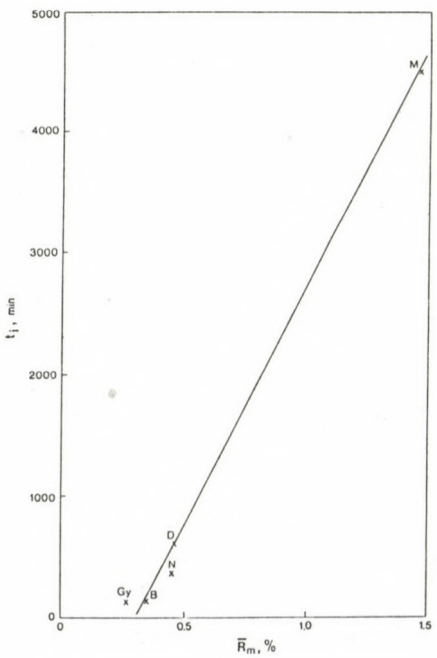

Fig. 5. $\bar{R}_m$ vs. t_i relationship for different coals

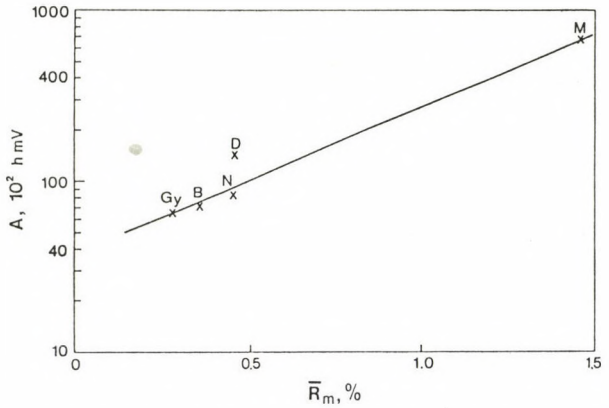

Fig. 6. Relationship between A and huminite or vitrinite reflection

Table III. Characteristic values of the redox potential curves and huminite or vitrinite reflexion for samples of Fig. 4

Age of samples	A, h·mV	t, min	$\bar{R}_m$, %
1. Pliocene	6636	115	0.27
2. Miocene	6967	140	0.35
3. Miocene	8208	360	0.45
4. Eocene	10391	620	0.46
5. Jurassic	14768	4550	1.46

Table IV. Analytical data for samples in Fig. 4

Age of samples	A^a, %	W^a, %	C^a, %	H^a, %	ϱ, g/cm^3
1. Pliocene	43.1	11.0	29.7	2.7	1.7053
2. Miocene	39.5	7.5	35.0	3.3	1.6992
3. Miocene	40.4	9.7	32.4	2.6	1.7224
4. Eocene	39.2	6.1	36.7	4.0	1.9299
5. Jurassic	11.8	0.9	77.7	4.0	1.4820

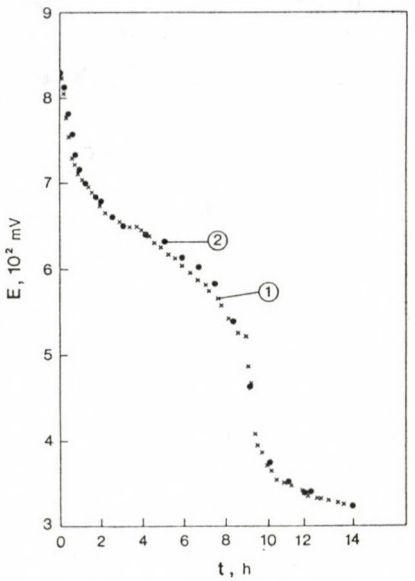

Fig. 7. Reproducibility of the redox potential measurements

Tables between the most characteristic values of the redox potential curves and the results of Rock-Eval pyrolysis as well as the huminite and vitrinite reflection, it is possible to draw the conclusion that the redox potential curves represent mainly the degree of carbonization of the coals, and can be used as a new method for its determination.

The advantages of the method: 1. Requires simple instrumentation; 2: Preliminary preparative work is not necessary (except grinding and sieving); 3. The reproducibility is very high; 4. The method is applicable to follow any change in the state of coals during or after physical and/or chemical treatment causing the increase of the degree of carbonization (beneficiation, etc.).

The time of measurement is rather long, but investigations to decrease it are already going on.

REFERENCES

Bod M, Bárdossy Gy 1959: In: Geochemical Proceedings of Eötvös

Loránd Institute Hungary, Vol. VIII, No. 1-2.

Kossuth G 1982: Personal communication

Krumbein W C, Garrels R M 1948: Journ. of Geol., 56, 13-19.

Milley J 1985: Acta Geod. Geoph. Mont. Hung., 20, 253-260.

Pitt G J, Millward G R 1979: Coal and modern coal processing: an introduction. Academic Press, London

Pustovalov L V, Sokolova E I 1957: Metodi izuchenyiya osadochnich porod. Gosgeoltekhizdat, Moscow

Verheyen T V, Johns R B, Espatalié I 1984: Geochim. Cosmochim. Acta, 48, 63-70.

Acta Geod. Geoph. Mont. Hung., Vol. 24 (1-2), pp. 195-208 (1989)

OUTLINES OF HISTORICAL EVOLUTION AND INSTITUTIONAL SYSTEM OF THE TECHNICAL-SCIENTIFIC RESEARCH OF HUNGARIAN MINING

G Faller

H-1014 Budapest, Dísz tér 8, Hungary

[Manuscript received June 5, 1988]

In interaction with the several thousand years old mining in the Carpathian Basin, scientific research and higher education came into being nearly at the same time. The first part of this paper presents some events, results and personalities from this process. The second part gives a review of Hungarian research institutions outside of the university: Hungarian State Institute of Geology, Eötvös Loránd Geophysical Institute, Geodetical and Geophysical Research Institute and Mining Chemical Research Laboratory of the Hungarian Academy of Sciences, Research Centre of the Mecsek Coal Mines, Projecting and Research Institute of the Aluminium Industry, Hungarian Research-Development Institute of the Hydrocarbon Industry and Central Institute of Mining Development. Then it hints at the activity of the Hungarian National Association of Mining and Metallurgy and of several bodies of the Hungarian Academy of Sciences and enumerates periodicals which publish the results of research and developments.

Keywords: blasting; Hungarian mining; mining history; mining research; Selmec academy

In the first part of this paper[1] some events of the history of the technical-scientific research of the Hungarian mining will be presented which are - in my opinion - significant on an international scale. In the second part the present institutional system of this activity will be summed up.

It cannot be the objective of this paper to give a full overview on mining history. By the way of introduction only a few, mostly well-known facts are mentioned, as follows. Regarding the very beginning of Hungarian mining, the Hungarians

[1]Paper presented at the Ninth Session of Meeting of Directors of National Mining Research Institutes in the framework of the United Nations European Economical Committee's Coal Committee on April 18, 1988.

(895 A.D) settled down with definite knowledge of mining technics in the Carpathian Basin where mining operations were carried out during the era of the Roman imperium, too. The knowledge and the development of mining and processing of precious metals are witnessed by the coins of the first king St. Stephen (976/977?-1038) and of his successors. The perfection of the mining of the Hungarian territory in the 13th century is documented by the Selmec miner's code of law issued in 1245 by King Béla the Fourth (1206-1270). Till the discovery of America the European money market was ruled by gold and silver coins minted in the Hungarian Kingdom. In the 13th century the Hungarian mining has produced 20-25 % of the gold production of Europe and of the territories being in an economical connection with it.

The Hungarian Kingdom had a considerable iron ore, copper ore and salt mining. The mining technics got a strong impetus by the blasting technology: the first blasting of the world in a mine adit has been carried out on February 8, 1627 by Gáspár Weindl in the adit Felső-Biber, belonging to Selmecbánya (Banska Stiavnica) at present in Czechoslovakia). At the same place a huge water-power system composed of 16 lakes has been constructed in 1699 on the basic idea of Máté Kornél Hell (1650-1743). This system actuated the water-driven mining machinery of European reputation of József Károly Hell (1713--1789). The first so-called fire engine in the mining of the European continent, the foregoer of the steam engine appeared presumably in Újbánya (Nova Bana in Czechoslovakia) in 1722.

In this paper neither the essential content nor the chronology can be presented how the mining science developed from the mining skill inherited by the sons from the fathers. In a high-grade simplification the Hungarian mining science - the scientific research - was born and developed together with the university education in mining.

In the important and advanced mining of the Carpathian Basin, the necessity of university education emerged relatively early: King Charles the Third (1685-1740) established a School of Officers of Mines (Bergschule) in 1735 at Selmecbánya. In

1763 Queen Maria Theresia (1717-1780) decreed to establish on the basis of this school an educational institution of mining and metallurgy with several professorates. Till 1770 three of them have been established. Hereby an effective university educational organization: the Mining Academy (Bergakademie) was developed practically in the same time as the oldest institutions of the world (Freiberg, Skt.Petersburg now Leningrade and Mexico City). Its history was compiled (1871) by my great-great father, Gusztáv Faller (1816-1881). The first professors were not only excellent specialists, but their scientific activity was of international significance. The first professor of the mining school was Samuel Mikoviny (1700-1750) born in Hungary who studied mathematics and natural sciences at the university of Altdorf near Nürnberg in 1721-23 and at the university of Jena in 1723-25. As he got his professorate in Selmecbánya he was the engineer of the county Pozsony (Bratislawa), further of the Court Chamber of Vienna, being at the same time major of the engineer corps. Numerous technical constructions are bound to his name. He is the founder of the Hungarian scientific cartography (among other works, 49 of his maps are known). He was elected member of the Prussian Royal Scientific Association (1733-34) (the Academy of Sciences in Berlin) mainly for the determination of the Ludolph-number with more decimals as previously known.

The other professors were also scientists of European reputation: in the professorate of metallurgy-chemistry-mineralogy - which was established as the first one in 1763 - we find baron Nikolaus Josef Jacquin (1727-1817) and in the professorate mathematics-physics-mechanics - the second one established in 1765 - Miklós Poda (1723-1798). The third mining professorate organized in 1770 had as its first professor Kristóf Delius Traugott (1728-1779) who studied mathematics and natural sciences at Wittenberg and mining and metallurgy at Selmecbánya. In his book "Anleitung zu der Bergbaukunst..." (1773) he summarized with scientific pretension all the theoretical and practical mining knowledge of the second half of the 18th century, creating a textbook which compiled geology, mining,

mineral processing and mining economy. This book was for many decades authoritative for the European university education in mining. In Hungarian the Appendix has been issued first, translated by János Mihalovits, the full work has been published - without the Appendix mentioned - in the precise and enjoyable translation of Gábor Boday (1972).

An outstanding event of the history of science in this period is the institution of the first international technical--scientific association of the world, that of the "Societät der Bergbaukunde", in Szkleno near Selmecbánya where the best experts from Europe and America met to study Ignác Born's (1742--1791) amalgamation process (that time Glashütte, now Sklené Teplice in Czechoslovakia) as described by my father, Jenő Faller (1975) (1894-1966). This group established an association which is considered pridefully as its foregoer by the World Mining Congress. The foundation of this association has been adequately commemorated at the sessions of the Comittee in 1986 (Session 58: Clausthal-Zellerfeld, Session 59: Wien). A comprehensive bibliography on Born was published at this occasion (Molnár 1986).

The technical-scientific research work on the field of mining at the academy of Selmecbánya has achieved international publicity in the second half of the 19th century when the academy started participation in the edition and publication of the common professional-scientific yearbooks of the institutions at Leoben and Pribram, and continued it till 1904. That was the "Berg- und Hüttenmännisches Jahrbuch" (Mining and Metallurgical Yearbook) (BuHJ) which was discussed by J Faller (1971) including the role of Gusztáv Faller. According to that the BuHJ was actually the continuation of the periodical journal of the technical school of mining in Vordernberg, started in 1842. The first volume came out in 1851 (Berg- und Hüttenmännisches Jahrbuch der Kaiserl. Königl. Montanlehranstalt zu Leoben. I. Band. Als Fortsetzung der vormals steier. stand. Lehranstalt zu Vordernberg der IV. Band. Redakteur: Direktor Tunner, Wien. In Commission bei Tandler und Compagnie. 1851.) Following the first one, the volumes edited alternately

in Leoben (red.: Peter Tunner) and in Pribram (red.: Johann Grimm) contained numerous studies by Hungarian specialists, but the Academy of Selmecbánya got involved in the editing work only after 8 years, thanks to the activity of Gusztáv Faller. In his edition volumes 1858/1859/VIII, 1861/1862/X, 1864/1865/XV and 1867/1868/XVII of the yearbook were published under the title "BuHJ der k.k. Schemnitzer Bergakademie und der k.k. Montanlehranstalten zu Leoben und Pribram..." (Mining and Metallurgical Yearbook of the Imperial, Royal Mining Academy at Schemnitz and of the Imperial, Royal Mining Technical Schools at Leoben and Pribram...). In this volumes he published during 10 years 21 studies. In this work he was supported by Ignác Curter (1812-1893), professor of metallurgy and chemistry who was responsible for the metallurgical papers in the volumes.

The institution developed in 1867 to an Academy of Mining and Forestry. It moved after the First World War to Sopron. Later the Academy passed through many changes, between 1952 and 1959 the faculties of mining and metallurgy moved as faculties of the Technical University for Heavy Industry (established in 1949) to Miskolc where in 1980 an Institute of Law has been added as fourth faculty. Not a long time ago an Institute of Economics has been founded, from which the fifth faculty, the Faculty of Economics is to develop.

In the meantime the production structure of the Hungarian mining has also undergone a significant transformation: the history of coal mining started in 1753, the bauxite-production in 1926. Hungarian experts who achieved considerable successes in Near East and elsewhere in the oil exploration, opened the first production wells in Hungary in 1937. Uranium ore mining has a past of about three decades. The dimensions, structure of production of the Hungarian mining are characterized by the following production data (in parentheses the time period is given for which according to my opinion the supply of economically exploitable minerals will be sufficient taking into account the present level of production):

- black coal 2.3 Mt (more than 100 years)
- brown coal 13.9 Mt (54 years)
- lignites 6.9 Mt (more than 100 years)

- croude oil	2.0 Mt	(15 years)
- natural gas	7.3 Gm^3	(15 years)
- bauxite	3.0 Mt	(26 years)
- manganese ore	0.1 Mt	(11 years)
- raw material for the concrete industry	8.2 Mt	(more than 100 years)
- stone for building and decoration	9.1 Mt	(more than 100 years)
- sand and gravel for the building industry	32.5 Mt	(30 years)
- raw material for the fine and raw pottery industry	6.3 Mt	(more than 100 years)
- different non-metallic minerals	5.7 Mt	(more than 100 years)

When calculating the period of supply the anticipated mineral resources have not been taken into calculation. At the moment the development works of an about 200 Mt capacity polimetallic (first of all copper) occurrence are suspended, basically due to lack of resources. The production of uranium ore is in consonance with the programme to build nuclear power stations.

The most important technical basis of the present Hungarian mining is the Mining Faculty of the Technical University for Heavy Industry. From the very rich scientific past of this faculty only two persons should be highlighted here due to their international significance: as forerunner of the present Hungarian school of theory of mine location and mining economy (Faller 1974) József Finkey (1889-1941), and that of the Hungarian school of the rock mechanics (Patvaros 1979) Péter Esztó (1885-1965) and Richard Richter (1920-1979). (The research work of the faculty is not dealt with here.)

According to the Hungarian scientific community, the mining should be handled in a proper system (Kapolyi 1981, 1989) which incorporates all the processes from exploration of mineral resources to utilization. Taking into account this aspect a few scientific institutions should be also mentioned which do not deal (or do not only deal) directly with the production of solid minerals. This will be followed by the presentation of the largest technical-scientific research and development

institution in the field of solid minerals, of the Central Institute for Mining Development. All these institutions are dating back directly or indirectly to the Scientific School of Selmecbánya-Sopron-Miskolc.

The Hungarian State Institute of Geology (Budapest) was established 1869 by King Ferenc József the First (1830-1916) as Hungarian Royal Institute of Geology. Miksa Hantken (1821-1893) was appointed director who started his studies in Vienna and finalized at the Academy of Selmecbánya between 1843 and 1846. This institute deals with systematic geological mapping of the country, is elaborating regional row-material prognoses and has a decisive role in the reconnaissance and exploration of new occurrences of coal, coloured and black metals, of raw materials of the building industry, etc. The international connections of this institute are traditional: since the time of its foundation geological expeditions have been sent abroad, it is taking part in international cooperative projects as in paleogeography and marsh-theory in regional prognoses etc.

The Loránd Eötvös Geophysical Institute (Budapest) established in 1919 is the oldest research institute of the world dealing with applied geophysics. The institute's name came from Loránd Eötvös (1848-1919) who became world known by the torsion balance constructed for the measurement of spatial changes of gravity. The institute is known for the development of geophysical instruments and methods and has wide-spread international connections. The activity of the institute involves numerous areas of coal exploration. These are: explanation of strata and tectonic conditions, determination of coal seam quality, geoelectric determination of faults between deep drill-holes, determination of geological correlations using seismic logging. Among in-mine geophysical methods the institute applies and develops at the first place seismic tomography.

The Geodetical and Geophysical Research Institute of the Hungarian Academy of Sciences (Sopron) has been established first as two independent research laboratories from the research staff of the two relevant university chairs of the Mining Faculty working that time in Sopron. The institute itself has

been founded by the fusion of these laboratories; in 1971 an Observatory of seismology (Budapest) has been added under the directorate of Antal Tárczy-Hornoch (1900-1986) who was well-known specialist of this area of sciences, being Doctor Honoris Causa of many universities and honorary member of several academies abroad (Somogyi 1986, Molnár 1986, 1988). Thus, the institute became an internationally recognized research centre. The activity of the institute involves:

- in the field of geodesy
  elaboration of adjustment methods
  geodetic networks
  photogrammetric blocks
  development of means and instruments to measure the accuracy of instruments
  tidal research,
- regarding geophysics
  development and elaboration of instruments
  measuring, processing and interpretation methods of tellurics and magnetotellurics
  investigations of terrestrial electric and electromagnetic fields
  investigation of the ionosphere and atmosphere
  determinations of earthquake risk.

From the point of view of mining, integrated geodynamic investigations based on changing geometrical and physical parameters are of interest. The institute is taking part in the work of the International Union of Geodesy and Geophysics, they carried out different projects together with Austrian and Finnish partner institutions.

The Oil Mining Department of the former Mining Research Institute (Budapest) continued its work from December 1, 1957 as the Oil Mining Research Laboratory of the Hungarian Academy of Sciences (Martos 1969, 1974) (in Sopron and later in Miskolc) and got Mining Chemical Research Laboratory of the Hungarian Academy of Sciences. At the very beginning they were engaged in basic research of the oil mining, their present activity involves also the solution of problems of physico-chemistry,

chemistry and measuring technics which are in connection with the exploration, development and preparation of other raw materials, first of all of coal. Among others up-to-date, computer controlled special measuring equipments with data collection have been developed in the laboratory (PVT-systems, edge plane stress measurement between different strata conditions, viscosity measurements, etc.) which are also used abroad (Austria, India, Poland).

Three remarkable research stations of mining companies and of trusts being active in mining are to be mentioned.

Research Centre of the Mecsek Coal Mines (Pécs). The Centre has been carrying out its scientific research and technical service activity since 35 years. They involve the prevention and fighting down of natural hazards and health damages. As basic method of regional protection against gas outburst hazards, protective seam exploitation has been developed, besides local protective measures as washing out of coal, stress decreasing drilling, provoking shot firing. Their local gas outburst prognoses are based on laboratory coal structure investigations, on "in situ" measurements; the qualification of effectivness of local protection is based on seismoacoustic measurements. For the cognition and observation of the preliminary condition of rock environment of mining operations and of the change of conditions due to exploitation, in-seam wave seismic logging and seismic tomography resp. are used. Their activity on the field of environmental protection is successful in the measurement of the effects of dust emissions and of harmful noise sources. Their dust-protective measures aim to reduce the hazards of silicosis and dust explosions; in regard of the protection against silicosis-hazards the above measures are supported by research in medical biology. The underground fire protection - besides traditional means - are supported by hardening plastic foam and foam generating equipments both developed in the Research Centre. The research and development activity is carried out partly in the framework of bilateral or multilateral international technical-scientific collaboration.

In the Hungarian Aluminium Trust established in 1963 technical research work is coordinated by the staff of the director

of mining using the aid of numerous institutions. They work mainly in the fields of production technology and environmental protection. In this latter field it is of essential significance that bauxite mining - as well as coal mining in the area - have an influence on the karstic water reservoir of the Transdanubian Central Mountains. In the directly connected mining - karstic water system the optimal compromise is to be ensured continuously (by means of a systematic water level observing network and of the modelling of the reservoir). Besides other research stations an essential role is played in this work by the Projecting and Research Institute of the Aluminium Industry (ALUTERV-FKI, Budapest); its foregoer has been established earlier than the Trust itself.

In the frame of the National Oil and Gas Trust the Hungarian Research-Development Institute of the Hydrocarbone Industry (SZKFI, Budapest) has been established 1980 from the fusion of three earlier research stations (High Pressure Research Institute, NAKI; Industrial Research Laboratories of Oil and Gas Mining, OGIL; Gastechnical Research and Testing Station, GKVA). The headquarters of SZKFI are in Százhalombatta with branch institutes in Budapest, Nagykanizsa, Szolnok and Szeged.

The institute is dealing with theoretical and applied research, investigations, experiments, pilot plant tests, especially in the field of geological raw-material exploration, hydrocarbon production, storage, transportation, processing and petrolchemistry. They are also engaged in the product-development of the oil industry, in quality-control, application-technics and motor-tests of products of the oil industry, further the application technics and technological development of structural materials used in gas supply, environmental protection and protection against corrosion. The institute has achieved considerable results in the application and development of purpose-oriented computer technics.

The institute has cooperation agreements with most similar institutions of the East-European countries. From wide-spread international connections, collaborations with Canadian (AOSTRA, SEFEL) and French (IFP, Petrofrance) companies are to

be mentioned. Staff members of the institute are working as experts and lecturers abroad, mostly in Lybia.

The SZKFI is a member of the Hungarian-Soviet ENERGOTECHNO Ltd which has been founded to solve tasks in the field of energetics, including research, development, management and engineering. As soon as the work of a preparatory team, composed of Hungarian and US experts will be finalized in 1988, a joint venture office OXY-SZKFI should be established for different kinds of services.

The most significant institution engaged in the research and development of the mining of solid mineral raw materials is the Central Institute of Mining Development (KBFI) which has been founded 1979 with the fusion of the earlier Mining Research Institute and Mining Projecting Institute (Simon 1979). Both predecessor institutes were founded after the second world war following the nationalization of mining.

As the first steps of the centralization of the mining projecting work, a Mining Machinery Designing Office (1949) and a Mine Projecting Office (1950) have been established. They were amalgamated in 1952 as Mining Projecting Institute (Bercsényi 1962). Its task has been defined very simply in its founding resolution: "... design of ground breaking, all planning, projecting, design works of any kind of mines and mining projects ...". In 1958 these tasks were extended, and the extension did not bring new tasks, but the definition is more detailed: "Studies and general projecting works of mining projects, mining plants, preparation plants, concentrations (within these, projecting of new establishments, reconstructions, extensions); technological design of establishments of mining investments; detailed design of buildings of the mining industry except of design of the public services".

The strictly technical-scientific research of the mining (independent from the universities) has been based on a government order in 1949 regarding the organization of industrial research. This order called into life - besides the existing five research institutes (among them the mentioned Institute of Geology, Institute of Geophysics, Institute of Oil and Gas

Experiments, Aluminium and Light Metal Research Institute) - five new research institutes, four central research laboratories and nine so-called research committees, among the latter the Coal Mining Industrial Research Committee (Martos 1969, 1974). As a result of the quick organisatory work of the committee, the Central Research Laboratory of the Coal Mining Industry has been founded in the same year from which - after one year - the Mining Research Institute has been established. (In the meantime its organization changed many times, e.g. some earlier independent institutions, as the Research Institute of Mine Safety and Blasting Technics which existed between 1950 and 1966 were amalgamated, some of its departments became parts of other institutions, as its mechanical department went over in 1954 to the Testing and Research Institute for the Application of Mining Machinery - founded in 1952 -, the latter institute has been completely amalgamated with the Mining Research Institute in 1955.)

The basic aim of the present Central Institute for Mining Development is the wide field of the technical-scientific mining research and mining planning, projecting and design. Its design and expert activity is in many aspects outranging the mining itself. The institute has also servicing activities, as sales of explosive and manufacturing of detonators. The headquarters are in Budapest, branch establishments are in Tokod and Tatabánya; the Central Mining Museum, opened in 1957 belongs to the institute (Faller J 1958) and it is the center of mining-historical research. The activity of the institute is not dealt with here.

When speaking about the present institutional system of the Hungarian mining research the following are to be mentioned

- the technical-scientific organization of the Hungarian mining engineers and mining technicians: the National Hungarian Association of Mining and Metallurgy (Faller J 1958) which supports (e.g. by technical periodicals, etc.) the technical development of the mining;
- the corporative-scientific activity of the Hungarian Academy of Sciences in the field of mining carried out in Section X,

Earth Sciences and Mining and of its Mining Scientific Committee and in its professional and regional committees; and
- professional periodicals, where the research-development results are published.

Among the 13 ordinary members of the Section X, Earth Sciences and Mining of the Hungarian Academy of Sciences there are 4 mining engineers and among the 4 corresponding members there is 1 mining engineer. The ordinary members are: László Kapolyi (system theory in mining, rock mechanics, economy of mineral resources, economy of raw materials and energy, complex utilization of energy carrying media), Ferenc Martos (mining, rock mechanics), Gusztáv Tarján (mineral processing), and János Zambó (mining), corresponding member: Ferenc Kovács (mine-location, economy of mining, mining technologies and mine safety).

I hope that with this mosaic-like picture it can be shown that it has been characteristic for the technical-scientific research of Hungarian mining of a respectable past that it had mutual research connections with the international scientific life. Today it is also the aim of the technical-scientific research to serve the Hungarian mining so that this work should simultaneously contribute to the augmentation of the universal mining science. This is the intention of the Hungarian experts and institutions when they take part in the work of international organizations as the World Mining Congress, the Permanent Coal Mining Committee of the COMECON, the Coal Committee of the European Economic and Social Council of the United Nations.

REFERENCES

Bercsényi J 1962: Bányászati Lapok, 95, 505-509.

Delius K T 1773: Introduction in the theory and praxis of mining, and into the knowledge of sciences of the mining treasury. Reprint, Mining Section of the National Hungarian Association of Mining and Metallurgy.

Faller G 1871: Die Geschichte und die jetzigen Verhältnisse der Schemnitzer Berg- und Forstakademie. Gedenkbuch zur hundertjährigen Gründung der königl. ungarischen Berg- und Forstakademie in Schemnitz 1770-1870. Schemnitz, 1-78.

Faller G 1974: Bányászati és Kohászati Lapok, Bányászat, 107, 511-516.

Faller J 1958: Bányászati Lapok, 91, 265-271.

Faller J 1971: Bányászati és Kohászati Lapok, Bányászat, 104, 192-199, 271-277.

Faller J 1975: Good luck! Events and pictures from the past of the mining. Műszaki Könyvkiadó, Budapest, 157-159.

Kapolyi L 1981: System and functional aspects of natural resources of mineral origin (in Hungarian). Akadémiai Kiadó, Budapest

Kapolyi L 1987: Mineral resources: A system analytical and functional approach. Springer Verlag, Wien-New York

Martos F 1969: Publications of the Mining Research Institute, 13, No. 3, 7-12.

Martos F 1974: Bányászati és Kohászati Lapok, Bányászat, 107, 2. spec. issue; Publications of the Mining Research Institute, 18, No. 2, K114-K121.

Mihalovits J 1937: Brief biography and smaller works of Delius Kristóf Traugott, the first professor of mining of the Mining Academy at Selmec (1770) (in Hungarian). Publishing Foundation of the Faculty of Mining, Metallurgy and Forestry of the Hung. Royal József Nádor University of Technical and Economic Sciences

Mikoviny S 1739: Epistola ad d.Jo.Jac. Marinonium occasione quaestionis de quadratura circuli nuper perperam motae at falso definitae a d. Joseph. Ign. Car. Leistnero. - Posterior eiusdem epistola. - Nucleus controversiae de quadrate circuli. Wien

Molnár L 1986: Bányászati és Kohászati Lapok, Bányászat, 119, 203-204.

Molnár L 1988: Acta Geod. Geoph. Mont. Hung., 23, 153-164.

Molnár L Weiss A 1986: Ignaz Edler von Born and the Association of Mining (in German). Published by the ad-hoc Working Team for the Cooperation on the Field of Raw- and Basic Materials of Hungary and Austria, Vienna

Patvaros J 1979: Bányászati és Kohászati Lapok, Bányászat, 112, 791.

Simon K 1979: Bányászati és Kohászati Lapok, Bányászat, 112, 1. spec. issue; Publications of the Central Institute for Mining Development, 23, No. 1, K1-K2.

Somogyi J 1986: Acta Geod. Geoph. Mont. Hung., 21, 463-465.

Zsámboki L ed. 1983: Brief biography and technical literature activity of the lecturers of the Academy of Mining and Forestry at Selmec, 1735-1918. Miskolc

Ferenc Martos 70 years

Ferenc MARTOS, mining engineer, ordinary member of the Hungarian Academy of Sciences, retired deputy managing director of the Central Institute for Mining Development celebrated his 70th birthday in 1988.

When we appraise the life-work of Ferenc Martos, mining engineer and scientist we have to outline a rich, and continuously rising path of life of a resolute and diligent man who has been zealous to put into practice his ideas, but has been also ready to concessions.

He spent his childhood in Temesvár, studied at Bucharest and Temesvár (Timisoara), where he took his diploma in mining engineering in 1943. From 1942 to 1944, he worked with coal mines in Transylvania.

Ferenc Martos had a diversified life, since after leaving Rumania in 1943 and after the years being prisoner of war in the Soviet Union, he has built up his existence at the Hungarian State Coal Mines, then he worked in the Ministry of Mining and Energy. He displayed almost all of his activity in the Research Institute for Mining, where he started to work as an aspirant to Candidate's degree in 1951, has been head of the Department of Mine Exploitation since 1955 and of the Main Department of Mining since 1964. In 1966 he was appointed to director of the reorganized Central Institute for Mining Development until 1980, when he retired and since then he has helped our work as a scientific adviser.

His knowledge of foreign languages made him easy to utilize the newest foreign results in technical sciences within his own research work.

He recognized that an initial condition both of the management of mineral resources and of the protection of buildings and establishments on the surface is a detailed knowledge of the regularities of rock movements due to mining activities. Measurements and observations on surface and in mines as well as model experiments carried out under his guidance resulted in connections and generalized conclusions. These studies have determined for several decades the direction of the investigations of rock movements in Hungary. As appreciation of his activity and his results in rock movement

research he was qualified by the Hungarian Academy of Sciences Candidate in 1955 and Doctor of Technical Science in 1966. For his university lectures he was appointed titular university professor in 1967. He was elected corresponding member of the Hungarian Academy of Sciences in 1973 and ordinary member in 1979. During ten years (1976-1985) he was chairman of the Section of Earth and Mining Sciences of the Academy. A book on mine working methods in Hungary published with him as editor in 1963, filled a gap in the literature, a monograph on water protection of mines published in 1975 met international interest, and has helped to obtain information well-applicable in the practice. His handbook on "Damages due to Mining" is a basic aid for university education, too.

He is a founding member of the International Bureau of Rock Mechanics; the Hungarian Section of the International Society of Rock Mechanics is working under his chairmanship and he has been active in the Organizing Committee of Mining World Congresses. In the Hungarian Society of Mining and Metallurgy he has been a member of the governing body since 1951, secretary general between 1954 and 1960 and at present he is vice-chairman of the society. In the editorial board of the mining journal Bányászati Lapok he has played a determining role since a longer time.

His activity in committees of the Hungarian Academy of Sciences is remarkable, his work in the editorial board of the periodicals Acta Geodaetica Geophysica et Montanistica and Magyar Tudomány contributed to raise their scientific level. He has published a high number of papers. His lectures held at international symposia and conferences as well as his activity in the Comecon Technical-Scientifical Council of Deep-Working are most remarkable.

It is nearly thirty years ago that we became colleagues of him and he directed, tought and advised us during many years. He never made his authority felt but ensured wide possibilities for everybody to unfold his creativity.

At his 70th birthday he was congratulated in the Central Institute for Mining Development by his colleagues and followers and we wished him a long and happy life in good health and good luck!

J Bese and J Bodonyi

BOOK REVIEW

E A BASKOV: The Fundamentals of Paleohydrogeology of Ore Deposits. Springer Verlag, 1987, 253 p., Figs 60, Tables 38

This book is really an interdisciplinary work, the reader gets a collection of relationships between hydrogeology and metallogeny that are usually not interrelated. Experts dealing with these two subjects and with all problems of geochemistry and sedimentary petrology may have useful information when studying this volume.

Chapter I summarizes the significance of paleohydrogeological reconstruction and the history of this branch of science and makes an outlook to show the relation of paleohydrogeology to other branches of science. Chapter 2 introduces the forms of occurrence, the position and quantity of water in the earth crust. Formation waters developed in the sediments overlying the continental crust are assigned to two groups: waters in platform type sediments and waters in geosyncline type sediments. Based on large number of references the composition of the types and the character of ion transport are discussed here. Large-scale generalized profiles serve to illustrate the position of formation waters of different composition in some artesian regions. The geological processes in the course of which the dissolved material gets the formation water are reviewed, the characteristic concentrations of trace elements are also listed and finally some recent ore deposits are mentioned.

Based on the dissolved salt and gas composition, on the oxidation state and on the total salinity waters are assigned to seven main types. In this relation the genesis and geological environment of each type are summarized.

Chapter 3 deals with the methodology of paleohydrogeology. In order to construct the lithological maps a special petrological classification is introduced. Based on this classification and taking into account the state of transformation overprinting the hydrological features of each formation, as well as the tectonic history, the boundaries of the hydrogeological landscape units of a region can be constructed to different geological ages. Subsequently to the lithological classification and the areal distribution the interpretation follows that takes into consideration both the paleohydrodynamic and the reservoir parameters. In this respect the changes of porosity and permeability related to the compaction and lithification of the sequence as well as the measure of release of water are dealt with in particular. By means of the discussed paleohydrogeological methods the processes of water release-migration-precipitation that proceeded in the course of basin evolution due to different reasons (diagenesis, coalification, metamorphism, volcanic activity etc.) can be traced and interpreted. The significance of this type of interpretation is emphasized and the complete analysis extending over the mineralogical, megatectonic and crustal-thermal environments is demonstrated.

Chapter 4 is probably most interesting for geologists. Here the ion movement and metal concentration during the metallogenesis are introduced according to the geological-paleohydrogeological environments. A lot of geological structure and profile of ore deposits are demonstrated and supplemented with the interpretation of paleohydrogeological aspects.

The book is a valuable and pragmatic work though the reader feels sometimes the lack of results of the up-to-date analytical methods, e.g. maturation of the organic matter, stable isotope data, this, however, does not deteriorate the essence of the volume. I do believe that this book

provides valuable aid to solve not only metallogenic problems but to carry out more particular geochemical interpretations in the field of different geological-hydrological phenomena.

J Dunkl

OSTRACODA IN THE EARTH SCIENCES

edited by **P. De Deckker,** *The Australian National University, Canberra, A.C.T., Australia,* **J.-P. Colin,** *Esso Research, Bègles, France and* **J.-P. Peypouqet,** *Université de Bordeaux I, Talence, France*

This book endeavours to bring about a greater understanding of the usefulness of ostracods in many aspects of geological sciences, and provides suggestions for future research. It is principally intended for the non-specialist, and shows many appplications of ostracods to help solve geological problems and phenomena. Topics reviewed assume no prior knowledge of palaeontology, and thus terminology is kept simple. There is an exhaustive index, and an appendix supplying additional references on significant sources of information on ostracods.

The book aims to deliver information on ostracods to those people not usually interested in the literature of palaeontology and also to awaken an interest in the Ostracoda by referring to more specialized articles published elsewhere. It will therefore be of interest to general geologists, as well as to those involved in petroleum exploration, and students of palaeoenvironments.

Contents: Illustration of ostracods. Ostracods and palaeoceanography *(R.H. Benson)*. The importance of ostracods in biostratigraphic analysis *(J.P. Colin, F. Lethiers)*. Chronoecology, a non-taxonomic application of ostracods *(D. van Harten)*. Palaeobathymetry on the continental shelf based on examples using ostracods from the Gulf of Alaska *(E.M. Brouwers)*. Ostracods and sea-level changes: case studies form the Quaternary of North and South Carolina, U.S. Atlantic coast *(T.M. Cronin)*. Determining Late Neogene and Quaternary palaeoclimates and palaeotemperature regimes using ostracods *(J.E. Hazel)*. Ostracoda and palaeogeography *(R.C. Whatley)*. Ostracods and palaeosalinity reconstruction *(J.W. Neale)*. Ostracods and the transition between fresh and saline waters *(P. Carbonel)*. The use of ostracods to reconstruct continental palaeoenvironmental records *(P. De Deckker, R.M. Forester)*. Stable isotopes from lacustrine Ostracoda as tracers for continental palaeoenvironments *(G.S.Lister)*. Amino acid racemization in fossil non-marine ostracod shells: a potential tool for the study of Quaternary stratigraphy, chronology, and palaeotemperature *(W.D. McCoy)*. Sediment transport detected from the analysis of ostracod population structure: an example from the Alaskan continental shelf *(E.M. Brouwers)*. Population structure of ostracods: Some general principles from the recognition of palaeoenvironments *(R.C. Whatley)*. Applications of ostracods in quantitative geology *(R.C. Reyment)*. Appendix. Genus and species index. Subject and locality index.

1988 xii + 302 pages
US$ 84.25 / Dfl. 160.00
ISBN 0-444-43011-3

ELSEVIER SCIENCE PUBLISHERS

P.O. Box 211, 1000 AE Amsterdam, The Netherlands
P.O. Box 1663, Grand Central Station, New York, NY 10163, USA

The Dutch Guilder price is definitive. US$ prices are valid only in the USA & Canada.

Developments in Palaeontology and Stratigraphy, 10

BIOGEOGRAPHY AND PLATE TECTONICS

by **J.C. Briggs,** *University of South Florida, St. Petersburg, FL, USA*

The author of this book traces the changing relationships among the various biogeographic regions, and demonstrates how such changes may often be correlated with the gradual geographic alteration of the Earth's surface. He analyses recent information about the distribution of widespread groups of terrestrial and freshwater vertebrates, invertebrates and plants, and discusses the biogeographical effects of the movement of oceanic plates.

It is particularly important to obtain dependable information about certain critical times in the history of continental relationships. We need to know when the terrestrial parts of the earth were broken apart and when they were joined together. The present investigation makes it clear that we cannot depend entirely on evidence from plate tectonics, nor will purely biological evidence suffice. This book thus provides much of interest to systematists working on contemporary groups of plants and animals, paleontologists, evolutionary biologists, and professors teaching courses in biogeography.

1987 xii + 204 pages
US$ 81.50 / Dfl. 155.00
ISBN 0-444-42743-0

ELSEVIER SCIENCE PUBLISHERS

P.O. Box 211, 1000 AE Amsterdam, The Netherlands
P.O. Box 1663, Grand Central Station, New York, NY 10163, USA

The Dutch guilder price is definitive. US$ prices are valid only in the USA & Canada.

treble underlining: bold-face italics
red underlining: Greek letters
green underlining: script letters

Rules for mathematical-physical notations:

trigonometric, logarithmic, analytic symbols, symbols for units and functions are in roman type (not underlined)

letter symbols in mathematical and physical formulas, scalars, and subscripts of algebraic and physical quantities are in italics (underlined)

vectors, matrices, operators in probability theory are in bold-face roman type (double underlining) tensors, operators and some special functions are in script letters (green underlining). These cannot be bold.

Greek letters (red underlining) cannot be bold or extra bold type (thus they cannot be used for vectors or tensors)

void upper lines e.g. for vectors

avoid possible confusion between o (letter) and 0 (zero), l (letter) and 1 (one), ν (Greek nu) and v.u. (letters) etc.

explain ambiguous or uncommon symbols by making marginal notes in pencil

be careful about superscripts and subscripts

formulae must be numbered consecutively with the number in parentheses to the right of the formula. References in text to the equations may then usually be made by the number in parenthesis. When the word equation is used with a number, it is to be abbreviated. Eq. or Eqs in the plural the International System of Units (SI) should be used.

Authors are liable for the cost of alteration in the *proofs*. It is, therefore, the responsibility of the author to check the text for errors of facts before submitting the paper for publication.

3. *References* are accepted only in the Harvard system. Citations in the text should be as:

... (Bomford 1971) ... or Bomford (1971)

... (Brosche and Sündermann 1976) ...

... (Gibbs et al. 1976b) ...

The list of references should contain names and initials of all authors (the abbreviation et al. is not accepted here); for *journal articles* year of publication, the title of the paper, title of the journal abbreviated, volume number, first and last page.

For *books* or *chapters in books*, the title is followed by the publisher and place of publication.

All items must appear both in the text and references.

Examples:

Bomford G 1971: Geodesy. Clarendon Press, Oxford

Brosche P, Sündermann J 1976: Effects of oceanic tides on the rotation of the earth. Manuscript. Univ. of Bonn

Buntebarth G 1976: Temperature calculations on the Hungarian seismic profile-section NP–2. In: *Geoelectric and Geothermal Studies (East-Central Europe. Soviet Asia), KAPG Geophysical Monograph.* Akadémiai Kiadó, Budapest, 561–566.

Gibbs N E, Poole W G, Stockmeyer P K 1976a: An algorithm for reducing the bandwidth and profile of a sparse matrix. *SIAM J. Number. Anal.*, 13, 236–250.

Gibbs N E, Poole W G, Stockmeyer P K 1976b: A comparison of several bandwidth and profile reduction algorithms. *ACM Trans. on Math. Software.* 2, 322–330.

Szarka L 1980: Potenciáltérképezés analóg modellezéssel (Analogue modeling of potential mapping). *Magyar Geofizika,* 21, 193–200.

4. *Footnotes* should be typed on separate sheets.

5. *Legends* should be short and clear. The place of the tables and figures should be indicated in the text, on the margin.

6. *Tables* should be numbered serially with Roman numerals. Vertical lines are not used.

All the illustrations should contain the figure number and author's name in pencil on the reverse.

Figures will be redrawn. Therefore the most important point is clearness of the figures, even pencil-drawings are accepted (with a duplicate).

Photographs and *half-tone* illustrations should be sharp and well contrasted.

If a specific reduction or enlargement is required, please indicate this in blue pencil on the figure.

The editors will send information to the first author about the *arrival* and acceptance of the papers. A galley proof is also sent to the first author for *correction*. Hundred *offprints* are supplied free of charge.

Periodicals of the Hungarian Academy of Sciences are obtainable at the following addresses:

AUSTRALIA
C.B.D. LIBRARY AND SUBSCRIPTION SERVICE
Box 4886, G.P.O., *Sydney N.S.W. 2001*
COSMOS BOOKSHOP, 145 Ackland Street
St. Kilda (Melbourne), Victoria 3182

AUSTRIA
GLOBUS, Höchstädtplatz 3, *1206 Wien XX*

BELGIUM
OFFICE INTERNATIONAL DES PERIODIQUES
Avenue Louise, 485, *1050 Bruxelles*
E. STORY-SCIENTIA P.V.B.A.
P. van Duyseplein 8, *9000 Gent*

BULGARIA
HEMUS, Bulvar Ruszki 6, *Sofia*

CANADA
PANNONIA BOOKS, P.O. Box 1017
Postal Station "B", *Toronto, Ont. M5T 2T8*

CHINA
CNPICOR, Periodical Department, P.O. Box 50
Peking

CZECHOSLOVAKIA
MAD'ARSKA KULTURA, Národni třida 22
115 66 Praha
PNS DOVOZ TISKU, Vinohradská 46, *Praha 2*
PNS DOVOZ TLAČE, *Bratislava 2*

DENMARK
EJNAR MUNKSGAARD, 35, Nørre Søgade
1370 Copenhagen K

FEDERAL REPUBLIC OF GERMANY
KUNST UND WISSEN ERICH BIEBER
Postfach 46, *7000 Stuttgart 1*

FINLAND
AKATEEMINEN KIRJAKAUPPA, P.O. Box 128
00101 Helsinki 10

FRANCE
DAWSON-FRANCE S.A., B.P. 40, *91121 Palaiseau*
OFFICE INTERNATIONAL DE DOCUMENTATION ET LIBRAIRIE, 48 rue Gay-Lussac
75240 Paris, Cedex 05

GERMAN DEMOCRATIC REPUBLIC
HAUS DER UNGARISCHEN KULTUR
Karl Liebknecht-Straße 9, *DDR-102 Berlin*

GREAT BRITAIN
BLACKWELL'S PERIODICALS DIVISION
Hythe Bridge Street, *Oxford OX1 2ET*
BUMPUS, HALDANE AND MAXWELL LTD.
Cowper Works, *Olney, Bucks MK46 4BN*
COLLET'S HOLDINGS LTD., Denington Estate,
Wellingborough, Northants NN8 2QT
WM DAWSON AND SONS LTD., Cannon House
Folkstone, Kent CT19 5EE
H. K. LEWIS AND CO., 136 Gower Street
London WC1E 6BS

GREECE
KOSTARAKIS BROTHERS INTERNATIONAL BOOKSELLERS, 2 Hippokratous Street, *Athens-143*

HOLLAND
FAXON EUROPE, P.O. Box 167
1000 AD Amsterdam
MARTINUS NIJHOFF B. V.
Lange Voorhout 9–11, *Den Haag*
SWETS SUBSCRIPTION SERVICE
P.O. Box 830, 2160 Sz Lisse

INDIA
ALLIED PUBLISHING PVT. LTD.
750 Mount Road, *Madras 600002*
CENTRAL NEWS AGENCY PVT. LTD.
Connaught Circus, *New Delhi 110001*
INTERNATIONAL BOOK HOUSE PVT. LTD.
Madame Cama Road, *Bombay 400039*

ITALY
D. E. A., Via Lima 28, *00198 Roma*
INTERSCIENTIA, Via Mazzé 28, *10149 Torino*
LIBRERIA COMMISSIONARIA SANSONI
Via Lamarmora 45, *50121 Firenze*
SANTO VANASIA, Via M. Macchi 58
20124 Milano

JAPAN
KINOKUNIYA COMPANY LTD.
Journal Department, P.O. Box 55
Chitose, *Tokyo 156*
MARUZEN COMPANY LTD., Book Department
P.O. Box 5050 Tokyo International, *Tokyo 100-31*
NAUKA LTD., Import Department
2-30-19 Minami Ikebukuro, Toshima-ku, *Tokyo 171*

KOREA
CHULPANMUL, *Phenjan*

NORWAY
TANUM-TIDSKRIFT-SENTRALEN A.S.
Karl Johansgata 43, *1000 Oslo*

POLAND
WEGIERSKI INSTYTUT KULTURY
Marszalkowska 80, *00-517 Warszawa*
CKP I W, ul. Towarowa 28, *00-958 Warszawa*

ROUMANIA
D. E. P., *Bucuresti*
ILEXIM, Calea Grivitei 64–66, *Bucuresti*

SOVIET UNION
SOYUZPECHAT — IMPORT, *Moscow*
and the post offices in each town
MEZHDUNARODNAYA KNIGA, *Moscow G-200*

SPAIN
DIAZ DE SANTOS Lagasca 95, *Madrid 6*

SWEDEN
ESSELTE TIDSKRIFTSCENTRALEN
Box 62, *101 20 Stockholm*

SWITZERLAND
KARGER LIBRI AG, Petersgraben 31, *4011 Basel*

USA
EBSCO SUBSCRIPTION SERVICES
P.O. Box 1943, *Birmingham, Alabama 35201*
F. W. FAXON COMPANY, INC.
15 Southwest Park, *Westwood Mass. 02090*
MAJOR SCIENTIFIC SUBSCRIPTIONS
1851 Diplomat, P.O. Box 819074,
Pallas, Tx. 75381-9074
READ-MORE PUBLICATIONS, INC.
140 Cedar Street, *New York, N. Y. 10006*

YUGOSLAVIA
JUGOSLOVENSKA KNJIGA, Terazije 27, *Beograd*
FORUM, Vojvode Mišića 1, *21000 Novi Sad*

Acta Geodaetica, Geophysica et Montanistica Hungarica

VOLUME 24, NUMBERS 3–4, 1989

Akadémiai Kiadó, Budapest

AGGM 24 (3–4) 213–480 (1989) HU ISSN 0236-5758

ACTA GEODAETICA, GEOPHYSICA et MONTANISTICA HUNGARICA
A Quarterly Journal of the Hungarian Academy of Sciences

Acta Geodaetica, Geophysica et Montanistica (AGGM) publishes original reports on geodesy, geophysics and minings in English.

AGGM is published in yearly volumes of four numbers by

AKADÉMIAI KIADÓ
Publishing House of the Hungarian Academy of Sciences
H–1054 Budapest, Alkotmány u. 21.

Manuscripts and editorial correspondence should be addressed to

AGGM Editorial Office
H–9401 Sopron P.O. Box 5

Subscription information

Orders should be addressed to KULTURA Foreign Trading Company
H–1389 Budapest P.O. Box 149

Acta Geodaetica, Geophysica et Montanistica Hungarica is abstracted/indexed in Geographical Abstracts, GeoRef Information System, Science Abstracts

INSTRUCTIONS TO AUTHORS

Manuscripts should be sent to the editors (MTA Geodéziai és Geofizikai Kutató Intézete, AGGM Editorial Office. H–9401 Sopron, P.O. Box 5. HUNGARY) Only articles not submitted for publication elsewhere are accepted.

Manuscripts should be typewritten in duplicate, double-spaced, 25 lines with 50 letters each. The papers generally include the following components, which should be presented in the order listed.

1. Title, name of author(s), affiliation, dateline, abstract, keywords
2. Text, acknowledgements
3. References
4. Footnotes
5. Legends
6. Tables and illustrations

1. The *affiliation* should be as concise as possible and should include the complete mailing address of the authors. The *date of receipt* of the manuscript will be supplied by the editors. The abstract should not exceed 250 words and should clearly and simply summarize the most important methods and results. 5–10 significant expressions describing the content are used as *keywords*. Authors may recommend these keywords.

2. The *text* should be generally in English and as short and clear as possible. From Hungarian authors papers are also accepted in Hungarian.

The section heading should *not* be underlined or in capitals.

Please note that underlining denotes special types:

– single underlining: italics
– double underlining: bold-face roman

CONTENTS

Acta Geod. Geoph. Mont. Hung., Vol. 24 (3-4), pp. 213-236 (1989)

ON THE RELATION BETWEEN THE GRAVITY FIELD AND LITHOSPHERIC FEATURES IN THE GREEK AREA

M Doufexopoulou, P Milas, B Nakos, A Papafitsorou

Higher Geodesy Laboratory, National Technical University of Athens,
157 73 Zographou, Heroon Polytechniou 9, Greece

[Manuscript received February 5, 1987]

The results of studies of the gravity field in the Greek area are presented and discussed in relation to the tectonic background. The occurrence of the African tectonic plate and its subduction under the Aegean together with the Hellenic trench and the Alpine fold, disturb the gravity field of the region at a wide range of wavelengths. The abrupt Moho depth changes indicate among other features a possible lack of isostasy and the need of mass modeling in order to explain the long wavelength variations of the gravity field.

The referenced F.A. anomalies to GRM3L1 geopotential model, truncated at degree 30 were further smoothed by a statistically estimated complete Bouguer reduction with the use of 5'×5' mean topographic heights. The resulted gravity anomaly signal contains major lithospheric information indicated by the directivity diagrams. Statistical evaluation of the distance dependent Bouguer coefficient at $1^{o}\times1^{o}$ blocks indicated the presence of • densities in the area between the Hellenic arc and the Alpine fold which can be considerably different from the one used in the standard earth models.

Further research is needed with denser and more extended data.

Keywords: gravity field; Greece; lithospheric signal; modelling

INTRODUCTION

The Greek area, a part of the Eastern Mediterranean, is one of the more interesting areas in Europe from a geophysical point of view. This area has been the object of several geophysical studies (e.g. Papazachos and Comninakis 1971, Woodside 1976, Makris 1973, 1977) which indicate the presence of active tectonic stress fields, unbalanced masses and energy released from tectonic activity at various depths.

The estimation of the earth's gravity field is the main object of physical geodesy and methods that deal with this

problem involve the gravity field modeling under the assumption that the anomalous gravitational potential T fulfills Laplace's equation $\nabla T = 0$, at least outside the surface of the earth. These methods are approximation methods for harmonic functions, and no assumption is made about the density distribution which actually generates the gravity field.

For geodesy, the gravity field modeling is a direct problem with unique solution, while for geophysics it is an inverse problem without unique solution. In geophysically complex areas the geodetic gravity field modeling needs a second order approximation, involving the geophysical inversion which is not restricted to the short wavelength variations due to terrain, but it may be needed also for longer wavelengths. These wavelengths can be related to the tectonic features of the region and may come from deep mass sources.

The gravity field of the Greek area, although mostly complicated, is not yet adequately modeled for a geodetic purpose (i.e. representation of an accurate geoid). This is partly due to the great complexity of the area and partly to the fact that the available data belong to different institutions with various objectives. Therefore, a systematic study of an hybrid gravity field modeling/geophysical inversion demands a collaboration of all institutions, in the frame of a long term project.

This work is an attempt to:

- describe the data which are available at the Higher Geodesy Laboratory of the N.T.U. of Athens
- present previous results which were obtained using a part of these data
- present new results in order to extend previous investigations.

The theoretical background consists of statistical concepts at a great part and of geophysical information. Frequent use of related references will prevent repetitions.

It is worth mentioning that in spite of the generally accepted use of the high degree and order geopotential models (G.M.) to refer the gravity field data in modeling problems (e.g. Tscherning 1983, Forsberg 1984, Schwarz 1985), this con-

sideration is not valid for the Greek area. As it will be shown in the following, it seems that local mass modeling would be more appropriate, at least in some regions, in order to replace the medium wavelength variations of the gravity field.

THEORETICAL CONSIDERATIONS

Gravity field modeling is needed in physical geodesy and geophysics. The approach of modeling is different for each purpose. In physical geodesy it is a direct problem in which the disturbing gravitational potential T must be a harmonic function. In geophysics it is an inverse problem, where the observed gravity field must be generated from an assumed mass model.

The gravitational disturbing potential T at a point $P(r,\varphi,\lambda)$ is generated by a density anomaly distribution $\Delta\rho$:

$$\tilde{T}(P) = k \int_V \frac{\Delta\rho}{r}\, dV \qquad (1)$$

where r is the distance between P and the center of mass of the disturbing mass element, dV is the volume of this element, k is the gravitational constant and $\Delta\rho$ is the difference between the actual density distribution and a "normal" density distribution which generates the normal potential U

$$\Delta\rho = \rho - \rho_o \,. \qquad (2)$$

Any density distribution $\Delta\rho$ can satisfy (1) because any radial symmetric normal density distribution ρ_o can generate the normal potential U, provided that the value kM is correct (M is the mass of the Earth). So, ρ_o must be chosen.

The potential T can also be expressed by the usual spherical harmonic expansion:

$$\tilde{T}(P) = kM \sum_{n=2}^{nmax} \sum_{m=0}^{n} \left(\frac{R}{r}\right)^n (\bar{C}^{*}_{nm} \cos m\lambda - \bar{S}^{*}_{nm} \sin m\lambda)\, P_{nm}(\sin\varphi) \,. \qquad (3)$$

The approximation $\tilde{T}(P)$ in (3) is split up as successive approximations with increasing degree in of expansion:

$$\tilde{T}(P) = \tilde{T}_1 + \tilde{T}_2 + \tilde{T}_3 + \ldots \quad (4)$$

where $\tilde{T}_1$, $\tilde{T}_2$ ... are the components relative to the increasing degree n and are related to the depths of the sources of the disturbing mass in the interior of the earth.

The observable gravity field quantities g, N, ξ , n, etc. in the usual spherical approximation are expressed as linear functionals L(T) of T and have different "sensitivity" to the disturbing mass sources. This is because the depth of the source affects differently each of the above quantities (e.g. Meissl 1971), since the physical characters of these quantities are different.

Any set of observed gravity field quantities on the earth can be considered to satisfy a statistical collocation model:

$$x = A\,X + s + n \quad (5)$$

where $x = L(T)$, $A\,X$ is the trend part, s is the random signal and n is the noise.

Linearization of (5) can be applied when the trend part is properly expressed:

$$x - A\,X = s + n \quad (6)$$

However the trend elimination may be viewed as a structural one in which the components of the parameter vector X

$$X = X\,(x_1, x_2, x_3, \ldots) \quad (7)$$

are related to geophysical characteristics.

So, the traditional reference of L(T) to a geopotential model (G.M.)

$$L(T) - L(T_{GM}) = L(\Delta T) \quad (8)$$

can be viewed as a kind of structural trend elimination for the low-end part of the medium wavelengths of the gravity field (see Table 3.1 in Schwarz 1985). For this aspect, the coefficients C_{nm},S_{nm} of the spherical harmonic expansion are considered to be related to the depth of the disturbing mass sources which generate the gravity field.

This consideration is opposed to the usual reference of L(T) to high degree G.M. (n = 180), not only because of the errors in the estimation of high degree coefficients (e.g. Rapp 1981) but also because the relation between the depth of sources and the affected degree and order of coefficients C_{nm} and S_{nm} is not well defined. One may adopt that for degrees $n \geq 30$ the coefficients contain lithospheric information (e.g. Bjerhammar 1981).

The most important and best known density anomalies are in the earth's interior those associated with topography. They include the gravitational effect of the visible topographic masses (orthometric heights), the bathymetry and the isostatic compensation. These effects account for the major part of the gravity field variation, at least for wavelengths $\lambda < 1000$ km. In a global statistical study for the earth's gravity field (Jordan 1978) it is estimated that about 97 % of the gravity anomalies are due to the lithosphere. However, the gravity anomalies for λ = 500 to 170 km may result from density variations beneath the lithosphere (Parsons and Daly 1983), while this range shares causes of isostasy and lithospheric flexure for topography (Jordan 1978).

In geophysically complex areas usual characteristics are the thickening of the crust and phenomena in the earth's lower lithosphere which tend to establish the isostatic equilibrium. The isostatic equilibrium is considered as a static, thermal and kinematic one. Both characteristics have as surface expressions the generation of topography and the motion of tectonic units (isostatic motions, rotation of plates). Typical examples of deeply compensated regions (through anomalous density values in upper mantle) are sea trenches.

For such areas the task to model analytically the gravity

field may be difficult because:

- medium wavelengths can be associated to different tectonic units which may have been brought to different elevations by vertical actions and compressive forces with source origin at the lower lithosphere
- the wavelengths associated with the topography will be contaminated by crustal flexure and density contrasts which do not belong to the visible masses.

Therefore the linearization of the gravity field modeling involves a wide range of wavelengths-and this problem may be viewed in relation with the statistical information contained in the gravity field functionals L(T). This information is useful for the detection of structural trends and is related to:

- the type of the functional (gravity anomaly, undulation, deflection of the vertical) and its sensitivity to the gravitational attraction of the topographic masses
- the resolution of the data (minimum detectable wavelength)
- the geographical covering of the data (maximum detectable wavelength).

The results of the inversion for medium wavelengths can be interpreted as statistical averages on which the high frequency part of the gravity field is superimposed. The geoid may offer a possibility to check linearity for medium wavelengths through the relation to the undulation of the Moho (e.g. Doufexopoulou 1984).

The covariance functions of the gravity field functionals are widely used for the prediction/estimation of the gravity field. The two basic parameters, the variance C_0 and the correlation distance ξ (e.g. Moritz 1976) control the quality of the above quantities.

The power spectrum of a quantity can be viewed as the decomposition of the variance in narrow bands of frequency. Therefore the variance of an experimental covariance function is a direct measure of the power existing in the data field, for recognizing purposes. The correlation distance indicates the frequencies in which the power is concentrated. A small correlation distance indicates power in high frequencies. So the

experimental (empirical) computation of the covariance function (C.F.) can be used as an alternative to the frequency analysis methods (Fourier transforms etc.), especially for recognition. Moreover the computation of the 2-D C.F. allows, in some cases, the detections of structures related to the tectonic background (e.g. Meskó 1977).

In principle, the free air gravity anomalies give anisotropic C.F. and the orientation of anisotropy is related to the topography, provided that no serious geological changes occur in the area under examination. For small areas, the F.A. anomalies are related to the topographic elevations:

$$g_{FA} = a + bh + s \tag{9}$$

where a and b are coefficients and h is the topographic elevation. The coefficient a can be interpreted as a mean Bouguer anomaly for the region, while b is a representative Bouguer coefficient. For the standard density of the surface masses 2.67 gr/cm^3, b is 0.1119 mgal/m. However, when the Bouguer coefficient cannot be assumed as constant, but is varying with the distance, it can be estimated as (Heiskanen and Moritz 1967):

$$b = \frac{Cov(\Delta g, h)}{Cov(h,h)} \tag{10}$$

An interpretation of this relation can be found with the use of the convolution integral of gravity anomaly-topography (e.g. Doufexopoulou 1985). For small areas where the flat earth approximation can be used, the Bouguer coefficient is:

$$b = 2\pi k\rho h \tag{11}$$

where ρ is the density of the topographic masses.

Thus, when the Bouguer coefficient is estimated analytically for a region with the regression (9), an estimation about the surface mass density can be obtained under the essential assumption of the linear relation between gravity anomaly and topography. If the estimated values of b (or ρ) differ

considerably from the standard ones (b = 0.1119 mgal/m, p = = 2.67 gr/cm^3), either the data are noisy, or the density is not the standardly adopted. However, even in the case of noisy data, the variation of b (or p) at various sample regions in an area indicates the variation of subsurface mass densities.

The covariance function of terrain elevations indicates the terrain variability:

$$c^h(s) = M\{ h(\tau) \cdot h(\tau+s) \} \quad \text{for } \tau = 0 \text{ to } \tau \text{ max} \tag{12}$$

(where $C^h(s)$ is the covariance estimate for distance s, τ is the sampling interval) and can be used for the estimation of the order of terrain corrections in an area (Sünkel 1981) from the formula:

$$T.C. = 3\pi kp \frac{C_0^h}{\xi} \tag{13}$$

where C_0^h is the variance of the topographic elevations, ξ is the correlation distance, p is the density, and T.C. is the order of the terrain correction.

The order of terrain corrections over different sample regions within an area can be used as a numerical filter to the gravity anomaly data for the elimination of high frequencies.

On the other hand, the selected degree of truncation of the G.M. to refer the local gravity data corresponds to a high pass filtering. Thus, with this kind of crude high and low pass numerical filtering, the gravity anomaly data include the part which is considered as a signal of the local gravity field, and can be related to structural anomalies within the lithosphere.

The computation of 2-D C.F. of the "filtered" gravity data will give azimuth dependent covariance values. These values can be used for the construction of the directivity diagrams (Meskó and Kis 1977) as following:

Diagrams are obtained by summation of covariance values along azimuths:

$$I_R(a) = \int_0^R \varphi(r \cos a, r \sin a)\, dr \tag{14}$$

where (a) is the continuous covariance with arguments (x,y) expressed in polar coordinates. Instead of the continuous function, the experimental values of the covariance are available at distances s = id and orientations a. Therefore:

$$I_R(a) = \sum_{i=0}^{n} \varphi(id,a) \qquad (15)$$

where $\varphi(id,a)$ is the experimental value of the covariance of data points for distance id and azimuth a,d is the data interval. For reasons of statistical stability, the upper limit of summation n should be at least

$$n = \frac{L}{5d} \qquad (16)$$

where L is the length of the data block.

The upper limit of summation n acts as a parameter for the identification of linear features. The large peaks in I_R values correspond to linear structural features, provided that n is sufficiently large.

This geophysically originated method can be used to confirm structures (tectonic plate boundaries, faults, etc.) for which results from other methods contradict.

DESCRIPTION OF DATA

For several regions of Greece data files including mean height values are available at the Higher Geodesy Laboratory of the N.T.U. of Athens, These values have been calculated after manual digitization of contour lines from topographical maps. The scale of these maps was selected in respect to the grid size of each file.

The whole procedure includes two phases. The first one concerns the digitization and a linear registration model. In the second phase, the mean height values with their standard deviations are calculated through an algorithm based on the linear integration of contour lines.

The available data files containing mean heights are:

1. 5'×5' grid of mean height values. It is located in Western Greece between $\lambda = 19^{o}$ to 24^{o} and $\varphi = 36^{o}$ to 42^{o}. As initial source map, the series of 1:1 M scale bathymetric maps of Mediterranean (I.O.C. (Head Department of Navigation and Oceanography, USSR, 1981)) with 200 m contour line interval was used.
2. 1'×1' grid of mean height values. It is located at Etoloakarnania area and covers a region of 1^{o} 0.5^{o}.
3. 15"×15" grid of mean height values. It is located at Zakynthos island and Delvinaki area which extend from $\lambda = 20^{o}37'$ to $20^{o}57'$ and $\varphi = 37^{o}40'$ to $37^{o}57'$ and from $\lambda = 20^{o}15'$ to $20^{o}35'$ and $\varphi = 39^{o}45'$ to $40^{o}05'$, respectively.

For both 2 and 3 sections the series of 1:50 K scale topographic maps of HAGS with 20 m contour line interval were used as source maps.

The data files containing free air gravity anomalies extend from $\lambda = 20^{o}$ to 27^{o} and $\varphi = 35^{o}$ to 41^{o}, and contain 5300 5'×5' mean values, as well as 672 15'×15' means. These files have been created through manual digitization of the free air gravity anomaly map of Greece which is published by the Greek Military Service. The scale of the map is 1:1 M with a contour interval 10 mgal. The uncertainty of the 5'×5' mean values is estimated to 4 mgals (Doufexopoulou 1985). The 15'×15' mean values file is produced from the 5'×5' one by simply averaging the 9 5'×5' values which occur within each 15'×15' block. The uncertainty of the 15'×15' values is 12/9 mgals, applying the law of propagation of variances.

PREVIOUS AND RECENT ANALYSIS AND RESULTS

In the frame of a local gravity field study for the geoid approximation (Doufexopoulou 1985) it was early indicated that the free air anomalies pattern shows anisotropic characteristics in the empirically computed 2-D covariance functions (Doufexopoulou 1982). In addition, strong inhomogeneities were indicated by a wide range of variance value parameters which could not be explained by the terrain. The values of variance generally

showd an increase towards East and South and this investigation suggested the need of a more systematic study of the area from a geodynamical aspect.

Although during these computations a digital terrain model for the reduction of the gravity data was not available, the preferred orientation of anisotropies and the inhomogeneity indicated that the reasons for the interpretation had to be looked for also within deeper mass structures than the terrain. The two major tectonic blocks (African and Aegean plates) and the subducting slab of the African plate introduce disturbances of medium wavelengths in the gravity field and the lithospheric signal is masked. So, elimination of structural trends is of importance in order to study in detail the fine structure of the gravity field.

With the use of the Moho depth model and of altimetric undulations, the linear correlation between these data was checked over the African and Aegean plates (Doufexopoulou 1984). This correlation is expected to hold for the flexure model of isostatic compensation (e.g. Sandwell 1984). Results are presented in Table I. No correlation exists over the Aegean while over the Southwestern part of the country the linear correlation is confirmed.

Table I. Correlation between geoid undulations and Moho depths over the African tectonic plate (from Doufexopoulou 1984)

Geoid undulation	Degree of harm. expansion	Correlation coef.
GEM10B	36	0.755
GEM10C	180	0.567
Altimetric (Geos 3+Seasat)	360	0.801
Gravimetric (Stokes)	360	0.711
Gravimetric (collocation)	360	0.814

The geoid can be used for the medium wavelengths study of the gravity field because the undulations N have sources at deep lithospheric features (e.g. Kaula 1972, see also Schwarz 1985

Table 3.1). In addition, the undulations may be considered as low pass filtered gravity anomalies, through e.g. Stokes kernel. The low frequency part of the geoid (degrees ≤ 36) can be well modeled with the use of G.M. because the C_{nm} , S_{nm} coefficients are well defined in those G.M. which also contain altimetric data. In addition, the spherical harmonic coefficients $n < 36$ come mainly from lower lithosphere and deep mass layers.

The technique which is mostly followed in local gravity field modeling concerns the combination of a G.M. and local data. The G.M. is used as a reference field for the local data. The remaining residual gravity field data can be considered as a signal presenting the local features of the field. High degree and order ($n \geq 180$) G.M. may not be suitable for this purpose, in spite of the advantages it may offer (e.g. decrease of local data coverage, use of flat approximation, etc.). These advantages may be questioned from the aspect of geophysical inversibility of high degree coefficients, as well as the increase of errors in the coefficients above $n = 120$ (Rapp 1981).

For the Greek area the choice of a conforming reference G.M. was studied from the aspect of its geophysical "inversibility" and the power distribution at different degrees of expansion. Four G.M.-s were studied, GEM10B, GRIM3B, GRM3L1 (n=36) and RAPP81 (n=180) (Doufexopoulou and Papafitsorou 1986). As criteria for the choice were used:

- the correlation of undulation components between different degrees of expansion of the G.M with the Moho depths
- the behaviour of the index of inhomogeneity for various reference degrees of the local 15'×15' anomaly data. As index of inhomogeneity the ratio of the higher to the lower variance of referenced anomalies was considered. The higher and lower variances refer to three subregions, into which the whole area was divided, in order to investigate the inhomogeneity of the gravity field
- the construction of the variance spectra of the geoid undulations for the G.M.

The details of these computations can be found in the above mentioned reference. Significant correlations obtained are

presented in Table II. In Table III the variances referred to G.M. local anomalies are shown for the four models and three subregions. Figure 1 shows the index of inhomogeneity for the RAPP81 G.M.

Table II. Correlation coefficient between computed components of undulation from G.M. and Moho depths for African and Aegean tectonic plates

Region \ GM	expan.	GRM3L1	GRIM3B	GEM10B	RAPP81
African	22-30	0.174	0.201	-	0.300
	30-36	0.876*	0.819*	0.794*	0.623*
	45-60				0.697*
Aegean	22-30	0.648*	0.648*	-	0.604*
	30-36	0.552	0.529	0.808*	0.842*
	45-60				0.179

*represents significant (numerical) correlation

Table III. Variances of $\Delta g(F.A)$ referenced to GM for regions I, II, III (Local field of 15'×15' anomalies. Unit: $mgal^2$)

Region \ Model	n	GRM3L1	GRIM3B	GEM10B	RAPP81
I	30	821	838	-	806
	36	669	704	871	678
II	30	7574	7818	-	7043
	36	7132	6999	7590	6840
III	30	882	959	-	800
	36	5835	530	941	591

Since the Greek area was recently partly covered with 5'×5' mean topographic heights (or depths), a further analysis of the gravity field has been done. The studied area extends from $\varphi = 38^{o}$ to 41^{o} and from $\lambda = 20^{o}$ to 23^{o} and includes

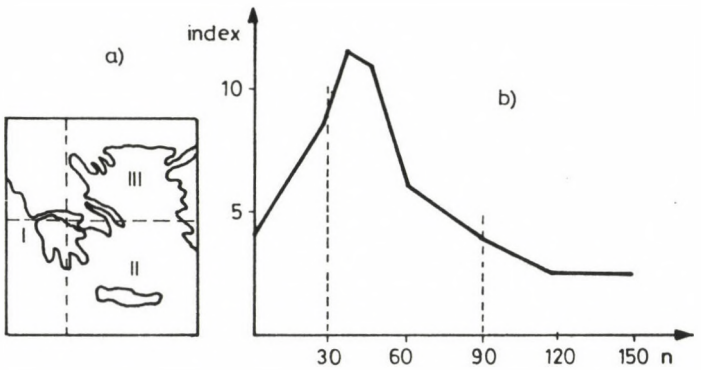

Fig. 1. a) Division of Greece in regions I, II, III for studying the inhomogeneity of gravity anomaly field. b) Index of inhomogeneity, for the Rapp81 G.M., of the local gravity anomaly field. (Higher/lower variance value of referenced gravity anomalies for regions I, II, III)

part of the Alpine fold, as well as major tectonic faults and plate boundaries (Fig. 2). For this area both 5'×5' mean free air anomalies and topography exist. The Moho depths, estimated from seismic and gravity data (Makris 1973) are presented in Fig. 3.

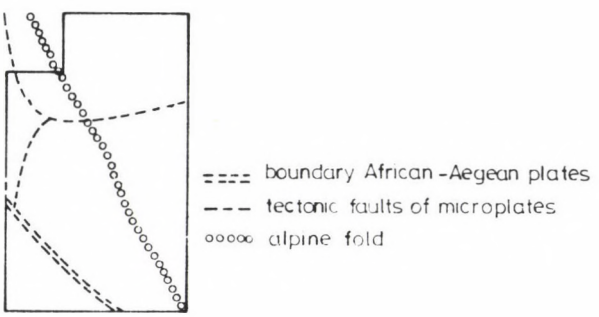

Fig. 2. Main pattern of the region in the present study

The main purpose of this study was to create a file of gravity anomalies whose major variations could be attributed to the lithosphere for further modeling. For that, GRM3L1 G.M., truncated at n = 30, was at first subtracted from the mean

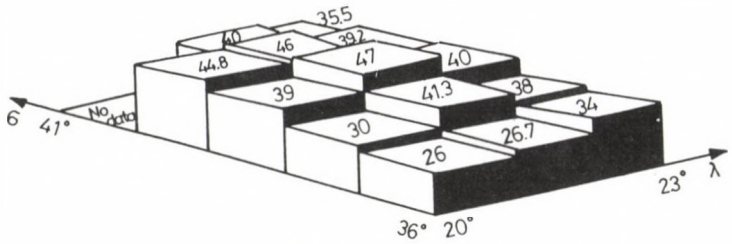

Fig. 3. Moho depth values (km), Makris (1973)

5'×5' free air anomaly values and the referenced 5'×5' Δg^r's:

$$\Delta g^r = \Delta g - \Delta g_{GRM3L1}$$

are considered to contain information coming mainly from the lithosphere and the topography (Figs 4, 5). The topography was used to estimate a crude complete "Bouguer" reduction (plate and terrain correction) (Fig. 6). The subtraction of these reductions from the Δg^r's (Fig. 7) acts as a low pass filter to the referenced gravity anomalies, and so the major part of the terrain influence is reduced. The process is as follows:

In each $1^o \times 1^o$ block of the study area the mean $1^o \times 1^o$ height was subtracted from the original 5'×5' mean height values of the block. The $1^o \times 1^o$ local mean topography was preferred to the global $1^o \times 1^o$ values of the spherical harmonic expansion because it represents better the local topography in this complex area.

A covariance and cross covariance computation for $(\Delta g, h)$ and (h,h) was performed for each $1^o \times 1^o$ block and the correlation distance ξ and variance C_o^h were found. Thus, the order of the terrain correction for each $1^o \times 1^o$ block was computed from Eq. (13). In this computation the standard rock density 2.67 gr/cm^3 was used. For two of the blocks the order of terrain correction (for the standard density) is larger than the uncertainty of the data (7 and 12 mgals). The isolines of the so computed filtered Bouguer map fit well to the analytically computed Bouguer anomalies of a detailed gravity survey for Peloponesos (Makris et al. 1973).

The relation (10) was used for an empirical estimation of the Bouguer coefficient in each block. Naturally, the wavelengts

Fig. 4. Free Air Anomalies (Contour interval 20 mgal)

Fig. 5. Topography (Contour interval 500 m)

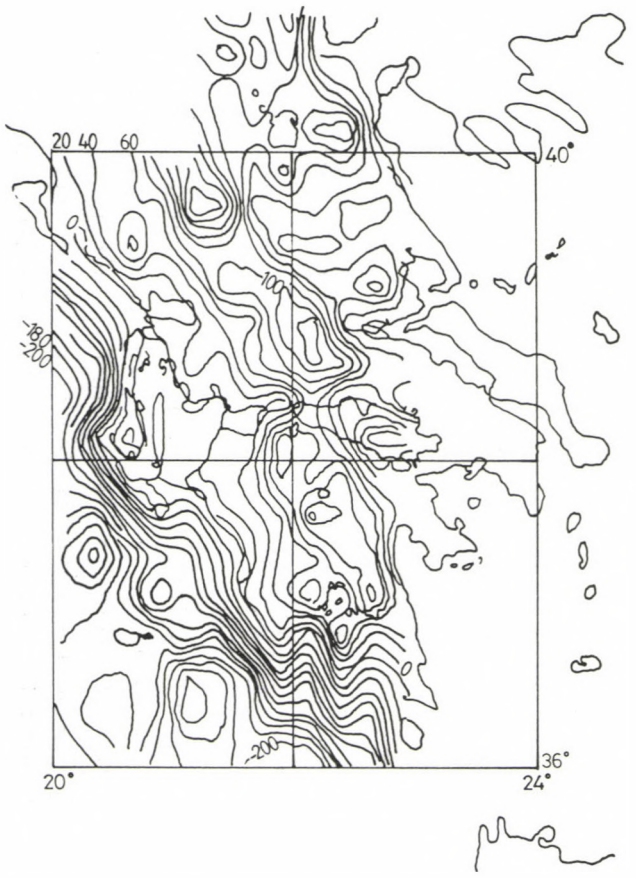

Fig. 6. Terrain Reductions (Bouguer plate + Terrain Corr.) (Contour interval 20 mgal)

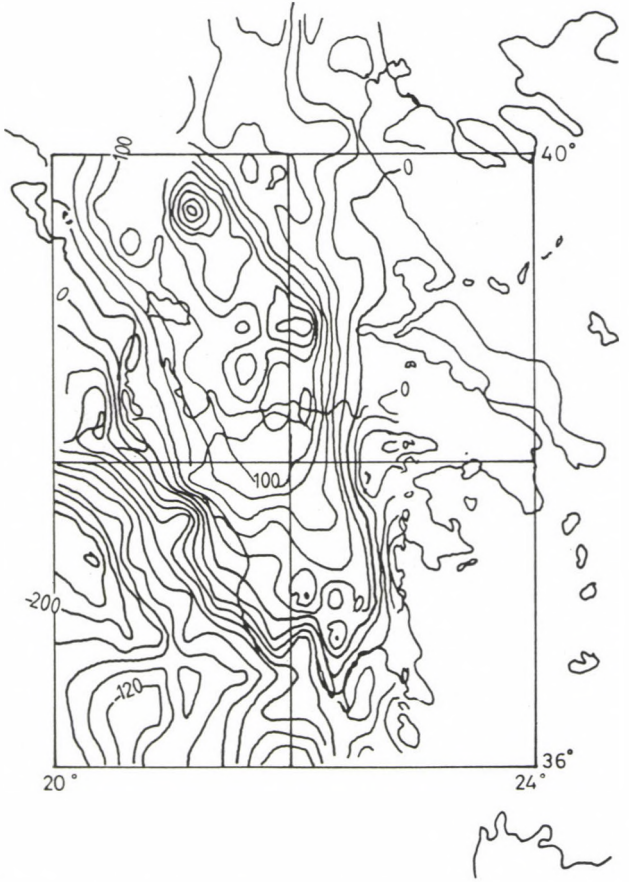

Fig. 7. Residual Gravity Anomalies (Contour interval 20 mgal)

existing in the data to not allow an absolute estimation of the coefficient, but it was expected that some information about the density disturbances could be received from the variations of the so-computed b values in each block. The results of this computation are presented in Fig. 8. Abrupt variations of coefficient b occur in two blocks, while in one block there exists a discontinuity from positive to negative values. The three blocks are located at the South-western part of the area, between the boundary of the African and the Aegean plates and the Alpine fold (Fig. 8).

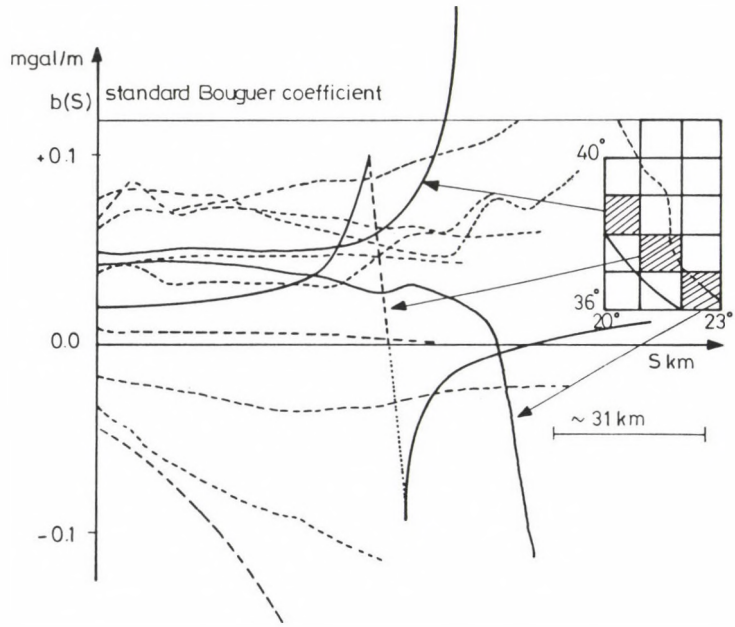

Fig. 8. Plots of distance dependent Bouguer coefficients, statistically derived, for all the $1^{0}\times1^{0}$ blocks. Shaded blocks indicate possible presence of disturbing masses, corresponding to full-line Bouguer coefficient function in the Fig. 8

After the application of the high and low pass "filters" on the data, the anomalies are considered to be mainly lithospheric signals. In order to check this consideration, the empirical 2-dimensional covariance function of the "filtered" data was computed for three regions within the area, and direc-

tivity diagrams were plotted, according to Eq. (15). The azimuths along which the covariance values were calculated are at every 22.5^{o}.

In the northern region ($2^{o} \times 2^{o}$) the preferred azimuth is North-South. For the southern region ($3^{o} \times 3^{o}$) the preferred azimuth is at 135^{o}, almost parallel to the boundary of the African and Aegean tectonic plates. However, for the middle region ($3^{o} \times 3^{o}$) the preferred azimuth of the 2-D covariance function is slightly pronounced at 157.5^{o}, while the directivity diagram has an elliptical shape with small eccentricity. Since within this region the tectonic pattern is more complicated (see Fig. 2) a recomputation of the directivity diagram was done for every 10^{o}, in order to distinguish other important orientations which could be related to the tectonic features. The directivity diagrams are presented in Fig. 9.

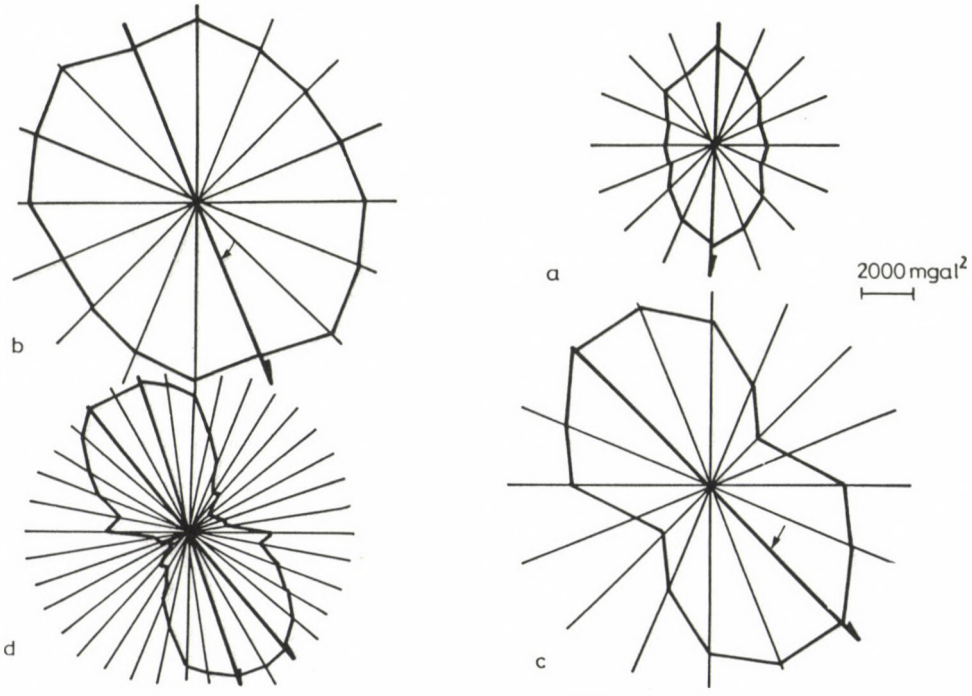

Fig. 9. Directivity for a (north), b (middle), c (south) region, d (as c with higher resolution in directivity azimuth). Arrows present significant directions related to linear features

CONCLUSIONS AND DISCUSSION

It should be pointed out that the rather large grid (5'×5') of the mean values in gravity anomaly and topography does not allow the study of the very short wavelength variations of the gravity field. Since these variations are due to the terrain, the statistically reduced gravity anomalies can be considered as a partly filtered lithospheric signal.

In spite of this problem with the original data files, the tectonic background of the Greek area gives strong enough signal and it is possible to get significant indications on the order of wavelengths which disturb the regional gravity field.

From Table II it can be observed that longer wavelengths disturb the gravity field in the Eastern part of the country, but the total power of the gravity field, as indicated by the variance values of gravity anomalies (Tables III and IV) is considerably lower than that in the Western part (region II in Fig. 1). This suggests that the variations in the Western part are due to shallower masses than the ones in the Eastern part.

Table IV. Variances of Δg(F.A.) referenced to RAPP81 for various degrees of truncation and for regions I, II, III (unit: $mgal^2$)

RAPP81	30	36	45	60	90	120	150	Local data
I	806	678	718	768	621	492•	621	1557
II	7045	6840	5632	4339	2384	1437•	2384	6904
III	800	591	499•	726	655	548	586	1545

The variations of the inhomogeneity index (Fig. 1) indicate that high inhomogeneity is introduced within the whole area when the local gravity anomaly data are referred to a G.M. of degrees 30 ÷ 90 of the harmonic expansion. The corresponding wavelengths are 1200 ÷ 400 km (following the empirical rule $\frac{180}{n}$). For degrees greater than 90 of the reference G.M., the

residual field becomes smooth (Table IV) but whithout any significance for inversion. However, the variance of the referenced gravity anomalies in region II is still high, suggesting that there may exist local sources. An optimal degree of the reference G.M is 30 ÷ 36 degrees, if the power sources of the gravity field are to be studied. From the four checked G.M-s, the GRM3L1 seems to fit better in the Greek area.

The statistically estimated order of terrain corrections (Table V) is greater than the uncertainty of the data in the South-western part of the region(recent study) within the same blocks for which the statistical estimations of the distance varying Bouguer coefficient show abrupt or discontinuous changes. These blocks (Fig. 10) are located between the two main plates' boundary and the Alpine fold. A mass model should be needed to interpret the gravity field there.

Since the critical wavelengths of the gravity field variations are 1200 ÷ 400 km, the "filtered" (referenced to GRM3L1 and Bouguer reduced) gravity anomalies should contain lithospheric signal. This is indicated by the directivity diagrams (Fig. 9). The ones for the middle and southern region give significant azimuths which are almost parallel to the boundary

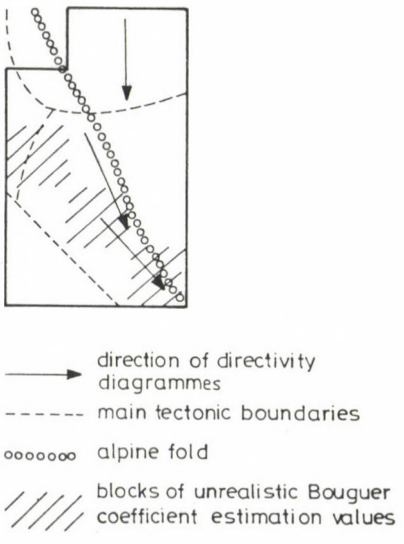

Fig. 10. Direction of directivity diagrams and the pattern of main tectonics on the region in study

Table V. Statistical parameters for topography, $1^{o} \times 1^{o}$ blocks, 5'×5' samples and variances of "filtered" gravity anomalies (present work)

Area, top left corner lat, long	Mean elevation $1^{o} \times 1^{o}$ (m)	Variance m^2	Correlation distance (arcmin)	Order of terrain correction (mgal)	Type of region	Variance "filtered" gravity anomalies	Ratio: Corr. distance sampling interval
41^{o}, 21^{o}	830	87.796	9.69	2	land	5475 $mgal^2$	1.938
41^{o}, 22^{o}	688	182.857	13.69	2	land	* 711 $mgal^2$	2.738
40^{o}, 20^{o}	988	253.525	13.46	3	land	9233 $mgal^2$	2.692
40^{o}, 21^{o}	970	201.344	15.96	2	land	15622 $mgal^2$	3.192
40^{o}, 22^{o}	318	77.185*	6.00	2	land	* 1150 $mgal^2$	1.200
39^{o}, 20^{o}	334	1247.767	28.48	7	sea	2586 $mgal^2$	5.696
39^{o}, 21^{o}	819	175.385	19.35	2	land	12836 $mgal^2$	3.870
39^{o}, 22^{o}	387	372.585	9.97	6	land	* 3887 $mgal^2$	1.994
38^{o}, 20^{o}	-860	1508.676	24.24	10	sea	28512 $mgal^2$	4.848
38^{o}, 21^{o}	381	634.094	28.88	4	sea	4435 $mgal^2$	5.776
38^{o}, 22^{o}	429	225.715	15.57	2	land	* 3365 $mgal^2$	3.114
37^{o}, 20^{o}	-2212	65.786*	12.72	1	sea	23277 $mgal^2$	2.550
37^{o}, 21^{o}	-194	1819.098	25.56	12	sea	14936 $mgal^2$	5.112
37^{o}, 22^{o}	697	1572.357	21.16	12	sea	* 3567 $mgal^2$	4.232

of the tectonic plates. The diagram for the northern region gives a N-S azimuth, for which there is no clear explanation, or the origin lies within the thick crust.

The gravity field of the Greek area is suggested to be object of further research, priority given to the computation of isostatic gravity anomalies, as soon as the computation of mean heights is completed. Standard isostatic models (Pratt or Airy) are not expected to give a smooth gravity anomaly field. Seismic information together with a mass model (considering e.g. the lithospheric flexure) may give satisfying results in the gravity field interpretation. The identification of the isostatic or tectonic origin of mass disturbances may assist the geodynamical interpretation of time dependent control networks. Collaboration with scientists from other geo-sciences is important for the investigation of the gravity field.

REFERENCES

Bjerhammar A 1981: Longwave heterogeneities as seen in the upper mantle. 7th E.G.S. Meeting, Uppsala, Sweden

Doufexopoulou M 1982: In: Proceedings of the III Inter. Symposium "The use of artificial satellites for Geodesy and Geodynamics", Hermioni, Greece

Doufexopoulou M 1984: In: Proc. of the Intern. Symposium "Space techniques for geodynamics", Tome 1, Sopron, Hungary

Doufexopoulou M 1985: Study of the gravity field in Greece for the geoid approximation (in Greek). Ph.D. Thesis, N.T.U. of Athens

Doufexopoulou M, Papafitsorou A 1986: Inversibility of geopotential models for local gravity field approximation. Presented at the Intern. Symposium "The figure and dynamics of the Earth, Moon and other planets", Prague, Czechoslovakia

Forsberg R 1984: Local covariance functions and density distributions. Department of Geodetic Sciences, O.S.U. Scientific report No. 6, 1984, Columbus, Ohio

Heiskanen W, Moritz H 1967: Physical Geodesy. W H Freeman and Company, San Francisco

Jordan S K 1978: J.G.R., 83, 1816-1824.

Kaula W 1972: In: The nature of the solid earth. Ed. by E Robertson, U.S. Geological Survey, Silver Spring Maryland

Makris J 1973: Bull. Geol. Soc. of Greece, 10, I. 206-213.

Makris J 1977: The crust and upper mantle of Aegean region

obtained from deep seismic soundings. Publ. Inst. Geoph. Pol. Acad. Sci. A-4 (115).

Makris J, Mavridis L, Menzel H, Stavrou A, Veis G 1973: Zeitschrift für Geophysik, 39, 929-936.

Meissl P 1971: A study of covariance functions related to the Earth's gravitational potential. O.S.U. Report, No. 151, Columbus, Ohio

Meskó A, Kis K 1977: Acta Geol. Acad. Sci. Hung., 21, 325-335.

Moritz H 1976: Covariance functions in Least Squares Collocation. O.S.U. Report, No. 242, Columbus, Ohio

Papazachos B C, Comninakis P K 1971: J.G.R., 76, No 35, 8517-8533.

Parson B, Daly S 1983: J.G.R., 88, B2, 1129-1144.

Rapp R 1981: The Earth's gravity to degree and order 180 using Seasat Altimeter data, terrestrial gravity data and other data. Report No. 322, Department of Geodetic Sciences, O. S.U., Columbus, Ohio

Sandwell D 1984: J.G.R., 89, B2, 1089-1104.

Schwarz K P 1985: In: Proceedings of Local gravity field approximation, Beijing China

Sünkel H 1981: Point mass models and the anomalous gravity field. Department of Geodetic Science and Surveying, Report No. 328, O.S.U., Columbus, Ohio

Tscherning C 1983: In: Proceedings of the 18th General Assembly of IAG-IUGG, Hamburg

Woodside J 1976: J.G.R., No. 47, 1947-1968.

Acta Geod. Geoph. Mont. Hung., Vol. 24 (3-4), pp. 237-249 (1989)

DETERMINATION OF TRANSFORMATION PARAMETERS WITH THE METHOD OF THE LEAST SUM OF ABSOLUTE VALUES

J Somogyi and J Závoti

Geodetic and Geophysical Research Insitute of the Hungarian Academy of Sciences, H-9401 .Sopron, POB 5, Hungary

[Manuscript received July 7, 1988]

The paper deals with the determination of transformation parameters with the method of the least sum of absolute values. It gives a solution for the three dimensional transformation and a solution for the two dimensional version compared with Fuchs' method.

Keywords: Helmert transformation; least sum of absolute values; L1--norm; robust estimation; similarity transformation

1. INTRODUCTION

The theory of mathematical statistics has been enriched in the last decades with a new direction, with the robust estimates. The appearance of this direction is connected with the fact that the conditions in the parameter estimations (e.g. Gaussian distribution, linearity, independence) are seldom fulfilled. Moreover, the spread of automatization involves the danger that gross errors remain undetected what on its turn decreases the reliability of estimations if classical methods are used.

Robust estimation methods enable automatical exclusion of outliers, further they enable to decrease the effect of "contaminated" measurement results on the parameter estimation.

Efforts to exclude gross errors have appeared simultaneously with the advent of data processing. This is especially true in case of surveying where sampling refers to small data samples in a statistical sense of the word. This makes a checking of data easier being a very important phase of processing as the general method of parameter estimation, the least squares method resulting in the arithmetical mean, gets

erroneous if there are undetected erroneous values.

As a consequence of the rapid development of measurement and computation techniques, the demand for automatized data processing refers to surveying, too. Photogrammetry and space methods necessitate the processing of large data sets which led to the application of robust estimation methods together with classical data processing methods. Such tendencies do exist, but their spread is hampered by the adherence to classical methods.

The method of the least sums of absolute values (or the L1-norm) is a most effective method to filter gross errors. There were several experiments to introduce it into surveying (e.g. Fuchs 1982, Hahn and Bull 1984, Ebong 1985, Kampmann 1986, Burstedde and Cremer 1986).

In the following possibilities are presented using the L1-norm for the adjustment of two- and three-dimensional coordinate transformations playing an important role in surveying.

2. PRINCIPLE OF THE LEAST SUM OF ABSOLUTE VALUES

The method is known for a long time, it has been proposed by Laplace in 1773. The object function to be minimized can be given in the following form (L1-norm):

$$\Phi(X-\bar{X}) = \sum_{i=1}^{n} |X_i-\bar{X}| = \min . \qquad (1)$$

The minimum is found by partial derivation of Eq. (1) by making the obtained ω-function equal to zero:

$$\sum\omega(|X-\bar{X}|) = \sum_{i=1}^{n} \operatorname{sign}(X_i-\bar{X}) = 0 . \qquad (2)$$

This equation estimates the location parameter (expected value) by the median. Its distribution function is flatter than that of the Gaussian distribution thus it tolerates more outliers. Parameters should be determined by linear programming, being more complicated than the usual computation algorithms in

surveying. The dynamic development in the field of computation techniques, however, will enable the spread of linear programming in the practice of surveying, too.

3. SOLUTION OF THE HELMERT-TRANSFORMATION ON THE BASIS OF THE L1-NORM

Let us consider a set of points $P(x_i, y_i)$, $i = 1, 2, \ldots n$. Be the points to be transformed $Q(x_i+dx_i, y_i+dy_i)$, $i = 1, 2, \ldots n$ (supposing that dx_i and dy_i are small values) and the coordinates after transformation be $(x_i+v_{x_i}, y_i+v_{y_i})$.

The formula for the Helmert-transformation is:

$$\begin{aligned} x_i+v_{x_i} &= (x_i+dx_i) \cos d\varphi - (y_i+dy_i) \sin d\varphi + mx_i+c_x \\ y_i+v_{y_i} &= (x_i+dx_i) \sin d\varphi + (y_i+dy_i) \cos d\varphi + my_i+c_y \end{aligned} \qquad (3)$$

where $d\varphi$ = the angle of rotation,
m = the scale factor,
c_x, c_y = the parameters of translation.

One has in a first approximation:

$$\begin{aligned} v_{x_i} &= mx_i - d\varphi\, y_i + c_x + dx_i \\ v_{y_i} &= my_i + d\varphi\, x_i + c_y + dy_i \end{aligned} \qquad i = 1, 2, \ldots n \qquad (4)$$

The measure of fitting, r_i, should fulfil the following inequality on the basis of the corrections:

$$\sqrt{v_{x_i}^2 + v_{y_i}^2} \leq r_i; \qquad r_i \geq 0 \qquad (5)$$

Now the minimum of the following target function is to be found:

$$\sum_{i=1}^{n} r_i \longrightarrow \min \qquad (6)$$

Equations (4), (5), (6) define a non-linear optimization problem. It

can be solved by the algorithm proposed by Fuchs (1982).

It can be easily seen that Eq. (5) can be approximated by an infinite number of inequalities of the form:

$$v_{x_i} \cos\alpha + v_{y_i} \sin\alpha \leq r_i \qquad 0 \leq \alpha < 2\pi . \tag{7}$$

As initial values let us select a finite number of angles at each point:

$$\alpha_{ij} = (j-1)\frac{\pi}{2} \qquad j = 1, 2, 3, 4 . \tag{8}$$

With this, the initial problem of Eqs (4), (5), (6) can be re-written as a linear programming problem:

$$(x_i \cos\alpha_{ij} + y_i \sin\alpha_{ij})\, m + (x_i \sin\alpha_{ij} - y_i \cos\alpha_{ij})\, d\varphi$$

$$+ \cos\alpha_{ij}\, c_x + \sin\alpha_{ij}\, c_y - r_i \leq -(dx_i \cos\alpha_{ij} + dy_i \sin\alpha_{ij}) \tag{9}$$

$$-\sum_{i=1}^{n} r_i \rightarrow \max \qquad r_i \geq 0$$

$$i = 1, 2, \ldots n \qquad j = 1, 2, \ldots k_i .$$

It is advantageous to use the dual of this linear programming problem:

$$-\sum_{j=1}^{k_i} \pi_{ij} \leq 1 \qquad i = 1, 2, \ldots n$$

$$-\sum_{i=1}^{n}\sum_{j=1}^{k_i} \pi_{ij} \sin\alpha_{ij} = 0$$

$$-\sum_{i=1}^{n}\sum_{j=1}^{k_i} \pi_{ij} \cos\alpha_{ij} = 0$$

$$-\sum_{i=1}^{n}\sum_{j=1}^{k_i} (x_i \sin\alpha_{ij} - y_i \cos\alpha_{ij})\pi_{ij} = 0 \tag{10}$$

$$- \sum_{i=1}^{n} \sum_{j=1}^{k_i} (x_i \cos \alpha_{ij} + y_i \sin \alpha_{ij}) \pi_{ij} = 0$$

$$- \sum_{i=1}^{n} \sum_{j=1}^{k_i} (dx_i \cos \alpha_{ij} + dy_i \sin \alpha_{ij}) \pi_{ij} \rightarrow \max$$

$$\pi_{ij} \geq 0 .$$

For the solution of the dual linear programming problem we suggest the use of the two-phase simplex method, as this two-phase simplex method can be used for the solution of any linear programming task. The only condition - namely that the free term be non-negative - can be easily fulfilled. The optimum solution of the primal task is obtained from the dual solution if at the end of the first phase all artificially introduced variables are eliminated from the set of basis variables. The solution is then $\bar{m}^{(1)}$, $\bar{d}\rho^{(1)}$, $x_x^{(1)}$, $c_y^{(1)}$, $\bar{r}_i^{(1)}$. Equation (4) enables the computation of the corrections $v_{x_i}^{(1)}$, $v_{y_i}^{(1)}$ and from Eq. (5) one gets:

$$r_i^{(1)} = \sqrt{v_{x_i}^{(1)\,2} + v_{y_i}^{(1)\,2}} \qquad (11)$$

At points where the inequality

$$\bar{r}_i^{(1)} \leq r_i^{(1)} \qquad (12)$$

does not hold, let us determine the angle:

$$\tau_{ij} = \arctan \left(v_{y_i}^{(1)} / v_{x_i}^{(1)} \right) \qquad \begin{matrix} i = 1, 2, \ldots n \\ k_i^{*} = k_i + 1 \end{matrix} \qquad (13)$$

These angles add to Eq. (9) further inequalities. Thus iterations can be carried out till the difference of the absolute values of two subsequent angles τ computed by Eq. (13) is in all points less than a given lower limit ($\varepsilon = 0.01$).

4. DIRECT DETERMINATION OF THE TRANSFORMATION PARAMETERS IN THREE DIMENSIONS USING THE L1-NORM

The general form of the similarity transformation in three dimensions is:

$$\underline{\underline{X}} = m\underline{\underline{R}}\underline{\underline{x}} + \underline{\underline{X}}_0 \tag{14}$$

At it is well-known the spatial transformation is composed of three phases: translation, scaling and rotation around the three coordinate axes. From the point of view of mathematics, the third phase is the most interesting one, as the coefficients of the orthogonal rotation matrix $\underline{\underline{R}}$, are non-linear functions of three independent parameters. For this reason iteration is generally used to determine the rotation elements with the aid of linear equations derived from the transformation formulas (14) by derivation. To avoid the iterative procedure one can chose the way of direct determination of the elements of matrix $\underline{\underline{R}}$ what is very often used in photogrammetry (see e.g. Thompson 1958-59, Schut 1958-59, Somogyi 1969).

The translation can be eliminated with the reduction to the gravity centres of the coordinate systems and also the calculation of scale can be easily done. The three independent parameters determining the elements $a_{11} \ldots a_{33}$ of matrix $\underline{\underline{R}}$ should be denoted by α, β and γ. Equation (15) gives $\underline{\underline{R}}$ in terms of these parameters.

$$R = \begin{bmatrix} \frac{1+\alpha^2-\beta^2-\gamma^2}{1+\alpha^2+\beta^2+\gamma^2} & \frac{2(\alpha\beta-\gamma)}{1+\alpha^2+\beta^2+\gamma^2} & \frac{2(\alpha\gamma+\beta)}{1+\alpha^2+\beta^2+\gamma^2} \\ \frac{2(\alpha\beta+\gamma)}{1+\alpha^2+\beta^2+\gamma^2} & \frac{1+\beta^2-\alpha^2-\alpha^2}{1+\alpha^2+\beta^2+\gamma^2} & \frac{2(\beta\gamma-\alpha)}{1+\alpha^2+\beta^2+\gamma^2} \\ \frac{2(\alpha\gamma-\beta)}{1+\alpha^2+\beta^2+\gamma^2} & \frac{2(\alpha+\beta\gamma)}{1+\alpha^2+\beta^2+\gamma^2} & \frac{1+\gamma^2-\alpha^2-\beta^2}{1+\alpha^2+\beta^2+\gamma^2} \end{bmatrix} \tag{15}$$

The following linear equations can be written for the calculation of these parameters:

$$\begin{aligned} 0 + (Z_i+z_i)\beta - (Y_i+y_i)\gamma &= (X_i-x_i) \\ -(Z_i+z_i)\alpha + 0 + (X_i+x_i)\gamma &= (y_i-y_i) \qquad i = 1, 2, \ldots n \qquad (16) \\ (Y_i+y_i)\alpha - (X_i+x_i)\beta + 0 &= (Z_z-z_i). \end{aligned}$$

Here X, Y and Z mean the coordinates in the first system reduced to the gravity centre, and x, y, z the coordinates in the system to be transformed after reduction to the gravity centre and to the correct scale.

The simplex table is developed according to Eq. (16) in the following form:

$$\begin{aligned} a_{i,1} &= 0 \\ a_{i,2} &= Z_i+z_i \\ a_{i,3} &= -Y_i-y_i \\ a_{i+n,1} &= -Z_i-z_i \\ a_{i+n,2} &= 0 \\ a_{i+n,3} &= X_i+x_i \\ a_{i+2n,1} &= Y_i+y_i \\ a_{i+2n,2} &= -X_i-x_i \\ a_{i+2n,3} &= 0 \\ b_i &= -(X_i-x_i) \\ b_{i+n} &= -(Y_i-y_i) \\ b_{i+2n} &= -(Z_i-z_i) \quad . \end{aligned} \qquad i = 1, 2 \ldots n \qquad (17)$$

For the determination of the unknowns α, β, γ from 3n overdetermined equations, Barrodale and Roberts' (1973) algorithm is used on the basis of the L1-norm. This algorithm computes the values α, β, γ for which the sum of the absolute values of the residuals is a minimum:

$$e = \sum_{i=1}^{3n} \left| b_i - a_{i,1}\alpha - a_{i,2}\beta - a_{i,3}\gamma \right| \qquad (18)$$

In the next step the elements $a_{11} \ldots a_{33}$ of the rotation matrix $\underline{R}$ are determined using the values found for α , β , γ . Lastly, the corrections are obtained from the following equations:

$$\begin{aligned} v_{x_i} &= X_i - a_{11}x_i - a_{12}y_i - a_{13}z_i \\ v_{y_i} &= Y_i - a_{21}x_i - a_{22}y_i - a_{23}z_i \qquad i = 1, 2, \ldots n \\ v_{z_i} &= Z_i - a_{31}x_i - a_{32}y_i - a_{33}z_i \ . \end{aligned} \tag{19}$$

In these formulas, coordinates refer to the gravity centres of the corresponding systems of coordinates and the coordinates x_i, y_i, z_i, include the scale $\underline{m}$. The scale is determined by averaging from the distances between the distances the gravity centre and the coordinates which appear in the adjustment.

Gross errors in the initial data may influence the resulting scale, as this unknown is not determined using the L1-norm. The effect of the gross errors can be eliminated from the scale by prescribing an upper limit for the discrepancies then the equation system (16) is solved using the L1-norm. If the discrepancy for an arbitrary point is more than this limit, the programme re-starts the computation without taking into account all the points outside of the prescribed limit. The iteration is continued till all discrepancies in Eqs (16) are less than the prescribed limit - supposing that the remaining points are sufficient for the determination of the unknowns. (In the opposite case a less rigorous limit should be chosen.)

The direct determination of the elements of the rotation matrix $\underline{\underline{R}}$ as described here enables to reduce the solution of the three-dimensional transformation according to the L1-norm to a simple linear programming. The non-linear inequality (5) occurring in the Helmert-transformation can be avoided; it would result in the solution of a convex optimization by iterations (Meissl 1968). This inequality is in case of the three-dimensional transformation:

$$\sqrt{v_{x_i}^2 + v_{y_i}^2 + v_{z_i}^2} \leq r_i \tag{20}$$

and it refers in a geometrical sense to radii r_i belonging to a sphere. The iterative solution of such a convex programme is much more complicated, as instead of a circle, a sphere is to be approximated by polyhedrons.

The programme LTRANS developed on this basis can be advantageously used for the adjustment of spatial transformation problems. The solution is equivalent with other robust adjustment methods (Somogyi 1987). The same programme can also be adopted for the robust adjustment of planar similarity transformation parameters by introducing $z_i = Z_i = 0$. This programme is essentially quicker than our programme HTRANS based on the algorithm developed by Fuchs (1982) what follows from the difference of the two principles of optimization.

5. NUMERICAL EXAMPLES FOR DIFFERENT SOLUTIONS

Finally some numerical examples will be given for the solution of planar and spatial transformation based on the L1-norm to show the effect of the robust method. The simulated test net consists of 15 points with the coordinates given in Table I, their projections on the plane are represented in Fig. 1.

Coordinates x, y and z were obtained by rotating the system X, Y, Z by a value of:

$a_{11} = 0.999833$	$a_{21} = -0.012213$	$a_{31} = -0.013529$
$a_{12} = 0.012012$	$a_{22} = 0.998818$	$a_{32} = -0.014804$
$a_{13} = 0.013708$	$a_{23} = 0.14639$	$a_{33} = 0.999798$

and by multiplying them with the scale factor $m = 0.79$. Points 10 and 14 have gross errors. The errorfree values are given in parantheses. Discrepancies after the adjustment are given in Table II together with the transformation parameters resulting from the adjustment. The robust effect of the L1-norm adjustment is clearly visible. Erroneous values do not influence the reliability of the parameter estimation.

Table III containes the two-dimensional simulated version of the point field of Fig. 1. Coordinates x and y were obtained

Table I

P	X	Y	Z	x	y	z
1	100	600	50	85.222	473.527	31.406
2	425	490	120	341.643	384.317	84.508
3	410	700	70	331.247	549.753	42.720
4	750	640	80	599.341	499.197	47.686
5	575	575	130	461.038	450.123	89.809
6	830	460	240	662.555	358.101	175.311
7	600	400	180	479.666	312.235	131.080
8	770	240	370	614.483	186.415	281.204
9	560	150	510	449.272	118.973	395.079
				(.278)	(.823)	
10	450	250	320	361.713	196.311	245.016
11	340	50	430	273.686	41.185	335.413
12	150	100	380	123.544	81.933	297.367
13	270	220	270	218.276	174.286	207.798
				(.757)	(.847)	(.633)
14	225	465	150	183.872	366.896	110.683
15	50	300	290	45.481	239.828	225.011

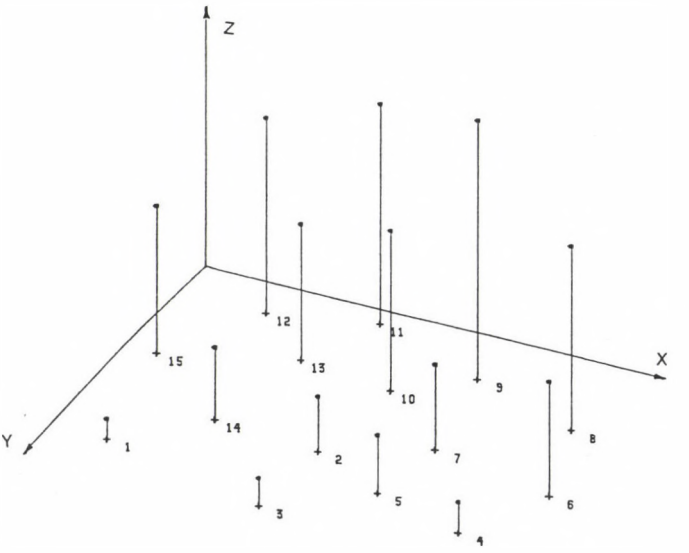

Fig. 1.

Table II

P	v_x	v_y	v_z	Parameters after adjustment
1	0.000	0.000	.001	0.9998339 = a_{11}
2	0.001	0.000	.000	0.0120130 = a_{12}
3	0.000	0.000	.000	0.0137083 = a_{13}
4	0.000	0.000	.000	
5	0.001	0.000	.000	-0.0122135 = a_{21}
6	0.000	0.000	.000	0.9998183 = a_{22}
7	0.000	0.000	.000	0.0146382 = a_{23}
8	0.000	0.000	.000	
9	0.001	0.000	.000	-0.0135300 = a_{31}
10	-0.558	0.616	.001	-0.0148032 = a_{32}
11	0.000	0.000	.000	0.9997989 = a_{33}
12	0.000	0.000	.000	
13	0.000	0.000	.000	1/m = 1.2658234
14	-0.143	0.063	-.066	
15	0.001	0.000	.000	

by a rotation by $\alpha = 15^{0}$ of the system X, Y and by miltiplying it with the scale factor m = 0.79.

Original coordinates of the erroneous points 10 and 14 are given in parantheses. The adjustment was carried out by both methods. Discrepancies after the adjustment are found in Table IV. The two solutions give practically the same result with the difference that the computer times on the HP 2100 of our Institute are in a ratio 1:25; and the ratio further deteriorates for HTRANS with respect to LTRANS with the increasing number of points in the adjustment.

REFERENCES

Barrodale I, Roberts F D K 1973: SIAM, Journal of Num. Analysis, 10, 839-848.

Burstedde J, Cremer K 1986: Allgemeine Vermessungsnachrichten, 6, 228-234.

Ebong M B 1985: Manuscripta Geodaetica, 10, 32-36.

Table III

P	X	Y	x	y
1	100	600	-46.372	478.295
2	425	490	224.120	460.808
3	410	700	169.736	619.988
4	750	640	441.452	641.722
5	575	575	321.203	556.340
6	830	460	539.303	520.725
7	600	400	376.062	427.913
8	770	240	538.501	340.579
9	560	150	396.656	228.964
			(270)	(780)
10	450	250	292.796	282.638
11	340	50	249.224	107.673
12	150	100	94.016	106.978
13	270	220	161.049	223.084
			(616)	(838)
14	225	465	76.731	400.887
15	50	300	-23.186	239.148

Table IV

P	LTRANS		HTRANS		Parameters after adjustment
	v_x	v_y	v_x	v_y	
1	.000	.000	.000	.000	
2	.001	.000	.001	.000	sin α = .2588193
3	.001	.000	.001	.000	cos α = .9659257
4	.000	.000	.000	.000	
5	.001	.000	.000	.000	1/m = 1.2658231
6	.000	.000	.000	.000	
7	.000	.000	.000	.000	
8	-.001	.000	.000	.000	
9	-.001	.000	.000	.000	
10	-.597	.346	-.596	.346	
11	.000	.000	.001	.000	
12	.000	.000	.000	.000	
13	.000	.000	.001	.000	
14	-.157	-.023	-.156	-.023	
15	.000	-.001	.000	-.001	

Fuchs H 1982: Manuscripta Geodaetica, 7, 151-207.

Hahn M, Bull R 1984: Allgemeine Vermessungsnachrichten, 11-12, 440-450.

Kampmann G 1986: Allgemeine Vermessungsnachrichten, 4, 139-147.

Meissl P 1968: Österreichische Zeitschrift für Vermessungswesen, 56, 140-149.

Schut G H 1958-59: Photogrammetria, 15, 149.

Somogyi J 1969: Acta Geod. Geoph. Mont. Hung., 4, 451-458.

Somogyi J 1987: DGK, Reihe B, Heft Nr. 287.

Thompson E H 1958-59: Photogrammetria, 15, 163.

Acta Geod. Geoph. Mont. Hung., Vol. 24 (3-4), pp. 251-272 (1989)

ASYMPTOTIC BEHAVIOUR OF ERROR ESTIMATIONS. NEED FOR A PRACTICE IN ERROR ESTIMATION ON NEW BASES

B Hajagos and F Steiner

University for Heavy Industry, Chair of Geophysics, H-3515 Miskolc, Egyetemváros, Hungary

[Manuscript received January 15, 1987]

The paper discusses the asymptotic uncertainty of the accuracies determined from the sample standard deviation and from the semi-interquartile range of the sample for the supermodel $f_a(x)$ introduced by Csernyák and Steiner (1982). The sample standard deviation (which is used at present predominantly) turned out to be advantageous only in the neighbourhood of the Gaussian distribution (i.e. only for sterile distributions). For a wide range of distributions occurring in the practice the sample standard deviation is asymptotically unusable (its relative efficiency is zero with respect of the efficiency of the semi-interquartile range). The more and more sophisticated geophysical algorithms necessitate, however, a more and more accurate error determination both with respect to input data and to the comparison of algorithms for the same purpose (e.g. for the comparison of sets of deviations). Therefore the authors think that the entire error calculation should be developed on new bases. Investigations presented in this paper show that such a base should be the semi-interquartile range. An advantageous solution seems to be the quantity U proposed by Steiner (1985a).

Keywords: asymptotic uncertainty; efficiency of estimation; interquartile range; robust estimations

1. MUTUAL CONVERTIBILITY OF ERROR CHARACTERISTICS FOR SOME GIVEN TYPE OF RANDOM DISTRIBUTION

Any measurement or any indirect determination made by the engineer or by the scientist has some error - this very simple fact or commonplace has never been disputed. (This fact is emphasized in mathematical statistics by a consequent use of the terminus "estimate" in all cases when engineers speak generally about "determinations"). It is, however, much less evident how the error, the measure of uncertainty is to be determined (or estimated). This is true even if, nearly automatically, the square root of the quantity

$$\tilde{\sigma}^2_{emp} = \frac{1}{n-1} \sum_{i=1}^{n} x_i^2 \qquad (1a)$$

or that of

$$\sigma^2_{emp} = \frac{1}{n} \sum_{i=1}^{n} x_i^2 \qquad (1b)$$

(being asymptotically the same) is computed as a measure of uncertainty; this quantity is called standard deviation of the sample, or sample dispersion. (In Eqs (1a) and (1b) the deviations obtained from an adjustment with an arbitrary number of unknowns concerning the quantity z, are denoted by x_1, x_2, ..., x_i, ..., x_n.)

On the basis of the probability theory one could think in the first moment that using the scale parameter of the density function f(x), or of the distribution function F(x) of the given type of random distribution, multiplied by a well-defined constant, yields an arbitrarily defined error, thus it is equivalent to carry out the error computations for any error characteristics, as any of them can be transformed in all others. If e.g. one supposes a Gaussian distribution with the scale parameter σ, and the symmetry point in the origin, i.e. the density function is

$$f_G(x) = \frac{1}{\sigma\sqrt{2\pi}} e^{(-x^2/2\sigma^2)} \qquad (2)$$

then in a general case the semi-interquartile range defined by

$$Q = \frac{1}{2} \left[F^{-1}(0.75) - F^{-1}(0.25)\right] \qquad (3)$$

is obtained by the product

$$Q = 0.6745\sigma \qquad (4)$$

The product (Eq. 4) can be naturally used in the inverse

direction, too: Rényi (1954) hints on p. 594 of his book at the possibility that in case of a Gaussian distribution, σ can be estimated from the sample by determining Q_{emp} (basically by using Eq. 3), and then using Eq. (4). It is further well known that for a Gaussian distribution, the occurrence probability of an error being greater than $1.96\,\sigma$ is only 5 percent (the level of significance being 95 %), that of greater than 2.58σ, 1 percent (the level of significance being 99 %) and that of greater than 3σ, 3 per mille. This list could be continued infinitely by listing the constant multiplicators for the errors corresponding to different levels of significance (in the sense used above). Even with such a list, only the case of the Gaussian distribution would be exhausted: multiplicators transforming errors defined differently can also be listed for any other type of distribution.

2. PUTTING THE QUESTION STATISTICALLY. THE BASIC CONDITION IS AN INCREASE OF THE ACCURACY PROPORTIONALLY WITH $\sqrt{n}$ IN THE DETERMINATION OF THE ERRORS

The proper (practically important) problem is which of the error characteristics can be more accurately determined, thus the problem has more a statistical, than a probabilistic character. Namely if σ can be (in percents) more accurately determined than Q, then e.g. Q can also be determined via σ_{emp} more accurately than if Q_{emp} would be immediately determined. (The index "emp" refers to empirical values coming from samples.) And vice versa: if Q_{emp} is more accurate for a certain distribution than σ_{emp}, then a more accurate estimate is obtained for σ_{emp} via Q_{emp} than if σ_{emp} would be directly determined. (In this case the existence of σ should be supposed.) As the requirements for processing and/or interpreting algorithms are increasing in earth sciences, too, rough estimates for error characteristics to describe the so-called deviation systems may be insufficient to characterize both the data set and the results (e.g. the adjustment results). It is namely known that if an algorithm yields results with 10 percent

error surplus, then the efficiency decreases by 20 percent what is hardly allowed in case of expensive data sets of earth sciences. A deviation in the errors by 10 percent can be detected, however, only if the errors themselves are determined with errors not surpassing 1-2 percents. Such an accuracy can be reached even from great data sets only if the error decreases in the usual way, i.e. proportionally with $1/\sqrt{n}$.

Error formulas in textbooks (Cramér 1958) contain $\sqrt{n}$ really in the denominator. In the following it will be shown that for certain types of distributions and for certain types of error definitions this is purely formal due to the divergence of other factors in these formulas.

3. ERRORS IN THE DETERMINATION OF INTERQUANTILE RANGES (q(p)-s). ADVANTAGES OF THE USE OF THE SEMI-INTERQUARTILE RANGE Q

For sake of simplicity in the following only cases will be treated when the density function f(x) of x is unimodal, continuous and symmetrical for the origin. In such a case (see p. 370 at Cramér 1958) the distribution of the Q_{emp}-s is asymptotically Gaussian with the following semi-interquartile range:

$$Q_{Q_{emp}} = \frac{1}{\sqrt{n}} \cdot \frac{0.6745}{4 \cdot f(Q)} \quad . \tag{5a}$$

It is more advantageous to use in comparisons the relative error:

$$Q_{Q_{emp}}/Q = \frac{1}{\sqrt{n}} \cdot \frac{0.6745}{4 \cdot Q \cdot f(Q)} \equiv E_{Q_{emp}}/\sqrt{n} \quad . \tag{5b}$$

It should be remarked that the interquantile ranges can be determined for other values of p ($0 < p < 0.5$), too, on the basis of the deviations $x_1, x_2, \ldots, x_n$; the definition of q(p) is:

$$q(p) = F^{-1}(1-p) - F^{-1}(p) \quad , \tag{6}$$

i.e. values to the left and to the right from a central

interval of the length q(p) have the same probability p (i.e. the values smaller than -q(p)/2 and greater than +q(p)/2 have the same probability p). The problem is naturally if any other choice should be more advantageous instead of Q = q(0.25)/2, i.e. any increase in the accuracy could be reached in this way.

In order to answer this question, the error measured by the semi-interquartile range of the numerical determination of q(p) should be obtained (based on Cramér 1958) again in a relative sense, i.e. divided by q(p):

$$Q_{q(p)_{emp}}/q(p) = \frac{1}{\sqrt{n}} \frac{2 \cdot 0.6745}{q(p) \cdot f(q(p)/2)} \sqrt{p(0.5-p)} = E(p)/\sqrt{n} . \qquad (7)$$

By substituting p = 1/4, Eq. (5) is found again (and $E_{Q_{emp}}$ is equal to E(0.25)).

The analytical form of E(p) is given in the following for some random distributions.

a) For uniform distribution:

$$E(p) = 0.6745 \sqrt{\frac{1}{0.5-p}} ; \qquad (7a)$$

b) For the Laplace-distribution:

$$E(p) = \frac{0.6745}{p \cdot \ln \frac{1}{2p}} \sqrt{p(0.5-p)} ; \qquad (7b)$$

c) For the Cauchy-distribution:

$$E(p) = \frac{\pi \cdot 0.6745 \cdot [1+(\tan[\pi(0.5-p)])^2]}{\tan[\pi(0.5-p)]} \cdot \sqrt{p(0.5-p)} ; \qquad (7c)$$

d) for the distribution $f_{CS}(x)$ defined by Csernyák (1982):

$$E(p) = \frac{\ln 2 \cdot 0.6745 \cdot 2^{(1/2p)}}{2p^2 \cdot (2^{1/2p} - 2)} \sqrt{p(0.5-p)} . \qquad (7d)$$

The distribution $f_{CS}(x)$ has the density function:

$$f_{CS}(x) = \frac{2 \cdot \ln 2}{(4|x| + 2) \cdot \ln^2 (4|x| + 2)} , \qquad (8)$$

and it is of infinite entropy, thus it has very heavy flanks. The practically occurring distributions cannot be naturally selected in the engineering practice, therefore, if it is necessary, Eq. (8) is used as a model of the density function. Naturally it may also occur that one has a much more advantageous situation and the actual distribution can be modelled by the Laplace-distribution's density function:

$$f(x) = \frac{1}{2} e^{-x} \qquad (9)$$

(In this case not only the entropy, but moments of any order are finite, too.)

If the E(p)-curves corresponding to Eqs (7a) and (7b) are plotted, cases are considered which are extremely advantageous and disadvantageous, respectively. Figure 1 shows that E(p) of the Laplace-distribution has a minimum at about p = 0.1, i.e. if the samples are from such a distribution, the error (or the scale parameter) can be estimated more effectively from an interval which contains about 80 percent of the data (from all interquantile ranges); in such a case the error of the error determination can be estimated for great n-s from the formula $0.838/\sqrt{n}$. In case of the $f_{CS}(x)$ distribution the most effective estimation is made from a sample containing the central third of all values, and in that case the error of the determined error is $1.693/\sqrt{n}$. Therefore when the engineering practice uses nearly always the value of $2Q_{emp}$ (if an interquantile range is determined and not the most common method, the determination of σ_{emp} is applied), a very wise choice is made: for a distribution of unknown type, the determination is made for a p-value of 0.25 which yields both for very advantageous and very disadvantageous cases an accuracy in the determination of the error not too far from the optimum. (For the Laplace-distribution E(0.25) = 0.9731, the minimum E(p) is only by 14 percent less, for the $f_{CS}(x)$ distribution E(0.25) = 1.8701, and the minimum is in that case less only by 9.5 percent.) is reached which is. It should be added that the Cauchy-distribution which has an important role in earth sciences, has its minimum just at

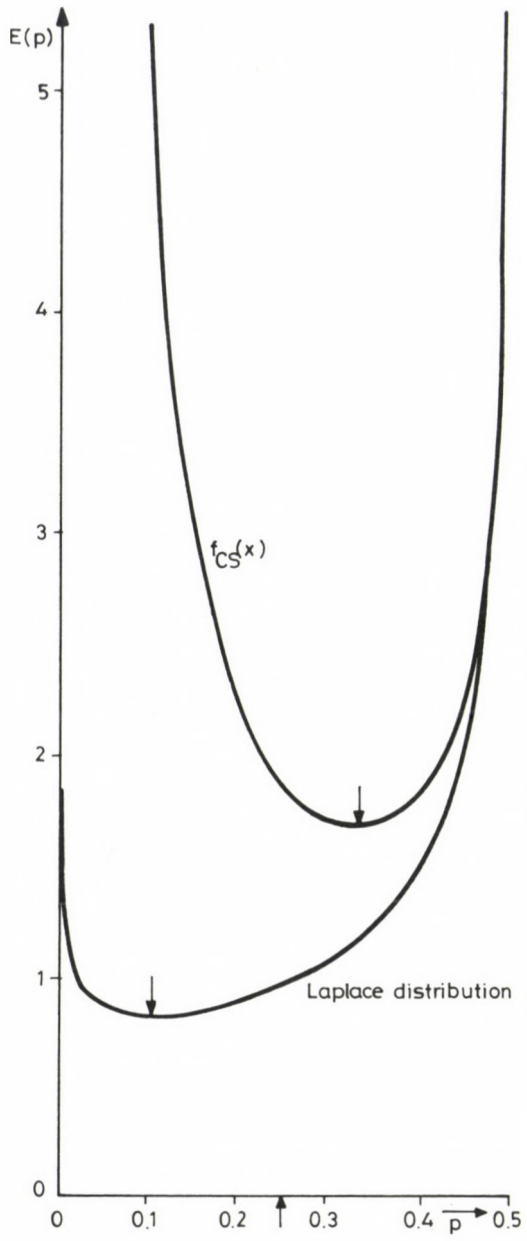

Fig. 1. The function E(p) characterizing the relative errors of the estimation of the semi-interquantile range q(p) in a "very advantageous" and in a "very disadvantageous" case. (This error is computed as $E(p)/\sqrt{n}$, where n is the number of elements in the sample.) The semi-interquartile range Q can be estimated advantageously in both cases

p = 0.25 (and it is symmetrical around this point, see the curve to a=2 on Fig. 5, or directly Eq. (7c)).

A further well known practical advantage of the use of Q should be mentioned here, too: Q is the probable error in the sense that the absolute values of the deviations (i.e. the errors) have values both greater and less than Q with a probability of 0.5.

4. ERRORS OF THE DETERMINATIONS OF Q FOR THE DISTRIBUTION TYPES OF THE FAMILY $f_a(x)$

Two kinds of $E(0.25) = E_{Q_{emp}}$ have been mentioned hitherto, whereby the value 1.8701 corresponding to a very unfavourable case does not differ by more than a factor of two from the value 0.9731 for a very favourable case. This means that the error in the error estimation is rather insensitive for the (mostly unknown) type of the distribution. For a systematic study some known singular types of distributions are naturally insufficient: a supermodel should be used.

On the basis of Csernyák and Steiner (1982), the distribution family $f_a(x)$ should be defined as follows:

$$f_a(x) = \frac{1}{c(a) \cdot (1+x^2)^{a/2}} \qquad a > 1 \ , \qquad (10)$$

where

$$c(a) = \frac{\sqrt{\pi} \cdot \Gamma\left(\frac{a-1}{2}\right)}{\Gamma\left(\frac{a}{2}\right)} \ . \qquad (10a)$$

a=2 yields the density function of the Cauchy-distribution; in case of $a \to \infty$ $f_a(x) \to f_G(x)$. Steiner (1988) presented the analytical forms of the distribution functions $F_a(x)$ for integer values of a, further comfortable tables for c(a) and Q.

The general equation (5) yields easily $E_{Q_{emp}} = E(0.25)$ for the family $f_a(x)$:

$$E_{Q_{emp}} = \frac{1}{4Q} \, 0.6745 \cdot c(a) \cdot (1+Q^2)^{a/2} \ . \qquad (11)$$

$E_{Q_{emp}}$ can be advantageously plotted vs. $(a-1)^{-1}$ (see Fig. 2); beginning with the Gaussian distribution (i.e. from $a = \infty$, i.e. from $(a-1)^{-1} = 0$). $E_{Q_{emp}}$ is monotonously increasing from 0.7867 till 1.3426 for $f_a(x)$ belonging to $a = 1.6$. (It is characteristic for the range of the values of $E_{Q_{emp}}$ that if the percentual error of the estimate Q_{emp} would be always computed with the formula $100/\sqrt{n}$, a maximum distortion of 27 percent would be made in the very wide range of types studied.)

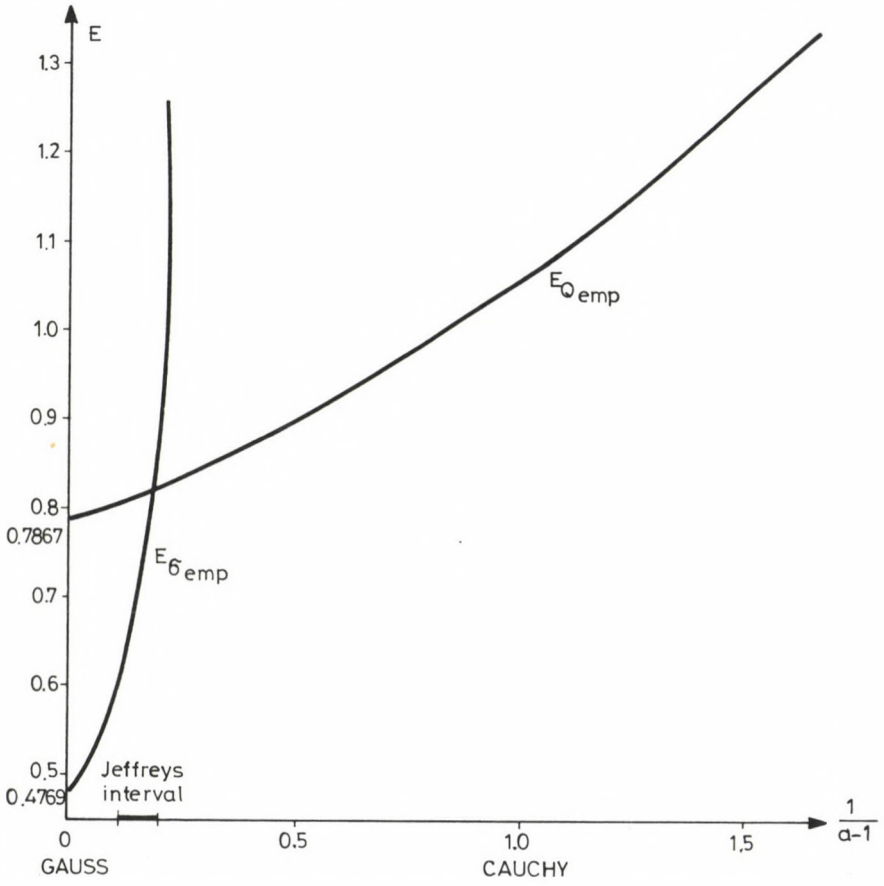

Fig. 2. The curves of $E_{Q_{emp}}$ and of $E_{\sigma_{emp}}$ for the distribution types of the supermodel $f_a(x)$. (The errors are to be computed as $E/\sqrt{n}$ in both cases.) $E_{\sigma_{emp}}$ is approximating infinity if $(1-a)^{-1}$ tends to 0.25, i.e., a tends to 5

5. ERRORS OF THE DETERMINATIONS OF σ_{emp} IN A GENERAL CASE AND FOR THE DISTRIBUTION TYPES OF THE FAMILY $f_a(x)$

In an overwhelming majority of the practical cases, σ_{emp} is computed as mentioned already several times. The ratio $Q_{\sigma_{emp}}/\sigma$ should be studied in the following for different types of distributions. For this quantity the notation $E_{\sigma_{emp}}$ is introduced.

Cramér (1958, p. 364) tells us that the quantities σ^2_{emp} computed according to Eq. (1) have asymptotically a Gaussian distribution with a semi-interquartile range of:

$$Q_{\sigma^2_{emp}} = \frac{0.6745}{\sqrt{n}} \sqrt{\int_{-\infty}^{\infty} x^4 f(x)\,dx - \sigma^4}\,. \qquad (12)$$

If n is really very big, then $Q_{\sigma^2_{emp}}$ is very small with respect to σ^2, i.e. the semi-interquartile range $Q_{\sigma_{emp}}$ of the quantities σ_{emp} is obtained by the division of the expression in Eq. (12) by 2σ. The relative error of the error estimation by σ_{emp} is obtained accordingly from the following formula:

$$Q_{\sigma_{emp}}/\sigma = \frac{1}{\sqrt{n}} \frac{0.6745}{2\sigma^2} \sqrt{\int_{-\infty}^{\infty} x^4 f(x)\,dx - \sigma^4} \equiv E_{\sigma_{emp}}/\sqrt{n}\,. \qquad (13)$$

Let us carry out the following investigations on the distribution types of the supermodel $f_a(x)$.

Introductorily it should be remarked that σ exists only if $a > 3$, its value is in such cases $1/\sqrt{a-3}$ (Csernyák and Steiner 1982). It is surprising for the first glance that the integral in Eq. (13) exists only for $a > 5$: that means that for distributions with $a \leq 5$, at increasing n values, an error decreasing with $1/\sqrt{n}$ should not be expected (although, as it has been shown, this is the basic condition). By substituting the values of the integral and of σ into Eq. (13), one gets:

$$E_{\sigma_{emp}} = \frac{0.6745}{\sqrt{2}} \sqrt{\frac{a-2}{a-5}}\,, \qquad (a > 5)\,. \qquad (14)$$

This curve of $E_{\sigma_{emp}}$ is also presented on Fig. 2: the curve starts in case of a Gaussian distribution (at $1/(a-1) = 0$) at a value being significantly less than the curve $E_{Q_{emp}}$, but then it increases very quickly toward infinity.

If both curves are represented on a common figure, several comparisons become possible, nevertheless it is advantageous to compute the relative efficiency, too:

$$e_r = E^2_{Q_{emp}} / E^2_{\sigma_{emp}} \tag{15}$$

being for the family $f_a(x)$

$$e_r = \frac{c^2(a)}{8Q^2} \cdot \frac{a-5}{a-2} \cdot (1+Q)^a \ , \tag{15a}$$

if $a > 5$, and zero if $a \leq 5$. The curve of e_r is presented on Fig. 3.

At $a = 6.5, e_r = 1$; in case of this distribution type it makes no difference if the error of the deviation set is determined via σ_{emp} or via Q_{emp}. This distribution is an element of the distributions in the so-called Jeffreys-interval characterized by $6 < a < 10$ (see e.g. Steiner 1985) which was described by Jeffreys as the interval where distributions are found which may occur in the practice, too, but an even better approximation of the Gaussian distribution is very unlikely.

The Jeffreys-interval was found also by Csernyák (1987) as being an intermediate range which was yielded on ground of a simple and easily acceptable mathematical definition for the "sterile" distributions, i.e. for distributions having significantly shorter flanks than the commonly occurring distributions. The inscriptions "sterile distribution" - "real distributions" on Fig. 3 indicate just this circumstance.

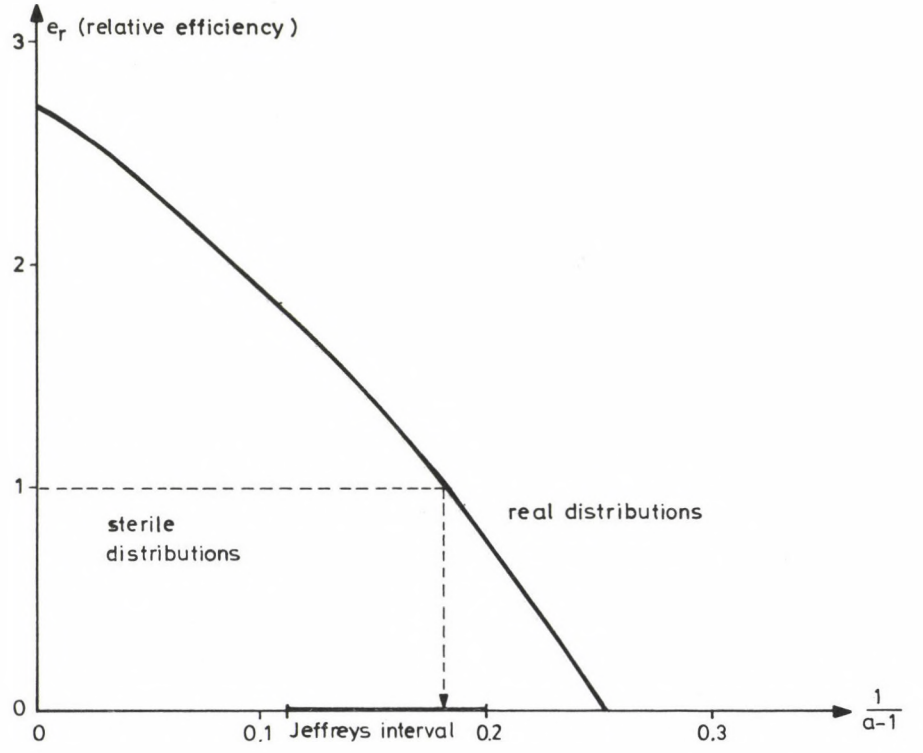

Fig. 3. Relative efficiency of the sample standard deviation in relation to the empirical sample semi-interquartile range for different types of distributions

6. THE RANGE OF TYPES $f_a(x)$ MODELLING THE BEST THE MOST FREQUENTLY OCCURRING DISTRIBUTIONS IN THE PRACTICE. THE DOGMA ABOUT THE OVERWHELMING OCCURRENCE OF THE GAUSSIAN DISTRIBUTION IN PRIMARY DISTRIBUTIONS

There are contradictory opinions about the occurrence of the Gaussian distribution in the practice. Early authors (and present ones who could not change their mind in this respect) have supposed that errors follow practically always a Gaussian distribution; at present the opinion prevails that a Gaussian distribution is found only with a negligible probability. Some corresponding texts are quoted by Steiner (1985) where he also emphasized that estimates have in the majority of cases

Gaussian distributions independently of the occurrence probability of random variables of different distribution types in the practice.

The previous comparison between ancient and recent authors is somewhat unjustified against the ancient ones as some rather early authors (50-100 years ago) have already mentioned the fact that practical distributions may differ from the Gaussian one (cited by Steiner 1985, 1986). It is more correct to say that authors with proper theoretical knowledge and possessing sufficiently large data sets deny the overwhelming occurrence of the Gaussian distribution in primary data, whereas theoretical mathematicians and authors following them accept this preponderance. As a theory behind this acceptance it is quoted sometimes that if the error is the results of the addition of an infinite number of infinitely small errors, then the distribution is really of Gaussian type. This premissa is, however, never fully true. But if this condition is not fulfilled then the real distribution will only approximate the Gaussian distribution, the actual distribution corresponds e.g. to $f_a(x)$ belonging to a = 5. Whether this distribution type is near to the Gaussian one or not, can be judged by means of Fig. 4. One of the three curves represents $f_5(x)$, the other two are $f_G(x)$-es according to Eq. (2), in case of the first Q, in case of the second, σ is the same as that of $f_5(x)$. The small difference in the density functions is not felt sufficient for the change of the error of an error characteristic from an advantageous value to an infinite one (see also the rapid decrease to zero of the curve e_r in Fig. 3 at 1/(a-1) = 0.25, i.e. at a = 5, or the infinite value of the curve of $E\sigma_{emp}$ at the same place). Thus the reliability of the error estimation is strongly influenced by the fact, that the error estimation by σ_{emp} is extremely sensitive for a change of the distribution type, and in a wide range of distributions, it is assymptotically of no use. (For finite n-s, Csernyák is carrying out investigations to close this problem with satisfying results: from these results it will be known what is the most probable value of σ_{emp} for a given value of n, even if σ is infinite).

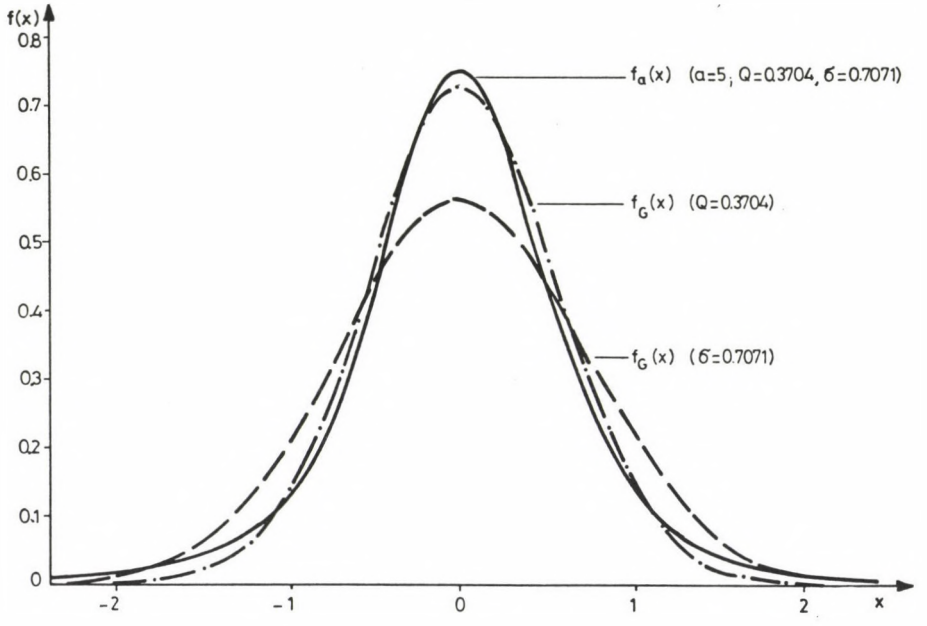

Fig. 4. The density function of the supermodel $f_a(x)$ for the type parameter value a = 5, together with two Gaussian density functions in the same system of coordinates. The deviation of the types is hardly considered important

Mathematicians have no competence to speak about the frequency of occurrence of the different distribution types; as mathematics is the science to reach conclusions from given premissae (the very mistake is not made by the mathematician when he is speaking about corresponding results, but by those who expect the answer from the mathematicians). Such a statement is in its more general form by far not new. Seneca wrote in his Ethical Letter 88: "the mathematics is so to say a surface science, it builds on foreign bases. It accepts the starting points and from them it continues toward the end point".

Thus the study of the occurrence of types is a task for practical experts. (For this purpose, uptodate methods should be used; concerning the dangers of the application of the χ^2-test, see e.g. Hajagos' (1987) paper.) Ferenczy and Takács

(1986) reported on the results of the type determinations on borehole data systems using different methods; they found distributions in the Jeffreys-interval, too, but the bulk of the deviation-systems fulfilled not only $a < 6$, but also $a < 4$, and even $a < 2$ was present. Taking into account Steiner's (1988) statements, the distribution types can be modelled by $f_a(x)$-es belonging to the values a in the interval $6 > a > 1.8$, and in a wider sense in the interval $10 > a > 1.6$ (e.g. the distribution of the deviations after adjustment); the occurrence of distribution outside of the last interval has a very low probability.

Investigations concerning distribution types made on data sets of a very high number of elements can lead evidently to different results in different disciplines. In earth sciences there is a very great amount to be made, too, but a considerable change in the statements above is not to be expected belonging the distribution types occurring there.

7. THE NEED FOR A NEW DEFINITION OF THE ERROR. PROPOSAL TO USE THE QUANTITIES U AND $\bar{U}$, RESPECTIVELY, IN THE NORMAL PRACTICE

The previous sections contain the necessary minimum information about the type of deviations occurring in the practice; they help those who have little practice in this topic to understand the main points. Now returning to our original task, we have to demand from the practically applicable error definition that its reliability should depend as slightly as only possible from the actual type of error distribution.

One might as well say at first sight that Q_{emp} has according to our investigations this property. This is true, nevertheless, a further development to make it more adequate is necessary.

The first remark is that it seems to be useful to take into account not only $2Q = q(0.25)$, but some other $q(p)$-s belonging to $p \neq 0.25$, as it has been shown already in Fig. 1 that $q(p)$-s can be determined with similar accuracy in a rather wide range (where $E(p)$-s differ only slightly). Since then, we have got acquainted with the family $f_a(x)$, and also with the

types of distributions to be expected in earth sciences. In the following we shall concentrate on the inaccuracies connected with the determination of q(p)-s for these types of distributions.

General equation (7) gives the following recipe in case of the family $f_a(x)$ for the determination of $E(p) = \sqrt{n} \cdot Q_{q(p)_{emp}}/q(p)$.

$$E(p) = \frac{0.6745}{F_a^{-1}(1-p)} \cdot c(a) \cdot \left\{1 + \left[F_a^{-1}(1-p)\right]2\right\}^{\frac{a}{2}} \sqrt{p(0.5-p)}, \quad (16)$$

where $F_a^{-1}(.)$ is the inverse function of the $F_a(x)$ distribution function belonging to $f_a(x)$ (in a general case it cannot be given in an analytical form; for a=2, it is $\tan[\pi(0.5-p)]$, see also Eq. (7c)).

Figure 5 shows the curves E(p) on the basis of Eq. (16) for a=1.26; 2; 3; 4; 6; 10. This series is complemented with the E(p)-curve belonging to $a=\infty$, i.e. to the Gaussian type distributions, being on the basis of Eq. (7)

$$E(p) = \frac{0.6745\ \sqrt{2\pi}}{\Phi^{-1}(1-p)} \exp\left\{\left[\Phi^{-1}(1-p)\right]^2/2\right\} \cdot \sqrt{p \cdot (0.5-p)} \cdot \quad (17)$$

This formula can be easily evaluated by using tables of the function $\Phi(x) = (2\pi)^{-1/2} \int_{-\infty}^{x} e^{-t^2/2}\, dt$. Figure 5 contains the E(p) curves belonging to the uniform distribution, too (Eq. (7a)), as it can be easily seen that with $p \to 0.5$, the E(p)--curves have to converge to this function if the distribution function can continuously be derived in the symmetry point, i.e. if the density function f(x) can be approximated by a constant value in the vicinity of the symmetry point. - The E(p)-curve of the Gaussian distribution is in a surprisingly wide interval very near to the E(p)-curve of the uniform distribution yielding a further proof for the fact that the Gaussian distribution is very similar to the character of an absolutely sterile, in the practical earth sciences never occurring distribution type. -

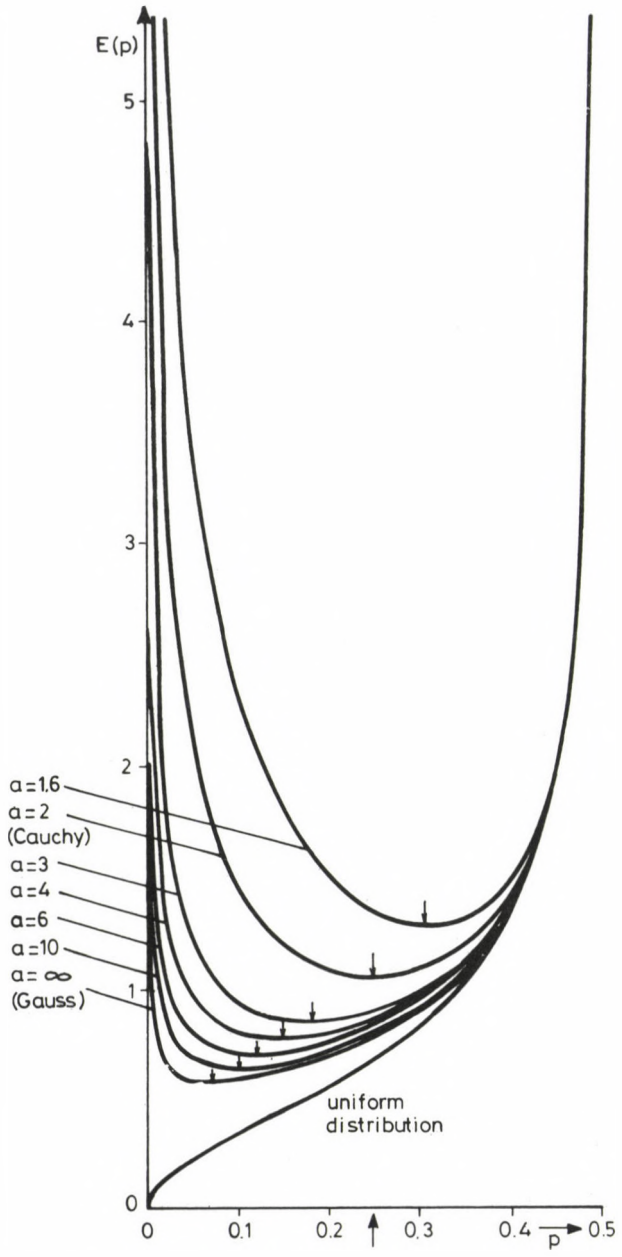

Fig. 5. Functions E(p) for some distributions $f_a(x)$ which may model practically occurring cases, for the Gaussian distribution and for the uniform distribution

The E(p) curves corresponding to the type-parameters a = 1.6; 2; 3; 4 in Fig. 5 have very similar broad minima to those of the curves in Fig. 1 - that means that in addition to 2Q = q(0.25), a rather wide range of q(p)-s around p = 0.25 should be taken into account, as it has been proposed earlier.

The first step of development could be that the determination of 2Q itself is made more accurate by taking into account some neighborous empirical values of q(p). The value of $q(0.25)_{emp}$ for a given empirical system of deviations is, however, very similar even in the included fluctuation to the value of $p(0.25 \pm \Delta p)$ (where Δp is a small value), therefore we suppose that due to the interdependence, no significant increase can be expected. Anyway the data series of the $q(p)_{emp}$-values determined from the sample informs us about the value a in $f_a(x)$ being most applicable for the modelling, i.e. about the type of the distribution which determines the multiplicative factors for high values of n corresponding to the actual $q(p)_{emp}$. It is evident that an investigation aiming at completeness should consider the E(p)-curves in Fig. 5, too. Therefore this task is wide enough to make out a separate paper. It is sufficient here to add that if in the following $2Q_{emp} = (0.25)q_{emp}$ is mentioned any of the corrected or uncorrected quantities could be understood.

Having discussed the advantageous properties of q(0.25) and summarized the ways for its determination, attention must be called to some disadvantages, too.

The notion of the semi-interquartile range does not reflect the properties of the set of deviations (actually possible errors) outside of the interval with the length of $2Q_{emp}$: it has no effect if the deviations greater and smaller making out the half of the data lie near to this interval or they are very far from it. Q_{emp} remains unchanged in both cases - while it is expected that the single numerical value called "error" should characterize the whole system of the deviation data, including some information about the errors outside of the interquartile range.

It is inevitable to characterize the errors by a single

numerical value in spite of being aware the fact that the approximately complete information about the error would be obtained by the set of $q(p)_{emp}$-s determined for all possible p-s. These if the deviation set $x_1, x_2, \ldots x_n$ has been indexed according to the increasing value of the elements, can be summarized by the step function defined by the following differences:

$$q(p)_{emp} = \begin{cases} x_n - x_1 & , \text{ if } 0 < p < \frac{1}{n} \\ x_{n-1} - x_2 & , \text{ if } \frac{1}{n} < p < \frac{2}{n} \\ \vdots & \\ x_{n-i} - x_{1+i} & , \text{ if } \frac{i}{n} < p < \frac{i+1}{n} \\ \vdots & \\ x_{n-[n/2]-1} - x_{[n/2]} & , \text{ if } \frac{[n/2]-1}{n} < p < \frac{[n/2]}{n} \\ 0 & , \text{ if } \frac{[n/2]}{n} < p < \frac{1}{2} \quad . \end{cases} \tag{18}$$

Having this, many different weightings can be proved in order to transform the series of $q(p)_{emp}$-s into a single value of product sums which corresponds to our ideas. In any case, it can be accepted as basic requirement without any further investigation that if q(p) is integrated according to the weight function it should be used as an error characteristics of the distribution with the density function f(x). It can be shown, however, that by choosing any kind of weight function there is an f(x) with so heavy flanks that the result of the weighted integration of the corresponding q(p) is unlimited (Csernyák and Steiner 1984). That means that a generally applicable characteristics cannot be obtained by this way. In certain fields of science where the occurrence of too heavy flanks can be excluded with good reasons, an error defined so can be eventually used; in the earth sciences, as a simplification, the use of errors constructed on this basis is also possible for special purposes, but in a general case the present authors propose an other

method to take into account the whole of the function $q(p)_{emp}$.

For the characterization of the uncertainty of random distributions Steiner (1985) has introduced the following quantity:

$$U = 24 \int_0^{0.5} q(p) \frac{q(0.25)\cdot(0.5-p)^2}{q(p)+q(0.25)} dp \qquad (19)$$

This quantity is for all kinds of distributions limited, and the question if it takes into account in proper way the flanks, can be decided on the basis of the following values taken from the tables at Steiner (1985). U is given here in all cases for the distribution characterized by unit q(0.25)-value (i.e. for Q = 0.5):

type of the distribution	U
a) symmetrical U-distribution	0.50
b) uniform distribution	0.59
c) Laplacian distribution	0.67
d) Cauchy-distribution	0.77
e) the distribution $f_{CS}(x)$ (see Csernyák 1982)	0.82

In case a, one cannot speak of flanks; in case b, this is no more true, as here outside of the interquartile range deviations x occur , too, but else the distribution being defined for only a finite interval is absolutely sterile. The distribution c may model certain practical cases; theoretically any value of x may occur, but as all moments are limited, the flanks are not very well developed. This is the case, however, for the distribution d, where no limited moments exist. The especially heavy flanks of case e is demonstrated by its unlimited entropy, as it has been mentioned; the entropy is in case d limited yet. (The value 0.63 for the Gaussian distribution is the average of the values of the uniform and Laplacian distributions.)

It can be seen that the value of U increases with the increase of the heaviness of the flanks. It can be formulated so that the surplus due to the flanks increases (the maximum being 7/16 = 0.4315 if Q = 0.5), but the dominant quantity in U remains Q. (A comparative theoretical investigation of U, as

compared to other definitions of uncertainty and for the super-model $f_a(x)$ has been published by Hajagos and Steiner 1988.)

The authors of the present article propose that the practice of the error computation should be based on the quantity defined by Eq. (19), where $q(p)$ is the $q(p)_{emp}$ referring to the practical data systems, given by Eq. (18). If the so obtained quantity is denoted by $\bar{U}$, the (corrected or uncorrected) Q_{emp} by $\bar{Q}$, then it can be easily seen on ground of

$$\bar{U} = 48 \cdot \bar{Q} \int_0^{0.5} \frac{(0.5-p)^2 \; q(p)_{emp}}{2\bar{Q}+q(p)_{emp}} \, dp \qquad (19a)$$

(and from Eq. (18)) that

$$U = 48 \cdot \bar{Q} \cdot \sum_{i=0}^{[n/2]-1} \frac{x_{n-i}-x_{1+i}}{x_{n-i}-x_{1+i}+2\bar{Q}} \cdot \left[\frac{i^2}{n^3} - i\left(\frac{1}{n^2} - \frac{1}{n^3}\right) + \frac{1}{4n} - \frac{1}{2n^2} + \frac{1}{3n^3} \right] \qquad (20)$$

is that formula which should be used for practical data systems.

x x x

As long as the demand for the error value was not more as a gross information, may be correct only for the order of magnitude, the use of σ_{emp} seemed to be adequate for the majority of the cases. We have seen, however, that requirements changed in time considerably and σ_{emp} is only seldom able to fulfil them (only in sterile cases). The increased demands necessitate a very detailed, many sided investigation of the quantity $\bar{U}$, too, but these cannot be made in the frame of the present paper. Some preliminary Monte Carlo-investigations for the Cauchy-distribution have proved that the integral in Eq. (19) is very well approximated already for small n-s by the sum in Eq. (20). The same investigations have further shown that the asymptotic formulas for the errors of the $q(p)$-s can be used for small values of n, too.

REFERENCES

Cramér H 1958: Mathematical Methods of Statistics. Princeton University Press, Princeton

Csernyák L 1982: Bemerkung zum Artikel "Uer häufigste Wert etc" von B Hajagos. Publications of the Technical University for Heavy Industry, Series A, Mining, 37, No. 1-2

Csernyák L 1988: Flanken-Diagnostik. Publications of the Technical University for Heavy Industry, Series A, Mining (in press)

Csernyák L, Steiner F 1982: Untersuchungen über das Erfüllungstempo des Gesetzes der grossen Zahlen. Publications of the Technical University for Heavy Industry, Series A, Mining, 37, No. 1-2

Ferenczy L, Takács E 1986: Increase of the efficiency and reliability of a quantitative borehole interpretation system based on probability theory (in Hungarian). Manuscript, Miskolc

Hajagos B 1988: Normalitätsuntersuchungen mit Hilfe der χ^2-Probe an Stichproben, die aus Studentschen Mutterverteilungen stammen. Publications of the Technical University for Heavy Industry, Series A, Mining (in press)

Hajagos B, Steiner F 1989: Acta Geod. Geoph. Mont. Hung. (present issue)

Rényi A 1954: Probability theory. Tankönyvkiadó, Budapest

Seneca 1960: Consolationes, Ethical Letters. Hungarian edition. Europa, Budapest

Steiner F 1985a: Ein möglicher Kennwert der Unbestimmtheit der einzelnen Messergebnisse. Publications of the Technical University for Heavy Industry, Series A, Mining, 38, No. 3-4

Steiner F 1985b: Robust estimations. University textbook. Tankönyvkiadó, Budapest

Steiner F 1986: Most frequent values (Modern adjustment methods for users) (in Hungarian). Manuscript, Miskolc

Acta Geod. Geoph. Mont. Hung., Vol. 24 (3-4), pp. 273-287 (1989)

INVESTIGATION OF THE UNCERTAINTY OF A SINGLE MEASUREMENT IN THE SUPERMODEL $f_a(x)$

B Hajagos and F Steiner

University for Heavy Industry, Chair of Geophysics, H-3515 Miskolc, Egyetemváros, Hungary

[Manuscript received November 29, 1985]

The demand to characterize the uncertainty of a single measurement by an adequate value is well founded. The uncertainty measures deduced from Fisher's information and from the entropy (denoted here by F and H, respectively) cannot be used for arbitrary density functions. A common setback of both F and H is that in cases approximating digital sampling then get zero i.e. they cannot be considered as robust quantities.

The uncertainty U defined by Steiner (1986) has for all distributions a finite value and it is a robust quantity. This paper shows for the supermodel $f_a(x)$ introduced by Csernyák and Steiner (1982) the connection of U with the interquartile range, and with F and H, respectively. Between the Cauchy distribution and the Gaussian distribution - especially in the Jeffreys-interval - the deviations of U, F and H are not significant. A practically important remark: in the mentioned interval it is the simplest to characterize the uncertainty by the dihesion ε.

Kevwords: interquartile range; robust estimation; uncertainty

The engineering practice has to prepare for significant changes in the interpretation of data systems, as well as in the description of their accuracy. Namely, it became more and more accepted that the supposition about the frequent occurrence of the Gaussian, i.e., the so called normal distribution, as a parent distribution is not correct, see e.g. Mosteller and Tukey (1977): "Some misinterpret the word ""normal"" to mean ""the ordinarily occurring"" - but, so far as we know, distributions that exactly fit this formula never occur in practice .." Consequently, in all practical cases efficient algorithms cannot be developed on ground of the unalterated least squares principle: recent results in mathematical statistics have clearly shown the low efficiency (or even complete failure) of algorithms based on the Gaussian distribution (i.e., of the

least squares algorithms) in case of data systems resulting from distributions differring from the Gaussian type. A single title of a recent paper may symbolize this situation: "Götterdämmerung Over Least Squares Adjustment" (Krarup et al. 1980).

This change necessitates not only the preparation and introduction of new program systems, but some general questions should also be solved for which do not exist ready-made answers available in mathematical statistics to be relied upon in such situations.

It is a basic demand that the experimenter should be informed about the uncertainty of his measurement and this uncertainty ought to be presented in a numerical form. The numerical characterization of the uncertainty of a single measurement is one of the primary tasks to be solved; this problem is attacked in this paper for a rather general supermodel, namely the distribution family $f_a(x)$.

The precedents of this paper were published by the group at the Chair of Geophysics of the University for Heavy Industry Miskolc (e.g. the first steps by Csernyák and Steiner 1984, and some general suggestions by Steiner 1986), but it seems advantageous in this paper to deal first with this problem based only on general ideas of mathematical statistics.

The so-called Fisher-information, meant as the "information content of a single measurement" is defined by (e.g. Cramér 1958):

$$I \equiv \int_{-\infty}^{\infty} \frac{\left(\frac{\partial f(x;T)}{\partial T}\right)^2}{f(x;T)}\, dx \qquad (1)$$

where $f(x;T)$ is the probability density function of the measurement result and T the location parameter.

The quantity

$$F \equiv \frac{1}{\sqrt{I}} \qquad (2)$$

could be called "Fisher-uncertainty", and at a first glance it could be considered as the uncertainty of a single measurement

as this quantity has the same character as x itself (as known from the minimum scatter sense of $1/\sqrt{I}$) and, as it was already mentioned, "I" refers to a single measurement.

The condition of the existence of the integral in Eq. (1) means some restrictions for f; in the practice, however, it would be better to have a definition of the uncertainty without restrictions. This demand is fulfilled by the interquartile semi-extent q used often in the practice and involved also in the probability theory: it means the half of the length of the interval, outside of which greater and smaller values occur with the same probability 1/4 (thus the name quartile).

The value q is the half of the value of a function q(p), belonging to p = 0.25: q(p) gives for any p between 0 and 0.5 the interval outside of which greater and smaller values occur with the same probability p. Thus, q(p) is a function which gives all the possible quantile extents and as such it defines fully the distribution for symmetrical distributions; some authors (e.g. Box et al. 1978) deal even before the distribution- and density functions with this function, as the most primary characteristic. - The connection between the distribution function F(x) and the function q(p) is evidently the following:

$$q(p) = F^{-1}(1-p) - F^{-1}(p) \ .$$

It can be said that q(p) informs fully about the uncertainty of a single measurement - but in the technical practice an individual analysis of the q(p)-distribution is impossible, moreover, it is inevitable for comparisons to characterize the distribution by a single numerical value. For this the simplest way is to use the half of the value of q(p) for the symmetry point of the possible values of p, p = 0.25, i.e. q = q(0.25)/2 as the numerical value characterizing the uncertainty. It seems to be even more evident for the choice of these values if it is said that the deviation of x from the symmetry point in absolute value can be with the same probability smaller and greater than q.

It is surely insufficient to consider only one or a few

distribution models for the decision about the applicability of some definition of the uncertainty. from a practical point of view. Thus, a general supermodel is selected for testing purposes: namely the supermodel $f_a(x)$, defined by Csernyák and Steiner (1982), which has the elements for a value of the $(1 < a < \infty)$

$$f_a(x) = \frac{1}{c(a)\left[\sqrt{1+x^2}\right]^a}, \tag{3}$$

where

$$c(a) = \frac{\sqrt{\pi} \cdot \Gamma\left(\frac{a-1}{2}\right)}{\Gamma\left(\frac{a}{2}\right)}. \tag{3a}$$

The general character of supermodel $f_a(x)$ is shown by the facts that for $a \to 1$, the distribution has flanks characterized by const/x, being no more a density function. On the other side for $a \to \infty$, one gets the Gaussian distribution. The so-called Jeffreys-interval with $6 < a < 10$ includes the distributions with the shortest flanks which occur with not negligible probabilities. The supermodel $f_a(x)$ contains the Student-distributions, thus e.g. for $a = 2$, the Cauchy-distribution, too.

Two different kinds of uncertainty parameters can be best compared by their ratios. Therefore the ratios of the Fischer--uncertainty (F) and of the interquartile semi-extent q is calculated for all a-s, and the results are represented as a function of 1/(a-1) (see Figs 1a and 1b; on Fig. 1b the 1/(a-1) values are considerably larger). As it is known (Hajagos 1985), F is given for the family $f_a(x)$ defined by Eq. (3) simply as

$$\sqrt{\frac{a+2}{a(a-1)}}.$$

Concerning the use of the function 1/(a-1), the Gaussian distribution belongs to the abscissa value of 0, the Cauchy-distribution to the abscissa value of 1, and thus figure 1a shows the range in details where the greatest interest is concentrated.

The curve F/q is sufficient to show that for the present

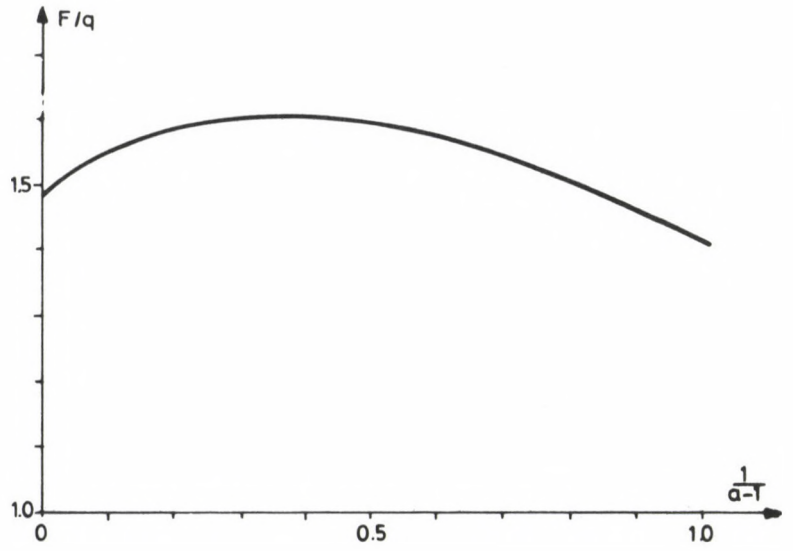

Fig. 1a.

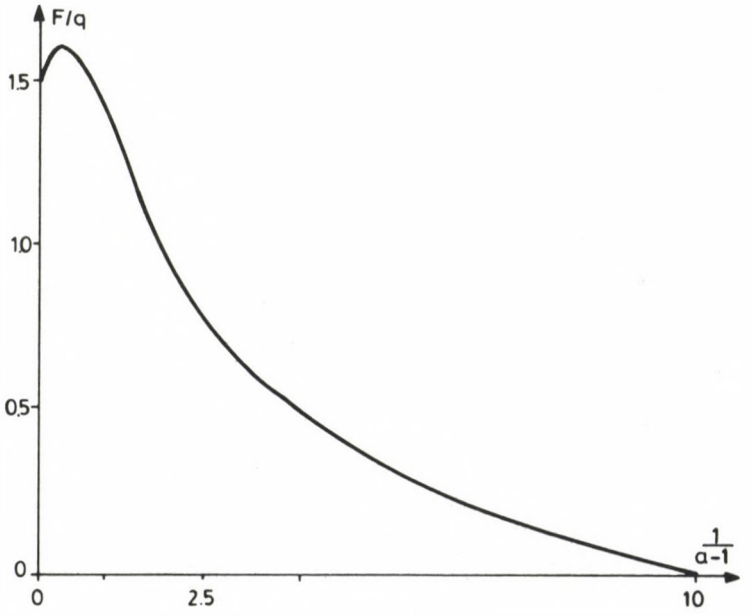

Fig. 1b.

purpose none of the quantities F and q is perfectly applicable. At high values of a (i.e. at low abscissa values) when $f_a(x)$ has extremely short flanks, and the distributions do not differ very significantly from the Gaussian distribution, too great deviations from the Fisher-uncertainty are now welcomed, whereas the deviations of the ratio F/q from the value 1 are not insignificant in this section. Further F cannot be used generally, as the ratio F/q decreases at a = 1.1 to 0.01 (see Fig. 1b). The probability that the deviation of a single measurement from the symmetry point is less than F, is here hardly more than 20 percent, and in the practice an error limit, with 80 percent of the occurring errors being greater than it, cannot be used.

This emphasizes again the advantages of q, but in addition to the objections mentioned, some other disadvantages of the interquartile semiextent as parameter of uncertainty should not be left unmentioned. From the point of view of q it is namely unimportant if the distribution has short or long flanks (or if these flanks are completely absent, as in case of the U-distributions, consisting of two Dirac- δ-s of the same value 0.5 at different x values as a density function).

Steiner (1985) proposed a measure of the uncertainty denoted by U which is based on q, but which takes also the flanks into account. The definition is the following:

$$U = 24 \int_0^{0.5} \frac{1}{\frac{1}{2q} + \frac{1}{q(p)}} (0.5-p)^2 \, dp \, , \qquad (4)$$

where the integrand contains the harmonic mean of the constant 2q and of the value q(p) changing with p multiplied by a weight function which emphasizes the flanks. The norming factor 24 was found by Steiner (1985) with the help of the U-distribution consisting of two Dirac- δ-s; namely from the point of view of the uncertainty of a single measurement this distribution plays the role of a standard: only in case of this distribution is the uncertainty unambiguously given.

The increase of the uncertainty U defined by Eq. (4) against q, if the flanks of the distribution are longer, is

shown in Fig. 2. In case of the Gaussian-distribution (for 1/(a-1) = 0) the surplus is roughly 25 percent; with increasing lengths of the flanks the ratio U/q increases, too, according to the expectation. As the figure shows, the surplus is in case of the Cauchy-distribution (at 1/(a-1) = 1) already 45 percent.

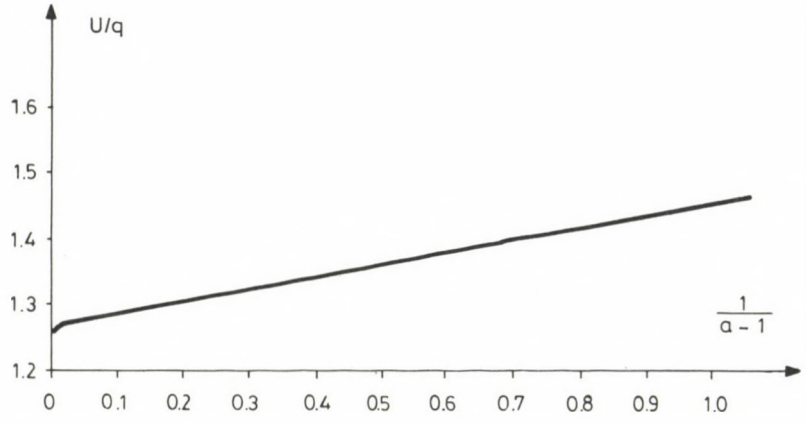

Fig. 2.

As Steiner (1985) has shown that the maximum of U/q is 1.875, thus the surplus due to the flanks cannot be more than 87.5 percent.

In order to have a better idea about U, it can be mentioned here that a densification around the symmetry point may decrease the value of U by maximally 12.5 percent. (This can be easily shown by putting two Dirac- δ-s at the x values +q and -q with the value (0.25 + d), a third to the origin with a value of (0.5 - 2d), and then U is calculated for these distributions. If d is let to approach zero, the above value is obtained.)

According to that, U can be well used as a measure of the uncertainty. Its estimation can be easily made by Eq. (4): only q(p) is to be calculated as a step function on the basis of the data system as a first step.

Let us now compare the Fisher-uncertainty with U for the

supermodel $f_a(x)$ (curve F/U in Fig. 3). For distributions with short and very short flanks, in the range $3 < a < \infty$, this ratio is nearly constant and not far from 1 (roughly 1.2). For the Gaussian distribution one gets $U = \sigma \cdot 0.85$ (where σ denotes the square root of the second moment at the symmetry point, being in this case F); the difference of 15 percent is already in the range hardly perceptible in the technical practice for a single measurement, therefore a discussion U against F or vice versa is not necessary.

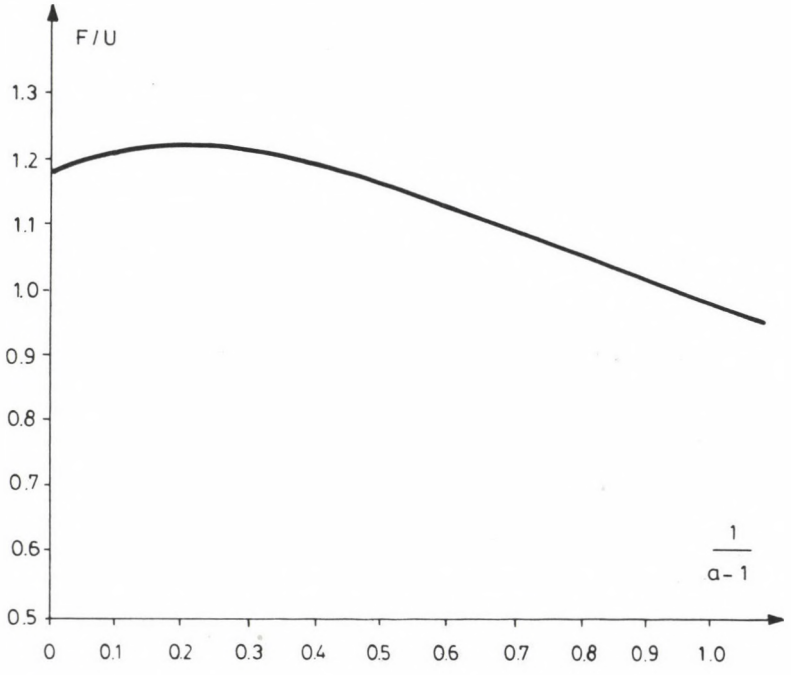

Fig. 3.

An other fact: for the Cauchy-distribution $U \approx F$, the difference is only 2.5 percent. This is curious, as the Cauchy--distribution is from all possible probability distributions that one which has from many points of view specific characteristics; namely it is the only distribution where the best weight function in the estimation of the location parameter is identical with the density function (Hajagos 1985)

The Fisher-uncertainty F fails not only in case of distributions with long flanks (as discussed in connection with Fig. 1b), but leads to irrealistic values in other cases, too. If e.g. a symmetrical distribution is produced from two Gaussian distributions with the symmetry points x = -1 and +1 with the same small value of the parameter σ , Eq. (1), and therefore Eq. (2) defining F can be used without problems (there are e.g. no problems with the derivation), but the result decreases infinitely if $\sigma \to 0$, in spite of the fact that at the limit we get the already mentioned U-distribution, where the uncertainty of a single measurement is just 1. The same result is obtained if F approximates a series of Dirac- δ-s corresponding to a digital apparatus. Any measure of the uncertainty is, however, expected to yield realistic results even in such cases, as it is easily done by the quantity U defined by Eq. (4).

Speaking of uncertainty, the entropy H(f) should also be mentioned which has the following definition:

$$H(f) = \int f(x) \cdot \ln \frac{1}{f(x)} \, dx \, , \qquad (5)$$

where the integration is to be carried out for all ranges of x where $f(x) > 0$.

The problem with the digital values appears in H(f) similarly to F. If e.g. f(x) has the value $1/(4\Delta)$ in the intervals $-1-\Delta < x < -1+\Delta$ and $1-\Delta < x < 1+\Delta$, and else it is zero, then $H(f) = \ln(4\Delta)$ approximates $-\infty$, if $\Delta \to 0$, in spite of the fact that the limiting case is here the same U-distribution, as in the previous considerations, and where the uncertainty of a single measurement as an estimate of the symmetry point is just 1.

Naturally, the definition of Eq. (5) is not applicable in the practice without a suitable transformation as it does not fulfil the precondition that a stretching of the f(x) scale by a factor of c should increase the measure of uncertainty also by c. This is, however, no problem, as it can be easily seen that any value of const. $e^{H(f)}$ has already this property. (This transformation, however, does not change the problem with the

mentioned digital data systems, only the result changes from $H(f) \to -\infty$ to $e^{H(f)} \to 0$; $e^{H(f)}$ is from this point of view quite analogous to the Fisher-uncertainty.)

In the following the uncertainty measure H based on the entropy is defined as:

$$H = \frac{e^{H(f)}}{2\sqrt{\pi \cdot e}} .$$

The choice of the constant multiplicator can be understood from Fig. 4: the value of H approximates F at increasing a; the deviation is at a = 14 only 1.1 percent, at the beginning and end of the Jeffreys-interval 2.3 and 6.3 percent, respectively, and the difference is even at a = 4 only 14 percent.

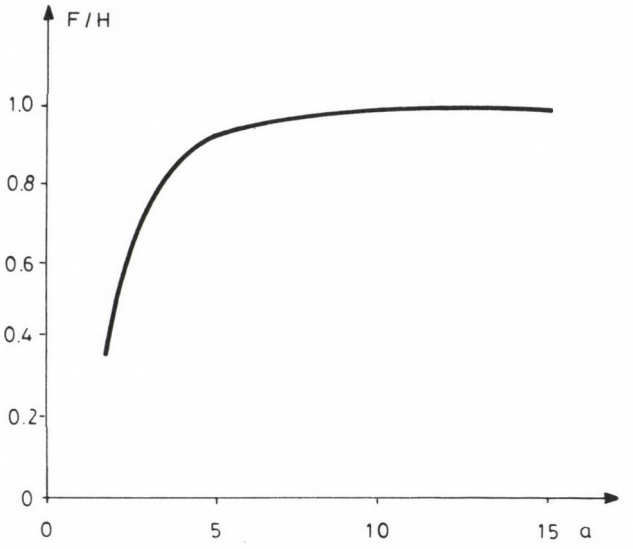

Fig. 4.

H is compared to U in Fig. 5. The ratio H/U vs. 1/(a-1) starts for 1/(a-1) = 0 at the same place in the same direction, as the curve F/U in Fig. 3 due to the choice of the constant multiplicator, but the ratio H/U increases significantly as the flanks get longer in spite of the decrease in the same situation at the curve F/U.

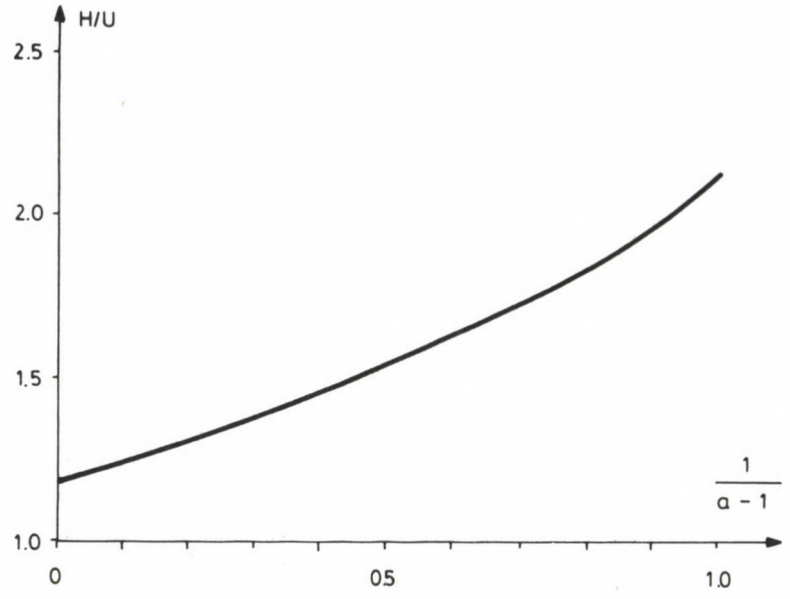

Fig. 5.

The too high sensitivity for the flanks is thus a shortcoming of H; and leads in case of the Cauchy-distribution to H = 2U. Now the question could be raised whether H expresses even more correctly than U the influence of the flanks on the measure of the uncertainty. It is easy, however, to give a negative answer, to this question, as it is known that distributions with infinite entropy do exist, too (Csernyák 1982) which define, however, very precisely a value by their symmetry point; the value H = ∞ means that such distributions cannot be described and treated on this basis. (As it was already shown, U is for all distribution finite.)

As conclusion, some short comparisons should be given.

Steiner (1973) has defined the most frequent value M; its uncertainty-pair is the dihesion ε (Steiner used firstly the more complicated term "reciprocal cohesion"). Csernyák (1971) has shown that ε coincides with the value q of a Cauchy--distribution being most similar to the actual distribution according to a criterion deduced from the Schwarz-unequality (see also the notion of affinity defined by Bhattacharyya; see e.g.

in Mathai and Rathie 1975). ε has therefore a most illustrative content, and its reciprocal, in accordance with the concept of the most frequent value, measures the density around the symmetry point for unimodal distributions. Thus, ε as a measure of uncertainty, characterizes only the range of great values of the density function f(x). The curve ε/U represented in Fig. 6 has consequently a decreasing tendency: the dihesion ε does not take into account the distant parts of the flanks. The numerical values of ε/U differ, however, in the range $3.1 \leq a < \infty$ by less than 10 percent from unity, and therefore here ε can be used without problems as a quick estimate of U, if one has a data-system, but the uncertainty of the single measurements is to be found, too. If the value of a is even less (less than 3), then ε can be also used for the estimation of the uncertainty, but this estimate gets increasingly optimistic, and in case of the Cauchy-distribution, ε is by 31 percent less than U (Fig. 6). - The asymptotic scatter of M, A_M, yields in its turn the best estimate for U just in the vicinity of the Cauchy-distribution (Fig. 7). As known, A_M

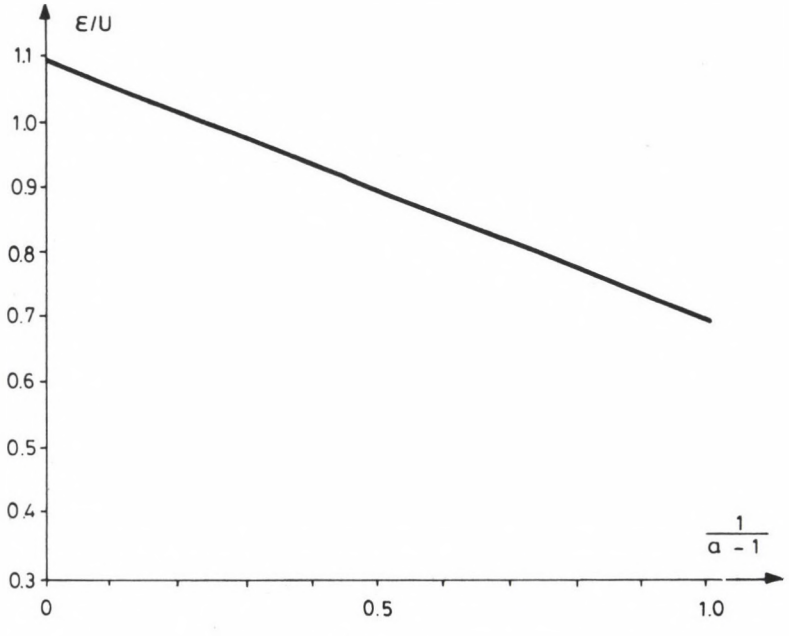

Fig. 6.

can be estimated from a data system (Csernyák and Steiner 1983) as

$$\varepsilon \sqrt{\frac{n}{\text{sum of the weights}}}$$

where n is the number of data in the sample.

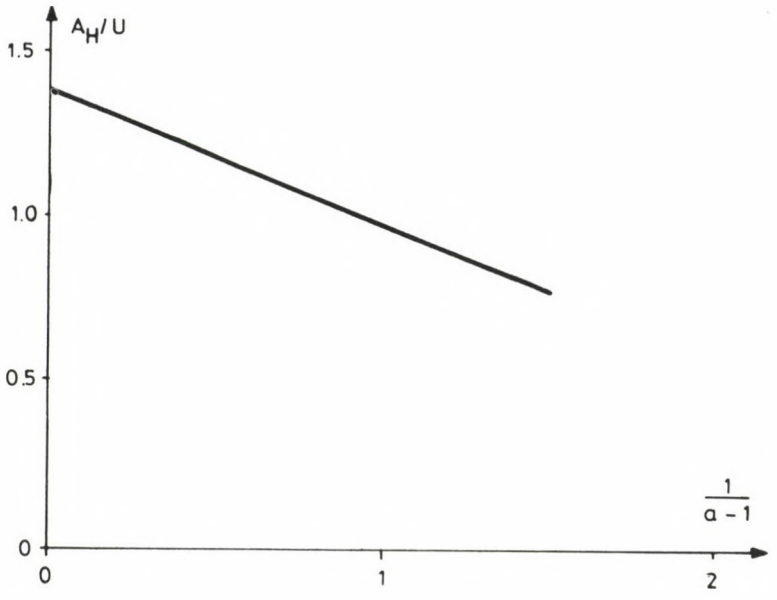

Fig. 7.

At last let us see the curve σ/U in Fig. 8. The curve can be constructed at any reduction of the ordinates only till a value of 0.5 of the abscissa, as for $a \leq 3$ holds $\sigma = \infty$ (more accurately the second moment is not interpreted in this case). Even there, where the interpretation of σ means no problem, the sensitivity of σ is so high for the distant parts of the flanks that this quantity is worthless for the characterization of the uncertainty outside of the immediate vicinity of the Gaussian distribution. σ has significance only as the asymptotic scatter of the averages (if it does exist), therefore it is advisable to read the introductory texts of books on probability theory, dealing with the interpretation

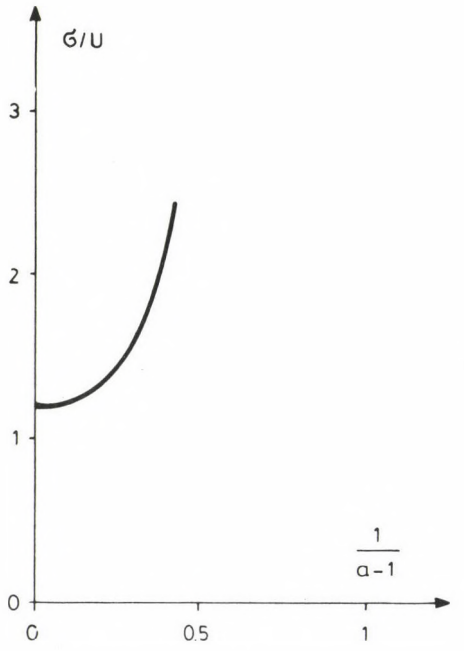

Fig. 8.

of σ , with reservation. (More details of the problem are discussed by Steiner 1982.)

ACKNOWLEDGEMENT

The authors thank Professor L Csernyák for reading the manuscript and for valuable comments.

REFFRENCES

Box G E P, Hunter W G, Hunter J S 1978: Statistics for Experimenters. John Wiley and Sons, New York

Cramér H 1958: Mathematical Methods of Statistics. Princeton University Press, Princeton

Csernyák L 1973: Acta Geod. Geoph. Mont. Hung., 8, 397-401.

Csernyák L 1982: Publications of the Techn. Univ. for Heavy Ind., Series A Mining, 37 (1-2).

Csernyák L,Steiner F 1982: Publications of the Techn. Univ. for Heavy Ind., Series A Mining, 37 (1-2).

Csernyák L, Steiner F 1983: Acta Geod. Geoph. Mong. Hung., 18, 135-140.

Csernyák L, Steiner F 1984: Acta Geod. Geoph. Mont. Hung., 19, 235-248.

Hajagos B 1985: Publications of the Techn. Univ. for Heavy Ind., Series A Mining, 40 (1-4).

Krarup T, Juhl J, Kubik K 1980: In: 14th Congress of the International Society of Photogrammetry, 369-378.

Mathai A M, Rathie P N 1975: Basic Concepts in Information Theory and Statistics.Wiley Eastern Limited, New Delhi

Mosteller F, Tukey J W 1977: Data Analysis and Regression. Addison-Wesley, Reding, Mass.

Steiner F 1973: Acta Geod. Geoph. Mont. Hung., 8, 381-396.

Steiner F 1982: Publications of the Techn. Univ. for Heavy Ind.. Series A Mining, 37 (1-2).

Steiner F 1985: Publications of the Techn. Univ. for Heavy Ind., Series A Mining, 38, (3-4).

Acta Geod. Geoph. Mont. Hung., Vol. 24 (3-4), pp. 289-307 (1989)

METHODS TO INCREASE THE RESISTENCY OF THE COMPUTATION OF THE GENERAL MOST FREQUENT VALUE

B Hajagos and F Steiner

University for Heavy Industry, Chair of Geophysics, H-3515 Miskolc, Egyetemváros, Hungary

[Manuscript received November 5, 1986]

The general adjustment according to the most frequent value (M_k-adjustment) has excellent robust properties, but its resistency is in certain fields of exploration geophysics insufficient as it has been found by L Zilahi-Sebess (1987). Two methods to increase the resistency ($M_{k;b}$-, and $M_{k;c}$-adjustments) are proposed in the present paper. If proper parameters are used to increase the resistency, the excellent efficiency of the M_k--adjustment is only slightly deteriorated, and in addition, the necessary number of steps of the iterations may decrease significantly, if an $M_{k;b}$- or an $M_{k;c}$-adjustment is used instead of the M_k- adjustment.

Keywords: efficiency of estimation; most frequent value; resistency; robust estimation

1. INTRODUCTION

1.1 Definition of the general most frequent value The M_k-adjustment

Let $z_1, z_2, \ldots, z_i, \ldots, z_n$ be a sample of n elements (e.g. the results of measurements carried out on the same physical quantity). If M_k is the so-called location parameter ("real value"), then the quantities x_i, the so-called deviations are defined as

$$x_i = z_i - M_k. \tag{1}$$

The computation of the general most frequent value is - according to Huber's (1981, page 43) nomenclature - a so-called M-estimation where the weight function is

$$\varphi_k(x) = \frac{(k\varepsilon)^2}{(k\varepsilon)^2+x^2} \quad . \tag{2}$$

The quantity ε , the dihesion in this formula fulfills the following equality:

$$\varepsilon^2 = \frac{3\sum_{i=1}^{n} \frac{x_i^2}{(\varepsilon^2+x_i^2)^2}}{\sum_{i=1}^{n} \frac{1}{(\varepsilon^2+x_i^2)^2}} \quad . \tag{3}$$

By a correct choice of the parameter k an estimation of high efficiency can be realized. If e.g. k=1, then: the weighted average

$$M_k = \frac{\sum_{i=1}^{n} \varphi_k(x_i)\, z_i}{\sum_{i=1}^{n} \varphi_k(x_i)} \tag{4}$$

yields an estimation with an efficiency of 100 percent for samples from a Cauchy-distribution in respect of the location parameter (i.e. for the symmetry point of the distribution); if the actual distribution is approximately of a Gaussian type, a high k-value (e.g. k=5) renders the estimation of high efficiency based on Eq. (4).

The double iteration algorithm defined by Eqs (3) and (4) is called the computation of the general most frequent value (for more details see Steiner 1985, for the foundation of the method: Hajagos 1985). If the measurements aim not only the determination of a single constant, but there is again a great quantity of measurements in order to make the results more reliable, then Eq. (4) is substituted by an adjustment according to the method of the least squares with the quantities $\varphi(x_i)$ as weights, and this is called an M_k-adjustment. In such a case the deviations x_i are to be defined more generally than

in Eq. (1): they are the deviations of the measured and computed values, respectively, for the same independent variable(s); on the close connection between adjustment and location parameter, see Steiner (1985). These detailed considerations refer in the quoted paper only to k=1, but mutatis mutandis they are also valid for k > 1. As a last step Eq. (4) is substituted by a weighted adjustment, where the weights correspond to Eq. (2). (This adjustment yields Eq. (4) when only one constant value is computed.) Thus it is not only legal, but also more general if one speaks of an M_k- adjustment instead of "the estimation of the most frequent value based on the parameter k".

1.2 Family of distributions $f_a(x)$

The robustness of estimations can be most easily described by the efficiency in a wide range of random distributions. To test this character, it is insufficient to carry out the investigations for some discrete distributions, but it is more adequate to investigate distribution families containing types varying in one (or more) parameter(s) continuously, i.e. so-called supermodels.

The introduction of the supermodel $f_a(x)$ proved to be useful from several points of view (Csernyák and Steiner 1982). The type parameter a (a > 1) defines according to the following density function, different symmetrical distributions by its different values:

$$f_a(x) = \frac{1}{c(a)\left(\sqrt{1+x^2}\right)^a} \quad (a > 1) \; . \tag{5}$$

(The norming factor c(a) can be expressed by the gamma-function as follows:

$$c(a) = \frac{\sqrt{\pi} \cdot \Gamma\left(\frac{a-1}{2}\right)}{\Gamma\left(\frac{a}{2}\right)} \; . \;) \tag{5a}$$

Equation (5) is a standardized form; in a general case one has

$$f_a(x;S;T) = \frac{S^{a-1}}{c(a)\cdot\left(\sqrt{S^2+(x-T)^2}\right)^a}, \qquad (5b)$$

with the scale parameter S and the symmetry point T. The quoted paper gives more information on the family $f_a(x)$ and it shows several bell-shaped curves according to Eq. (5). Here we show only one of them: the continuous curve of Fig. 1 is the density function corresponding to a=8 and S=4 (and to T=0).

If it is to be determined for a value of k what is the efficiency of the estimation of the location parameter (symmetry point) in a sample from $f_a(x)$, then one needs on the one hand the efficiency of the optimum, i.e. in the present case of the maximum likelihood estimation, too (Cramér 1946), - this is after Hajagos (1985) (a+2)/a(a-1) - on the other the assymptotic variance for the M_k-estimation. According to Huber (1981) the assymptotic variance of the estimation of the location parameter can be computed for M-estimations defined by the weight function $\varphi(x)$ being symmetrical with respect to the origin for S=1 as follows

$$A^2 = \frac{\int_{-\infty}^{\infty}[x\cdot\varphi(x)]^2\cdot f(x)\,dx}{\left[\int_{-\infty}^{\infty}[x\cdot\varphi(x)]'\cdot f(x)\,dx\right]^2} \qquad (6)$$

but since Eq. (2) presented the weight function $\varphi(x) = (1+x^2)^{-1}$ for S=kε , one needs to write out the general formula, too:

$$A^2 = S^2\,\frac{\int_{-\infty}^{\infty}x^2\cdot\rho^2\left(\frac{x}{S}\right)\cdot f(x)\,dx}{\left[\int_{-\infty}^{\infty}\left[x\cdot\rho\left(\frac{x}{S}\right)\right]'\cdot f(x)\,dx\right]^2}. \qquad (6a)$$

Thus, the variance A_k^2 of the M_k-estimation defined by the weight function in Eq. (2) is computed as

$$A_k^2 = \frac{\int_{-\infty}^{\infty} \frac{x^2 \cdot (k\varepsilon)^4}{[(k\varepsilon)^2 + x^2]^2} f(x)\, dx}{\left[\int_{-\infty}^{\infty} \frac{(k\varepsilon)^4 - x^2\,(k\varepsilon)^2}{[(k\varepsilon)^2 + x^2]^2} f(x)\, dx\right]^2} \qquad (7)$$

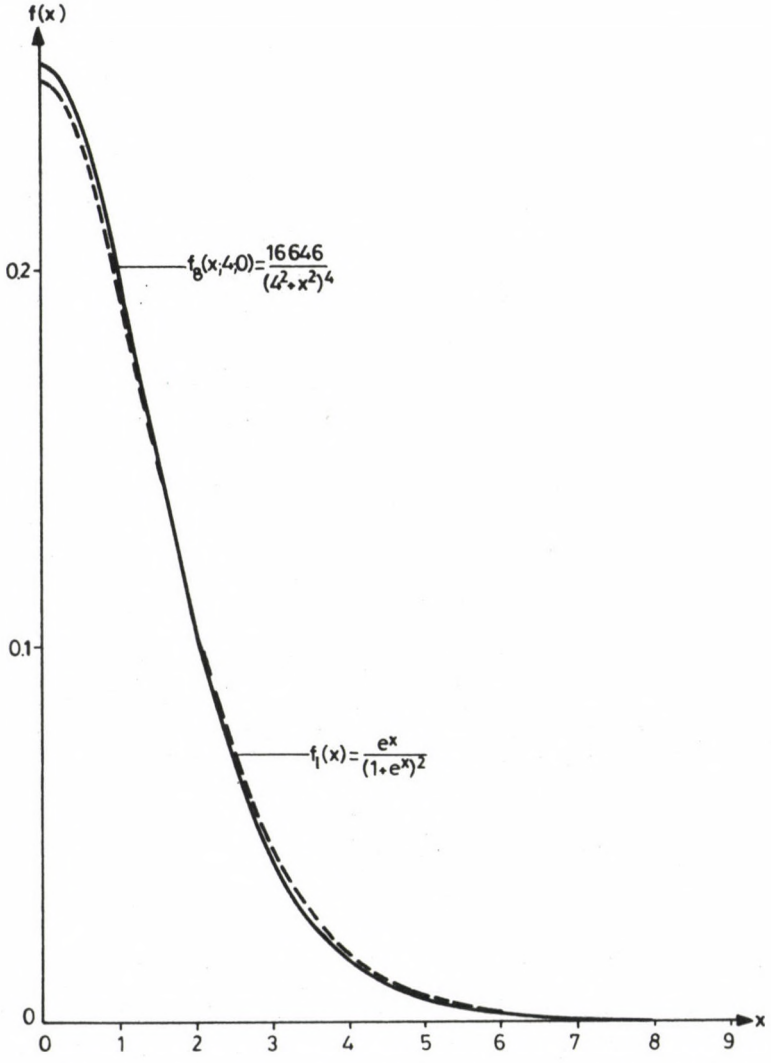

Fig. 1. Density function $f_1(x)$ of the logistic distribution and the curve $f_8(x;4;0)$

After substituting $f(x) = f_a(x)$, one gets the values denoted by $A_k^2(a)$, and the efficiency e is obtained as

$$e = \frac{a+2}{a\cdot(a-1)\cdot A_k^2(a)} . \qquad (8)$$

The curve of the efficiency for the value k=1.9 computed from Eq. (8) is presented as the top curve of Fig. 2, denoted by M_k in function of 1/(a-1).

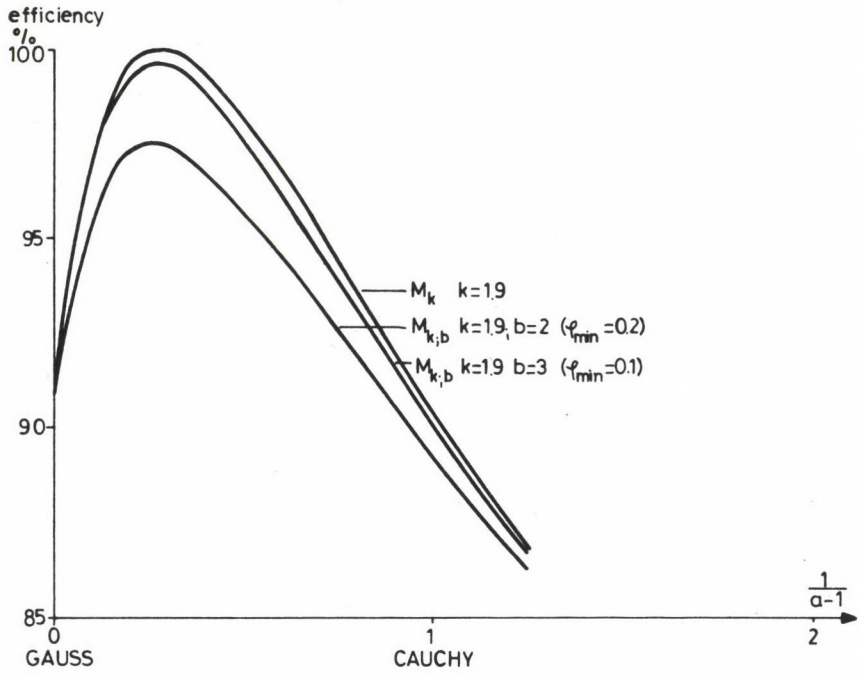

Fig. 2. Efficiency curves of the $M_{k;b}$-adjustment to different values of φ_{min} (or b) and to k=1.9 for the supermodel $f_a(x)$

2. INCREASE OF THE RESISTENCY BY TRUNCATING ACCORDING TO THE WEIGHT MINIMUM: $M_{k;b}$-ADJUSTMENT

2.1 Remarks to the efficiency-curves of the M_k-adjustment

The topmost curve on Fig. 2 shows an efficiency over 90 percent in the whole range $0 < 1/(a-1) < 1$. It can be easily

shown that $f_2(x)$ is the Cauchy-distribution, that $a \to \infty$ yields the Gaussian distribution (normal distribution), and consequently the interval $0 < 1/(a-1) < 1$ covers distributions from the Cauchy-type to the Gaussian one: i.e., the robustness of the estimation fulfils all demands.

The topmost curve on Fig. 2 shows for a=4.4 an efficiency of 100 percent - but instead of the value k=1.9, any k-value greater than 1 yields an efficiency of 100 percent somewhere in the interval $0 < 1/(a-1) < 1$ (for e.g. $k > 5$, this is near to the Gaussian distribution, for $k \approx 1$, near to the Cauchy-distribution). Intuitively one can state that the members of the distribution family $f_a(x)$ are the eigendistributions of the computational algorithm of the general most frequent value. However, the criterion of objectivity is not hurt by studying the efficiency on the members of the $f_a(x)$-family, as on the one hand it contains many types of distributions (Cauchy, Gaussian, Student-distributions), on the other experimental distributions can be very closely modelled in most cases by a member of the $f_a(x)$-family. Let us consider e.g. the curve plotted on Fig. 1 by the dotted curve, being the density function of the so-called logistic distribution:

$$f_1(x) = \frac{e^x}{(1+e^x)^2} \tag{9}$$

which is very near to the density function with a=8 and S=4 (the type of the distribution is naturally determined exclusively by the value of a). It can be shown that the optimum approximation is at a=7.9 and S=4.06 being somewhat closer to the logistic distribution as the previously mentioned one; the most convincing datum on the quality of this approximation $f_{7.9}(x;4.06;0)$ is the value of efficiency, being equal to 99.79 percent.

If such a distribution is looked for, which lies far away from the supermodel $f_a(x)$, then the well-known Laplace-distribution should be chosen which is pointed at the symmetry point, as there all $f_a(x)$ density functions are essentially flat, bell-shaped curves. The density function of the standard

Laplace-distribution is:

$$f_L(x) = \frac{1}{2} e^{-|x|} . \qquad (10)$$

It is known that the sample median as an estimate for the symmetry point has an efficiency of 100 percent for this distribution. The reciprocal of the asymptotic scatter A_{med} is for the median and for distributions being symmetrical to the origin equal to 2f(0) yielding for Eq. (10) $A^2_{med} = 1$; in comparison, A^2 from Eq. (7) computed with $f(x) = f_L(x)$ and k=1, $e=A^2_{med}/A^2$ is 86.4 percent. That means that in case of a distribution being far from the family $f_a(x)$, the efficiency is rather high, too; the model can be even adapted for $f_L(x)$.

The previous survey was necessary, but the following remark is more important.

One of the most important and for the practice outstanding notion of the theory of robust estimations is the function IC(x), namely, IC(x)/n yields for a given algorithm of the determination of the location parameter and for a given random distribution how much does the estimated value of the location parameter change if to a sample with a (high) number of elements n an (n+1)-th element with a value x is added. It is known that IC(x) is proportional to $x \cdot \varphi(x)$ (Huber 1981), therefore for the M_k-adjustments:

$$IC_k(x) = \text{const.} \frac{x \cdot (k\varepsilon)^2}{(k\varepsilon)^2 + x^2} . \qquad (11)$$

The absolute value of this function decreases slowly with increasing |x| (especially for high k-values), i.e. in such cases outliers can influence significantly the result, or in other words: the resistency of the M_k-adjustment cannot be always regarded as sufficient. Such a case of geophysical interpretation is dealt with by Zilahi-Sebess (1987) and therefore he used as weights instead of $\varphi(x)$ from Eq. (2) its square. This is the so-called M^*-adjustment which has a much better resistency as illustrated by the curves in Steiner (1985).

As a short summary, the M_k-adjustment has excellent

robustness but its resistency is insufficient in some cases for the practice.

2.2 The truncation according to φ_{min} and its effect on the efficiency

In this section we propose the use of the following weight function:

$$\varphi_{k;b}(x) = \begin{cases} \varphi_k(x), & \text{if } \varphi_k(x) \geq \varphi_{min} \\ 0, & \text{if } \varphi_k(x) < \varphi_{min} \end{cases} \tag{12}$$

which may seem at a first glance somewhat too drastic or arbitrary modification. The value φ_{min} is the least non-zero weight, else the weights from the M_k-adjustment are used. Such a modification of the algorithm needs only a slight change in an M_k-adjustment program, beyond a limit, however, i.e. for the ranges

$$|x| > bk\varepsilon = k\sqrt{\frac{1-\varphi_{min}}{\varphi_{min}}} \tag{13}$$

it yields absolute resistency: for $|x| > bk\varepsilon$ $IC_{k;b}(x) = 0$.

It is to be investigated what is the effect of such a change in the weights on the efficiency.

The first step is to found the expression of Eq. (6) for the special case of Eq. (12). Due to the discontinuity of the function $x \cdot \varphi_{k;b}(x)$ at $x = \pm bk\varepsilon$, the function $\left[x \cdot \varphi_{b;k}(x)\right]$ contains also a term of the form

$$\frac{b(k\varepsilon)^3}{(k\varepsilon)^2+(bk\varepsilon)^2} \cdot \delta(x-bk\varepsilon)$$

where δ is the Dirac-delta. The result is then:

$$A^2_{k;b} = \frac{\int_{-bk\varepsilon}^{+bk\varepsilon} \frac{x^2\,(k\varepsilon)^4}{\left[(k\varepsilon)^2+x^2\right]^2}\, f(x)\,dx}{\left[\int_{-bk\varepsilon}^{+bk\varepsilon} \frac{(k\varepsilon)^4-x^2\cdot(k\varepsilon)^2}{\left[(k\varepsilon)^2+x^2\right]^2}\, f(x)\,dx - \frac{2b(k\varepsilon)^3}{(k\varepsilon)^2+(bk\varepsilon)^2}\cdot f(bk\varepsilon)\right]^2}. \qquad (14)$$

By substituting $f(x) = f_a(x)$ one gets a value to be denoted by $A^2_{k;b}(a)$; the efficiency is now naturally:

$$e = \frac{a+2}{a\,(a-1)\,A^2_{k;b}(a)}. \qquad (8a)$$

The computations of the efficiency have been carried out for the values $\gamma_{min} = 0.02$; 0.1 and 0.2 (i.e. according to Eq. (13) for the values b=7; 3 and 2). Figure 2 shows only the efficiency curves for the values b=3 and b=2, as the curve obtained for a truncation at $\gamma_{min} = 0.02$ was practically identical with the curve of the original curve M_k (which refers here to $\gamma_{min} = 0$, or to $b = \infty$). Figure 2 shows that for $\gamma_{min} = 0.2$ the decrease in the efficiency is about half percent in the type-range near to the Gaussian one, but it approaches the value of 3 percent at a=4 which may be a little bit too much. The decrease of the efficiency by maximum half percent due to a truncation at $\gamma_{min} = 0.1$ is, however, practically always negligible.

The question could be also risen how far the truncations after γ_{min} "cut" into the mother-distributions $f_a(x)$, or more concretely: what is the measure of the neglection from the mother distribution (regarding them only from this point of view). The answer does evidently depend on a and it can be simply given if the explicit form of the distribution function $F_a(x)$ is known. For the cases a=2, 3 and 4 and for a values greater than 4 the distribution functions are the following:

$$F_2(x) = \frac{1}{2} + \frac{1}{\pi}\arctan x; \quad F_3(x) = \frac{1}{2} + \frac{x}{2\sqrt{1+x^2}}; \quad f_4(x) = F_2(x) + \frac{1}{\pi}\frac{x}{1+x^2};$$

$$F_a(x) = F_{a-2}(x) + \frac{1.3. \ \ldots \ .(a-4)}{2.4. \ \ldots \ .(a-3)} \frac{1}{2} \frac{x}{(1+x^2)^{\frac{a-2}{2}}} \qquad (a \geq 5 \text{ and odd}); \qquad (15)$$

$$F_a(x) = F_{a-2}(x) + \frac{2.4. \ \ldots \ .(a-4)}{1.3. \ \ldots \ .(a-3)} \frac{1}{\pi} \frac{x}{(1+x^2)^{\frac{a-2}{2}}} \qquad (a \geq 6 \text{ and even}).$$

The quantity of the data neglected from the mother-distribution is shown in Fig. 3 in comparison to all data in the mother-distribution for the range $0 < 1/(a-1) < 1$. Even if these values cannot be neglected in the vicinity of the Cauchy--distribution (e.g. for $\gamma_{min} = 0.1$, about 10 percent), it is not necessary to be anxious: the efficiency-curves of Fig. 2 give answer to all questions being important from a practical point of view. Figure 3 is presented here only to enable a comparison with the most ancient robust estimation method, with the "α-truncated average". The aim of this comparison is here just to emphasize differences: a similar truncation rate does not yield similar results in the two cases due to several causes. The α-truncated average gives equal weights within the untruncated range, differring from the $M_{k;b}$-adjustment. Using $\alpha = 10$ percent yields anyway very good efficiencies for the so-called Jeffreys-range including the best practical data systems with $6 < a < 10$, as Fig. 4 shows (that is why Stigler 1981 in his paper with a provoking title could conclude to the advantageous feasibility of the use of the $\alpha = 10$ percent--truncated average), but outside of this interval the efficiency of the α-truncated average decreases quickly; that means that the method is not robust enough. For the computation of e the formula from Huber (1981), p. 58 applied to the $f_a(x)$-functions can be used:

$$A^2 = \frac{2}{(1-2\alpha)^2} \left\{ \int_0^{F_a^{-1}(1-\alpha)} x^2 \cdot f_a(x)\, dx + \alpha [F_a^{-1}(1-\alpha)]^2 \right\}. \qquad (16)$$

A perhaps even more serious setback of this method is that it

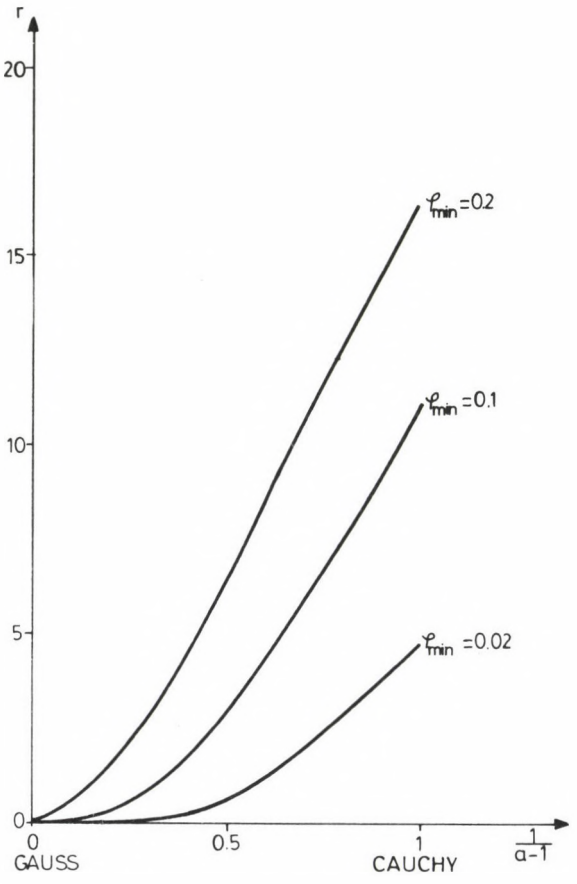

Fig. 3. The percentual r-values of neglected data in case of the truncation of flanks corresponding to different ϱ_{min}-values, and those referring to mother distributions of the supermodel $f_a(x)$

supposes tacitly: the number of outliers to be represented on the left and right hand sides, respectively, of the x-axis is the same. If this is not fulfilled, i.e., all outliers are found e.g. on one side of the axis, then the α -truncated estimation does not yield an undistorted estimation even if all outliers are eliminated by a proper choice of the value of α as in such a case a similar quantity of the mother distribution is eliminated on the other side - what makes the originally symmetric mother distribution asymmetric. Evidently such a distortion cannot be caused by the truncation according to the

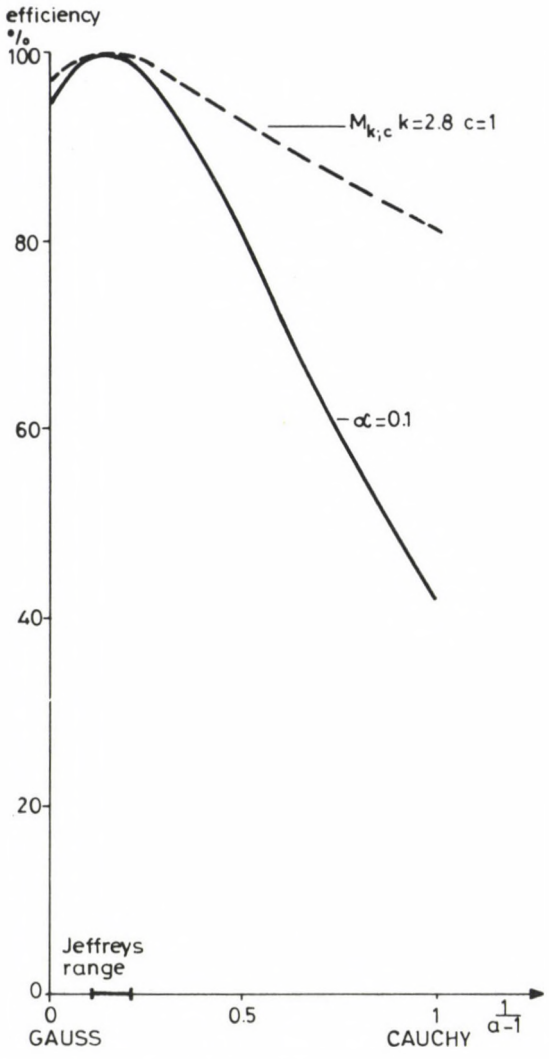

Fig. 4. The efficiency curve of the α-truncated average for α=0.1 (full line). The range of the optimum efficiencies covers the Jeffreys--range, but outside the efficiency decreases rapidly. The low robustness and the possibility of the occurrence of distortions as well as the computational difficulties of such an adjustment are important setbacks of the method which is therefore not proposed for the practice. The dotted line shows for comparison the efficiency curve of the $M_{k;c}$-adjustment (see Section 3) for k=2.8 and c=1; in this case, the Jeffreys-range is again preferred but the robustness is much higher (in the vicinity of a=2 the efficiency is twice of that at α=0.1), and the $M_{k;c}$-adjustment is free from the other two setbacks, too

weight, i.e. by the $M_{k;b}$-adjustment.

3. INCREASE OF THE RESISTENCY BY THE $M_{k;c}$-ADJUSTMENT

3.1 Truncation by a continuously derivable weight function

It has been shown in the previous section that the $M_{k;b}$--adjustment has advantageous properties from the points of view of both robustness and resistency, only aesthetic points of view are hurtful (by the sudden truncation). It is, however, no practical point of view whether a succesful mathematical method be aesthetic or not, but the present authors think that more "aesthetic" solutions are often more advantageous, too, from one or other practical aspect.

Let us define the weight function as follows:

$$\varphi_{k;c}(x) = \begin{cases} \dfrac{(k\varepsilon)^2}{(k\varepsilon)^2+x^2} & \text{, if } |x| \leqslant ck\varepsilon \\ \dfrac{1}{1+c^2}\, e^{\frac{c^2}{1+c^2}\left[1-\frac{x^2}{(ck\varepsilon)^2}\right]} & \text{, if } |x| > |ck\varepsilon. \end{cases} \tag{17}$$

It can be easily seen that not only this weight function is continuous, but its first derivate, too. Concerning the resistency, $IC_{k;c}(x) = \text{const.}\; x\varphi_{k;c}(x)$ decreases so quickly for high values of $|x|$ that practically it is a truncation after weight (it should be mentioned that $IC_k(x)$ from Eq. (11) decreases with increasing x very slowly, namely, as $1/x$).

The most important questions remain the same, namely how far will be changed the efficiencies when substituting $\varphi_k(x)$ by $\varphi_{k;c}(x)$. The asymptotic variance $A^2_{k;c}$ is obtained by substituting Eq. (17) into Eq. (6) as:

$$A^2_{k;c} = \frac{\int_0^{ck\varepsilon} \frac{x^2\,(k\varepsilon)^4}{[(k\varepsilon)^2+x^2]^2} f(x)\,dx + \int_{ck\varepsilon}^{\varepsilon} \frac{x^2}{(1+c^2)^2} e^{\frac{2c^2}{1+c^2}\left[1-\frac{x^2}{(ck\varepsilon)^2}\right]} f(x)\,dx}{2\left[\int_0^{ck\varepsilon} \frac{(k\varepsilon)^4 - x^2\,(k\varepsilon)^2}{[(k\varepsilon)^2+x^2]^2} f(x)\,dx + \int_{ck\varepsilon}^{\infty} \frac{1}{1+c^2}\left\{1-\frac{2x^2}{(k\varepsilon)^2\,(1+c^2)}\right\} e^{\frac{c^2}{1+c^2}\left[1-\frac{x^2}{(ck\varepsilon)^2}\right]} f(x)\,dx\right]^2} \tag{18}$$

By substituting $f_a(x)$ or $F(x)$ one obtains $A^2_{k;c}(a)$, and the efficiencies are similarly computed as before from

$$e = \frac{a+2}{a\,(a-1)\,A^2_{k;c}(a)} \qquad (8b)$$

As an example, let us consider the dotted curve on Fig. 4; for k=2.8 and c=b one gets estimations preferring the Jeffreys--range similarly to $\alpha = 0.1$, but the efficiencies are here everywhere higher; at a=2, the ratio of the efficiencies is already around 2.

3.2 Discussion

Figure 5 presents efficiency-curves (in addition to the original efficiency curve known from Fig. 2) for c=1.5 and c=1 (the value of k is in all three cases as before, 1.9). In the

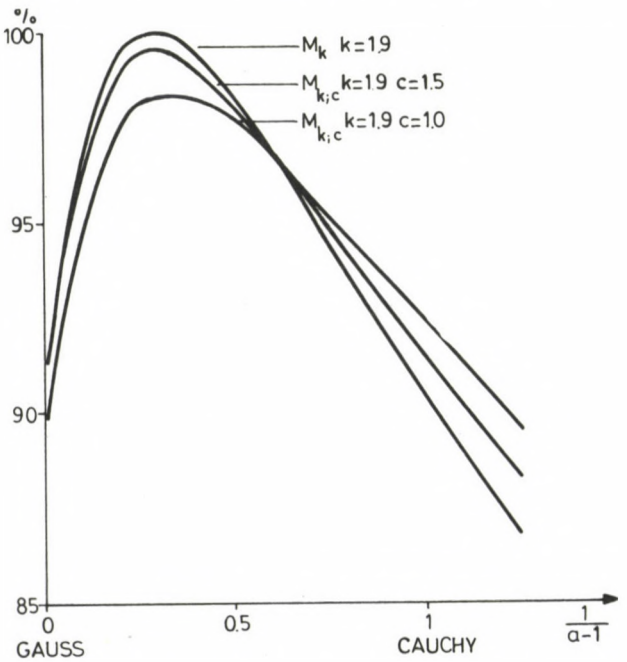

Fig. 5. Efficiency curves of the $M_{k;c}$-adjustment for different values of c, and for k=1.9 in the supermodel $f_a(x)$

interval $0 < 1/(a-1) < 0.5$ the maximum decrease of the efficiency is for c=1.5, 0.5 percent, for c=1, 2 percent; this is for c=1 sometimes allowed, for c=1.5, it is always allowed; the situation is therefore very similar to that found in connection with Fig. 2 for the $M_{k;b}$-adjustment.

It is somewhat surprising that in the vicinity of the Cauchy-distribution the continuous truncation does not decrease, but in opposite, it increases the efficiency. That means that the practical utility of the aesthetic point of view proved itself.

The fact that the dependence of the efficiency on c may be of different character for different values of a is illustrated in Fig. 6a and 6b beginning with the minimum c-value suggested, 0.5 at a=4 and a=2, respectively. It is to be decided if these differences are realistic?

Concerning Fig. 6a, the weight function $\varphi_k(x)$ with k=1.9 differs hardly from the optimum weight function for $f_4(x)$ (this is shown by the efficiency greater than 99.9 percent of Figs 2 and 5 on the M_k-curves); thus it is evident that a significant change like the transition from $\varphi_k(x)$ to $\varphi_{k;c}(x)$ at c=1 (and even more at c=0.5)may result only in a decrease of the efficiency.

A different situation is found at a=2, i.e. at the Cauchy--distribution: here 100 percent efficiency would be yielded by k=1, therefore k=1.9 results in a more emphasized effect of the flanks of the Cauchy-distribution than the optimum algorithm would allow (these flanks, more exactly the too high weights attributed to them cause the averaging to be a zero efficiency). Both weight functions (represented on Fig. 7 by dash line and dotted line, respectively) show significant deviations at high x-values. The curve with full line in Fig. 7 is the weight function $\varphi_{k;c}(x)$ corresponding to k=1.9 and c=1: it is nearer to the optimum weight function, as expected in case of $|x| > 2k\varepsilon$ than to the weight function corresponding to k=1.9.

It has been mentioned in several cases that if the type range of the actual distributions is known then the value k can be chosen so that an efficiency of 100 percent is approximated.

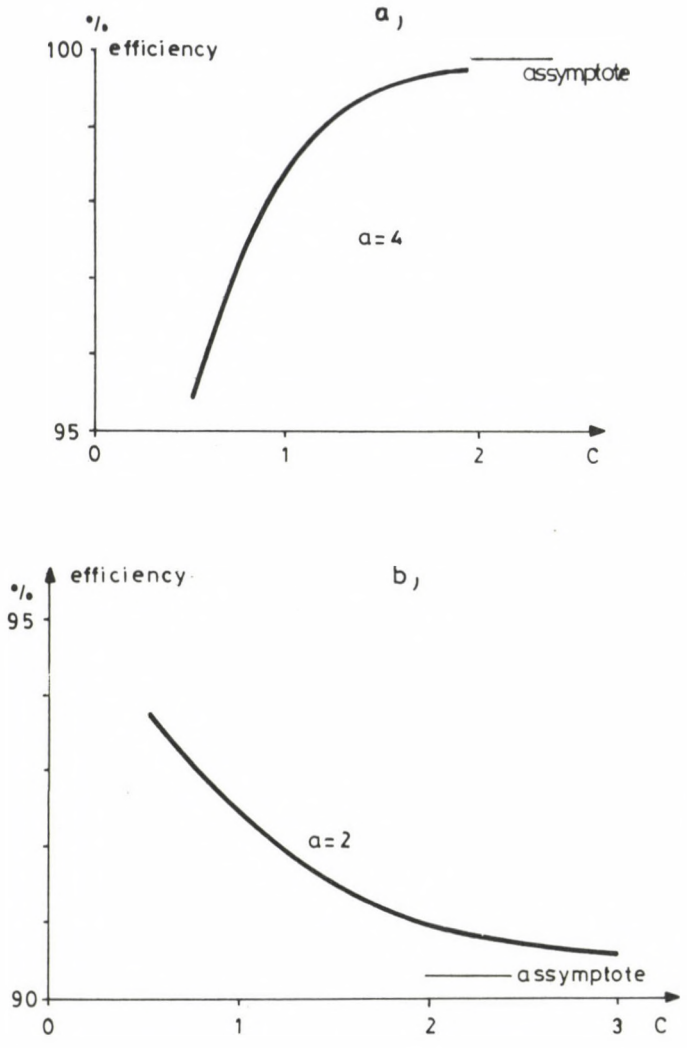

Figs 6a and 6b. Changes of the efficiency vs. c for a fixed value of k (k=1.9) and for different values of a (a=4 and a=2)

For given deviation-sets x_i the type-range can be determined by the know-how No. 34 of the University for Heavy Industry, Miskolc; to the centre of the range of types obtained an optimum k-value can be attributed. Then the resistency can be increased by an appropriate choice of the value c (or of φ_{min}).

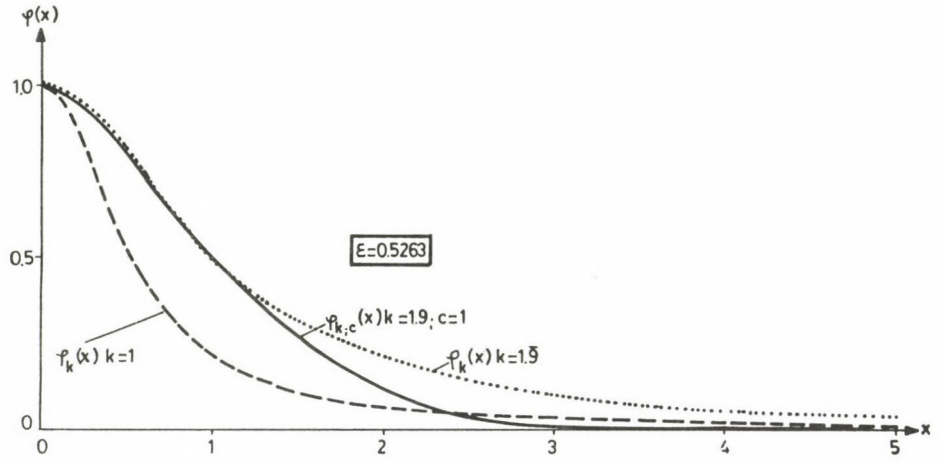

Fig. 7. Weight functions $\varphi_k(x)$ of the M_k-adjustment in case of $\varepsilon=0.5263$, and for k=1 and k=1.9; the weight function $\varphi_{k;c}(x)$ the $M_{k;c}$-adjustment for $\varepsilon=0.5263$, k=1.9 and c=1

All previous examples nave been presented for a single value of k, namely k=1.9. This seems to contradict the present conclusions. The authors of this paper have realized, however, that e.g. the new methods to define the type of distributions, but even the whole of the robust statistics is rather unknown to practical people, and they can spend only a very small fraction of the working hours by studying such questions. Thus the possibility to choose the values k and b (or of k and c) from a rather wide range can appear at the first glance as a factor of uncertainty. As experimental distributions are expected to be mostly within the Cauchy-Gaussian range, we propose the use of the value k=1.9 being an optimum for this full range in case of the weight function $\varphi_{k;c}(x)$, i.e. of the $M_{k;c}$-adjustment with c=1.5, and in case of the $M_{k;b}$-adjustment, with $\varphi_{min} = 0.1$. Thus, only two possibilities remain, and the authors propose to use the $M_{k;c}$-adjustment.

ACKNOWLEDGEMENT

The authors thank Professor L Csernyák for a thorough

discussion of the paper and for many useful advices.

REFERENCES

Cramér H 1946: Mathematical Methods in Statistics. Princeton Univ. Press, Princeton, N.J.

Csernyák L, Steiner F 1982: Publications of the Techn. Univ. for Heavy Industry. Series A, Mining, 37 (1-2).

Hajagos B 1982: Publications of the Techn. Univ. for Heavy Industry, Series A, Mining, 37 (1-2).

Hajagos B 1985: Publications of the Techn. Univ. for Heavy Industry, Series A, Mining, 40 (1-4).

Huber J P 1981: Robust Statistics. Wiley and Sons, New York

Jeffreys H 1961: Theory of Probability. Clarendon Press, Oxford

Steiner F 1985: Robust estimations (in the series Geophysical Data Processing) (in Hungarian). Tankönyvkiadó, Budapest

Stigler S M 1977: The Annals of Statistics, 5, 1055-1098.

Zilahi-Sebess L 1987: Publications of the Techn. Univ. for Heavy Industry, Series A, Mining (in press)

Acta Geod. Geoph. Mont. Hung., Vol. 24 (3-4), pp. 309-327 (1989)

INTERPRETATION OF GRAVITY AND MAGNETIC ANOMALIES USING RELATIVE HORIZONTAL AND TRUNCATED VERTICAL GRADIENTS

K Kis[1], K Kloska[2], F Kovács[2], S Tóth[3]

[1]Department of Geophysics, Eötvös Loránd University, H-1083 Budapest, Kun Béla tér 2, Hungary

[2]Department of Gravity and Geomagnetism, Geophysical Exploration Company, H-1068 Budapest, Gorkij fasor 42, Hungary

[3]Department of Geology, Geophysical Exploration Company, H-1062 Budapest, Népköztársaság útja 59, Hungary

[Manuscript received January 6, 1987]

The calculated gradients indicate the rate of change of gravity and magnetic anomalies. The amplitude and direction of the gradients are affected by the changes in the subsurface structure. The gradients are derived from the truncated derivatives of the potential field with respect to x, y and z. A Gaussian low-pass window has been used as a truncating function. The relative horizontal gradient is obtained from the truncated derivatives with respect to x and y after normalizing its maximum amplitude. The truncated vertical gradient is obtained from the truncated derivative with respect to z. The suggested procedure is illustrated by model calculations as well as field examples. It is applied to the Bouguer anomalies, and the vertical magnetic anomalies of the Nova prospecting area of Hungary. The Bouguer anomaly and the vertical magnetic anomaly maps of Nova are presented with the results of the gradient determinations on maps of the area. These latter results are interpreted and discussed.

Keywords: Bouguer-anomaly; gradients; gravity anomalies; interpretation; magnetic anomalies; truncation

INTRODUCTION

The torsion balance, as developed by Eötvös, was utilized in the gravitational exploration with great success. It measures the north and east components of horizontal gradient, the difference in the maximum and minimum curvatures and direction of minimum curvature of the equipotential surface of gravity. It does not react to the vertical changes in gravity (Heiland 1946, Jakosky 1950). The torsion balances have been replaced by gravimeters because of their greater accuracy and speed in exploration.

The horizontal and vertical gradients are determined from gravimeter measurements. The vertical gradient is measured using a tower and gravimeter. This procedure was initiated by Thyssen-Bornemisza and Stackler (1956). The application of this method was discussed and developed by Fajklewicz (1976); Anger and Liard (1982). The accuracy requirements were discussed by Hammer and Anzoleaga (1975). Kanasewich and Agarwal (1970) used the Fourier transform to obtain horizontal and vertical derivatives. Stanley and Green (1976) demonstrated that the horizontal and vertical gradients could be obtained my means of a Hilbert transformation.

The gradients of the magnetic field can be used to advantage in the interpretation of magnetic anomalies. They were used in ground magnetic prospecting (Hood and McClure 1975); in marine magnetic surveys (Eggers and Thompson 1984); in aeromagnetic surveys (Hood 1965). Barongo (1985) suggested a method for depth estimation of the magnetic sources using the vertical gradient profiles.

The normal or planetary variation of horizontal gravity gradients can be obtained by differentiation of the international gravity formula. It is sufficient to consider the Earth as an ellipsoid of revolution. The numerical values of the normal horizontal gradients are

$$g_x^{normal} = 8.122 \sin 2\varphi E \ , \qquad (1)$$

where E is the Eötvös unit (of $1E = 10^{-9}s^{-2}$)

$$g_y^{normal} = 0 \ , \qquad (2)$$

where φ is the geographic latitude. The normal variation of the radial gravity gradient can be calculated with sufficient accuracy by differentiating the Clairaut equation. The normal variation of radial gravity gradient is

$$g_r^{normal} = -3086 \ E \ . \qquad (3)$$

The radial and the latter used vertical gradients are opposite in sign.

The normal variation of vertical magnetic gradients can be determined with sufficient accuracy by considering the magnetic dipole field of the Earth. The numerical values of normal vertical magnetic gradients are

$$Z_x^{normal} = 0.0096 \sin \Theta \text{nTm}^{-1} , \quad (4)$$

$$Z_y^{normal} = 0, \quad (5)$$

$$Z_r^{normal} = 0.0288 \cos \Theta \text{nTm}^{-1} , \quad (6)$$

where Θ is the magnetic colatitude measured from the South pole. The vertical magnetic gradient quantities are given in nTm^{-1}.

DETERMINATION OF GRADIENTS

The aim of calculation is the determination of horizontal and vertical gradients of Bouguer anomalies and vertical magnetic anomalies. The north and east components of the horizontal gradient are given by the derivatives with respect to the variables x and y, and the vertical gradient is obtained by the derivative with respect to the variable z.

One of the possible methods for the calculation of the derivatives is the determination of two-dimensional sets of coefficients whose convolution with the input data, gives good approximations to certain derivatives of the input. This type of coefficients was presented by Kis (1983). The derivation of coefficients is as follows. The transfer function of the derivatives with respect to x, y and z are known and they are

$$S_{dx}(f_x,f_y) = j\, 2\, \pi f_x , \quad (7)$$

$$S_{dy}(f_x,f_y) = j\, 2\, \pi f_y , \quad (8)$$

$$S_{dz}(f_x,f_y) = 2\pi(f_x^2 + f_y^2)^{1/2}, \qquad (9)$$

where f_x and f_y denote the spatial frequencies measured along the x and y axis respectively.

Amplification in the high frequency range is undesirable, since this range possesses the lowest signal-to-noise level. As a consequence amplification of the high frequency components usually corresponds to the amplification of the high frequency noise. In order to remove the high frequencies, the theoretical transfer function is multiplied by the Gaussian window function,

$$S_{LP}(f_x,f_y) = e^{-\left(\frac{36}{m}\right)^2\left(f_x^2+f_y^2\right)} \qquad (10)$$

as suggested by Meskó (1984). This windowing corresponds to low-pass filtering of the input. The parameter m, in Eq. (10) modifies the cut-off frequency of the filter. The coefficients, i.e. the digital weight function, can be obtained by the numerical inverse Fourier transformation of the truncated theoretical transfer function. The numerical Fourier transformation of the coefficients is the actual transfer function or the frequency response of the truncated derivation. In the low frequency range the actual transfer functions are in accord with the theoretical.

The absolute value of the truncated horizontal gradient is given by the square root of the sum of the north and east components:

$$g_h = \left(g_x^2 + g_y^2\right)^{1/2} \qquad (11)$$

The maximum of this absolute value is determined and the horizontal gradients are divided by this maximum. In this manner the dimensionless relative horizontal gradients are obtained, and their magnitude varies between 0 and 1. The direction of gradients is given by the equation

$$\alpha = \tan^{-1}\frac{g_x}{g_y} \qquad (12)$$

The angle α is measured counterclockwise from the y-axis. The relative horizontal gradients are depicted by arrows whose lengths are proportional to their magnitude.

The truncated vertical gradients are presented in isoline form.

MODEL CALCULATIONS

The suggested procedure is illustrated by simple gravitational and magnetic model calculations.

The faults and contacts of beds are often modeled by vertical escarpment. The formula for gravitational field was given by Sazhina and Grushinsky (1971). It is as follows:

$$g(x) = G\varsigma\pi\left[(d_2-d_1) + 2d_2\tan^{-1}\frac{x}{d_2} - 2d_1\tan^{-1}\frac{x}{d_1} + x\log\frac{x^2+d_2^2}{x^2+d_1^2}\right], \quad (13)$$

where G is the universal constant of gravitation, ς is the density or density contrast, d_1 and d_2 are the upper and lower depths of the escarpment.

Figure 1 shows the gravity effect, the vertical gradient obtained analytically the truncated vertical gradient calculated by the suggested method and the relative horizontal gradients. The model dimensions are: $\varsigma = 200\ \mathrm{kgm}^{-3}$ the upper depth = = 500 m, 2000 m, 5000 m the thickness d_2-d_1 = 1000 m. The relative horizontal gradients were divided by the same maximum value. Thus, the magnitudes of relative horizontal gradients can be seen to be a function of depths which are comparable. As result of the applied truncation function, the amplitudes of the vertical gradients are always less than the analytical ones.

Similar model examples were calculated to illustrate the application of the method in the case of the vertical magnetic field of a magnetized step as given by Nabighian (1972):

$$Z(x) = \frac{\mu_0 J}{2\pi}\left[\left(\tan^{-1}\frac{x}{d_1} - \tan^{-1}\frac{x}{d_2}\right)\cos\Theta + \sin\Theta\log\frac{x^2+d_1^2}{x^2+d_2^2}\right], \quad (14)$$

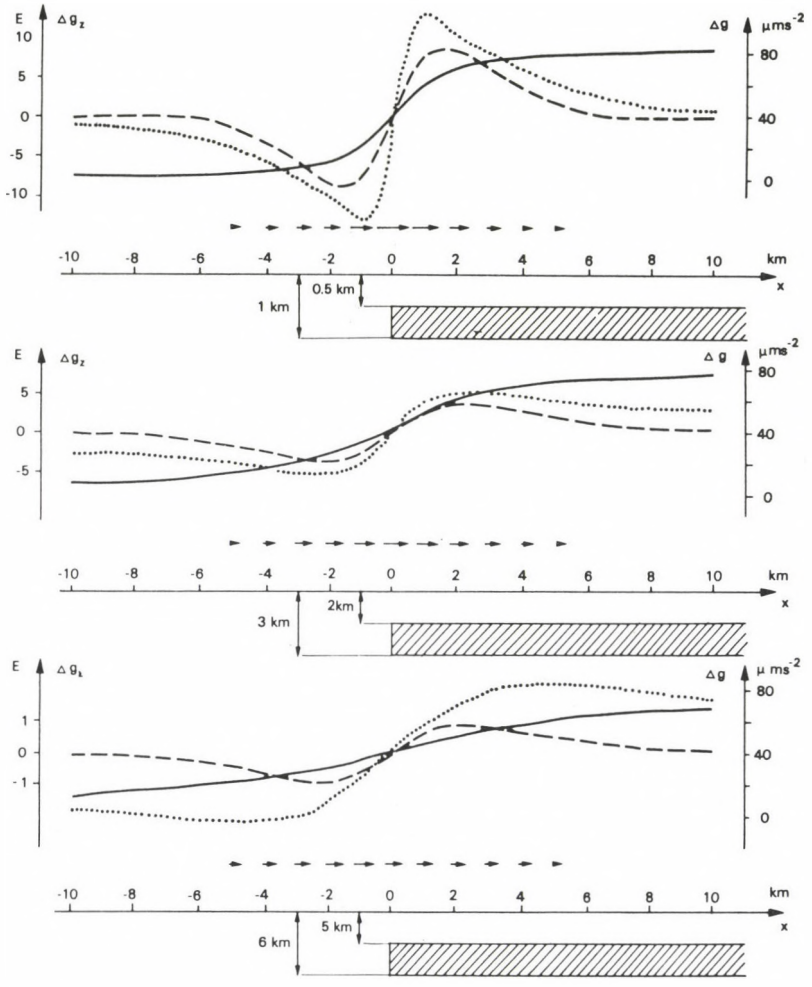

Fig. 1. The gravity effect (solid line, scale to the right), the truncated vertical gradient (dashed line, scale to the left), the analytical vertical gradient (dotted line, scale to the left), relative horizontal gradients (depicted by arrow) of the vertical escarpment placed in different depths

where μ_0 is the permeability of vacuum; J is the induced magnetization; d_1 and d_2 are the upper and lower depths of the magnetized step; I is the inclination of the earth's field and $\Theta = I-90^{\circ}$.

The model dimensions are: $J = 1\ Am^{-1}$, $I = 60^{o}$, $d_1 = 500$ m, 2000 m, 5000 m and $d_2 = 1500$ m, 3000 m, 6000 m respectively. Figure 2 shows the vertical magnetic effect of the step, the vertical gradient obtained analytically, the truncated vertical gradient calculated by this procedure and the relative horizontal gradients. In all of the three model examples, the relative horizontal gradients were divided by the same maximum value. Thus their magnitude expresses the effect of depth.

NOVA PROSPECTING AREA

Nova prospecting area is located in the southwest part of Hungary (Fig. 3).

The Bouguer anomalies of Nova (Fig. 4) were recorded by MÁELGI (Eötvös Loránd Geophysical Institute of Hungary). The gravity stations were distributed randomly, with the average sampling distance being 500 m. The surface density of the stations was approximately 1 station/km^2. The accuracy of the digitized data in a square grid of 1000 m sampling distance, was $\pm 1.0\ \mu ms^{-2}$. The range of Bouguer anomalies exceeds the noise level. The form of Bouguer anomalies expresses the effect of the geological structure unambiguously.

The vertical magnetic anomalies of Nova (Fig. 5) were also recorded by MÁELGI. The magnetic stations were distributed randomly with the average sampling distance being 1000-1500 m. The surface density of the stations was approximately 0.5/km^2. The accuracy of the digitized data, in a square grid of 1000 m sampling distance, was ± 10 nT. Two maxima separated by a narrow minimum zone can be seen in the anomaly map.

The following observations can be made on the subsurface structure of Nova (Figs 4 and 5). The observations are based on the investigations of the exploration wells and detailed seismic surveys (GKV 1972, GKV 1982). The Pre-Neogene basement consists of two main structural units: the Balaton crystalline swell and the central mountain facies belt.

The elements of the Balaton crystalline swell are detected in the southern part of Nova. Mica-schist, granite,

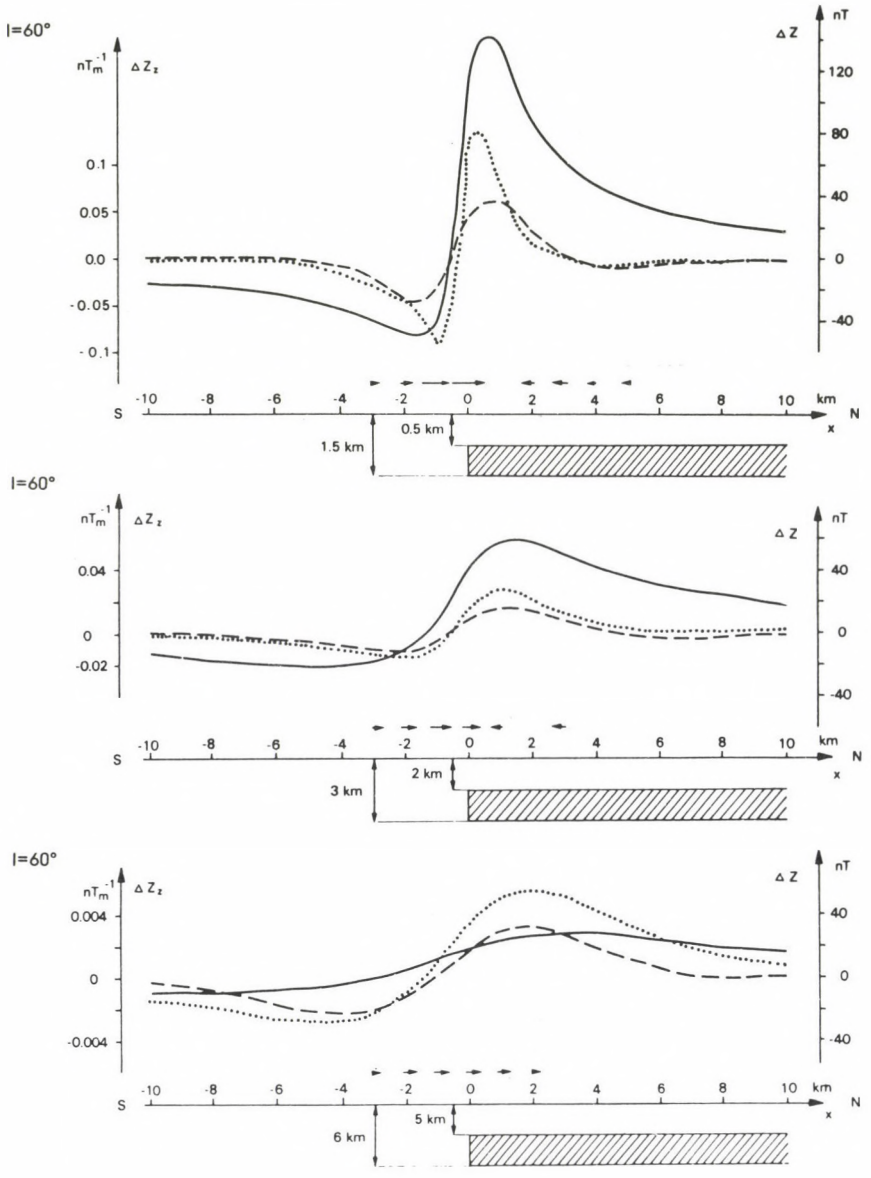

Fig. 2. Vertical magnetic field (solid line, scale to the right), the truncated vertical gradient (dashed line, scale to the left), the analytical vertical gradient (dotted line, scale to the left), relative horizontal gradients (depicted by arrow) of the magnetized vertical step placed in different depths

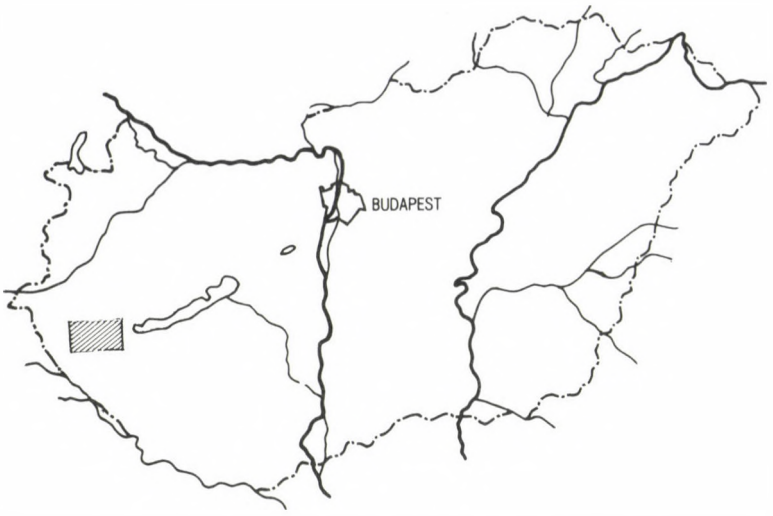

Fig. 3. Location of the Nova prospecting area

granodiorite, quartz-porphyrite were cored by exploration wells. The age of these rocks may be Precambrian, but the main mass is Paleozoic: Ordovician-Silurian metamorphic rocks, Carboniferous granite, Permian quartz-porphyrite. These rocks are located in an east-west emergent ridge in the Ortaháza-Pusztaederics-Hahót-Kilimán line. They subsided to greater depths along a structure to the north and south, as well as to the west from Ortaháza.

The rocks of the central mountain facies belt can be found north of the crystalline swell. Large amounts of sediments were deposited in the late Paleozoic-Mesozoic cycle. The products of exploration wells indicate that Permian rocks are probable located south of Dióskál. Triassic Dachstein limestone and dolomite formation is detected in the entire area. Jurassic detritus is found in a northeast-southwest direction in the vicinity of Bárszentmihályfa and Kehida. The position of the Liassic-Dogger rocks proves the presence of reverse fault zones. The limestone formation of Ugod and marl formation of Polány are the products of Upper-Cretaceous sedimentation.

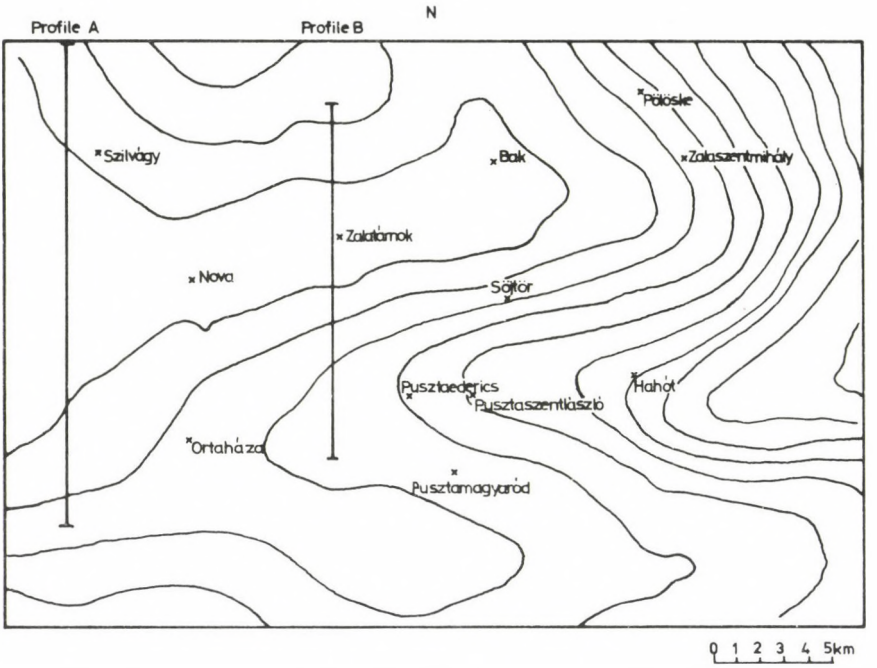
N
Profile A
Profile B
Pölöske
Szilvágy
Bak
Zalaszentmihály
Zalatárnok
Nova
Sójtór
Pusztaederics
Pusztaszentlászló
Hahót
Ortaháza
Pusztamagyaród
0 1 2 3 4 5km

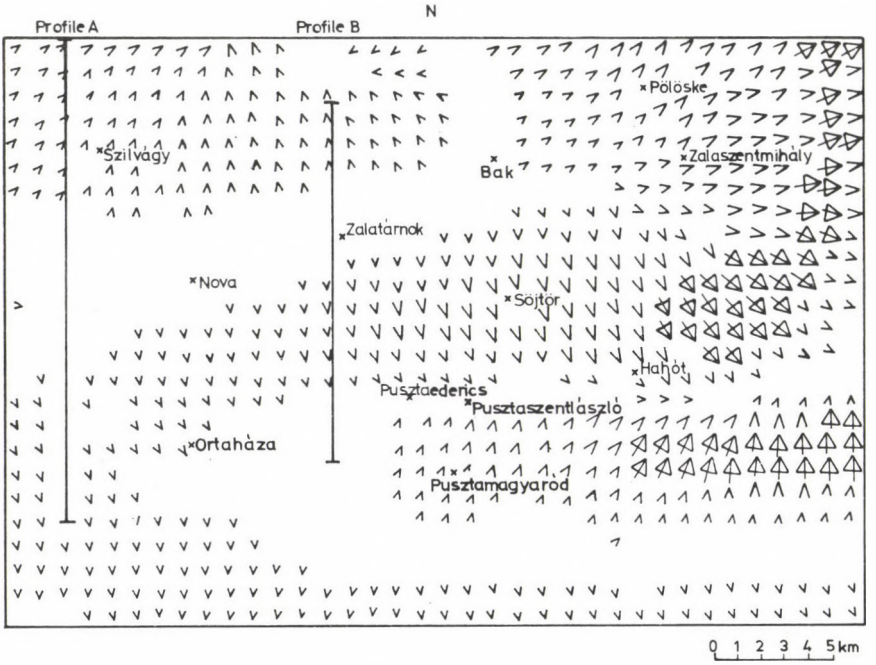
N
Profile A
Profile B
Pölöske
Szilvágy
Bak
Zalaszentmihály
Zalatárnok
Nova
Sójtór
Hahót
Pusztaederics
Pusztaszentlászló
Ortaháza
Pusztamagyaród
0 1 2 3 4 5km

Fig. 4.

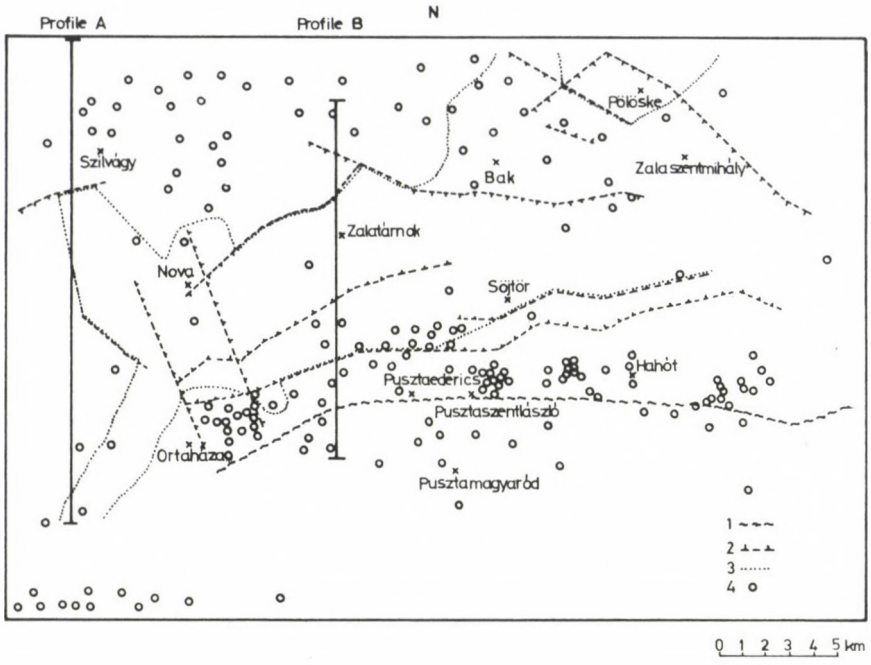

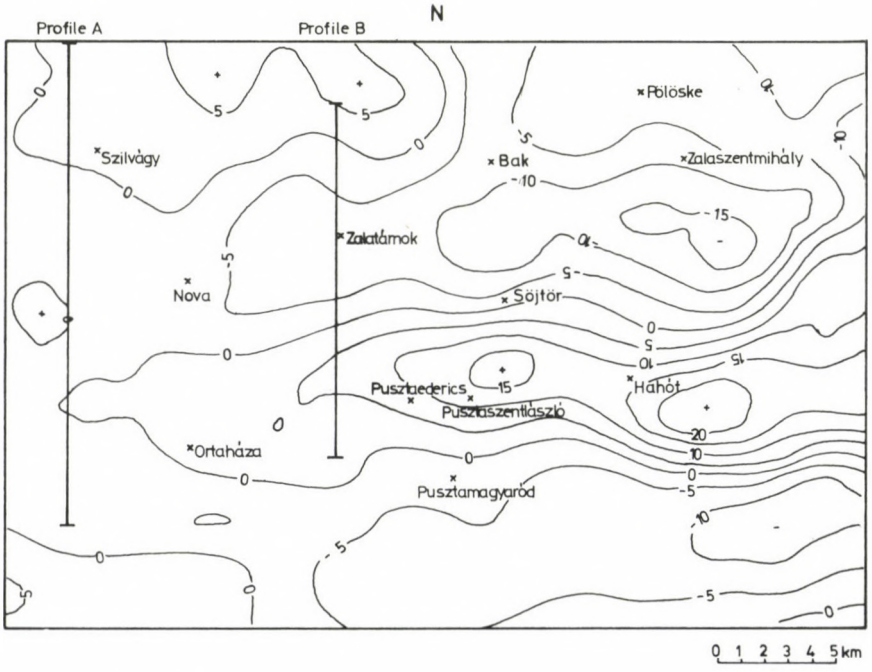

(Caption see p. 322)

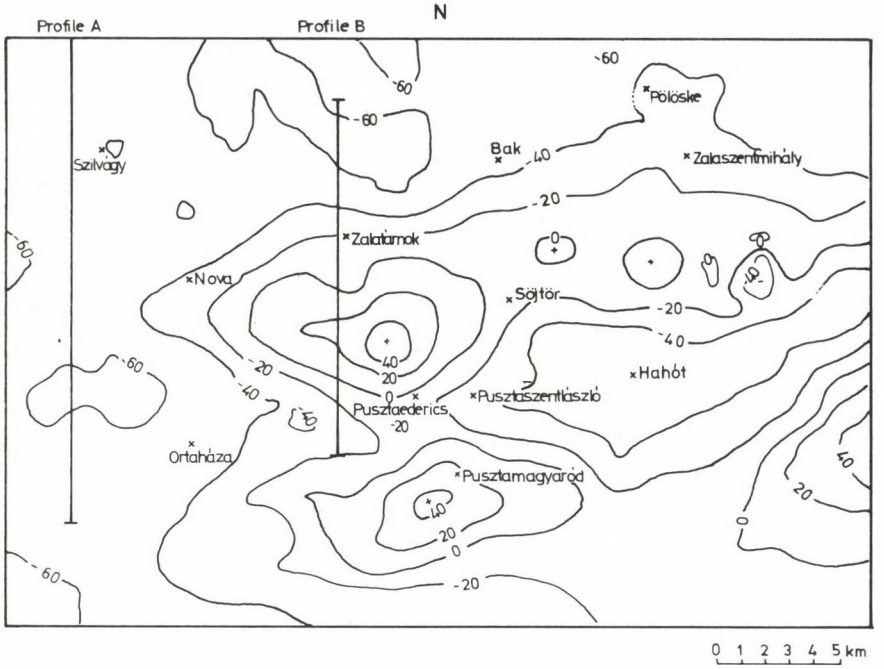
N
Profile A
Profile B
Szilvágy
Bak
Pölöske
Zalaszentmihály
Zalatárnok
Nova
Söjtör
Hahót
Pusztaederics
Pusztaszentlászló
Ortaháza
Pusztamagyaród
-60
-40
-20
0
20
40
0 1 2 3 4 5 km

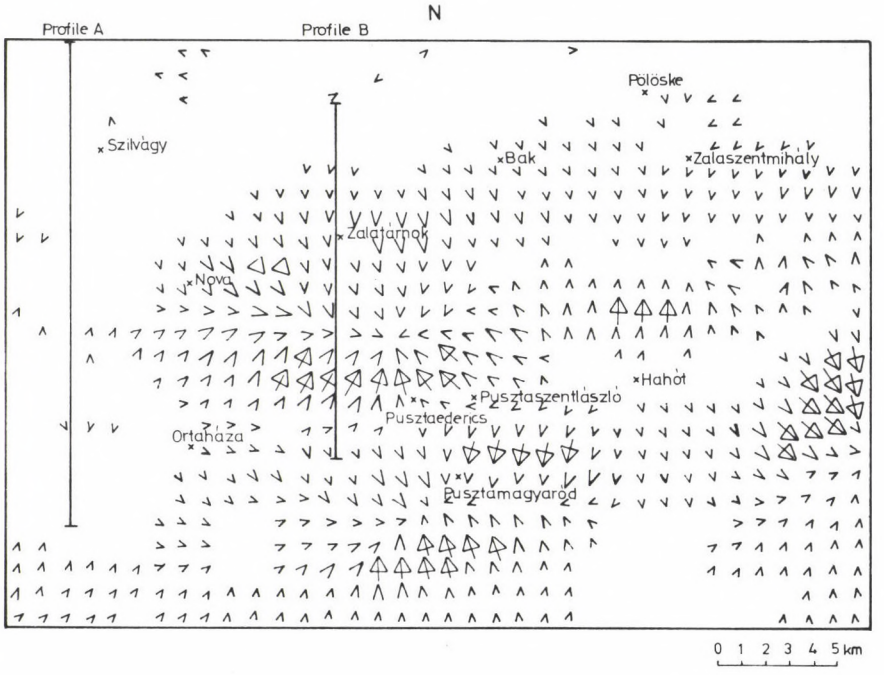
N
Profile A
Profile B
Szilvágy
Bak
Pölöske
Zalaszentmihály
Zalatárnok
Nova
Hahót
Pusztaszentlászló
Pusztaederics
Ortaháza
Pusztamagyaród
0 1 2 3 4 5 km

Fig. 5.

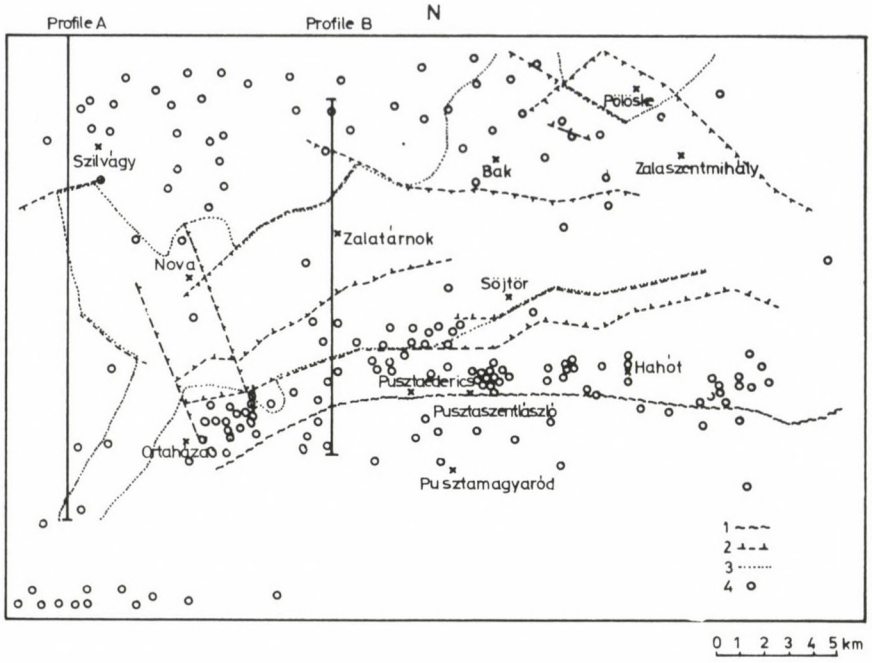

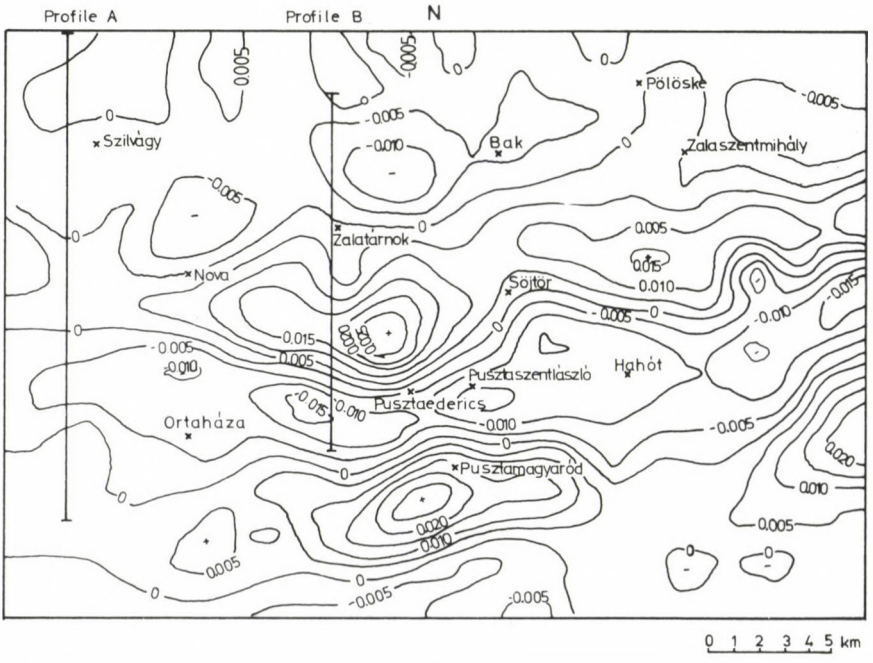

Caption see p. 322)

Fig. 4. Bouguer anomaly field over the Nova prospection area anomalies are contoured at 10 μms^{-2} (upper left). Pre-Miocene tectonic lines over Nova, symbols: 1. boundary of the Balaton crystalline swell and the central mountain facies belt, 2. tectonic lines, 3. boundary of the Eocene sediments, 4. exploration wells (top right). Relative horizontal gradients derived from the Bouguer anomalies (bottom left). Truncated vertical gradients derived from the Bouguer anomalies contoured in Eötvös units (bottom right). These figures show the position of profiles A and B, respectively

Fig. 5. Vertical magnetic anomaly field over the Nova prospection area anomalies contoured at nT (top left). Pre-Miocene tectonic lines over Nova, symbols: 1. boundary of the Balaton crystalline swell and the central mountain facies belt, 2. tectonic lines, 3. boundary of the Eocene sediments, 4. exploration wells (top right). Relative horizontal gradients derived from the vertical magnetic anomalies (bottom left). Truncated vertical gradients derived from the vertical magnetic anomalies contoured at nTm^{-1} (bottom right). These figures show the position of profile A and B, respectively

Eocene series are superimposed on the eroded surface of Mesozoic rocks with angular unconformity. Middle and Upper Eocene sediments were deposited simultaneously with subsidence of the basin. The deepest part of the basin is in the central zone of the area. This east-west trench of Zalatárnok contains more than 1000 m of the sedimentary complex.

An erosion period was dominant from Eocene to Miocene. Sedimentation started probably in Badenian, and it continued, with short hiatuses in Sarmatian as well as in Pannonian. The higher parts of the uplifted basin (mainly the Balaton crystalline swell) were covered by water in Late Miocene (Lower Pannonian). The Badenian-Sarmatian transgression period turned into a regressional filling cycle (Lower Pannonian) and terrestrial sediments were deposited as the last stage of the basin evolution.

GRADIENTS OF NOVA AND THEIR INTERPRETATION

The Bouguer anomalies and the vertical magnetic anomalies were sampled in a square grid with the sampling unit being 1 km. In the computations, we chose m = 9 for the parameter of the Gaussian truncation function (Eq. 10). The cut-off spatial

frequency was defined by the -3 dB point, and it gave a 0.15 km^{-1} cut-off spatial frequency.

Relative horizontal gradients of the gravity were computed from Bouguer and of the magnetics from vertical magnetic anomalies, respectively. The relative horizontal gradients were indicated by arrows if their magnitude was greater than 20 percent of the maximum value.

For the latitude, $\varphi = 47^{o}$, of Nova prospecting area, the normal value of the gravity gradient g_x is approximately 8.1 E from Eq. (1). The values of the truncated gradient g_x are 24.1 E maximum, and -21.2 E minimum. The computed gradient is three times the normal value. The numerical value of the truncated vertical gradient g_z has a maximum = 24.9 E, and a minimum = = -17.4 E which are a few thousandths of the normal value given by Eq. (3). The maximum of the truncated relative horizontal gradients is 25.9 E.

For the colatitude of $\Theta = 130^{o}$ for the Nova prospecting area, the normal value of the gradient Z_x of the vertical magnetic field is 0.0074 nTm^{-1} given by Eq. (4). The truncated maximum Z_x is 0.020 nTm^{-1} and the minimum is -0.021 nTm^{-1}. The absolute extremum of the computed gradient is three times greater than the normal value. The maximum of 0.029 nTm^{-1} and the minimum of -0.018 nTm^{-1} of the truncated vertical gradient are approximately the same as the absolute magnitude of the normal vertical gradient of -0.0185 nTm^{-1} from Eq. (6). The maximum of the truncated relative horizontal gradients is 0.023 nTm^{-1}.

Relative horizontal gradients obtained from the Bouguer anomalies can be seen in Fig. 4. The relative horizontal gradients show the typical features along an east-west line (Orta-háza-Pusztaederics-Pusztaszentlászló-Hahót line). To the north and to the south of this zone the gradients are less. The arrows point to the south and to the north direction respectively. This type of variation of the arrows is characteristic of an uplifted ridge. In the northern part of the horizontal gradient map, a deeper zone can be indicated by smaller gradients along the Nova-Zalatárnok-Bak line. The boundary of this deeper

zone is indicated by gradients pointing outwards.

The uplifted ridge is a positive anomaly on the truncated vertical gradient map obtained from the Bouguer anomalies while the deeper zones show negative anomalies in the northern and southern part of the prospecting area.

Relative horizontal gradients obtained from the vertical magnetic anomalies can be seen on Fig. 5. The uplifted ridge in the middle part of the area shows smaller gradients. As compared to the gradients obtained from the Bouguer anomalies, its boundary is characterized by gradients pointing outwards. The relative horizontal gradients pointing concentrically inwards indicate a local maximum of the vertical magnetic anomalies in a direction south-east from Nova. The deeper zones are not characterized by outward pointing gradients.

The truncated vertical gradient anomalies obtained from the vertical magnetic anomalies can be also seen on Fig. 5. The uplifted ridge is indicated by negative vertical gradient anomalies. The deeper zones to the north and south are characterized by positive vertical gradients.

Detailed results from this method can be seen on Figs 6 and 7. Profiles A and B show the Bouguer profile, vertical magnetic profile, the truncated vertical gradients and the relative horizontal gradients in north-south plane. The geological section and the position of some exploration wells are shown on these figures.

The different zones appearing on the gradient maps are separated by tectonic lines. There are three different characteristic directions in the prospecting area: approximately east-west, northeast-southwest, and northwest-southeast. The directions are the results of different tectonic cycles, their age cannot be determined by this procedure. The northeast--southwest and the northwest-southeast directions are related to the Alpian tectonic cycle. It appears partially in the form of normal and partly of reverse faults. The reverse faults can be explained indirectly.

The discontinuity of the directions can be regarded as the result of a horizontal displacement. The results appear where

the main tectonic units, the Balaton crystalline swell and the central mountain facies belt, are in contact.

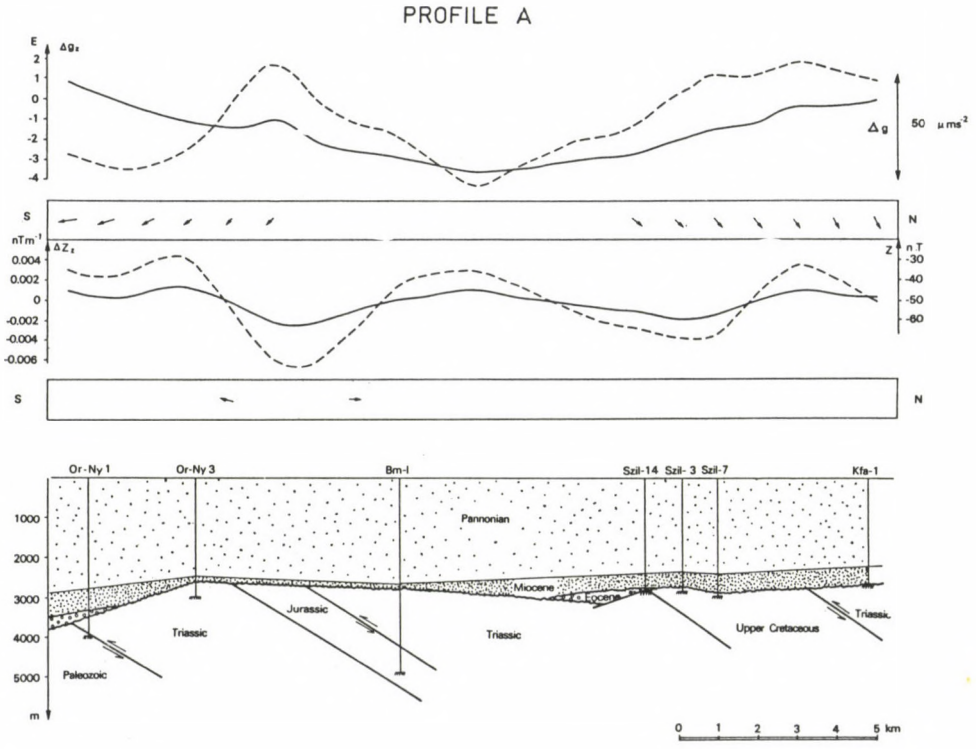

Fig. 6. The gravity profile A (solid line, scale to the right) its truncated vertical gradients profile (dashed line, scale to the left) its relative horizontal gradients (in a horizontal south-north plane). The vertical magnetic profile A (solid line scale to the right), its truncated vertical gradient profile (dashed line, scale to the left), its relative horizontal gradients (in a horizontal south--north plane). Geological profile A and the exploration wells along the profile A

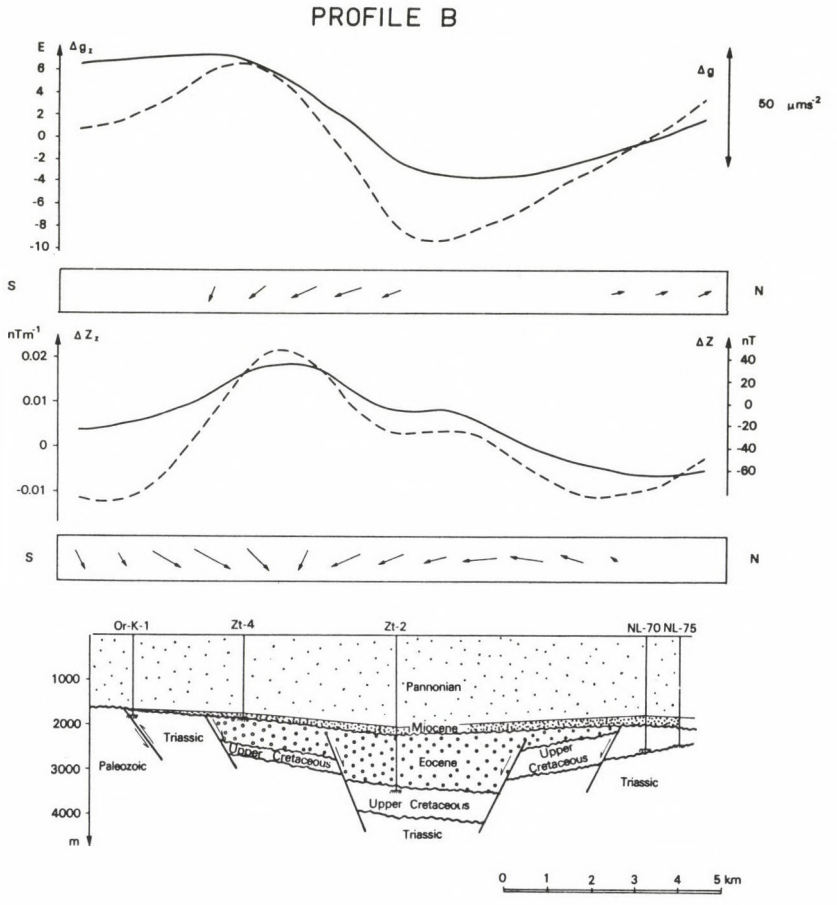

Fig. 7. The gravity profile B (solid line, scale to the right), its truncated vertical gradient profile (dashed line, scale to the left) its relative horizontal gradients (in a horizontal south-north plane). The vertical magnetic profile B (solid line, scale to the right), its truncated vertical gradient profile (dashed line, scale to the left), its relative horizontal gradients (in a horizontal south-north plane). Geological profile B and the exploration wells along the profile B

ACKNOWLEDGEMENTS

The authors thank Dr W B Agocs for critically reviewing the manuscript and Dr L Cserepes for the permission to use his

subroutine LEVEL. The computations were done by the computer CDC-3300, the maps were drawn by the plotter CALCOMP-936 of the Research Institute for Computing Methods and Automatization of the Hungarian Academy of Sciences. The permission for using the computing facilities is being highly acknowledged.

REFERENCES

Anger C A, Liard J O 1982: Geophysics, 47, 919-925.

Barongo J O 1985: Geophysics, 50, 963-968.

Eggers D E, Thompson D T 1984: Geophysics, 49, 771-779.

Fajklewicz Z J 1976: Geophysics, 41, 1016-1030.

GKV Report on the seismic survey of Bak-Szilvágy prospection territory. No. 105, 1972 (in Hungarian), GKV (Geophysical Exploration Company) Database

GKV Report on the seismic survey of Zalatárnok prospection territory. No. 181, 1982 (in Hungarian), GKV (Geophysical Exploration Company) Database

Hammer S 1970: Geophysics, 35, 153-157.

Hammer S 1979: Geophysics, 44, 99-101.

Hammer S, Anzoleaga R 1975: Geophysics, 40, 256-268.

Heiland C A 1940: Geophysical Exploration. New York, Prentice Hall

Hood P 1965: Geophysics, 30, 891-902.

Hood P, McClure D J 1965: Geophysics, 30, 403-410.

Jakosky J J 1950: Exploration Geophysics. Trija Publishing Company, Los Angeles

Kanasewich E R,Agarwal R G 1970: Journal of Geophysical Res., 75, 5702-5712.

Kis K 1983: Acta Geod. Geoph. Mont. Hung., 18, 501-511.

Meskó A 1984: Digital Filtering: Application Geophysical Exploration for Oil. Akadémiai Kiadó, Budapest, Pitman Publishing Ltd., London, Halsted Press, New York

Nabighian M N 1972: Geophysics, 37, 507-517.

Sazhina N, Grushinsky N 1971: Gravity Prospecting. Mir Publishers, Moscow

Stanley J M, Green R 1976: Geophysics, 41, 1370-1376.

Thyssen-Bornemisza S, Stackler W F 1956: Geophysics, 21, 771-779.

Acta Geod. Geoph. Mont. Hung., Vol. 24 (3-4), pp. 329-341 (1989)

REDUCTION TO THE MAGNETIC POLE OF TOTAL FIELD MAGNETIC ANOMALIES AND DETERMINATION OF ITS PARAMETERS BASED ON POISSON'S RELATION

K Kis[1], K Kloska[4], F Kovács[2], S Tóth[3]

[1]Geophysical Research Group of the Hung. Acad. Sci. L. Eötvös University, H-1083 Budapest, Kun Béla tér 2, Hungary

[2]Department of Gravity and Magnetics, Geophysical Exploration Company, H-1068 Budapest, Gorkij fasor 42, Hungary

[3]Hungarian Hydrocarbon Institute, H-2443 Százhalombatta, POB 32, Hungary

[Manuscript received January 20, 1988]

Reduction to the magnetic pole of the total magnetic anomalies requires the determination of the direction of the magnetization. This determination is based on the minimization of a linearized objective function obtained from Poisson's relation. The suggested procedure was applied to the reduction to the magnetic pole of the total magnetic anomalies of the Tóalmás area of Hungary. The position of the calculated anomalies are in agreement with the geological structure of the area.

Keywords: magnetic anomaly; magnetization; Poisson's relation; Tóalmás anomaly

INTRODUCTION

The reduction of the total field magnetic anomalies to the magnetic pole improves the interpretation through universalizing the magnetic anomalies. The efficiency of this transformation has been discussed by Baranov (1957), Baranov and Naudy (1964), Bhattacharyaa (1965), Kanasewich and Agarval (1970), Cordell and Taylor (1971). The analysis summarized in this paper are continuations of previous results (Kis 1983, 1984). In the present paper, only the final results of the earlier investigations are presented. The interpretation of anomalies needs the aid of specialists in the field.

If the homogeneous magnetization of the source is accepted, the transfer function of reduction to the pole is as follows:

$$S_T(f_x,f_y) = \frac{f_x^2+f_y^2}{\left(N(f_x^2+f_y^2)^{1/2} + j(Lf_x+Mf_y)\right)\left(n\,f_x^2+f_y^2)^{1/2} + j(lf_x+mf_y)\right)} \qquad (1)$$

where f_x and f_y are the spatial frequencies measured along the x and y axes, respectively. L, M, N and l, m, n are the directional cosines of the magnetization, and of the Earth's magnetic field, respectively. The directional cosines can be expressed by the inclination α and declination β of the magnetization, and by the inclination I and declination D of the Earth's magnetic field:

$$\begin{aligned} L &= \cos\alpha\cos\beta & l &= \cos I \cos D \\ M &= \cos\alpha\sin\beta & m &= \cos I \sin D \\ N &= \sin\alpha & n &= \sin I \ . \end{aligned} \qquad (2)$$

The equations are valid in a Cartesian coordinate system in which the x,y,z axes point to North, East and downward, respectively.

The transfer function $S_T(f_x,f_y)$ has a finite discontinuity at $f_x=f_y=0$. This discontinuity can be eliminated if Eq. (1) is multiplied by the Gaussian band-pass window:

$$S_{BP}(f_x,f_y) = C(\exp(-(36\ f_r/m_1)^2)-\exp(-(36\ f_r/m_2)^2)) \ . \qquad (3)$$

The normalization factor C in the above can be expressed in the form

$$C = \frac{1}{\exp(-(36\ f_{r\ max}/m_1)^2)-\exp(-(36\ f_{r\ max}/m_2)^2)} \qquad (4)$$

where

$$f_{r\ max} = \frac{m_1 m_2}{36}\left(\frac{2}{m_1^2-m_2^2}\log\frac{m_1}{m_2}\right)^{1/2}$$

$$f_r^2 = f_x^2 + f_y^2 \ .$$

This band-pass window was suggested by Meskó (1984). The

parameters m_1 and m_2 of the band-pass window control the band which is passed. If the lower and upper cut-off frequencies f_L^c and f_U^c are defined by the -3 dB amplification then

$$f_L^c = \frac{0.01633\ m_2}{\xi} \quad \text{and} \quad f_U^c = \frac{0.01633\ m_1}{\xi} \tag{5}$$

where ξ is the sampling unit.

The output of the reduction is band-pass filtered because of the applied band-pass window.

DETERMINATION OF PARAMETERS OF REDUCTION

The transfer function of Eq. (1) shows that the reduction to the north magnetic pole requires the value of the direction of magnetization. Only the homogeneous magnetization was assumed when the transfer function of Eq. (1) was derived. The direction of the magnetization can be determined by the use of Poisson's relation

$$Z = \frac{\mu_0 J}{4\pi G \varrho} \frac{\partial}{\partial s} g_z \ . \tag{6}$$

In Eq. (6) Z is the vertical component of the magnetic field; μ_0 the permeability of vacuum; J the magnetization; G the universal gravitational constant; ϱ the specific density; $\underline{s}$ the unit vector pointing in the direction of magnetization; and g_z the vertical component of gravity. Poisson's relation implies the following assumptions:

1. the gravity and the corresponding magnetic anomalies are produced by same geological sources; and

2. the specific density and the magnetization are homogeneous.

If the directional derivative in Eq. (6) is expressed by the directional cosines, Poisson's relation can be written in a form given by Lundbak (1956):

$$Z = \frac{\mu_0}{4\pi G} p_1 \left(\cos p_2 \cos p_3 \frac{\partial}{\partial x} g_z + \cos p_2 \sin p_3 \frac{\partial}{\partial y} g_z + \sin p_2 \frac{\partial}{\partial z} g_z \right) \tag{7}$$

where

$$p_1 = \frac{J}{\varrho} \qquad p_2 = \alpha \qquad p_3 = \beta \ .$$

The application of Poisson's relation requires the derivatives of vertical gravity with respect to the variables x,y and z, and the transformation of the total magnetic field into the vertical magnetic field. The transfer function of the latter transformation is as follows

$$S_Z(f_x,f_y) = \frac{-(f_x^2+f_y^2)^{1/2}}{n(f_x^2+f_y^2)^{1/2} + j(lf_x+mf_y)} \ . \tag{8}$$

Calculation of the derivatives of the vertical gravity with respect to the variables x,y and z was carried out by the method proposed by Kis (1984). The theoretical transfer functions of the derivatives with respect to the variables x,y and z are as follow

$$\begin{aligned} S_{dx}(f_x,f_y) &= j\ 2\pi f_x \\ S_{dy}(f_x,f_y) &= j\ 2\pi f_y \\ S_{dz}(f_x,f_y) &= 2\pi(f_x^2+f_y^2)^{1/2} \ . \end{aligned} \tag{9}$$

The deviations have an undesirable amplification in the high frequency range. In order to remove this undesirable property of the theoretical transfer functions each of them is multiplied with the band-pass window given by Eq. (3). It has to be emphasized the same band-pass shown in Eq. (3) is used in the above four transformations.

The parameters were determined by the minimization of the objective function

$$\varphi(p) = \sum_i \Big(Z_i - \frac{\mu_0}{4\pi G} p_1(\cos p_2 \cos p_3 \frac{\partial}{\partial x} g_{zi} + \cos p_2 \sin p_3 \frac{\partial}{\partial y} g_{zi} + \sin p_3 \frac{\partial}{\partial z} g_{zi})\Big)^2 = \min \ . \tag{10}$$

The minimum is obtained by iteration after the linearization of the objective function.

TÓALMÁS PROSPECTION AREA

The Tóalmás area is located in the northern part of the Hungarian Plain (Fig. 1). Gravity and magnetic measurements were made by the Geophysical Exploration Company. The measurements were obtained on a square grid of 500 m spacing. The area extends 21 kms N-S and 14.5 kms E-W.

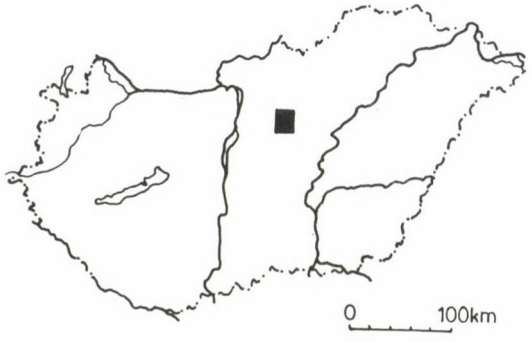

Fig. 1. Location of the Tóalmás prospection area

The Bouguer anomalies of the prospection area are shown in Fig. 2. The accuracy of the gravity measurements is $\pm 0.5\ \mu ms^{-2}$. A maximum zone striking SW-NE can be seen not only on the Bouguer anomaly map, but also on its band-pass windowed, and its vertical gradient (windowed by the same band-pass) maps. The maximum zone differs from its surrounding with its greater horizontal gradients. Minor anomalies can be seen north and south of the maximum zone.

The total magnetic anomalies, with an accuracy ± 2 nT, were obtained at the same stations. The total magnetic anomalies are presented in Figs 3 and 5. The maximum of the magnetic anomalies is located south of the gravity maximum. At other parts of the surveyed area minor anomalies are located.

Relatively few exploration wells were drilled in the

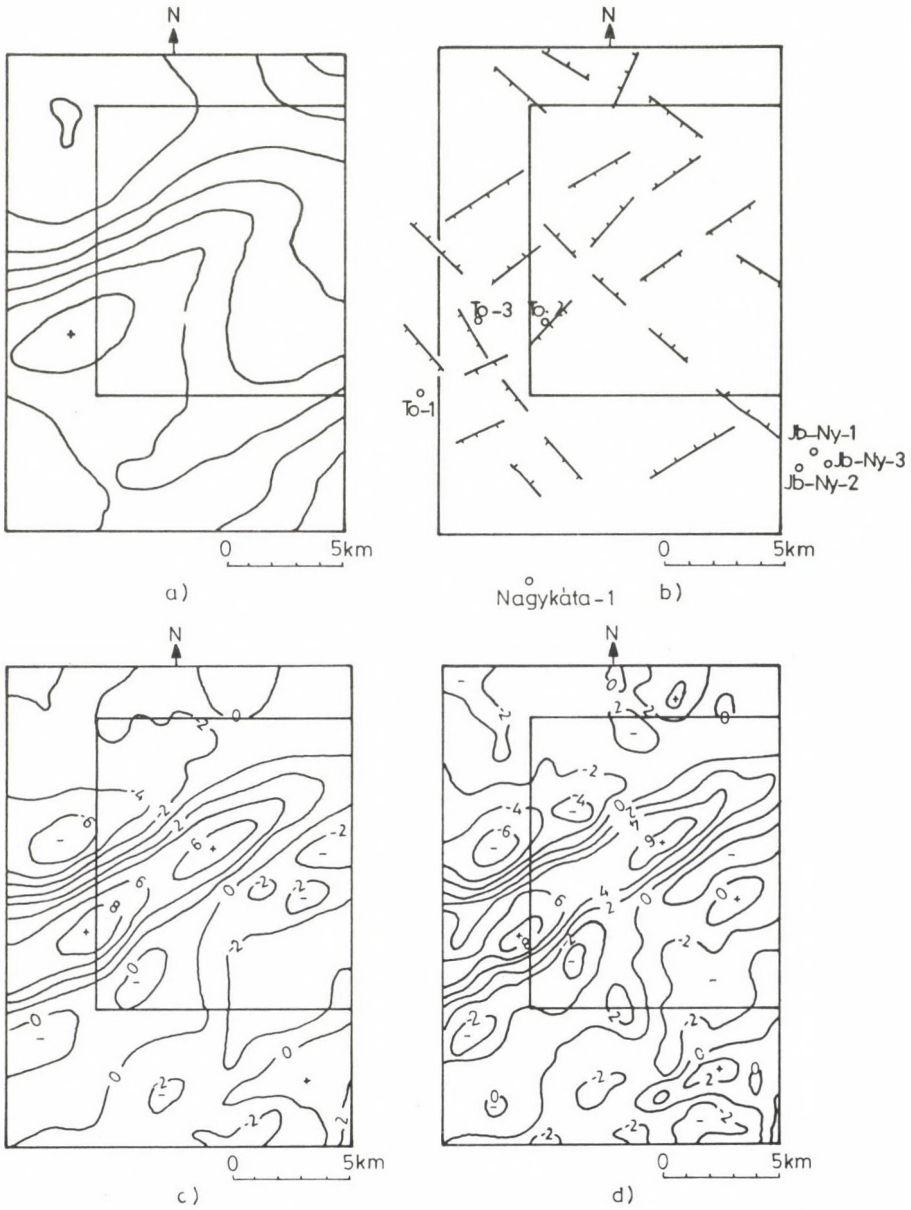

Fig. 2. (a) Bouguer anomaly field over the Tóalmás prospection area; anomalies are contoured at 10 μms^{-2}; (b) tectonic lines and well locations; (c) band-pass windowed Bouguer anomalies contoured in μms^{-2} units; (d) truncated vertical gradients derived from the Bouguer anomalies contoured in Eötvös units ($1E = 10^{-9}\ s^{-2}$). The inner frame indicates the two-dimensional box-car function

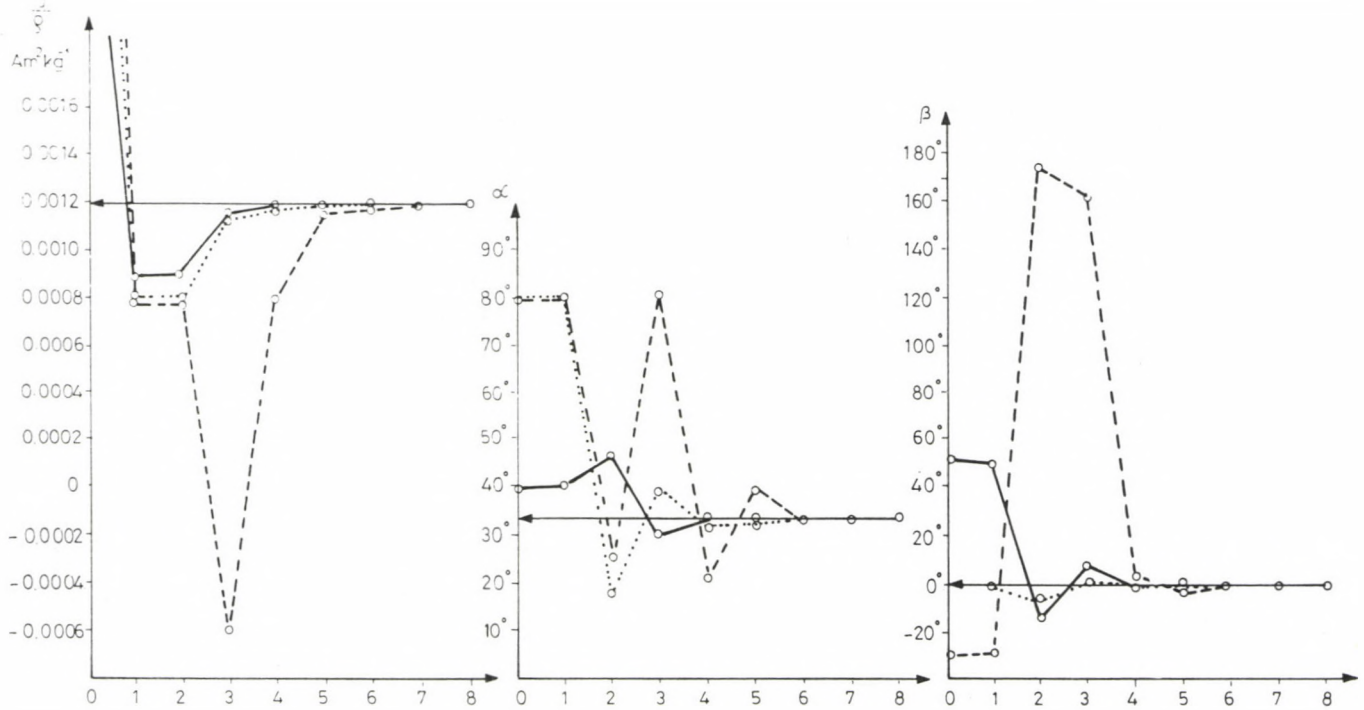

Fig. 4. The estimated values of the ratio J/ϱ and of the angles α and β as a function of the steps of iteration started (0th step) from three different values

(Fig. 3 see on next page.)

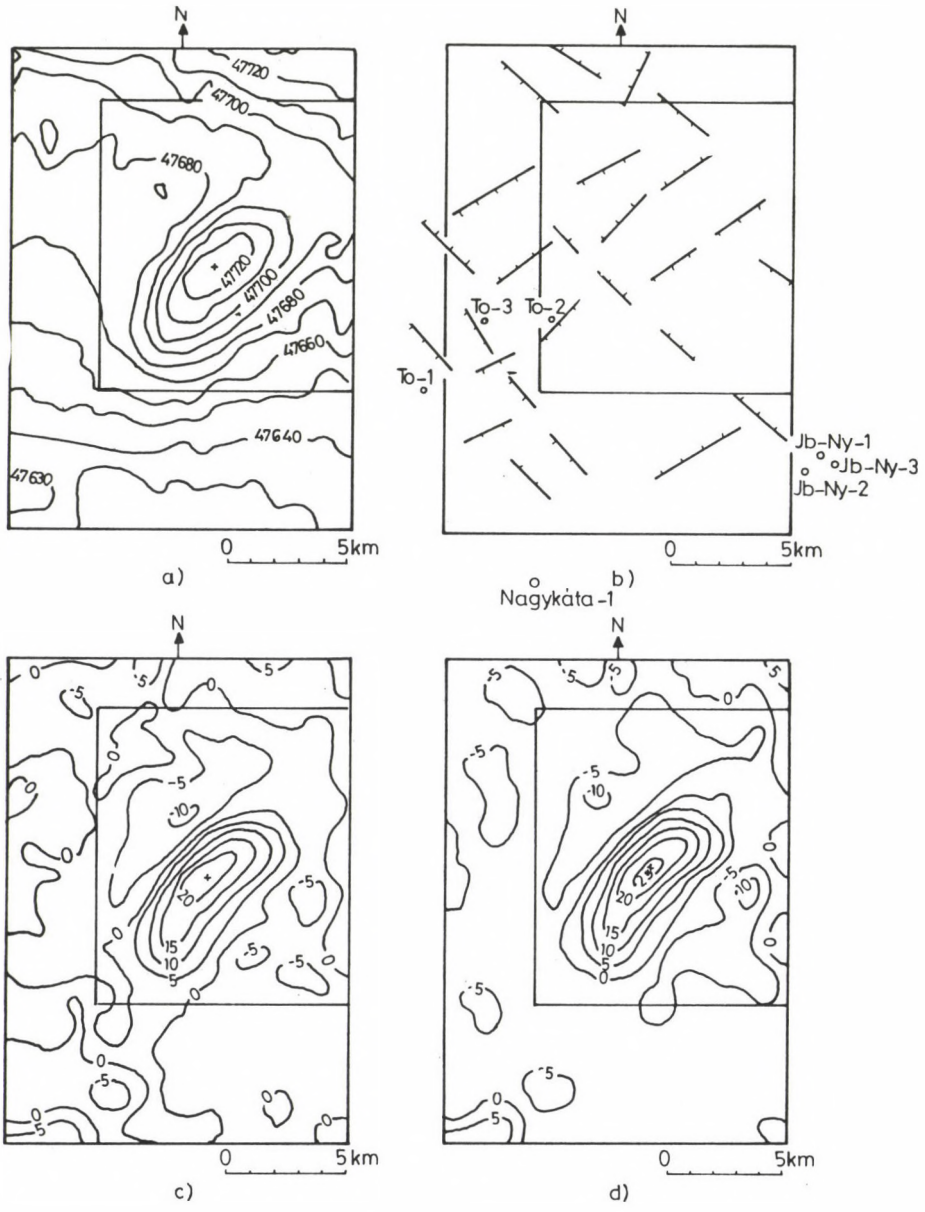

Fig. 3. (a) Total magnetic anomaly field over the Tóalmás prospection area; anomalies are contoured in nT units; (b) tectonic lines and wells; (c) band-pass windowed total magnetic anomalies contoured in nT units; (d) total magnetic anomalies transformed into band-pass windowed vertical magnetic anomalies contoured in nT units. The inner frame indicates the two-dimensional box-car function

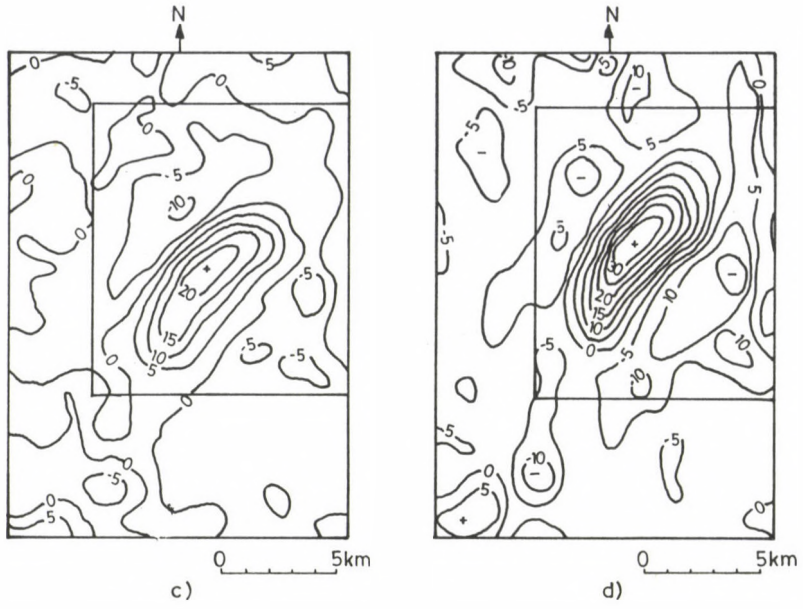

Fig. 5. Total magnetic anomalies of the Tóalmás area (see Fig.3) reduced to the north magnetic pole contoured in nT units. The inner frame indicates the two-dimensional box-car function (a and b see Fig. 3)

survey area (Figs 2, 3, 5). The geological structure of the area can be outlined by the results from the exploration wells. Refer to Fig. 2b for the well locations discussed below.

Three wells To-1, To-2, To-3 are in the western part of the area. The oldest rocks located at To-3 are probably Mesozoic diabase and shale. Eocene sediments, banded by volcanic tuff, followed the sequence in the well of To-1 and To-3. There are several short hiatuses in the Oligocene sedimentation. These layers were deposited in the off-shore (sublitoral) zone. Some slips can also be detected. All the three wells penetrated Middle and Upper Miocene rocks which consist of grey rhiolitic tuff (Galgavölgyi Rhyolitic Tuff Formation). The thickness of the Pannonian and younger sediments deposited on the Miocene layers varies between 1000-1500 m.

Well Nagykáta-1 (located in the southern part of the area) locates Triassic rocks in the basement. The upper Triassic limestone (2690-2820 m) is deposited on Triassic dolomite

(2820-3202 m). An Eocene conglomerate-sandstone-marl series are probably above the Triassic layers. Dominantly, schliren marl facies represents the Oligocene sediments. The Miocene consists of Badenian and Sarmatian sediments and Badenian andesite tuffs (1675-1888 m) which is the Mátra Volcanic Formation. The thickness of the Pannonian and younger sediments is approximately 1500 m.

The wells Jb-Ny-1, Jb-Ny-2, Jb-Ny-3 located in the South--East part of the area reached Upper Eocene rocks. Some Kupelian sediments represent the Oligocene. The characteristic section of the wells containes Miocene rhyolitic tuffs. Resedimented Badenian tuff (31 m in thickness) Sarmatian (or possibly Badenian) rhyolitic tuffs and rhyolitic agglomerate (211 m in thickness) were discovered by well Jb-Ny-1. An approximately 300 m thick rhyo-dacite-tuff series was recorded by well Jb-Ny-2 while the 180 m thick rhyolitic tuffs were penetrated by the well Jb-Ny-3. The thickness of the Pannonian and younger sediments is approximately 1600 m.

DISCUSSION

In the computations, the band-pass window Eq. (3) was used as a truncation function, and, its parameters were taken at $m_1 = 9$, $m_2 = 3$. The cut-off frequency as defined by the -3 dB point, the parameters m_1 and m_2, gave a lower $f_L = 0.0979$ km^{-1} and an upper $f_U = 0.2939$ km^{-1} cut-off spatial frequency. The band-pass window was applied both for gravity and magnetic anomalies (Figs 2, 3, 5).

The inputs of the determination are the derivatives of the Bouguer anomalies with respect to the variables x,y,z, and the total magnetic anomaly transformed into the vertical magnetic anomalies.

The derivatives were obtained by Kis' method (1984). The equations for these derivatives are given in Eq. (9). The truncation function was the band-pass window Eq. (3). The application of the band-pass window eliminates the undesirable enhancement of the derivatives. In Fig. 2, the band-pass

windowed derivative with respect to the variable z of the Bouguer anomalies is shown.

The input of the estimation based on Poisson's relation requires the transformation of the total magnetic anomaly into a vertical anomaly. The transfer function of this transformation is given by Eq. (8). The transfer function was windowed by the band-pass filter Eq. (3). The parameters in Eq. (8) were $I = 60^{o}$, $D = 0^{o}$. These are the average values of the magnetic inclination and declination in the survey area.

The optimum problem Eq. (10) was linearized by expansion into a first order Taylor series as developed by Al-Chalabi (1970) and Höpcke (1980). The linearized optimum problem was solved by iteration. The details of this calculation were presented by Kis (1984). The parameters are calculated by the iteration with the quotient J/ϱ and the direction of magnetization fixed by α and β. These three parameters can be determined unambiguously in point of potential theory, as shown by Skeels and Watson (1949).

The input data for the determination were windowed using a two-dimensional box-car function in order to have a limited extension of the data. This windowing contributed to the use of gravity and magnetic data which are from the same source. The windowing was suggested by Wilson (1970) and Chandler et al. (1981). The limited area of this study is indicated by the inner frame (in Figs 2, 3, 5). It extends 13 kms N-S and 11 kms E-W. The limited area was selected by the investigation of the gradient and band-pass windowed anomalies.

The parameters determined from of the iterations can be seen in Fig. 4. It shows three iterations with different initial values: $J/\varrho_0 = 10\ Am^2kg^{-1}$, $\alpha_0 = 40^{o}$, $\beta_0 = 50^{o}$; $J/\varrho_0 = 100\ Am^2kg^{-1}$, $\alpha_0 = 80^{o}$, $\beta_0 = -30^{o}$; $J/\varrho_0 = 100\ Am^2kg^{-1}$, $\alpha_0 = 80^{o}$, $\beta_0 = 0^{o}$. After the 7th iteration the oscillation of the parameters is less than one thousandth part of the iterated value. The results of the iteration are: $J/\varrho = 0.00118\ Am^2kg^{-1}$, $\alpha = 33^{o}$, $\beta = -1^{o}$.

The values α and β estimated by iteration decided the average values of the inclination ($I = 60^{o}$) and declination

($D = 0^{o}$) and were used to calculate the transfer function Eq. (1). The coefficients to reduce the total magnetic anomalies to the pole were obtained by numerical inverse Fourier transform of the transfer function of Eq. (1) truncated by the band--pass window of Eq. (3). The total magnetic anomalies reduced to the magnetic pole can be seen in Fig. 5.

The calculation based on Poisson's relation implies the following assumptions: the gravity and the corresponding magnetic anomalies are produced by same geological source; the density and the magnetization are homogeneous. If the assumptions according to Poisson's relation are fulfilled, then the magnetic field reduced to the pole and the derivative of the gravity anomalies with respect to the variable z are in correlation. The empirical correlation coefficient of the above mentioned two anomalies is 0.53 and its confidence interval of 99 percent 0.44-0.61. The ratio J/ϱ can be interpreted only in its range because the assumptions are fulfilled in 50 percent.

The position of the calculated anomalies are in accord with the tectonic lines (Fig. 2, 3, 5). The coincidence of the tectonic lines and the shape of the anomalies is especially good in the central and South-West zones of the survey area. The tectonic lines were probably developed before the deposition of the Paleogene sediments, and they were partly renewed by the Paleogene volcanic activities which occurred along other, new lines. The Miocene volcanic activities were scattering ones. Several hundred meters of tuffs confirm effective tectonics in the area. The volcanic centre was in a zone striking NE-SW in the central part of the area. The NE-SW and NW-SE main tectonic directions can be located with some local deviations. The tectonic lines in the direction NW-SE are younger according to the position of the calculated anomalies. They probably shifted the NE-SW zones horizontally. The tectonics of the Pannonian section cannot be detected by the current method. It can be supposed, indirectly, that the Triassic, partly, and the Paleogene and Neogene section may consist of porous beds which may be considered as hydrocarbon reservoirs.

ACKNOWLEDGEMENTS

The authors wish to thank Dr. W B Agocs for reviewing the manuscript. Computations were made on a CDC-3300 of the Research Institute for Computing Methods and Automation of the Hungarian Academy of Sciences. The permission for the use of the computing facilities is being greatly appreciated and acknowledged.

REFERENCES

Al-Chalabi M 1970: Bolletino di Geophysica Teorica ed Applicata, 12, No. 45-46, 3-20.

Baranov V 1957: Geophysics, 22, 359-383.

Baranov V, Naudy H 1964: Geophysics, 29, 67-79.

Bhattacharyaa B K 1965: Geophysics, 30, 829-857.

Chandler V M, Koski J S, Hinze W J, Brailes L W 1981: Geophysics, 46, 30-39.

Cordell L, Taylor P T 1971: Geophysics, 36, 919-937.

Garland G D 1951: Geophysics, 16, 51-62.

Höpcke W 1980: Fehlerlehre und Ausgleichrechnung. Walter de Gruyter, Berlin-New York

Kanasewich R G, Agarwal E R 1970: Journal of Geophysical Research, 75, 5702-5712.

Kis K 1983: Acta Geod. Geoph. Mong. Hung., 18, 173-186.

Kis K 1984: Acta Geod. Geoph. Mong. Hung., 19, 383-394.

Lundbak A 1956: Geophysical Prospecting, 4, 226-235.

Meskó A 1984: Digital Filtering: Applications in Geophysical Exploration for Oil. Akadémiai Kiadó, Budapest

Report on the detailed gravity and magnetic surveys in the prospecting area Tóalmás (in Hungarian). GKV Database, 1982, No. G-39.

Skeels D C, Watson R J 1949: Geophysics, 14, 133-150.

Wilson C D V 1970: Bolletino di Geofisica Teorica ed Applicata, 12, No. 45-46, 158-182.

Acta Geod. Geoph. Mont. Hung., Vol. 24 (3-4), pp. 343-367 (1989)

A PROBLEM OF AN OBDUCTING LITHOSPHERIC PLATE IN THE ALEUTIAN ARC SYSTEM. A FINITE ELEMENT ANALYSIS IN THE FRICTIONLESS CASE

J Nedoma[1], J Haslinger[2], I Hlaváček[3]

[1]General Computing Center Czech. Acad. Sci., 182 07 Prague 8 - Libeň, Pod vodárenskou věží 2, Czechoslovakia

[2]Mathematical-Physical Faculty Charles University, 110 00 Prague 1 - Malá Strana, Malostranské nám. 25, Czechoslovakia

[3]Mathematical Institute Czech. Acad. Sci., 115 67 Prague 1, Žitná 25, Czechoslovakia

[Manuscript received May 13, 1987]

A model of the Aleutian arc system is studied from the point of view of the plate tectonic concept based on the global geodynamic model given by Nedoma (1984). In the model problem we limit ourselves to a model in which the lithospheric plate is obducting with time onto the oceanic lithospheric plate. For numerical experiments an elastic rheology was applied. The mathematical analysis is based on the contact problem without friction. Details of numerical results are discussed.

Keywords: Aleutian arc; finite element method; numerical modelling; obduction; plate tectonics

1. INTRODUCTION

In order to review the general characteristics of the collision zones, an example is taken from the cross section of the Aleutian arc system in Fig. 1. The present study of the Aleutian arc is made within a plate tectonic concept based on the global geotectonic model given by Nedoma (1984, 1986). From a geometric point of view the investigations are based on the model (see Fig. 1a) given by Grow (1973) (see also Le Pichon et al. 1973).

The stresses in the lithospheric plate arise from several fundamental sources: tectonic stresses, thermally induced stresses, stresses resulting from the action of gravitational and magnetic body forces as well as of tidal body forces acting on the density distribution to the lithospheric plate. In the present study the influence of thermally induced stresses and

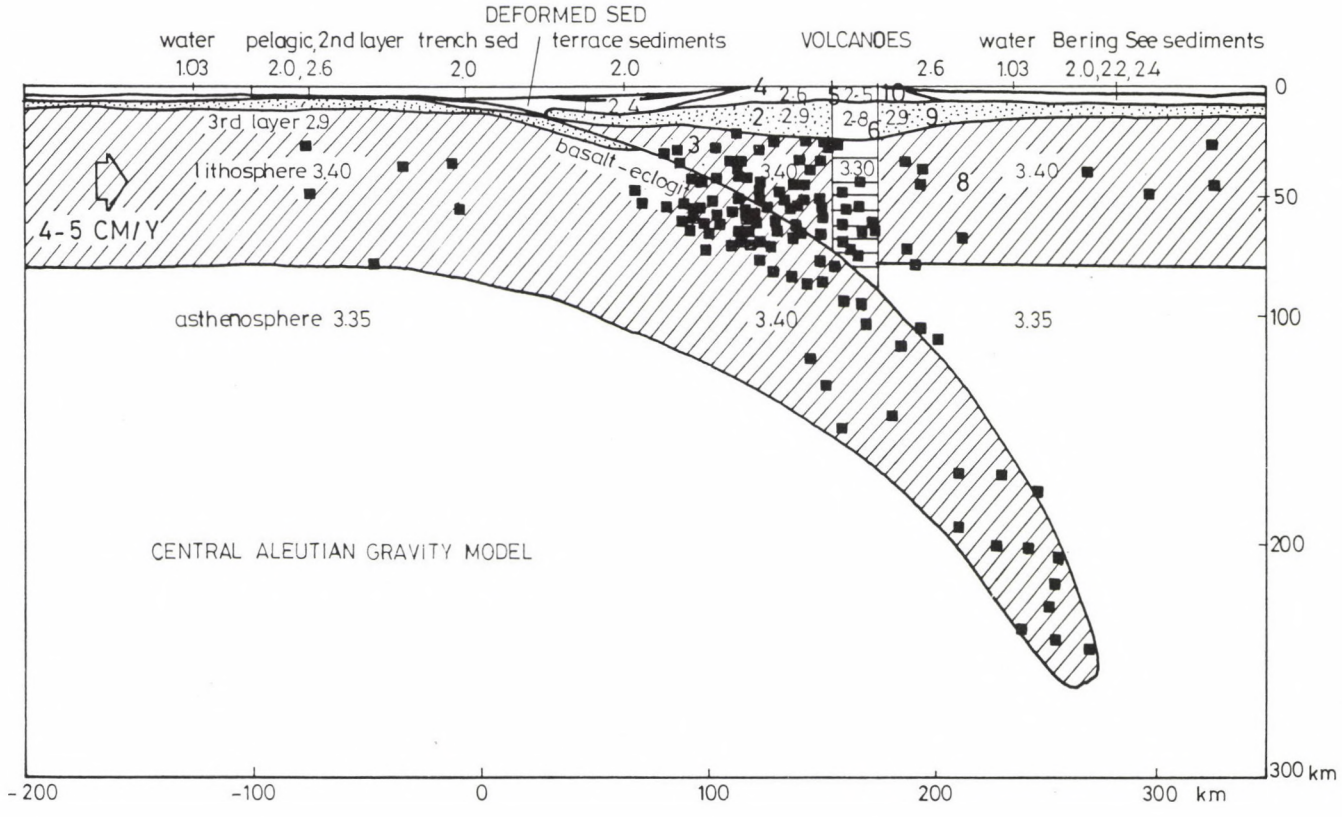

Fig. 1a. Schematic cross-section of the Central Aleutian arc after Grow(1972), see also Le Pichon et al. (1973). Numbers refer to types of rocks in Table I

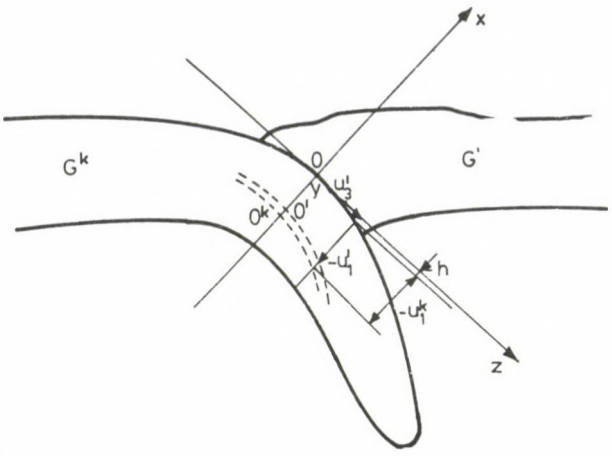

Fig. 1b. Derivation of the contact conditions

stresses resulting from the action of magnetic and tidal bodies will be neglected.

The present-day earthquake activity at the Aleutian arc is largely controlled by the geometry of the northern boundary between the North American and the Pacific plates. Stauder (1968, 1972) shows that earthquakes are located near the intersection of the Aleutian arc and the Bowers Ridge and that underthrust faulting occurs beneath the northern Aleutian Terrace and southern Aleutian Ridge, slip vectors are parallel with the Pacific plate motion vector and that normal-faulting earthquakes occur in association with the Aleutian Trench, the axes of least compressive stress are perpendicular to the local trench axis. The Aleutian volcanoes are located in the Aleutian arc, starting at Buldir Island eastward. As shown by Engdahl (1973), the Aleutian arc volcanism has a connection with the occurrence of earthquake activity beneath a depth of about 110 km and thus also with the subduction of the Pacific plate under the North American lithospheric plate The maximum depth of earthquakes is about 250-300 km and decreases westward along the arc. As was shown by Spence (1977) the dominant tectonic process occurring at the central Aleutian arc is the episodic occurrence of large thrust earthquakes and the subsequent subduction process

is characterized by episodic downslab pressure overload pulses. Recent seismic evidence indicates that the Benioff zone is segmented along its length by breaks (Stauder 1972, Van Wormers et al. 1974, etc.). The present relative motion in the region of Aleutian arc and Alaska due to Grow (1973), Grow and Atwater (1973) and Atwater (1970) is about 4 to 5 cm yr^{-1}. This estimation is based on an analysis of spreading in the eastern Pacific.

2. RHEOLOGY-MODEL

Many authors have treated the deformation of the lithosphere in the collision zones using thin elastic plate-theory (Le Pichon et al. 1973, Watts and Talwani (1974), Caldwell et al. (1976). In some other cases the elastic or elasto-plastic and visco-elastic theories are used (McAdoo et al. 1978, Turcotte et al. 1978, Park and Westbrook 1983). Generally the model considered can be thermoelastic to thermo-elasto-visco-plastic (Nedoma 1984, 1986). Laboratory measurements of creep in lithospheric rocks indicate that the strain rate is a nonlinear function of stress (Heard 1976) and of temperature. The strong temperature dependence of rheology is much more important in determining the character of flow in the mantle than is the nonlinear dependence of strain rate on shear stress (Schubert et al. 1976, Yuen and Schubert 1976). In order to model the obducting lithospheric plate an elastic or thermo-elastic rheology can be used. Such approximations are possible due to a short time period from the geological point of view. Since the collision of the lithospheric plates and blocks extends over several tens of million years, plates behave visco-elastic with a long memory approximating thermo-visco-plastic media. Experimental studies on the deformation mechanism of single crystals of olivine and of polycrystaline aggregates like dunite and lherzolite showed that the dominant mechanisms are nonlinear creeps. These experimental studies prove the previous assertions. It is well-known, however, that for time periods shorter than a characteristic time $t_c = \nu/\mu$, the upper

parts of the Earth behaves elastically while for longer times it behaves thermo-visco-elastically or even thermo-visco-plastically. Here ν is the effective viscosity at a given stress level defined by

$$\nu = \frac{\tau_2 + [(2/3\ \dot{e}_{ij}\ \dot{e}_{ij})^{1/2}\ \gamma^{-1}]^{1/n}}{(3\sqrt{2}\ \dot{e}_{ij}\ \dot{e}_{ij})^{1/2}} ,$$

where $\dot{e}_{ij}$ is the strain rate tensor, τ_2 is the yield stress (mean flow limit of the continental lithosphere),

$$\gamma = 1/L \int_L \gamma_0 \exp(-Q/RT)\ dx_3 ,$$

($\gamma \to \infty$ for the rigid perfectly plastic flow), where Q is an activation energy, R is the universal gas constant, L the thickness of the lithosphere (see Zienkiewicz et al. 1978) and μ is the elastic rigidity.

As it was shown by Cathles (1975) $t_c \sim 10^9 - 10^{12}$ s $\doteq$ $\doteq 20^2 - 10^5$ years, being sufficient for further investigations. Therefore the analysis can be based on the elastic rheology only (see Table I and the model at Fig. 1).

Table I

$[g/cm^3]$	2400	2900	3400	2600	2500	2800	3300	3400	2900	2800
$c_p[m/sec]$	3800	6410	7600	6200	6100	6300	7780	7900	6410	5950
$C_S[m/sec]$	2100	3700	4400	3600	3500	3680	4500	4560	3700	3400
type of rocks	1	2	3	4	5	6	7	8	9	10

The stress-strain relations of such materials are given by Hooke's or by Duhamel-Neumann s linear laws. The thermo-elastic rheology was analyzed in the geodynamic mechanism by Nedoma

(1982), this is a special case of the global model discussed by Nedoma (1984, 1986). Mathematical analyses of such simpler problems have been presented by Hlaváček and Livíšek (1977) for the elastic case and by Nedoma (1983) for the thermo-elastic case.

3. THE MODEL

In our considerations we shall use a simple model based on Grow's model of the Aleutian arc (Grow 1973). The simple model used assumes a lithospheric plate 80 km thick, of an average density 3400 g m^{-3} in the deeper parts of the lithosphere and of 2800 g m^{-3} in the crustal part of the lithosphere. Note also the implied accretion of about 15 km of deformed sediments of average density 2400 g m^{-3} at the leading edge of the overriding plate (see Fig. 1 and Table I). The geometrical surface configuration of the lithosphere is derived from the distribution of intermediate and deep earthquakes.

In order to give the equations of motion of the obducting plate moving along the asthenosphere, we shall assume in the first approximation that the obducting plate is formed by inhomogeneous isotropic materials. Following Nedoma (1982) we shall assume that the variability in time of sources in the lithospheric plate and the asthenosphere and the body and surface forces is slow and moreover that the motion of the lithospheric plate is uniform e.g. over the last several million years. Then the problem can be studied as a quasi-stationary one and the forces of inertia can be neglected. Moreover, such problems can be studied as a quasi-coupled problem in linear thermo-elasticity. In such a model problem both fields, i.e. the stress-strain field and the thermal field, are studied separately. For simplicity the investigations will be made in the plane (x_1,x_3) only. The geometry of the model problem discussed is due to Grow (1973) in the Fig. 1a.

Let Ox_1x_3 be the orthogonal Cartesian coordinate system. Let the obducted plate which is approximated by an elastic isotropic plate in the (x_1,x_3)-plane, occupy the region G with

the boundary ∂G at a time $t \in \langle t_1, t_2 \rangle$. The total boundary of the obducting lithospheric plate consists of three parts: the Earth's surface Γ_τ , the contact boundary Γ_α and the boundary Γ_u . The Earth's surface Γ_τ is represented by the Aleutian arc surface and of the boundary defined by the oceanic bottom. The contact boundary Γ_α consists of the contact boundary Γ_c between the obducting and subducting plates and is characterized by the collision zone, and of the contact boundary Γ_a between the obducting plate and the asthenosphere which is supposed to be rigid. Such an assumption is not correct from the geological point of view but it is so from a mathematical point of view according to the simple model assumed with time periods shorter than a characteristic time t_c. Such an approximation is more accurate than the models accepted for the Earth's crust only based on elastic rheology (Kasahara 1978) or for the lithosphere modelled as a rigid-visco-plastic medium resting without friction upon the asthenosphere (Vilotte et al. 1982), because such models are static ones only which do not render the shift of the lithosphere along the asthenosphere, while the model presented here renders the shift (since the model is simpler, the elastic rheology of the obducting lithosphere and the rigid rheology of the asthenosphere and of the subducting plate are used only). The boundary Γ_u is a fictitious boundary and is represented by the boundary defined in a sufficiently large distance from the collision zone, in the discussed case from the Aleutian trench where the magnitude of the displacement vector $\tilde{u}_0$ of the plate over the studied time period is given.

Further for simplicity we assume that the obducting elastic plate (the American plate) occupying the domain G rests on the rigid support - the asthenosphere and the subducting oceanic plate. It is convenient to choose the origin (0,0) as the point nearest to the trench axis.

It is well known that the stress field in the plate satisfies the equilibrium equations

$$\tau_{ij,j} + F_i = 0 \qquad i=1,3 \quad , \tag{3.1}$$

where $\vec{F}$ denotes the vector of body forces and τ_{ij} is the elastic stress tensor. Henceforth we use the summation convention: a repeated index means summation over 1 and 3. Moreover, prime and index means derivative.

The traction vector on the boundary

$$\tau_i = \tau_{ij} n_j \tag{3.2}$$

can be decomposed into the normal and tangential components

$$\tau_n = \tau_i n_i = \tau_{ij} n_j n_i, \quad \tau_s = \tau_i s_i = \tau_{ij} s_i n_j , \tag{3.3}$$

where $\vec{n} = (n_1, n_3)$ and $\vec{s} = (s_1, s_3) = (-n_3, n_1)$ are the outward normal and tangential unit vectors. The displacement vector can be decomposed into the normal and tangential components

$$u_n = u_i n_i , \quad u_s = u_i s_i . \tag{3.4}$$

Due to the presumption the collision model can be investigated within the range of linear elasticity. Generally the problem leads to a coupled contact problem in linear thermoelasticity or thermo-plasticity. But we limit ourselves to a special case in which attention is concentrated onto resulting tectonic effects in the obducting plate only. Then the problem is solved in linear elasticity. Therefore the stress-strain relation is given by Hook's law

$$\tau_{ij} = 2(\mu e_{ij} + \lambda e_{kk} \delta_{ij}) , \quad e_{ij} = e_{ji} = 1/2(u_{i,j} + u_{j,i}) \tag{3.5}$$

where λ , μ are Lamé's coefficients, δ_{ij} is Kronecker's symbol. Due to (3.1) one obtains

$$\mu_{i,jj} + (\lambda + \mu) u_{j,ji} + F = 0 \qquad i,j = 1,3 . \tag{3.6}$$

The elastic coefficients λ and μ are positive $\lambda(x) > 0$,

$\mu(x) \geq \mu_0 > 0$ almost everywhere in the plate and fulfil therefore the following condition

$$1/2\,(\lambda\vartheta^2 + 2\mu\, e_{ij}\, e_{ij}) \geq \mu\, e_{ij}\, e_{ij}\,, \quad \vartheta = e_{kk}\,, \tag{3.7}$$

almost everywhere in the plate.

BOUNDARY CONDITIONS

To investigate the stress-strain field in the obducting plate in a neighbourhood of the collision zone, conditions should be usually given characterizing the effect of the environment of the plate on the processes taking place within a limited region containing the collision parts of the lithospheric plates under study and asthenosphere. The interaction between the collising plates and their environment is modelled by the boundary conditions for the displacement vector $\tilde{u}$. In the model problem the boundary ∂G of the investigated region occupied by the obducting plate G consists of three parts Γ_u, Γ_τ, Γ_α. Then on the Earth's surface the surface forces Γ_τ are prescribed as caused by the weight of the oceans, of the atmosphere, and of the mountains above some approximate surface. Thus one has

$$\tau_{ij}\, n_j = P_i \tag{3.8}$$

on the Earth's surface Γ_τ. In the model problem the weight of the oceans, atmosphere, etc. are neglected so that $P_i = 0$.

On the contact boundary Γ_α the boundary conditions are deduced from the following consideration (see Haslinger and Hlavácek 1980): At the time $t \in \langle t_1, t_2 \rangle$ we assume that before the deformation the colliding plates G ($l = 1,2$, $l = 1$ is the obducting and $l = 2$ is the subducting lithosphere and the asthenosphere) and the asthenosphere were in contact along the whole contact boundary $\Gamma_\alpha = \overline{CC} \cup \overline{AA}$ (see Fig. 1a). Let the x_1-axis be the normal $\vec{n}^{(2)}$ and the x_2-axis be the tangent $\vec{s}^{(2)}$ at

point $0 \in \Gamma_\alpha$. During the deformation process the points $0^{(1)} \in \partial G^{(1)}$ and $0^{(2)} \in \partial G^{(2)}$ will be displaced in a different way, but plate $G^{(2)}$ can never penetrate into plate $G^{(1)}$. From this condition it follows that (Fig. 1b)

$$u_1^{(2)}(0,0) \leqq u_1^{(1)}(\bar{x}_1,\bar{x}_2) + h(\bar{x}_2) ,$$

where h is the function, describing the curve Γ_α and $(\bar{x}_1,\bar{x}_2) \in \Gamma_\alpha$ so that

$$u_2^{(1)}(\bar{x}_1,\bar{x}_2) + \bar{x}_2 \leqq x_2^{(2)}(0,0) .$$

Since the point $(\bar{x}_1,\bar{x}_2)$ is unknown, we shall for simplicity assume that $h(\bar{x}_2) = 0$, $u_1^{(1)}(\bar{x}_1, \bar{x}_2) \doteq u_1^{(1)}(0,0)$ which is correct for a flat contact boundary Γ_α and for derivatives and mutual shifts $|u_2^{(1)} - u_2^{(2)}|$ small in a neighbourhood of the origin. Moreover, by putting $u_1^{(2)} \equiv u_n^{(2)}$, $u_1^{(1)} = - u_n^{(1)}$ one obtains $u_n^{(1)} + u_n^{(2)} \leqq 0$, $u_n^{l} = u_i^{l} n_i$, $l = 1,2$ at a point $0 \in \Gamma_\alpha$

For the contact forces one obtains from the law of action and reaction

$$\tau_n^{(1)} = \tau_n^{(2)} , \quad \tau_s^{(1)} = \tau_s^{(2)} \leqq \text{on } \Gamma_\alpha .$$

On the other hand, the tangential component vanish in the case of zero friction and the normal contact force cannot be tensile, i.e.

$$\tau_s^{(1)} = \tau_s^{(2)} = 0, \qquad \tau_n^{(1)} = \tau_n^{(2)} \leqq 0.$$

Therefore if the colliding plates are not in contact then $u_n^{(1)} + u_n^{(2)} < 0$ and the contact forces are zero, i.e. $\tau_n^{(1)} = \tau_n^{(2)} = 0$. If there is a contact, then $u_n^{(1)} + u_n^{(2)} = 0$ and $\tau_n^{(1)} = \tau_n^{(2)} < 0$. Altogether one has

$$u_n^{(1)} + u_n^{(2)} \leqq 0, \quad \tau_n^{(1)} = \tau_n^{(2)} \leqq 0, \quad u_n^{(1)} + u_n^{(2)} \quad \tau_n^{(1)} = 0,$$

$$\tau_s^{(1)} = \tau_s^{(2)} = 0 \ .$$

Further, since the stress-strain field in the obducting plate is studied for simplicity (see previously) we shall assume that the subducting plate and the asthenosphere are rigid, i.e. $\tilde{u}^{(2)} = 0$. Thus in the summary one has the following contact conditions on the contact boundary Γ_c :

$$u_n \leqq 0 \ . \tag{3.9a}$$

If $u_n < 0$ at some point of the contact boundary, the support does not produce a reaction and thus $\tau_n = 0$. If $u_n = 0$, i.e. if there exists a contact between the obducting plate and the support (i.e. the Pacific plate and the asthenosphere), then it exerts a normal force $\tau_n \leqq 0$ in the moving North American obducted plate. Hence

$$\tau_n \leqq 0 \quad \text{and} \quad u_n \tau_n = 0 \tag{3.9b}$$

at the contact boundary Γ_c .
We refer to these conditions (3.9a,b) as to Signorini's conditions. If no friction is considered at the contact, the tangential stress component vanishes, i.e.

$$\tau_s = 0 \tag{3.9c}$$

at the contact boundary Γ_c

To model the shifting of the obduced North American plate the value of the displacement vector is determined in a distance sufficiently far from the collision zone (it is the boundary Γ_u). The values of the displacement vector components can be determined from the knowledges of the speed of the North American plate per year and the recent vertical movements, thus

$$\tilde{u} = \tilde{u}_0 \tag{3.10}$$

at the fictitious boundary Γ_u.

4. SOLUTION AND ACCURACY OF THE APPROXIMATION

The problem considered will be solved numerically by the finite element technique. Suppose that the American obducting plate occupying the domain G rests on a rigid support by a part $\Gamma_\alpha = \Gamma_a \cup \Gamma_c$ of the boundary ∂G (see above). Under the assumption of small displacement and of linearly elastic materials formed the obducting American plate we shall consider the problem (3.6)-(3.10), where we assume the body forces $\vec{F} \in [L^2(G)]^2$, and the surface load $\vec{P} \in [L^2(\Gamma_\tau)]^2$.

Let us define the set of virtual displacements V as the set of all sufficiently smooth functions satisfying the prescribed value of displacement $\vec{u}_0$ on the fictive boundary Γ_u i.e.

$$V = \left\{ \vec{v} \mid \vec{v} \in W^1(G) = [H^1(G)]^2, \quad \vec{v} = \vec{u}_0 \quad \text{on } \Gamma_u \right\} .$$

Further we define the set of admissible virtual displacements K as a set of all functions of the space of virtual displacements V for which the normal displacement component on the contact boundary is less or equal to zero, i.e.

$$K = \left\{ \vec{v} \in V : v_n \leq 0 \quad \text{on the contact boundary } \Gamma_\alpha \right\} .$$

Multiplying (3.6) by $\vec{v} \in K$, integrating over G, using Green's theorem and boundary conditions the potential energy L_0 is obtained as

$$L_0(\vec{v}) = 1/2 \int_G \tau_{ij}(\vec{v}) e_{ij}(\vec{v}) \, dx - \int_G F_i v_i \, dx - \int_{\Gamma_\tau} P_i v_i \, ds . \qquad (4.1)$$

From modern convex analysis (see e.g. Ekeland and Temam 1976) it is known that the solution of this problems tends to minimize the generalized potential energy over the set of admissible displacement fields. The problem (4.1) is equivalent with the problem (in the literature known as the variational or weak formulation): find a displacement vector $\vec{u}$ from the set of admissible virtual displacements K so that

$$B(\vec{u},\vec{v}-\vec{u}) \geq S(\vec{v}-\vec{u}) \quad \text{for all} \quad \vec{v} \in K \ , \tag{4.2}$$

where

$$B(\vec{u},\vec{v}) = \int_G (\lambda \operatorname{div} \vec{u} \operatorname{div} \vec{v} + 2(\mu e_{ij}(\vec{u}) e_{ij}(\vec{v})) \, dx = \int_G \tau_{ij}(\vec{u}) e_{ij}(\vec{v}) \, dx \ , \tag{4.3a}$$

$$S(\vec{v}) = \int_G F_i v_i \, dx + \int_{\Gamma_\tau} P_i v_i \, ds \ . \tag{4.3b}$$

It is easy to show that the set K (the set of admissible virtual displacements) (Ekeland and Temam 1976) is weakly closed. The functional $L_o(\vec{v})$ is strictly convex and weakly lower semicontinuous (Hlaváček and Lovíšek 1977, Nedoma 1983). Thus we find $L_o(\vec{v}) \to \infty$ as $\| \vec{u} \| \to \infty$ what shows that the functional L_o has a minimum. It can be shown that if the weak solution is smooth enough, then it represents a classical solution of the problem, and any classical solution of (3.6-3.10) is a weak solution (see Hlaváček et al. 1987).

The numerical solution of the problem is based on the finite element technique. For simplicity piecewise linear triangular elements are used. We assume that the obducting plate occupying the domain G is approximated by a polygonal bounded domain. Then we divide the domain G into relatively small-sized triangles. Denote h the maximum side of all triangles generating a regular triangulation τ_h. Let V_h be the set of linear finite elements. Further we define the set of admissible approximate virtual displacements K_h as

$$K_h = \left\{ \vec{v} | \vec{v} | V_h |^2, \ v_n \leq 0 \text{ on the contact boundary } \Gamma_c \ , \ \vec{v}=\vec{u}_o \text{ on } \Gamma_u \right\}.$$

The aim is to minimize the functional $L_o(\vec{v})$ over the set of admissible approximate virtual displacements K_h. An estimate

of the rate of convergence of the FEM approximation to the accurate solution is of an order O(h) (Hlaváček and Lovíšek 1977, Nedoma 1979, 1983). These problems lead to minimization of a quadratic form on a set with linear constraints. Such problems are problems of quadratic programming. In our case it is solved on the basis of the method of conjugate gradients (Glowinski et al. 1976).

Since the analysis of the model problem is mathematically non-trivial and represents a new approach in mathematical and theoretical geophysics we discuss the problem only briefly. For more details see Nedoma (1983) analysing the problem studied from the mathematical point of view. At the end we shall show a continuous dependence of the solution on the given data $(\vec{u}_0,\vec{P},\vec{F})$. From the physical point of view it reflects the fact that the solution of the model problem which approximates the geodynamic process at time $t \in \langle t_1,t_2\rangle$ only changes a little for small changes in the given displacements and surface and body forces. The consideration is the following: Let

$$V_0 = \left\{ \vec{v} \mid v \in W^1(g),\ \vec{v} = 0 \text{ on } \Gamma_u \right\},\quad K_0 = \left\{ \vec{v} \in V_0,\ v_n \overset{\leq}{=} 0 \text{ on } \Gamma_\alpha \right\} .$$

Let $\vec{u}=\vec{u}_0+\vec{w}$, $\vec{v}=\vec{u}_0+\vec{\omega}$, $\vec{w},\vec{\omega} \in K_0$. It is readily seen that (4.2) is equivalent with the following inequality

$$\vec{w} \in K_0,\ B(\vec{w},\vec{\omega}-\vec{w}) = S(\vec{\omega}-\vec{w}) - B(\vec{u}_0,\vec{\omega}-\vec{w}) = S_1(\vec{\omega}-\vec{v}) \text{ for all } \vec{\omega} \in K_0. \quad (4.4)$$

Let us define the auxiliary problem as follows: find $\vec{z} \in V_0$ so that

$$B(\vec{z},\vec{y}) = S_1(\vec{y}) \quad \text{for all} \quad \vec{y} \in V_0 . \quad (4.5)$$

Note that there exists a unique solution of this problem. Then (4.4) is written in the following form

$$B(\vec{w},\vec{\omega}-\vec{w}) = B(\vec{z},\vec{\omega}-\vec{w}) \quad \text{for all} \quad \vec{\omega} \in K_0 . \quad (4.6)$$

It is easy to see that (4.6) is equivalent to the problem of

minimizing the functional $B(\tilde{w}-\tilde{z},\tilde{w}-\tilde{z}) - B(\tilde{z},\tilde{z})$ over the set K_o. If we introduce the inner product $B(\tilde{u},\tilde{v})$ in the space V_o, then V_o becomes a Hilbert space and the minimizer coincides with the projection Π_{K_o} of the element $\tilde{z}$ onto the set K_o, i.e.

$$\tilde{w} = \Pi_{K_o} \tilde{z} \ . \tag{4.7}$$

In addition to the triple $\{\tilde{u}_o,\tilde{P},\tilde{F}\}$ let us consider also a "perturbed" triple $\{\tilde{u}_o,\tilde{P}',\tilde{F}'\}$ which represents the measured values of $\tilde{u}_o,\tilde{P},\tilde{F}$ obtained from the geophysical prospecting data. Let $\tilde{z}'$ and $\tilde{w}'$ be the solutions of the problems (4.5) and (4.4) respectively, with $\{\tilde{u}_o',\tilde{P}',\tilde{F}'\}$. It is well known that the solution of the problem (4.5) depends continuously on the data, i.e.

$$\|\tilde{z}-\tilde{z}'\|_{W^1} \leq C(\|\tilde{u}_o-\tilde{u}_o'\|_{W^1} + \|\tilde{F}-\tilde{F}'\|_{[L^2(G)]^2} + \|\tilde{P}-\tilde{P}'\|_{[L^2(\Gamma_T)]^2} \equiv$$
$$\equiv C(\{\tilde{u}_o,\tilde{P},\tilde{F}\} - \{\tilde{u}_o',\tilde{P}',\tilde{F}'\}) \ . \tag{4.8}$$

Similarly one has

$$\tilde{w}' = \Pi_{K_o} \tilde{z}' \ . \tag{4.9}$$

Let us denote by $\|w\|_E^2 = B(w,w)$. Then due to (4.7) and (4.9) one gets

$$\|w-w'\|_E = \|\Pi_{K_o} \tilde{z} - \Pi_{K_o} \tilde{z}'\|_E = \|\tilde{z}-\tilde{z}'\|_E = C\|\tilde{z}-\tilde{z}'\|_{W^1} \ .$$

From the Korn inequality (Hlaváček et al. 1987) in V_o results that

$$\|\tilde{w}-\tilde{w}'\|_{W^1} \leq C_o \|\tilde{z}-\tilde{z}'\|_{W^1} \ .$$

Combining the later inequality with (4.8) one obtains

$$\|\tilde{w}-\tilde{w}'\|_{W^1} C(\{\tilde{u}_o,\tilde{P},\tilde{F}\} - \{\tilde{u}_o',\tilde{P}',\tilde{F}'\}) \ .$$

Substituting for $\tilde{u} = \tilde{u}_o + \tilde{w}$, $u' = \tilde{u}_o' + \tilde{w}'$ one obtains

$$\|\tilde{u}-\tilde{u}'\|_{W^1} = (\|(\tilde{u}_0+\tilde{w})-(\tilde{u}_0'+\tilde{w}')\|_{W^1}) \leq \|\tilde{u}_0-\tilde{u}_0'\|_{W^1} + \|\tilde{w}-\tilde{w}'\|_{W^1} \leq$$

$$\leq C(\{\tilde{u}_0,\tilde{P},\tilde{F}\} - \{\tilde{u}_0',\tilde{P}',\tilde{F}'\}) \ .$$

The last inequality verifies the continuous dependence of the solution on the geophysical measured data which physically means that the results from the numerical analysis correspond to the geophysical reality.

5. RESULTS

In the present paper the Aleutian arc is studied within a plate-tectonic concept. The investigations are based on the model given by Grow (1973) and Table I. This model assumes a 80 km thick lithospheric plate, with densities between 2400 kg/m^3 and 3400 kg/m^3, velocities of seismic P waves between 3800 m/sec and 7900 m/sec and of S waves between 2190 and 4560 m/sec. Its surface configuration is obtained from the distribution of intermediate and deep earthquakes. Note also the implied accretion of sediments of about 15 km at the leading edge of the overriding plate and of about 5 km of sediments in the Behring See.

The collision of the lithospheric plates itself is the actual cause of the large stresses and strains in the lithosphere. The lithosphere thus behaves like a stress guide. To appreciate the part played by this process in tectonogenesis, we study this problem in greater details. One of the main aims of the paper is to show that the mathematical model of collision zone under the assumption discussed above is more correctly described by the variational inequalities (see section 4). As it was shown such model problems accurately approximate the shift of the obducting lithospheric plate along the subducting lithospheric plate and the asthenosphere, while the classical approach corresponds to the static models of the crust or the lithosphere, resting on their support (Kasahara 1978, Vilotte et al. 1982), which on the contrary do not allow

shifting of the obducting lithospheric plate along the subducting lithosphere and the asthenosphere. As indicated by the numerical results, in the obducting invasion plate an internal transfer mass will occur at the place, where it has grown thicker and which is not very far from the head of the plate, accurately at the place of the Aleutian arc. Moreover the invasion makes the North American plate deformed. Its deformation is accompanied by enormous stresses.

The main results are illustrated in Figs 2-10. At Fig. 2 the displacement vector $\tilde{u}$ (in $m/10^k$ years) is shown for the time period $t = 10^4$ years and for the case without friction at the contact boundaries North American (Pacific plates and North American plate) asthenosphere and without any surface loading on the Earth's surface. Figures 3 and 4 illustrate the horizontal u_1 and vertical u_3 components of the displacement vector $\tilde{u}$, respectively. Figure 3 represents the horizontal displacement component u_1 with values between 70 $m/10^4$ yrs at the head of the plate to of about 280 $m/10^4$ yrs at a distance 300 km from the Aleutian trench, it shows the inner shifts of the lithospheric material in the plate in a horizontal direction. It is evident from it, that slower shifting occurs at the head of the obducting plate and faster shifting occurs behind the Aleutian arc. Figure 4 represents the vertical displacement component u_3 and proves the elevation of the Aleutian arc as well as of the head of the obducting plate (short dashed lines) and the depression in the domain behind the Aleutian arc (longer dashed lines) i.e. at distances of about 280-310 km. Numerical results indicate changes in its appearance with the uplift ~ 33 $m/10^4$ yrs at the head of the plate and with the greatest value of uplift of about 38.5 m at the distance ~ 140 km from the Aleutian trench (i.e. in the region of the Aleutian arc) and further with depressions with greatest values of about 55 $m/10^4$ yrs at the distance ~ 280 km from the Aleutian trench. The numerical results prove the observed facts in these regions. So these results are in an agreement with observations in the Behring See, where basins like the Aleutian and Bowers ones occur. Their evolution continues also in present time due to geodynamic processes.

Figure 5 demonstrates the normal component of the

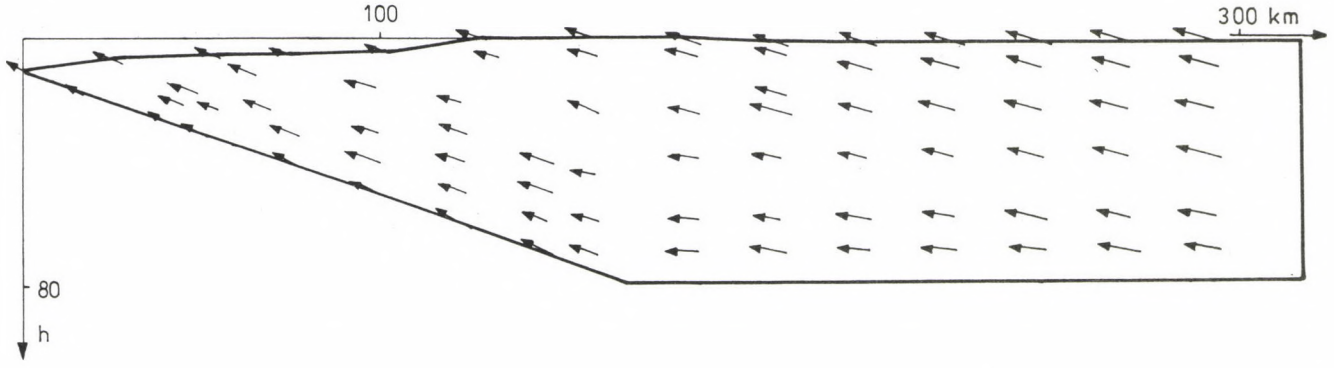

Fig. 2. Display of the displacement vector $\vec{u}$ [m/10^k yrs] for the time period t = 10^4 yrs

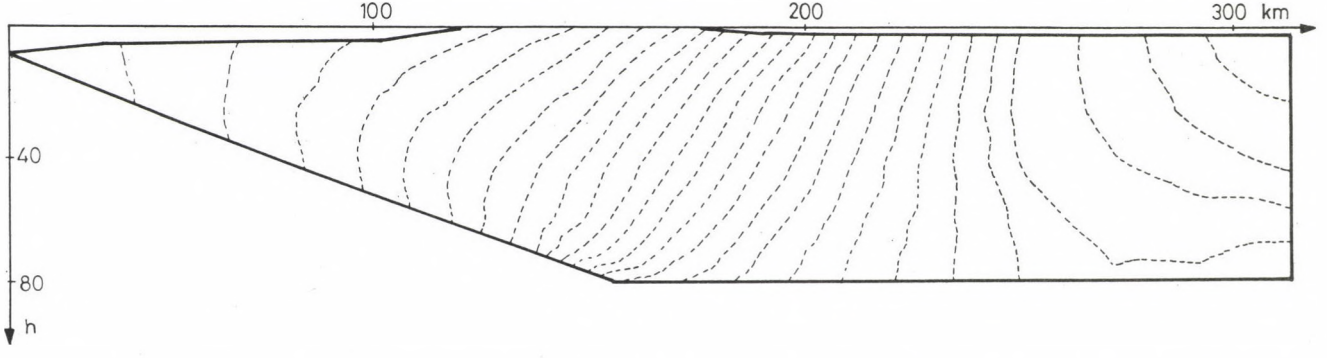

Fig. 3. Display of the horizontal component u_1 of the displacement vector $\vec{u}$ with values between 70 m/10^4 yrs at the head of the plate to of about 280 m/10^4 yrs at the distance ~ 300 km from the Aleutian trench

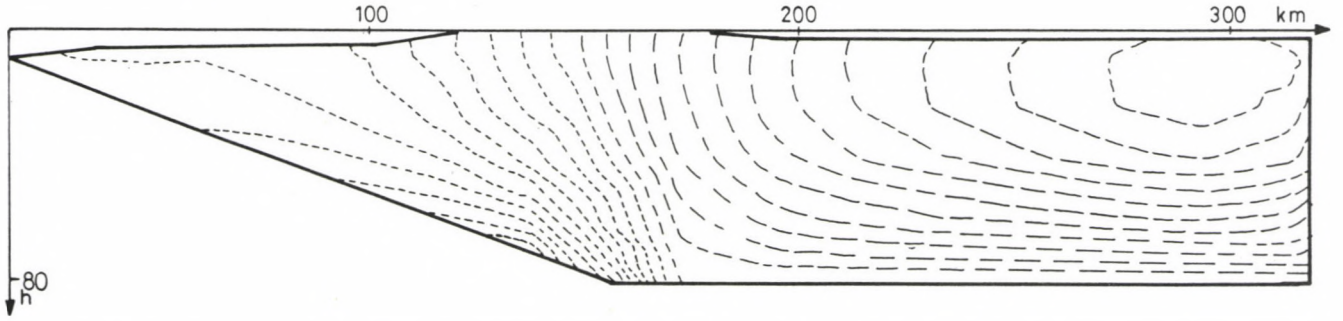

Fig. 4. Display of the vertical component u_3 of the displacement vector $\vec{u}$ (short dashed lines correspond to the elevation, longer dashed lines to the depression) with the greatest value of uplift of about 38.5 m at the distance ~140 km from the Aleutian trench (i.e. in the region of the Aleutian arc) and with the uplift ~33 m/10^4 yrs at the head of the plate and with the depression with greatest value of about 55 m/10^4 yrs at the distance ~280 km from the Aleutian trench

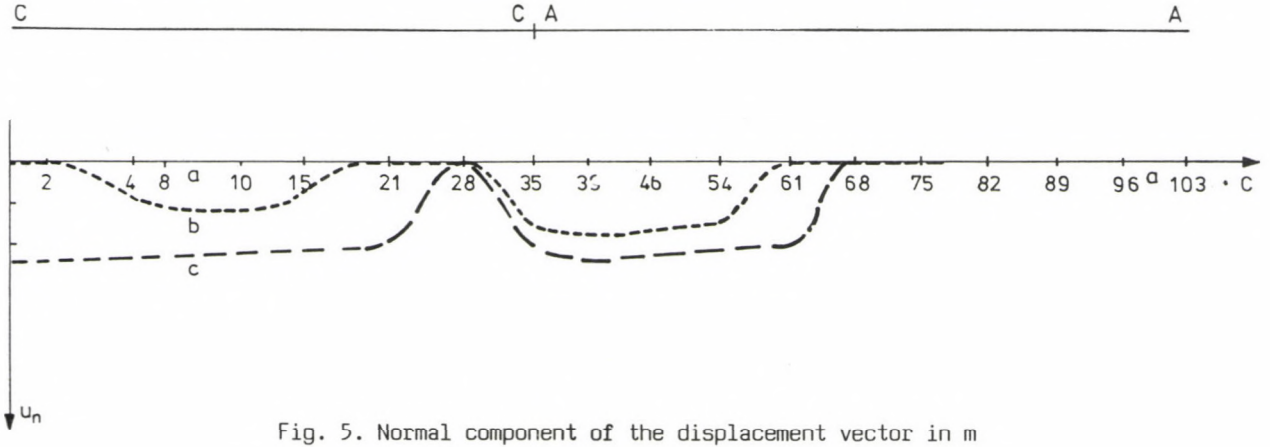

Fig. 5. Normal component of the displacement vector in m

displacement vector. There are three curves $\underline{a}$, $\underline{b}$, $\underline{c}$ in the figure. Curve $\underline{a}$ corresponds to a very short time period ~ max 10^4 yrs. During these time periods the colliding obducted plate, as $u_n = 0$ is only shifted. Curves $\underline{b}$ and $\underline{c}$ correspond to greater time periods of $\sim 10^5$ and 10^6 years for which $u_n < 0$. The places where the obducted plate bulges out, result in the subduction zone and in the region behind the Aleutian arc on the bottom of the lithosphere, i.e. on the contact boundary with the asthenosphere. The space where the lithosphere have bulged out are immediately filled by melted material from the subducted zone. Volcanous chambers are created here in the first case and asthenospheric material in the second case, respectively. Partial melting in these regions is assumed also by Anderson and Sammis (1970). The conditions describing these processes are the so-called contact conditions, discussed in Section 3 - Eqs (3.9a-c) and are derived by Nedoma (1986) for the generalized model problem.

Figures 6-8 display results for the stress components τ_{xx}, τ_{zz}, τ_{xz} as well as for the normal component τ_n of the stress vector $\vec{\tau}$ on the contact boundary Γ_c. In Figs 6 and 7 the greatest value, corresponding to greater values of compressive stresses, occurred in the lower part of the contact in the subduction zone and at distances between 180 km to 250 km on the contact boundary with the asthenosphere. The anomalous regions of greater compressive stresses correspond to anomalous places with a great gradient of the vertical component of the displacement vector $\vec{u}$ (see Fig. 4) and to places where the normal component u_n of the displacement vector is equal to zero i.e. $u_n = 0$ (see Fig. 5). The τ_{xz} component of the stress tensor is shown in Fig. 8. The zones where the faults may occur are indicated. A domain, where the sign of the τ_{xz} component changes is observed. At the contact of the obducted plate with the subducted one the normal component of the stress vector is characterized particularly by a compressive maximum closer to the lower edge of the lithosphere (Fig. 9). Zones of tensile stresses are created at a certain distance on both sides of the compressive stress maximum. As a result of the compressive and

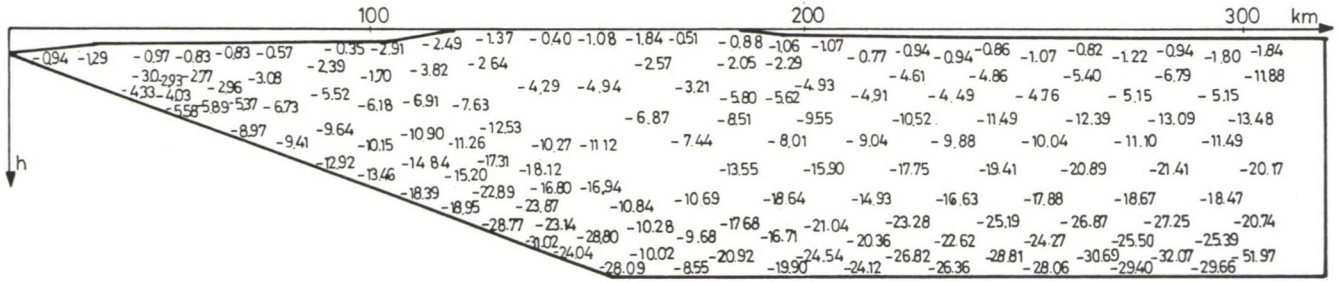

Fig. 6. Display of the stress tensor component τ_{xx} in 10^9 Newton m^{-2}

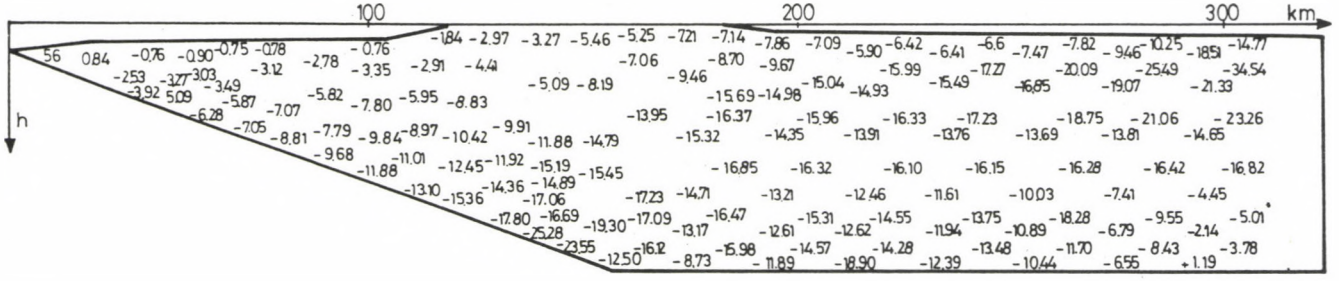

Fig. 7. Display of the stress tensor component τ_{xz} in 10^9 Newton m^{-2}

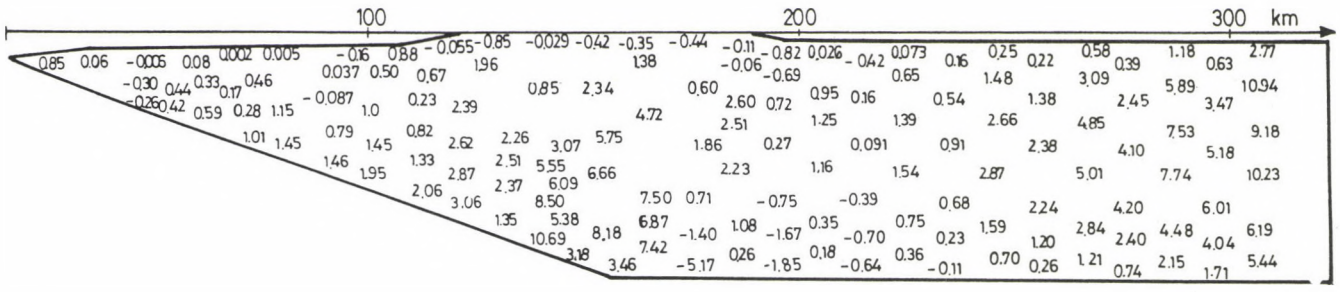

Fig. 8. Display of the stress tensor component τ_{zz} in 10^9 Newton m^{-2}

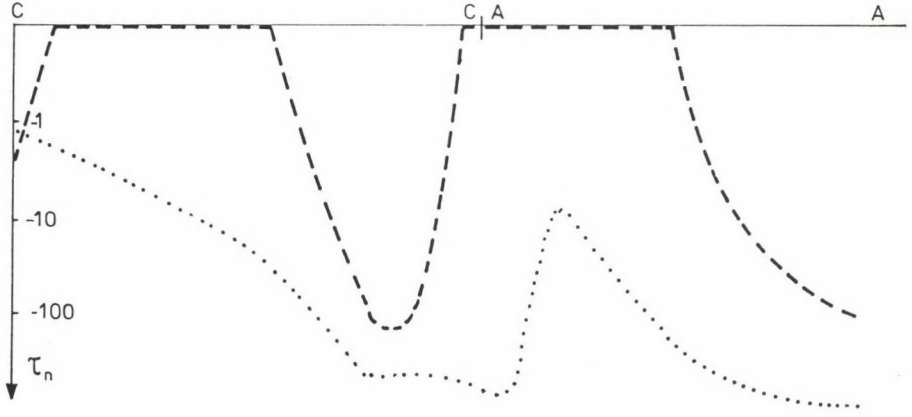

Fig. 9. Normal component of the stress vector in 10^9 Newton m^{-2}, t $\sim$ 10^4 and 10^5 yrs

tensile stresses, faults appear which often reach up to the Earth's surface at places where volcanoes occur.

The last figure (Fig. 10a, b) shows the main stresses in the obducting North American Plate for the time periods $t \sim 10^4$ yrs and $t \sim 10^5$ yrs. By the result of the geotectonic processes for the time period $\sim 10^4$ yrs are the compressive stresses in the obducting plate (Fig. 10a), while for the greater time period $\sim 10^5$ yrs (the Fig. 10b) the result of geotectonic processes is characterized by greater compressive stresses at the contact boundary between the obducting and subducting plates Γ_c in the region under the origin of the Aleutian arc. In this place the subducting Pacific plate is thus strongly loaded. At about one half of the contact boundary Γ_c and in the region at the heel of the bottom part of the subduction zone, but now at the contact boundary of the North American plate with the asthenosphere, the tensile stresses originate and are displayed up to the Earth's surface in two regions in the domain of the Aleutian arc. These tensile stresses produce deep faults. These faults reach up to the Earth's surface in places where volcanoes are found.

Theoretical gravity profiles can be determined directly from the best-fitting deflection profiles $u_3(x)$, using the well-known Bouguer relation.

REFERENCES

Anderson D L, Sammis C 1970: Phys. Earth. Planet. Interiors, 3, 41-50.

Atwater T 1970: Geol. Soc. Am. Bull., 81, 3513-3536.

Caldwell J G, Haxby W F, Karig D E, Turcotte D L 1976: Earth Planet Sci. Lett., 31, 239-246.

Cathless L M 1975: Viscosity of the Earth's Mantle. Princeton University Press, Princeton, N.J.

Ekeland I, Temam R 1976: Convex Analysis and Variational Problems. North Holland, Amsterdam

Engdahl E R 1973: Nature, 245, 23-25.

Glowinski R, Lions J L, Trémolliéres R 1976: Analyse numérique des inéquations variationnelles. Dunod, Paris

Grow J A 1973: Geol. Soc. Am. Bull., 84, 2169-2192.

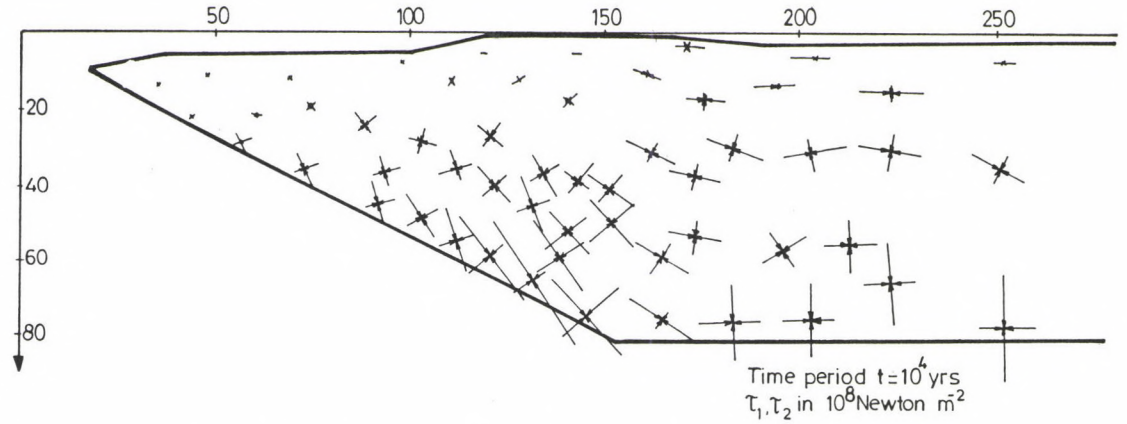

Fig. 10a. The main stresses in the North American plate for $t \sim 10^4$ yrs

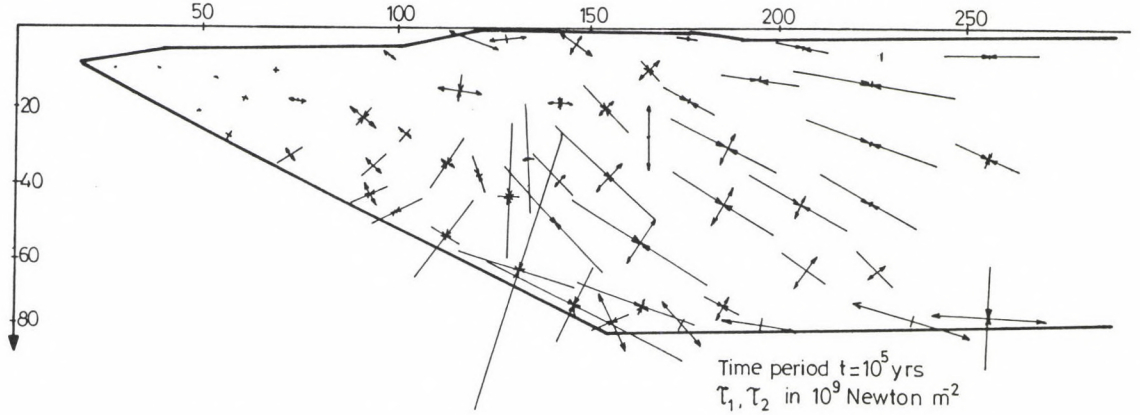

Fig. 10b. The main stresses in the North American plate for $t \sim 10^5$ yrs

Grow J A, Atwater T 1973: Geol. Soc. Am. Bull., 81, 3715-3721.

Haslinger J, Hlaváček I 1980: Apl. Mat., 25, 324-347; Apl. Mat. (1981), 26, 263-290.

Heard H C 1976: Phil. Trans. R. Soc. Lond. A., 283, 173-186.

Hlaváček I, Lovíšek J 1977: Apl. Mat., 22, 215-228.

Hlaváček I, Haslinger J, Nečas J, Lovíšek J 1987: Solution of variational inequalities in mechanics. Springer Verlag, New York, Heidelberg (in press)

Kasahara J 1978: Bull. Earthquake Res. Inst., 53, 339-357.

Le Pichon X, Francheteau J, Bonin J 1973: Plate Tectonics (Developments in Geophysics, 6), Elsevier, Amsterdam, London, New York

McAdoo D C, Caldwell J G, Turcotte D L 1978: Geophys. J. R. astr. Soc., 54, 11-26.

Nedoma J 1979: The Use of the Variational Inequalities in Geophysics. Proc. of the Summer School "Algorithms and Software of Numerical Mathematics", Nové Město n. M., 1979, MFF UK Praha, 1980 (in Czech.)

Nedoma J 1982: Gerlands Beitr. Geophysik, 91, 1, 75-89.

Nedoma J 1983: Apl. Mat., 28, 393-407.

Nedoma J 1984: Gerlands Beitr Geophysik, 93, 4, 231-260.

Nedoma J 1986: Gerlands Beitr. Geophysik, 95, 1, 36-62; 2, 89-105.

Park M J M, Westbrook G K 1983: Geophys. J. R. astr. Soc., 74, 905-914.

Schubert G, Froidevaux C, Yuen D A 1976: J. Geophys. Res., 81, 3525-3540.

Spence W 1977: J. Geophys. Res., 82, 2, 213-230.

Stauder W 1968: J. Geophys. Res., 73, 7693-7701.

Stauder W 1972: J. Geophys. Res., 77, 2072-2080.

Turcotte D L, McAdoo D C, Caldwell J C 1978: Tectonophysics, 47, 193-205.

Van Wormers J D, Davies J, Gedney L 1974: Bull Seismol. Soc. Am., 64, 1467-1475.

Vilotte J R, Daguieres M, Madariaga R 1982: J. Geophys. Res., 87, B13, 10,709-10,728.

Watts A, Talwani M 1974: Geophys. J. R. astr. Soc., 36, 57-90.

Yuen D A, Schubert G 1976: J. Geophys. Res., 81, 2499-2510.

Zienkiewicz D C, Jain P C, Ouate E 1978: Int. J. Solids Structure, 14, 15-38.

Acta Geod. Geoph. Mont. Hung., Vol. 24 (3-4), pp. 369-384 (1989)

GEOMAGNETIC SUDDEN IMPULSES AND PULSATION ACTIVITY

J Verő and L Holló

Geodetical and Geophysical Research Institute of the Hungarian Academy of Sciences, H-9401 Sopron, POB 5, Hungary

[Manuscript received January 10, 1988]

Geomagnetic pulsation activity is analyzed around geomagnetic SI-s. A definition is given for the SI-s used here which differs from the internationally accepted definition. It is shown that these SI-s strongly influence the pulsation activity and the changes after the SI-s are not closely correlated with the changes in interplanetary parameters. If none of the interplanetary parameters changes after the SI, there is no change in the pulsation activity. It is suggested that in the latter case the SI is due to K-H instability and it is no SI in the proper sense.

Keywords: dynamic spectrum; geomagnetic pulsations; interplanetary magnetic field; solar wind; sudden impulse

1. INTRODUCTION

Veldkamp (1960) was the first to note that a geomagnetic sudden impulse (SI) may influence geomagnetic pulsations. During the strong giant pulsation event of July, 1958, an SI occurred at 0930 UT. Previously pulsations with periods of 12 s were observed. Simultaneously with this impulse they disappeared. The period of Pg changed from 95 s before the SI to 105 s after it. During the event the amplitude of Pg decreased, but after it, it became especially strong.

This earliest described event indicates two types of changes in the pulsation activity around SI-s. One of them may be called "Hirasawa-effect": it means a change of the pulsation periods, mainly of Pc5, during SI-s (Hirasawa et al. 1966). The authors supposed that the change is connected to the change in the dimension of the magnetosphere; that means that changes of the period should be parallel to the change of the magnetic

field and cease after the SI had ceased. They have analyzed three such events.

Troitskaya et al. (1968) found several cases of the SI^--effect. (SI^+ and SI^- mean positive and negative SI-s at lower latitudes.) The SI interrupted previously existing pulsation activity - mostly of longer periods - or, the period changed - this was typical for Pc2-3. They attributed the disappearance of pulsations to the stabilization of the magnetopause against K-H instability. One event of this paper (December 14, 1965) was presented in more details by Troitskaya and Gul'elmi (1967), where it can be seen that after the SI^-, pulsations of much shorter periods appear. Such events (3 after SI^- and two after SI^+) were studed in more details by Tátrallyay and Verő (1973) and they found the following sequence of events both for SI^- and SI^+:

longer period pulsations (Pc4-5)
SI
shorter period pulsations (Pc2-3).

The last two steps do not overlap.

In spite of the similarities, there are significant differences between negative and positive SI-s, e.g. Pc2-3 amplitudes are smaller at low latitudes after an SI^+. At higher latitudes the Pc2-3 activity is substituted by Pc1 after SI^+, thus Nurmijärvi (58^o) records Pc2-3, and Sodankylä (64^o), Pc1 (Verő 1975, 1986).

Early speculations about the effect of SI-s were concentrated on a change in the dimension of the magnetosphere (e.g. Sen 1968) which may be valid for the Hirasawa-effect, but not for the post-SI changes. The latter needs some source mechanism active after the SI, too, such as e.g. a change in interplanetary parameters lasting longer time after the impulse.

Associations between different type pulsations and geomagnetic impulses have been discussed by many authors. In the following some types of such pulsations are listed which differ from those treated in this paper.

Damped-type longer period (Pc4) pulsations are excited at the plasmapause during impulses (Lanzerotti et al. 1973,

Fukunishi 1979). They seldom reach middle latitudes (Verő 1975). ULF emissions of different types (Pc1, Pi1) are also excited simultaneously with SI-s or after a delay of a few minutes, or the characteristic period of such existing emissions changes at the time of SI-s. Hirasawa (1981) found such enhancements after positive SI-s, Olson and Lee (1983) and Kangas et al. (1986) did not discriminate SI-s of different sign in similar studies. Allan et al. (1985, 1986) discussed impulse-excited cavity and field line resonances in the magnetosphere, but these pulsations differ essentially from the here discussed ones by having longer periods and occurring at higher latitudes. However, a propagation to lower latitudes with local resonant periods cannot be excluded here. Pulsations associated with flux transfer events (Gillis et al. 1987) are connected to geomagnetic variations other than SI.

2. BASIC MATERIAL

The basic material for the investigations was a list of SI-s selected on a routine basis for the years 1979-1983 as discussed in Section 3. Interplanetary medium data for this rather high geomagnetic activity period are available (King 1986). Only SI-s recorded on quick-run earth current records were used, making a total of 237 events. Pulsation data were taken from the quick-run records: a part of the data is from the pulsation catalogue compiled on a routine basis, others from a re-evaluation to achieve better time resolution. In 15 minute intervals before and after the SI, the amplitude of pulsations have been determined using the same method as for the catalogue. Thus for these periods before and after the SI, the active period ranges were selected (0-5, 5-10, 10-15, 15-20, 20-25, 25-30, 30-40, 40-60, 60-90, 90-120 s, 2-5 and 5-10 min), and to each active range, an amplitude value has also been attributed.

Based on experience of about 30 years with these pulsation data, we consider spectra obtained from 50-100 hours of data as stable, i.e. comparable with each other. In case of spectra

from subsequent hours (e.g. before and after an SI), spectra obtained from 10 and 20 events may be compared, too, as here the spectra are less influenced by changes in the subjective estimation.

3. DEFINITION OF SI-S USED IN THIS PAPER

In the present investigation SI-s listed in the Reports of Nagycenk Observatory (47.2^{o}) were used for the years 1979-1983. As SI-s are selected for these Reports by a criterion differring from the generally accepted one, it should be discussed in some details.

There is only a rather vague internationally accepted criterion for selecting SI-s, namely "SI-s are impulses which cannot be qualified as SSC-s". In Nagycenk we use instead of this the following one: "An SI is a geomagnetic impulse which is clearly distinguishable from its surroundings, has a duration of about 5-10 minutes and after it, the pre-SI level of the geomagnetic field returns." This definition excludes many storm-time impulses, but includes smaller ones in quiet intervals. The difference of SI-s and SSC-s lies mainly in the return of the field to the pre-event level.

Okamoto and Fujita (1987) published a list of 479 SI-s and 789 SSC-s from the observatory Kakioka for the years 1957-1985. The amplitude distributions of these events and of the Nagycenk SI-s are given in Table I.

These figures show that Kakioka is cautious with small amplitude SI-s. In Nagycenk, there are considerably more SI-s in the low amplitude category (but the percentage is less than for Kakioka SSC-s which can be more easily distinguished especially with a lower noise level at lower latitude), but the large amplitude events lack in Nagycenk due to the criterion that they should be clearly distinguished from the surroundings.

There are even more significant differences in SI-s discussed by different authors. So e.g. from 6 SI-s mentioned in papers cited in the Introduction, only one appears in the Nagycenk list, and even from the 5 used by Tátrallyay and Verő (1973)

Table I. Distribution of SSC and SI amplitudes at Kakioka and Nagycenk

Amplitude	Distribution in percents Kakioka SSC	Kakioka SI	Nagycenk SI
0-10 nT	42	10	27
10-30 nT	42	63	70
30-50 nT	12	21	3
50 nT	4	6	<1
Number of events/year	28	17	50

(from Nagycenk records), only 3 are listed.

The justification for using the Nagycenk list lies in the fact that it is quite homogeneous, at least during the interval studied and it is thought to be nearly complete as it is made from lists compiled from magnetic and earth currents records independently. Further justification is derived from a comparison of changes between the pre- and after-event hours (i.e. in 2 hours) of the interplanetary parameters V and |B| after Nagycenk SI-s (N = 237) and a similar set of random times. Table II shows the results of this comparison.

Table II. Signatures of SI-s and similar values in the random sample

Percents of all events	SI-s	random sample
a) $\Delta\|B\| > 2$nT	30	3
b) $\Delta V > 20$ km/s	30	11
a and b simultaneously	49	13
average $\Delta\|B\|$	$\pm$2.2 nT	$\pm$1.45 nT
average ΔV	$\pm$25.4 km/s	$\pm$8.0 km/s
c) $\Delta\|B\| > 1$ nT and $\Delta V > 10$ km/s simultaneously	76	45

The values indicate that SI-s selected in Nagycenk are accompanied by realistic changes in interplanetary parameters, the average changes in |B| being 1.5 times, in V three times more than in case of a random sample.

On the basis of the present investigation and the data presented in this section, the Nagycenk list of SI-s represents a set of geomagnetic variations which does not correspond to the generally accepted SI-s as it includes significantly more small amplitude and less large amplitude events, it is, however, rather homogeneous and indicates occasions when interplanetary parameters change more quickly than normal.

4. CHANGES OF THE PULSATION ACTIVITY AROUND SI-S

In the present paper pulsations activities are compared during a longer time interval (1 hour) before and after the SI event. The immediate effect of the SI (Hirasawa-effect) is not considered. Thus, pre- and post-shock interplanetary conditions are compared from the point of view of pulsation excitation. In case of "normal" conditions, the dependence of the pulsation activity on IMF parameters is rather well known (e.g. Verő 1986), the |B|-dependence of the position of the peak in the pulsation spectrum can be approximated by $T = 160/|B|$. This approximation is used for comparison throughout the paper.

4.1 Changes of parameters |B| and Θ, and the change in the pulsation activity

A) As the first step of the investigation, |B| values of the hours (n-1) and (n+1) were compared. The limit for a change in |B| was chosen in 20 percent, of the value of the hour (n-1) thus the following three groups were obtained:

a) increasing |B| (48 events)

b) decreasing |B| (48 events)

c) unchanged |B|, 141 events, about 60 percent due to a rather severe selection criterion in a and b. Results are presented in Fig. 1 both for the amplitudes and occurrence frequencies of the 12 period ranges listed in Section 2. The

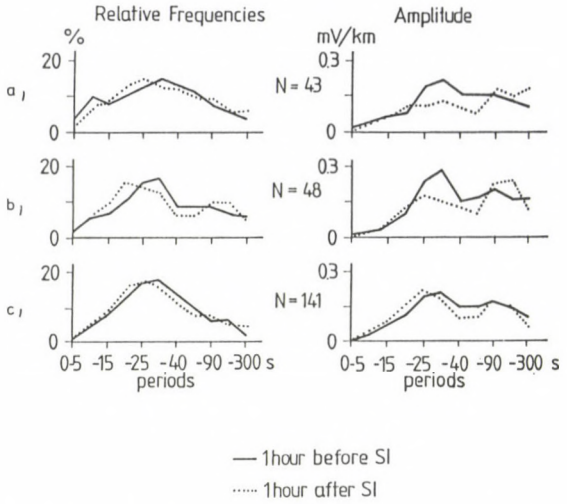

Fig. 1. Changes of the pulsation spectra after SI-s, left: relative occurrence frequency spectra, right: amplitude spectra, first row: |B| increased by more than 20 percent, second row: |B| decreased by more than 20 percent, third row: the change in |B| is less than 20 percent. In Figs 1-4, the error of an average relative occurrence frequency G can be easily obtained from 2N half-hourly occurrence values (0 or 100) as $\mu_G = \sqrt{G(1-G)/2N}$, being here 3-10 percents. These values are, however, overestimated from the point of view of a difference corresponding to adjacent period ranges, as these values are strongly correlated

peak of the occurrence frequency shifts in all cases to shorter periods, in the cases a and c, from 27 to 22, and in the case b, i.e. when |B| is decreasing, from 27 to 17 s. The latter shift is just opposite to what was expected, as according to the proportionality between f and B (f = 1/T = 6B), in this case longer periods would appear. In the amplitudes there is a drop in the Pc3-4 range if |B| does change, else they are essentially constant irrespecting a shift in the peak period similar as in the case of the occurrence frequencies. The drop is in both cases (a and b) about 30-40 percent, in the case c there is a slight amplitude increase of less than 10 percent. Outside the Pc3-4 range, the changes around SI-s are insignificant.

B) In the case of the cone angle of the IMF (i.e. the angle between the Earth-Sun direction and the direction of the IMF), only "advantageous" (A, less than 45^{o}) and

"disadvantageous" (D, more than 45^{o}) ranges have been separated. Transitions A-D and D-A occur in 12 percent of all cases, A-A in 20 percent, and 56 percent belongs to D-D. The pulsation activity shifts towards somewhat shorter periods in the cases A-A and D-D (Fig. 2), the height of the peak of the spectrum does not change significantly (naturally, in the D-D case, the pulsation activity is much lower). In the D-A case, there is a drop of the amplitudes by about 20 percent, in the A-D case this drop amounts to about 40 percent. Here the drop in the D-A case is inexpected, as a turn of the IMF to an advantageous direction should result in an increase of pulsation amplitudes.

The results of Sections A and B can be summarized as follows: after SI-s, the average pulsation activity changes in two respects: periods get shorter and amplitudes smaller. The first

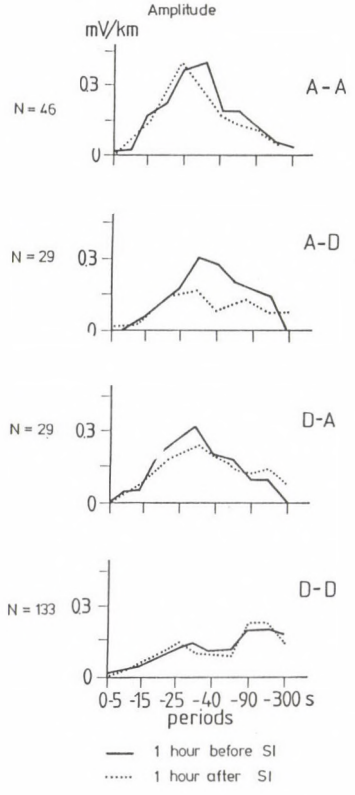

Fig. 2. Changes of the amplitude spectra of pulsations after SI-s with different changes in the cone angle (A means advantageous, D disadvantageous cone angle)

is true for all types of IMF-changes studied, the second, the amplitude drop appears only if any of the interplanetary parameters has significant changes simultaneously with the SI. Any kind of changes in these parameters resulted in a drop of the amplitude in the hour following the SI.

C) As it has been found that the actual values of the IMF parameters do not play a significant role in determining the changes of the Pc3-4 activity around SI-s, only the fact counts if these parameters did change, another, non-IMF parameter, namely the amplitude of the SI-s has also been studied. Daytime events have been divided into three groups with electric amplitudes less than 5; 5-10 and more than 10 mV/km, corresponding to magnetic amplitude limits of 10 and 20 nT. As here only daytime events have been considered, the number of events is less, but even in the third group it is 23. Figure 3 shows the results: in the small amplitude group, there is an activity maximum in the Pc3-4 range which drops after the SI by about 40 percent. The spectrum has a similar shape before medium amplitude SI-s, but there is no significant change after the SI. In the case of the large SI-s, the spectrum is different even

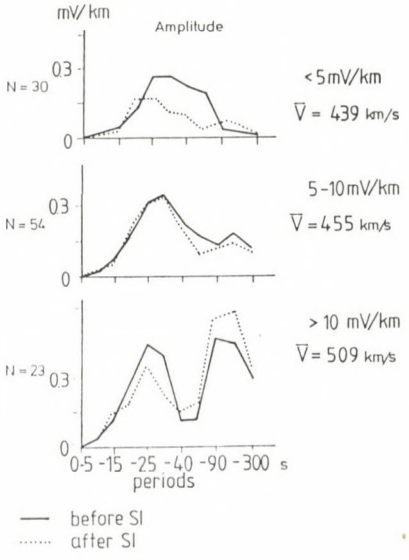

Fig. 3. Changes of the amplitude spectra of pulsations after SI-s of different amplitude (amplitudes in the electric field less than 5, 5-10 and more than 10 mV/km). Average solar wind velocities are indicated, too

before SI-s: there is a strong peak in the long period, Pc5 range which gets even more accentuated after the SI, as the Pc3-4 peak decreases, the Pc5 peak increases.

These results suggest that very small amplitude SI-s are physically different from larger ones as they cause a strong decrease in the Pc3-4 activity (even 1 h after the SI).

4.2 Connections between the trend of interplanetary parameters and pulsation spectra around SI-s

As the investigations described in Section 4.1 did not result in an unambiguous connection between changes of the IMF and those of the pulsation spectra after SI-s, a second investigation has been carried out based on the trends of all interplanetary parameters in King et al's (1986) book. The trends have been taken from the graphical representations, and disturbed sections and spikes around SI-s were separated as independent groups. In the following only a few typical examples are chosen for illustration.

A) If V increases in the time interval around the SI, Pc3-4 activity decreases sharply after the SI, while Pc5 activity increases. If the SI occurs in a decreasing V-period, then the pulsation activity shifts to shorter periods and it is damped after the SI, too. If there is no change in V around the SI, the activity of the pulsations hardly changes (Fig. 4 left).

Thus the change of the Pc3-4 activity is in no relation to the change of V around the impulse. If V changes, the pulsation activity decreases independently of the sense of the change in V. Else the pulsation activity remains at a constant level, too.

B) The situation is similar with the trends in $|B|$. The maximum shifts toward shorter periods both if $|B|$ decreases or increases (Fig. 4 right). Here occurrence frequency spectra are shown, as they express better these period changes. The change of the amplitudes is insignificant.

C) In case of all other parameters, the results are generally similar to the previous ones. If there is some change in any of the interplanetary parameters around the SI, then the pulsation activity decreases after it. If the change is abrupt,

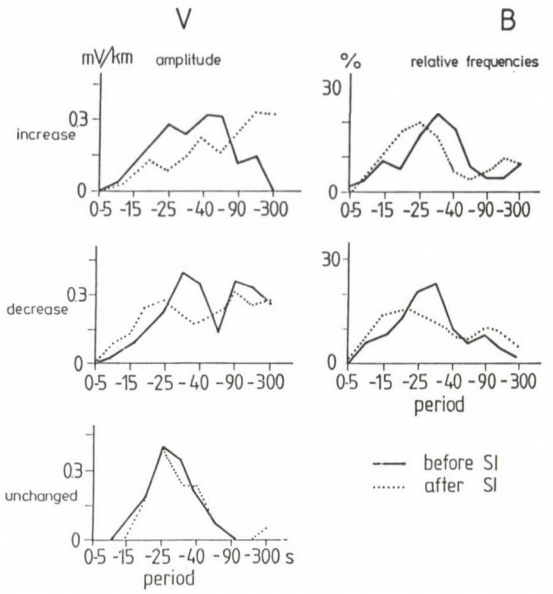

Fig. 4. Changes in the spectra of pulsations, if V and |B| had different trends in a time interval of a few hours (left: for V, amplitude spectra, right: for |B|, occurrence frequency spectra)

e.g. in the case of spikes in the B_z-component, the decrease of the pulsation amplitudes may reach a factor of three. If the parameter does not change or if it is disturbed, then the pulsation activity decreases slightly or remains after the SI at the same level where it had been earlier.

5. PULSATION ACTIVITY AND IMF PARAMETERS AROUND TWO CHARACTERISTIC SI-S

Figure 5 shows the analogue record, amplitude and dynamic spectra (component E_y) of an SI-event (Event 1) on December 8, 1979, from 0830 UT. The three main parameters of the interplanetary medium are given in Table III for this event. Solar wind velocity and cone angle did not change significantly, whereas |B| increased from 3 to 11 nT. The dynamic and amplitude spectra show that before the SI, there is pulsation activity with periods of about 60 s, corresponding to the actual |B|

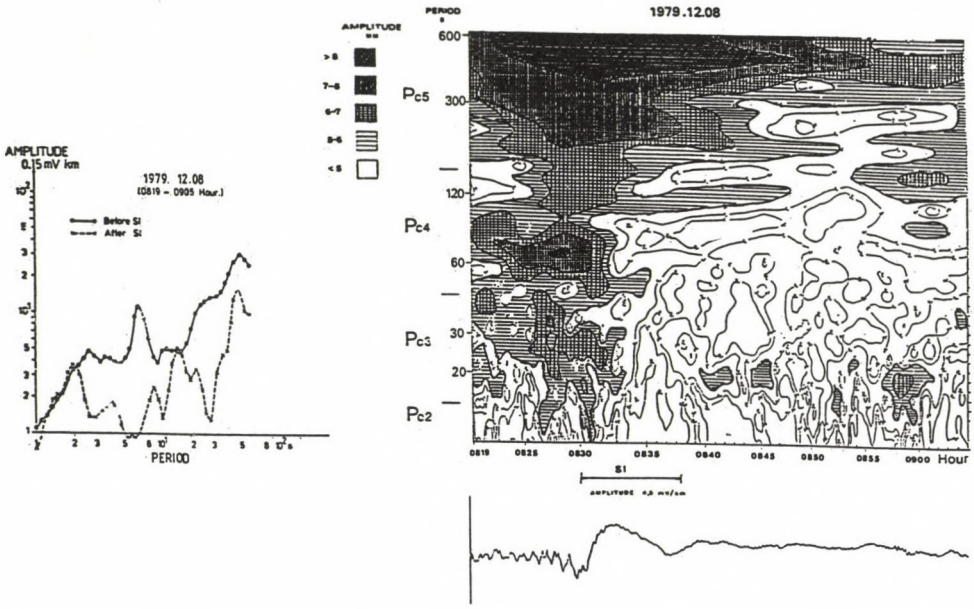

Fig. 5. Changes of the pulsation spectra around Event 1 on December 8, 1979. Left, amplitude spectra from digital records before and after the SI, right bottom, the analogue record (E_y, the left side line is 10 mV/km), right top, dynamic spectrum of the event with the same time scale as the analogue record. Isolines are drawn for amplitudes corresponding to exponents of 2, i.e. the amplitude increases between two isolines by a factor of 2 (E_y component)

Table III. Interplanetary parameters around the December 8, 1979, SI

	Before	During the SI	After	
|B|	2.9	11.1	10.6	nT
V	323	326	359	km/s
Θ	37	39	50^{o}	

value (160/2.9 ≈ 55), after the SI, the 18 s peak corresponds again rougly to the IMF magnitude (160/10.6 ≈ 15 s). The drop in the pulsation amplitudes starts around 0832 in the short period part, and after a switch-off, some activity appears

again at 0840, but with rather low amplitudes. In the Pc4 range, the switch-off is at least for the time interval studied final. In the Pc5 range, maximum amplitudes are experienced during the SI, afterwards the activity is low.

The other event (Event 2, March 16, 1981) is presented in Fig. 6, with the same kinds of data. IMF data are for this event in Table IV.

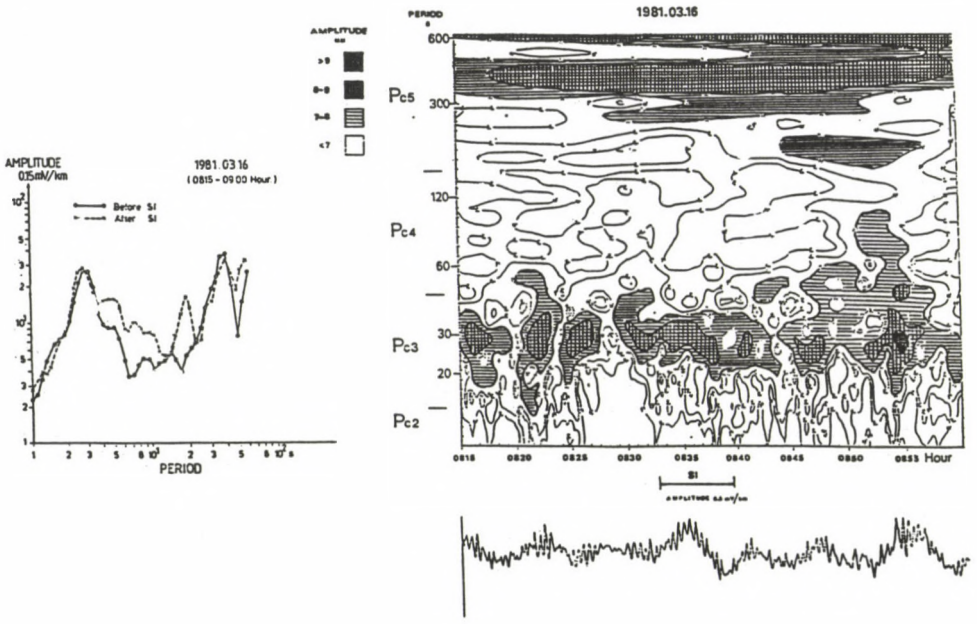

Fig. 6. The same as Fig. 5, but for Event 2 (SI of March 16, 1981)

Table IV. Interplanetary data around the March 16, 1981, SI

	Before	During the SI	After	
$\|B\|$	6.4	6.8	6.4	nT
V	560	549	538	km/s
Θ	43	15	8^{o}	

Among the IMF-parameters, only Θ changes significantly at the SI; it may be that this change from a rather disadvantageous direction of the IMF before the SI to an advantageous one after it balances the amplitude drop at the time of the SI. Namely as the dynamic spectrum shows, the pulsation activity remains constant during the whole time interval with a peak slightly longer (28 s) than that corresponding to the $|B|$-value ($160/6.4 \approx 25$ s). This period did not change during the event. The peak in the Pc5-range (400 s) had similarly rather constant amplitudes. (The SI-event was identified originally on the E_x-record, where the amplitude peaks in a value several times greater than before and after it; analogue records and dynamic spectra are shown here for the E_y component, where the pulsation activity is stronger). This latter fact deserves special attention, it means that both before and after the SI, there is a rather high amplitude Pc5 activity which continues without interruption similarly to the Pc3 activity.

6. DISCUSSION

Geomagnetic impulses have a very complex effect on pulsations. In the introduction some of these effects have been mentioned e.g. the Hirasawa-effect (shortening of Pc5 periods during the impulse), several effects on short period pulsations and the switching of Pc3-4 type activities. Both the statistical material and the examples of events presented here could only show the effects on Pc3-5; however, the investigation did not cover specially the Hirasawa-effect (Event 2 did not show it, for Event 1, see later). Concerning the effect of the changes in the solar wind-parameters simultaneously with the SI, it is evident that such a change is a precondition for any effect in the pulsation spectrum. This is clearly shown by Event 2, where the solar wind parameters change slightly, and there is no effect in the pulsation activity. If, however, there is a significant change in any of the solar wind-parameters V, $|B|$ or Θ, then the SI causes a switch-off of the pulsations; afterwards in some minutes pulsations may reappear, but

generally with shorter periods. The shortening of the period is independent of the sign of the change say in $|B|$, thus after the impulse the activity does not correspond always to that expected on the basis of the actual IMF-parameters, some "transitory" activity appears. This transitory pulsation activity will be investigated in a future paper.

There is an important point which needs clarification: what is the character of the SI-s like Event 2? In that connection it is to be reminded that such SI-s occur mostly in time intervals when both before and after the SI some Pc5 activity exists (as in the rather extreme case of Event 2 the situation is). We suppose that in such cases the SI is a sudden enhancement of a Pc5 activity due to the immediate effect of the Kelvin-Helmholtz instability. This would explain why there is no effect on Pc3-4 pulsations which originate from a different (upstream) source, further perhaps the result in Fig. 3, too, where for small SI-s, a strong decrease was found, less for larger SI-s. The small SI-s are accordingly mostly due to changes in solar wind parameters. SI-s due to an enhancement of the K-H instability are more often in the medium group, as small enhancements cannot be distinguished from background activity (which is present around such events, but absent around events originating in the solar wind). The large SI-s are again mostly of solar wind origin, they are what is normally called SI, i.e. SSC-s without subsequent storm. This conclusion is to be checkd by interplanetary data of higher time resolution.

It is to be added to these considerations that the pulsation activity is deviating from normal even before the SI. Moreover, as in case of Event 1, there is a precursor of the SI (e.g. Pc3-5 activity increased about 5 minutes before the SI extending to period ranges not active previously). That is why it is difficult to tell if there is any period change in the Pc5-range according to the Hirasawa-effect. The situation is somewhat similar in the second group of SI-s, too, as here the pre-existing Pc5-activity is a signal for the possibility of the excitation of KH-instability.

Summarizing SI-s have rather important effects both on the

activity and the spectrum of pulsations. We do not consider impossible that impulses play a very important role in the excitation of the Pc3-4 pulsations, too, as implicitely supposed by Allan et al. (1985, 1986) and Gillis et al. (1987), even if for other types of long period geomagnetic variations.

REFERENCES

Allan W, Poulter E M, Junginger H 1985: Planet. Space. Sci., 33, 159-173.

Allan W, Poulter A M, White S P 1986: Planet. Space. Sci., 34, 1189-1200.

Fukunishi H 1979: J. Geophys. Res., 84, 7191-7200.

Gillis E J, Rijnbeek R, Kling R, Speiser T W, Fritz T A 1987: J. Geophys. Res., 92, 5820-5826.

Hirasawa T 1981: In: Memoirs of National Institute of Polar Research. Tokyo, March, 127-151.

Hirasawa T, Nishida A, Nagata T 1966: Rept. Ionosph. Space. Res. Japan, 20, 51-56.

Kangas J, Aikio A, Olson J V 1986: Planet. Space. Sci., 34, 543-553.

King J H 1986: Interplanetary medium data book 1977-1985. National Space Data Center, NASA

Lanzerotti L J, Fukunishi A, Hasegawa A, Chen L 1973: Phys. Rev. Lett. 31, 624-628.

Okamoto A, Fujita S 1987: In: Memoirs of the Kakioka Magnetic Observatory, 22, 21-23.

Olson J W, Lee L C 1983: Planet. Space. Sci., 31, 295-302.

Reports of the Nagycenk Observatory, 1979-1983. Geodetic and Geophysical Research Institute, Sopron

Sen K 1968: J. Geomagn. Geoelect. 20, 225-243.

Tátrallyay M, Verő J 1973: J. atmos. terr. Phys., 35, 1507-1513.

Troitskaya V A, Gul'elmi A V 1967: Space Sci. Rev., 7, 689-695.

Troitskaya V A, Schepetnov P V, Gul'elmi A V 1968: Geomagnetizm i Aeron., 9, 363-366.

Veldkamp J 1960: J. atmos. terr. Phys., 17, 320-324.

Verő J 1975: Acta Geod. Geoph. Mont. Hung., 10, 247-253.

Verő J 1986: J. Geophys., 60, 106-119.

Acta Geod. Geoph. Mont. Hung., Vol. 24 (3-4), pp. 385-393 (1989)

EXPANSION OF TRIGONOMETRIC FUNCTIONS IN TERMS OF SPHERICAL HARMONICS

A Hajósy

Department of Geophysics, Eötvös University, H-1083 Budapest,
Kun Béla tér 2, Hungary

[Manuscript received May 12, 1988]

The expansion of a data set into surface spherical harmonics is a rather time-consuming problem in computer terms. The expansion presented in this paper reduces this computer time by orders of magnitude.

Keywords: Fourier expansion; spherical harmonics

INTRODUCTION

In processing results of measurements, the data are usually approximated by partial sums of series expansions. The expansion is chosen in conformity with the physical meaning of the data, while the approximation is done normally by a least-squares fitting. It may occur, however, that this numerical problem can be solved much more simply by using another expansion which is not directly related to the physics of the problem. If it is known how the terms of this latter series can be expanded into the previous one, then the calculation of the coefficients can be significantly simplified.

This simplification is summarized in the following. Let the values of the function f be known at the points x_i. Then, with a set of functions $\{p_n\}$ which corresponds to the physical meaning of the problem, the coefficients of the expansion

$$f(x) \approx \sum_{n=0}^{N} u_n \cdot p_n(x)$$

are calculated using the weighting function r and the

least-squares principle

$$\sum_i r(x_i) \cdot \left[\sum_{n=0}^{N} u_n \cdot p_n(x_i) - f(x_i) \right]^2 = \text{minimum} .$$

Now suppose that the same problem is numerically much simpler with some other set of functions $\{q_n\}$ and a different weight s. Consider the functions $\{q_n\}$ as linear combinations of the members of set $\{p_n\}$:

$$q_n(x) = \sum_{k=0}^{n} a_{nk} \cdot p_k(x) , \qquad a_{nn} \neq 0, \qquad n = 0, 1, \ldots .$$

The required coefficients $\{u_n\}$ can be obtained from the numbers a_{nk} in the following way. First the coefficients $\{v_n\}$ corresponding to the set $\{q_n\}$ are obtained:

$$f(x) \approx \sum_{n=0}^{N} v_n \cdot q_n(x) ,$$

where

$$\sum_i s(x_i) \cdot \left[\sum_{n=0}^{N} v_n \cdot q_n(x_i) - f(x_i) \right]^2 = \text{minimum} .$$

The coefficients $\{u_n\}$ are calculated as linear combinations of v_n and a_{nk}:

$$u_k = \sum_{n=k}^{N} v_n \cdot a_{nk} , \qquad k = 0, 1, \ldots, N ,$$

since

$$\sum_{n=0}^{N} v_n \cdot q_n(x) = \sum_{n=0}^{N} v_n \cdot \sum_{k=0}^{n} a_{nk} \cdot p_k(x) = \sum_{k=0}^{N} \sum_{n=k}^{N} v_n \cdot a_{nk} \cdot p_k(x) .$$

Many geophysical quantities (e.g. the stationary part of the geomagnetic field, geoid heights, topography of the Earth) can be expressed by expansion into surface spherical harmonics. Their use is justified by the fact that the spherical harmonics are particular solutions to Laplace's equation.

The present paper is a study of the relationship between the surface harmonic expansion and the classical Fourier series. Approximating a data set by Fourier series is a simple problem from the numerical point of view. This is not true, however, for the surface spherical harmonic approximation. Very long computer time as well as accuracy problems arise owing to the complexity of the spherical functions. If, however, the terms of the Fourier series can be expanded into surface spherical harmonics, then, following the reasoning presented above, the coefficients of the spherical harmonic expansion can be given as linear combinations of the Fourier coefficients.

FOURIER EXPANSION OF THE SURFACE SPHERICAL HARMONICS

The domain of definition of the surface spherical harmonics is the unit sphere. They can be defined in various ways. Their construction with a linear combination of the sine and cosine functions will be treated here. The set of spherical surface harmonics with the usual notation is:

$$\left\{1,\ P_n^0(\cos\varphi),\ \cos m\lambda\ P_n^m(\cos\varphi),\ \sin m\lambda\cdot P_n^m(\cos\varphi)\right\}_{n=1\ m=1}^{\infty\quad n}, \tag{1}$$

$$\varphi\in[0,\pi],\qquad \lambda\in[0,\ 2\pi).$$

The elements of set (1) are linearly related to the elements of the following subset of the two-variable Fourier system:

$$\left\{1,\ \cos n\varphi,\ \cos 2n\lambda\cdot\cos n\varphi,\ \sin 2m\lambda\cdot\cos n\varphi,\right.$$
$$\left.\cos(2m-1)\lambda\cdot\sin n\varphi,\ \sin(2m-1)\lambda\cdot\sin n\varphi\right\}_{n,m=1}^{\infty}, \qquad (2)$$
$$\varphi\in[0,\pi]\quad,\quad \lambda\in[0,\ 2\pi)\ .$$

It is to be noted that both (1) and (2) represent a full orthogonal set on the unit sphere $\varphi\in[0,\pi]$, $\lambda\in[0,\ 2\pi]$ with the weighting functions $\sin\varphi$ and 1 (=identity), respectively.

The functions of (1) and (2) show that the linear relationship requires only the Fourier coefficients of the single-variable functions P_n^m:

$$P_n^m(\cos\varphi) = \sum_{k=0}^{n} \alpha_{nk}^{m} \begin{cases} \cos k\varphi, & \text{if } m \text{ is even,} \\ \sin k\varphi, & \text{if } m \text{ is odd.} \end{cases} \qquad (3)$$

The simplest way to express α_{nk}^{m} is a recursion which progresses with increasing m:

$$\alpha_{nk}^{m} = (-1)^{m-1}\ 2k\cdot\alpha_{nk}^{m-1} + (n+m-1)\ (n-m+2)\cdot\alpha_{nk}^{m-2}\ , \qquad (4)$$
$$m = 2,\ 3,\ \dots\ ,$$

$$\overset{0}{\alpha}_{nk} = \begin{cases} 0, & \text{if } n+k \text{ is odd,} \\ 2^{1-2n}\cdot\binom{n-k}{\frac{n-k}{2}}\binom{n+k}{\frac{n+k}{2}}, & \text{if } n+k \text{ is even, } k\neq 0, \\ 2^{-2n}\binom{n}{\frac{n}{2}}^{2}, & \text{if } n \text{ is even, } k=0\ . \end{cases} \qquad (5)$$

$$\alpha_{nk}^{1} = k\cdot\overset{0}{\alpha}_{nk} \qquad (6)$$

The recursive relationship (4) together with the initial conditions (5) and (6) determines uniquely the coefficients α_{nk}^{m}. The law (4) is directly obtained from the recursion law

of the spherical functions (Heine 1878):

$$P_n^m(\cos\varphi) = -2\cdot\frac{dP_n^{m-1}(\cos\varphi)}{d\varphi} + (n+m-1)\,(n-m+2)\cdot P_n^{m-2}(\cos\varphi)\ .$$

The initial conditions (5) and (6) are identical to well-known formulas.

SPHERICAL HARMONIC EXPANSION OF THE TERMS OF FOURIER SERIES

This expansion is far more complicated than the above-mentioned inverse problem. In the early years of this century, Schuster (1903) investigated this question with the aim of simplifying the numerical calculations. He expressed the trigonometric functions as infinite series of spherical harmonics:

$$\left.\begin{matrix}\cos n\varphi\\ \\ \sin n\varphi\end{matrix}\right\} = \sum_{k=n}^{\infty} b_{nk}^m\cdot P_k^m(\cos\varphi)\ , \qquad \begin{matrix}\text{if m is odd,}\\ \\ \text{if m is even.}\end{matrix}$$

He published explicit formulas for the coefficients b_{nk}^m (Schuster 1903). In the same paper he warned that these series expansions, being infinite, should be used with great care in numerical approximations. Since then, authors dealing with the geomagnetic field have often discussed this problem (Schmidt 1938, Fanselau 1959), especially the question of convergence of Schuster's expansion.

The present paper will give a similar "complementer" expansion:

$$\left.\begin{matrix}\cos n\varphi\\ \\ \sin n\varphi\end{matrix}\right\} = \sum_{k=0}^{n} a_{nk}^m\cdot P_k^m(\cos\varphi)\ , \qquad \begin{matrix}\text{if n is even,}\\ \\ \text{if m is odd.}\end{matrix} \qquad (7)$$

First of all the number of terms used in (7) is to be considered. Let m be a fixed, positive, even number. The subset (8) of the spherical harmonics of the order m contains linearly

independent functions, since $\alpha^{m}_{nn} \neq 0$:

$$\left\{ P^{m}_{n}(\cos\varphi) = \sum_{k=0}^{n} \alpha^{m}_{nk} \cos k\varphi \right\}_{n=m}^{N} . \tag{8}$$

It is to be noted that, if $n < m$, $P^{m}_{n}(\cos\varphi) \equiv 0$ as a definition.

The subset (8), composed of the spherical harmonics of the order m up to degree N, has (N-m+1) elements: On the other hand, the definition shows that these functions can be expressed as linear combinations of (N+1) linearly independent cosine functions. Therefore the set (8) can be suitably completed with m additional cosines to obtain a new set with (N+1) independent elements:

$$\left\{ P^{m}(\cos\varphi), \quad \cos j\varphi \right\}_{n=m,\ j=0}^{N \quad m-1} .$$

The spherical harmonics of odd order can be similarly completed with properly chosen sine functions.

Now the sine and cosine functions are expanded as linear combinations of the new, complete sets in the following way:

$$\left.\begin{matrix} \cos n\varphi \\ \\ \sin n\varphi \end{matrix}\right\} = \sum_{k=m}^{n} a^{m}_{nk} \cdot P^{m}_{k}(\cos\varphi) + \sum_{k=0}^{m-1} a^{m}_{nk} \cdot \begin{cases} \cos k\varphi , & \text{if m is even,} \\ \\ \sin k\varphi , & \text{if m is odd.} \end{cases} \tag{9}$$

It can be proved that the numerical computations, final aim of this study, require only the first sum of (9), i.e. the coefficients a^{m}_{nk} with $k \geq m$. These coefficients can be calculated with a recursion law which, similarly to that explained above in the inverse problem, progresses with increasing m:

$$a^{m}_{nk} = (-1)^{m-1} \cdot \frac{2(m-1)n}{(m-2)(k+m)(k-m+1)} a^{m-1}_{nk} + \\ + \frac{m}{(m-2)(k+m)(k-m+1)} a^{m-2}_{nk} , \qquad k=m,\ m=3,\ 4,\ \ldots \tag{10}$$

$$a^{o}_{nk} = \begin{cases} 0 , & \text{if } n+k \text{ is odd,} \\ -\dfrac{2^{2k}(2k+1)n\binom{n-k}{\frac{n-k}{2}}}{(n+k+1)(n-k-1)(n+k)\binom{n+k}{\frac{n+k}{2}}} , & \text{if } n+k \text{ is even,} \end{cases} \tag{11}$$

$$a^{1}_{nk} = \frac{1}{n} \cdot a^{o}_{nk} , \tag{12}$$

$$a^{2}_{nk} = -\frac{(3k^2+3k+2)\,n}{(k+2)(k+1)k(k-1)} \cdot a^{1}_{nk} + \frac{2n^2}{(k+2)(k+1)k(k-1)}\, a^{o}_{nk} . \tag{13}$$

The recursion (10) together with the three initial conditions determines uniquely the coefficients a^{m}_{nk}. It is interesting to note that the recursion formula of the numbers α^{m}_{nk} in the inverse expansion is valid from m=2 upwards while now it is valid only from m=3. This was one of the difficulties in establishing (10).

The proof of the validity of (10) is rather lengthy and goes beyond the scope of this paper. It can be found in the author's unpublished thesis (Hajósy 1978).

APPROXIMATION OF A DATA SET WITH SURFACE SPHERICAL HARMONICS

Let $f(\varphi_i, \lambda_j)$ be discrete values of the function f defined on the unit sphere and consider the problem of approximating this function with a sum of surface spherical harmonics up to degree N. The coefficients of this sum can be calculated with the aid of expansion (9) in the following way. First the Fourier coefficients U^{m}_{n}, V^{m}_{n} are calculated:

$$f(\varphi,\lambda) \approx \sum_{n=0}^{N} \sum_{m=0}^{N} \left[U^{m}_{n}\cos m\lambda + V^{m}_{n}\sin m\lambda\right] \cdot \begin{cases} \cos^{n}\varphi , & \text{if } m \text{ is even,} \\ \sin^{n}\varphi , & \text{if } m \text{ is odd.} \end{cases}$$

The surface harmonic expansion in question is the following:

$$f(\varphi,\lambda) \approx \sum_{n=0}^{N} \sum_{m=0}^{n} \left[C_n^m \cos m\lambda + S_n^m \sin m\lambda \right] P_n^m(\cos\varphi) ,$$

where

$$C_n^m = \sum_{k=n}^{N} U_k^m \cdot a_{kn}^m ,$$

$$S_n^m = \sum_{k=n}^{N} V_k^m \cdot a_{kn}^m .$$

As a consequence of this expansion, the normal equations of the coefficients contain only scalar products of simple sine and cosine functions calculated at the points (φ_i, λ_j). In other words, there is no need to evaluate complicated spherical functions. (E.g. when 500 data are approximated by an expansion of degree 10, the computer time is reduced to one tenth. Increasing the degree of the expansion, the time reduction becomes even more significant since the time required by the trigonometric approximation is proportional to a lower power of the degree than that required by the direct spherical harmonics expansion.)

This method made it possible to carry out efficient calculations concerning the geoid and other geophysical quantities despite limitations of the available computers. These calculations support the geodynamic theory of Professor Barta.

REFERENCES

Fanselau G ed. 1959: Geomagnetismus und Aeronomie. Band III, VEB Deutscher Verlag der Wiss., Berlin

Hajósy A 1978: Approximation of data systems by surface spherical functions (in Hungarian). Thesis, Eötvös University, Budapest

Heine E 1878/1881: Handbuch der Kugelfunktionen. 2. Aufl., Berlin

Schmidt Ad 1937, 1938: Terrestr. Magnet. Atmosph. Electr. 42, 347-354; 43, 135.

Schuster A 1903: Philosoph. Transact. Roy. Soc. London, Ser. A, 200, 181-223.

Acta Geod. Geoph. Mont. Hung., Vol. 24 (3-4), pp. 395-415 (1989)

A CRITICAL REVIEW OF THE MAGNETOTELLURIC INFORMATION ON THE UPPER MANTLE

A Ádám[1] and G F Panza[2]

[1]Geodetic and Geophysical Research Institute of the Hungarian Academy of Sciences, H-9401 Sopron, POB 5, Hungary

[2]Università degli Studi di Trieste, Istituto di Geodesia e Geofisica, I-34100 Trieste, via dell'Università 7 and International School for Advanced Studies, Italy

[Manuscript received June 10, 1988]

Deep magnetotelluric soundings allow to outline two conductive layers in the upper mantle. The one closer to the surface can be quite well correlated with the low velocity layer detected by surface waves; the deeper one is much more poorly resolved and can only tentatively be associated to phase transitions. Lateral variations in electromagnetic properties seem to be present in the whole upper mantle.

Keywords: asthenosphere; deep sounding; magnetotellurics; phase transition; upper mantle

1. INTRODUCTION

It is well known that in case of magnetotellurics (MT) the resistivity distribution in the Earth's interior is determined by the time variations of the horizontal components of the electromagnetic (EM) field (E_x, E_y, H_x, H_y) of different period (Cagniard 1953). At a given period the so determined apparent resistivity is related to the penetration depth of the EM field. Using very long periods of the EM field such as the quiet daily variations (S_q) and its harmonics, the apparent resistivity at a depth of some hundred km can be calculated.

Therefore magnetotellurics represent an important research tool, to be used in combination with seismic waves analysis, for the investigation of the deep interior of the Earth. In fact, from the resistivity in the upper mantle we can infer not only its thermal properties but also variations in the physical state of the rocks, as partial melting and phase transitions. Due to the continuous increase of the temperature with

increasing depth, the resistivity decreases in the upper mantle. Furthermore the resistivity decreases in the asthenosphere due to partial melting. Finally abrupt resistivity decrements can be due to different phase transitions in the crystal structure of the mantle rocks.

2. THEORETICAL MODEL CALCULATIONS

The resolving power of MT soundings in the depth range of the asthenosphere and of the phase transitions can be studied by numerical modelling.

For the asthenosphere Vanyan and Shilovski (1979) calculated MT models. The resistivity distribution used by these authors for stable (shield) areas (1) and for mobile, orogenic belts (2) are shown in Fig. 1. Model (1) corresponds to that called by Vanyan (1980) the "normal resistivity profile". The magnetotelluric sounding curves characterized by different surface conditions, i.e. by different horizontal conductances (S_1), have been calculated for different conductance values, S_a, of the asthenosphere (S_a = 0-20000 Siemens). As shown in Fig. 2, on the MT sounding curves, the asthenosphere with its top at 90 km can already be distinguished from the normal resistivity profile in case of about 2-3 kSiemens, thus at least the depth to the top of the asthenosphere can be well determined. This is the basic idea of the IAGA ELAS (Electric Resistivity of the Asthenosphere) started in Seattle in 1977 and coordinated nowdays by an Interassociation Working Group.

The olivine-spinel (β) phase-transition can cause a conductivity rise of about one order of magnitude as demonstrated by laboratory measurements of Akimoto and Fijusawa (1965). According to these experiments our model curves in Figs 3 and 4 show resistivity decreases of one order of magnitude at the depths of 400 and 700 km. The resistivity decrease at 400 km appears on the magnetotelluric sounding curves in Figs 3 and 4 differing from the reference MT curve due to the section without phase transition. The same resistivity change at a depth of 700 km is hardly to be distinguished on the MT sounding curves.

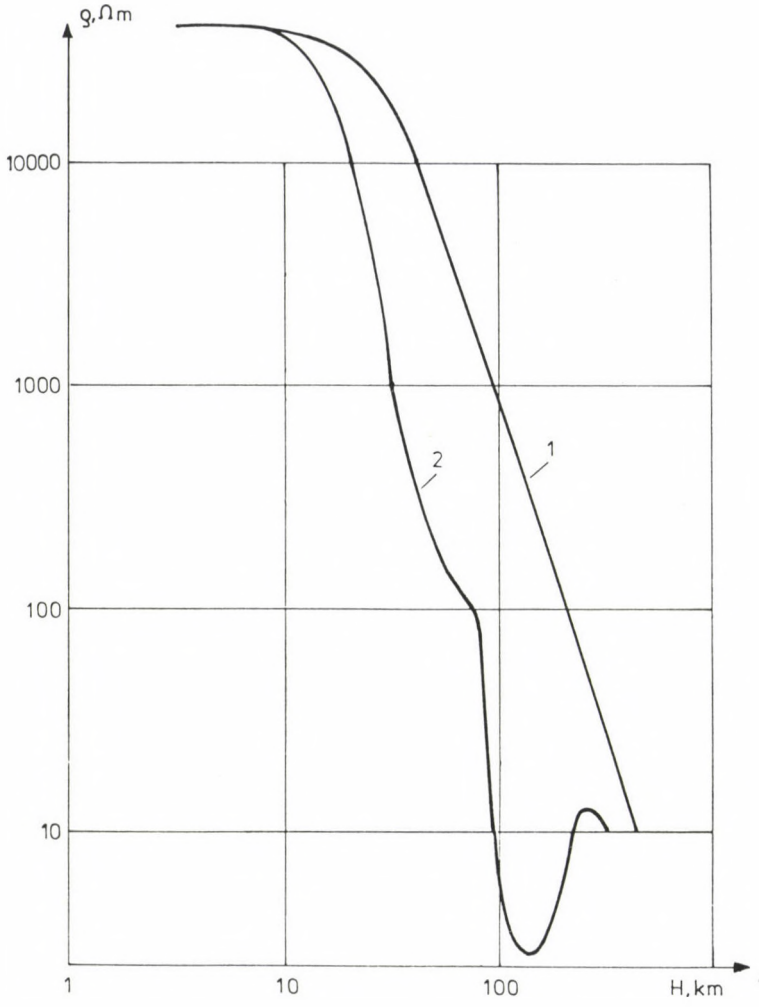

Fig. 1. Resistivity vs depth function for stable (1) and active zones (2) (Vanyan and Shilovski 1979)

These numerical calculations argue only to a certain degree with the statement of Parkinson's review (1986) concerning the efficiency of wide range magnetotellurics: "Effective probing is to a depth of the order of 200 km" because near-surface inhomogeneities, distorting the resistivity distribution deduced from the MT field data, may decrease the resolving power of the

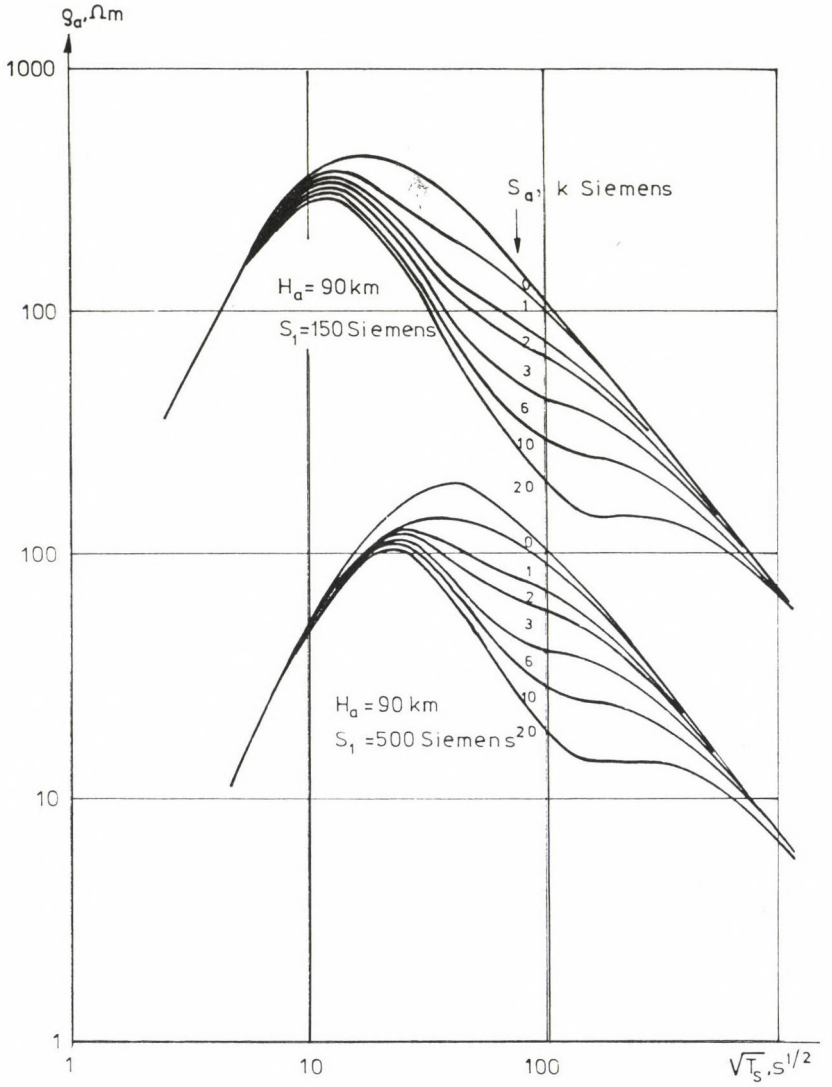

Fig. 2. Synthetic MT sounding curves for different conductance values in the asthenosphere, S_a, (Vanyan and Shilovski 1979), H_a is the depth of the top of the asthenosphere, S_1 is the surface conductance

MT method and its penetration depth. Therefore it is very important to find measuring sites for deep sounding without near surface inhomogeneities and all field distortions should be taken into account.

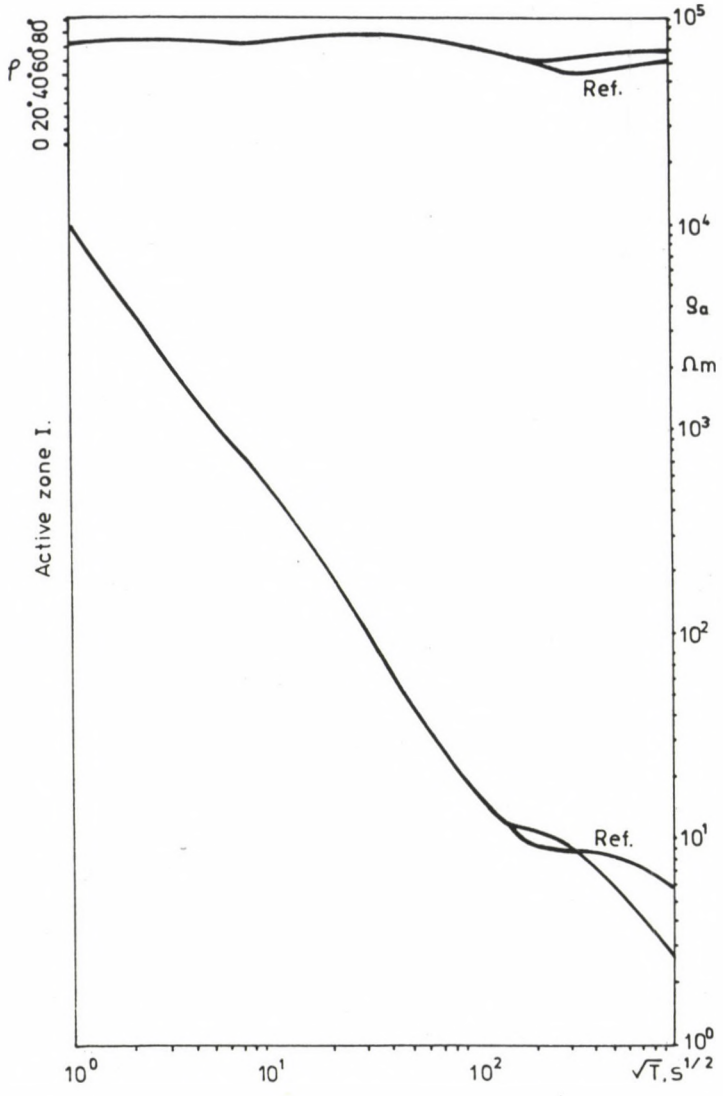

Fig. 3a. Synthetic MT sounding curves (resistivity, ϱ_a, and phase, φ) demonstrating the apparent resistivity decrease due to the phase transition at 400 km in case of active asthenosphere (see curve 2 in Fig. 1). For comparison, a reference MT curve is also given corresponding to the section without phase transition

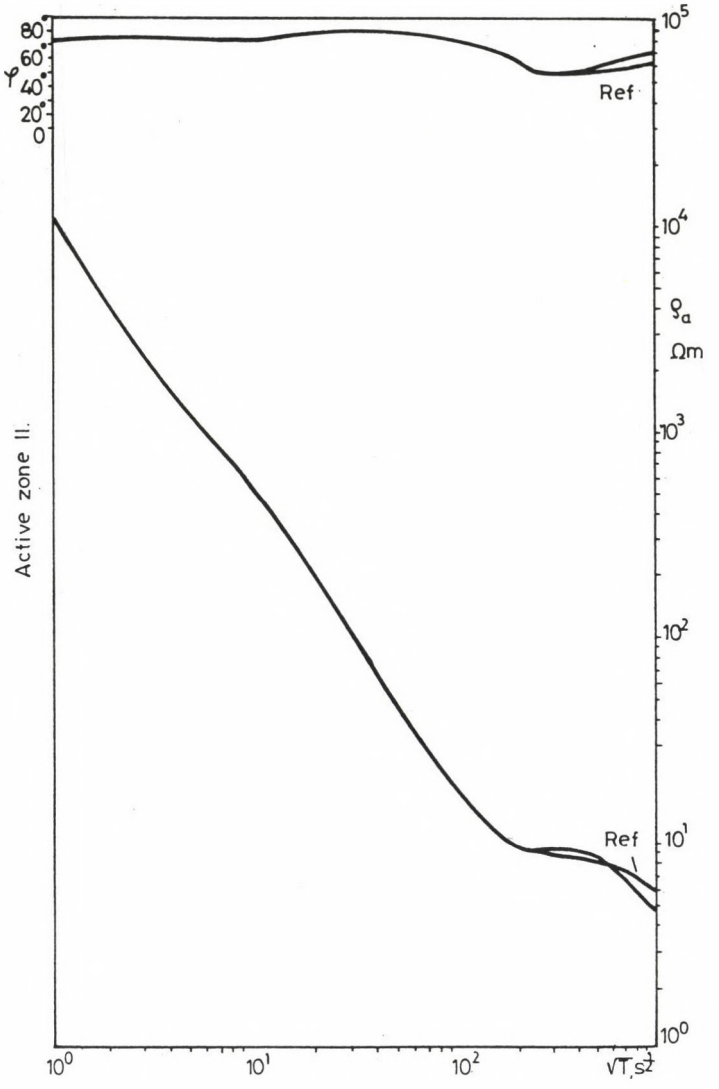

Fig. 3b. Synthetic MT sounding curves (resistivity, ϱ_a, and phase, φ) demonstrating the apparent resistivity decrease due to the phase transition at 700 km in case of active asthenosphere (see curve 2 in Fig. 1). For comparison, a reference MT curve is also given corresponding to the section without phase transition

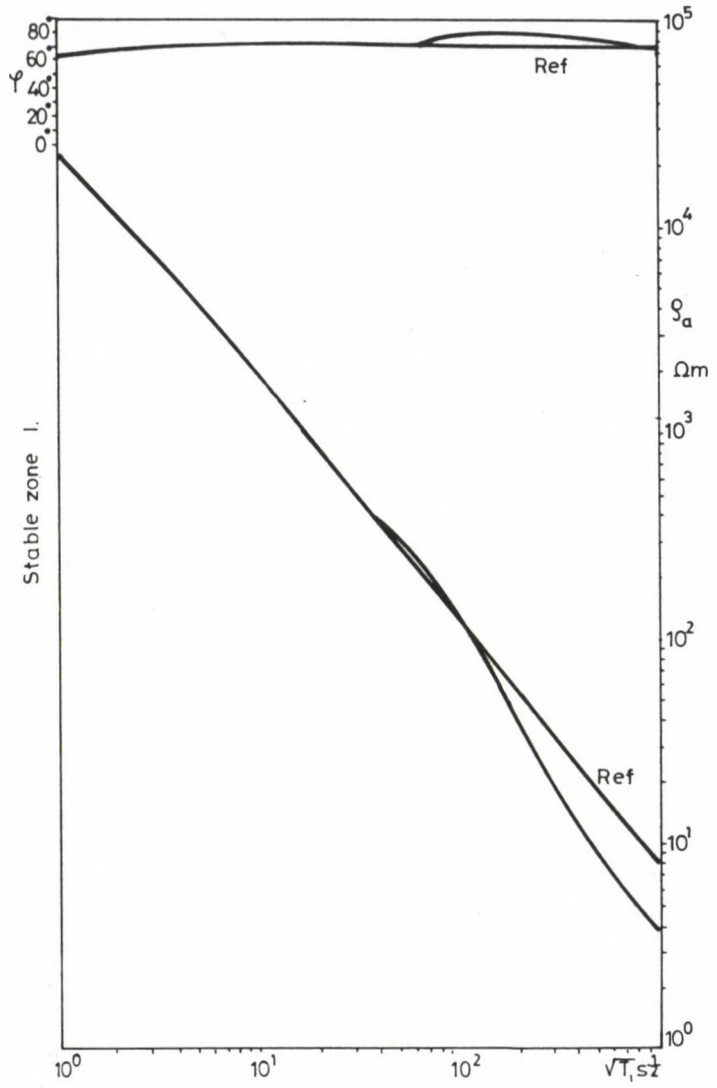

Fig. 4a. Synthetic MT sounding curves demonstrating the apparent resistivity decrease due to the phase transition at 400 km in case of stable zones without asthenosphere (see curve 1 in Fig. 1). For comparison, a reference MT curve is also given corresponding to the section without phase transition

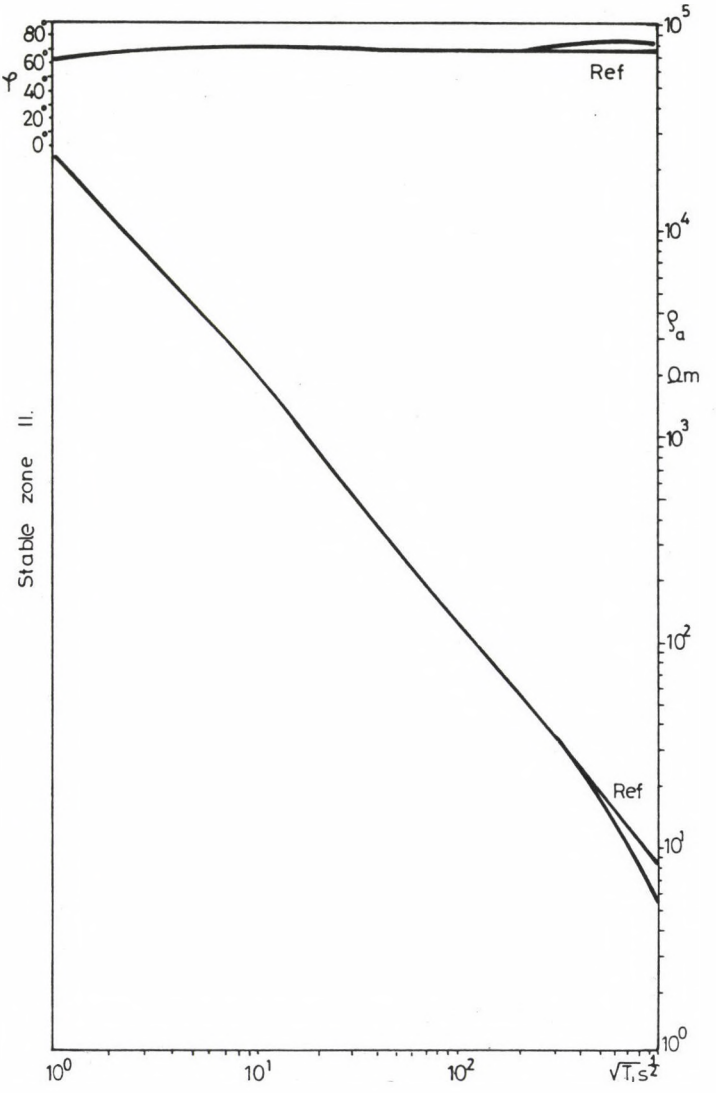

Fig. 4b. Synthetic MT sounding curves demonstrating the apparent resistivity decrease due to the phase transition at 700 km in case of stable zones without asthenosphere (see curve 1 in Fig. 1). For comparison, a reference MT curve is also given corresponding to the section without phase transition

3. CONDUCTIVITY DISTRIBUTION IN THE UPPER MANTLE ON THE BASIS OF MT MEASUREMENTS

Let us start from the MT sounding curves of the Nagycenk observatory, in the western part of Hungary, lying above 1500 m thick sedimentary layers of low resistivity (Fig. 5). The S_q variation and its harmonics were also applied to determine these curves (Ádám et al. 1981). As the anisotropy is low and there is no static shift due to changes in the sediments thickness, the extreme values of the resistivity (ϱ_{max} and ϱ_{min})

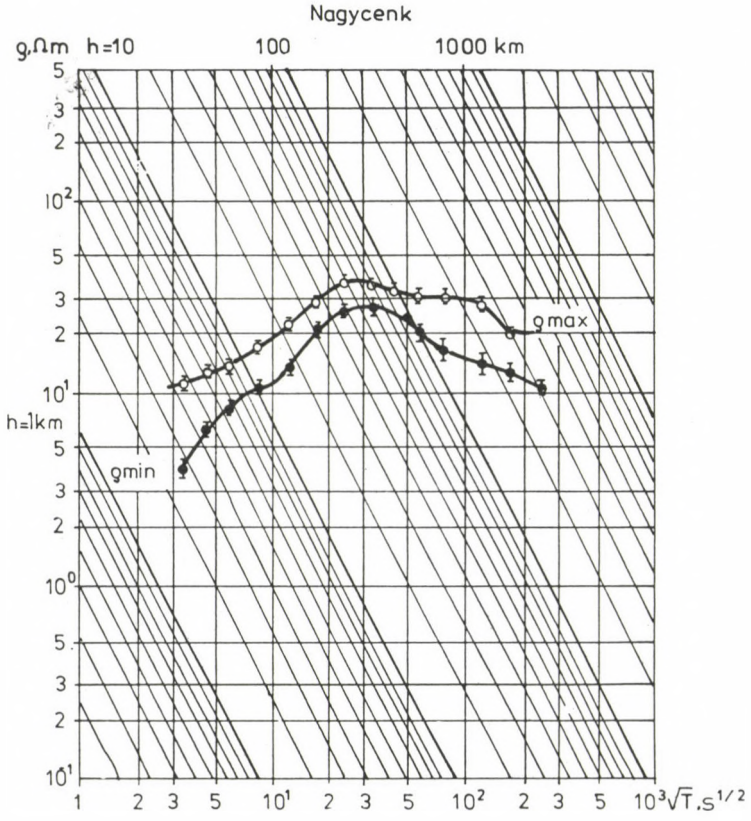

Fig. 5. Deep magnetotelluric sounding curves measured in the Nagycenk observatory (W-Hungary) (Ádám et al. 1981)

give practically the same values for the depth of the asthenosphere at about 80 km (78 and 83) and for the depth of the phase transition at about 300 km (298 and 308 km), see Table I. This table contains the horizontally stratified resistivity Earth model with the corresponding error limits. The low depth

Table I

Layer sequence corresponding to the Nagycenk magnetotelluric sounding curves. Part a) corresponds to ϱ_{min}, part b) corresponds to ϱ_{max}. Δh = thickness (km), ϱ = resistivity (Ωm), S = conductance (Siemens)

NAGYCENK

ϱ_{min} a)

layer number	Δh [km]	ϱ [Ωm]
1	1.60	2.30
2	16.00 ± 2.50	200.00^{+500}_{-60}
3	1.00	1.50
4	60.00 ± 9.0	80.00 ± 50.00
5	230.00 ± 40.00	6.00 ± 0.80
6		0.10

$S_1 = 690 \pm 70$ Siemens

$/\Delta h_2 = 1.6 \, ^{+1.6}_{-1.2}$ km/

$S_3 = 650 \pm 120$ Siemens

$/\Delta h_3 = 1 \, ^{+10}_{-1}$ km/

ϱ_{max} b)

layer number	Δh [km]	ϱ [Ωm]
1	1.50 ± 0.40	8.00 ± 1.00
2	4.00 ± 1.50	16.00 ± 3.00
3	8.00 ± 3.00	28.00 ± 5.00
4	15.00 ± 15.00	45.00 ± 10.00
5	55.00 ± 10.00	$90.00^{+50.00}_{-25.00}$
6	15.00	8.00
7	200.00 ± 25.00	20.00 ± 4.00
8		0.10

$S_6 = 1900 \pm 1250$ Siemens

$/\Delta h_6 = 15 \, ^{+13}_{-8}$ km/

of the top of the asthenosphere is well checked by other MT measurements in the Pannonian Basin as well as by high heat flow data (called "red spot") (Ádám et al. 1982).

A surface waves dispersion profile running from Sardinia to Istria indicates that the seismological discontinuity usually placed at a depth of about 400 km is about 100 km shallower (Scalera et al. 1980). Should these seismological evidences be correlable with the results of MT measurements in the Pannonian Basin, the existence of a very broad thermal perturbation in the upper mantle could be proposed as a working hypothesis for future seismological and electromagnetic investigations.

3.1 In Fig. 6 the depths of the top of the asthenosphere

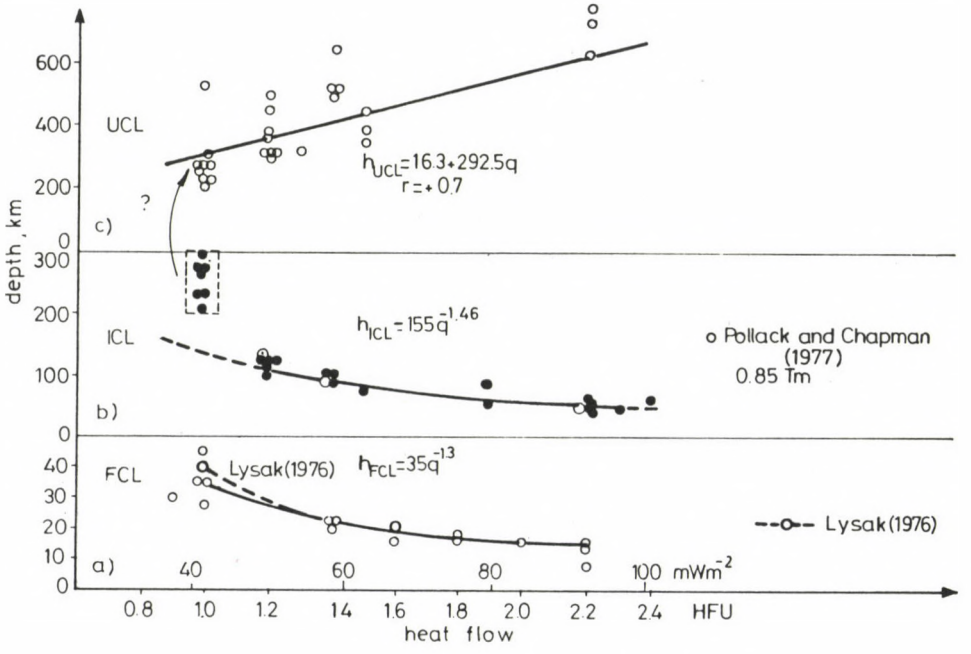

Fig. 6. Empirical relations between surface heat flow and the depth of the top of the conductive layers in the crust (FCL) or in the upper mantle (ICL, UCL); FCL = First Conducting Layer, ICL = Intermediate Conducting Layer, UCL = Ultimate Conducting Layer (Ádám 1978)

(ICL = Intermediate Conducting Layer) published mainly in the monograph "Geoelectric and Geothermal Studies" (Ádám 1976b) are plotted against heat flow values. In the same figure similar empirical relations are given for the crustal (FCL = First Conducting Layer) and for the second upper mantle (UCL = Ultimate Conducting Layer) conducting layers corresponding to the phase transition. Latter ones were completed and reinterpreted since their first publication by Ádám in 1976a (Ádám 1980, 1987).

Accordingly to the resolving power of surface waves with respect to upper mantle properties (Knopoff and Chang 1977, Knopoff and Panza 1977, Panza 1981) the top of the asthenosperic low velocity layer can be determined with an uncertainty of about 30 km, while its thickness can be resolved within about 50 km. The good agreement between the depth of the top of the asthenosphere derived from surface waves dispersion and from magnetotelluric deep soundings has been recently described by Calcagnile and Panza (1987). Their relation, for Europe, is shown in Fig. 7 and nicely agrees with the empirical relation given in Ádám (1978) (Fig. 6b).

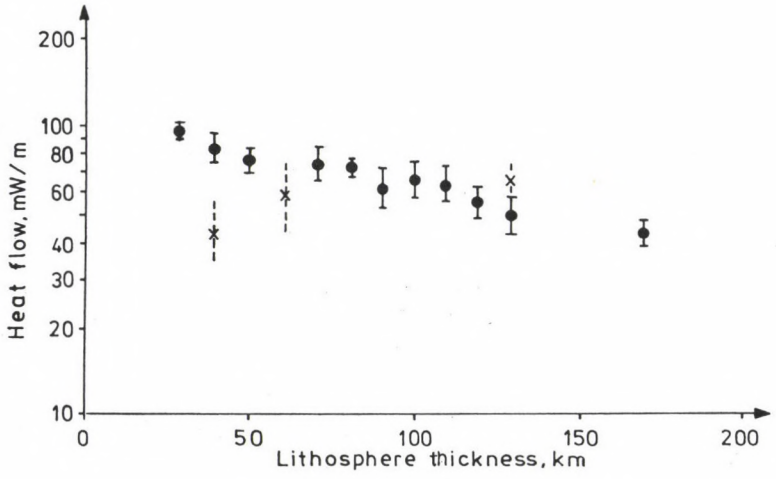

Fig. 7. Surface heat flow versus depth of the top of the low velocity asthenospheric layer determined from surface wave dispersion in Europe (Calcagnile and Panza 1987)

According to Rokityansky (1982): "The resolving power of the available global Geomagnetic Deep Soundings (GDS) data is inadequate to determine the depth where the conducting layer lies" therefore the role of magnetotellurics in determining the electric parameters of the asthenosphere is indisputable among the EM induction methods.

3.2 In regard to the conducting layer, possibly corresponding to the olivine-spinel phase transition, the results of different autnors should be confronted:

a) Parkinson (1986) shows the averaged global resistivity distributions for continental and oceanic models to a depth of about 300 km, based on deep MT soundings (Fig. 8) and maintains that the two curves come close to each other only below 150 km.

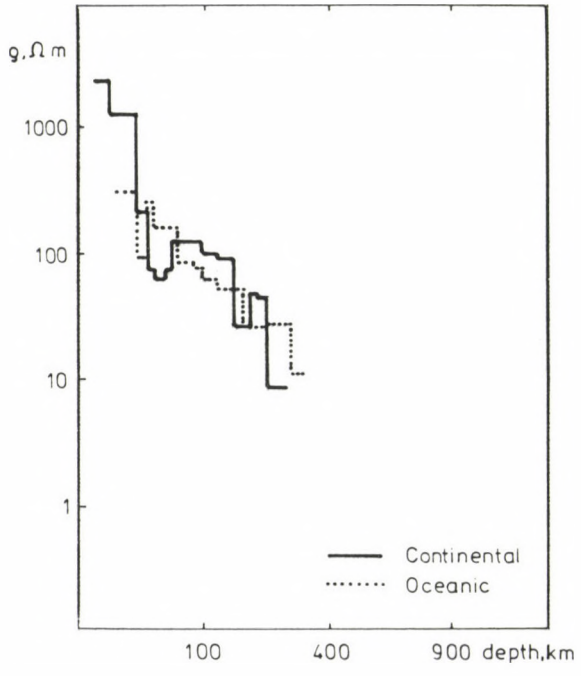

Fig. 8. Distribution versus depth of the average apparent resistivity for continental and oceanic models (Parkinson 1986)

b) A variant of Vanyan's normal resistivity profile was published recently by Berdichevsky et al. (1986) (Fig. 9).

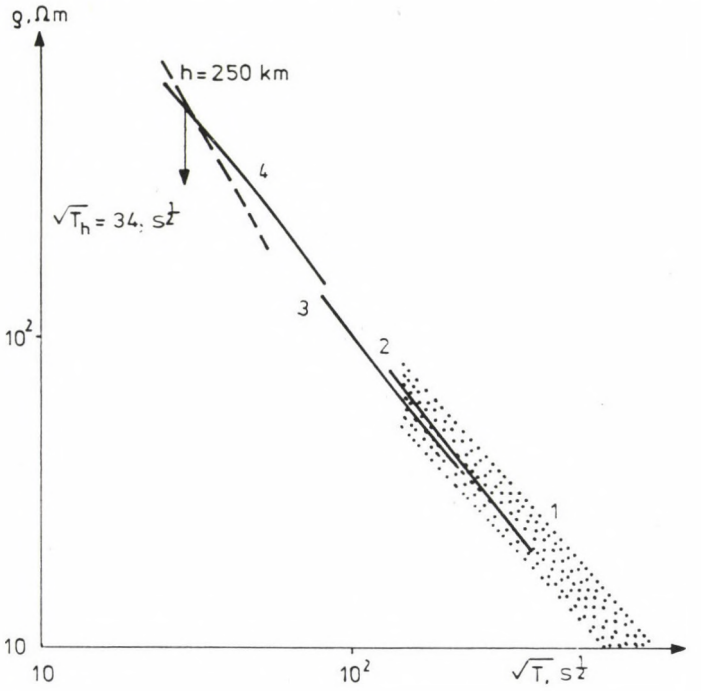

Fig. 9. A summary of magnetotelluric (MT) and magnetovariational (MV) data below a depth of 250 km (Berdichevsky et al. 1986). (1) MV sounding, (2) MT sounding of the northern part of the Pacific Ocean, (3) MT sounding of the southern part of the Turan basin, (4) MT sounding of the North-Western part of the Russian platform. All curves are reduced to the basement

c) Rokityansky discusses Vanyan's normal resistivity profile on the basis of MT measurements in Central Karelia, the most homogeneous part of the Baltic Shield, and in the Murmansk massif (Fig. 10). According to his opinion there are at least two normal profiles in these regions as the short period part of the MT curves varies from region to region. Vanyan's normal curve N_1 and Krasnobaeva's curve N_2 meet each other only at the periods of the daily variations.

Certainly, there is a discrepancy between e.g. Parkinson's

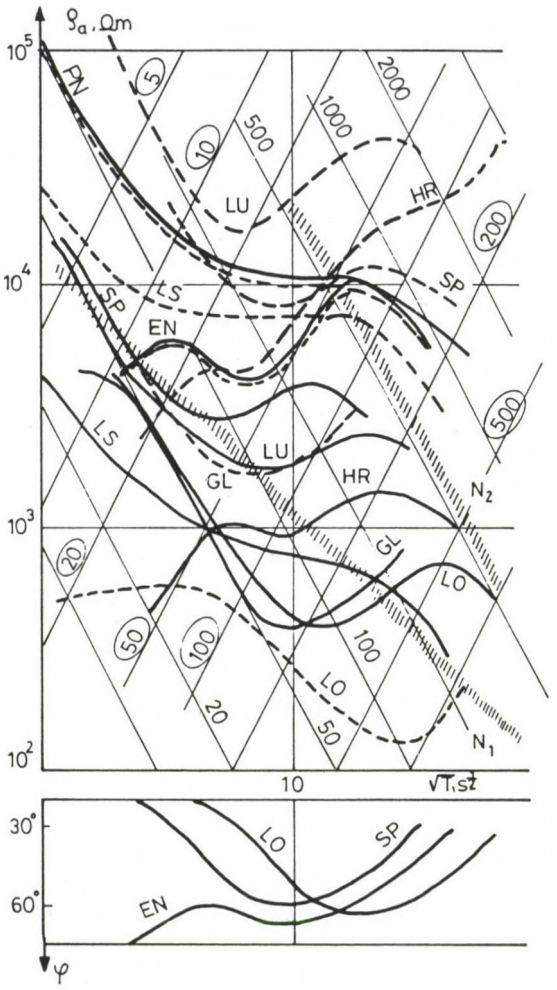

Fig. 10. MT sounding curves on the Murmansk Massif on the Kola Peninsula (Krasnobajeva et al. 1981). Solid lines: longitudinal curves (measured in 120° direction from north). Dashed lines: transverse ones (measured in 30° direction from north). N_1: normal curve according to Vanyan et al. (1980). N_2: normal curve according to Krasnobajeva et al. (1981). (5): conductance (S) values in Siemens. 10: depth to the conducting layer in km

layer sequence and Vanyan's continuous normal resistivity profile. In the latter case, the relatively small conductivity jump due to phase transition can became indistinct at the background of the continuous resistivity decrease as it was shown by

numerical models. There is no general agreement concerning the inversion of such MT curves.

4. RESISTIVITY MODELS DERIVED FROM GLOBAL GEOMAGNETIC SOUNDINGS

On the different MT curves presented above, except Parkinson's ones, below 200 km, it does not appear a resistivity variation with large gradient as can be seen on the global geomagnetic sounding curves. Campbell (1985) concluded on the basis of his newest calculations: "Distinct discontinuities seemed to be evident near 225 to 300 km and near 450 to 600 km". This deeper conductivity jump is confirmed by the figure of Isikara (personal com.) in which the results of different authors are collected (Fig. 11). An earlier statement of Anderssen et al. (1979) can be cited, too: "One many therefore be tempted to identify the discontinuities at 565 and 720 km with the seismic discontinuities at 450 and 650 km, but a more sophisticated inversion of the data will be necessary ...". According to Rokityansky's (1982) newest view: "Thus, while not completely excluding the existence of an electrical conductivity jump by two orders of magnitude, the experimental evidence gives no indication that it does exist. .... At the same time, the data convincingly indicate that within a depth range of 500-1200 km the electrical conductivity rises by approximately three orders of magnitude.

This questions could be answered only by a more detailed study of the whole data set of GDS, but this is not the aim of present study.

5. MT LAYER MODELS IN THE DEPTH RANGE CORRESPONDING TO THE PHASE TRANSITION AND THEIR RELATION TO OTHER PHYSICAL PARAMETERS

On the basis of the global geomagnetic soundings and of our numerical calculations, the increase in conductivity in MT sounding curves seems to be probable if its depth well approximates that of the conductivity anomalies appearing on the

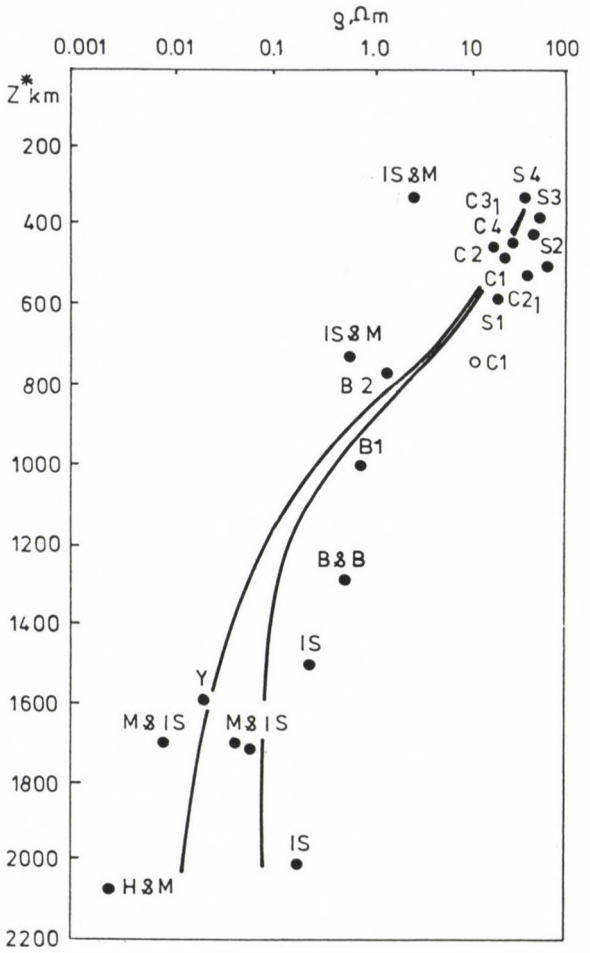

Fig. 11. Isikara's summarizing figure on the results of the recent global geomagnetic soundings: resistivity vs depth (personal com.)

global geomagnetic sounding curves.

Although the continental MT data can express strong local geologic effects (noise), an attempt was made to order the depth values of these so-called ultimate (generally second) upper mantle conductivity anomalies in function of heat flow values (Ádám 1980, Fig. 12).

If the regression, in Fig. 12, expressing the gradient +dP/dT in correspondence of the rock phase transition, is not

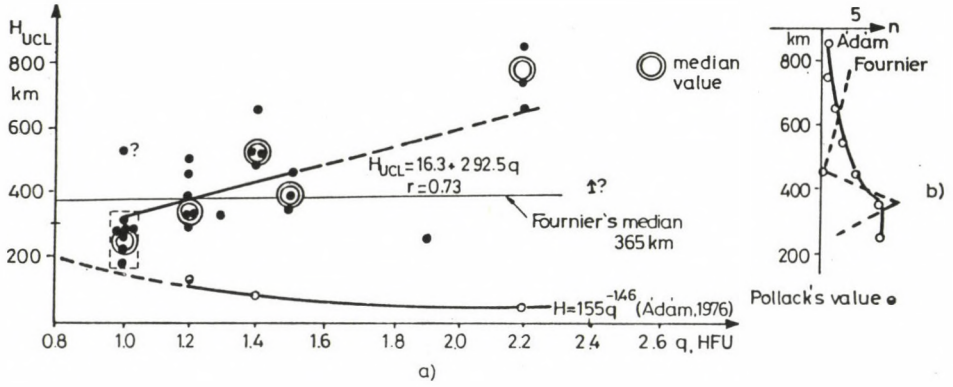

Fig. 12. MT depth values referring to the phase transition in function of heat flow (a), number of data vs depth (b), according to Ádám (1980) and Fournier (1978)

taken into account because of the low correlation coefficient (r = 0.73), an average depth value of 300-400 km can be deduced both from Ádám's and Fournier's data for a second conductivity increase in the upper mantle. In case of the data gathered in the East European Platform it is questionable whether the depth values of 250-300 km correspond to the asthenosphere or to the phase transition. According to seismological data in the shield area (Panza 1984), they represent more probably phase transitions than partial melting. In fact S-wave velocities in the upper mantle under shields are not low enough to require partial melting. Of course if partial melting occurs in very thin layers it cannot be detected by surface waves and by MT soundings. Therefore, these data are associated to the UCL. Figure 12 also shows that these values lie well above the curve characterizing the asthenosphere. In Parkinson's figure (Fig. 8) a conductivity jump in the depth range 200-300 km is clearly visible. Here both the oceanic and the continental MT curves refer to very old formations (E-Canadian shield and Mariana graben).

Vanyan (1979) concludes from the comparison of different

MT sounding curves and his normal resistivity profile that "the temperatures at depths greater than 300-400 km are nearly the same for all geotectonic zones". On the other hand Schultz et al. (1986) recently emphasize that "significant lateral heterogeneity in mantle conductivity structure is required by the data". Menvielle et al. (1986) came to the same conclusion by analysing the four harmonics of the daily variation. Duba and Shankland's (1986) recent statement is in good agreement with latter conclusions. They calculated even for a depth of 600 km a difference of about 250^{o}C in "representative temperature" between active (e.g., Baikal rift) and stable (e.g., N- and Central America) areas.

6. CONCLUSIONS

The magnetotelluric deep soundings can give informations about two conductivity increases in the upper mantle. While the conductivity increase due to partial melting in the asthenosphere can be studied in detail by magnetotellurics and the results are in good correlation with other physical parameters, such as surface heat flow and the S-wave velocity decrease determined on the basis of surface wave dispersion analysis, in the depth range of the phase transition - possibly the olivine--spinel transition - the MT method reaches the limit of its resolving power and hence, as an optimum, only a probable average value for the depth (300-400 km) of the phase transition can be given.

The continuous resistivity decrease due to the continuous temperature increase in the Earth's interior shows regional variations even in case of the crystalline shields (Rokityansky 1983). The most recent EM soundings and temperature calculations based on them seem to outline the presence of lateral heterogeneities in the whole tectonosphere of the upper mantle till the lower mantle.

REFERENCES

Ádám A 1976a: Acta Geod. Geoph. Mont. Hung., 11, 503-509.

Ádám A ed. 1976b: Geoelectric and Geothermal Studies. KAPG Geophysical Monograph. Akadémiai Kiadó, Budapest

Ádám A 1978: Phys. Earth Planet. Int., 17, No. 2, P21-P28.

Ádám A 1980: J. Geomagn. Geoel., 32, 115-125.

Ádám A 1987: Phys. Earth Planet. Int., 45, 209-215.

Ádám A, Verő J, Cz Miletits J, Holló L, Wallner Á 1981: Acta Geod. Geoph. Mont. Hung., 16, 333-351.

Ádám A, Vanyan L L, Varlamov D A, Yegorov I V, Shilovski A P, Shilovski P P 1982: Phys. Earth Planet. Int., 28, 251-260.

Akimoto S J, Fujisawa H 1965: J. Geophys. Res., 70, 443-449.

Anderssen R S, Devane J F, Gustavson S A, Winch D E 1979: Phys. Earth Planet. Int., 20, P15-P21.

Berdichevsky M N, Vanyan L L, Dmitriev V I 1986: Fizika Zemli, 12, 24-38.

Cagniard L 1953: Geophysics, 18, 605-635.

Calcagnile G, Panza G F 1987: PAGEOPH, 125, 241-254.

Campbell H W 1985: A comparison of upper mantle subcontinental electrical conductivity for North America, Europe and Asia. J. Geophys. (in press)

Counil J L, Menvielle M, LeMouel J L 1987: PAGEOPH, 125, 319-340.

Duba A G, Shankland T J 1986: Upper mantle temperature heterogeneity inferred from electrical conductivity. In: Abstracts of the Eighth IAGA Workshop on Electromagnetic Induction in the Earth and Moon, Neuchatel, Switzerland. Abstract 2-3

Fournier H 1978: Recent work in magnetotelluric soundings of the lower crust and uppermost mantle. Review lecture at the 4th IAGA Workshop on Electromagnetic Induction in the Earth and Moon, Murnau, FRG

Isikara A M 1980: Personal communication

Knopoff L, Chang F-S 1977: J. Geophys., 43, 299-310.

Knopoff L, Panza G F 1977: Ann. Geofis., 30, 491-505.

Krasnobajeva A G, D'Yakonov B P, Astafyev P F, Batalova O V, Vishenev V S, Gavrilova I E, Zhuravlyova R B, Kirollov S K 1981: Fizika Zemli, 6, 65-73.

Panza G F 1981: In: R Cassinis ed.: The Solution of the Inverse Problem in Geophysical Interpretation. Plenum Publ. Co., New York, 39-77.

Panza G F 1984: The deep structure of the Mediterranean-Alpine region and large shallow earthquakes. Mem. Soc. Geol. It., 29 (in press)

Parkinson W D 1986: The global conductivity distribution. In: Review papers of the Eighth Workshop on Electromagnetic Induction in the Earth and Moon, Neuchatel, Switzerland

(5-1)-(5-7)

Rokityansky I I 1982: Geoelectromagnetic Investigation of the Earth's Crust and Mantle. Springer Verlag, Berlin, Heidelberg, New York

Rokityansky I I 1983: Geoelectromagnetic studies of the Baltic and Ukrainian Shield: Review of some results. In: S E Hjelt ed.: The Development of the Deep Geoelectric Model of the Baltic Shield, Part 2. Proceedings of the 1st project symposium, Oulu, Department of Geophysics, University of Oulu, Rep. No. 8.

Scalera G, Calcagnile G, Panza G F 1980: Boll. Geof. Teor. Appl., 23, 11-16.

Schultz A, Larsen J C, Constable S C 1986: Lateral heterogeneity in mid-mantle electrical conductivity structure, and constraints on vertical gradient in mantle conductivity. In: Abstracts of the Eighth IAGA Workshop on Electromagnetic Induction in the Earth and Moon, Neuchatel, Switzerland, Abstract 5-4

Vanyan L L 1979: Deep geoelectrical models: geological and electromagnetic principles. In: Abstract of the symposium: Electrical Conductivity and the Characteristics of the Asthenosphere in Canberra, IUGG General Assembly, 525

Vanyan L L 1980: IAGA News, No 19, 73-84.

Vanyan L L, Shilovski P P 1979: Apparent resistivity curves for interpretation of deep magnetotelluric soundings. Soviet Working Group on ELAS Project. Manuscript distributed at the ELAS Conference in Sukhumi

Acta Geod. Geoph. Mont. Hung., Vol. 24 (3-4), pp. 417-439 (1989)

MEASURE OF THE LINEAR DEPENDENCE

B Hajagos[1] and F Steiner[1]

University for Heavy Industry, Chair of Geophysics, H-3515 Miskolc, Egyetemváros, Hungary

[Manuscript received July 14, 1988]

Taking as basis the supermodel $f_\alpha(x)$ which includes all symmetric stable probability distributions and properly models many cases in earth physics, the generation of the linear dependence and of the determination of the value r characterizing the measure of the dependence can be carried out easily, well arranged and without additional conditions. The paper presents the exact formulas for its determination together with simple approximative methods and draws attention to the distortions in the traditional method of determination of the correlation coefficient, e.g. that it is not resistant, further that irrealistically high coefficients near to 1 may be obtained by the traditional method even in case of medium dependences if the distribution has heavy flanks, i.e. if the actual distribution is far from the Gaussian one.

Keywords: correlation; Gaussian distribution; linear dependence; robust estimation

1. INTRODUCTION

There is a lot of practical problems in every field of science which are connected - according to the terminology of probability - with the dependent or independent character of random variables. If a deterministic dependence is evident, moreover its analytic form is also known (from physical principles or empirically) and a random variable appears only so to say secondarily in the connections as an additive component, then an adjustment method is to be used (e.g. based on the least squares method, using the L_1-norm or the method of the most frequent value (Steiner 1988)). It may be superfluous in such cases to ask about the measure of the dependence of a random variable η from an other random variable ξ which question can be answered practically only by introducing

strongly simplifying assumptions.

Concerning these simplifications it is normally avoided to emphasize (especially in practical applications) that the measure

$$\frac{\sum_{i=1}^{n}(x_i-\bar{x})(y_i-\bar{y})}{\sqrt{\sum_{i=1}^{n}(x_i-\bar{x})^2}\cdot\sqrt{\sum_{i=1}^{n}(y_i-\bar{y})^2}} \qquad (1)$$

computed from the set of data (x_i, y_i), containing n elements from the distributions η and ξ, is an adequate measure only if certain conditions are fulfilled, e.g. if the dependence is a linear one ($\bar{x}$ and $\bar{y}$ are the corresponding algebraic averages). The classics of mathematical statistics (Cramér 1946, Rényi 1971) do not forget to tell this (and Rényi even proposes a generalization which, unfortunately, did not prove useful in practice). The general use of Eq. (1) is connected with the comfortable property that its value lies between +1 and -1 and this property remains in case of gross errors, too. A value near zero means independence.

The possiblity that the value determined from Eq. (1) and lying between +1 and -1 can be very far from a realistic value is presented by a simple example in Fig. 1. The measured values x_i and y_i have both an expected value of +100 and unit scatter, both are distributed according to the Gaussian law and they are independent. From the 100 sample of these values one has a gross error, resulting in a pair of values (0, 0) (let us say due to an error in the power supply). For this sample Eq. (1) does not yield a value near zero as sign of the independence - what should be expected as the values of x and y are independent - but the resulting coefficient is +0.989, indicating a very close connection. The expression in Eq. (1) is therefore far from being resistant (i.e. it is very sensitive for gross errors), that is why the reliability of coefficients computed according to Eq. (1) may be questioned even in cases much less accentuated than in the example mentioned.

Some further remarks follow about the restricted

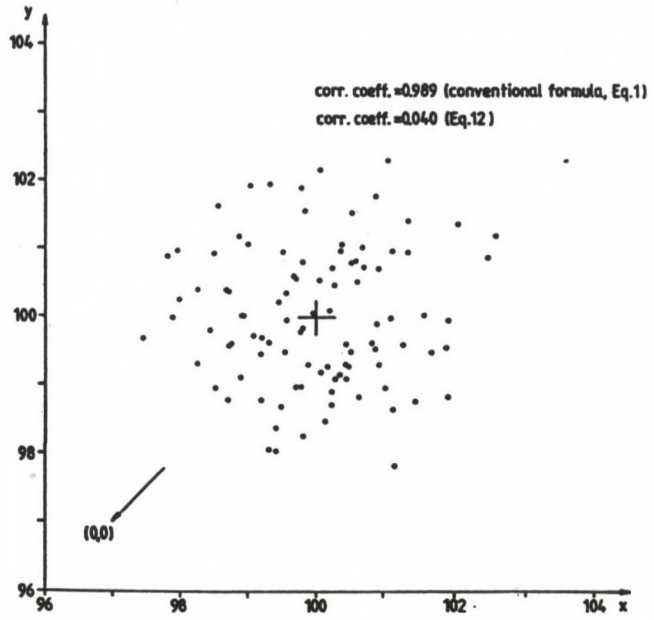

Fig. 1. Random data pairs from a two-variable Gaussian distribution in case of independent x and y. One of the data pairs (0, 0) is burdened by a gross error. The traditional correlation coefficient is 0.989

applicability of Eq. (1) at the end of the present paper.

2. GENERATION OF A LINEAR DEPENDENCE

In the following a simplified discussion is striven at according to Einstein's principle (which refers here both to the construction of the model and to the definition and the method of determination of the measure of dependence): "whatever you do, do it in the simplest way - but even simpler do not do it".

2.1 Family of distribution types $f_\alpha(x)$

Let us define the family of types (supermodel) $f_\alpha(x)$ with the parameter α ($0 < \alpha \leqslant 2$) as follows:

$$f_\alpha(x) = \frac{1}{2\pi} \cdot \mathcal{F}\left\{e^{-|t|^\alpha/\alpha}\right\}, \qquad (2)$$

where $\mathcal{F}$ denotes the Fourier-transformation.

It is easy to show that $\alpha = 2$ yields the standard Gaussian distribution, $\alpha = 1$ the Cauchy-distribution with the density function

$$\frac{1}{\pi} \frac{1}{1+x^2} \tag{2a}$$

(Erdélyi 1954). For other $f_\alpha(x)$-s, no analytic form is known; thus $f_\alpha(x)$-s are computed numerically from the formula

$$f_\alpha(x) = \frac{1}{\pi} \int_0^\infty e^{-|t|^\alpha/\alpha} \cos(xt)\, dt \,. \tag{2b}$$

The curves of $f_\alpha(x)$ for some values of α are presented in Figs 2a and 2b. Evidently the members of this supermodel fulfil the various practical demands as models of really occurring error distributions (distributions with both strong and slight flanks appear in the supermodel).

Concerning the emphatic aspect of simplicity, a first glance at Eq. (2b) would tell us that it is not fulfilled by it. Using, however, personal computers and modern quadratures (e.g. Hajósy 1989), the program computing the value of the integral in Eq. (2b) yields in a very short time the values of $f_\alpha(x)$; the time of computation is subjectively as imperceptible as the computation time of Eq. (2a) with only four elementary operations.

It is evident from Eq. (2) that the characteristic function of $f_\alpha(x)$ is $e^{-|t|^\alpha/\alpha}$. (The notion of the characteristic function and the formulas in connection with it are supposed to be known.) This form of the characteristic function shows that a linear combination of distributions with different scale parameters but with the same α yields a distribution of the family $f_\alpha(x)$ with just the same parameter α, too (as the characteristic functions are to be multiplied in this case); that means that all distributions $f_\alpha(x)$ are stable

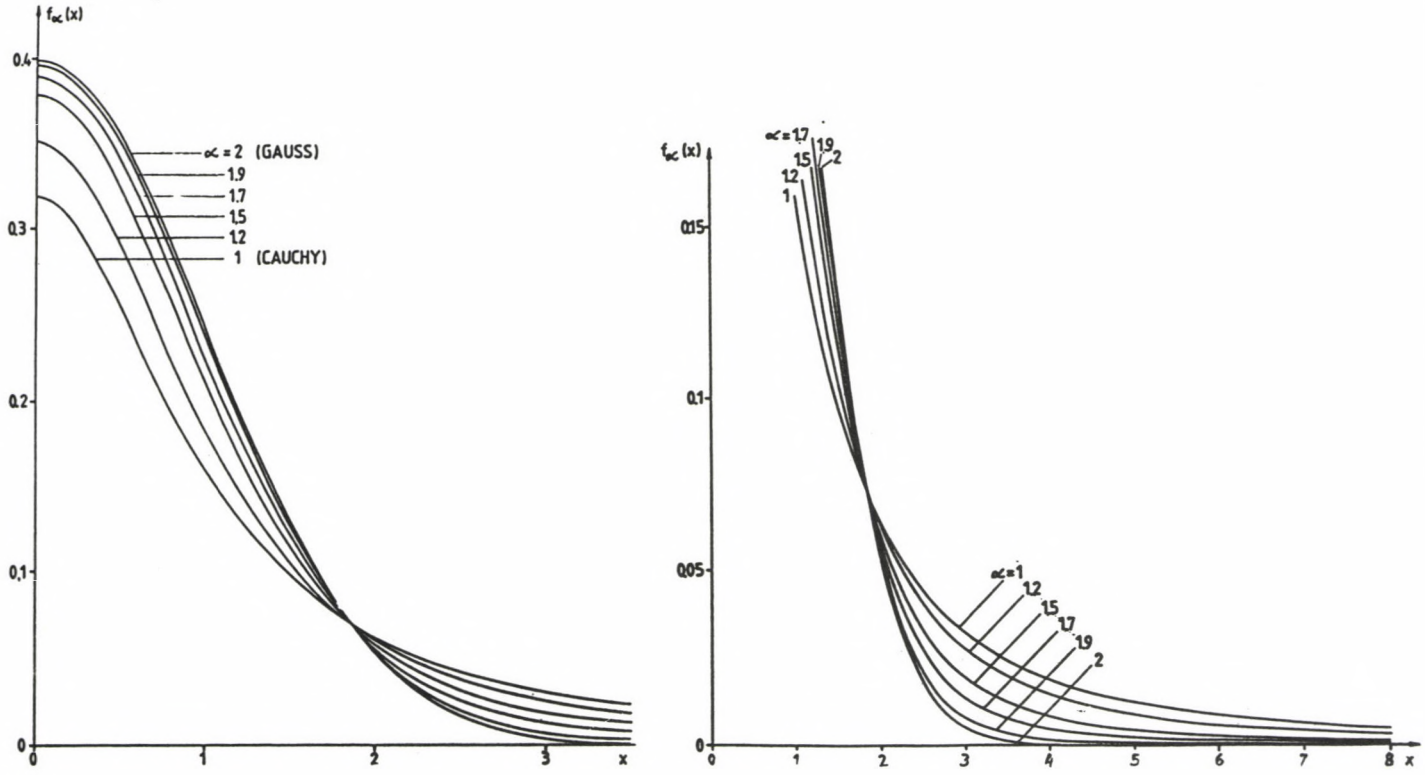

Fig. 2. Symmetrical stable distributions for some values of the parameter

distributions. An analysis of the analytic form of the characteristic function valid for all possible stable distributions (e.g. Gnedenko and Kolmogorov 1951) shows that the family $f_\alpha(x)$ is equivalent with the class of all symmetric stable distributions: there is no symmetric error distribution outside of the supermodel $f_\alpha(x)$ which would be at the same time stable, too.

These facts explain the very simplicity of the supermodel $f_\alpha(x)$: its origin lies much deeper than the level of any, already at present outdated aspect of computation technics. As it will be shown the problem of the dependence can be treated in a concise or "pure" way, i.e. without open or implied additional assumptions.

2.2 Genaration of a dependence of a given measure

In the following a fixed α-value and a pre-selected definition of the scale parameter (the latter consequently) will be used. This definition of the scale parameter may be any interquantile semi-range (e.g. the inter-quartile or inter-sextile semi-range), dihesion (definition at Steiner 1988) or any other resistant parameter. (The scatter as scale parameter can be used in this family $f_\alpha(x)$ only if $\alpha = 2$, as it is infinite for all $\alpha < 2$, see Gnedenko and Kolmogorov (1951). The dangers of the use of the scatter as scale parameter were stressed by Steiner (1982), even in case of a finite scatter.)

Let us consider from $f_\alpha(x)$-s with a given α the distribution - with the same aspect of simplicity in view - which has a unit scale parameter S. This distribution is valid for both random variables ξ and ζ ; in this case, the random variable

$$\eta = r\xi + (1-|r|^\alpha)^{1/\alpha}\zeta \qquad (-1 \leq r \leq 1) \qquad (3)$$

has exactly the same distribution. (If a streching of s-times is necessary to get a unit scale parameter S, the characteristic function of $r\xi$ is $\exp(-|r|^\alpha|st|^\alpha/\alpha)$ and that of the second term on the right side of Eq. (3) is $\exp(-(1-|r|^\alpha)|st|^\alpha/\alpha)$, thus the product of these, i.e. the characteristic function of η is $\exp(-|st|^\alpha/\alpha)$ and this is exactly the same, as those of

ξ and of ζ .)

Equation (3) describes the possible simplest connection i.e. the proportionality between η and ξ . Naturally this proportionality with the factor r is only one component of η , the other component is a fully independent statistical noise. Equation (3) produces really very simply a dependence of a certain level.

3. DETERMINATION OF THE VALUE OF r

3.1 Determination of the location parameter. The effectivity of the computation of the general most frequent value for the type family $f_\alpha(x)$

In the practice, the data pairs $(x_i \; y_i)$ corresponding to the variables ξ , η are measured, and accepting Eq. (3) as a model, the problem is to determine the dependence y on x, i.e. to determine the value of r. In order to ensure a fulfillment of the conditions of Eq. (3) (namely zero location parameter and unit scale parameter), the data sets x_i and y_i are standardized separately, i.e. in the following the data sets

$$\hat{x} = \frac{x_i - T_x}{S_x} , \quad \hat{y} = \frac{y_i - T_y}{S_y} \tag{4}$$

are used.

Concerning the location parameter, it should be resistant similarly to the scale parameter, and it is the better, the more robust it is. Theoretically it could be proposed - and this would be the most consequent way as the family $f_\alpha(x)$ of distributions is chosen as supermodel in the present paper - if a substituting distribution would be selected from the family $f_\alpha(x)$ somewhere between $\alpha = 2$ (Gaussian distribution) and $\alpha = 1$ (Cauchy-distribution), (say $\alpha = 1.5$), and then according to Hajagos (1982), the corresponding estimation of the location parameter would be used. (Hajagos (1982) gives the conditions when the proposed estimation of the location parameter causes minimum loss of information.) This method, however, does

not yield a practically advantageous algorithm for the determination of the location parameter.

Let us try to use the generalized most frequent value which was proven by Steiner (1988) to be applicable with high efficiency to a wide range of distributions. This is a value M_k for the data set z_i ($i = 1, 2, \ldots n$) which fulfils the equation

$$M_k = \frac{\sum_{i=1}^{n} \frac{z_i}{(k\varepsilon)^2 + (z_i - M_k)^2}}{\sum_{i=1}^{n} \frac{1}{(k\varepsilon)^2 + (z_i - M_k)^2}} . \qquad (5)$$

ε having the character of a scale parameter fulfils the following equation:

$$\varepsilon^2 = \frac{3 \sum_{i=1}^{n} \frac{(z_i - M_k)^2}{[\varepsilon^2 + (z_i - M_k)^2]^2}}{\sum_{i=1}^{n} \frac{1}{[\varepsilon^2 + (z_i - M_k)^2]^2}} . \qquad (6)$$

(It is exactly identical with the dihesion in a symmetrical case, in an asymmetric case it is approximately equal with it.)

The only problem in the determination of M_k is the choice of the value k. The choice depends on the condition whether the value of α in the given measurement situation is known or not in the sense that $f_\alpha(x)$ with this α is the best model from the family $f_\alpha(x)$. If it is unknown (and perhaps this is the more frequent situation), then according to Steiner (1988), $k = 2$ should be chosen. In this case the efficiency of the determination of M_k in function of α corresponds to the full curve in Fig. 3; at $\alpha = 1.5$, the maximum effectivity is 99.5 percent, and even at the ends of the intervals (at $\alpha = 1$ and $\alpha = 2$) it decreases only to 90 percent. The computation of the efficiencies denoted by $\underline{e}$ was carried out according to the formula

$$e = \frac{\dfrac{1}{\displaystyle\int_{-\infty}^{\infty} \left(\frac{f'_{\alpha}(x)}{f_{\alpha}(x)}\right)^2 \cdot f_{\alpha}(x)\,dx}}{\dfrac{\displaystyle\int_{-\infty}^{\infty} \frac{x^2}{(4\varepsilon^2+x^2)^2} f_{\alpha}(x)\,dx}{\left[\displaystyle\int_{-\infty}^{\infty} \frac{4\varepsilon^2-x^2}{(4\varepsilon^2+x^2)^2} f_{\alpha}(x)\,dx\right]^2}} \qquad (7)$$

The multiple fracture has not been re-arranged, in order to show clearly in the nominator the well-known Cramér-Rao-limit (the reciprocal of the Fischer-information), and in the denominator, the asymptotic variance M_k belonging to k = 2 (i.e. M_2) (see Steiner 1988). The curve of the Cramér-Rao limit is shown in Fig. 4 (here the limit is interpreted as minimum asymptotic scatter)

If the value α corresponding adequately to the given problem is known, then the efficiency can be further improved. By substituting k^2 into Eq. (7) for the three numbers "4", $\underline{e}$ gives the efficiency of the computation of M_k for the actual value of k. The optimum k (k_{opt}) can be found therefore to each α with which the determination of M_k has the highest efficiency. The curve of these values k_{opt} is shown in Fig. 5, the efficiencies determined with the actual k_{opt} values in Fig. 3 are shown by dotted line. The latter curve is in the whole range studied so near to 100 percent that it shows clearly the close connection between the supermodel $f_{\alpha}(x)$ and the type family $f_a(x)$.

3.2 Definition of the values S^+ and S^-. Points corresponding to values (r,α) on the plane (S^-, S^+)

According to the previous section, the location parameter is estimated with the optimum M_k or (and this may be the more frequent case) M_2 is used for this purpose. In the following the index 2 is omitted from M if it is computed using k = 2, and the corresponding value for the set x_i is denoted by M_x,

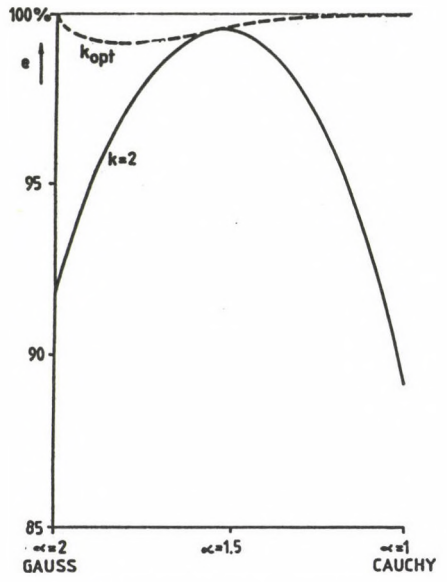

Fig. 3. Effectivity of the most frequent value calculations in the type family $f_{\alpha}(x)$ at k = 2 (full line), and using the actual optimum k (k_{opt})

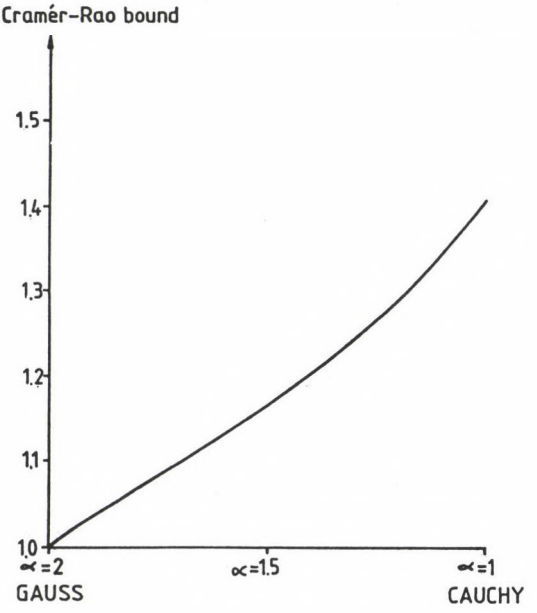

Fig. 4. Minimum asymptotic scatters for the type family $f_{\alpha}(x)$

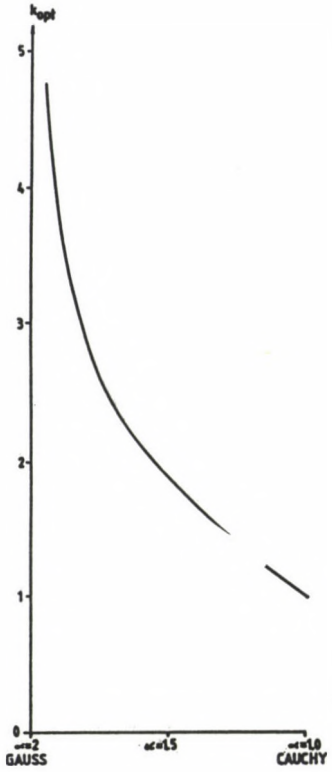

Fig. 5. Optimum k (k_{opt}) for the type family $f_\alpha(x)$

for the set y_i by M_y - these two quantities are thus the quantities T_x and T_y, as denoted generally in Eq. (4). On the other hand if a resistant scale parameter is chosen - which can be the values ε_x and ε_y, being at disposal from the results of the computations of M, or the interquartile semiranges Q_x and Q_y of the samples - then there is no more problem with the standardization of the sets x_i and y_i. If the latter scale parameter is chosen, the simple transformations

$$\hat{x}_i = \frac{x_i - M_x}{Q_x} , \quad \hat{y}_i = \frac{y_i - M_y}{Q_y} \tag{8}$$

are to be carried out.

After these preparations the original question can be put: how does indicate the set of data-pairs x_i, y_i taken from the sampling of the random variables ξ , η the dependence or

independence of y_i-s from the x_i-s?

At this point it is especially important to choose the most simple way - and even the fact should be omitted that if certain conditions are fulfilled, Eq. (1) gives an acceptable measure of the dependence. (That means that it would be misleading to test some seemingly obvious generalizations of Eq. (1) by solving our generally set problem.)

If ξ and η have independent and symmetrical distributions, the distributions of $(\xi + \eta)$ and of $(\xi - \eta)$ will coincide, i.e. the scale parameter of the differences $(\hat{x}_i - \hat{y}_i)$ denoted by S_{x-y} coincides (in correspondence to the previous discussion e.g. to the interquartile semi-range) with the scale parameter of S_{x+y} of $(\hat{x}_i + \hat{y}_i)$, computed in a similar way, naturally, with some statistical noise. (These noises will be shown in the following by Monte-Carlo examples.)

If this approximative coincidence is not the case, there is no independence - in such a case one of the scale parameters S_{x+y} and S_{x-y} will be greater than the other.

Let us denote in the following the smaller of the scale parameters by S^-, the greater by S^+. If the dependence is close ($|r|$ in Eq. (3) is high), then an S^--value significantly less than 1 is expected. (In case of $r = 1$, the set of the differences $(x_i - y_i)$ contains only 0-s, therefore any definition of the scale parameter yields $S_{x-y} = 0$.)

At a first glance it seems to be sufficient to determine the values of S^- to be able to conclude to r. As S^- is the smaller of the values S_{x+y} and S_{x-y}, the sign of r is also available: if $S^- = S_{x-y}$, r is positive, if $S^- = S_{x+y}$, r is negative.

Concerning the absolute value of r, S^- does not only depend on it, but also on α. Using the characteristic functions of $f_\alpha(x)$, the equalities

$$S^- = [(1-|r|)^\alpha + (1-|r|^\alpha)]^{1/\alpha}$$
$$S^+ = [(1+|r|)^\alpha + (1-|r|^\alpha)]^{1/\alpha} \qquad (9)$$

can be easily proved which correspond on the plane (S^-, S^+) to the system of curves $|r| = \text{const}$ and $\alpha = \text{const}$ (see Fig. 6a).

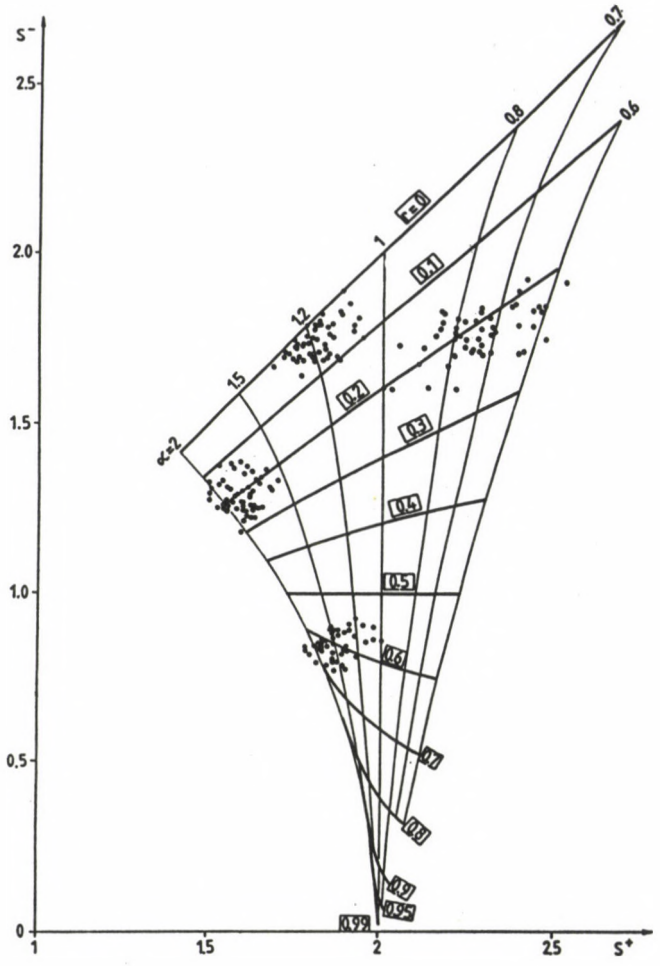

Fig. 6a. Illustration of the simultaneous determination of r and α. The points of the clusters are obtained from Monte-Carlo trials

If |r| is near to 1, the determination of |r| from the data pair (S^-, S^+) is by no means unambiguous (see the magnified Fig. 6b), not even in case of large n. Otherwise the determination of |r| is unambiguous (disregarding statistical errors) even if the value of α is unknown. If the value of α is known, |r| can be determined unambiguously even if its value is near to 1.

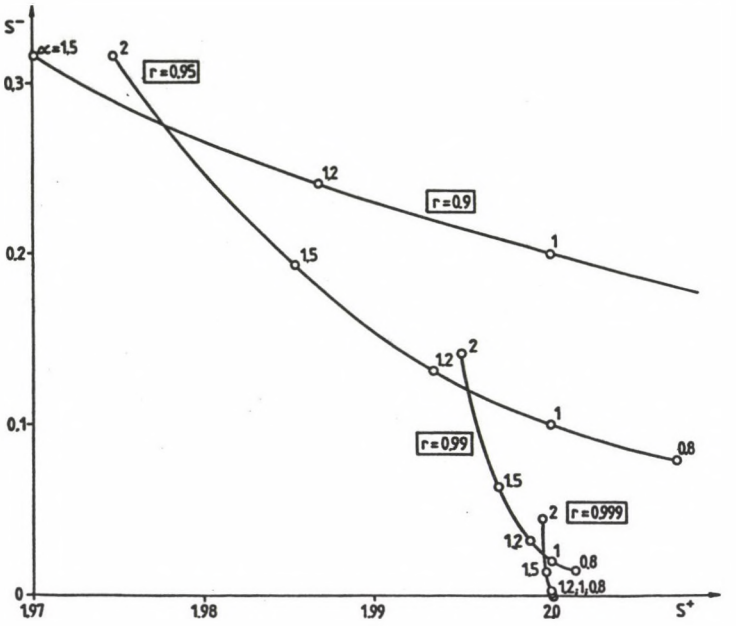

Fig. 6b. Bottom magnified part of Fig. 6a

3.3 Results of the Monte-Carlo experiments for the determination of r

In this section, experiments for the determination of r are presented for the following four pairs of parameters: r = 0.2 with α = 0.75 and α = 1.8; r = 0 with α = 1.2; and r = 0.6 with α = 1.5. Based on Eq. (3), 1000 randomly selected data pairs of x_i and y_i were generated, the most frequent values of x_i and y_i were computed (with k = 2), and the empirical interquartile semi-range has been accepted as scale parameter. Using this parameter, the data sets of x_i and of y_i have been standardized (Eq. 8), then the interquartile semi-range of the sets of the sums and differences formed (S^- and S^+). The values of |r| and α have been determined from Eq. (9).

The values S^- and S^+ have been plotted as small circles in the plane S^-, S^+ of Fig. 6a. By repeating 50 times this

procedure for a given pair of values (r, α) information is obtained about the accuracy of the determination of the data pair (r, α) for a given n.

The clusters of points in Fig. 6a give evidence for the applicability of the method.

3.4 Approximative determinations of r

It has been shown that for any distribution of the supermodel $f_\alpha(x)$ (with a scatter shown by the Monte-Carlo experiments, and depending on n) the data pairs S^- and S^+ yield unambiguously the value of $|r|$ till a limit of $|r| \approx 0.8$ (at higher values of $|r|$, it yields an interval) without the knowledge of α, i.e. of the type of the distribution.

For a practical computation, the solution of Eq. (9) is to be programmed; this programme is not too difficult, but it is by no means a routine task. Therefore, if somebody wants to know the connection between two physical quantities approximately (and, on the other hand, only occasionally), it is possible that he should like to spare this programming and prefers to use some alternative simplified method. That is why we consider in the following such simplifications and some simpler cases - and their studies proves to be useful from other points of view, too.

The simpler case is if α is a priori known (from previously made measurements under similar conditions). Then by taking the α-th power of Eq. (9) and substracting them the following results is obtained:

$$(S^+)^\alpha - (S^-)^\alpha = (1+|r|)^\alpha - (1-|r|)^\alpha . \qquad (10)$$

As there are library programmes for the determination of the roots of equations with one unknown, Eq. (10) can be easily solved. Nevertheless, and approximative formula for $|r|$ is given here:

$$r \approx \frac{(S^+)^\alpha - (S^-)^\alpha}{2^\alpha} . \qquad (11)$$

(It should be re-emphasized that the definition of the scale parameter is arbitrary, the user may choose the inter-quartile semi-range or any other - the only condition to be fulfilled is that if the definition is applied directly to a distribution itself, a finite value should be obtained.)

Equation (11) yields $|r|$ values somewhat greater than the realistic ones, but the maximum deviation is only 0.0268 (at $\alpha = 1.425$ and at $|r| = 0.63$), meaning a deviation of 4.3 percent. The maximum of the percentual error is only 6 percent (at $\alpha = 1.44$ and $|r| \to 0$); this means a deviation e.g. at $r \approx 0.1$ of some 10^{-3} parts. (In an iterative solution of Eq. (9), the approximative value $|r|$ yielded by Eq. (11) can be used as an initial value for a subsequent part of the iteration $|r|$ with the next value of α .)

Equation (11) yields accurate values at $\alpha = 2$ and $\alpha = 1$:

$$|r| = \frac{(S^+)^2 - (S^-)^2}{4} , \qquad \text{if} \quad \alpha = 2 \qquad (12)$$

$$|r| = \frac{S^+ - S^-}{2} \qquad \text{if} \quad \alpha = 1 . \qquad (13)$$

In Eq. (12), being valid for the Gaussian distribution, the empirical scatter can also be chosen (but only here); it is easy to show that in such a way Eq. (1) is obtained. (It should be remembered that according to our convention both the sets x_i and y_i are transformed to make a unit scale parameter.) It follows that even if it is ensured in an actual case that the distribution is very near to the Gaussian one, the use of Eq. (12) is proposed instead of Eq. (1), too, from the point of view of resistance: in the example of the Introduction containing a single outlier (Fig. 1) if the interquartile semi-range is accepted as scale parameter (and for simplicity, the median as location parameter), Eq. (12) yields $r = 0.040$ and according to the Monte-Carlo results, this value differs from the correct $r = 0$ only due to statistical noise. Equation (12) gives therefore correct information about the value of r even if Eq. (1) yields the value $r = 0.989$, being in the actual case completely

irrealistic. Equation (12) can be considered for Gaussian distributions (and for distributions being near to the Gaussian one) as a resistant generalization of Eq. (1). The measure of dependence introduced according to Eq. (3), is rightly considered - in a more general sense - as a measure of the correlation (correlation coefficient).

In extreme cases - e.g. in the case of $\alpha = 0.75$ of the distribution $f_\alpha(x)$ which is surely extreme from the point of view of the Gaussian distribution - Eq. (12) may give a computed r value being somewhat greater than 1 if the true $|r|$ value is also near to unit - but Eq. (12) never yields irrealistic values as $r = 0.989$ in case of independent variables. As this paper shows, the present authors consider the problem of the determination of r as a two-variable problem even in the framework of the supermodel $f_\alpha(x)$. Even if simplifications are allowed, it should not be expected that a formula give correct values for $\alpha = 0.75$, if it yields correct values at $\alpha = 2$: the strongly different character of the two density functions (Fig. 9) makes such an expectation irrealistic. (Some further remarks will follow at the end of the present paper in connection with the interpretation of Fig. 8.)

As a rough approximation, a formula is given for the case when the value α defining the type of the distribution is completely unknown and a quick orientation is necessary about $|r|$:

$$|r| \approx \frac{S^+ \cdot \sqrt{S^+} - S^- \cdot \sqrt{S^-}}{2 \cdot \sqrt{2}} \quad . \tag{14}$$

Figure 7 shows the values computed from Eq. (7) as computed r-s (r_o) vs. the true values of the correlation coefficient (denoted here by r_t). The curve belonging to $\alpha = 1.5$ is nearly a straight line of 45^o - but this is hardly surprising from a comparison of Eqs (14) and (11), and from what has been said about the latter. Equation (14) gives an r value less than the correct r_t, as a maximum by 0.08 (and by 12 percent, respectively) for the Gaussian distribution, for the Cauchy-distribution this value can be greater by maximum 0.15 than the correct

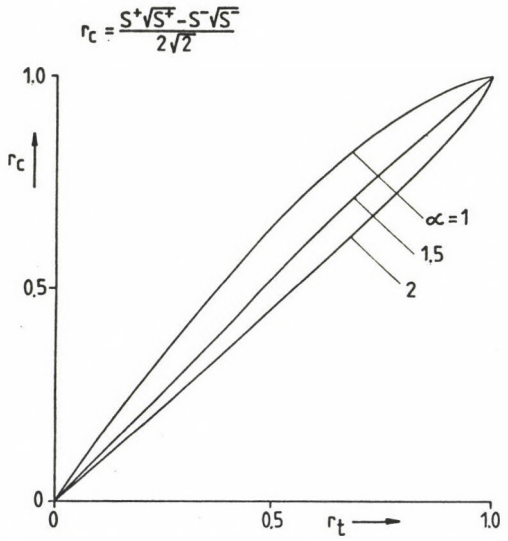

Fig. 7. Errors due to the approximative formula, Eq. (14) (r_t is the true correlation coefficient, r_c its computed value)

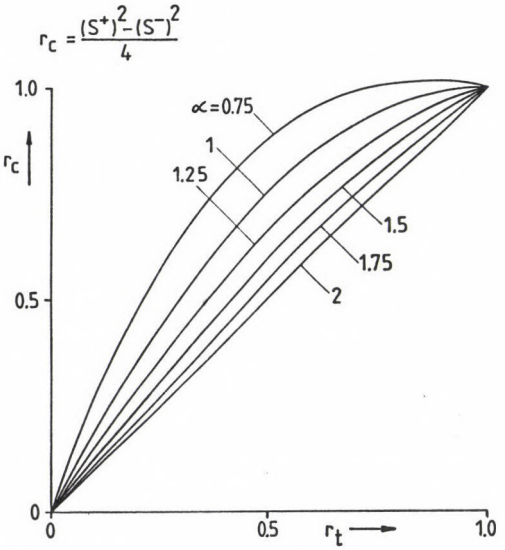

Fig. 8. Errors with the approximative formula, Eq. (12) (r_t and r_c as in Fig. 7). This figure explains why the correlation coefficient is often higher than expected or estimated

r-value. It should be added that Eq. (14) gives correct results at distribution types $f_\alpha(x)$ which are near to the distributions of data resulting from very carefully made measurements (see the definition of the Jeffreys-interval given by Steiner (1988); see also the Jeffreys-quotation in Kerékfy (1978)).

Let us return to Eq. (12) being in case of the Gaussian distribution a resistant form of Eq. (1), and let us see what r_c values would be obtained by it, if this formula would be universally accepted. The r_c values computed by Eq. (12) are shown vs. the true value r_t in Fig. 8. The formula is correct, as mentioned, for $\alpha = 2$, thus the corresponding curve is a 45^o straight line. For smaller α-s, the r_c-values computed from Eq. (12) (i.e. supposing a Gaussian distribution) are in an increasing rate higher than the realistic r (r_t) values: r_c may be greater than 0.9 (in case of the Cauchy-distribution), if $r_t = 0.7$; or r_c is nearly 0.5 in case of $\alpha = 0.75$ if r. etc. (The density function for $\alpha = 0.75$ is shown

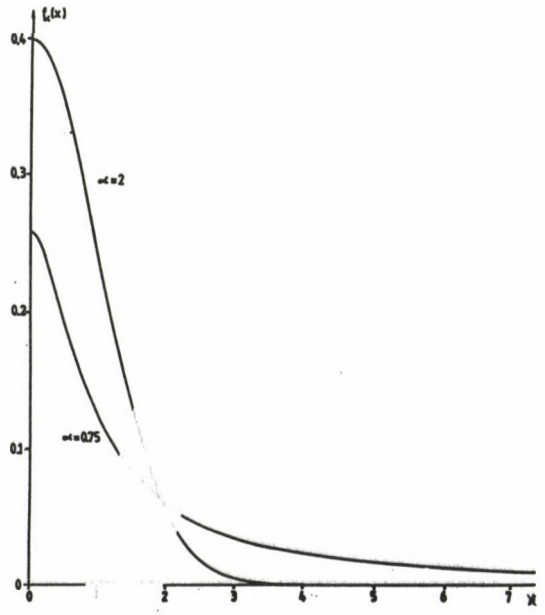

Fig. 9. The curve f x) corresponding to $\alpha = 0.75$ compared to the density func ı of the Gaussian distribution

illustrate the difference, the Gaussian density function is also plotted.) The deviations of the actual distributions from the Gaussian one result in correlation coefficients being much higher than the correct ones - and this remind us at many cases from the practice, when Eq. (1) gave too high correlation coefficients even if a visual inspection did not confirm this close connection. Such a situation can be interpreted as a frequent occurrence of distributions having heavier flanks than the Gaussian distribution. (On the other hand, this effect resulting in a too high apparent r may cause economical and other consequences of decisions which were based on apparently very close connections being in reality rather poor ones.)

These great deviations from the correct correlation coefficient remind us again at Einstein's remark quoted earlier: "do everything in the simplest way, but even simpler do not do it". The acceptance of the Gaussian distribution as an always valid general model is an oversimplification, which is unallowed in earth sciences even in cases if correlation coefficients are to be computed.

Figures 10a and 10b show the median of the r values from different formulas for the three cases of (r, α) characterized by $r \neq 0$, the full range and (by double line) the interquartile range. This figures are presented partly as supplement to Fig. 8, partly as a comparison of the results obtained from Eqs (11) and (1).

The upper part of Fig. 10a shows cases being near to the Gaussian distribution: $\alpha = 1.8$. The denominator of Eq. (1) contains empirical scatters; the S-values in Eq. (11) are empirical interquartile semi-ranges. As in case of a Gaussian distribution the asymptotic scatter of the latter is by 65 percent higher than the corresponding parameter for the empirical scatter (e.g. Hajagos and Steiner 1988), hence the greater statistical noise in the values computed by Eq. (11) can be understood. Thus if it is not only so much sure that the distribution is very near to the Gaussian one but also the occurrence of outliers are absolutely excluded, then Eq. (1) may be advantageously applied. It should be, however, reminded at the

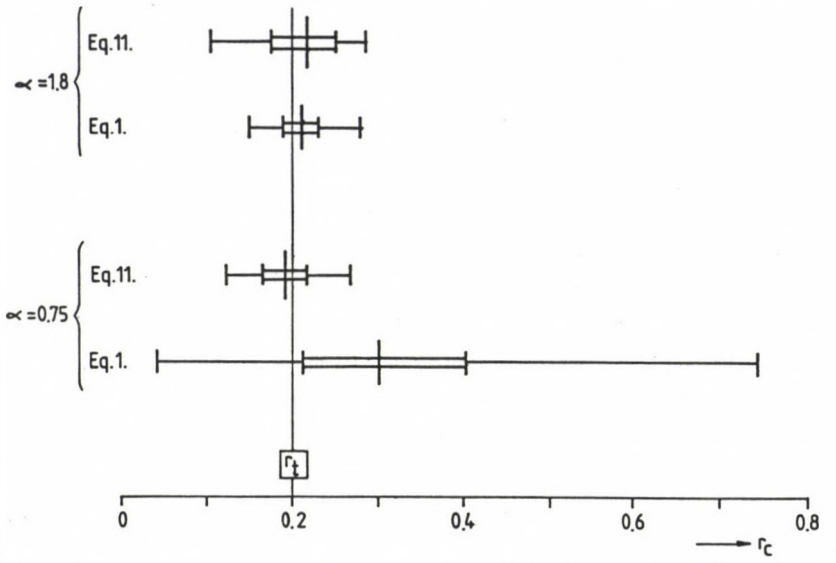

Fig. 10a. Systematic and random errors of different formulas for r

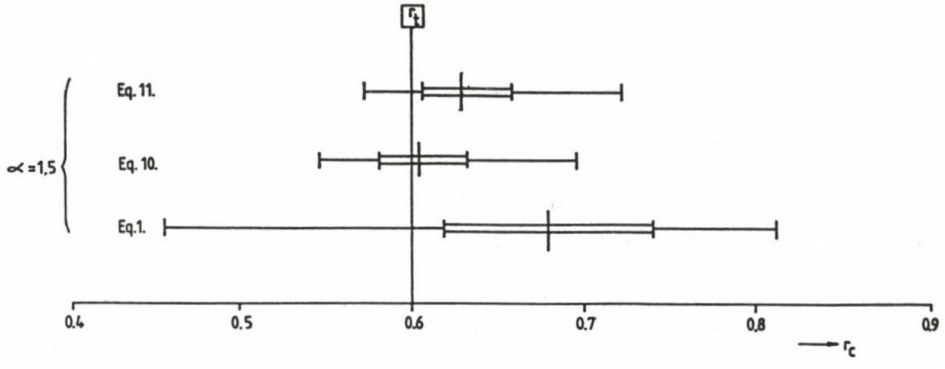

Fig. 10b. Systematic and random errors of different formulas for r

very high sensitivity of this formula against gross errors and at the systematic distortion in case of distributions significantly differring from the Gaussian one; that is why the

application of Eq. (1) is not recommended in most problems of earth physics.

The systematic distortion of Eq. (1) and the significantly higher scatter of the values obtained by them is evident in Fig. 10b and in the bottom part of Fig. 10a. The median value corresponding to the simple approximative formula, Eq. (11) in Fig. 10b is near to the greatest possible deviation of the latter formula (the deviation itself is in accordance with the values cited after Eq. 11); the distortion of Eq. (1) should be qualified as unacceptable in spite of the fact that the distribution $f_{\alpha}(x)$ with $\alpha = 1.5$ has no extremely stong flanks and it can be considered in many practical cases as a valid model.

If the approximation yielded by Eq. (11) does not fulfil the accuracy demands, the value of r should be determined as a root of Eq. (10). Figure 10b shows the results of this proper method, too; the result is surely acceptable. It could be objected that Eq. (10) supposes the knowledge of the actual value of α, i.e. of the type of the distribution. The bottom cluster of points in Fig. 6b shows, however, that the uncertainty of r does not increase in case of an unknown α, in the investigated r-domain.

REFERENCES

Cramér H 1946: Mathematical Methods of Statistics. University Press, Princeton

Csernyák L, Steiner F 1982: Publ. of the Techn. Univ. for Heavy Industry, Ser. A., Mining, 37 (1-2), 47-64.

Erdélyi A ed. 1954: Tables of Integral Transforms. McGraw-Hill, New York

Gnedenko B V, Kolmogorov A N 1951: Limiting distributions for the sum of random variables (in Russian). Akadémiai Kiadó, Budapest

Hajagos B 1982: Publ. of the Techn. Univ. for Heavy Industry, Ser. A., Mining, 37 (1-2), 95-114.

Hajagos B, Steiner F 1989: Acta Geod. Geoph. Mont. Hung., (present issue)

Hajósy A 1989: Acta Geod. Geoph. Mont. Hung. (present issue)

Kerékfy P 1978: Alkalmazott Matematikai Lapok, 4, 327-357.

Rényi A 1971: Wahrscheinlichkeitsrechnung. (Mit einem Anhang über Informationstheorie). 3. Auflage. Dtsch. Verl. der Wissenschaften, Berlin

Steiner F 1982: Publ. of the Techn. Univ. for Heavy Industry, Ser. A., Mining, 37 (1-2), 79-88.

Steiner F 1988: Geophysical Transactions, 34, 138-260.

Acta Geod. Geoph. Mont. Hung., Vol. 24 (3-4), pp. 441-447 (1989)

DETERMINATION OF TYPE USING SAMPLE WIDTH

L Csernyák

University for Heavy Industry, H-3515 Miskolc, Egyetemváros, Hungary

[Manuscript received October 17, 1988]

The paper gives sets of curves which show the number of sample elements needed for a decision for or against Gaussian distribution, or for or against any other distribution type in the supermodel $f_a(x)$ at a given level of significance.

Keywords: Gaussian distribution; sample range; supermodel $f_a(x)$; type of a probability distribution

Data sets in earth sciences may belong to a number of different distribution types. It is known that from the (mostly supposed as symmetrical) distributions only the Gaussian one (and others very near to it) enable us an effective use of the algorithms based on the L2-norm. This paper gives a very simple statistics using the range of the sample to decide if the Gaussian distribution can be adapted for the actual distribution (i.e. traditional methods can be used with an acceptable statistical effectivity) or this hypothesis should be rejected.

Such a statistics decides against the use of the Gaussian distribution in case of Gaussian data sets containing some outliers, too, as traditional methods may give in such cases false results.

The distribution function of the random variable ξ be F, the sample containing n elements from ξ : ξ_1, ξ_2, ..., ξ_n. There are many procedures to decide from the sample if the hypothesis about the original distribution F is correct or not. In the present paper it will be shown that based on the range of the sample it can be rather effectively distinguished to which other distribution of the family the sample belongs.

The supermodel $f_a(x)$ (the so-called generalized Student--distributions) has been intensively studied by the Miskolc team (e.g. Steiner 1988). It is defined by the density functions:

$$f_a(x) = \frac{1}{c(a)} \frac{1}{(1+x^2)^{a/2}} \qquad 1 < a < \infty \ .$$

Here a = 2 corresponds to the Cauchy-distribution, the limit distribution is at $a \to \infty$ (standardizing to the variance) the Gaussian one. In the following this family is studied, including the Gaussian (the so-called normal) distribution, too.

Be ξ_1^* the smallest of the sample elements $\xi_1, \ldots \xi_n$, and ξ_n^* the greatest among them. In such a case the range of the sample is the difference

$$R_n = \xi_n^* - \xi_1^* \ .$$

The distribution function W_n of the random variable R_n can be given in a general case as

$$W_n(r) = n \int_{-\infty}^{\infty} \left[F(r+u) - F(u)\right]^{n-1} f(u)du \ ; \qquad r \geq 0 \ ,$$

if the density function f exists (Cramer 1946, Rényi 1968). As not each member of the family f_a has a finite variance, standardization is made to the interquartile range (2q), i.e. the quotient

$$R_n/2q$$

is being studied, where

$$\int_{-q}^{q} f_a(x)\, dx = \frac{1}{2} \ .$$

Figures 1 to 6 show the values of R for different n-s for

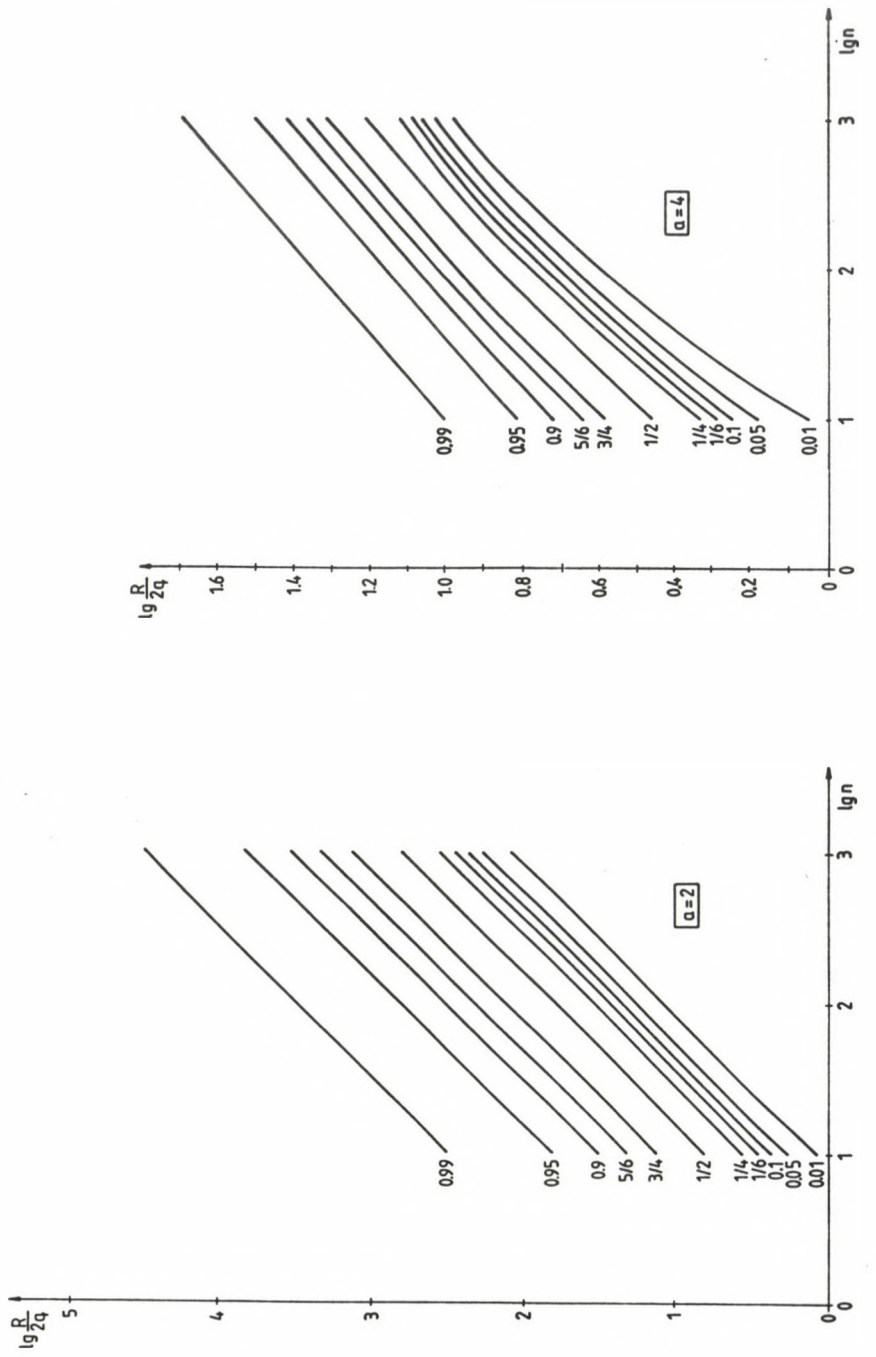
lg R/2q
5
4
3
2
1
0
0
1
2
3
lgn
0.99
0.95
0.9
5/6
3/4
1/2
1/4
1/6
0.1
0.05
0.01
a=2

Fig. 1.

lg R/2q
1.6
1.4
1.2
1.0
0.8
0.6
0.4
0.2
0
0
1
2
3
lgn
0.99
0.95
0.9
5/6
3/4
1/2
1/4
1/6
0.1
0.05
0.01
a=4

Fig. 2.

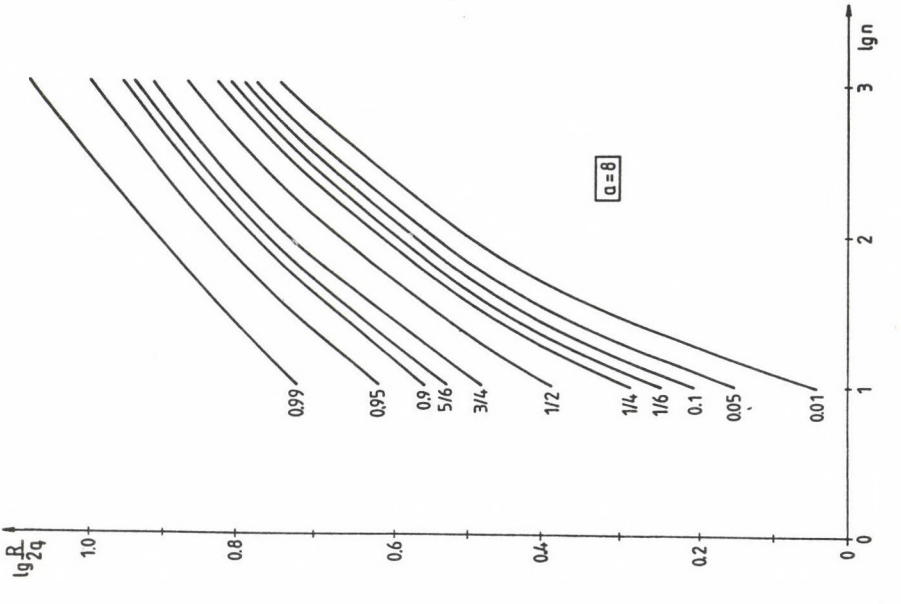
lg R/2q
1.0
0.8
0.6
0.4
0.2
0
0
1
2
3
lgn
0.99
0.95
0.9
5/6
3/4
1/2
1/4
1/6
0.1
0.05
0.01
a=8

Fig. 3.

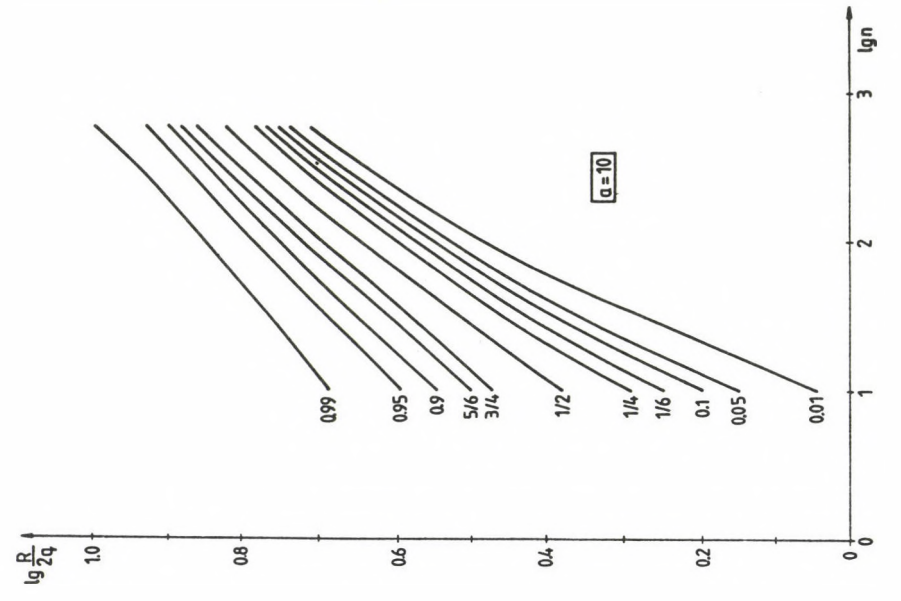
lg R/2q
1.0
0.8
0.6
0.4
0.2
0
0
1
2
3
lgn
0.99
0.95
0.9
5/6
3/4
1/2
1/4
1/6
0.1
0.05
0.01
a=10

Fig. 4.

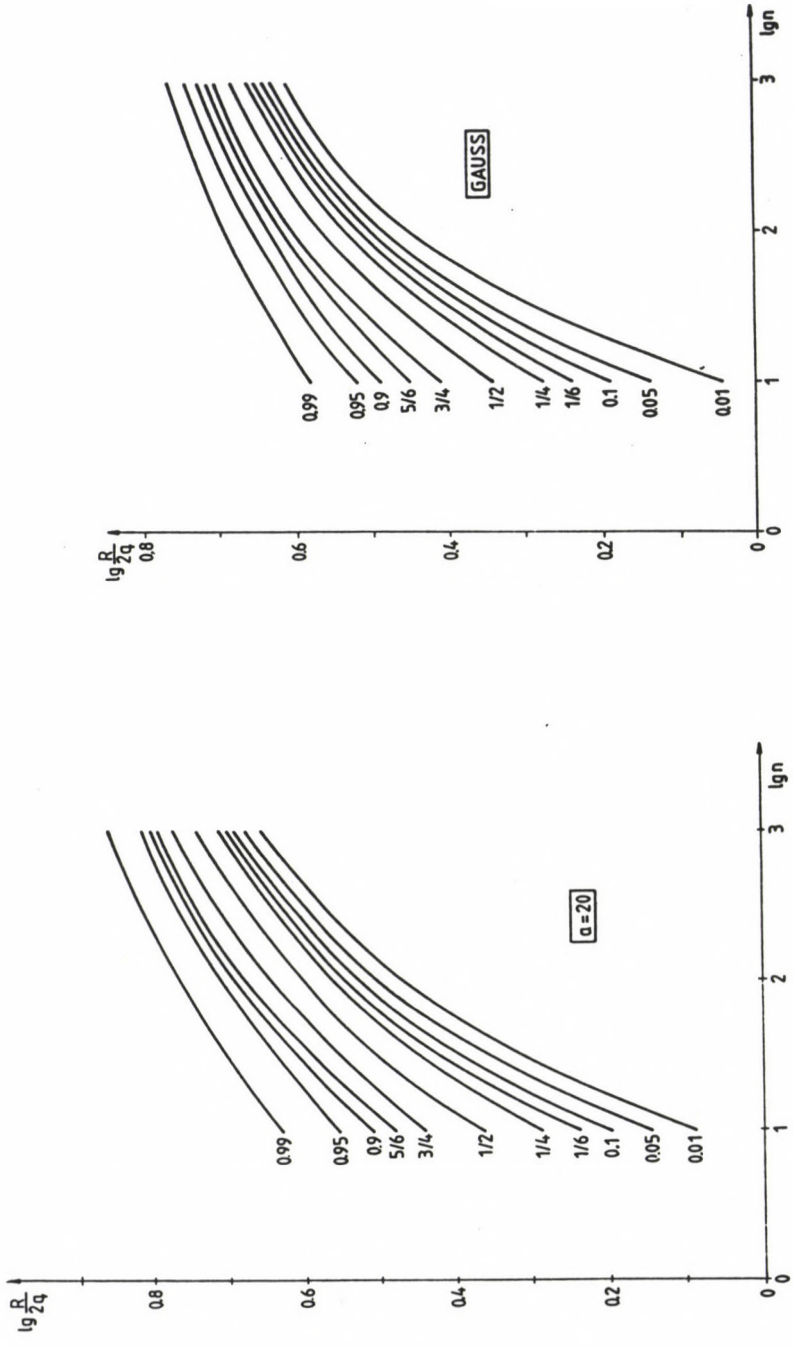
lg R/2q
0.8
0.6
0.4
0.2
0
0
1
2
3
lgn
a=20
0.99
0.95
0.9
5/6
3/4
1/2
1/4
1/6
0.1
0.05
0.01

Fig. 5.

lg R/2q
0.8
0.6
0.4
0.2
0
0
1
2
3
lgn
GAUSS
0.99
0.95
0.9
5/6
3/4
1/2
1/4
1/6
0.1
0.05
0.01

Fig. 6.

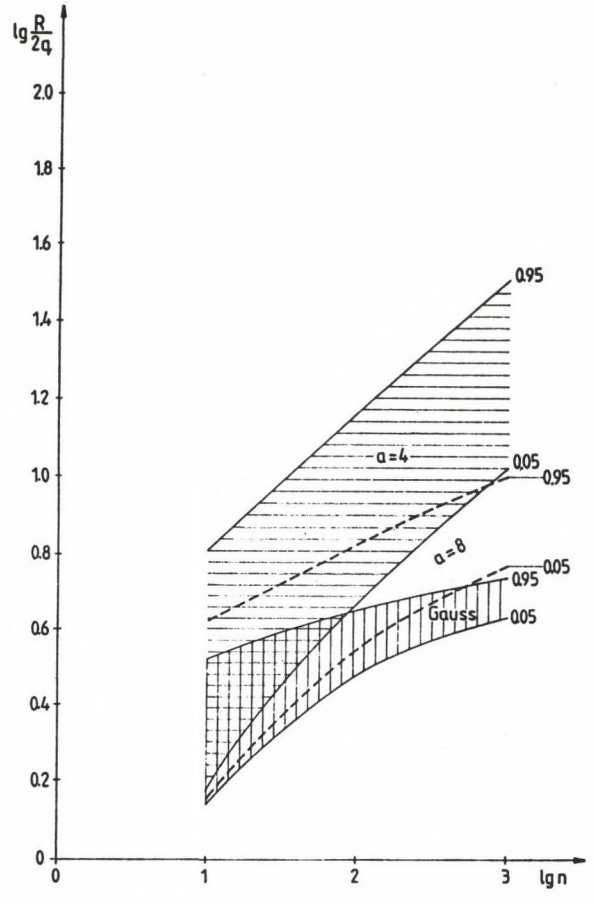
lg R/2q
2.0
1.8
1.6
1.4
1.2
1.0
0.8
0.6
0.4
0.2
0
0
1
2
3
lg n
0.95
a=4
0.05
0.95
a=8
0.95
0.05
Gauss
0.05

Fig. 7.

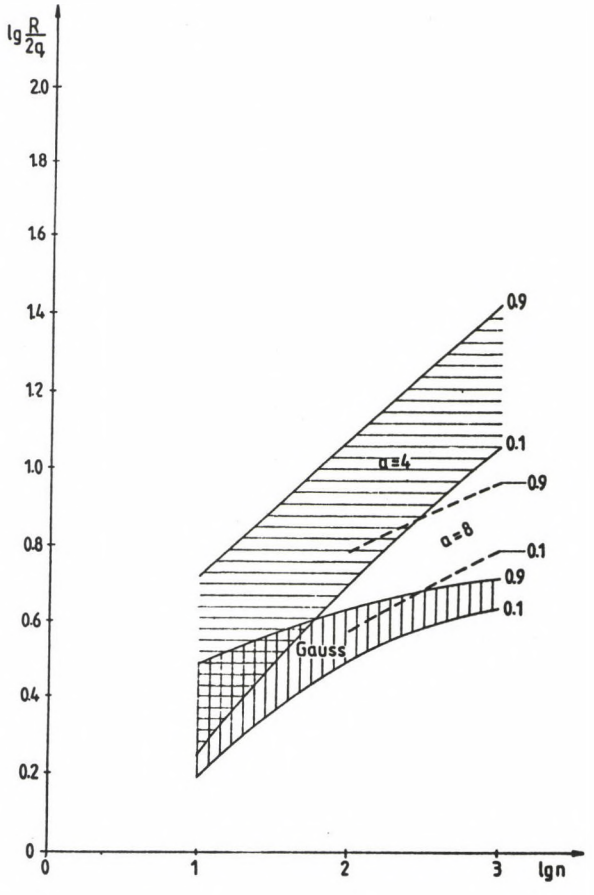
lg R/2q
2.0
1.8
1.6
1.4
1.2
1.0
0.8
0.6
0.4
0.2
0
0
1
2
3
lg n
0.9
a=4
0.1
0.9
a=8
0.1
0.9
Gauss
0.1

Fig. 8.

which the probabilities 0.01; 0.05; 0.1; 1/6; 1/4; 1/2; 3/4; 5/6; 0.9; 0.95; 0.99 are reached by $W\left(\frac{R}{2q}\right)$.

Figure 6 refers to the Gaussian distribution. It shows that e.g. for a sample having 100 elements (lg n = 2) the probability for $\lg R_{100}/2q > 0.69$ is 0.01, if the sample is from a Gaussian distribution. Thus it can be rejected at a probability level of 99 percent that the distribution is a Gaussian one if $\lg(R_{100}/2q)$ is greater than 0.69.

Figures 7 and 8 show that these probability levels separate well in case of samples having more than 100 elements the Student-distributions with the density functions f_4, f_8 and the Gaussian distributions.

For example with n = 1000, if

$$\lg \frac{R_{1000}}{2q} = 0.97$$

the Gaussian distribution can be rejected at least at a level of significance of 95 percent (Fig. 7), and the Student-distribution f_8 at a level of at least 90 percent (Fig. 8).

A few (one or two) outliers may significantly influence the range of the sample. Therefore, if this effect is to be eliminated, it is recommended to carry out the proposed type determination in a modified form, namely using instead of the sample range the interquantile range $F^{-1}(1-\delta) - F^{-1}(\delta)$ with a small δ-value. The distribution function for these data of the sample cannot be given in a general form, but Monte-Carlo computations have been started in this problem.

REFERENCES

Cramér H 1946: Mathematical Methods of Statistics. Princeton University Press, Princeton

Rényi A 1968: Probability theory (in Hungarian). Tankönyvkiadó, Budapest

Steiner F 1988: Geophysical Transactions, 34 (2-3), 139-260.

Acta Geod. Geoph. Mont. Hung., Vol. 24 (3-4) pp. 449-452 (1989)

A 450 KM LONG RUPTURE ZONE BETWEEN THE CZECH-MORAVIAN HILLS, SOUTHERN TRANSDANUBIA AND KISKUNSÁG

L Moldvay

H-1113 Budapest, Elek u. 3/B, Hungary

[Manuscript received November 3, 1988]

The crust in the Carpathian Basin has been extensive since the Early, according to several authors since the Late Miocene. Later no folding or overthrust came into being, only some smaller blocks moved mainly vertically. In the Bakony Mts horizontal displacements of up to 5 km-s were found.

In the Alpine-Carpathian region an extensive system exists due to the moving of the Carpathians away from the Alps (or to a mutual moving off). This 450 km long zone could be called Hungarian-Moravian extension zone.

The huge extensive rupture system is compared with a polyethylene model. Both indicate fan-like ruptures crossed by transversal bowed zones.

Keywords: Carpathian Basin; Czech-Moravian Hills; Kiskunság; rupture zone; Transdanubia

It is generally accepted that the crust of the Carpathian Basin has been extensive since the Early, according to others since the Late Miocene. Therefore in the area of Hungary no more foldings or overthrusts have developed since the Early and Late Miocene, respectively. Smaller blocks moved mainly vertically, they rose or sank. There are, however, results which found horizontal movements in the Bakony Mts up to 5 km (Mészáros 1983).

Photogeologic, endogenous morphological, hydrographical, seismological studies yielded new data about the area, and they enabled together with traditional geological results to detect in all its connections a huge extensive system in Hungary, with continuations in Austria and in a part of Moravia. This extension is evidently due to a movement of the Carpathians away from the Alps, or from a relative movement of both away from each other. Such a rupture system could give answer to a lot of questions which remained unanswered till now. This zone could

be called Hungarian-Moravian extension zone. Its length is 450 km. This short report intends to communicate only this fact.

In Central and Eastern Hungary, signatures of an extensive zone like that in Transdanubia are not to be found. With this system, the horizontal movements in the Bakony Mts can be well explained.

The extension zone is presented in Fig. 1 which shows among other phototectonic lines given by Sikhegyi (1985) (1:1 000 000 map), and river beds. The connection of the two systems of lines is evident. The system is similar to two open fans placed at opposite positions. The tips of the fans are connected by radii with the closing perimeters of the fans; between the radii bowed internal lines appear. Parts of the Hungarian Central Mts fit to the SE photogeological lines. At the tips, the Little Hungarian Plain and the Moravian Basin are found (1, 2 in the Figure).

The system closes at North by the Czech-Moravian Hills, at South by the Mecsek and Villány Mts and the Kiskunhalas graben. Its huge dimension fits well to the dimension of the two chain mountains. This system may help an understanding of the Central European region and partly of the Balkan peninsula, too. The seismological data of the area should be re-interpreted in the light of this zone.

A model for this extension zone was found at Shinozaki and Howe (1968).This model supports the idea. Figure 2 shows ruptures on a polyethylene plate due to moving off and having the same double fan structure as was found between Mecsek Mts and Kiskunság on the one side, and the Czech-Moravian Hills on the other. It is characteristic for both that the ruptures are crossed by transversal stripes. The surface, morphological and hydrographic situation in Hungary fits well with Sikhegyi's (1985) interpretation of the satellite image. The radial system of the tectonic system is especially well visible on older striped and hydrographic maps.

A detailed study of the extension zone should be started in the near future.

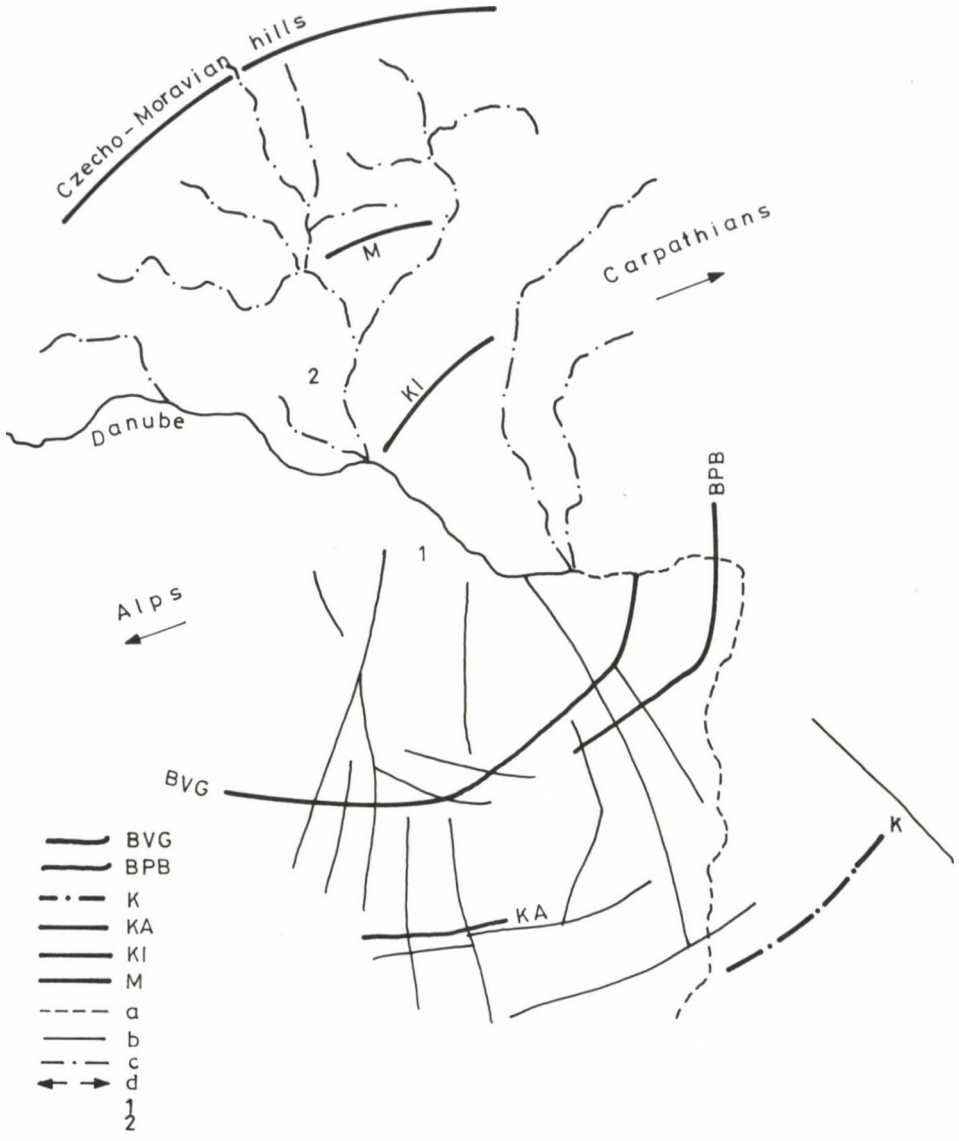

Fig. 1. The map of the extension zone. BVG - Bakony, Vértes, Gerecse geoanticline, partly on the cover of the Upper Pannonian, after Moldvay; BPB - Budai Mts, Pilis, Börzsöny geoanticline, partly on the cover of the Upper Pannonian; K - Kiskunhalas Badenian-quarternary graben, after Körössy and Moldvay; KA - Kaposvár high zone; KI - Little Carpathians; M - Mars Mts; a - Danube; b - Phototectonic lines after Sikhegyi (1985); c - river beds in Czechoslovakia; d - arrows indicating divergence; 1 - Little Hungarian Plain; 2 - Moravian Basin

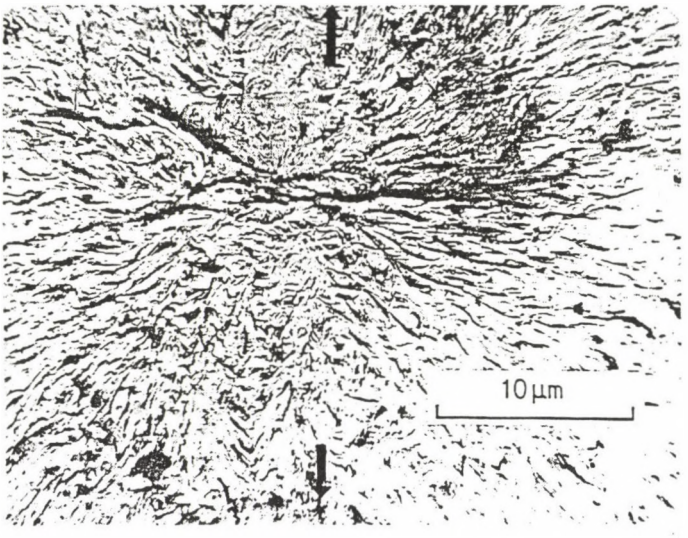

Fig. 2. Shinozaki and Howe's (1968) model for the extension zone

REFERENCES

Mészáros J 1983: In: Annual Rept. of the Geol. Inst., 1981, 483-502.

Shinozaki D M, Howe R 1968: Journ. Material Sci.

Sikhegyi F 1985: Structural elements in Hungary from satellite images, map with a scale of 1:1000000, manuscript (in Hungarian)

Acta Geod. Geoph. Mont. Hung., Vol. 24 (3-4), pp. 453-469 (1989)

EXPLORATION OF COAL SEAMS BY THE MEASUREMENT OF THE ELECTRIC FIELD OF A BURIED VERTICAL AC ELECTRIC DIPOLE

E Takács

University for Heavy Industry, Department of Geophysics, H-3515 Miskolc, Egyetemváros, Hungary

[Manuscript received January 17, 1989]

The imaginary and real parts of the electric field of a vertical AC electric dipole are investigated in the equatorial plane and in its vicinity. The dipole is buried in a coal seam having an electric resistivity higher by one order of magnitude than its host rock. The effect of the coal seam on the components of the electric field is analyzed. The responses of real and imaginary current systems are different to stratification and to discontinuities. Proposals are made with some examples for the exploration of the seam, of the cover and basement.

Keywords: coal seam; mining geophysics; transillumination; vertical electric dipole

1. INTRODUCTION

DC measurements yielded favourable experiences about the use of the exploration of the coal seam complex and of its embedding in a mine (Csókás et al. 1986). Based on this result it is worth investigating if a similar arrangement - earthened vertical electric dipoles at the boundary of the coal seam complex in workings or in boreholes - can be applied for frequency sounding. The purpose of the present paper is therefore to study the characteristics of the vertical electric field of a vertical, elementary electric dipole in a stratified space in the equatorial plane. This task is carried out by an algorithm from Takács et al. (1986). No similar study is known to the author about the effect of the stratification on the electric field in a seam of low resistivity contrast.

The coal seam has a resistivity higher than its embedding. The investigations are carried out therefore for horizontally

stratified sections where the resistivity of the layer in which the dipole is buried, is higher than that of the embedding. One of the models contains three layers representing a high resistivity intermediate layer between underlying and cover. The other model has four layers corresponding to the situation of the base seam when a high resistivity dolomite or limestone appears near to the seam.

A section consisting of horizontal layers is the basic model for the exploration of seam underlying and cover. Further the knowledge of the field is necessary for the detection of lateral inhomogeneities too, as in such cases the basis for the investigation is the deviation of the field from that in the basic model.

2. CHARACTERISTICS OF THE ELECTRIC FIELD OF A BURIED AC VERTICAL ELECTRIC DIPOLE

2.1 Character of the frequency sounding curves

Frequency sounding curves are presented in Figs 1 and 2. They show curves for the mentioned sections and for a homogeneous space corresponding to the embedding rock. Transmitter and receiver are in the centre of the 250 ohmm layer at a distance of R = 50 m. The locations of discontinuities intercept the location of change of sign, i.e. of the zero crossing. Negative fields are denoted by broken line.

In case of the three-layer section (Section A) the value of both the real and imaginary field components and the shape of the curves change with respect to those in a homogeneous medium. The increase of the quasi-stationary part on the curves of $|E_Z(f)|$ and of Re $E_Z(f)$ with respect to the homogeneous case is the basis of the DC measurement. With an increase of the frequency, however, the EM field starts to contract and the effect of the coal seam gets correspondingly enhanced. Consequently the effective resistivity of the volume affecting the measurement increases. Thus the explored volume is determined both by spacing transmitter-receiver and by frequency. Due to the continuously changing volume in consequence of a changing

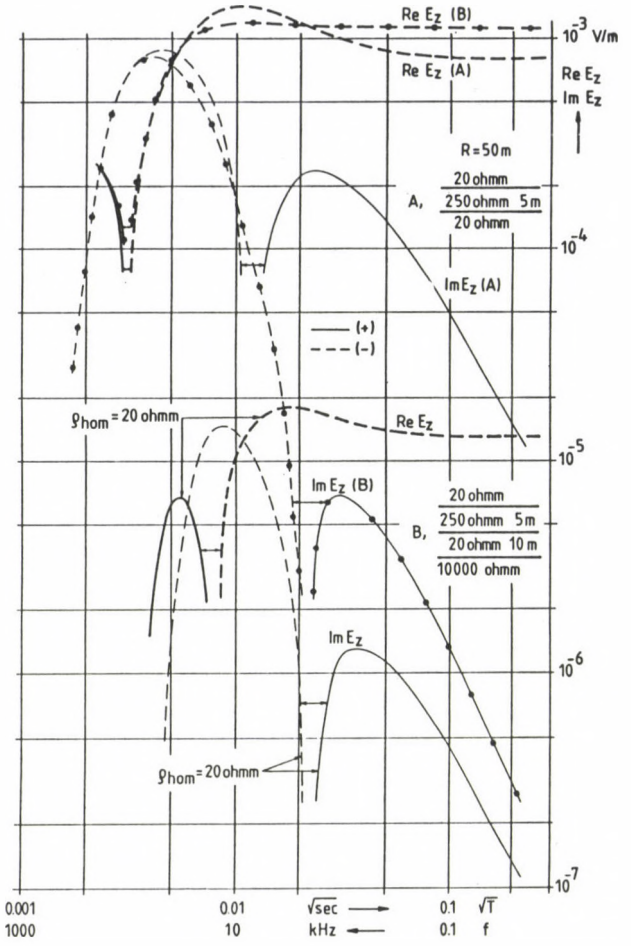

Fig. 1. Frequency sounding with real and imaginary components in the 250 ohmm layer of the given sections and in a homogeneous space of 20 ohmm, transmitter-receiver spacing R = 50 m

frequency, the characteristic points of the curves - maxima, minima, sign changes - shift both in resistance and frequency from the corresponding initial values in homogeneous space. That is just how the effect of the stratification appears and - as expected - that of lateral inhomogeneities, too.

In Figs 1 and 2 there is practically no difference between three- and four-layered curves at the highest frequencies. This

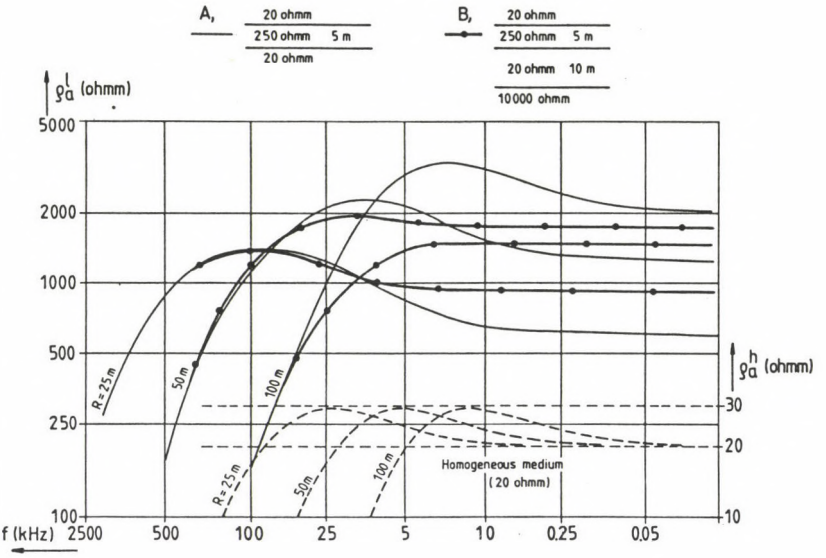

Fig. 2. Frequency sounding curves with the amplitude in the 250 ohmm layer of the given sections, and in a homogeneous space of 20 ohmm, transmitter-receiver spacings R = 25, 50 and 100 m

is due to a concentration of the EM field in the seam when the high resistivity basement does not exert any influence.

A comparison of the three- (A) and four-layered (B) curves at lower frequencies shows that the field of an inductive character (near to the maxima of Im E_z, Re E_z) decreases in case of the four-layered curves, while in the quasi-stationary part the field increases. The significant decrease of the inductive Im E_z component at low frequencies is of special significance. In this frequency range the curve Re E_z is influenced by geometrical, Im E_z by inductive effects, resulting in opposite changes due to the effect of the basement.

The effect of the change in the parameters of the sections at the given spacing transmitter-receiver has else the same sign as the sign of the change in the specific resistivity is along the equatorial plane. An increase of the effective resistance in the space outside of the plane of the dipoles - an increase in resistivity, thicker seam, high resistivity embedding

- decreases the field.

2.2 Definition of the apparent resistivity based on characteristic points of frequency-sounding curves

The changes connected to the layering appear successively vs. frequency; they can be hardly identified in case of complicated, dynamically changing curves. Therefore it is advantageous to attach apparent resistivities to different frequencies. In other words: be given the resistivity of a homogeneous space in which the same measurement arrangement yields characteristic points at the same frequency as in the layered space.

Apparent resistivities can be taken from the curves in Fig. 3 which shows the absolute value and the real and imaginary components vs. R/δ - where R is the distance of the station, δ the skin depth - for the ratio of the AC fields at a frequency f and of the DC field and for the phase in the homogeneous space. A concrete value of R/δ belongs to each characteristic point of the curve, to a selected level between them or to a phase. In case of areal measurement with a spacing R measured values of a given characteristics belong to a fixed frequency. If the corresponding value R/δ of the homogeneous field is attributed to this frequency, a skin depth, and from it - as the frequency is known - an apparent resistivity $\varrho_a^*(f)$ can be computed. The phase can be especially well used for the determination of the apparent resistivity, as it changes monotonously after the first zero crossing, and its values are restricted to the range of $\pm 90^0$. As it shall be discussed later, real and imaginary components reflect elements of the geological structure in different ways. Thus, a common application of the apparent resistivities, determined from the real and imaginary components may be of use. Namely the value $\varrho_a^*(f)$ computed from the amplitudes or from the phases averages their information at frequencies where the magnitude of the components is similar.

2.3 Effect of the seam on the field and on the location of the characteristic points

The increase of the field in consequence of the seam is

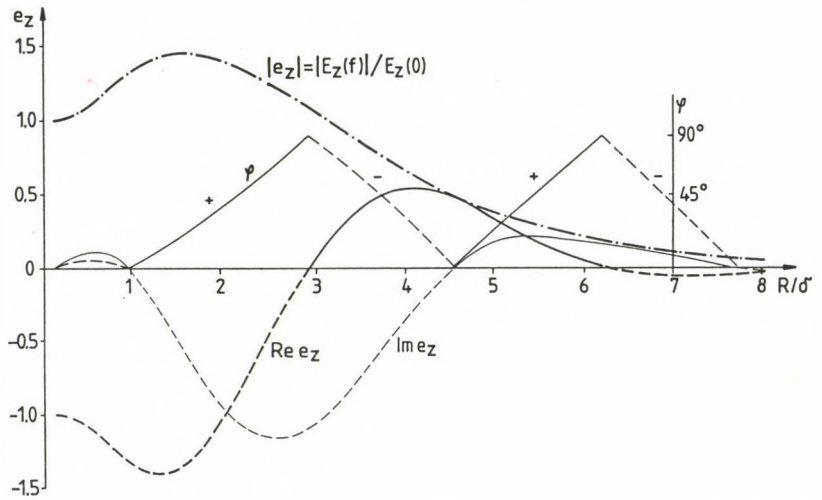

Fig. 3. Electric number e_z of the real and imaginary components and of the amplitude and phase vs. ratio of the transmitter-receiver spacing and skin depth δ in a homogeneous space

shown in Fig. 4 for characteristic points of the curves referred to the same points obtained in a homogeneous space (stationary part, maxima, minima, zero crossings) for a three--layer-section. The increase is significantly more than the ratio of the resistivities and increases with the spacing (see Fig. 3). Index 1 refers to the layered, index h to the homogeneous space. The maximum of the absolute value is an exception as the effect of the seam differs on the real and imaginary current loops, respectively. The rate of the increase is higher at lower frequencies, mainly for the imaginary component. At higher frequencies - i.e. at the location of the maximum Re E_z - where the field is concentrated into the seam, the change is slower. The figure shows the curve $\varrho_a(0)^1/\varrho_a(0)^h$ of the apparent resistivity of the DC geometrical sounding, too, further the value $\varrho_a(f_{max})^1/\varrho_a(0)^1$ computed from the formula of the apparent resistivity of the DC sounding. Latter value is 1.46 for a homogeneous space.

The presence of the seam changes significantly the position of the extrema and of the zero crossings on the frequency

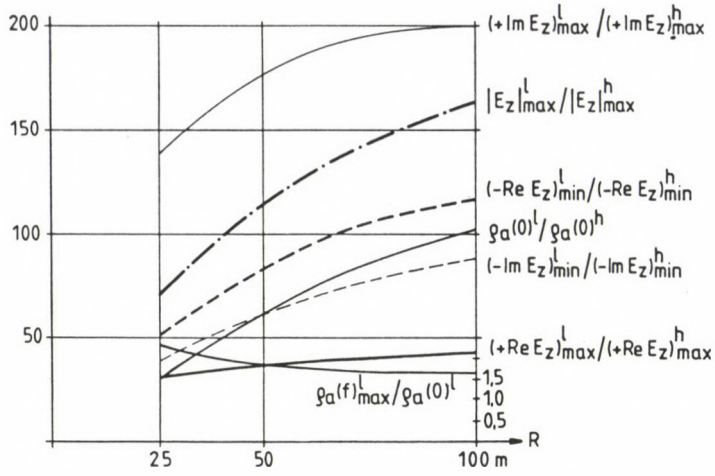

Fig. 4. Ratio of the fields in the 250 ohmm layer of the three-layer--section - index l - and of the 20 ohmm homogeneous space - index h - in case of different transmitter-receiver spacings at the characteristic points of the frequency sounding curves. ϱ_a values are determined by the factor of the geometrical sounding from the amplitude value

axis. Their shift is shown in Fig. 5. Here the values are related again to values at a frequency which would belong to the same characteristic points in a homogeneous space of a resistivity corresponding to that of the host rock. The characteristic points shift in each case toward higher frequencies due to the presence of the seam - as the effective resistance of the volume within the contracting current system increases. This effect, however, decreases with an increasing spacing R. According to the principle of the geometrical sounding the volume affecting the measurement increases if the spacing increases. The greater the volume the less is the effect of the seam, but it remains significant. At greater distances the curves are more similar to those in homogeneous space. The curves of the characteristic points - with the exception of that of $\mathrm{Im}\,E_z = 0$ - follow each other from bottom as they develop in a homogeneous space with increasing frequency. In this sequence $\mathrm{Im}\,E_z = 0$ would, however, follow the curve $\mathrm{Im}\,E_z = \max$. This

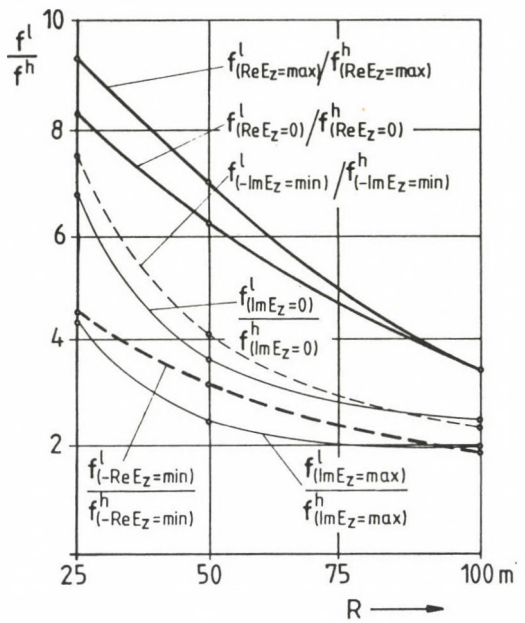

Fig. 5. The ratio of the frequencies belonging to the characteristic points of the frequency sounding curves in case of the three-layer-section (1)- and of the 20 ohmm homogeneous space (h) vs. transmitter-receiver spacing

fact speaks again about the different influence of the seam on the real and imaginary current systems. This is especially true for the low frequency, inner current system in the immediate vicinity of the transmitter.

The apparent resistivities from the characteristic points of the three-layer-section are presented in Fig. 6. For a better comparison of data at different spacings, the apparent skin depth ϱ_a is shown on the abscissa axis of Fig. 6. At higher frequencies - i.e. at low values of δ_a - ϱ_a^* approximates the real resistivity of the seam in consequence of the concentration of the current loop in the seam. Figure 6 illustrates again the different character of the inner imaginary current loop.

The EM field in the three-layer-section A is shown in Fig. 7 in the equatorial plane for the full practical range of

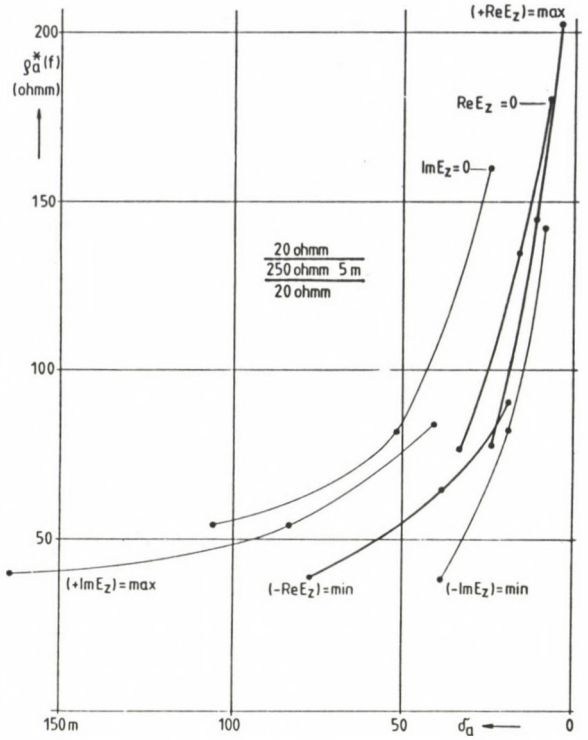

Fig. 6. The apparent resistivity for the characteristic points of the frequency sounding curves for spacings R = 25, 50, 100 m measured in the 250 ohmm layer of the section vs. apparent skin depth

spacings at three - rather low - frequencies. There is a chain of current loops of opposite signs which contracts both laterally and vertically if the frequency increases. A more detailed study in the vicinity of the seam shows that not only the zero crossings, but also the distributions outside of the seam differ for the real and imaginary components. That is why apparent resistivities computed from the real and imaginary components do not coincide, as the geological structure influences the two resistivities differently.

2.4 Character of the horizontal electric field

In the practice asymmetrical sections - with different

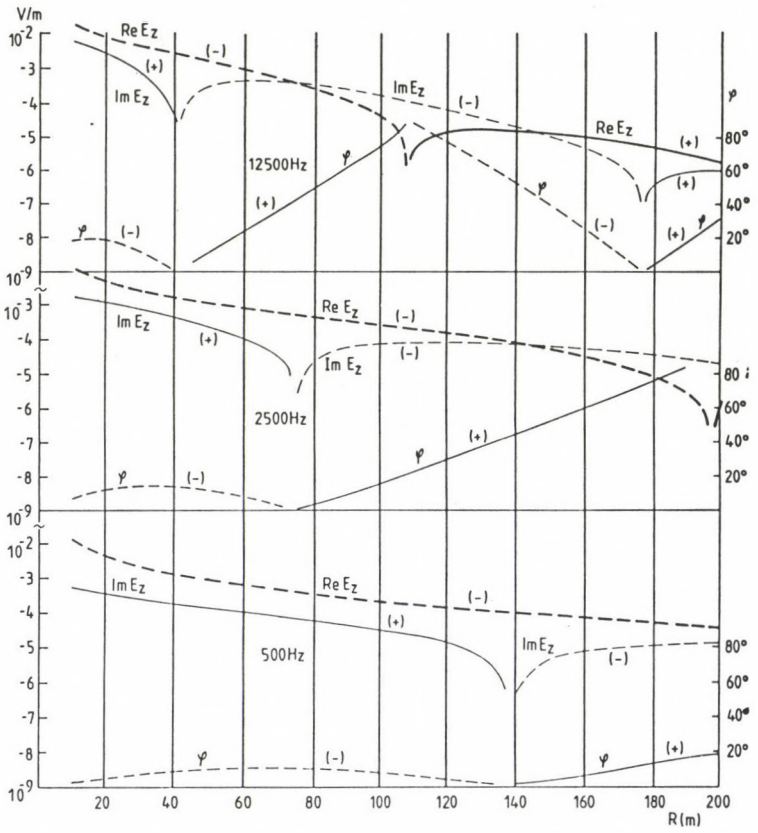

Fig. 7. Real and imaginary fields and phases in the three-layer section, in the 250 ohmm layer vs. distance from the transmitter (R)

basement and cover - do occur. Such a section is the four-layer section, too. The vertical electric field itself did not show the asymmetry of the section. Thus e.g. the curves for a cover of 10 ohmm and a basement of 30 ohmm practically coincide with the curves of a seam embedded into a 20 ohmm underlying and cover. The different horizontal components of the electric field at the bottom and top boundary of the layer, however, hint at a difference between basement and cover. The low frequency parts of the curves of the real and imaginary components of the horizontal field differ from each other (Fig. 8) and the ratio of the real components coincides in the quasi-stationary part - independently of the spacing R - with the ratio of the

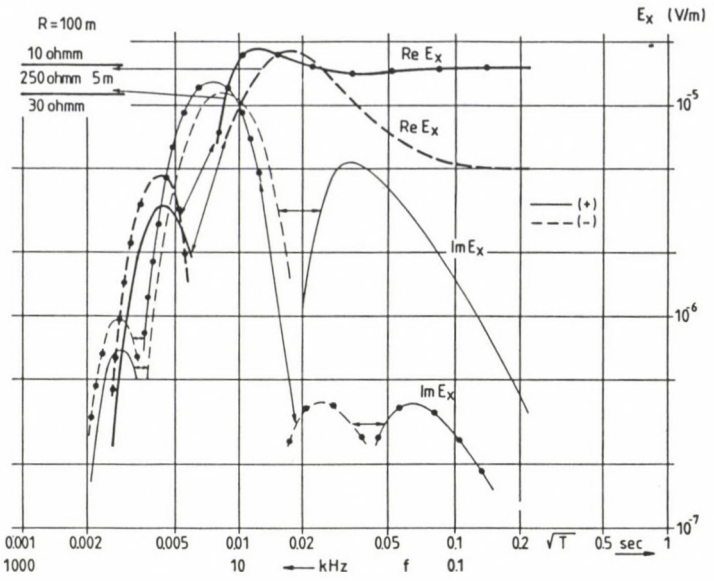

Fig. 8. Frequency sounding curves for the horizontal electric field of a vertical electric dipole, for R = 100 m, at the upper and lower boundary (dotted) of the 250 ohmm layer in the asymmetric section

resistivities of cover and basement. At higher frequencies the curves approximate each other, as the field is reorganized from both directions toward the seam. In the vicinity of the equatorial plane of the transmitter the horizontal component has a value of zero, therefore the information from the upper and lower loops seems to separate. This fact is shown by the different positions of the maxima of the real and imaginary components on the frequency axis on the curves belonging to the upper and lower boundary of the layer, further by the fact that curves measured at the roof and at the underside differ slightly according to the resistivities.

3. POSSIBILITIES FOR PRACTICAL USE

On the basis of the characteristics of the EM field presented in Section 2, the underground frequency sounding has the following advantages in mining geophysics.

There are several kinds of data for the determination of

the distribution of the resistivity in the space between the workings and boreholes - real and imaginary components, absolute value, phase - in contrast to a single value of $\Delta U/I$ from DC measurements. An interpretation based on the shape of the curves - i.e. on the characteristic points - is more reliable even in case of shunting metal objects in the vicinity of the transmitter than if only amplitudes were used.

The basis for DC imaging is the deviation from the value computed for a normal - horizontally stratified - section, that is why values in the normal section should be exactly known. This is a difficult problem concerning the resistivity of the seam, as the curve of the geometrical sounding is to be known till great spacings R. In case of frequency sounding the situation is more advantageous. From the point of view of induction, the effect of the seam is stronger at small spacings, thus a small spacing R is more advantageous for the determination of the resistivity of the seam. This is not only an advantage in measurement technics, but also the probability of a lateral homogeneity is less within a small spacing transmitter-receiver. A simple approximative method has been developed for the practical determination of the average resistivity of the rock volume near to the equatorial plane - ϱ_i^* -, i.e. of the seam. This method is based on two facts. First, the location of the characteristic points at low frequencies, and consequently that of the value $\varrho_a^*(f)$ computed from them is primarily determined by the low resistivity vicinity, $\varrho_{vicinity} = c(f)\,\varrho_a^*(f)$, second, the apparent resistivity belonging to the geometric sounding within given distance R is determined by the ratio $(\varrho_a)_{R \to \infty} = \varrho_i^{*2}/\varrho_{vicinity}$. ϱ_i^* is a characteristic value for the rock volume between the electrodes and it can be suitably used for tracing the change in the seam. Figure 9 shows the results of a measurement with a transmitter-receiver spacing of R = 70 m made in a seam. Layout 9 crossed a fault across the working which thrusted the seam.

The shape and the level of the frequency sounding curves differ from those computed for a laterally homogeneous section, especially at the point near to the fault.

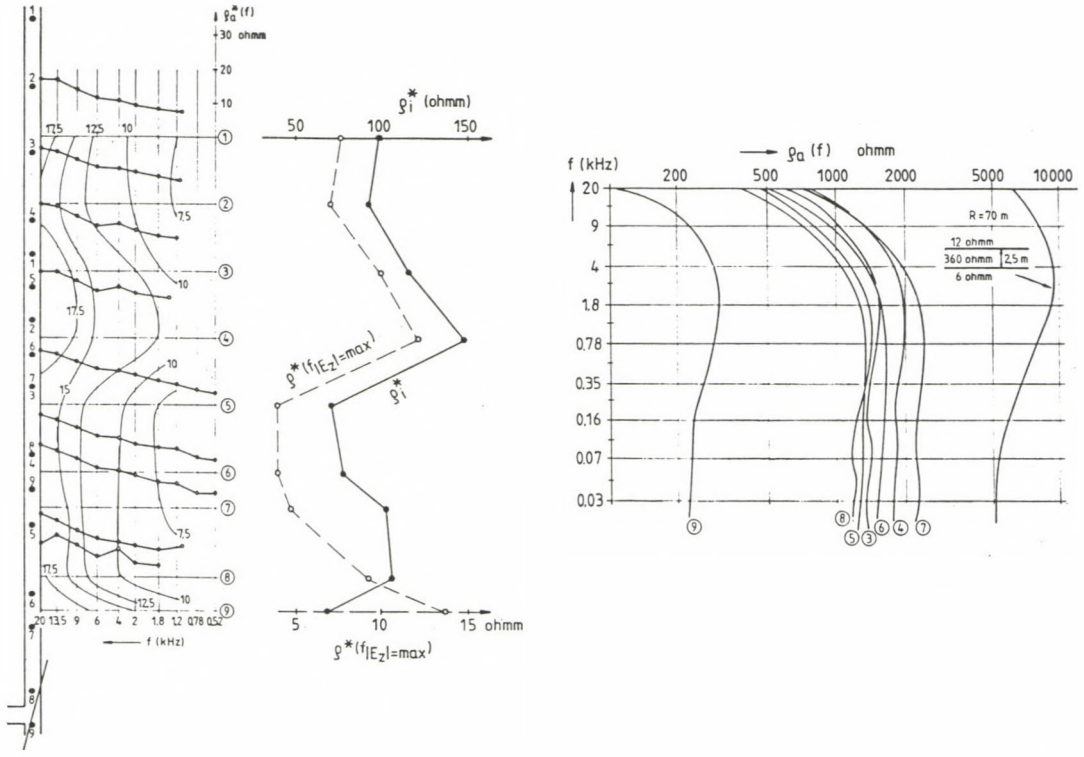

Fig. 9. Results of a frequency sounding along a working with a transmitter-receiver spacing of R = 70 m. $\varrho_a(f)$ is the frequency sounding curve computed from the field amplitude with the factor of the geometrical sounding. $\varrho_a^*(f)$ is the apparent resistivity computed by Fig. 3, and ϱ_i^* the average resistivity of the rock volume in the equatorial plane

The measurements have shown that the fault is even in the vicinity of station 1 near to the working, as ϱ_i^* is everywhere significantly less than the characteristic resistivity of the seam, 360 ohmm. The direction of the fault changes significantly near to stations 4-5. In the curves $\varrho_a^*(f)$ of stations 3-8 there is hardly any maximum indicating the proximity of a high resistivity layer either in the basement or in the cover of the seam. The increase of the value $\varrho_a^*(f)_{max}$ at station 9 - characterizing the complete volume which influences the measured value - is caused by a shift of this layer. $\varrho_a^*(f)$ computed from the plot $|e_z(R/\delta)|$ in Fig. 3 increases with the frequency and this is due to a slightly increasing effect of the seam.

It has been shown that the electric field is restricted to the immediate vicinity of the seam even at rather low frequencies, and this fact is advantageous from several respects, e.g. in the tomographic investigation of the seam.

Several measurements indicated the possibility of a determination of the continuity of the seam based on transillumination between two points at several frequencies without any change in the configuration of the measurement. It is highly probable that the location of discontinuities can also be determined by this method.

By transilluminating a seam from a borehole toward the working, it was experienced at several stations that the apparent resistivity $\varrho_a^*(f)$ does not increase continuously with increasing frequency - as expected for a continuous seam - but after an initial increase, the curve descends (Fig. 10). At the same time the field is also weaker than expected. As both transmitter and receiver dipoles were in the seam, this effect can be explained by an intermediate discontinuity of the seam. Toward station 9 the curve $\varrho_a^*(f)$ has significantly higher values and correspondingly the seam should be continuous.

Based on the characteristics of the EM field mentioned in connection with Figs 1 and 8, layers embedding the seam can be investigated by this measurement system, e.g. the depth of the high resistivity basement and inhomogeneities in it. For this purpose the inner real and imaginary current loops should be

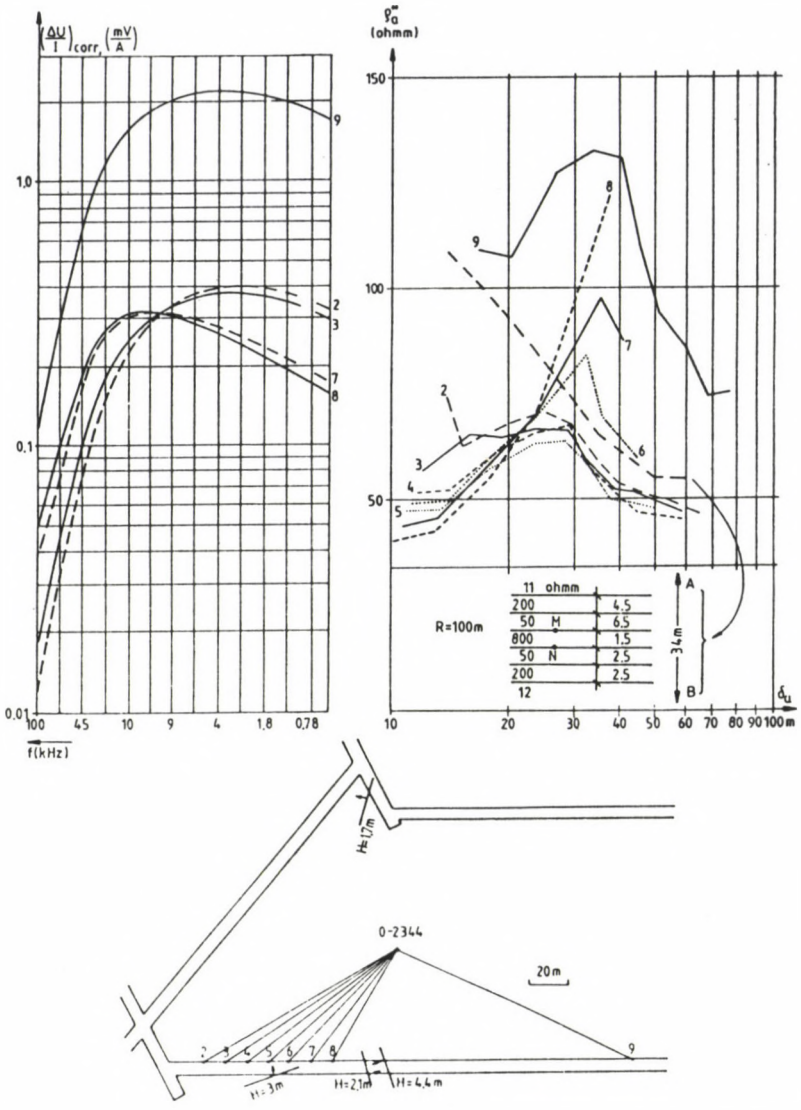

Fig. 10. The curves $\varrho_a^*(\varrho_a)$ resulting from transillumination between borehole and stations 2-8 in the seam, start to decrease above a limit δ_a. This decrease is caused by faults of 2.1 and 4.4 m found in the working. In an intact seam the curves would remain continuously increasing

used in the immediate vicinity of the transmitter at low frequencies. It is more advantageous to use a low value of R in

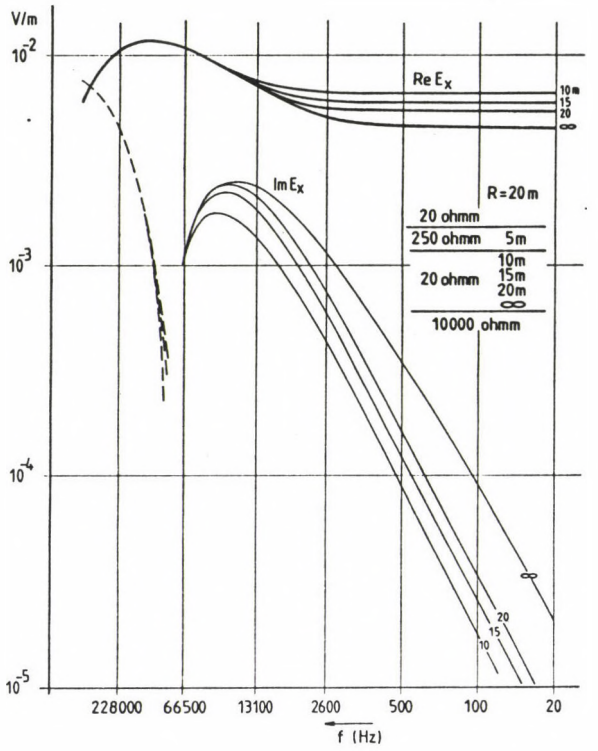

Fig. 11. The changes of the depth of the 10000 ohmm basement are reflected at small transmitter-receiver spacings and low frequencies in the horizontal electric field at the bottom of the coal seam

order to involve a smaller rock volume. The possibility of such a profiling with the horizontal electric field - it is best to use only one frequency - is presented in Fig. 11. The basement can be explored till a depth corresponding to the spacing R. The imaginary component is more sensitive for changes in the depth of the basement. The common use of the real and imaginary components is, nevertheless, more advantageous. Changes of these components measured in the logs of identical sign indicate changes in the rock in the vicinity of the equatorial plane, changes of opposite signs indicate, however, changes in the cover or in the basement. Effects from the upper and lower space can be distinguished by the horizontal component. In this paper the possibilities for an investigation of the cover and

basement should only be indicated without discussing the details.

4. CONCLUSIONS

The electric field of a vertical electric dipole in the seam is influenced in the low frequency range, too, by the horizontal layering - by the seam, by the cover and basement - and by their inhomogeneities. The character of these effects hints at the causes and this is the basis for the application of the frequency sounding in mines. Complete information can be obtained by a simultaneous use of amplitudes and phases or real and imaginary components, respectively.

REFERENCES

Csókás J, Dobróka M, Gyulai Á 1986: Geophysical Prospecting, 34, 1067-1084.

Takács E, Nagy J, Mádai F 1986: Geophysical Transactions, 32, No. 1, 43-56.

PROFESSOR JÁNOS CSÓKÁS IS 70 YEARS OLD

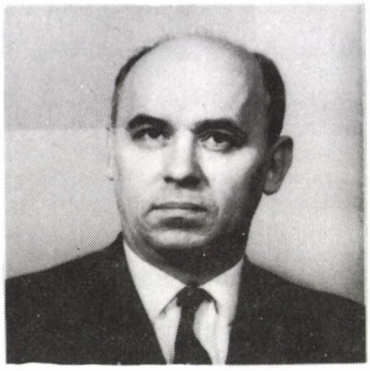

Professor János Csókás, former head of the Department of Geophysics at the Technical University for Heavy Industry, has turned to 70 on December 15, 1988. The professor who instructed generations of geophysicists, the scientist who developed several domains of geophysics, was greeted on this occasion by the community of Hungarian geophysicists.

Having obtained a Ph.D. degree in physics-mathematics at the "Pázmány Péter" University János Csókás started as a geophysicist in 1941 with the Hungarian-American Oil Industries Co. Ltd. Here he dealt with Eötvös-torsion balance and gravimetric measurements, data processing and interpretation. When geophysical education was to be started he was invited by Professors Tárczy-Hornoch and Kántás to the Department of Physics at the Technical University in Sopron. Since 1951 he has been at the new Department of Geophysics where he organized the training of geophysicists, compiled the curriculum and formed the spiritual atmosphere that survived till now. As recognition of his work he became associate professor in 1953. In 1956 he took over the Department of Geophysics. The Department of Geophysics was transferred in 1959 to Miskolc to the Technical University for Heavy Industry as a part of the Faculty of Mining. In 1956-59 he was assistant manager with the Eötvös Loránd Geophysical Institute, but continued his work in Sopron, too. He was appointed professor in Miskolc in 1959.

He led the Department of Geophysics till 1983. He has continued, however, to fulfil his duties as professor and lecturer with his usual commitment by helping the work of the Department of Geophysics.

Professor Csókás' activity as a lecturer and department leader has been characterized in every period of his career by a great pretension to be up-to-date and by the wish to create human contacts and cooperation with the students.

He considered it important that theory, instruments and results of the geophysical measurements should have a suitable place in education. For their sake he created educational connections, first of all with Eötvös Institute, with the Geophysical Company and with other institutions. He built up international connections of the department including the Mining Academy in Freiberg, the Mining University in Moscow and the Geophysical Institute of the Ruhr University in Bochum.

As a university lecturer he was the first to deal with the radiological examination of borehole samples. Later he led gravity, magnetic and geoelectric research for bauxite supported by the Hungarian Academy of Sciences.

He received academic awards several times. He took part in the introduction of the telluric and magnetotelluric methods in Hungary. He constructed the principle of an instrument for detection of gases solved in sludge. His candidate dissertation on this subject was published in 1959. He introduced a thermal instrument to detect underground fire and karst water in mines which was successful in coal and bauxite mining. A paper by Professor Csókás and co-authors on the focussed geoelectric sounding met international interest and the method became patented. He contributed to the measurement of the seismic effect of mining explosions.

With a co-author he developed the theory and an instrument for remanence logging. He pointed out possibilities to apply susceptability logging and developed an instrument for this purpose. For the in situ qualification of coal deposits and for well logging in mines he constructed further instruments. His method for the determination of the filtration coefficient in water-bearing sand layers proved to be succesful, too.

Several of his publications inform us about exploration methods of raw materials in the silicate industry. He proposed a special geoelectric method, the layer profiling, for the location of holes. This method was later introduced into archeology, too. He realized the dynamic determination of the rock-mechanical coefficients of borehole samples and found a relationship for their conversion into static values.

From the early seventies on Professor Csókás paid attention to mining geophysics where he did pioneering work and became an advocate of the applied geophysics in mines. An outstanding result of his scientific activity is a geoelectric method for mining geophysics. The method of seam-sounding is unique even in international comparison. This procedure makes it possible to determine the tectonic disturbances in coal deposits. In recognition of his great results in this field he got the degree Doctor of Sciences in 1980. The interest from foreign countries is demonstrated by the fact that the second research project has been started in co-operation with the Geophysical Institute of the Ruhr University in the frame of a DFG-MTA collaboration. The Hungarian project leader is Professor Csókás.

Professor Csókás incorporates the type of the creative scientists who considers that a university professor should also have social commitments. Besides his intense teaching and research work he has led an active public life. In his posts he has served passionately progress and rationality.

The greatest satisfaction of a person loving his profession is the result of his work. For Professor Csókás this satisfaction is based both on the achievements of his former students and on his personal contribution to the development of Hungarian geophysics.

Professor Csókás is owner of many awards: among them Order of Labour (1971) and Gold Medal for Merit in Mining (1979). The Association of Hungarian Geophysicists awarded him honorary membership (1974) and "Egyed László" Medal (1986).

Let us wish Professor János Csókás many creative years to follow at the occasion of his 70th birthday on behalf of his students, colleagues and of every Hungarian geophysicist.

E Takács

BOOK REVIEWS

K KRAUS and W SCHNEIDER: Fernerkundung. Band 1, Physikalische Grundlagen und Aufnahmentechniken. Dümmler-Verlag, Bonn, 1988. 291 pp, 137 figs, 15 tables

Remote sensing is one of the fastest growing techniques available to experts concerned with environmental problems from fields of diverse geosciences.

This textbook has been prepared primarily for use in introductory courses in remote sensing. It gives a very nice summarization of the physical fundamentals and sensor techniques.

Chapter I of the book describes the necessary definitions.

Chapter II summarizes the fundamental characteristics of electromagnetic radiation. The next chapter deals with different sensors, aerial photography, different scanners, radar systems.

Chapter IV describes taking different imagery; aerial photography, multispectral photography and imagery, microwave imagery, satellite imagery.

The book is very clearly written and will help all geodesists who are interested in remote sensing.

J Somogyi

•

G H FRIEDRICH and P M HERZIG eds: Base Metal Sulfide Deposits in Sedimentary and Volcanic Environments. Proceedings of the DMG - GDMB - SGA Meeting, Aachen, 1985. Springer Verlag, Berlin-Heidelberg, 1988. 290 pp, 155 figs, 46 tables

The book is the fifth in a series of Special Publications of the Society for Geology Applied to Mineral Deposits. This Proceedings Volume presents a collection of carefully selected papers on current research on the geology and metallogeny of base metal sulfide deposits in Europe, Africa and Australia, held at the DMG (Deutsche Mineralogische Gesellschaft) - GDMB (Gesellschaft Deutscher Metallhütten- und Bergleute, Fachsektion Lagerstättenforschung) - SGA (Society for Geology Applied to Mineral Deposits) Joint Meeting on Ore Deposits Aachen, FRG, September 16-19, 1985.

The present compilation is an overview of current research activities and results on base metal sulfide deposits in classical mining districts. Since such deposits with different ore compositions occur in a wide variety of geological and lithological settings of almost any age, the volume is organized along the lines of the classical host-rock classification.

Some of the papers give general view of the formation of different types of deposits with respect to their hosting environment. In the light of new concepts of the evolution of sedimentary basins and the ore forming processes in the volcanic environment some apparently well established ore genetic models seem to be reinterpreted. In his paper Large suggests a strict correlation between an evolutional stage of extensional basins and the sediment-hosted massive sulfide mineralization which stage is marked by sedimentological and lithological indications. His results highlight the possibility of using preliminary stratigraphical analysis of sedimentary sequences for their potential of hosting such mineralization.

On the other hand there are intensive local studies on ore deposits both in sedimentary and volcanic environments. In a very detailed study Herzig - discussing the genetic questions of the Agrokipia B sulfide

deposit, Troodos, Cyprus - presents a brilliant example of applying new concepts and complex methods in the examination of a deposit.

Part I focuses on sediment-hosted deposits including examples of Kupferschiefer and Copperbelt-type, as well as lead-zinc mineralization in carbonate host rocks.

Part II covers the volcanic and volcanic-sediment hosted base metal sulfides describing research on hydrothermal Cyprus and Kuroko-type, Iberian Pyrite Belt, Turkish copper deposits and sulfide ore deposits in alpine volcano-sedimentary sequences.

The book contains 16 papers and a useful subject index.

This volume provides valuable information to researchers and explorationists on geological, lithological, geochemical and tectonic parameters of ore formation.

F Gondi

STUART TURNER ed.: Applied Geodesy (Global Positioning System - Networks - Accelerators - Mathematical Geodesy). Springer-Verlag, Berlin, Heidelberg, New York, London, Paris , Tokyo, 1987. 393 pp, 190 figs, 25 tables

This book is Vol. 12 of Lecture Notes in Earth Sciences and was originally published as Internal Report under the title: Proceedings of the CERN Accelerator School of Applied Geodesy for Particle Accelerators, Geneva 1987. Lectures by 25 authors have been grouped under four main topics.

Chapter I. Global Positioning System and V.L.B.I. contains 6 lectures with the following topics: GPS, its Development and Deployment. GPS Receiver Technology. Precise Positioning with the GPS. GPS Orbit Determination Using the Double Difference Phase Observable. Very Long Base Interferometry.

Chapter II. Surface Geodetic Networks and Underground Geodesy also comprises six lectures which are the following: The LEP Trilateration Network. Deviation of the Vertical, Comparison between Terrameter and GPS Results- and How to Get There. Geodetic Networks for Crustal Movements Studies. Gyroscope Technology, Status and Trends. Underground Geodesy.

Chapter III. collects seven lectures in the topic of Applied Geodesy for Particle Accelerators. They are the following: High Precision Geodesy Applied to CERN Accelerators. Three-Dimensional Adjustments in a Local Reference System. Computer Aided Geodesy (I) Installation Procedure. Computer Aided Geodesy (II) Instrumentation. Applied Metrology for LEP (I) Computing and Analysis Methods. Applied Metrology for LEP (III) Data Logging and Management of Geodetic Measurements. Metrology for Experiments.

Chapter IV deals with Mathematical Geodesy involving three lecture: between Three- and Two-Dimensional Geodesy. On Continuous Theory for Geodetic Networks.

For the construction of large accelerators it is necessary to use geodetic techniques to ensure precise positioning of the machines' components. The increasing dimensions of new accelerators dictates the use of the best geodetic methods in the search for the greatest precision. At the same time, the powerful computer methods now available for solving difficult problems are also applicable at the instrument level where data collection can be automatically checked.

This book collects the most important measuring methods and calculations for this purpose.

The book is an up to-date work and gives a useful help to the readers involved in these subjects.

J Somogyi

K SCHNÄDELBACH (H Ebner Hrsg.): Ingenieurvermessung 88. Beiträge zum X. Internationalen Kurs für Ingenieurvermessung. Band 1. Dümmler-Verlag, Bonn, 1988, 328 pp, 128 figs, 14 tables

This book is a collection of lectures held on the X. International Meeting of Surveyors in Munich.

The articles are related to the following two topics: A) Instrumentation and Data Collection. B) Plotting Systems and Interpretation.

Topic A: A new concept for a partial automation of levelling system. The Hannover pendulum - a computer controlled mechanical pendulum measuring the position of the wire at any height without mechanical contact. A suggestion, how the surveying of a water body can be performed with the help of instruments, a surveyor affice should have at his disposal. Strapdown - inertial navigation system. The hybrid application of a combined INS-GPS system in surveying. An apparatus for calibrating horizontal and vertical - circle systems of electronic theodolites. A computer controlled total station to measure distances and horizontal and vertical angles. TOPOMAT a modulor fully automated polar measuring system. A summary of the executed experiences and examinations of the Wild DIOR 3002. Information about the Mekometer ME 5000. Description of a two-colour distance meter. Conditions and possibilities of electronic total stations and field computers. Conception of a fully automated measurement system. A measurement method allowing an automatic and permanent enforcement of the measurements.

Topic B: Digital Close-range photogrammetry. Functional aspects of a typical real-time vision system. "On-line" coordinate measurement with theodolites. The pros and cons of Kalman-filtering technique against the elastical deformation analyses. Theodolite measurement systems in industry, software construction, operating systems, expert systems and information-systems in engineering. CAD - graphic system. The acquisition, management and analysis of spatial information in informationsystems. The concept of a Geo-informationsystem. Hybrid graphic in geoinformationsystem. Development of Land Information Systems.

The book gives very useful information for practicioners.

J Somogyi

K SCHNÄDELBACH (H Ebner Hrsg.): Ingenieurvermessung 88. Beiträge zum X. Internationalen Kurs für Ingenieurvermessung. Band 2. Dümmler-Verlag, Bonn, 1988, 421 pp, 216 figs, 16 tables

This book is the second part of collected lectures held on the X. International Meeting of Surveyors in Munich. The articles join the following three topics:

C) Surface construction and industrial establishment.

D) Structural engineering and underground construction.

E) Environment and construction monitoring.

Topic C: Special equipment for control of parabolic antennas. Geodetic problems related to the construction of the building of a Water-Water-Energy Reactor of atomic power stations. The mathematical and elastomechanical principles governing the formfinding and analysis of thin prestressed surface structures. The formfinding and determination of working drawings for sophisticated spatial timber structure. Test controlling measurement of a bridge across a valley and an automatic pipe jacking measurement. About lateral refraction in engineering surveying. Using photogrammetry in surface engineering. Basic concepts in the use of TRANSIT and GPS for marine

platform positioning. Investigation of displacements and deformations of dry dock. A geographic information system. Three-dimensional survey techniques and their industrial applications.

Topic D: Tunnel-networks. The use of GPS in an Alps-crossing tunnel. The engineering-surveying problems of the planning and construction of railway tunnels. The use of the GYROMAT by the construction of the EUROTUNNEL. The geodetic control by the construction of a new large accelerator.

Measuring and surveying for the railway network of the Zürich S-Bahn. Checkingpoint system for the construction and the maintenance of a railway track. A system providing the data for the horizontal and vertical alignment of railway design. The interpretation of geotechnical measurements by tunnel constructions. Geographic information system developed by Wild. A modern, comprehensive network information system. Geographic-Technical Information Systems.

Topic E: The concept and design of a hybrid network: Special computer-controlled display and warning systems for engineer surveying. Automation of data collection and processing of deformation measurement. Photogrammetric monitoring in building construction. Photogrammetric deformation surveys. Terrain and image data processing for environmental surveillance. The development of a nation-wide environmental information system. The state of the art for the application of the deformation analysis.

The book gives useful information for those interested in this three topics.

J Somogyi

H MILITZER and F WEBER eds: Angewandte Geophysik. Band 3. Seismik. Akademie Verlag, Berlin and Springer, Vienna - New York, 420 pp, DM 68

This is the last volume of a three volume series on Exploration geophysics, written by R Schmöller and F Weber from the Leoben University in Austria and B Forkmann, H Militzer and R Rösler from the Freiberg Mining Academy in the GDR. It is meant as a handbook for university students in geophysics at both universities.

In the Introduction, Militzer gives an outline of the development of seismics, being the most important method in exploration geophysics. The following parts deal with seismic waves, petrophysical principles, principles of instruments and methods, seismic methodology, determination of the velocity, processing of reflexion data, interpretation and representation of seismic data, geological interpretation and with selected special seismic methods. All these parts are very richly illustrated in many cases from the countries of the authors, thus they have direct access to the data and are therefore characteristic for the area. Attention is paid to special problems, as e.g. deep seismic measurements in Central Europe. The different points of view from the two countries add to the value of the book as it helps to avoid bias or prejudice. Both mathematical principles and seismic instruments are adequately dealt with, being important for students of geophysics as well as for practicizing geophysicists. This book is and will be for several years an unavoidable companion for anybody dealing with geophysics in a German speaking country.

J Verő

W D STUART and K AKI eds: Intermediate-Term Earthquake Prediction. (Reprint from Pure and Applied Geophysics, 126, 1988, no. 2-4) Birkhäuser, Basel, 1988

The reprint volume contains the material of the international conference, "Physical and Observational Basis of Intermediate-Term Earthquake Prediction" in Monterey, California, November 14-17, 1986, sponsored by the US Geological Survey. It contains three main parts, the first on "Hydrologic and Geochemical Precursors" (100 pages), the second on "Seismologic and Geodetic Precursors" (250 pages), and a third on "Mechanical Models" (190 pages). The bulk of the papers are from US authors, in each part with one or two Japanese contributions indicating that mainly results from these two countries are to be found here. Roughly one half of the volume contains reviews, the other half original contributions in restricted sense. As a whole, the book gives a clear picture on methods which are considered in these two countries as most hopeful for intermediate-term earthquake prediction. These methods are based on the following phenomena: hydrological precursors, geochemical precursors, seismic quiescence, retardation of fault creep rates. Observational material for the prediction may be very different, e.g. groundwater monitoring is carried out in Japan by an amateur network (Catfish Club), while seismologists have extended networks - nevertheless in the latter case any change in the network may cause changes in detectability (lower limit in magnitude of detected earthquakes) and this is one of the most serious problems in the determination of seismic quiescence.

People interested in earthquake prediction obtain uptodate information about the present situation in this field from the book, with emphasis on methods used in the two mentioned countries. This restriction is a drawback of the volume, even if the numerous excellent reviews try to collect data and results from other countries, too. Geomagnetic and geoelectric methods are e.g. nearly completely omitted. Anyway, the increasing number of successful predictions, reported and explained here shows that it can be strongly hoped that more sophisticated methods of earthquake prediction combined with large observational networks may result in the near future in significant developments in this field.

J Verő

H FRÖHLICH: Vermessungstechnische Handgriffe. Basiswissen für den Aussendienst. Dümmler-Verlag, Bonn, 1988, 93 pp, 109 figs

In field work there are a lot of knacks which make easier the measurements. This book gives a help for technical people who are unskilled in practical surveying. For this reason the text is combined with lifelike figures.

J Somogyi

J BOISSONNAS and P OMENETTO eds: Mineral deposits within the European Community. Springer-Verlag, Berlin, Heidelberg, New York, London, Paris, Tokyo, 1988, 558 pp, 221 figs

After the oil crisis in 1973-74 the Council of Ministers of the European Community adopted a series of multiannual research programmes,

among others the programmes on "Primary Raw Materials" (1978-81) and "Metals and Mineral Substances" (1982-85). With the help of the research and development programmes of the European Community a collection of research papers originated mostly from the 1982-85 programme has been published in this volume which represents the 6th Special Publication of the Society for Geology Applied to Mineral Deposits.

The book is divided into three parts. The first part consists of the papers dealing with the tungsten and more or less associated mineralizations, such as tin, lithium, molybdenum and tantalum. The problems connected with the chromite and platinum group elements are discussed in the 2nd part, while the new results concerning the base metal, phosphate and placer mineral deposits are outlined in the 3rd part. This threefold division corresponds roughly to the three major geological environments: granites, ultrabasic rocks and sedimentary rocks.

Most of the papers are the results of the cooperation of scientists from at least two countries, thanks to the "contact groups" set up by the programme management.

The scope and subject matter varies from the individual deposits to the metallogenic provinces. Special attention is paid on the questions of exploration methodology. Thus, first of all structural and geochemical techniques are described.

This selection of papers gives a real picture on the present state of the Western European research in the field of economic (ore) geology.

P Árkai

REN JISHUN, JIANG CHUNFA, ZHANG ZHENGKUN, QIN DEYU under the direction of Prof. HUANG JIQING: Geotectonic Evolution of China. Science Press, Beijing and Springer-Verlag, Berlin, Heidelberg, New York, London, Paris, Tokyo, 1987, 203 pp, 30 figs, 14 plates

The present monograph is a brief explanatory text to the "Geotectonic map of China" in scale of 1:4000000 finished in 1978, as well as a further elucidation of the previous work "An outline of the tectonic characteristics of China" written by Huang Jiquing et al. (1977). This book presents the condensed summary of the enormous geologic work made by thousands of Chinese geologists in the last forty years.

The first chapter of the monograph outlines the theoretical and methodologic background of the further, detailed discussion. Although the authors of the book acknowledge the important changes caused by the theory of plate tectonics, they do not apply them fully in their interpretations. Discussing the main problems of geotectonics, special attention is paid to the specific features of continental and oceanic crusts, their contacts and relationship. The contrasting characteristics of mobile belts and platforms and their transformations are also outlined. The authors emphasize the significance of the polycyclic evolution of crustal parts including the stabilization of mobile belts as well as the re-activation of stable areas. In the view of this Chinese geotectonic school the deep fractures of different origin play an important role in the tectonic classification of the given area.

The subdivision and characterization of the tectonic cycles of China (Chapter II) is followed by the description of the main tectonic units (paraplatforms, platforms, geosynclinal fold regions, epicontinental and marginal sea basins) in Chapter III. After a more detailed explanation of geosynclinal evolution, deep fractures and deep-seated structures

(Chapters IV and V) the final (VIth) part of the book gives the genetic interpretation of the geotectonic evolution of China from the Archean up to the Alpine cycles. Beginning with the Indonesian (Triassic) cycle, plate movements are introduced to explain the evolution of the Tethys-Himalayan and the marginal-Pacific domains.

Until now very few, sporadic data have been published in English about the geology, and especially about the tectonic conditions of China. This fact gives an extraordinary value to this book. This volume provides basic data to everybody who is interested in the geotectonic evolution of Eurasia, or who intend to colour the white areas in plate tectonic models.

P Árkai

J GANGULY and S K SAXENA: Mixtures and mineral reactions. Springer-Verlag, Berlin, Heidelberg, New York, London, Paris, Tokyo, 1987, 291 pp, 108 figs

The 19th volume of the well-known series of the Springer-Verlag ("Minerals and Rocks", editor in chief: P J Wyllie, editors: A El Goresy, W von Engelhardt and T Hahn) presents an excellent summary of the enormous progress which has been achieved in the last twenty years in the konwledge of physicochemical changes of rocks based on the thermodynamic analysis of equilibria and reactions of solid solutions (minerals).

In addition to the concepts of the classical thermodynamics, solid solution, atomic ordering and interaction are outlined in the present work in order to solve different subsolidus (first of all metamorphic) petrological problems.

Although the book assumes familiarity with the basic principles of thermodynamics, the first chapter contains an up-to-date review of different basic thermodynamic functions (activity, fugacity, standard states, excess functions etc.), the interpretation of ideal and dilute solutions.

This is followed by the description of the mixing models and activity--composition relations of the real solid solutions. Chapter 3 deals with the phase separation in solutions with a detailed investigation of P-T dependence of unmixing as well as of the displacement of binary solvi due to a dilute third component. After the calculation methods of heterogeneous chemical reactions and equilibria (Chap. 4) thermodynamic properties of the most important mineral solid solutions (garnets, olivine, pyroxenes, micas, feldspars, nepheline-kalsilite, spinels and rhombohedral carbonates) are described (Chap. 5). The discussion of exchange equilibrium and inter--crystalline fractionation provides the theoretical basis of one of the most important application of the subject, namely the geothermometry and geobarometry (Chap. 6). This topic is closely related with the thermodynamics of cation ordering and with the relationships between order-disorder state and thermal history (Chap. 7). The last chapter (estimation and extrapolation of the thermodynamic properties of minerals and solid solutions) gives a stable basis for further developments.

The main text is completed with three appendices. The first one contains diverse, mainly theoretical topics such as crystal field theory, electronegativity, interdiffusion coefficient, temperature - time - transformation (TTT) diagram, while Appendix B deals with the geothermometric and geobarometric applications of continuous and discontinuous reactions. The behaviour of fluids under high pressure and temperature is outlined in Appendix C.

The structure of the text is logical, clear, well organized. The complete list of references and the well selected, didactic figures highly

increase the scientific value of the book.

This volume of the series "Minerals and Rocks" can be recommended to graduate students and geologists (mainly petrologists and geochemists) who intend to start or develop their knowledge in the field of geothermometry and geobarometry of metamorphic rocks, or who want to understand the nature of geologic processes reaching (more precisely, approaching) equilibrium.

P Árkai

V A MILASHEV: Explosion pipes. Springer-Verlag, Berlin, Heidelberg, New York, London, Paris, Tokyo, 1988, 249 pp, 51 figs

According to the author, the explosion pipes (or diatremes) are very common among geological formations. The explosion pipes which are the results of magmatic gas eruptions are characterized by peculiar shape, size, intrusive contacts, diverse infillings and mineralizations.

Although a lot of works have been published on the different aspects of diatremes, a monograph-like summary of the present state of our knowledge was lacking so far. This book intends to fill this gap.

The book consists of three main chapters. In the first and second ones the basic properties of kimberlite and lamproite pipes as well as the non-kimberlite diatremes are described, including the morphology, types, internal (endogenous and exogenous) structure, xenolith content, contact effects and raw material occurrences of the pipes. The main attention is focused on the temporal and spatial distributions of kimberlites, their structural controls and other factors of their localization. The hypotheses on the character of kimberlitic magma chamber are critically evaluated. The non-kimberlitic diatremes (Chapter 2) are connected mainly with alkali--basaltoid - carbonatite, trachyte and basaltic trap formations of the continental crust.

Chapter 3 presents an up-to-date synthesis of the mechanism and conditions of pipe formatioin. Evaluating the physical state of the materials involved in diatreme formation, and the dynamics and mechanism of the process, the energetics of this peculiar phenomenon is described.

The author collected and interpreted all of the available data. The structure of the book is clear, the figures are didactic. Both specialists, field geologists and students may profit this excellent monograph.

P Árkai

PRINTED IN HUNGARY

GÉPKOOP–GRAFITYP GM
Budapest

treble underlining: bold-face italics
red underlining: Greek letters
green underlining: script letters

Rules for mathematical-physical notations:

trigonometric, logarithmic, analytic symbols, symbols for units and functions are in roman type (not underlined)

letter symbols in mathematical and physical formulas, scalars, and subscripts of algebraic and physical quantities are in italics (underlined)

vectors, matrices, operators in probability theory are in bold-face roman type (double underlining) tensors, operators and some special functions are in script letters (green underlining). These cannot be bold.

Greek letters (red underlining) cannot be bold or extra bold type (thus they cannot be used for vectors or tensors)

void upper lines e.g. for vectors

avoid possible confusion between o (letter) and 0 (zero), l (letter) and 1 (one), ν (Greek nu) and v.u. (letters) etc.

explain ambiguous or uncommon symbols by making marginal notes in pencil

be careful about superscripts and subscripts

formulae must be numbered consecutively with the number in parentheses to the right of the formula. References in text to the equations may then usually be made by the number in parenthesis. When the word equation is used with a number, it is to be abbreviated. Eq. or Eqs in the plural the International System of Units (SI) should be used.

Authors are liable for the cost of alteration in the *proofs*. It is, therefore, the responsibility of the author to check the text for errors of facts before submitting the paper for publication.

3. *References* are accepted only in the Harvard system. Citations in the text should be as:

... (Bomford 1971) ... or Bomford (1971)

... (Brosche and Sündermann 1976) ...

... (Gibbs et al. 1976b) ...

The list of references should contain names and initials of all authors (the abbreviation et al. is not accepted here); for *journal articles* year of publication, the title of the paper, title of the journal abbreviated, volume number, first and last page.

For *books* or *chapters in books*, the title is followed by the publisher and place of publication.

All items must appear both in the text and references.

Examples:

Bomford G 1971: Geodesy. Clarendon Press, Oxford

Brosche P, Sündermann J 1976: Effects of oceanic tides on the rotation of the earth. Manuscript. Univ. of Bonn

Buntebarth G 1976: Temperature calculations on the Hungarian seismic profile-section NP–2. In: *Geoelectric and Geothermal Studies (East-Central Europe. Soviet Asia), KAPG Geophysical Monograph.* Akadémiai Kiadó, Budapest, 561–566.

Gibbs N E, Poole W G, Stockmeyer P K 1976a: An algorithm for reducing the bandwidth and profile of a sparse matrix. *SIAM J. Number. Anal.*, 13, 236–250.

Gibbs N E, Poole W G, Stockmeyer P K 1976b: A comparison of several bandwidth and profile reduction algorithms. *ACM Trans. on Math. Software.* 2, 322–330.

Szarka L 1980: Potenciáltérképezés analóg modellezéssel (Analogue modeling of potential mapping). *Magyar Geofizika,* 21, 193–200.

4. *Footnotes* should be typed on separate sheets.

5. *Legends* should be short and clear. The place of the tables and figures should be indicated in the text, on the margin.

6. *Tables* should be numbered serially with Roman numerals. Vertical lines are not used.

All the illustrations should contain the figure number and author's name in pencil on the reverse.

Figures will be redrawn. Therefore the most important point is clearness of the figures, even pencil-drawings are accepted (with a duplicate).

Photographs and *half-tone* illustrations should be sharp and well contrasted.

If a specific reduction or enlargement is required, please indicate this in blue pencil on the figure.

The editors will send information to the first author about the *arrival* and acceptance of the papers. A galley proof is also sent to the first author for *correction*. Hundred *offprints* are supplied free of charge.

Periodicals of the Hungarian Academy of Sciences are obtainable at the following addresses:

AUSTRALIA
C.B.D. LIBRARY AND SUBSCRIPTION SERVICE
Box 4886, G.P.O., *Sydney N.S.W. 2001*
COSMOS BOOKSHOP, 145 Ackland Street
St. Kilda (Melbourne), Victoria 3182

AUSTRIA
GLOBUS, Hochstadtplatz 3, *1206 Wien XX*

BELGIUM
OFFICE INTERNATIONAL DES PERIODIQUES
Avenue Louise, 485, *1050 Bruxelles*
E. STORY-SCIENTIA P.V.B.A.
P. van Duyseplein 8, *9000 Gent*

BULGARIA
HEMUS, Bulvar Ruszki 6, *Sofia*

CANADA
PANNONIA BOOKS, P.O. Box 1017
Postal Station "B", *Toronto, Ont. M5T 2T8*

CHINA
CNPICOR, Periodical Department, P.O. Box 50
Peking

CZECHOSLOVAKIA
MAD'ARSKA KULTURA, Národni třida 22
115 66 Praha
PNS DOVOZ TISKU, Vinohradská 46, *Praha 2*
PNS DOVOZ TLAČE, *Bratislava 2*

DENMARK
EJNAR MUNKSGAARD, 35, Nørre Søgade
1370 Copenhagen K

FEDERAL REPUBLIC OF GERMANY
KUNST UND WISSEN ERICH BIEBER
Postfach 46, *7000 Stuttgart 1*

FINLAND
AKATEEMINEN KIRJAKAUPPA, P.O. Box 128
00101 Helsinki 10

FRANCE
DAWSON-FRANCE S.A., B.P. 40, *91121 Palaiseau*
OFFICE INTERNATIONAL DE DOCUMENTATION ET LIBRAIRIE, 48 rue Gay-Lussac
75240 Paris, Cedex 05

GERMAN DEMOCRATIC REPUBLIC
HAUS DER UNGARISCHEN KULTUR
Karl Liebknecht-Straße 9, *DDR-102 Berlin*

GREAT BRITAIN
BLACKWELL'S PERIODICALS DIVISION
Hythe Bridge Street, *Oxford OX1 2ET*
BUMPUS, HALDANE AND MAXWELL LTD.
Cowper Works, *Olney, Bucks MK46 4BN*
COLLET'S HOLDINGS LTD., Denington Estate,
Wellingborough, Northants NN8 2QT
WM DAWSON AND SONS LTD., Cannon House
Folkstone, Kent CT19 5EE
H. K. LEWIS AND CO., 136 Gower Street
London WC1E 6BS

GREECE
KOSTARAKIS BROTHERS INTERNATIONAL BOOKSELLERS, 2 Hippokratous Street, *Athens-143*

HOLLAND
FAXON EUROPE, P.O. Box 167
1000 AD Amsterdam
MARTINUS NIJHOFF B. V.
Lange Voorhout 9–11, *Den Haag*
SWETS SUBSCRIPTION SERVICE
P.O. Box 830, 2160 Sz Lisse

INDIA
ALLIED PUBLISHING PVT. LTD.
750 Mount Road, *Madras 600002*
CENTRAL NEWS AGENCY PVT. LTD.
Connaught Circus, *New Delhi 110001*
INTERNATIONAL BOOK HOUSE PVT. LTD.
Madame Cama Road, *Bombay 400039*

ITALY
D. E. A., Via Lima 28, *00198 Roma*
INTERSCIENTIA, Via Mazzé 28, *10149 Torino*
LIBRERIA COMMISSIONARIA SANSONI
Via Lamarmora 45, *50121 Firenze*
SANTO VANASIA, Via M. Macchi 58
20124 Milano

JAPAN
KINOKUNIYA COMPANY LTD.
Journal Department, P.O. Box 55
Chitose, *Tokyo 156*
MARUZEN COMPANY LTD., Book Department
P.O. Box 5050 Tokyo International, *Tokyo 100-31*
NAUKA LTD., Import Department
2-30-19 Minami Ikebukuro, Toshima-ku, *Tokyo 171*

KOREA
CHULPANMUL, *Phenjan*

NORWAY
TANUM-TIDSKRIFT-SENTRALEN A.S.
Karl Johansgata 43, *1000 Oslo*

POLAND
WEGIERSKI INSTYTUT KULTURY
Marszalkowska 80, *00-517 Warszawa*
CKP I W, ul. Towarowa 28, *00-958 Warszawa*

ROUMANIA
D. E. P., *Bucuresti*
ILEXIM, Calea Grivitei 64–66, *Bucuresti*

SOVIET UNION
SOYUZPECHAT — IMPORT, *Moscow*
and the post offices in each town
MEZHDUNARODNAYA KNIGA, *Moscow G-200*

SPAIN
DIAZ DE SANTOS Lagasca 95, *Madrid 6*

SWEDEN
ESSELTE TIDSKRIFTSCENTRALEN
Box 62, *101 20 Stockholm*

SWITZERLAND
KARGER LIBRI AG, Petersgraben 31, *4011 Basel*

USA
EBSCO SUBSCRIPTION SERVICES
P.O. Box 1943, *Birmingham, Alabama 35201*
F. W. FAXON COMPANY, INC.
15 Southwest Park, *Westwood Mass. 02090*
MAJOR SCIENTIFIC SUBSCRIPTIONS
1851 Diplomat, P.O. Box 819074,
Pallas, Tx. 75381-9074
READ-MORE PUBLICATIONS, INC.
140 Cedar Street, *New York, N. Y. 10006*

YUGOSLAVIA
JUGOSLOVENSKA KNJIGA, Terazije 27, *Beograd*
FORUM, Vojvode Mišića 1, *21000 Novi Sad*